FACULTY OF CHEMISTRY
ORGANIC CHEMISTRY
DEPARTMENT

Doctoral program:
Organic Chemistry in the chemical
& pharmaceutical industry

CENTRO DE INVESTIGACIÓN
PRÍNCIPE FELIPE

POLYMER THERAPEUTICS
LABORATORY

POLYMER DRUG CONJUGATES FOR THE TREATMENT OF NEURODEGENERATIVE DISORDERS

INMACULADA CONEJOS SANCHEZ

Doctoral Thesis UV/ 2013
Thesis Director: María Jesús Vicent Docón

Dr. María J. Vicent Docón, Ph.D. in Chemistry and Head of the Polymer Therapeutics Laboratory at the Centro de Investigación Príncipe Felipe (Valencia, Spain)

CERTIFIES, that the work

"POLYMER DRUG CONJUGATES FOR THE TREATMENT OF NEURODEGENERATIVE DISORDERS"

has been developed by Inmaculada Conejos Sánchez under her supervision

in the Centro de Investigación Príncipe Felipe in Valencia, as a thesis project in order to obtain a Ph.D. degree in Chemistry from the University of Valencia, Department of Organic Chemistry.

Dr. María J. Vicent Docón

To the fourth pillars of my life:
Lorenzo, Luisa, Silvia y Felipe.

A los cuatro pilares de mi vida:
Lorenzo, Luisa, Silvia y Felipe.

ABBREVIATIONS

%ωt = drug loading in weight percent
4TP = 4-thiopyridine
Ab = antibody
ACN = acetonitrile
AML = acute myeloid leukemia
anh. = anhydrous
APS = ammonium persulfate
ATRP = atom transfer free-radical polymerization
BBB = blood brain barrier
Boc = Tertiary-Butyloxycarbonyl
BSA = bovine serum albumin
CMC = critical micelle concentration
CNS = central nervous system
cPEP = cyclic peptide
Cu = cupper
Cy = cyane
Cys = cysteine
DB = diblock
DCC = N,N´-dicyclohexylcarbodiimide
ddH2O = milliQ water
DIC = N,N'Diisopropylcarbodiimide
DIEA = di-isopropyl ethylamine
DLS = dynamic light scattering
DMF = dimethylformamide
DMTMM·Cl = 4-(4,6-dimethoxy[1,3,5]triazin-2-yl)-4-methylmorpholinium chloride
DOTA = 1,4,7-tetrazacyclododecane-1,4,7-10-tetraacetic acid
DOTA-NH2 = tert-butyl 2,2´,2´´-(10-(2-(2aminoethylamino)-2oxoethyl)-

1,4,7-tetrazacyclododecane-1,4,7-triyl)triacetate

DOTAtBu = t-butyl protected DOTA

Doxy = doxycycline

DP = degree of polymerisation

DTNB = 5,5'-dithiobis-(2-nitrobenzoic acid)

DTPA = N,N-bis(2-(2,6-dioxomorpholino)ethyl)glycine

DTR = dextran texas red

DTT = 1,4-dithiothreitol

FAP = familial amyloidotic polyneuropath

FBS = fetal bovine serum

FITR = Fourier transform infrared spectroscopy

FLI = fluorescence imaging

Fmoc = Fluorenylmethyloxycarbonyl

FPLC = fast protein light chromatography

Ga = galium

GA = glutamic acid

Gd = gadolinium

Gly = glycine

GPC = gel permeation cromatography

Hb = haemoglobin

HMDS = hexamethyldisilazanes

HOBt = Hydroxybenzotriazole

HPLC = high preasure light cromatography

HPMA = N-(2-hydroxypropyl)methacrylamide

HUVEC = human umbilical vein endothelial cells

i.p. = intraperitoneal

i.v. = intravenous

IHC = immunohistochemistry

LCMS = liquid chromatography-mass spectrometry

LRP1= low-density lipoprotein receptor-related protein-1

m/z = mass/charge

MOPS = 3-(N-morpholino)propanesulfonic acid

MRI = magnetic resonance imaging

MS = mass spectrometry

MSME = multi slice multi echo

MTT = 3-(4,5-dimethyl-2-thiazolyl)-2,5-diphenyl-2H-tetrazolium bromide

MW = molecular weight

NA = normal amine

NCA = N-carboxyanydride

NCS = neocarzinostatin

NHS = N-hydroxysuccinimide

NIR = near infrared

NMR = nuclear magnetic resonance

NMV = net magnetization vector

NPC = nuclear pore complex NPC

NRI = near infrarred

OG = oregon green cadaverine

p/p=protein / peptide

PB = phosphate buffer

PBLC = poly(benzyl-L-glutamate)

PBS = phosphate buffer saline

PCS = photon correlation spectroscopy

PD = pharmacodynamics

PDC = polymer drug conjugate

PDEPT = polymer-directed enzyme produrg therapy

PDI = polydispersity index

PEG = polyethylene glycol

PEI = poly(ethyleneimine)

PELT = polymer-enzyme liposome therapy

PEP1 = RAGE peptide-Gly

PEP2 = RAGE peptide-Gly-Cys

PET = positron emission tomography

PGA = poly-L-glutamic acid

PK = pharmacokinetics

PLL = polylysine

PMDTA = N,N,N´,N”,N”-Pentamethyldethylenetriamine

PNS = peripheral nervous system

PPC = polymer protein conjugate

PT = polymer therapeutics

RAFT = reversible addition-fragmentation chain-transfer

RAGE = receptor for advanced glycation end products

RAGE pep = RAGE peptide

RBC = reed blood cells

Rh = rhodamine (N-(6-Aminohexyl)rhodamine 6G-amide bis(trifluoroacetate))

ROP = ring-opening polymerisation

RP = reverse phase

RP-HPLC = reverse phase high pressure liquid chromatograpy

RT = room temperature

s.b. = subcutaneous

SANS = small angle neutron scattering

SAS = small angle scattering

SAXS = small angle X-ray scattering

SCID = severe combined immune deficiency

SDS = sodim dodecyl sulphate

SDS-PAGE = sodium dodecyl sulphate polyacrilamide gel electrophoresis

SEC = size exclusion chromatography

SMA = poly-(styrene-co-maleic acid)

SPECT = single photon emission computed tomography
SPR = surface plasmon resonance
T1-W= T1-weighted
TB = triblock
TBO = triblock labeled with Oregon Green
TEMED = tetramethylethylenediamine
Tf = transferrin
TFA = trifluoroacetic acid
TfR = transferrin receptor
THF =tetrahydrofuran
TJ = tight junction
TNBS = 2,4,6-Trinitrobenzenesulfonic acid
tR = retention time
TTR = transthyretin
UPCL = ultra performance light chromatography
UV = ultraviolet
v/v= volume/volume
WB = western blot
FDA = Food and Drug Administration
RNP = radionuclide purity
RY = radiochemical yield
ID = injected dose
AAS = atomic absortion spectroscopy
LSGS = low serum growth supplement
PMSF = phenylmethylsulfonyl fluoride
FOV = field of view
AIC = Akaike information criterion
AUC = area under the curve
rf = radio-frequency

ACKNOWLEDGEMENTS

"Feeling gratitude and not expressing it is like wrapping a present and not giving it". *William Arthur Ward*

Me es inevitable no extenderme en estas primeras páginas, ya que mucha de la gente a la que debo agradecer el estar aquí hoy no leerá más que estas palabras, ¡¡y hay tanta a la que reconocer todo este esfuerzo plasmado en papel! Puede resultar empalagoso y extremadamente largo, pero voy a darme el lujo.

La primera persona a la que debo haber comenzado esta aventura es sin duda mi directora de tesis, María Jesús. Gracias por haberme guiado en esta experiencia llamada doctorado. He tenido la oportunidad de crecer en tu grupo a la par que éste lo hacía. Haber llegado hasta aquí es fruto de tu optimismo y tus conocimientos, tus ganas de explorar y tu infinita capacidad de superación, cualidades que admiro. Gracias por haberme contagiado tu entusiasmo y por tu ayuda durante estos años. Ha sido un honor aprender de ti. Gracias por estar ahí y haber sido más que una directora de tesis, por entender mi alocada forma de ser y mis prisas, por tu apoyo, comprensión y por haber creído en mí. Gracias.

Y una jefa no es una jefa si no tiene un grupo a su cargo! Y ese grupo es el siguiente punto en la lista de agradecimientos. Más que un grupo es ya una familia. He tenido la suerte de encontrarme con buena gente, que se preocupan por ti más allá del trabajo y te demuestran un cariño y respeto impagables. Os voy a echar mucho de menos y costará no veros día tras día.El número de personas que han pasado por el i-36 puede definirse como incontable, al menos yo perdí la cuenta! Y aunque me costó entender que la gente "llega y se va", he conseguido aprender algo de cada una de esas personas. No nombraré a todos (porque si no podría escribir un buen anexo), pero están más que incluidos en estas palabras de cariño y agradecimiento. Todo

empezó contigo Vane, aprendí a tu lado a desenvolverme entre lab y lab, a pasar horas y horas entre risas y lágrimas, y seguir adelante día tras día, año tras año. Aprendí a echar de menos y a escribir emails interminables. Gracias por todos esos momentos que forman parte de nuestra historia y por esta amistad. Nuestra representante más internacional, Gabrielísima, una sonrisa venezolana que aunque se caiga el mundo es capaz de luchar en silencio contra todo pronóstico. Mi hijita. He aprendido mucho de ti, y sé que al otro lado del charco siempre tendré un hogar. Te deseo toda la felicidad del mundo, te la mereces más que nadie. Coralie completa el inicial grupo de doctorandas. Merci beacoup "chica Desigual" porque no habría logrado permanecer sin ti entre tanto ratoncito esas largas horas en animalario y durante esta ardua tarea llamada tesis. Entre otras cosas! :) Gracias por estar siempre pendiente, por tu constancia y ánimos; y sin duda tu tesis demostrará todo el intenso trabajo que has realizado. Lo lograremos! Amparísima, ver como lograste tu Cum Laude fue uno de los días más emocionantes de mi vida. Sin duda la investigación tiene la suerte de tenerte en sus filas. Gracias por tu locura y por tus ratos en el i36, espero que me hayas perdonado ya haberte "robado" la mesa! Para MH tengo más que palabras, un agradecimiento sincero por estar desde el principio en esta andadura. Por haber sufrido y celebrado cada una de las cosas que han sucedido entre esas cuatro paredes, por toda tu ayuda día a día. Gracias, gracias y gracias! Voy a echar muchísimo de menos tus *buenos días*! Lucile y Fabiana, los primeros pilares del i36. Gracias por vuestra paciencia y por ser prueba de que se sobrevive a la tesis! Gracias Fabs por el tiempo que dedicaste a mis primeros pasos por el i-36. Anita, eres (además de la dueña de las pipetas más codiciadas del i-36 ;D) un ejemplo a seguir, ojalá y sea capaz de alcanzar el punto de buen hacer, constancia y pulcritud que tu atesoras. Mil gracias por tu ayuda y predisposición, una "animalario's girl" a la que debo mucho y de la cual he aprendido un buen pellizco de lo presentado en este trabajo. Gracias por tus consejos y estar siempre ahí para animarme. Esther, gracias por tu sonrisa permanente y tu ayuda sin pedir nada a cambio, siempre y

cuando fuera. Tengo el placer de haberte conocido y sé que nos une algo más que el jamón! Muito obrigada menhina. Te admiro, de corazón. Y sí, estaremos en contacto :P. El grupo fue creciendo, nuevos Postdocs: Ximo, Rut, Rich, Marina. Los vecinos del despacho de al lado que daban vidilla a los *group meetings* y siempre han estado ahí cuando había que juntar cabezas para sacar algo adelante o para darte ánimos en los días de bajón. Gracias por vuestra comprensión y tantos y tantos ratos de fructíferas discusiones, almuerzos y cafés. Amaya, un apreciado fichaje que nos ha traído una positividad inocente desde "tierras lejanas". Deseo que tu tesis refleje todo el empeño que pones en ella, todo saldrá bien! Ha sido todo un placer contar contigo en esta última etapa y sin duda aun quedan muchos ratos por disfrutar juntas. En los últimos meses el lab ha recibido mucho género másculino :) Juanjo, Vicent, mil gracias por soportarme en este último tramo en el que he sido más bien poco sociable. Os deseo toda la suerte del mundo en este i-36! Gracias también a Matthias, por detenerse a ver mis problemas y sentarse a solucionarlos. Gracias por tus quejas y por escuchar las mías. He aprendido mucho de ti y espero seguir haciéndolo. Vielen dank chico. Y te dejo para el final Aroa, porque acabar esto no habría sido posible sin ti. Has sido el aliento del final de la carrera. Un viento fresco que me dio fuerzas para acabar cuando el barullo me impedía seguir. Voy a echarte de menos compi, muchísimo! He aprendido mucho de ti y contigo, nunca olvidaré nuestras andanzas a deshoras por el lab, nuestros skypes y meetings, nuestros momentos Máxima… y millones de cosas más. Te debo mucho... Gracias por tu ayuda y tu positividad que tanto me encanta. Todo te irá bien amiguita, sabes que no lo dudo, y espero no estar muy lejos para verlo contigo.

Mención especial al *PGA team*, tres personitas que hemos empleado tiempo, ánimo y un número indefinido de reuniones para sacar el trabajo adelante. ¡Aroa y Rich: somos un equipo! Las lecciones han sido aprendidas. Siempre me quedará el buen recuerdo de nuestro duro trabajo, lo mucho que nos recompensaban los buenos resultados y las risas juntos. Multitone!!

Gracias también a Carmen, Marta, David, Gianni, Harald, Ángela, Yentl y Andreu, porque vuestras manos han colaborado literalmente en este proyecto. Por esos experimentos que hemos compartido y han llegado por fin a puerto.

Gracias al Dr. Antonio Pineda, a Martina y Rodrigo por todas las veces que me han prestado su ayuda en los experimentos de RMN. Gracias por estar siempre para echar una mano, ayudarme a solucionar cualquier problema y tener una paciencia infinita con mis prisas.

Gracias al Dr. Vicente Felipo y al Dr. Omar Cauli, por ser parte de este trabajo y por su paciencia conmigo. Omar, mil gracias por tu disposición con tantos experimentos y pruebas que hemos ido tanteando y desarrollando, por tus ideas y estar siempre pendiente de mí, profesional y personalmente. Has sido una gran ayuda para mí en todos estos años. Siempre lo tendré presente.

Gracias al equipo de proteómica: Luz, Esther y Virginia. Gracias por compartir vuestros conocimientos y siempre tener una respuesta para mis atolondradas ideas, por vuestra paciencia infinita con mis MALDI exprés y vuestras sonrisas. Sois geniales.

Gracias también al Dr. M.A. Morcillo y su equipo, por toda la ayuda en los experimentos *in vivo* con radioactividad, por su buen trabajo y su ayuda en todo momento.

Mi estancia en Porto debo agradecérsela a nuestra colaboradora la profesora Maria Joao Saraiva. Gracias por acogerme esos tres meses en ese lugar perdido a orillas del Atlántico. A todo su grupo y muy especialmente a Isabel, por enseñarme todo cuanto aprendí allí y por estar siempre al otro lado del email cuando la necesitaba.

En todo este tiempo en el CIPF he conocido personas luchadoras con fe en la ciencia y el buen hacer, buenas personas con las que cruzarse por el pasillo alegraba el día. Gracias a todos por vuestros ratos y por solucionarme tantas dudas. Lucía, Roberto, Imelda, Carmen, Laura M., Rosa, Lorena, Rafa, Ana, Ali, Mara, Salva,

Natalia, Nacho, Amador, Ismail, Alba, Mar, Paqui, Susana, Tatiana, Andrés, Viviana, Amparo,….

Fuera de lo profesional, tus amigos siguen ahí sin entender porqué pasas semanas y semanas sin dar señales de vida. Permanecen pendientes de ti, insistiendo en que debes cambiar el chip, consiguen que veas más allá de tu negatividad y reconozcas todo lo que has logrado. Se esfuerzan por comprender qué les haces a los ratones, qué es eso de que se te mueren las células y en qué consiste eso de "sintetizar" vehículos que transportan cosas al cerebro. Debo agradecer a todo este elenco de amistades el apoyarme estos años, el celebrar conmigo mis triunfos y el hacerme ver todo lo bueno que tiene la vida si tienes unos amigos indescriptiblemente perfectos. A mis cedrillenses y cedrillensas, gracias por vuestras llamadas, los findes de charretas y vuestra contagiosa ilusión. Gracias Maco por siempre quitarme la venda que me pongo en los ojos y animarme sí o sí a seguir adelante y ver todo de una forma distinta, por tu apoyo y consuelo día a día. Gracias Vane por aguantar mis pataletas y ayudarme a que ser como soy no me autodestruyese ;), gracias por tu aliento y tu sonrisa. Gracias Tere por estar pendiente de cada movimiento, de alegrarte por cada pequeño logro y de sentir mi dolor como propio. Gracias a todos mis tajadinos por sus besos y abrazos tan reconfortantes en los findes por Cedrillas, y a ese adorable grupo representativo que vino a visitarme durante mi estancia en Porto, muitos beijinhos! A mis turolenses (Montse&Alf, Mapi, Yoli) por nuestras quedadas y por estar incondicionalmente dispuestos a todo, "en lo bueno y en lo malo". A los zoqueros, por esos findes de desconexión. A mi familia Erasmus, por estar cerca independientemente de los kilómetros que nos separaran. Y por supuesto a mis *kimicolocas*, esas chicas que siempre, contra viento y marea, siempre: están a mi lado. Soportando mi adicción al trabajo y comprendiéndome aun siendo absolutamente incomprensible. Gracias por vuestras "llamadas de atención", por ese amor y amistad tan incondicional que nos procesamos. Sé que siempre, estemos donde

estemos, estaremos unidas. La Uni me concedió este regalo que son vuestras sonrisas perpetuas de por vida. Guille+Pablo, sois dos más ;).

Ya casi por último, y sí por ello más importantes: mi hermana y mis padres. Esa comprensión sobrehumana que supera todos los límites que alcanza mi razón. Sabéis bien que no me soporto ni yo misma, y vosotros sois capaces de respaldarme a fe ciega y sin preguntas, de tener un tacto silencioso y darme los abrazos y ánimos más curativos que existen. Si llego a ser doctora, es gracias a vosotros. Vuestro ejemplo y apoyo me ha traído hasta aquí y nunca os daré las gracias las suficientes veces. Os amo y adoro, os debo esto y mucho más. Y *Tatiuska*, siempre serás la más grande, este doctorado es tan tuyo como mío. Gracias a todos mis tíos: Fernando, Feli, Laura, Luis,…y mis superprimos. Por su paciencia con mi impaciencia, porque todos los cafés y cervezas que hemos tomado juntos han sido una subida de moral y apoyo impagables. Gracias por creer en mí. A mis abuelos Lorenzo, Pilar, Fausto y Adoración, por ser el principio de todo y haber impreso su huella en mí, gracias por darme todo cuanto amo y necesito en esta vida. A través de vuestros ojos siempre me he sentido y me siento tremendamente protegida.

Y si alguien tiene derecho a reclamar cada palabra escrita aquí ese eres tú: Felipe. Mi equilibrio y parte de la brújula sin la cual no comprendo mi vida. Mi agradecimiento será eterno por todos y cada uno de los días que ha durado esta etapa. Espero que toda la vida que tengo por delante sea bastante para agradecerte que siempre veas más allá de lo que yo puedo soñar. Gracias por existir y hacerme existir. Tu simple sonrisa es capaz de curar mi alma. Gracias también a Puri y Felipe por su apoyo, y al resto de mi ahora familia política, por su interés y el ánimo que me han dado.

Y con todas estas palabras no quiero dejar la impresión de que esto haya sido “estar con la cabeza debajo del agua” todo el tiempo. No. Con estas palabras sólo quiero dejar constancia de que este

trabajo habría sido imposible llevarlo a cabo sin la aportación de cada una de estas personas. Gracias por estar en mi vida y compartir hoy esto. Igual parece demasiado agradecimiento para tan poca página…pero el crecimiento no ha sido solo profesional, en lo personal he logrado alcanzar unas cuantas metas que, al empezar el camino no parecían plausibles y…se han cumplido. Vero, gracias por tu parte. Por tu empeño y valentía, por sostenerme este penúltimo año que daba por perdido. Para ti mi “gracias” en mayúsculas. GRACIAS.

ABSTRACT

ABSTRACT

The design of second generation polymer conjugates is directed towards four main research areas: the synthesis of novel polymeric carriers with defined architectures, an exhaustive physico-chemical characterization through leading techniques, the use of combination therapy pursuing synergism and improved treatments and their application on novel molecular targets other than cancer, including the crossing of different biological barriers. These guidelines have been addressed in this thesis in which the main purpose was to build polymer-drug conjugates (PDCs) for the treatment of neurodegenerative disorders.

Based on the well established properties of the poly-glutamic acid (PGA) as polymer carrier, a versatile and simple methodology for the preparation of well-defined polyglutamate nanocarriers has been described. For the first time non-nucleophilic tetrafluoroborate anions were used as NCA initiators allowing a multigram scale polyglutamate synthesis with defined molecular weight (up to 1200 units), low polydispersity (<1.2) and controlled end-chain functionality. Systems obtained encompass homopolymers (PGA_n), diblocks (DB, PEG_m-PGA_n, PGA_n-PEG-X) and triblock copolymers (TB, PEG-PGA_n-PEG-X). The reason behind this design is based on: (i) the availability of points for site-specific conjugation (group X) (for peptide, protein, antibody, etc binding), (ii) the study of the different cell trafficking and (iii) in vivo fate depending on polymer solution conformation and its effect on the expected biological output. In addition, deprotection methodology of PBLG (poly-benzyl-L-glutamates) was optimised yielding 100% benzyl removal without damaging co-polymers structure as well as maintenance of the adequate stereoselectivity. Then, post-polymerisation modification on the PGA block enabled specific and orthogonal conjugation of different bioactive molecules such as targeting ligands, labelling probes or drugs.

Cytotoxicity of the novel nanocarriers was evaluated in HUVEC cells to secure their cell viability. Continuing with the *in vitro* assays,

investigation of the precise mechanism of internalisation in the same cell model was performed aiming to explore possible differences based on the size and shape in solution of the different carriers. In all cases endocytosis was the preferred cell uptake mechanism and a lysosomotropic drug delivery was observed.

Historically, many studies with PDCs have been focused on cancer treatment. Once the clinical benefits of these systems have been demonstrated, their use in other diseases has been also encouraged, in particular in the area of tissue regeneration and repair. In the present work, neurodegenerative disorders have been faced up. When damage in the central nervous system (CNS) is involved, drug must surpass a biological obstacle known as blood-brain barrier (BBB). Conjugation of a targeting ligand for blood-brain barrier (BBB) crossing though receptor-mediated endocytosis was the strategy selected for drug delivery into the brain. Ligands towards the transferrin receptor (TfR) (e.g. transferring (Tf), monoclonal antibody OX26 (mAbOX26), iron-mimicking cyclic peptide (cPEP) or Angiopep-2) were covalently linked to our polyglutamates trying to favor the BBB entry by active targeting. Molecular probes for fluorescence optical imaging, contrast agents for MRI or tracers for positron emission tomography (PET) were conjugated to our systems, with and without targeting ligands in order to monitor conjugate biodistribution comparing their BBB crossing capability. In most of the cases, the polymer platform linkage with the ligand was a disulphide bond. The bioreversible union allows the ligands to be released following transcytosis. All of the polyglutamate systems proved to have an appropriate biodistribution, where non-specific accumulation in any organ was observed and body elimination followed renal excretion. Regarding the targeted systems, TB-Tf was found in rat brain after tissue homogenation although in very low percentage. Aiming to increase the percentage, the natural ligand Tf which presents receptor saturation under physiologic conditions was substituted by an antibody able to selectively target this receptor with greater efficiency. mAbOX26 was successfully linked to the carrier but issues related to solubility issues limited a proper detection in brain.

Consequently, peptide ligands were used instead. cPEP was directed to TfR and Angiopep-2 to the lipoprotein receptor-related protein-1 (LRP1). This last peptide is the most advanced for BBB crossing in phase II clinical trials. After the results obtained, PGA homopolymer and DB were the carriers selected for further studies. Monitoring of these targeted systems did not show BBB crossing may be due to low availability of the peptide motifs for receptor recognition. Currently other polyglutamates with different structures are being tested to surpass this inconvenience.

When CNS is not involved but peripheral nervous system (PNS), brain entering is not a major problem. FAP (familiar amyloidotic polyneuropathy) is a rare amyloidotic disease where PNS is the main organ affected. A mutation in the protein transthyretin (TTR) promotes its aggregation ending up in fibril formation whose deposits promote organ failure. As a first proof of concept, treatment of FAP by means of PDCs was proposed. Continuing with the polymeric platforms exploited in this work, PGA and PEG were selected for conjugation of two bioactive molecules able to disrupt amyloid fibrils (doxycycline) and to suppress cytotoxicity promoted for the early aggregates (RAGE peptide). Two families of conjugates were synthesised following a rational design based on the extracellular target of the compounds and the properties and requirements of each drug. Total drug loading was varied as well as the linkage alternating biodegradable (disulphide) and non-biodegradable (amide) bonds. After *in vitro* screening in appropriate FAP models, Doxy conjugates showed higher activity than the parent drug at same concentration and RAGE peptide conjugates maintained the original activity. The best candidate of each library (PGA-CONH-Doxy and PEP1-PEG-PEP1) was selected and a full physico-chemical characterisation was performed in order to explain the activity found. Both conjugates proved by LCMS or HPLC techniques to be stable under the *in vitro* conditions used implying non requirement of drug release to achieve activity while the others not. Furthermore, the conjugates demonstrated stability in plasma and non haemolytic activity confirming their suitability for intravenous

administration. Studies on solution conformation by dynamic light scattering (DLS) showed marked differences in the RAGE peptide conjugates where more stable and smaller conjugates (R_h=0.6-3nm) corresponded to the most active ones. Regarding the PGA-Doxy, different ωt% loading did not show major differences in conformation in SANS (small angle neutron scattering) analysis corroborating the similar activity found with the selected conjugates.

Previous to *in vivo* activity evaluation, biodistribution of the conjugates were performed resulting in non-specific organ accumulation and elimination via the kidney.

Finally, combination therapy was proposed as a helpful tool due to the target species of the TTR aggregation cascade coexist in the advance stages of the disease. Initially, conjugation of both agents in the same polymer matrix (PGA homopolymer, DB or TB) was suggested but due to the unknown space among respective targets, individual PDCs were first tried and combination of the single conjugates was suggested as alternative. Thus, *preliminary in vitro* and *in vivo* studies with both conjugates (PGA-CONH-Doxy and PEP1-PEG-PEP1) were performed. Comparing the obtained results of immunohistochemistry analysis from single conjugates administration and their combination (without control samples) it could be concluded that the combination group showed lower deposition of non-fibrillar TTR. Histological analysis of the organs evidenced normal patterns in morphological tissue structures implying the safety of the administered conjugates. In any case, PGA-Doxy effect is planned to be evaluated in old FAP mice as well as a dose optimisation study should be performed in order to finally proved conjugates effectiveness in FAP.

CHAPTER I.

GENERAL INTRODUCTION

(Chapter co-written with A. Duro-Castano)

CHAPTER I. GENERAL INTRODUCTION

Nanomedicine has been defined as "the use of nano-sized tools for the diagnosis, prevention and treatment of disease and to gain increased understanding of the complex underlying patho-physiology of disease. The ultimate goal is improved quality-of-life". This relatively young field has been expanding significantly thanks to science and engineering advances and it is poised to revolutionise how medical and pharmaceutical industries approach the 21st century's pharmaceutical care challenges. Currently, about 40 nano-products for health care are in routine clinical use. Among the nanotechnologies that this term involves, polymer therapeutics (PT) is underlined as the most successful first generation nanomedicines [1]. Initial hallmarks of PT started in the 70s when the concept of polymer-drug conjugate was coined [2] and the "lysosomotropic drug delivery" described [3]. One decade after the development of the first polymer-anticancer conjugate entered clinical trials (CT28068, PK1, 2-hydroxymethacrilamide copolymer-doxorubicin (HPMA-Dox) conjugate) [4]. Up to now, a first generation of polymer conjugates has resulted in several products in the market (PEGylated proteins and polymeric drugs) and a growing number of polymer-drug conjugates in clinical development mainly as anticancer agents [5-8]. The acquired knowledge has built a solid source of background information from which a novel generation of polymer therapeutics is emerging. Together with the aim of meeting regulatory demands, this second bundle is supported by four main strategies: (1) the synthesis of novel polymeric carriers with defined architectures, (2) the implementation of better physico-chemical characterisation methods, (3) the use of polymer-based combination therapy to increase specificity and efficacy of the treatments always looking for synergysm and (4) the application of PDC to new molecular targets other than cancer, including the crossing of different biological barriers [8].

One of this potential novel targets are the neurodegenerative disorders. Aging of population leads to a growing incidence of

neurodegeneration [9]. The bottleneck for treating the vast majority of these diseases relies on the difficulty for drugs in crossing the protective barrier that surrounds the brain: the blood-brain barrier (BBB). Within an extensive rational design, polymer conjugates bring together all the basic requirements to overcome this barrier and become a successful therapy for neurodegeneration treatment.

The aim of this thesis covered the four explained lines as it was focused in the design, synthesis and characterisation of novel polymer carriers based on poly-L-glutamic acid (PGA) to construct polymer-drug conjugates (PDCs) for neurodegenerative disorders treatment. In the cases were the central nervous system (CNS) is involved, active targeting for blood-brain barrier (BBB) crossing entangled ligand conjugation to the polymeric platform. When it is the peripheral nervous system (PNS) the major organs affected, this requirement is not required. As a first application of PDC in the neurodegeneration field, herein the treatment of a rare amyloidotic disease FAP (Familial Amyloid Polyneuropathy) was proposed by means of novel PDCs as simple agents and in combination therapy.

I. 1 NEURODEGENERATIVE DISORDERS

One of the major challenges for the 21st century medicine is to find effective treatments to face the growing incidence of neurodegenerative diseases. These are tightly related to aging population due to constant and considerable increasing of life expectancy, environmental cues and/or disordered immunity and less with host genetics [10, 11]. It is predicted than disability and mortality caused by central nervous system (CNS) disorders will increase up to 15% in 2020 [12] and 65-year old population will rise from approximately 14% in 2010 to 26% in 2100 [13] (FIGURE I. 1) with the consequent growing number of affected individuals.

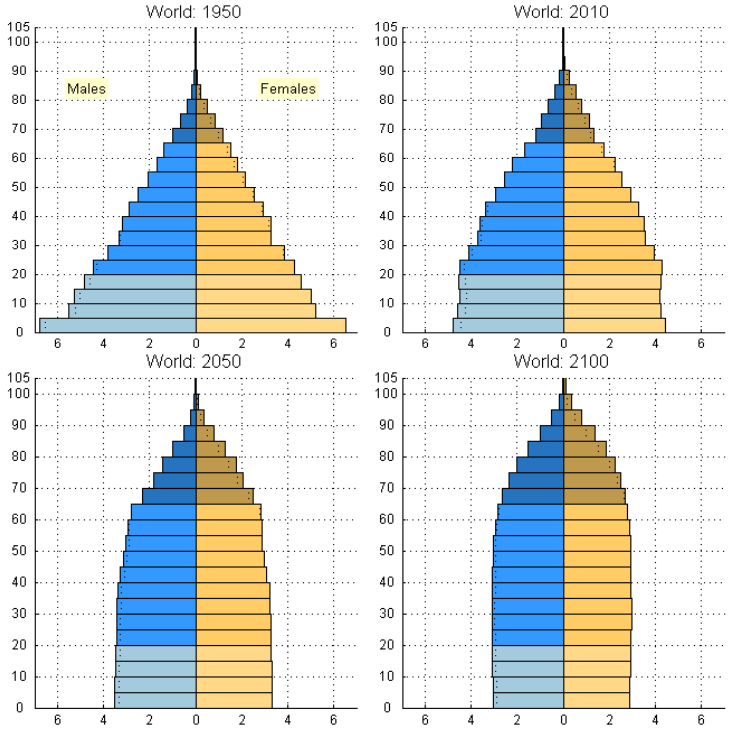

FIGURE I. 1 United Nations prediction for aging in world population. From ref [13].

Renowned examples as Alzheimer's and Parkinson's diseases (AD and PD), stroke, Huntington's disease (HD), multiple sclerosis (MS) and HIV-1-associated dementia (HAD) are only part of the vast number of common neurodegenerative disorders. Most of them have been well described in terms of pathology and disease mechanism although successful treatment strategies have been at best palliative and manage only the symptoms [14-16], receiving no benefit from currently available medication.

In western countries, an epidemic progression of chronic diseases such as neurodegenerative disorders (together with cardiovascular and metabolic afflictions) is expected to be the main cause of death in the next few decades. Moreover, these types of

pathologies already poses a heavy economic and social burden and it is predicted than in few decades their impact will increase considerably. This context establishes the urgent need for developing novel therapeutic strategies to face neuropathological diseases. Two main objectives in this field comprise specific site-directed drug delivery systems and the development of early diagnosis methodology.

Regarding causes of the neurodegenerative disorders, abnormal accumulation, aggregation and modification of certain proteins, effects of viral infections, disrupted blood flow, alterations in tissue homeostasis and immunological damage are the main reasons [10]. Scientific efforts have been concentrated in understanding key molecules and pathways in physiological processes as well as drug discovery for treating the different diseases. In addition, it has been recognised that neurological disorders may be multisystemic in nature which hinders their treatment, i.e. specific neuron death due to a cascade of multiple deleterious molecular and cellular events rather than a single pathogenic factor [17].

However, in spite of the assembled knowledge, many drugs remain ineffective in the treatment due to the inability to effectively deliver and retain them within the brain. Here is found one of the major bottleneck in neurodegeneration treatment: the different biological barriers that must be surpassed for successful drug delivery and avoidance of peripheral side-effects.

I. 1. 1 NERVOUS SYSTEM

Neurological disorders involve affection to the nervous system in the body, being characterised by the gradual and progressive loss of cells from the affected organs. Also the emerging symptoms vary depending on the region affected in the CNS or the PNS. CNS is composed by the brain and the spinal cord while PNS comprises cranial, spinal and autonomic nerves that connect CNS to the rest of the body.

Nervous system main function is based on communicate the whole body with the brain and within the brain through electric stimulus. It controls muscles, organs, glands and several basic processes such as heartbeat, breathing, digestion, urination, blood flow regulation or homeostasis maintenance among others. Higher functions such as thinking and memory are also regulated [18].

Nervous tissue is composed mainly by *neurons (*FIGURE I. 2), which transmit nerve messages and *glial cells or neuroglia* that primarily provides neurons insulation, physical support, metabolic assistance and protection.

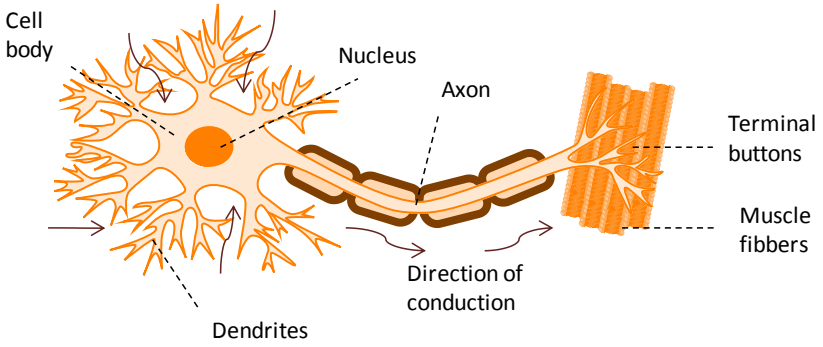

FIGURE I. 2 Neuron is the fundamental structural unit of the nervous system. Its structure consists of a spherical central portion (the *cell body* or *soma*), processes called *dendrites* are implied in bioelectric impulses reception toward the cell body and one *axon* that transmit impulses away from the cell body and reach its destination. Ending portion of the axon presents a branched morphology named *nerve terminal (boutons),* which communicate with the next neuron or organ.

Glial cells outnumber neurons by ten to one[19]. Unlike the neurons, they do not participate directly in synaptic interactions and electrical signalling. There are several types of glial cells: (i) *Schwann cells* are PNS structures that wrap neuronal axons to form a protecting cover known as the myelin sheath. Furthermore, they assist in the conduction of impulses as myelinated nerves conduct faster that

unmyelinated ones, (ii) *oligodendrocytes* have the same functions than Schwann cells (among others) but are allocated in the CNS, (iii) a*strocytes* are present in the capillaries of the brain and constitute part of the blood-brain barrier (BBB) (further explanation on BBB section I.3.1) and (iv) m*icroglia* are smaller scavenger cells found in CNS and are in charge of remove cellular waste and protect against microorganisms [19-21].

I. 1. 2 BARRIERS IN THE PERIPHERAL NERVOUS SYSTEM

Protection of PNS is not as restrictive as for the CNS. The PNS is not protected by spine bone and skull or by a structure like the BBB. Peripheral nerves tend to lie deep under the skin except in specific sites as the elbow joints. This feature exposes them to physical damage causing pain, loss of sensation or muscle control. This damage promotes neuronal regeneration with support cells aid. Nerve regeneration, for example after a transection, will take place but over months. Typical treatments after injury relies on surgery or use of an autologous nerve graft to guide restoring of the PNS function [22]. Peripheral neuropathy can be also caused by other circumstances such genetic, metabolic or inflammatory conditions as well as vitamin deficiency, infectious diseases or poisoning.

I. 1. 3 BARRIERS OF THE CENTRAL NERVOUS SYSTEM

Drug delivery to the CNS by means of a systemic approach is a highly challenging prospect in drug development. To achieve CNS access, therapeutics must overcome three barrier layers, which control molecular exchange between blood and neural tissue or its fluid spaces.

These barriers include: the blood-brain barrier (BBB) formed by the cerebrovascular endothelial cells between blood and brain interstitial fluid (ISF), next the choroid plexus epithelium between blood and ventricular cerebrospinal fluid (CSF) and finally the arachnoid epithelium between blood and subarachnoid CSF (components localised in FIGURE I. 3). In unison, these barriers govern

the passage of substances to the brain [23].

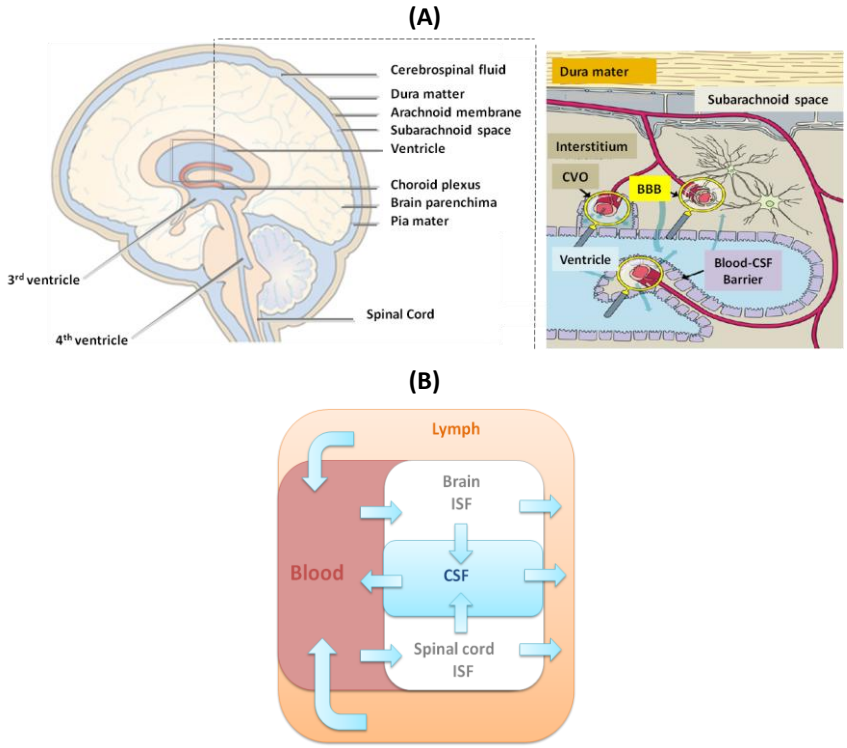

FIGURE I. 3 (a) The brain is protected by three membranes: the outermost dura mater, the arachnoid membrane and the innermost pia mater. The last two ones are known as the leptomeninges. On the right it is zoom insert inicating where is located the blood-brain barrier. Adapted from refs [24] and [25].(b) Fluid compartments in the CNS. Redrawn from ref. [12]. ISF=Interstitial fluid. CSF=Cerebrospinal fluid. BBB=blood brain barrier.

I. 1. 3. 1 Blood-brain barrier (BBB)

Since its discovery by Paul Ehrlich in 1885 [26], BBB has been baptized as the most critic nearly insurmountable cellular barrier in the human beings. This natural barrier guards brain and spinal cord, separating them from the blood flow by an active and restrictive cellular complex [23].

All organs into the body are connected to the circulatory system, which by means of blood is supplying through the capillaries:

nutrients and essential components for their sustention. Brain is not an exception but it has an extraordinary overprotection compared with the rest of the organs. Human brain posses around 100 billion capillaries, achieving approximately a total surface area of $20m^2$ and 650km of brain capillary endothelium [27]. Before reaching the brain from these capillaries, a densely packed brain capillary endothelial cell (BCEC) layer with tight junctions must be surpassed: the BBB. In humans, thickness of this barrier is estimated to be around 300 to 500nm. It allows the passage of specific nutrients and metabolites but effluxes or prevents the entrance of non-desired substances, maintaining a stable microenvironment (named brain homeostasis) and free of inflammation or attack from harmful endogenous compounds or exogenously introduced such as drugs.

Tight junctions (TJs) in the apical region of brain endothelial cells possess a unique intercellular occlusion profile [23] (FIGURE I. 4). They are composed by complex network of parallel, interconnected, transmembrane and cytoplasmatic strands of proteins (junctional adhesion molecule-1, occluding, claudyns and cytoplasmic accessory proteins). Furthermore, they provide significant transendothelial electrical resistance (TEER) ($8000V/cm^2$) to bone marrow microvascular ECs. Below TJs, *adherens junctions* (AJ) are found, completing BBB as a physical barrier. This structure is formed by transmembrane glycoproteins (cadherins) bond to the cytoskeleton, achieving a higher tightening structure between the adjacent brain endothelial cells [20].

Together with TJs, brain endothelium is characterised by remarkably lower degree of endocytosis activity (see FIGURE I. 11) than peripheral endothelium. *Free diffusion* is allowed for small gaseous molecules such O_2 and CO_2 as well as small lipophilic agents. In the case of small hydrophilic molecules (i.e. amino acids, glucose, etc) or larger and/or hydrophilic essential molecules (i.e. hormones transferring for iron, insulin, etc), it is required a *specific transport system* such GLUT1 glucose carrier, amino acid carrier LAT1,

transferrin receptors, insulin receptors, or lipoprotein receptors to regulate their transcellular traffic. A family of efflux transporters prevent entrance of undesired compounds. Transport mechanisms through this barrier are explained in section I.4. Finally, low and selective permeability is also attributed to lack of fenestrations and great number and volume of mitochondria in endothelial cells, as well as the lack of lymphatic drainage [28].

Besides the BCECs, extracellular base membrane, pericytes, astrocytes, microglia and neurons are been described to be functional contributors in the BBB. As a whole, these components form the "neurovascular unit" (NVU) (FIGURE I. 4). Research studies on each component functions and their relative contribution to the BBB has been carried out achieving results detailed below, but still there is information largely unknown.

Pericytes are the next critical components of the BBB that are located along the vascular endothelium in an intimate position regarding BCECs (approximately in a ratio 1:5-6 BCECs). Both are separated by a layer of basal lamina. Among their functions have been suggested their role in ECs proliferation, microvascular capillary flow control, normal regulation of BBB, efflux transporters expression (i.e. ATP- binding cassette (ABC) transporters) and has an important role during initiation of angiogenesis both in CNS and non-CNS tissue [29-31]. Recently, it has been demonstrated that pericytes deficiency increases BBB permeability to water and a range of low and high molecular mass tracers, as well as they regulate BBB specific gene expression patterns in endothelial cells and induce polarisation of astrocytes [32]. In addition, it has been recently proved that age-dependent vascular damage in pericyte-deficient mice precedes neuronal degenerative changes, learning and memory impairment and neuroinflammatory responses. Thus, pericytes control key NVU functions required for BBB maintenance and proper neuronal structure and function [33, 34].

Astrocytes are a class of macroglial cells in the CNS. Astrocytes

project endfeet forms a net, surrounding the endothelial cells (FIGURE I. 4). They have been described to significantly influence neurovascular structure, maintenance and integrity; participating in nutrition and metabolic support of neurons. Furthermore, they preserve TJs integrity and induce P-gp expression. Together with pericytes and the basement membrane, they have been suggested to play a role in TJs formation [28]. Current research remark astrocytes as ECs survival support in hypoxic and ischemic conditions, when acute hypoxic insult is suffered astrocytes protect the endothelial barrier. However, in prolonged stages pericytes are more protective. This difference is attributed to their intrinsic modulation of specific signalling pathways and subsequent released factors [34].

The *basement membrane* is a specialised extracellular matrix which separates BCECs and pericytes from the surrounding extracellular space [35]; it engulfs them without acting as a barrier for small molecules diffusion. Its main function is anchoring the cells in place and regulates cellular functions of the BECs through signalling molecules on the abluminal BCECs surface.

Finally, *microglia* is the 20% of the total glial cell population in the CNS and its activity deals with identifying and neutralising foreign objects, responding to minor pathological changes and starting a coordinated neuroinflammatory response [12]. This glia sheet, which derives from systemic circulating monocytes and macrophages, is essential for the barrier integrity and transcellular transport through it [30].

Apart from constituting a morphologic obstacle due to the named cell complex, BBB is also a metabolic barrier thanks to a combination of intracellular and extracellular enzymes [37].These enzymes handle drug and nutrients metabolism. Examples can be found in ref. [38]. This elevated enzymatic activity has to be taken into account once the drug arrives there, in order to prevent rapid degradation or deactivation.

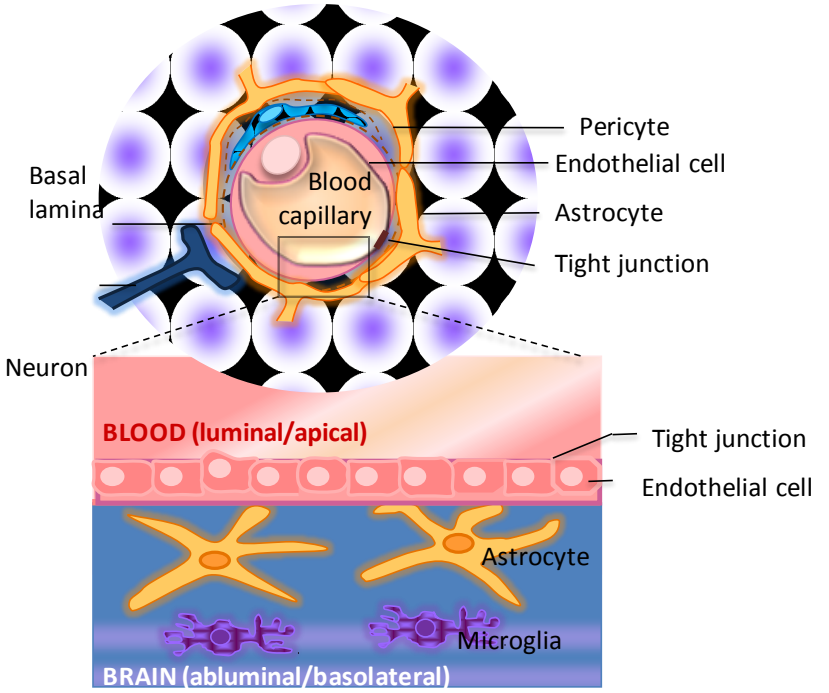

FIGURE I. 4 Components of the neurovascular unit (NVU).Redrawn from ref. [36].

I. 1. 3. 2. Blood-cereborspinal fluid barrier (BCSFB)

Morphologically, BCSF barrier is located in the choroid plexus and meninges. It is about 1000 times smaller than BBB. The choroid plexus, which is the principal source for the cerebrospinal fluid (CSF), is formed by cuboidal epithelial cells that contain apically localised tight junctions to prevent paracellular transport. On the contrary as BBB endothelial cells, endothelial cells of the choroid plexus capillaries posses fenestrations and lack tight junctions, forming a leaky endothelium [25].

One of the barrier faces is the ventricle, where CSF flows out to the subarachnoid space surrounding the brain and the spinal cord. Then, it returns to blood by different via (FIGURE I. 3). Although there is absence of a cellular barrier preventing diffusion from the ventricular surface into the brain tissue, the low diffusion speed and

high turnover rate of CSF prevents penetration of large molecules into deep tissue layers [30]. As the BBB, BCSFB is also an enzymatic barrier.

I. 1. 4 TRANSPORT MECHANISMS ACROSS THE BBB

As it has been already named, transport systems regulate passage from systemic circulation into the brain (influx) when turned back to blood circulation (efflux). Both types of solute movements are present in this endothelium, defining a unidirectional concentration-dependent profile. Importantly, net flux is a critical parameter in drugs reaching therapeutic concentrations within the CNS [12]. The different pathways are pictured in FIGURE I. 5. Basically, transport can be subdivided in passive and active processes.

I. *1. 4. 1 Passive transport*

Solute gradient by simple diffusion proceeds from low to high concentrations and includes:

(a) Paracellular (aqueous) diffusion (FIGURE I. 5(a)). Apparently, small water-soluble molecules are uptake through the TJs and diffuse through the BBB. However, this pathway is remarkably diminished in comparison with the rest of the organs due to the high TEER at the TJs.

(b) Transcellular (lipophilic) diffusion (FIGURE I. 5(b)). Among the passive diffusion mechanism, transcellular diffusion constitutes the most favoured. Lipid-soluble substances such as oxygen, carbon dioxide, alcohol or steroid hormones penetrate ECs through their plasma membrane. Either paracellularly or transcellulary, are non-saturable and non-competitive pathways. Most of CNS drugs enter via this route [39].

(c) Saturable (carrier-mediated) transport (CMT) (FIGURE I. 5(d)). Expression of these carriers is often polarised to

optimise substrate transport into the brain, which means they are co-localised on both the luminal and abluminal membranes of the BCECs and thereby operates in both directions. The process is more selective than those named before and it has been suggested to involve formation of transient narrow pores induced by binding of the respective substrate to the carrier that allows only its passage. An example is the glucose transporter 1 (GLUT1), in charge of glucose trafficking through BBB [40].

I . 1. 4. 2 Active transport

In cases where transport requires energy, the passage is carried out by means of an electrochemical gradient. Mainly, active transport task relies on vesicle formation. As it has been previously cited, endocytosis is remarkably diminished in the brain. However, more specific subtypes of this mechanism may take place. The general term is *transcytosis*, a group of phenomena which allows passage of a molecule through the cellular cytoplasm from blood capillary to brain parenchyma. It implies a double process across the BBB layer: endocytosis and exocytosis, and can be divided into specific (receptor-mediated transcytosis) or nonspecific (adsorptive-mediated transcytosis) processes. Implicated transporters are commonly named ATP-binding cassette (ABC) transporters.

(d) Receptor-mediated transcytosis (RMT) (FIGURE I. 5(e)). Essential molecules with high size required for normal function in the brain are delivered through specific receptors. RMT uses vesicular trafficking mechanism of the endothelium to transport nutrients into the parenchyma. Process could be divided into three steps: (i) Ligand binds its specific receptor localised at the luminal membrane of the BCECs, inducing a modification of the receptor either through cross-linking or conformational

change. This binding induces an endocytic event which produces aggregation of both components within pits, (ii) then the coated pits trigger the formation of bigger vesicles (aprox. 100nm diameter) and cross the cytoplasm while they transform into endosomes (acidic pH), where dissociation occurs. Afterwards, free receptor is recycled to cell surface or degraded through lysosomes. (iii) Finally, the ligand containing vesicles can be packed into export vesicles to be exocytosed on abluminal face, achieving BBB crossing. Complete crossing could be not achieve due to some of the vesicles could fuse with a lysosome and be degraded and others could bind a second intracellular receptor system.
Therapeutic compounds are able to cross the BBB after association or conjugation to the ligands of these receptors forming molecular "Trojan horses" [41].

Sometimes RMT is preferred as drug delivery route for BBB crossing possibly due to CMT involves molecular movement through a small pore while RMT use transcytosis [29] and macromolecules could be transported.

The three best-studied receptors are (i) the *insulin receptor (IR)*, where insulin binds changing its shape to form a tunnel for the entry of molecules such as glucose, (ii) the *transferrin receptor* (TfR) which mediates cellular uptake of iron by means of its natural ligand: the protein transferrin (Tf), which acts as carrier. TfR is expressed in BCECs, choroid plexus epithelial cells and neurons among other tissues. Iron-TfR complex is transcytosed across BCECs without intraendothelial degradation [42] and (iii) the *low-density lipoprotein receptor related proteins 1 and 2* (LDP-1 and 2). These multifunctional endocytic receptors mediate internalisation and degradation of several ligands

in different metabolic pathways. LRP receptor interacts with apoliprotein E (apoE), APP (amyloid precursor protein) and lactoferrin among others.

(e) Adsorptive endocytosis (AE or adsorptive-mediated transcytosis AMT) (FIGURE I. 5(f)). Molecules as peptides or proteins with basic isoelectric point (called “cationic”) can be uptake by the brain trough AE, such as protamine, histone or albumin [30, 43]. Binding process is mediated by electrostatic interactions between positive charged moieties of the molecule and the negative charged region of the plasma membrane surface region, which initiates endocytosis [44]. Main difference from RME is that AE do not involve specific plasma membrane receptors. Furthermore, AE presents lower affinity but higher capacity than RMT.

(f) Efflux transport systems (FIGURE I. 5(c)). Localised at the BBB as well as in the BCSFB, efflux systems reinforce barrier properties by extruding undesired substances from the brain or the CSF pulling them in the blood circulation, maintaining homeostasis. ATP family of efflux transporters include P-glycoprotein (P-gp), breast cancer resistance protein (BCRP) and multidrug resistance related proteins (MRPs). P-gp can actively transport many hydrophobic amphipathic drugs out of the brain, i.e. loperamide [28, 45].

There are examples of transporters driving a non-energy dependent mechanism such as the organic anion transporter (OAT) and organic anion transporter poly-peptide (OATP), that have dual function as efflux and influx transporters [46].

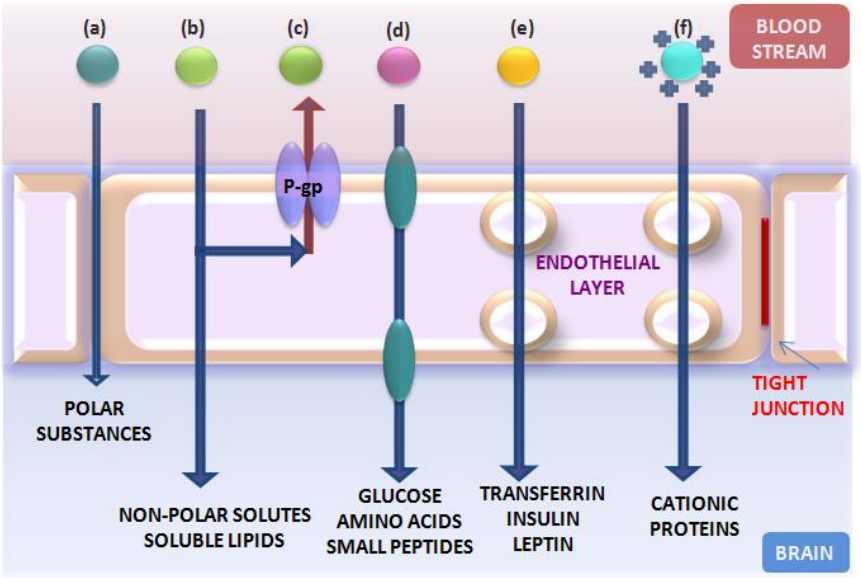

FIGURE I. 5 Transport mechanisms in the BBB (redrawn from ref. [23]). (a) Paracellular pathway for diffusion of small amounts of water-soluble compounds. (b) Transcellular lipophilic pathway for diffusion of lipid soluble agents. (c) Efflux transport systems restrict the penetration of many substances into the brain turning them to blood stream. (d) Saturable transport responsible for the transfer of essential polar solutes. (e) Receptor-mediated endocytosis is the mechanism used for transport essential proteins. (f) Adsorptive endocytosis. Cationisation increases the uptake of poorly transportable local plasma proteins.

I. 1. 5 BBB UNDER PATHOLOGICAL CONDITIONS

BBB role during degenerative development is unknown. Scientists discuss if BBB is the starting cause, participates in the process or if BBB is damaged as a final result of degeneration. Relying on the specific disease it could be a different answer but it is referred to display a significant causal part or involvement in the initial degenerative process. However, all neurological diseases studied up to date have suggested, at least, that BBB dysfunction results from the pathogenic process. Nevertheless it has been proposed that barrier dysfunction results from the own pathological process. It is

noteworthy to remark the existence of a common neuropathological condition inflammation and inflammatory mediators are involved in BBB disruption. Their mediators have been suggested to be targeted or controlled for opening or closing the BBB [28, 47]. BBB cohesion along all the disease states is a relevant parameter for understanding the disease as well as for therapeutic strategy design.

Experts remark the importance of using different targeting strategies depending on what to treat, only BBB or the brain plus the BBB [48].

During neurodegenerative processes BBB disruption is a common feature in infections, tumours and acute or chronic neurodegenerative disorders [47]. Its permeability and protective mechanisms such as TJs opening, P-gp up or down-regulation among others, are usually diminished in disease state. This impact can be defined as an advantage for providing a window of opportunity for drugs unable to cross the BBB to reach their target inside the brain by means of paracellular route. Several studies on this field have prove this affirmation [47]. However, researchers highlight that although this aspect may benefit drug efficacy, increasing of BBB impairment could lead to higher rates of neurodegeneration. For example, in AD restoring BBB integrity will confer better output than increase drug transport due to the BBB leakage. BBB disruption allows pathogens entrance to in the brain, aggravating or accelerating the disease. On the other hand, brain tumours can increase also BBB permeability, possibly caused by TJ complex disturbance, growth factors accumulation and proinflammatory cytokines [49].

It has been already tested in animal models and cell studies that transport processes in disease state such AMT and RMT are enhanced but it has to be still confirmed for CNS human disorders [48].

I. 1. 6 MIMICKING THE BLOOD BRAIN BARRIER

As important as the development of novel materials and BBB

targeting vectors is their biocompatibility and efficient investigation towards a successful therapeutic output. *In vitro* testing is considered a powerful tool for the screening of drug and materials and also comparing their performance and evaluating their ability for controlled drug release depending on the pursued objective. However, a step further must be done and studies on animal models complete the experimental panel to determine the effectiveness of the proposed treatment. Due to the inherent BBB complexity, *in vitro* methodologies for mimicking BBB remain sub-optimal.

I. 1. 6. 1 In vitro methodologies

By mimicking BBB *in vitro*, it is possible to pursue two different objectives: (i) to gain knowledge about how to cross this barrier enhancing drug transport into the brain and (ii) to discover how to reduce or prevent its disruption during injury. Then, the main objective combining both statements is how to maintain the barrier during injury but also facilitate selective opening to enable drug access.

Since contribution of individual cell types is crucial, identification and targeting of cell-specific mechanisms may gain better results than have been currently obtained using more global approaches. *In vitro* model systems are decisive in this respect. *In vitro* methodologies simplify experimental work, allowing investigation and interpretation of experiments that are impossible or complicated to perform *in vivo*. Additionally they are versatile, easy to be implemented and inexpensive although unable to fully recreate all aspects of a real situation and limited by the type of brain cells used.

An *in vitro* BBB model should include: (i) a restricted paracellular pathway, (ii) brain capillary endothelial cell characteristics, (iii) functional expression of BBB specific transport mechanisms, and (iv) *in vivo*-like BBB modulation and reproducibility [50].

Lately, co-culture of several cell types makes these systems

more relevant. Presence of astrocytes in BCECs vicinity is crucial for BBB development, upregulating Pg-p expression, enhance cell-cell tight junctions and inducing specific enzymes or transporters [29]. Triple culture systems has been also studied adding pericytes to the co-cultures named [51].

Next step on BBB modelling through *in vitro* assays considers the dimensional feature: 2D and 3D models and blood flow properties.

The strength of *2D model* lies on the ability to directly asses barrier function within an endothelial monolayer. Experimental setting up consists of ECs cultured on one side of a cell-culture insert with porous filter membrane (transwell system), allowing formation of a monolayer and induction of cell polarity (FIGURE I. 6). Correct function is assessed by means of TEER measurements or permeability assays that evaluate the diffusion/extravasation of labelled proteins and/or cells through the monolayer. As results with endothelial monocultures revealed poor TEER values (10-100Ω, compare to real situation where TEER>1000Ω)) and higher permeability, co-cultured was studied allowing a closer recreation. Even though higher TEER values were obtained, the degree of induction remains significantly lower than the *in vivo* situation [33].

Microfluidic-systems to simulate the real environment have been also tested in 2D systems by applying flow-induced shear stress across the monolayer [52-54].

2D models have facilitated studies on cell-cell interaction and external influences by pharmacological compounds to barrier function but they do not take into account the 3D dimensional structure of blood vessels and real complex cellular interactions in BBB are also missed.

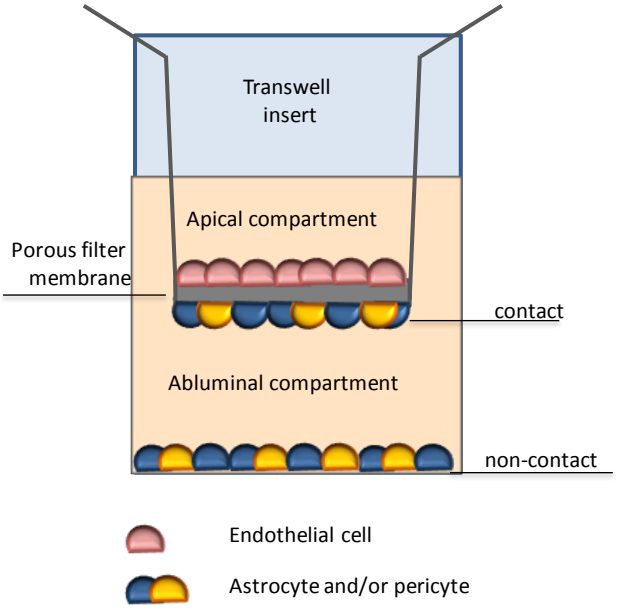

FIGURE I. 6 *In vitro* assembly of the 2D transwell system within a multiple-well plate. Several co-culture models are also used for this system, even with three cell lines. Closer recreation of cell interaction is achieved by growing astrocytes on the opposite face of the porous membrane (contact model), on the bottom of the well (non-contact model) or used astrocyte-conditioned media harvested from growing astrocyte cultures. Redrawn from ref. [33].

A step further towards *in vivo* recreation is the use of *3D models*, in which cellular movement and organisation of dynamic cell-cell interactions is included. Within this system there are two different approaches. On one hand, 3D collagen matrix models grow endothelial cells in type I collagen matrix promoting their organisation into tube-like structures [55]. Co-culture with other two cell lines suggested again to confer better analogy to BBB, allowing them to display their unique morphology [33, 56]. Main drawback lies in the difficulty of assessing tightness of the formed tubes as well as the TJs formation and the absence of flow. On the other hand, there are 3D flow systems trying to simulate the shear stress triggered by blood flow across the apical surface of the cells. In these models

microvascular ECs grown in three dimensions are exposed to flow [57]. Its influence has been demonstrated to be important for endothelial cell differentiation and metabolism. These advanced systems allowed to achieve enhanced TEER values, lower permeability output and longer lifetimes. Nevertheless, due to their technical demand and high cost they have not been adopted in researcher laboratories. Also, doubts on the percentage of correlation with cellular organisation *in vivo* have been reported [33].

I. 1. 6. 2 In vivo studies

In vitro models avoid the current exhaustive examination of animal experiments and the difficult data translation but it is becoming clear that BBB complexity need to be addressed directly by *in vivo* studies, in particular when active transport mechanisms are evaluated.

Concerning RMT methodology, antibodies or peptide targeting moieties have presented a vast variety of different results between *in vitro* and *in vivo* [58], which often do not agree. Studies differ either on the carrier exploited, complicating the selection of the best targeting residue, or the methodology used to detect BBB passage by biodistribution (optical imaging with near-infrared (NIR) dyes, radioactivity emission with different isotopes (PET, SPECT), magnetic resonance imaging (MRI),…) and activity studies [59-70].

Recently, zebrafish has emerged as a premier vertebrate organism to model and analyze complex BBB cellular interactions *in vivo*, thus, providing a profitable tool to complement drug discovery development studies [71, 72]. Furthermore it has demonstrated to express mutated disease-associated human proteins in specific neurons to rapidly model aspects of neurological disorders [73].

I. 1. 7 DELIVERY STRATEGIES TO THE BRAIN. DRUG TARGETING

Although important research efforts have been devoted in

targeting and targeted drug delivery to the brain, Markets are still waiting to find the Holy Grail in CNS-related diseases: BBB crossing. Until now, drug delivery to the brain has been partly accomplished through several methods, including invasive or systemic approaches (pharmacological or physiological). Most of them combine biology, nanotechnology and even biophysics to achieve this common goal. As this thesis deals with nanomedicine, an extensive number of examples are described in section III related to this strategy.

Route of administration is a key choice to make when designing pharmacological approaches to cross BBB and is highly influenced by the selected active principle. Delivery pathway can be driven by patient acceptability, important properties of the drug (i.e. solubility, stability), and ability to target the disease location or effectiveness in dealing with the specific disease. Fortunately, the use of drug delivery carriers can diminish the drawbacks of free agents, enhancing therefore its possible therapeutic value in the preferred route of administration [74].

I. 1. 7. 1 Invasive approach

Invasive approaches are based on mechanical breaching the BBB and posses the advantage of delivering higher concentration of the therapeutic compound due to a direct injection into CSF or parenchymal space [75]. Subsequently, this reduces drug concentration in peripheral environment and undesired effects. Several animal studies by means of this type of drug administration have demonstrated its efficiency and efficacy, either by using a mini-osmotic pump or acute injections through a cannula permanently implanted in the skull. However, for human use alternative methods are required as the use of these inventions for extensive periods compromise BBB, resulting in patients susceptible to injury and infection [76]. Invasive techniques include cerebral (intraparenchymal), intraventricular (transcranial), intrathecal (intra-CSF) delivery and BBB disruption.

Intracerebral delivery means drug delivery into parenchymal

space of the brain, by direct injection (bolus or infusion) via intrathecal catheters, controlled release matrices, microencapsulated chemicals or recombinant cells [39]. Main limitation of bolus relies on low drug diffusion characteristic of this tissue and large dose is required. On the other hand, infusion (also named convection enhanced diffusion (CED)) phenomena drive drugs to a larger tissue region and provides higher drug amount as well as its distribution and maintenance over time. Delivery of nanoparticles (NPs) through CED has been already demonstrated [69, 77-80]. However, some brain areas are difficult to fully saturate with infusate and delivery also depends on catheters placement [81]. It must not be forgotten that invasive neurosurgery needed give rise the usual risks associated such as stroke, infection, edema or temporary loss of neuronal functions. Long-term risks could be neurological scars and displacement of functional brain leading to permanent deficits.

Another method which implies brain surgery is the placement of intracerebral *implants*, biodegradable/non-biodegradable drug impregnated wafers placed for controlled drug delivery at the brain target site. Made of polymeric materials, drugs are encapsulated inside it and released by diffusion which present the same limitations named before[39]. Invasive neurosurgery drawbacks already detailed justify the desirable reduction of frequency for implant placing, which always will depend on the individual patient and the specific neurological disease. Small implant sizes as well as longer and better controlled drug release (i.e. by means of drug conjugation to the polymers) will confer important advantages to this system. Most successful implants reported to date have only been able to alleviate disease symptoms in animal models of neurological disease from two to eight months [76] and investigators highlight the challenging issue of their translation to human studies and their commercialisation. An example of a polymer implant depot with these characteristics is already in the market: Gliadel® (MGI Pharma, Bloomington, USA) [82]. As a local delivery system, anticancer drug only reaches adjacent areas of the implant [78] (more details in section III).

Disruption of the BBB is based on producing leakages in the TJs between the endothelial cells. It has been studied different techniques such as physical stimuli (ultrasound, microwave or electromagnetic fields) and through a chemical substance for promoting hyperosmolar nature, i.e. have higher hypertonicity or osmotic pressure [83], i.e. mannitol, bradykinin or alkylglicerols. Apart from undesired effects for affecting other tissues in the body, these alternatives are relatively costly and unwanted blood components can enter in the brain causing irreversible damage [84].

I. 1. 7. 2 Systemic drug administration approach

By systemic administration BBB becomes the obstacle to be circumvented by the drug. Great number of CNS drugs and polymer-based drug delivery systems containing biomacromolecules are administered systemically, mostly via intravenous (IV) injection. In comparison to other administration types, IV is a non-invasive method that does not disrupt BBB that prevents from a possible brain damage. Taking profit of the vast capillary brain surface where each neuron is perfused by its own capillary, the drug delivery approach through a transvascular route encourages brain drug targeting [85]. However, BBB together with rapid clearance from the extracellular fluid, decrease drug accumulation. Furthermore, brain availability of drug through IV route is directly influenced by the half-life of a drug in plasma, the rate of metabolism, non-specific binding to plasma proteins and the restriction of permeability of the compound across the BBB and into peripheral tissues [78]. Pathological states like gliomas reduce or suppress this endothelial barrier, thus enabling higher drug concentration to enter the brain. However, diseases such as AD or PD do not.[86]

Apart from IV, intra-arterial delivery or transnasal route are other alternatives of systemic drug administration. For example, intranasal delivery of drugs proteins by cationic liposomes has been demonstrated [87, 88].

Depending on the main strategy followed, two main tendencies have been defined to achieve BBB crossing.

I. 1. 7. 3 Pharmacological approach

Molecules such alcohol, nicotine or benzodiazepine enter passively in the brain crossing the BBB. This ability could be achieved for small molecules (<500g/mol) with low hydrogen bonding capability and lipophilic profile[89]. Thus, mimicking these characteristics and by means of chemical modification of a known active CNS bioactive drug this could end up in its passage to the brain. Alternatives as methylation, halogenation or blockage of C or N-terminal have been successfully exploited [30]. Unfortunately, some of these drug variations affect the activity and also lipophilicity increasing could promote P-gp exclusion among other disadvantages. Use of colloidal drug carriers such as liposomes, nanoparticles or nanogels are also included in this category [30].

I. 1. 7. 4 Physiological approach

As previously stated, transport systems offer the possibility of being used as a large molecule entry to the brain (FIGURE I. 7). This includes receptor-, carrier- or adsorptive-mediated endocytosis. See explanation of each transport foundation in section I.4 Drugs can be derived, encapsulated or conjugated to carrier systems together with a targeting moiety. Numerous advantages such as drug protection against plasma degradation support this strategy.

Carrier mediated transcytosis (CMT*)* is used for molecules mimicking nutrient structures and essential compounds. As an example, dopamine transformation to levodopa can cross BBB by LNAT (large neutral amino acid transporter), used for four decades in Parkinson's treatment [90].

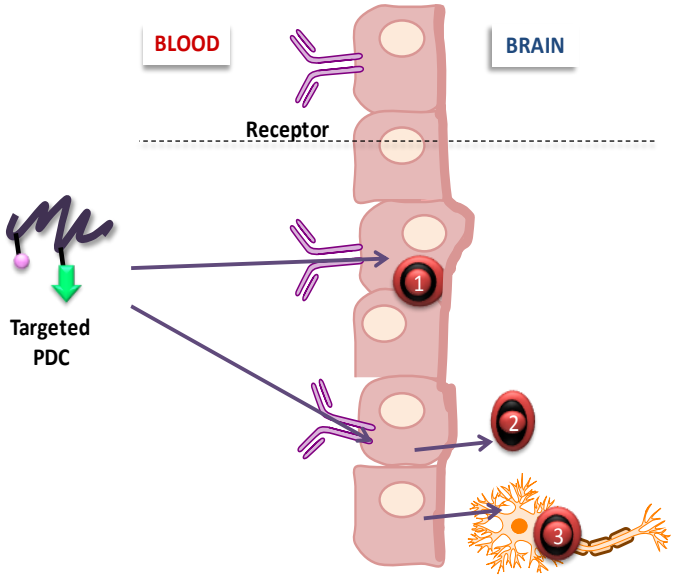

FIGURE I. 7 Differential PDC targeting to the BBB/brain. For conjugate design it is important to ensure where the target is located. (1) Intracellular targets in the brain capillary endothelial cells. 2. Extracellular target in the brain's extracellular space and /or neuron/glial cell surface. 3. Intracellular targets in brain cells (neurons, astrocyte, dendritic cells and pericytes). Adapted from ref. [48].

Recent appearance of cell-penetration peptides (CPPs) and also several proteins take profit of their positive charge and its amphipathic characteristics to cross BBB through *AMT* [43]. CPPs have been conjugated either covalently or non-covalently to poorly penetrating drugs (i.e. doxorubicin [91]), nanoparticles (i.e. cholesterol NPs [92]) or liposomes (i.e. cholesterol-poly(ethylene glycol) (PEG) [61]) have achieved activity once in the brain. SynB vectors, penetratin and TAT are some examples of effective CPPs. Proteins like albumin conjugated to PEG-PLA nanoparticles have demonstrated brain delivery in mice by the same mechanism [93]. However, AMT is a non-specific process: the adsorptive process can occur in blood vessels in other organs. Furthermore, toxicity and immunogenicity due to cationic profiles has to be defined for these

systems.

On the other hand, *RMT* provides a supported opportunity for active targeting of BBB, especially when the target receptor is over-expressed in the diseased condition or in the affected tissue as brain capillary endothelium in this case. In addition, many drug delivery strategies have been built up around RMT and AMT, although the RMT pathway has been preferred due to its higher specificity, especially for toxic agent delivery such as anticancer drugs. In RMT, cargo molecules associated with targeting ligands can be transported across the BBB, receiving for it the name of "Trojan horse approach" [94, 95]. A special remark is done with transferrin receptor in next paragraphs due to its importance in the present work.

Insulin receptor is an extensively characterised RMT system used for transporting drugs and genes into the brain. Pardridge *et al.* have successfully constructed a radiolabelled amyloid-beta-peptide conjugated to monoclonal antibody (mAb) that binds the human insulin receptor as a diagnostic prove for AD, and lately a chimeric form of the human insulin receptor mAb on adult monkeys showing rapid transport into the primate brain after i.v. achieving approximately 4% of the injected dose [96-100]. Despite its efficiency, this approach is considered risky because its involvement in glucose brain homeostasis. As for transferrin, the in vivo application of insulin is limited due to the high concentrations needed that could result in lethal overdosing [101].

Other receptors exploited are the low-density lipoprotein receptor related proteins 1 and 2 (LRP1 and LRP2 receptors) due to their diverse range of molecules and mediators such as ApoE, HIV-1 TAT protein, lactoferrin among others; diphtheria toxin receptor (DT_R), acetylcholine receptors,….

More recently, glutathione (GSH) has been also investigated as targeting moiety. GSH is and endogenous tripeptide in charges of detoxification of intracellular metabolites. BBB express transporters for this molecule [102]. Gaillard *et al*. started in June 2011 a clinical

trial to evaluate GSH PEGylated liposomal doxorubicin (2B3-101, to-BBB technologies, The Netherlands) as a novel option for brain cancer treatment administered i.v. [103]. Currently, this approach is in phase I/II clinical trial, in patients with primary and metastatic brain tumours. Within the same technology, a brain-targeted liposomal methylprednisolone is being developed for neuroinflammation [104].

Additionally, drug must block efflux pumps to remain into the brain [105, 106]. Transport influx systems in the cerebral endothelial play a key role in the delivery of essential substances to the brain and are usually overexpressed in tumours.

I. 1. 8 TRANSFERRIN RECEPTOR AS TARGET

Transferrin receptor is by far the most widely portrayed RMT system for drug targeting to the brain. It is a transmembrane glycoprotein consisting of two 90kDa subunits linked by a disulfide bridge. Each subunit binds one molecule of transferring (Tf). TfR mediates cellular uptake of iron bound to Tf (FIGURE I. 8). Mainly, it is expressed in hepatocytes, erythrocytes, intestinal cells, monocytes as well as in endothelial cells of the BBB, choroid plexus epithelial cells and neurons [107]. TfR presence is not studied in all brain diseases but remains clear that iron availability in the brain plays a fundamental role in their progression [108]. Therefore, iron metabolism may influence the efficacy and safety of TfR-mediated targeting to the brain. Furthermore, it is over-expressed in malignant cells [109].

Transferrin is the natural ligand of this receptor. Member of Fe-binding glycoproteins (such as lactoferrin, melanotransferrin and ovotransferrin), it is mainly synthesised in the liver [110]. It is a single chain 80kDa protein folded in two lobes. Each lobe can bind one iron ion, virtually irreversible at physiological pH [110]. After binding TfR, the receptor-ligand complex is endocytosed via clathrin-coated vesicles forming endosomes. In these structures pH reaches approximately 5.5, where Fe^{3+} is released from the protein and transported to the cytosol. The remaining apo-Tf (Tf without iron) has

higher affinity for the TfR at low pH and is recycled back to the luminal side of the endothelial cell. Apo-Tf is released from the receptor at physiological pH and binds iron again. It has been demonstrated that Tf has a bi-directional transport [111, 112].

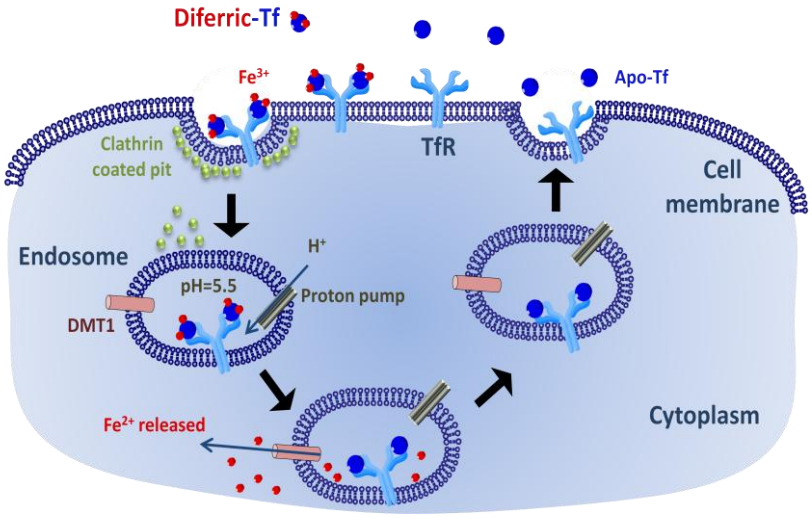

FIGURE I. 8 Cellular uptake of iron by the transferrin system via receptor mediated endocytosis. Redrawn from ref. [113]

Brain drug targeting by TfR strategy can be achieved either by using its endogenous ligand Tf or by using an antibody directed against the TfR. Each of these vectors has its advantages and disadvantages. Tf has been already reported as targeting moiety although *in vivo* its endogenous concentration in serum is already significant to compete for the TfR. Not only in brain but also in tumours, Tf has been used for the delivery of anti-tumour agents or gene therapeutics using polycation-based drug carriers [101, 114].

Monoclonal antibodies (mAbs) constitute other targeting motif option. Intensive research has been performed with a mAb against the rat TfR, the OX26 as a targeting vector [112, 115]. It binds to a different region than Tf, diminishing interferences with endogenous Tf. Several studies have demonstrated drug delivery across BBB with similar or higher efficiency than Tf, i.e. other mAb as

RI7217 or 8D3 [116]. Functionalised carriers used include liposomes, lipoplexes or cationic amphiphilic systems among others [117-122].

The mechanism of transcytosis for these ligands is not yet fully elucidated but in any case brain drug delivery via for TfR has been shown as a promising strategy . By this approach, vasoactive intestinal peptide (VIP), brain-derived neurotrophic factor or epidermal growth factor (EGF) among others have been transported into the brain parenchyma [101]. In addition, Pardridge *et al.* concluded that repetitive administration of cell surface specific mAbs did not result in down-regulation of BBB receptors [123]. This fact is relevant due to inherent chronic treatment necessary in neurodegenerative disorders. However, mAb OX26 targets rat TfR and does not bind human TfR, making difficult its translation to clinical setting. Apart from immunogenic reactions, humanised or chimeric antibodies preparation is a tedious task which could end up in loss of affinity and risks on iron homeostasis affection.

Recently, Atwal *et al.* and Yu *et al.* engineered a low-affinity bispecific monoclonal antibody with double targeting profile: the enzyme β-secretase (BACE1) and the TfR, reaching therapeutic concentrations in mouse brain and inhibiting BACE1 activity [64, 124]. This interesting therapy was proposed for AD in order to reduce production of the aggregation-prone amyloid peptides, thus decreasing amyloid plaque formation and slow disease progression. Again, this achievement stimulates attempts RMT use to increase brain uptake of therapeutic antibodies for brain disorders.

Making the most of all resources for TfR, novel targeting vectors to this receptor are already under study. Small and non-immunogenic peptide ligands for the human TfR are in the pipeline of development [101].

Despite the difficulties encountered so far and the low percentage of BBB crossing (unusually higher than 4% of the administered dose [96-100]), it could be said that, the potential for receptor-mediated targeting to the brain is very high. Not only the

selected targeting ligand is a key parameter for specific drug delivery but also other parameters could clearly influence the fate of the systems i.e. particle size, material, surface properties, density and conformation of targeting ligand. Improvement of drug selectivity is a critic parameter in all diseases. Concerning this issue, targeting offers an elegant approach to increase not only patient survival but also their quality of life [125]. Among the different types of targeting, benefit of their employment relies on the disease and its tissue characteristics, the chemical and biological properties of the bioactive agent used and the rate and time-course of administration.

I. 2 POLYMER THERAPEUTICS

I. 2. 1 DEFINITION AND CLASSIFICATION

'Polymer Therapeutics' (PT) was coined by Prof. Ruth Duncan to define a family of new chemical entities (NCEs) considered the first polymeric nanomedicines [126]. Polymer therapeutics encompasses a variety of complex macromolecular systems, their common feature being the presence of a rationally designed covalent chemical bond between a water-soluble polymeric carrier (with or without inherent activity) and the bioactive molecule(s). Although a tripartite design has been typically described for these systems, inclusion of targeting moieties and/or imaging agents has modified this concept [7].

Polymer therapeutics includes five compound families: *polymeric drugs,* polymers with inherent activity [127, 128]; *polymer-protein conjugates* [2, 6, 126]; *polyplexes* which are multi-component systems developed as non-viral vectors for gene/small interfering ribonucleic acid (siRNA) delivery [129, 130] *, polymeric micelles* where the bioactive agent is covalently bound [131, 132] and *polymer-drug conjugates* [126] (FIGURE I. 9). These nanosystems hold features such as a tailored drug loading, an incorporation of drug combinations or intelligent linker design tailored for specific biological conditions within the target organ or cell. Furthermore, the versatility of synthetic

chemistry and the inclusion of bioresponsive elements and biomimetic features provide scope for polymer therapeutics in comparison with other nanopharmaceutics [126].

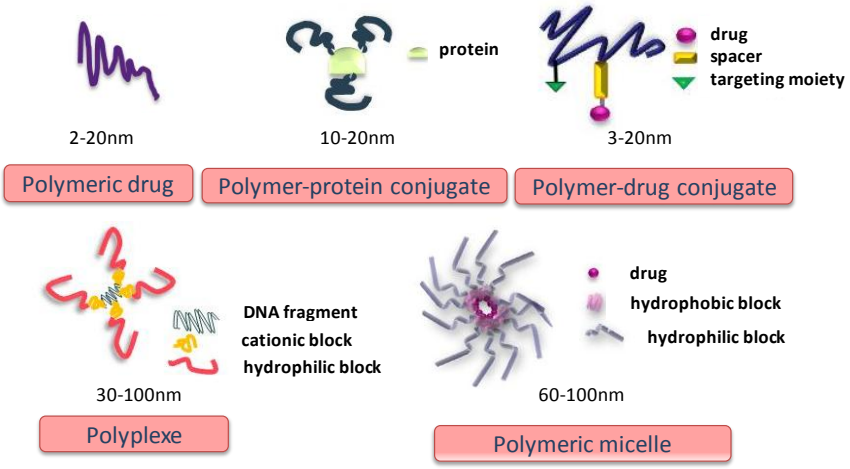

FIGURE I. 9 Schematic representation of polymer therapeutics families. Redrawn from ref. [126].

As any other delivery system, central objective of PT is (i) to release therapeutics at the desired body site (*targeting*) and (ii) to maintain the drug concentration within a therapeutic window for a desired duration (*controlled drug release*) [133].

Relying on the delivery route, bioavailability in the bloodstream allows for distribution to virtually all tissues. IV is the preferred route of administration when using polymer therapeutics as profits of the fastest drug distribution in comparison to other parenteral routes explored (i.e. subcutaneous (SC), intramuscular (IM) or intraperitoneal (IP)) and therefore, could enhance the benefits of intrinsic targeting mechanisms such as the EPR effect. Major obstacles to overcome after IV injection include tissue-specific issues, particularly BBB, tumour microenvironment, cell

compartmentalisation, hepatic clearance or renal filtration.

After more than two decades, development of these novel entities have result in several products in the market (PEGylated proteins and polymeric drugs) (TABLE I. 1) and a growing number of polymer-drug conjugates in clinical development (TABLE I. 2), mainly as anticancer agents via parenteral administration [5-7]. Knowledge acquired on biodistribution, clearance, mechanism of action and stability of these conjugates *in vivo* has helped to design an improved second generation of polymer therapeutics.

Product name	Technology	Indication	Route of admin.	Information source
Polymer-protein conjugates				
Zinostatin stimalmer®	Styrene maleic anhydride-neocarzinostatin, (SMANCS)	Cancer- hepatocellular carcinoma	Local admin. via hepatic artery infusion	Yamanouchia Japan
Oncaspar®	PEG-asparaginase	Cancer -acute lymphocytic leukaemia (ALL)	IV/IM	Enzon
Peg-intron®	PEG-Interferon alpha 2b	Hepatitis C	SC	Schering-Plough
Pegasys®	PEG-Interferon alpha 2a	Hepatitis C	SC	Roche
Neulasta™	PEG-hrGCSF	Chemotherapy-induced neutropenia	SC	Amgen
Adagen®	PEG-adenosine deaminase	Severe combined immune deficiency syndrome	IM	Enzon
Somavert®	PEG-HGH antagonist	Acromegalia	SC	Pfizer
Mircera®	PEG-EPO (polyethylene glycol-epoetin beta)	Treatment of anemia associated with chronic kidney disease	IV/SC	Roche
Krystexxa™ (pegloticase)	PEG-uricase	Chronic gout	IV	Savient farmaceuticals
Cimzia (certolizumab pegol)	PEG-anti-TNF Fab	Rheumatoid arthritis, Crohn's disease	SC	UCB
Polymer-aptamer				

conjugate				
Macugen$_{TM}$	PEG-aptamer (apatanib)	AMD	Intravitreous	OSI-Eyetech
Polymeric drugs				
Copaxone®	Glu,Ala,Tyr copolymer	Multiple sclerosis	SC	Teva
Renagel®	Phosphate binding polymer	End stage renal failure	Oral	Genzyme (Daiichi) licensed)
Welchol®	Cholesterol binding polymer	Type 2 diabetes	Oral	Genzyme

TABLE I. 1 First generation marketed polymer therapeutics. From refs. [1, 134] IV=intravenous, IM=intramuscular, SC=subcutaneous.

Product name	Technology	Indication	Adm.	Stage	Information source
Polymer-protein conjugates					
ADI-PEG 20	PEG-arginine deaminase	Cancer-hepatocellular carcinoma, melanoma	IV	Phase I/II	Phoenix Pharmalogics-Polaris Group
Hemospan® MP4OX	PEG–haemoglobin	Delivery of O2 in post surgery and trauma patients	IV	Phase I/II	Sangart
CDP 791	PEG-anti VEGFR-2 Fab	Cancer-NSCLC	IV	Phase II	UCB Pharma
Polymer-aptamer conjugates					
ARC1779	PEG-anti-platelet-binding function of von Willebrand Factor	Thrombotic microangiopathies	IV	Phase II	Archemix
E10030	PEG-anti-PDGF aptamer combination with Lucentis®	AMD	Local intravitreal	Phase II	Ophthotech
Polymeric Drugs					
AMG 223	Phosphate binding polymer	Hyperphosphatemia in CKD patients on hemodialysis	Oral	Phase II	Amgen
VivaGel®	Lysine-based dendrimer	Microbicide	Topical	Phase III	Starpharma
Polymer drug-conjugates					

Opaxio® (CT-2103; Xyotax)	Poly-L-glutamic acid (PGA)-paclitaxel	Cancer-NSCLC, ovarian, glioblastoma, various other cancers and combinations	IV	Phase III	Cell Therapeutics Inc
Prolindac®	HPMA-copolymer-DACH platinate	Cancer-melanoma, ovarian	IV	Phase III	Access Pharmaceuticals
FCE 28068 (PK1)	HPMA copolymer-Dox	Breast, lung and colon cancer	IV	Phase II	Pfizer
FCE 28069 (PK2)	HPMA copolymer-Dox	Hepatocellular carcinoma	IV	Phase I/II	Pfizer
PEG-SN38	Multiarm PEG-camptothecan derivative	Cancer-several	IV	Phase II	Enzon Inc
IT-101 (Cyclosert® technology assembled into a NP)	Polymer-cyclodextrin-camptothecin	Solid tumours	IV	Phase II/III	Cerulean Pharma
NKTR-118	PEG-naloxone	Opioid-induced constipation	Oral	Phase II	Nektar
NKTR-102	PEG-irinotecan	Cancer-metastatic breast	IV	Phase II	Nektar
NKTR-105	PEG-docetaxel	Cancer-various	IV	Phase I	Nektar
XMT-1001	Polyacetal-camptothecin	Cancer-various	IV	Phase I/II	Mersana

(Fleximer® technology)	conjugate				
Polyplexes					
CALAA-01	Polymer-cyclodextrin nanoparticle-siRNA	Solid tumours	IV	Phase I/II	Cerulean Pharma
Polymeric Micelles					
SP1049C Biotransport$_{TM}$	Pluronic® based formulation of Dox	Cancer-upper GI, NSCLC colorectal	IV	Phase III	Supratek Pharma Inc
NK 105 (Nanocarrier® technology)	Paclitaxel block copolymer micelle	Cancer-stomach	IV	Phase II	NanoCarrier Co.-Nippon Kayaku Co
NK-6004, Nanoplatin$_{TM}$ (Nanocarrier® technology)	Cisplatin block copolymer micelle	Cancer	IV	Phase I/II	NanoCarrier Co.-TOUDAI TLO Ltd/
NC-4016	Oxaliplatin block copolymer micelle	Cancer	IV	Phase I	NanoCarrier Co. TOUDAI TLO Ltd/

TABLE I. 2 Polymer therapeutics in clinical development. From refs. [1, 134] IV=intravenous, IM=intramuscular, SC=subcutaneous, Adm=administration route, dox=doxorubicin.

I. 2. 2 PASSIVE TARGETING: EPR EFFECT

Many of the advantages of nanotherapeutics derive from their controlled sizes and size-dependent properties like the "enhance permeability and retention (EPR) effect". Described by Maeda *et al.* [135, 136], this phenomenon is based on the unique phatophysiological characteristics of most solid tumours, such as extensive angiogenesis (hypervasculature), defective vascular architecture and an impaired lymphatic drainage. Basically, once the macromolecule is in the bloodstream is extravasated to tumour tissue due to the "leakiness" of the angiogenic tumour vasculature and retained there, promoting their accumulation in the tumour interstitium more than in normal tissues (FIGURE I. 10). Systems in the range of nanometre size take profit of this passive targeting which considerably increases the therapeutic effect. This phenomenon is also operative in inflammation areas, which justifies the development and use of this class of nanovectors in infectious and inflammatory conditions [137]. The EPR effect is ultimately driven by the circulating plasma concentration of the polymer conjugate [138].

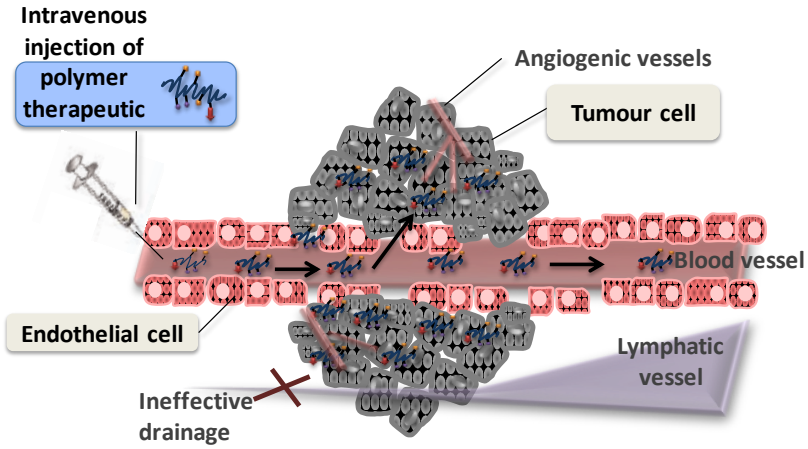

FIGURE I. 10 Schematic representation of the EPR effect. Adapted from ref. [139].

It has to be considered that the EPR effect has been described to be a highly heterogeneous phenomenon, it may change between different tumour regions, from tumour models as well as from patient to patient [140]. Typically, peripheral area is well-vascularised, there is a seminecrotic core and finally an avascular necrotic central region. All polymer therapeutics except one (FCE 28069, known as PK2) in the clinics relay on the EPR effect (TABLE I. 2) and now, the newer and more advanced systems are still mostly designed to fit this description [5, 141]. Simply utilising the hyperpermeability of this vasculature alone may not be possible to treat the entire tumour [142]. For this reason and others in the rest of scenarios, use of active targeting of polymer therapeutics will improve disease-to-normal tissue ratios.

I. 2. 3 BARRIERS AT THE CELLULAR LEVEL: ENDOCYTOSIS

Once the macromolecule is accumulated in the damage tissue drug release is seek either intracelullarly or in the extracellular matrix depending the location of the selected molecular target.

If an intracellular delivery is required, the first barrier of a therapeutic is breeching of the cell membrane, the fluid phospholipid bilayer sheet that excludes structures such as proteins from the cell interior, whilst retaining nanostructures such as ribosomes within. Normal uptake of nanoconjugates is achieved by endocytosis (FIGURE I. 11), governed by interactions with proteins and receptors on the cell membrane surface. However, there are exceptions to this with some PT that use electrostatic interactions to disrupt the cell membrane and gain entrance, i.e. polypropylenimine (PPI) [143]. The pH of the endosomal compartment drops during maturation to values of ≤ 5.5 because of the action of ATP-dependent proton pumps located in the membrane of the compartment [144]. As discussed, this drop in pH can be used for the breakdown of acid cleavable linkers, triggering the bioactive compound release within the cell.

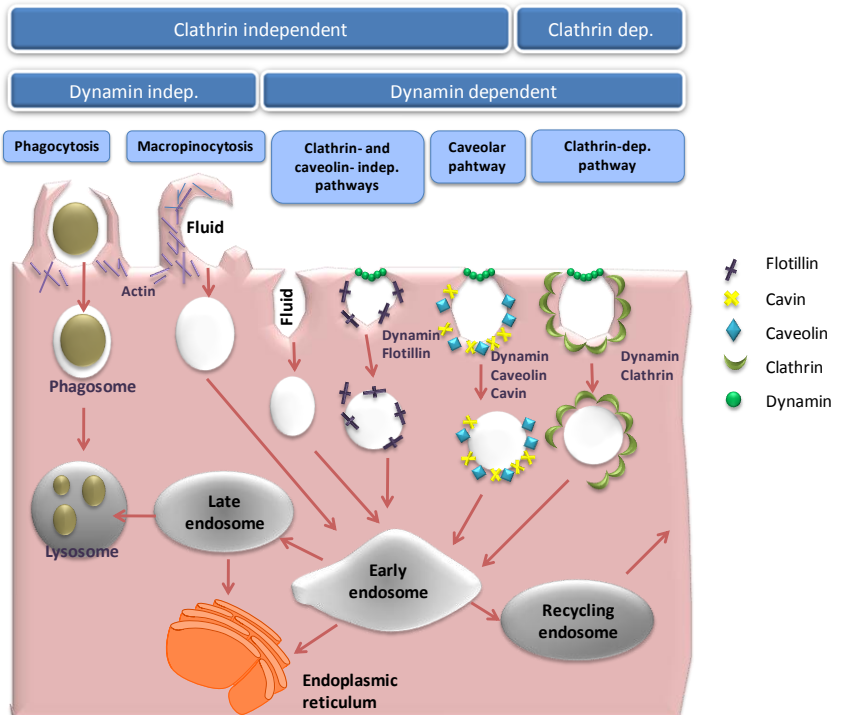

FIGURE I. 11 Mechanisms of extracellular uptake by endocytosis in a typical eukaryotic cell. *Endocytosis* defines the internalisation of the cell's plasma membrane to form vesicles that capture macromolecules and particles present in the extracellular fluid and/or bound to membrane-associated receptors. These vesicles undergo to a complex series of fusion events directing the internalised substances to an appropriate intracellular compartment. The endocytic pathways include clathrin-mediated, caveolae/lipid raft mediated, clathrin-, and caveolae-independent endocytosis, fluid-phase endocytosis, and phagocytosis. *Phagocytosis* involves the processing of large foreign particles by specialised cells such as macrophages, which form part of the reticuloendothelial system (RES). However, *clathrin-dependent endocytosis* consists first in the formation of endocytic vesicles (early endosomes) to trap the macromolecule. Depending on surface signals of membrane proteins to which nanostructures may be non-covalently linked, some may be trafficked along retrograde transport pathways for example via the Golgi apparatus and endoplasmic reticulum. Others may be carried through late endosomes to lysosomes where they may be degraded. Redrawn from [145] and [146].

Other pathways for release are possible within lysosomes as they contain a host of enzymes that are present for the breakdown of complex molecules such as lipids and proteins (known as lysosomotropic drug delivery usually used for small drugs or enzyme replacement therapies) (FIGURE I. 15). For example, the clinical performance of Opaxio^{TM}, a poly-L-glutamic acid(PGA)-paclitaxel (PTX) conjugate in Phase III trials as anticancer agent highly depend on the levels of the lysosomal enzyme cathepsin B. In fact, after finding a relation between oestrogen levels and cathepsin B expression in cancer patients, the latest clinical trials with Opaxio^{TM} have been design only to enrol women with oestrogen levels above 25pg/ml to ensure PTX release and therefore antitumor efficacy [147, 148].

Summarising, the performance of a PT is usually dependent on: efficient endosomal escape, retrograde trafficking and/or late endocytic/lysosomal activation for pharmacological activity [149].

On the other hand, it is important to recognise that the combination of hydrolytic enzymes and an acidic pH makes the intravesicle environment a hostile place for the therapeutic and can result in the inactivation of low Mw drugs as well as degradation of proteins, peptides and oligonucleotides that arrive there unless they are able to quickly escape to the cytosol. Escape from endosomal compartments can be achieved by disrupting the membrane bilayer (FIGURE I. 12, endosomotropic delivery). The use of pH-responsive endosomolytic systems is one of the preferred approaches to enhance cytosolic delivery for bioactives such as proteins, peptides or siRNA sequences. To date, the most successful example of this approach is CALAA-01, a transferrin targeted siRNA conjugate that consist on a self-assembling cyclodextrin containing polycation and anti-EWS-FLI1 siRNA-based nanoparticle (30-40 nm) pioneered by Davis *et al.* and developed by Cerulean Pharma in Phase I/II clinical trials (TABLE I. 2) [150, 151]. Similar strategy has been also followed by Kataoka *et al.* by means of polymeric micelles in order to enhance cytosolic delivery of

siRNA sequences [152]. Vesicle membrane disruptive properties can relay on the polymeric structure [153] or in protonable linked residues [154].

Beyond escaping the endosomal membrane barrier, the ultimate barrier is to deliver a therapeutic into the nucleus of the cell, particularly in gene therapy. It was reported in 1982 that anthracyclines can pass into the nucleus by passive diffusion from the cytoplasm through the nuclear pore complex (NPC) [155]. Polycations such as polyethylenimine (PEI), chitosan and polylysine (PLL) have shown initial success in interacting and facilitating the entry of genetic material into the nucleus [134]. Use of polymers as gene carriers has sparked a lot of interest in the field. Mainly due to the associated risks of using viral vectors, such as a reactivation of the virus, toxicity, gene control and targeting, which are either not present with polymers or can be controlled through the modification of the polymer properties such as Mw and architecture and also through conjugation of site specific markers or receptors.

In cases where endocytosis is diminished in the cell, polymer-directed enzyme prodrug therapy (PDEPT) is a useful tool for drug delivery [156] (detailed in section II.5.2 below). This system encompasses the combination of a polymer-drug conjugate carrying a single bioactive agent with a polymer-enzyme conjugate. The aim of the combination relies on appropriate and selective drug release from the polymer-drug conjugate at the desired site and is independent from endocytosis and the intracellular trafficking mechanisms. Another approach when these conditions are present is the use of plasma membrane disruptors such as melittin or cell penetrating peptides [134].

I. 2. 4 POLYMER CONJUGATION DESIGN THROUGH RATIONAL BASES

As mentioned, polymer conjugation of a protein or a drug is classified in two different families of PT. Biological purpose or rational

pursued in each case differs although both share a common structural composition: a polymer carrier, a linker or spacer and the bioactive agent.

I. 2. 4. 1 Polymer-protein conjugates (PPC)

Most therapies based on peptides, proteins or antibodies present as main limitation the short half-life time in blood, low stability, modest therapeutic effects and possible immunogenic responses. Conjugation of these bioactive molecules to polymeric platforms solves named drawbacks considerably enhancing their therapeutic output [126, 157]. From a historical perspective, PPC were among the earliest nano-therapeutic platforms explored for drug delivery which manage a successful clinical translation (TABLE I. 1).

History started in the early 90s. SMANCS, a conjugate of neocarzinostatin (NCS) and poly-(styrene-co-maleic acid) (SMA) for hepatocellular carcinoma treatment, was approved for clinical use in Japan [158]. Patients showed an extended blood half-life of NCS and markedly accumulation at tumour sites. Then followed the first enzyme conjugated to poly(ethylene glycol) (PEG) approved for clinical use in severe combined immune deficiency (SCID) syndrome: PEG-adenosine deaminase (Adagen®) [159]. Next advances on PPC were chased by an extensive use of this potential and well-stabilised technique: PEGylation, originally described in the 70s [160, 161], explained in detail in next section II.4.1.1.

For protein conjugation, the synthetic approach must offer reproducible site-specific protein modification. Semi-telechelic[1] polymers are required together with a linker that should not produce toxic or immunogenic by-products [126]. Bonds between the polymer

[1] SEMI-TELECHELIC: single group at one terminal end which avoiding crosslinked reactions and providing a specific point of linkage.

and the bio-agent have been adapted to specific release conditions [162]. Usually protein release is not desired as the main aim, mostly focus on enhancing its residence in blood stream, decrease its immunogenicity and avoid its proteolysis. Therefore, non-biodegradable bonds are utilised (i.e. Oncaspar®). When intracellular transport is needed, endosomotropic transport will require biodegradable linkers to release the protein through the endosome, impeding its lysosomal degradation (FIGURE I. 12).

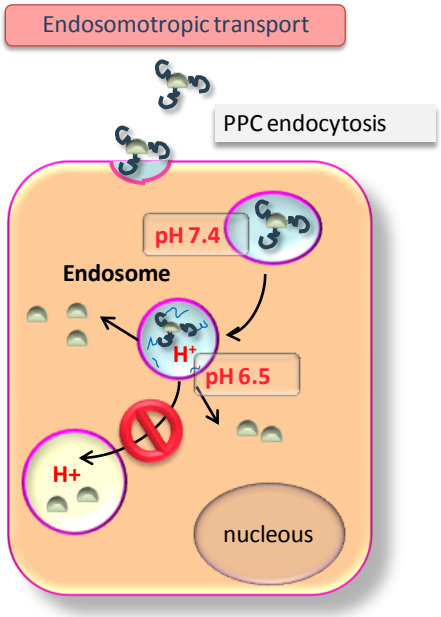

FIGURE I. 12 Intracellular transport mechanisms for polymer-protein conjugates (PPC). Endosomotropic transport (release trough endosomes): convenient pathway for intracellular trafficking of proteins or peptides. Redrawn from ref. [163].

PEGylation

PEGylation is a well-establish technology approved by the regulatory FDA (Food and Drug Administration) organism [164] with several examples in the market (TABLE I. 1). PEG has become one of the best defined polymer platform for biomedical applications [165].

PEG is a synthetic non-biodegradable polymer with semi-telechelic and low polydispersity (Mw/Mn varies from 1.01 for 5000Da to 1.1 in 50kDa PEG) [166]. Conjugation techniques have been developed since the first generation PPCs mostly based on linear monomethoxyPEGs or reaction conditions which could denaturise the protein. Currently, sophisticated methodology permits site-specific modification following protein mutagenesis or design of degradable PEG-protein linkages [126]. This non-ionic, hydrophilic polymer provides a steric shield to the conjugate avoiding recognition by immune system as well as increases molecule size, thereby reducing clearance from the bloodstream impeding rapid excretion through the reticulum endothelium system (RES) [167]. In addition, PEGylated products show less haemolysis[2] and could also diminish aggregation of erythrocytes. As mentioned for PPC, PEG augments duration of pharmacological activity, quality of life due to controlled release of the biomolecule and reduces toxic side effects. Thus, PEG conjugation has been defined as an effective strategy to alter the pharmacokinetic[3] (PK) profiles of a variety of biomolecules improving their therapeutic output and reaching a balance with their pharmacodynamics[4] (PD) properties to achieve novel therapies [168]. Considering all these advantages, dose frequency is reduced together with the drug amount required, improving patient compliance and reducing clinical cost. Veronese *et a*l. reported that the PEG conjugates have a favourable biodistribution, with preferred accumulation in the damage tissue (e.g. tumour, due to the EPR effect), and liver uptake values similar to other polymer–drug conjugates, such as (N-(2-

[2] HAEMOLYTIC: compounds that promote breakage of the red blood cell (RBC) membrane, releasing haemoglobin (Hb).

[3] PHARMACOKINETICS (PK): body processing of the drug/conjugate. It includes absortion, distribution, metabolism and excretion.

[4] PHARMACODYNAMICS (PD): drug action in the body. It includes the desired consequences of the treatment, i.e. therapeutic effect and the non-desired such as the side effects.

hydroxypropyl)methacrylamide)(HPMA) .

Final activity of the parent compound has to be reliable, thus site-specific chain location is critical. Shape and number of PEG chains, location next to an active site or a determinant region for active conformation could affect the expected activity. PEGylated proteins currently in the market used to follow non-specific site attachment strategies and were built with PEG sizes ranging from 5 to 40kDa and mainly trough amide bonding [169]. Only Cimzia® has a disulphide link by using a C-terminal cysteine reaction with maleimide [170]. Free cysteines as well as recombinantly placed ones are alternatives for site-specific conjugation with PEG derivates (i.e. disulfide, maleimide, vinylsulfone end groups). In parallel, to accomplish Mw limitation for safe renal elimination branched short PEG chains are proposed as alternative. Technical advances in controlled radical polymerisation (CRP) are able to form bioconjugates directly by polymerisation from modified proteins [171-173].

PEGylation has had lower impact for small drug conjugation because the limited drug loading capacity. However, use of PEG chains adsorbed or covalently attached to the surface of nanoparticles is a well established methodology [162, 174, 175] (FIGURE I. 13). PEG has demonstrated to be the perfect candidate to be grafted, conjugated or absorbed to the surface of nanocarriers or to be part of block-copolymers. Dye to its hydrophilic character PEG provides steric stability to the whole and allows bioactive ligands attachment, which remain at the outer part of the system (e.g. motifs for BBB crossing [47]).

Although PEG is in the market since the 90s, concerns about the fate of PEG and potential toxic effects have been started to be recently reported [176]. Among PEGylation drawbacks, adverse side effects in the body can be provoked by the progressive accumulation of the polymer upon repeated administration or the side products formed that lead to hypersensitivity reactions[162].

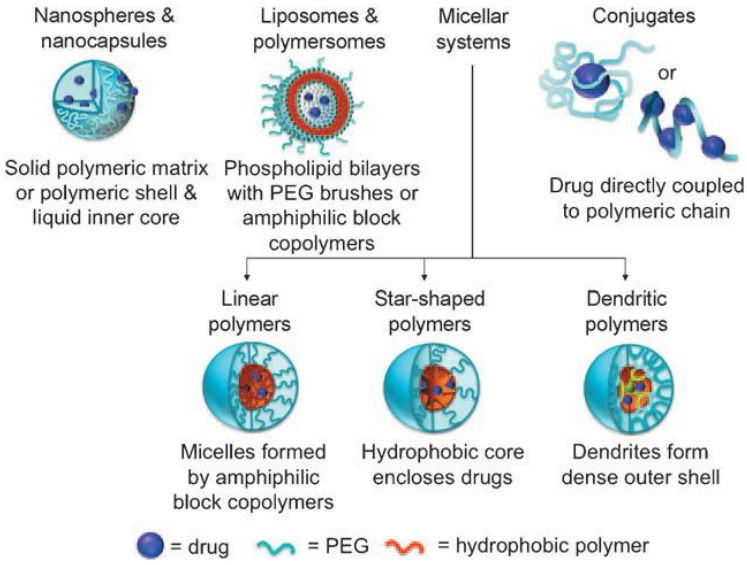

FIGURE I. 13 Examples of drug delivery systems where PEG is involved. From ref. [162].

Furthermore, its non biodegradability limits the usable Mw because for example, oligomers with <400Da have been found to be toxic in humans as a result of sequential oxidation into diacid and hydroxyl acid metabolites by alcohol and aldehyde dehydrogenase [177]. Not only for these reasons, PEG use in biomedical applications is being investigated as well as many alternatives for PEG are appearing [165].

I. 2. 4. 2 Polymer-drug conjugates (PDC)

Polymer drug conjugates are nano-sized systems where a small MW drug is covalently linked to a polymer [8, 178, 179]. PDC concept was born with polymer chemistry adaptation for drug conjugation developed by H. Ringsdorf on 1975, together with DeDuve's description of "lysosomotropic drug delivery" [2, 3].

Drug conjugation to a polymer not only enhances its aqueous poor solubility and protects it against degradation; it also changes its

PK at the whole organism and even subcellular level with the possibility to clearly enhance drug therapeutic value [5, 126, 141]. With a careful selection of the carrier, conjugation can yield long-circulating macromolecular systems that display passive targeting based on the EPR effect (detailed in section II.2) [180] and therefore lower systemic toxicity. It also limits uptake to the endocytic route, favouring lysosomotropic delivery with subsequent transfer of drug out of the endosomal/lysosomal compartment providing the opportunity to bypass mechanisms of drug resistance associated with membrane efflux pumps [126, 181]. This goal is directly related with the selection of the appropriate linker or spacer, which has to be stable during circulation and able to release the drug under certain environment.

Among the most used *polymer carriers* for suitable drug conjugation (FIGURE I. 14) the following examples are in the pipeline in PDCs design. These structures often provide a huge number of pendant groups (multivalent carrier) where apart from drug(s) conjugation, several molecules could be inserted, e.g. ligands for active targeting, stabilising moieties (like PEG), labelling motifs (fluorescent dyes, contrast agents,…), etc.

- HPMA: Initially developed as plasma expander, currently HPMA copolymers constitute one of the most studied polymer backbone for PDCs [126]. Its conjugates are mainly focused on cancer treatment with a special focus on the site-specific delivery of anti-cancer drugs. This neutral polymer is characterised by its water-solubility, biocompatibility and non-immunogenicity. Mayor drawback is the non-biodegradability which limits the Mw threshold for its safe body clearance. CFE28068 (PK1, HPMA-Dox, TABLE I. 2) was the first synthetic polymer entering in clinical trials.

- PGA (poly-glutamic acid): PGA is a polypeptide base on glutamic acid repeated units, each of them carrying a pendant

carboxyl group able for motif conjugation. It is water-soluble, non-toxic, biocompatible and biodegradable. In the body, such degradability is claimed by the cysteine proteases (particularly cathepsin B) which play the key role in the lysosomal degradation of this polymer. PGA has been conjugated to different class of drugs, e.g. anthracyclines, antimetabolites, DNA-binding drugs, taxol or camptothecin. Among these polymer-drug conjugates Opaxio™ (formerly Xyotax, PPX, CT-2103, TABLE I. 2) is in phase III for the treatment of non-small cell lung, ovarian carcinoma and has been recently designated as orphan drug in combination with radiotherapy for the treatment of glioblastoma. As mentioned in section I.2.1, Opaxio™ combines PTX covalently linked to PGA. PTX release is directly related to polymer degradation. Therefore, cathepsin B presence is a prerequisite in patients.

- Dextran: This polymer is a natural polysaccharide which monomer is sugar glucose, characterised by α-1,6 linkages with hydroxylated cyclohexyl units. It is water-soluble, biocompatible and biodegradable in blood and in the gastro-intestinal tract, although poorly degradable by mammalian enzymes, like other biopolymers such as alginates or chitosans [1]. Its hydroxyl groups are the linkage point for conjugation, via spacers.

- Dextrin, cyclodextrin and polyacetals : these novel polymeric carriers are on the second generation of PDCs and their mainly reliable due to their biodegradability [182]. PEG-polyacetals show pH dependent degradation [183-185] and dextrins are degraded by amylase [186]. These carriers have recently entered in clinical development (TABLE I. 2).

Within the PDCs design, selection of the *linker* may fulfil

several requisites. Connexion between drug and polymer backbone must remain stable during blood circulation and able to trigger drug release under specific conditions. Main reason is to achieve an effective intracellular drug release by lysosomotropic delivery (FIGURE I. 15). Once PDC is endocytosed, conjugate travels through endosomal pathway ending in lysosome vesicles. It is in this compartment where presence of proteolytic enzymes and/or acidic pH could promote carrier and/or linker degradation. Most drugs used in this macromolecular constructs are hydrophobic/lipophilic, therefore after the release they diffuse out to the cytosol, achieving the desired molecular target.

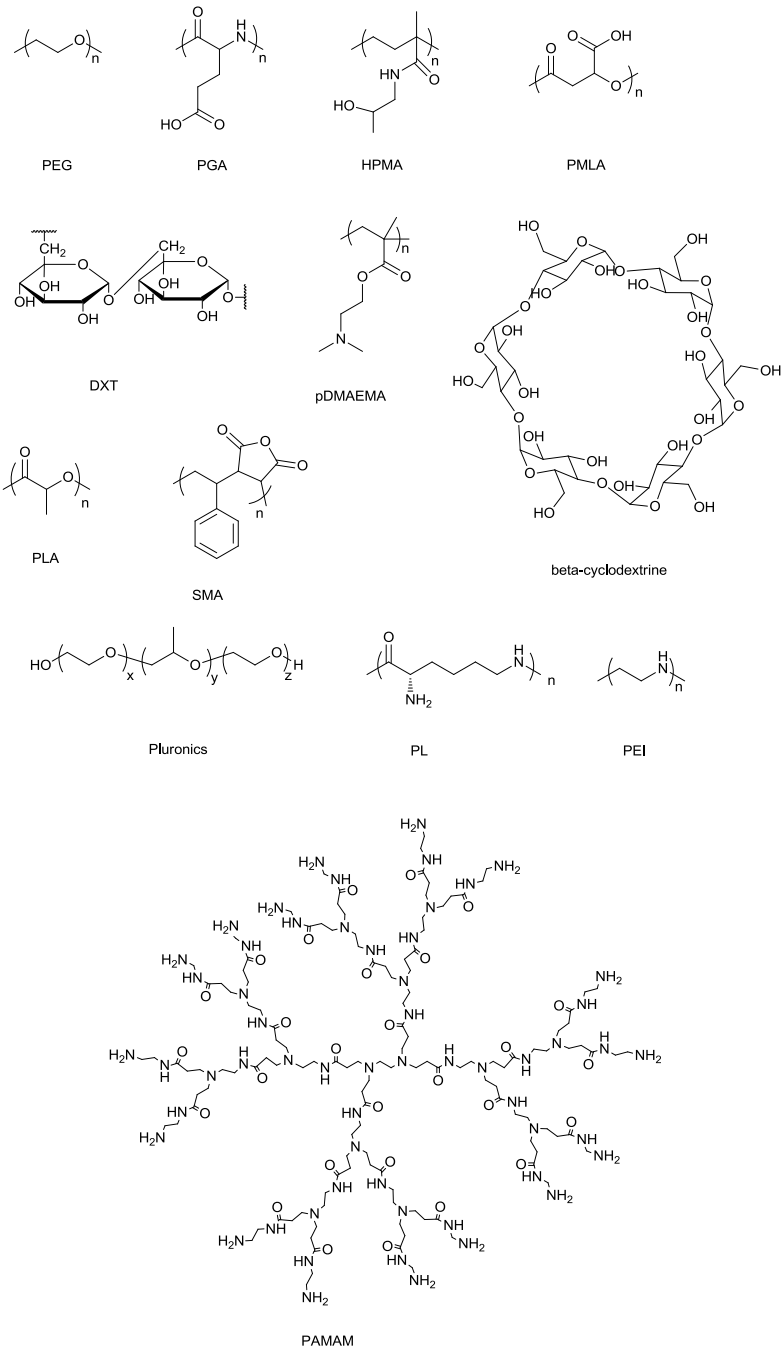

FIGURE I. 14 Examples of polymer used in the design of polymer therapeutics.

PGA=poly-L-glutamic acid, DXT=dextran, HPMA=N-(2-hydroxypropyl)methacrilamide, pDMAEMA=poly(dimethylamino)ethyl methacrylate, PEG=poly(ethylene glycol), PLA=polylactic acid, SMA=poly(styrene-maleic acid), PEI=polyethylenimine, PAMAM=polyaminoamines, PMLA=Poly(maleic acid), HPMA=N-(2-hydroxypropyl)methacrylamide, PL=Poly-L-lysine.

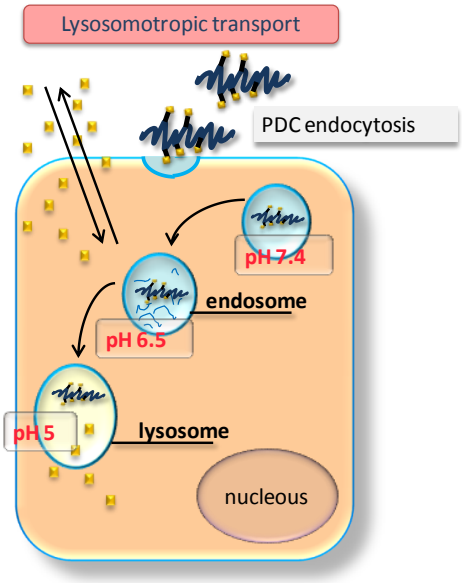

FIGURE I. 15 Intracellular transport mechanisms for polymer-drug conjugates (PDC). Lysosomotropic transport (release through lysosomes): optimal pathway for bioactive agents non susceptible to proteolytic degradation. Redrawn from ref. [163]

More than 16 polymer-drug conjugates are into clinical trials (TABLE I. 2) and as mentioned, possibly OPAXIO™ will be the first PDC into the market. PDCs initial field of application was focused on cancer therapy, bearing classical chemotherapeutic agents. Currently, future of PDCs for cancer treatment is centred in more specific targets and combination therapy, to increase efficacy and selectivity. Moreover, relationship between polymer architecture and conjugate PK at whole organism as well as at cellular level is a challenge area for PDC. As for PT in general, PDC also exploited lessons learned to search success in

the treatment of other human pathologies. Treatment of diabetes, hypertension, infections, digestive tract diseases or inflammation, as well as regenerative medicine applications or age-related diseases are already under study. FIGURE I. 16 briefly summarises the current state-of the art for PDCs [8].

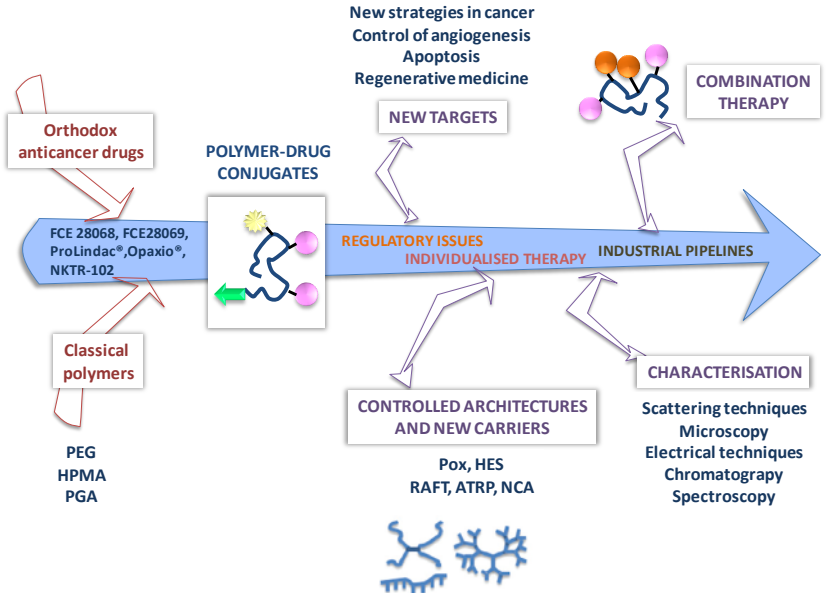

FIGURE I. 16 Current state-of-the-art technology with PDCs relies on established foundations from three decades of interdisciplinary research and is moved towards four accepted strategies: novel molecular targets in cancer as well as other disease, polymer-based combination therapy, new architectures and polymeric systems, and an exhaustive physico-chemical characterisation essential to clinical translation following regulatory indications. Deeper understanding on polymer conjugate features that govern clinical risk-benefit is leading to an appreciation of clinical biomarkers that will open new possibilities for personalised therapy. Redrawn from ref. [8].

I. 2. 5 CHALLENGES AND FUTURE OPORTUNITES FOR POLYMER CONJUGATES

First generation of polymer conjugates built a solid source of background information including optimisation of structures together with methodology development for characterisation, efficacy profiles

or pitfalls observed, clinical toxicities and side effect, setting up the different novel approaches that can take profit of all the experience obtained and improve it [140]. Practical and cost-effective design to use them as medicines for specific target indications, safe and effective in the context of the administration route, dose and frequency are guidelines in the current research [1].

For that purpose, four main strategies are followed: (i) the synthesis of novel polymeric carriers with defined architectures, (2) the search for better physico-chemical characterisation methods, (3) the use of polymer-based combination therapy to increase specificity and efficacy of the treatments and (4) their application for new molecular targets other than cancer, including the crossing of different biological barriers [8]. Besides, initial conjugates were developed for parenteral administration and after its successful proof-of-concept, rest of administration routes had been tested relying on each specific disease scenario.

Polymer conjugates also spans the field of diagnostic. Through a variety of imaging agents, several have been proposed as nanoprobes for monitoring. By means of tracer probe labelling, it is possible to build a single targeted conjugate to simultaneously report PK, targeting and clearance data *in vivo* and could also be used to report cellular and perhaps subcellular location of a biopsied sample *ex vivo.* Radiolabelled polymer based patient gamma camera imaging agents were already tested *in vivo* by Duncan *et al* more than one decade ago [126]. Other techniques as MRI, PET or optical imaging using near infra-red (NIR) fluorescent and luminescent probes are approaches under study in the area [1, 187-194]. For instance, an intravascular contrast agent, Gadomer-17 (SH L 643 A, Schering, Berlin, Germany) is a large dendrimer (Mw about 30-35kDa) containing 24 gadolinium ions transferred to the clinics although recently retired due to a non-adequate PK profile [195] . A step further in this direction encompasses the combination of therapeutic and diagnostic abilities into the same polymeric platform. This concept (“theranostics”) is

based on the “find, fight and follow approach” and offers the possibility of early detection, targeting and treatment of several diseases [1]. Relevant scientific studies meeting this new concept have been already reported [196-198].

In parallel, there is a growing effort to better understand the structure-activity relationships for defining safety and efficacy of these new therapeutics to meet with regulatory demand[1, 199]. First examples with polymer conjugates show that the panacea of enabling specific and individualised therapy through nanomedicine is becoming a feasible approach [200].

I. 2. 5. 1 Novel polymeric systems with well-defined architectures and exhaustive characterisation through physico-chemical methodologies

Addressing the necessity of more sophisticated biodegradable polymeric carriers with lower PDI and higher drug loading capacity, advances on polymer chemistry and physico-chemical characterisation techniques are ongoing implementations in the field.

Although well-tolerated in clinics, non-biodegradable polymers limit their use to certain Mw range for save renal elimination and possible risk of lysosomal accumulation has to be considered. Tendency on biodegradable polymers research is justified by their final use in applications as chronic or infectious diseases, for CNS disorders or tissue regeneration. Ideally, their hydrolytically or proteolytically backbone bonds would be cleaved ending up into small nontoxic metabolites eliminated through natural mechanisms. They are suitable for repeated parenteral administration and allow the use of higher Mw carriers to optimise PK as well as high polymer doses [7, 126]. Several examples are already under study, i.e. the lysosomal thiol-dependant proteases degradable polyglutamates [201], dextrins degradable by amylase and polyacetals which display pH-dependent degradation. In this thesis PGA-based carriers have been selected.

Concerning polymer manufacturing, several challenges must be faced to obtain reproducible and controlled systems. Polymers are inherently heterogeneous, and like macromolecules, their characterisation is hindered. In order to achieve the desired biodistribution, appropriate fate, biological activity and minimize side effects; crucial parameters must be exhaustively controlled along the polymer synthesis. Those parameters include chain length, Mw distribution, polydispersity, microstructure, charge localisation or hydrophilic-hydrophobic equilibrium and final conformation in solution [8, 138, 202, 203]. Depending on the polymerisation strategy followed, synthetic polymers get narrower dispersities than natural routes. Regarding microstructure of the polymeric chain, the relative stereochemistry (tacticity) [204] obtained after synthesis can directly influence on polymer degradation profile. Moreover, final conformational behaviour of the polymer is modulated by the nature and net charge of the macromolecular chain where microstructure plays a key role[205]. External stimulus could also undergo physical or chemical changes in responsive polymers depending on their tailored-composition (i.e. temperature-responsive micellisation or pH micelle dissociation) [133]. Surface charge or zeta potential (the electrical potential at the hydrodynamic slipping plane of a particle) is a determinant factor in the biological behaviour. It has been observed that negative or neutral surfaces significantly avoid nonspecific cellular uptake. Charge plays a key role in tubular reabsorption with positive charge leading to high retention in the renal cortex [197]. Thus, controlling these parameters over polymer sequences is an effective strategy for tuning macromolecular properties [185, 202, 204, 205]. Simultaneously to optimisation of polymerisation and bioconjugation processes, ease and scale up to pilot plant techniques have to been kept in mind for facilitate industry translation [206].

First generation of conjugates is based on few natural and synthetic polymers with linear, random-coil structures such PEG, HPMA copolymers or PGA (TABLE I. 1). Beyond linear polymers, the number of possible architectures is countless. To date, organic

synthesis and advanced polymerisation techniques can give birth multifaceted polymer carriers able to be engineered around the biological processes involved, rather than the current more opportunistic use as “carriers”. Modern synthetic approaches such as click chemistry [207] and/or controlled polymerisation methods (like RAFT, ATRP or ROP among others [165, 208-211]) have already yielded novel and well-defined polymer structure, i.e. multivalent polymers, graft and block copolymers, hyperbranched and star polymers, dendrimers and dendrons [66, 212-222] (FIGURE I. 17). These novel structures provide multivalent surfaces for the immobilisation of drugs and/or tracing agents, higher load capacity and the opportunity to exploit multiple pathways in cellular trafficking.

On the other hand, linker chemistry between the bioactive part and the polymer has evolved to be considered a key point in the conjugate rational design. Apart from enzymatic susceptible, non-enzymatic or pH-labile linkers, bioresponsive spacers are being developed to achieve more sophisticated and controlled constructs (i.e. self-immolative linkers) [7]. Linker selection will rely on the specific molecular target environment to trigger drug release.

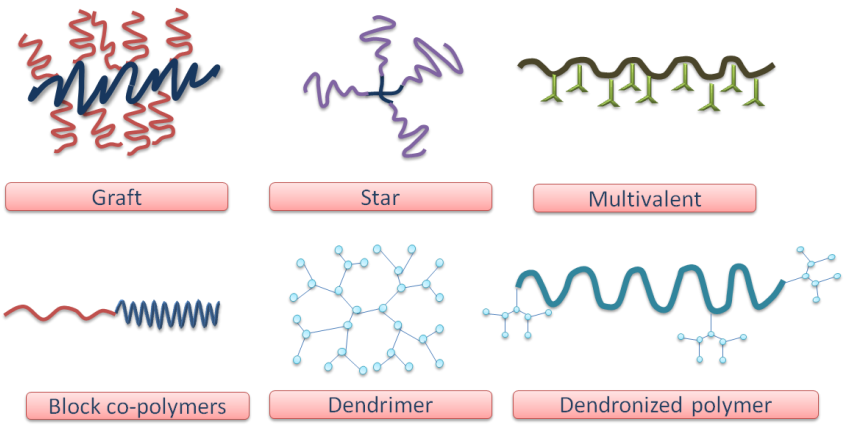

FIGURE I. 17 Example of several polymeric structures for PT applications. Adapted from ref. [126] .

All these evolved chemistry technologies increase the complexity of the final structures, therefore requiring exhaustive methodologies of characterisation. Clear understanding of physico-chemical behaviour makes a significant input toward a better understanding of its biological analysis which undoubtedly will smooth its acceptance in regulatory evaluation on the way to clinical development [199]. Sophisticated techniques have emerge in this concern, such as small-angle neutron scattering (SANS) for determine structure-activity relationships within conjugates [185, 223, 224], novel experiments trough NMR in solution such as pulse-field gradient spin-echo NMR (PGSE-NMR) to elucidate size, morphology and dynamics [182], and several imaging techniques for *in vivo* or *in vitro* monitoring of the conjugates [225-227].

Regardless, it has to be ensured that the chemistry used in conjugate synthesis will not cause toxicity or immunogenicity in biological systems as well as will not modify inherent properties of the bioactive compound. At last, it should be stressed that once drug is conjugated, characteristics of the polymer such conformation in solution or degradation profiles will vary. Final Mw, size and shape (in general solution conformation) of the entire system could end up in different biological behaviour, both at whole body and cellular level [74, 126].

I. 2. 5. 2 Polymer-based combination therapy

Disease progression underlies multiple molecular mechanisms. Unlike single agent therapy, multi-agent therapy can modulate different signalling pathways in diseased cells, thus maximising the therapeutic output and possibly overcoming mechanisms of resistance. Is becoming frequent the use of more than one drug or type of treatment in several human pathologies, e.g. cancer, malaria or HIV/AIDS. Polymer conjugates offer the advantage of carry multiple drugs in a unique platform obtaining the combination therapy approach [228].

There have been described four distinct types of polymer-based combination therapy. This includes (I) polymer-drug conjugate plus free drug(s), (II) polymer-drug conjugate plus polymer-drug conjugate, (III) single polymeric carrier carrying a combination of drugs and (IV) polymer-directed enzyme prodrug therapy (PDEPT) and polymer-enzyme liposome therapy (PELT) (FIGURE I. 18) [228].

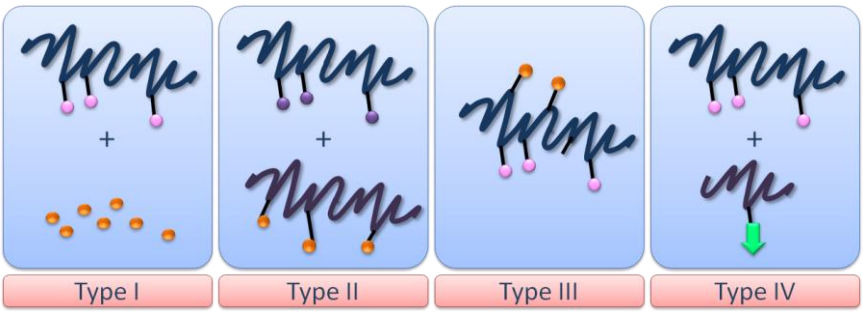

FIGURE I. 18 Schematic representation of the polymer-based combination therapy families: (I) combination of a polymer-drug conjugate carrying a single drug administered with a low molecular weight drug or a different type of therapy (e.g. radiotherapy), (II) combination of two different polymer-drug conjugates each containing a single therapeutic agent,(III) only one polymer main chain in which two or more drugs are conjugated and (IV) PDEPT relies on the combination of polymer-drug conjugate with a polymer-enzyme conjugate capable of the selective release of the drug at the targeted site. PELT is a comparable strategy where a polymer-enzyme conjugate is given in combination with the liposome to induce its degradation allowing release of the encapsulated drug. Redrawn from ref.[228].

Combination therapy approach is a growing area of research which started on cancer treatment, e. g. HPMA copolymer conjugate has been studied with different drug cocktails obtaining synergistic effects in tumour treatment (i.e. combining chemotherapy (doxorubicin (Dox)) and endocrine therapy (aminogluthemide); with conjugation of the antiangiogenic agent TNP-470 through an enzymatic cleavable linker and amino-bis-phosphonate alendronate; or the two drugs gemcitabine and Dox [7]). Nowadays, application of

this technology has created high expectancy on other diseases due to this first successful proof-of-concept. As first nanosystems in combination therapy, CPX-351 has been granted orphan drug status by the U.S. Food & Drug administration for the treatment of acute myeloid leukemia (AML) and is in two other clinical trials. This prodrug is a liposomal formulation of a synergistic 5:1 molar ratio of cytarabine and daunorubicin, two drugs used in hematologic malignancies [229].

It should be stressed that there are still many questions to address in order to optimise this polymer-based combinations. Rationale behind the design must consider the appropriate selection of drugs, best activity ratio and adequate polymer loading capacity for the desired drug cargo. Release kinetics will also play a key role depending on the selected linker for each drug. Again, complexity of the final system will require suitable techniques for characterisation and further *in vivo* investigations are required in each individual study to confirm that these systems are significantly synergistic, providing a more robust therapeutic effect than simple administration of the free drugs combined.

I. 2. 5. 3 Novel molecular targets

Recent anti-cancer approaches

First generation conjugate research was focused on anticancer agents. Conjugation of orthodox chemotherapeutic agents, i.e. Dox, to water-soluble carriers was developed and lead candidates raised the clinical arena [6]. Novel and sophisticated strategies for treating cancer are currently ongoing thanks to genomics and proteomics investigations on tumour molecular mechanisms. Recent studies have already reported the use of polymer conjugation techniques with drugs for specific inhibition of kinases and heat-shock proteins [230, 231], angiogenesis [232-234], chemoradiotherapy (combination of a

photosensitiser agent and a chemotherapeutic drug) [235, 236] and apoptotic[5] pathways [237-242]. In the last case, proapoptotic approach is related with cancer therapy but antiapoptotic has also applications in regenerative medicine [243]. Innovative tumour environment targeting has been achieved by PEG-rHuPH20 conjugate, able to reduce interstitial tumour pressure and enhance therapeutics passage by degrading hyaluronan (HA), a glycosaminoglycan polymer often accumulated in malignancy [244, 245].

Targeting diseases other than cancer

PT approaches towards novel molecular targets for other major human diseases than cancer is already a reality. High versatility and the favourable risk/benefit balance of these systems allow the design of effective treatments for novel molecular targets.

Initial studies up to date cover a broad spectrum of pathologies, trying to seek treatments for chronic and debilitating diseases of our aging increasing population. At present, Cimzia® (rheumatoid arthritis), Macugen® (age-related macular degeneration (AMD)) and Krystexxa® (chronic gout) are in routine clinical use (TABLE I. 1). Examples of ongoing studies are extensive review in reference [179] and summarised in TABLE I. 3. Attractive research is being carried out for tissue regeneration, i.e. by means of PGA-peptidil conjugate which acts as antiapoptotic inhibitor preventing inflammation-induced tissue damage [246, 247]; for corneal re-epithelialisation after injury through dextrin-rhEGF conjugates [248] or the anti-inflammatory therapy provided by multivalent dendritic polyglycerolsulfates designed to inhibit leucocyte trafficking [249]. Other pioneering approaches include a polymer conjugate for sepsis treatment based on PEG linked to a lipopolysaccharid (LPS)-neutralising small molecule which neutralise bacterial endotoxins [250] or bone targeting conjugates for

[5] APOPTOSIS: Programmed cell death pathway.

musculoskeletal diseases such osteoporosis and bone metastasis through [251].

Neurodegenerative disorders have been also targeted by polymer therapeutics and are reviewed in deep in next section due to the scope of this thesis.

DISEASE	POLYMER	DRUG	REF.
DIABETES	PGA	Phloridzin	[252]
HYPERTENSION	SMA	AHPP	[253]
HIV	PEG	Saquinavir	[254]
	SALP	Azidovudine	[255]
	Carregeenan	Azidovudine	[256]
	Dextrin	Azidovudine	[257]
	PHEA	Azidovudine	[258]
HEPATITIS	Dextran	Lamivudine	[259]
FUNGAL INFECTION	PEG	Amphotericin B	[260]
LEISHMANIASIS	Arabino-galactan	Amphotericin B	[261, 262]
	HPMA copolymer	Amphotericin B	[263]
	HPMA copolymer	NPC1161	[264]
SEPSIS	PEG	Peptoid 7	[250]
BOWEL CONSTIPATION	PEG	Naloxol	[265]
ULCERATIVE COLITIS	Dextran	Budesonide	[266, 267]
INFLAMMATORY BOWEL DISEASES	pDMAEMA	Dexamethasone	[268]
INFLAMMATION	Poyglycerol sulfates	-	[249]
RHEUMATOID ARTHRITIS	HPMA copolymer	Dexamethasone	[269]
	CDP	α-methylprednisolone	[270]

WOUND HEALING	PAMAM	Glucosamine	[271]
		Glucosamine-6-sulphate	
	Dextrin	rhEGF	[186, 248]
ISCHEMIA/injury reperfusion	PGA	APAF-1-inhibitors	[246, 272, 273]
	SMA	AHPP	[274]
	Modified dextran	17β-estradiol	[275]
	PEG	NO	[276]
OSTEOPOROSIS	HPMA copolymer	PGE_1	[269]
	HPMA copolymer	Alendronate	
	HPMA copolymer	D-Asp8	

TABLE I. 3 Polymer-drug conjugates under study targeting disease other than cancer. Updated from ref. [179].

SMA=copoly(styrene-maleic acid), AHPP=4-amino-6-hydroxypyrazolo[3,4-d]pyrimidine, PHEA=poly[α,β -(N-2-hydroxyethyl-DL-aspartamide)], PEG=poly(ethylene glycol), PGA=polyglutamic acid, HPMA=N-(2-hydroxypropyl)methacrylamide, GFLG=Glycin-Phenylalanin-Leucin-Glycin, AZT=Zidovudine, pDMAEMA=poly(dimethylamino)ethyl methacrylate, PAMAM=poly(amidoamine), CDP=linear cyclodextrin polymer (α-cyclodextrin + PEG), PGE_1=prostaglandin E_1, GGPNle=Glycin-Glycin-Prolin-NorLeucin, mPEG-PLA=methoxy-poly(ethylene glycol)-b-poly(lactic acid).

I. 3 POLYMER THERAPEUTICS FOR THE TREATMENT OF NEURODEGENERATIVE DISEASES.

Nanotechnology houses a helpful toolbox able to propose solutions to CNS drug delivery problems, such as controlled size and optimal delivery in defined conditions as well as specificity to site of action, generating drug targeting strategies precise enough to avoid damage to the delicate nervous system structures.

Development of strategies to reach central or peripheral nervous systems injured tissues and treat them is an objective pursued

by PT. Features conferred to the PT design will influence on the percentage of BBB crossing as well as on its pharmacokinetics and excretion inside the brain, which are key points that demand an exhaustive research. As mentioned, once achieved the site-specific area, polymer drug linkage can be tailored to be responsive against a particular enzymatic, pH or reductive environmental conditions. Administration routes existing for CNS drug delivery have been detailed in section I.7 and in each one it is possible to find examples of polymer therapeutics research. As explained, surpassing BBB by one or the other pathway displays a major issue for brain treatment. Although each alternative depends on the final application and the effectiveness of the given drug, undoubtedly a direct drug administration to the brain region, painless and safe provides an improved scenario.

PT possess all the requirements necessary for diagnosis and treatment of CNS disorders and brain tumours and therefore, constitute a promising field as BBB targeted drug delivery systems. Characteristics such as (i) specific strategies for active targeting by covalent binding of ligands or monoclonal antibodies of brain receptors, (ii) availability of different regions in the polymer backbone which serve for specific purpose, and (iii) sustained or controlled release of conjugated drugs through cleavable linkers in specific environmental situations, can be tailored to achieve this goal. It is noteworthy to emphasise that the PT studies described below are still at an early stage of development but the results are encouraging for future possibilities in achieving successful delivery of therapeutics to the CNS. Unlike other nanosystems, nanoconjugates are smaller in size so allow better penetration than the liposomes or non-conjugated micelles, less immunogenic and chemically more stable in plasma [277]. Proofs of nanosized particles translocation across BBB have been already achieved for several years [278, 279] but attaining inefficient percentage of total administered dose *in vivo*, typically less than 1% [1]. Potential of polymer structures usage for brain diseases

treatment was set by Gliadel® wafer (MGI Pharma, Bloomington, USA) [82]. This polymer depot was approved by FDA for brain therapy in high-grade malignant gliomas [101, 280]. This implantable polymeric system is made of a copolymer matrix based on 1,3-bis(p-carboxyphenoxy)propane and sebacic acid, loaded with carmustine. As a local delivery system, anticancer drug only reaches adjacent areas of the implant [78]. Unfortunately, this type of monolithic devices are beginning to lose popularity because researchers are developing materials to be implanted into deep brain regions that can disturb superficial brain tissue. Need of less invasive treatments through injectable formulations is already a reality [76].

Some of the main strategies adopted for crossing the BBB include innovative polymer-based therapeutics with covalently bound targeting ligands to mimic endogenous molecules (commonly named "Trojan Horses") [281], able to cross to brain parenchyma through receptors. PT systems used in this area include: *polymeric drugs*, *polymeric micelles*, *polyplexes* and *polymer conjugates* with linear or branch structures. Regarding polymer structures adopted by these compounds, few linear examples manage to cross BBB; most of them have vesicular conformation which favours the passage. Polymers in use for these purposes are shown in FIGURE I. 14. The most used polymers in this field are PEG, α-PGA, HPMA, poly-(L-malic acid), polyamidoamines (PAMAM) dendrimers, Pluronics®, poyethylenimine (PEI) and polylysine (PLL). Several examples of these formulations are given below; it must be highlighted that although goal of BBB crossing has been achieved, process has been very inefficient in terms of percentage of dose transferred. Usually maximum transfer *in vivo* is typically lower than 4% of the total administered dose [1].

Nanosized *polymeric micelles* are created when individual polymer chains (unimers) aggregate above a threshold concentration and temperature when dissolved in aqueous solution (known as the critical micelle concentration, CMC, and critical micelle temperature,

CMT, respectively). Hydrophobic drugs can be solubilised within its core, [282, 283] or covalently conjugated [284]. Studies involving polymeric micelles of Pluronic® block copolymers consisting of hydrophilic poly(ethylene oxide) (PEO) and hydrophobic poly(propylene oxide) (PPO) blocks (PEO-*b*-PPO-*b*-PEO) have been established as promising carriers for CNS drug delivery. The inherent amphiphilic character of this polymer gives surfactant-like properties and therefore interacts with hydrophobic surfaces and biological membranes [285]. In addition to the advantages conferred to the drug by micellisation, it has been discovered that Pluronic® unimers exhibit biological response modifying activities in drug formulations, therefore acting as a *polymeric drug* [286]. Depending on the aggregation state (unimer or micelle), this copolymer was shown to utilise multiple pathways to enter cells.[287] Pluronic® unimers are able to incorporate into membranes by changing their microviscosity and subsequently the translocation into cells is possible through caveolae-mediated endocytosis [287]. Once there, they can alter multiple cellular functions which includes inhibition of mitochondrial respiration, ATP depletion, inhibition of drug-efflux transporters (e.g. P-glycoprotein, multidrug resistance proteins and breast cancer resistance proteins), apoptotic signal transduction and gene expression [285]. Individual results from this make it possible to elucidate their activity within the brain.

Successful studies have shown brain accumulation through conjugation of targeting moieties i.e. polyclonal antibodies against brain α2-glycoprotein or insulin, which allowed BBB crossing through RMT of Pluronics®, either carrying a drug or a fluorescent probe [282]. They have also managed to increased analgesic effects with several opioid peptides [288] or polypeptide delivery to the brain via degradable disulfide linker (horseradish peroxidise, HRP as a model protein [289] and more recently leptin [290, 291]). In addition, Pluronics® are able to stimulate transcriptional activation of gene expression *in vitro* and *in vivo*.[285] Finally, to confirm that this system

has future promise in CNS drug delivery it must be remarked that a Pluronics®-based formulation of doxorubicin (SP1049C, Supratek Pharma) has advanced to Phase III in clinical trials to treat highly resistant tumours and could be the first FDA-approved polymeric micelle (see TABLE I. 2) [292].

Ljubimova et al. have designed a novel biodegradable nanoplatform based on poly-(β-L-malic acid) (PLMA) for IV treatment of gliomas [293, 294]. This *polymer conjugate* uses a tandem combination of monoclonal antibodies (mAbs) to enhance drug targeting across: (i) the BBB, thanks to an anti-mouse Tf antibody and (ii) the blood-tumour barrier (BTB) where antibody 2C5 targets tumour cell surface antigen. Through hierarchical addition, different molecules can be covalently attached at the same time to the polymer, e.g. with endosomal disrupting units, fluorescent dyes, drugs and PEG chains (as spacers and also as protection modules). Recent studies have shown that antisense oligonucleotides for tumour-specific protein inhibition (laminin-411) and the introduction of a trileucine endosome escape moiety have achieved specific accumulation in brain tumours and suppression of intracranial glioma growth [295]. PMLA-based delivery systems constitute an auspicious tool to treat brain tumours and for tumour imaging. However, this system entails drawbacks regarding the difficulties of chemical modification and the resulting technical limitations for high scale production [296].

PEGylation has also been explored as an alternative approach for enhancing brain entrance to non-penetrating peptide/proteins by reducing the interaction and/or specificity of the efflux transporters and enhance its stability and circulation. PEG conjugation to the opioid peptide DPDPE ((2,6-dimethyl-Tyr1,D-Pen2,D-Pen5)enkephalin) improved analgesic effect although therapeutic output has to be enhanced [297]. Several trials had been performed like PEGylation of growth factors for developing neurotherapeutic/neuroprotective conjugates (i.e. NGF (nerve growth factor) [298, 299], recombinant

human epidermal growth factor (rhEGF) [300], brain derived neurotrophic factor (BDNF) [299, 301-303]) or conjugation to OX26 antibody by avidin/biotin technology [304, 305]. As well in the neuroprotection field, Frank *et al.* achieved promised pre-clinical studies through PEGylation of the granulocyte colony-stimulating factor [306]. In a rodent model of Parkinson's disease, subcutaneous administration of a unique dose of the conjugate improved the PK profile in comparison with the non-modified counterpart together with improved motor performance. While current studies on PEGylation for BBB crossing are being carried out, PEG has became more popular as an extra complement (sterical stability shell, hydrophilic enhancing part, linker, etc) for the same final objective but not as the single carrier.

Regarding dendrimers, most research has been focused on glioma treatment. Polyamidoamines (PAMAM) have been evaluated for brain drug delivery. Sarin *et al.* have studied how PAMAM size influences its accumulation within malignant glioma cells by magnetic resonance and fluorescence imaging after IV administration, concluding that sizes of 11.1 to 11.9 nm in diameter were able to transverse BTB of malignant gliomas [307]. PAMAM-G5 dendrimer covalently linked to methotrexate (MTX) was constructed for targeting epidermal growth factor receptor-positive brain tumours by means of the antibody cetuximab (ICM-C225). By convection-enhanced delivery (CED) administration, the bioconjugate was selectively retained in rat gliomas [308]. More recently, successful *in vitro* experiments were performed with PAMAM-G4 dendrimers. By means of Tf conjugation, pH-bonded combination of Dox and tamoxifen demonstrated brain accumulation [309].

PAMAM dendrimers have also recently been tested *in vitro* for neuroinflammation treatment by its conjugation through a disulfide bond to N-acetyl-cystein (NAC), an anti-inflammatory agent [310]. Glutathione present in cell cytoplasm triggers drug release. Wu et al.

developed a vehicle for boron neutron capture therapy (BNCT) with a heavily boronated PAMAM dendrimer chemically linked to C225. *In vivo* studies by CED administration showed higher survival compared with control group [311]. Kannan *et al.* proved dendrimer conjugate localisation in astrocytes and activated microglia, cells responsible for neuroinflammation, after aubarachnoid injection in preliminary *in vivo* studies in cerebral palsy (CP) rabbit model [312, 313]. No targeting ligands were exploited. Same group already demonstrated that this conjugate improved myelination organisation, neuronal branching and neuronal injury after intrauterine administration in postnatal day 1 to 5 in the rabbit model, suggesting phenotype reversal [314].

An enhanced rate of transfer across biological barriers has been seen for dendrimers and hybrid dendritic architectures. Neutral and cationic systems have been demonstrated to have greater diffusivity in brain parenchyma after CED administration [312, 314]]. BBB crossing with non targeted dendrimers have been attributed to mixed cellular entry mechanisms, combining passive and others. However, as yet no dendrimers have been transferred into clinical trial for parenteral use other than the imaging agent Gadomer-17, mentioned above, which did not progress. The chemical simplification and systematic studies of dendrimer PK is enabling the optimisation of dendrimer structures with greater potential for parenteral use as therapeutics or imaging agents [315].

An increasingly popular field in the treatment of brain disorders is gene therapy using *polyplexes* as non-viral vectors. It should be remarked that cellular trafficking of these nanomaterials strongly depends on their composition, size, shape and surface characteristics as well as the cell line used for *in vitro* studies [287]. The surfaces of polyplexes are typically modified with hydrophilic and biocompatible polymers such as PEG or poly(hydroxypropylmethacrylate) (pHPMA) for *in vivo* applications, with the aim of increasing colloidal stability and solubility after its

systemic delivery by preventing aggregation and interaction with plasma proteins due to steric repulsions [316]. To improve the activity, acid-labile linkers between PEG and a polycationic block have been tested to expose the positively charged polyplex (after endosome hydrolysis) to enhance membrane disruption and cytosolic escape [317]. The design of polyplexes is often complemented by addition of brain-specific ligands for targeting neurodegenerative disorders. It has been shown that targeting moieties should be linked in distal ends of PEG to avoid masking receptor-ligand interaction [318]. Introduction of Nuclear Localisation Signal peptides (NLS) into polyplexes has been also attempted to achieve DNA delivery [316]. For example, recent studies pre-mixing NLS-PEG-trisacridine conjugate with DNA and biodegradable polyamines demonstrated significantly enhanced transfection into brain capillary endothelial cells [319]. Due to the cationic character of PAMAM, its use as non-viral vectors has been highly exploited. As a recent example, radio-labelled siRNA-PAMAM G7 dendriplexes incorporated in poloxamer 407 (Pluronic ®F127) and chitosan gels were proved to achieve BBB crossing after intranasal administration by radioactivity measurement [320].

Numerous targeting ligands have been conjugated to them to examine their potential for BBB passage. Angiopep-2 is an amino acid sequence endocytosed by the low-density lipoprotein (LDL) receptor-related protein (LRP-1) and to date is the most advanced technology in brain drug delivery. Its conjugation to three molecules of Paclitaxel (ANG1005, Angiochem Inc., Canada) is in two Phase I clinical trials for recurrent malignant gliomas and brain metastases of advanced cancer [280]. This peptide-drug conjugate is not a substrate for the P-gp efflux transporter and is therefore not pumped out of the brain as it happens with the free drug. Once in the brain, ANG1005 gains entry into tumour cells via LRP-1 mediated endocytosis and becomes activated in the tumour cell after the conjugated PTX is cleaved by esterases from the Angiopep-2 backbone, to release the active drug which leads to G2/M cell cycle point arrest and eventual tumour cell death (FIGURE I.

19). Angiopep-2 conjugated PEG-PAMAM dendrimer nanoparticles were observed to be internalised through clathrin- and caveolae-mediated endocytosis and partially by macropinocytosis. *In vivo* assays confirmed its passage through BBB and subsequent accumulation, showing higher efficiency in gene expression than non-modified dendrimers [321]. Transferrin-conjugated PEG-PAMAM dendrimer promoted gene expression in mouse brain after IV administration [322]. However, PAMAM safety has been always compromised its clinical development for systemic applications.

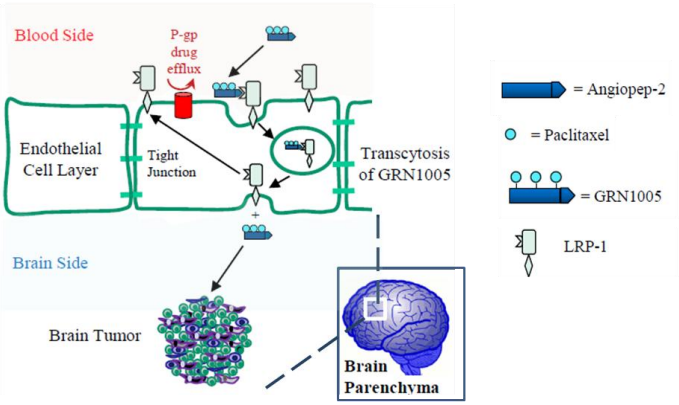

FIGURE I. 19 Mechanism of internalisation of Angiopep-2 as GRN1005. From ref. [323].

Number of targeting ligands tested to prove BBB crossing through RMT not involving polymer therapeutics is countless. For example, Zhan and colleges made up a micelle system with PLA-PEG encapsulating PTX, already functionalised with a 16-residue peptide named CDX, candid candoxin [60]. This peptide derived from the snake neurotoxin candoxin, which binds nAChrs with high affinity. They ensured BBB crossing by achieving higher survival in glioblastoma treatment and fluorescence detection of the system thanks to encapsulated infrared fluorescent dye (DiR). Another investigators anchored polysorbate 80 (P80) to dendritic poly(propyleneimine) (PPI) system encapsulating the anti-cancer drug docetaxel (DTX) [59]. RMT

through LDL receptors were targeted and demonstrated with *in vivo* experiments such as anti-tumour activity and biodistribution studies under a gamma camera. $^{99m}TcO_4^-$ was exploited for last purpose.

Arap-Pasqualini laboratory has designed, after a screening evaluation of small peptides library attached to viral particles, one peptide (CRTIGPSVC) that belongs to transferrin protein portion and it is currently being developed towards phase I human clinical trials. They confirmed that this peptide mimics the ligand of the Tf protein (iron), being able to bind, forcing the close conformation of the protein: "like if it were carrying iron". This closed form is the one binding to the receptors. Published work demonstrated BBB crossing with peptide-targeted phage particles in a mouse model of human glioblastoma [324].

Involving polymer therapeutics but not as the main actors, entails cell-based therapy transport. Batrakova *et. all* have developed a PEI-PEG complexed nanozyme loaded into bone marrow derived monocytes for Parkinson's disease treatment [325]. This system was able to attenuate oxidative stress due to sustained release of the antioxidant enzyme. Recent work based on similar electrostatic coupled enzymes (superoxide dismutase 1 (SOD1) and catalase) with cationic block copolymers (PEI-PEG or PLL-PEG) followed by covalent cross-linking to stabilise the nanoparticles, were radiolabelled and studied *in vivo* [326]. Results showed increased stability in blood and brain and increased accumulation in brain tissues, thus potentiating this formulation as antioxidant enzyme deliver system to CNS for oxidative stress reduction in neurodegenerative diseases.

Future possibilities with polymer therapeutics for brain delivery include the need of smart vector development and critical evaluation of currently existing ones. Also required its active targeting through novel ligands development in order to make the most of surface-mediated transcytosis as it is believed it constitutes a promising non-invasive strategy.

I. 1 4 FAMILIAL AMILOYD POLYNEUROPATHY (FAP): PROPOSAL FOR TREATMENT WITH POLYMER-DRUG CONJUGATES

Amyloidosis is the general term given to neurological diseases where an abnormal protein, known as amyloid, is misfolded and accumulated as deposits in organs and tissues disrupting their normal function. Some examples are given in TABLE I. 4. This large group of pathologies leads to cell damage, organ dysfunction and death. Amyloid proteins present difficulties to be removed by the body promoting their inherent accumulation. Amongst the different types of amyloidosis, where Alzheimer's and Parkinson's diseases are renowned examples, Familial Amyloid Polyneuropathies (FAP) constitute a group of inherited amyloidosis that affect mainly peripheral nerves [327]. One of the most common FAP is caused by transthyretin (TTR) misfolding and deposition in the peripheral nervous system, leading to neuronal toxicity and death[328].

Clinical syndrome	Precursor protein
Alzheimer´s disease	Aβ-protein
Primary Systemic Amyloidosis	Ig Light Chain
Secondary Systemic Amyloidosis	Serum Amyloid A
Senile Systemic Amyloidosis (SSA)	Transthyretin
Familial Amyloid Polyneuropathy (FAP)	Transthyretin
Finnish Hereditary Systemic Amyloidosis	Gelsolin
Type II Diabetes	Islet Amyloid Peptide
Non-Neuropathic Systemic Amyloidosis	Lysozyme
Cerebral Amyloid Angiopathy	Cystatin C
Atrial Amyloidosis	Atrial Natriuretic Factor
Familial Amyloidosis Type III	Apolipoprotein A-1
Hereditary Renal Amyloidosis	Fibrinogen

TABLE I. 4 A selection of diseases coupled to protein misfolding and amyloidosis and their precursor proteins.

TTR-related FAP has been selected herein as disease to be treated for the first time by means of rationally designed polymer-drug conjugates.

I. 4. 1 FAP CONCEPT

TTR-related FAP is catalogued as a rare disease, affecting around 8.000 patients around the world. Discovered in 1952 by the Dr. Corino de Andrade,[329] it is defined as a late-onset hereditary dominant neurodegenerative disorder. Its main characteristics are an ascending sensorimotor polyneuropathy and progressive autonomic dysfunction. The rate of evolution varies considerably depending on the protein mutation but usually manifesting itself upon the 40 decade of life and often becoming fatal 10 to 15 years after its onset. Initial symptoms are usually loss of sensibility and pain sensation in fingers and toes together with walking disability, but mainly dependent on the organ(s) involved. Furthermore, it leads to paresis, malabsorption and emaciation [330]. All of these symptoms critically disturb the quality and activities of patients' daily lives. As disease progresses, motor involvement comes out and ulcers or osteomyelitis may also occur. Later symptoms are cardiac dysfunction and renal failure.

The amyloidogenic mutated protein transthyretin (TTR) is the responsible of trigger the formation of extracellular deposits in several organs [331]. Prediction of the greatest extent and therefore the cause disease symptoms is difficult and peculiar of each individual. Although amyloid deposits may occur in any organ, peripheral nervous system is the most commonly affected, including nerve trunks, plexus and sensory and autonomic ganglia. In the peripheral nerves, tissues such as epineurium, perineurium and specially endoneurium are affected (FIGURE I. 20).

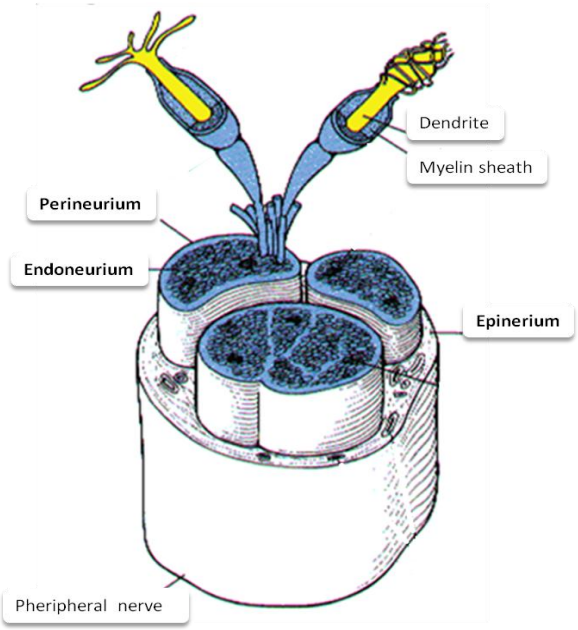

FIGURE I. 20 Structure of a nerve. Connective tissue wrapping. Adapted from ref. [332].

In the last one, deposits are usually closely opposed to Schwann cells or collagen fibrils [333]. Other organs involved are heart, intestine and kidney (FIGURE I. 21).

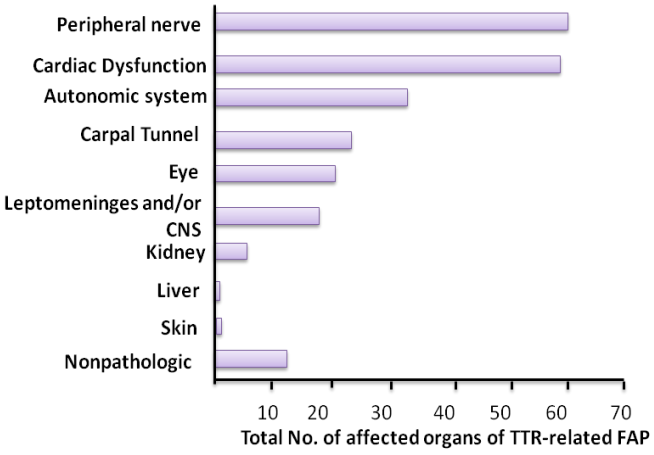

FIGURE I. 21 Amyloid-associated tissues in TTR related FAP patients. Redrawn from ref [328].

When heart is remarkably affected, the disease is denominated Familial Amyloid Cardiomyopathy (FAC). TTR amyloid fibrils infiltrate the myocardium leading to diastolic dysfunction progressing to restrictive cardiomyopathy and heart failure. Several specific mutations in TTR have been primarily associated. Heart involvement often causes congestive heart failure with tiredness, weakness and swelling of the feet due to water retention. Regarding intestine, it may cause diarrhea, constipation or both. Deposits can also occur in the eye, obstructing vision, and in minor frequency deposits may be found in the linings around the brain causing headache and stroke-like symptoms [334]. In some cases, there is reported direct involvement of the central nervous system (CNS) [335]. Amyloid deposition is localised in the leptomeninges in patients promoting cerebral infarction, haemorrhage, ataxia or even dementia. The mechanism by which the deposits lead to those symptoms remains unclear, but TTR synthesised by the choroid plexus could contribute to form them as it has been observed in patients following orthotopic liver transplantation [336].

I. 4. 2 ONSET OF THE DISEASE

FAP is found worldwide but there are endemic areas with higher frequency of patients found in Portugal, Japan and northern Sweden. Over 100 point mutations have been identified in TTR and associated with FAP; being the most common mutation the replacement of valine (V) with methionine (M) at position 30 in the protein sequence: V30M. Another common one is the replacement of V with an isoleucine at position 122: V122I where 3 to 4 percent of the African-Americans and 5 percent of some West African populations have this mutation. Most of the TTR gene mutations are thought to alter its natural structure impairing its ability to bind to other transthyretin proteins and altering its normal function.

In elderly people, TTR deposits may cause a condition named

senile systemic amyloidosis in which TTR does not have a mutation in its gene. Due to unknown reasons that remain unclear, TTR protein abnormally begins to form deposits. Heart is the common organ where this occurs, promoting slow progressive heart failure. Lungs, blood vessels and kidneys could be also affected. It has been estimated that 10 to 25 percent of population older than 80 suffer this disorder. For a patient with FAP, the age at which symptoms develop depends on the genetic mutation, ethnic background, and the penetrance of the disease [337]. The “penetrance” of a disease-causing mutation is the proportion of individuals with the mutation who exhibit clinical symptoms.

$$\text{penetrance} = \frac{\text{n heterocygotes with expressed trait}}{\text{total n heterocygotes}} * 100$$

Systemic variant of TTR circulates in the blood stream of asymptomatic patients; meanwhile it is deposited in several tissues in patients. Depending on which TTR mutation causes the disease, rate of progression varies. Reason for this difference is not known. The most abundant data pertain to the most aggressive variant with early disease onset: *TTR* V30M; from which following observations have been made:

- Variation in age of onset: The usual age of disease onset among *TTR* V30M gene carriers in Portugal, Brazil, and Japan is in the third to fourth decade of life. However, there are late-onset cases (as seen in Sweden) in which disease onset is in the fifth to sixth decade of life.
- Disease penetrance: In Portugal and Japan, more than 90 percent of *TTR* V30M gene carriers develop symptoms by middle age. However, in Sweden, disease penetrance is only 2 percent, and some V30M homozygous individuals remain asymptomatic.
- Some atypical Portuguese and Japanese kindred follow the late-onset, low-penetrance Swedish pattern.

- Some patients with no family history of amyloidosis and asymptomatic relatives with the variant gene carry the V30M variant.
- Disease onset is earlier in males than in females.
- Age of symptom onset is progressively earlier in successive generations. This feature is referred to as anticipation.

The explanation for the above observations is not well understood. Other genetic and/or environmental variables are thought to be at play. Anticipation, incomplete penetrance, and clinically sporadic cases in kindred's with unaffected allele carriers also have been observed with other *TTR* variants.

I. 4. 3 TTTR AND AMYLOID FORMATION PATHWAY

TTR gene is located on the long arm of the chromosome 18, at position 12.1 and codifies for 55kDa homotetrameric protein with four identical, monomeric subunits composed of 127 amino acids [338]. Each subunit has a molecular weight of 14kDa. 98 percent of this protein is synthesised in the liver and the other 2 percent in the choroid plexus of the brain and the retinal pigment in the eye [339] (FIGURE I. 22). TTR half life is 2 days. Main function of this protein is to act as carrier. TTR is the third transporter of thyroxine in plasma, carrying less than TBG (thyroxine-binding globulin) (70%) and albumin (15-20%). In the presence of normal levels of TBG, wide fluctuations in concentration of TTR or its removal from serum has little influence on the concentration of T4. Only 0.5% of circulating TTR in plasma is occupied by T4, which when is bond is not active. In the cerebrospinal fluid, TTR is the primary carrier of T4 as albumin is not present. This protein also acts as a carrier of retinol (vitamin A) through an association with RBP (retinol-binding protein). It takes part as a positive regulator in the delivery of RBP-bound retinol from plasma, preventing kidney filtration and enhancing RBP $t_{1/2}$ up to 16h. It enters by receptor-mediated endocytosis (RBP binds the receptor, retinol enters and TTR remains in plasma).

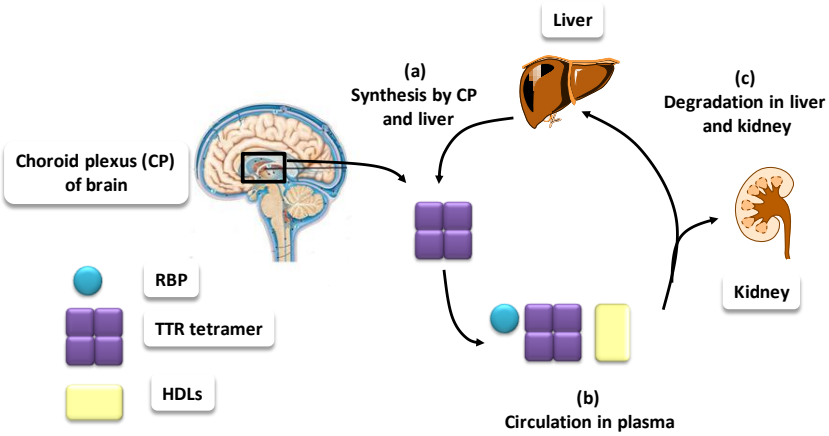

FIGURE I. 22 Synthesis, circulation and uptake of TTR pathways. From ref. [340].

It is a sensitive nutritional indicator with high impact in prognosis of oncologic patients. It is sensitive to proteins deficiency. Furthermore, it has been described that TTR binds A-beta protein, which plays the major role in the Alzheimer Disease (AD). It can act like a "chaperone" by preventing formation of A-beta amyloid aggregates and thereby it may halt progression of AD [341]. This disorder, also an amyloidotic disease, affects 5% of the population over the age of 65 years and 20% over 80 years of age.

Amyloid deposits are mainly composed by the precursor protein transthyretin, but there are several components associated such as serum amyloid P component (SAP), sulphonated glycosaminoglycans (GAGs), apoliproteins E and J, α1-antichymiotrypsin, several basement membrane components such as fibronectin, laminin and collagen type IV, complement proteins and metal ions. [342] Reasons for amyloid formation are not yet fully established. It is believed that several factors take part in the process that ends up in fibril formation. For example the inherent amyloidogenic potential of the protein that can be influenced or not by mutations, tissue and/or circulating factors as well as environment and genetic background. A singular characteristic involved in fibril

formation is the high content in β-content, present in most amyloidogenic proteins.

Regarding the specific mechanism by which TTR deposits and becomes pathological is not fully understood but it is currently accepted that the protein undergoes a series of events that lead to tetramer dissociation where the partially unfolded monomers self-assemble originating non-fibrillar aggregates, protofibrils and ending up in mature amyloid [343-345] (FIGURE I. 23). Structural studies *in vitro* concluded that fibrillar structures formed by TTR are polymorphic, exhibiting fibrils and oligomers of different diameters. The assembly dynamics evolves from oligomers of 5-8nm wide to short and thin fibrils with 4nm of diameter that twist over each other to end up in mature long fibrils of 8nm wide [346] .

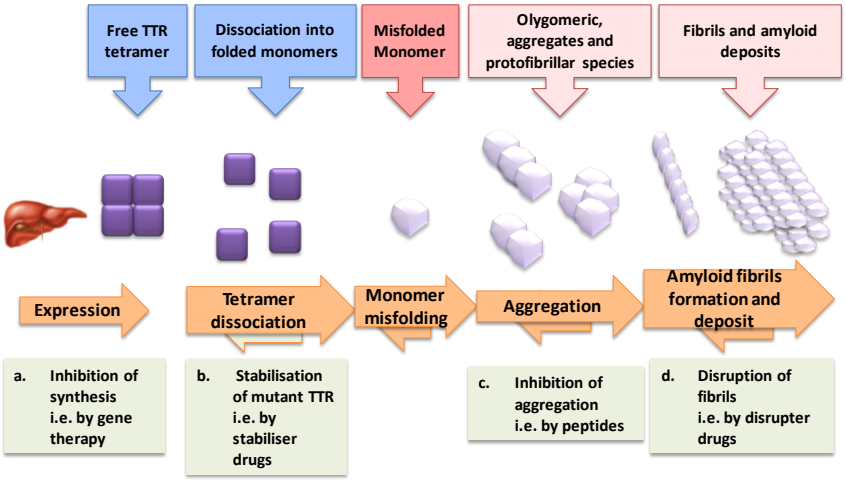

FIGURE I. 23 TTR amyloid cascade. In order for TTR to form amyloid, the tetramer must first dissociate (the rate-limiting step), and then the natively folded monomer must undergo partial denaturation to become competent to misassemble into a variety of aggregate morphologies, including oligomers and amyloid fibrils. Ligands (such as T_4; gray and red) stabilise the tetramer and thus prevent amyloidogenesis.

Existence of the different species has been proved “in vivo” from nerve biopsy samples of asymptomatic patients were small non-

fibrillar TTR aggregates were coexisting with amyloid deposits in later stages of the disease [347] .

Toxicity of the intermediate species has been studied by nerve and salivary glands analysis of FAP patients [348, 349]. Indeed, cytotoxicity of early TTR prefibrillar aggregates and not mature fibrils have shown oxidative and inflammatory responses in neuronal cells, induction of the NF-κB pathway and caspase-3 activation before amyloid fibrillar deposition, promoting cell dysfunction and death in the last stage [347]. Our collaborators, Saraiva et al., have previously contributed for the characterization of the dynamics of TTR fibril formation, including the characterization of the different TTR species generated along the process of fibril formation ([344]which allowed the screening of different drugs *in vitro*, acting at different stages of the amyloidogenic cascade [350, 351], and *in vivo* [346].

I. 4. 4 FAP DIAGNOSTIC

First step for amyloidosis diagnose is to detect amyloid. This can be shown in a tissue biopsy with the azodye Congo red (CR) [352] with the characteristic apple-green birefringence in polarised light. Next steps rely on determining if amyloid deposition is local or systemic and the type of amyloid as well as identify the responsible precursor protein. Ultrastructural analysis by electron microscopy [353], immunohistochemical staining for TTR, protein identification by mass spectrometry and genetic testing [354] are require for amyloid-associated TTR mutation. However, identification of disease-causing mutation is not considered as a final diagnostic because penetrance is variable [336, 337, 355]. Nevertheless, TTR amyloidosis is a predictable disease because gene mutations are detectable from birth in a genetic study. Early detection of the disease thanks to biomarkers may help in correct clinical treatment of the patients and delay the possible morbidity [356]. In the cases of non-hereditary ATTR, cardiac biopsy demonstrating amyloid deposits positive for TTR combined with lack of identifiable mutation in the TTR gene is necessary. Finally, a helpful

tool for ATTR diagnosis is the deposits found in the vitreous body with typical cotton wool inclusions due to approximately 20% of the protein is expressed in the retinal pigment epithelium of the eye [357].

CR method is commonly used in experimental studies of FAP. With polarised light, it is obtained a positive green birefringence due to amyloid-dye binding. In the early phases of FAP, TTR is already deposited in an aggregated *non-fibrillar form* negative by CR staining whereas in advanced stages these aggregates coexist with *mature amyloid fibrils* [356]. With age, short fibrils are easily observed by transmission electron microscopy (TEM), which are CR-positive. Furthermore, TTR initial aggregates are cytotoxic, both *in vivo* and *in vitro*, as evidenced by the presence of increased amounts of proinflammatory cytokines and oxidative stress markers such as nitrotyrosine, in tissues of FAP patients [349]and by apoptotic assays using a Schwannoma cell line [347].

I. 4. 5 FAP TREATMENT

Currently, there is not a specific pharmacologic therapy for ATTR. Available therapy is symptomatic. Effective FAP treatment alternatives are reduced to orthotropic liver transplantation (OLT), thus, suppressing the main source of mutant TTR [328, 358, 359]. Ideally, the transplantation should be performed as early in the disease course as possible. This therapy usually halts the illness progression resulting in amyloid clearance over time, but often with evolution of the cardiac amyloid affection. Besides, this strategy is extremely invasive, 100% of patients do not show clinical improvement and some of them have progression of their disease after transplantation.

This situation supports the urgent need to encourage medical research on new strategies for treating or preventing this disease. Together with this effort, complementary studies are carried out in identification and characterisation of the species formed along the

amyloid cascade process as well as biomarkers of each disease stage.

Less aggressive therapies for TTR amyloidosis treatment such as reduction of amyloidogenic TTR supply by other vias, stabilisation of the soluble circulating amyloid precursor, inhibition of aggregation of amyloidogenic intermediates and disruption of insoluble deposits have been proposed [340].

I. 4. 5. 1 Reduction of the supply of the amyloidogenic protein

Apart from OLT, another option is gene repair. Nakamura *et al.* reported that single-strand oligonucleotides (SSOs), induce targeted single-nucleotide exchanges in the TTR genes in both HepG2 cells secreting human wild-type TTR and liver from murine Val30Met TTR transgenic mice [360]. However, the level of gene conversion by SSOs was very low, with 11.1% and 7.9% conversion rate obtained, respectively. Inhibition of TTR synthesis has been also tested by Benson and co-workers [361]. They employed antisense oligonucleotides (ASOs) to inhibit hepatic expression of TTR. A transgenic mouse model carrying the human TTR Ile84Ser mutation was created and shown to express high levels of human mutant transthyretin. TTR ASOs suppressed hepatic TTR mRNA levels and serum TTR levels by as much as 80%. Finally, *Kurosawa et al*. had used small interfering RNAs (siRNAs) for the selective silencing of mutant Val30Met TTR in cell culture systems, identifying a siRNA that specifically inhibits mutant but not wild-type TTR expression even in cells expressing both alleles [362].

A gene-therapy study exploiting siRNA has been recently initiated by the company Alnylam [363]. *ALN-TTR01* is a systemically delivered RNAi therapeutic formulated in a first generation lipid nanoparticles (LNP) for the treatment of ATTR, including FAP and FAC. This vehicle is composed of cationic and fusogenic lipids, PEG and cholesterol. ALN targets a conserved region of the TTR gene in wild type and all known mutant forms; therefore it has the potential as a

therapeutic for all type of patients. Pre-clinical data demonstrated, for the first time, that treatment with an RNAi therapeutic could result in regression of pre-existing pathogenic TTR deposits in peripheral tissues. Additional data demonstrated its potential application for the treatment of ocular disease in ATTR. This therapeutic system is being improved using second generation LNP delivery technology developed in collaboration with Tekmira Pharmaceuticals Corporation, named *ALN-TTR02*.[176]

I. 4. 5. 2 Stabilisation of amyloidogenic protein precursor

Stabilisation of the TTR-tetramer to prevent formation of the destabilised monomer and its misfolding is another promising treatment option that under exploration [364] . Some nonsteroidal anti-inflammatory drugs such as *diflunisal* have been shown to stabilise TTR in serum [365]. Although this effect has not yet been demonstrated in patients with systemic amyloidosis, it may be represent great effect at the beginning of the disease, before clinical symptoms appear or in patients for whom re-transplantation is contraindicated.

Recently, Vindaquel® (tafamidis; previously named *Fx-1006A* developed by FoldRx Pharmaceuticals now property of Pfizer Inc.) has been approved by the EMEA and is in phase III in USA for TTR-FAP treatment in patients with stage 1 symptomatic polyneuropathy. It is a novel, selective and potent TTR stabiliser first described by Kelly and co-workers (FIGURE I. 24) [366]. Administrated by oral route, it reduces the burden of disease after 18 months compared to placebo, and appears to be safe and well-tolerated. This new chemical entity is able to stabilise wild type and variant TTR. It maintains neurologic function, reduces burden of the disease enhancing quality of live and improving nutritional state with similar side effects than the placebo group [367].

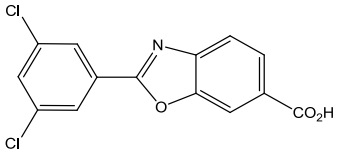

FIGURE I. 24 Tafamidis chemical structure.

As TTR crystal structure is well-known, there are other studies on protein stabilisers. They are able to fit in avoiding tetrameric structure destabilisation that ends up in fibril formation. For example, two palindromic ligands have been recently described to prevent TTR amyloid formation [368]. After the palindromic ligand is in place, the large number of ligand-protein contacts stabilises the complex with binding, which is irreversible under physiological conditions. These ligands are preferentially bound by and stabilise amyloidogenic variants, perhaps by virtue of improved access to the ligand site in these molecules, which bind T4 less avidly and are less stable than the WT. Furthermore, they have shown good oral bioavailability and a favourable PK profile.

I. 4. 5. 3 Disruption of amyloid fibrils

Within this therapeutic approach, the tetracycline doxycycline (doxy) is the most advanced compound in study. This drug demonstrated to be the most effective compound at disaggregating TTR mature fibrils [351]. Doxy was able to disrupt amyloid fibrils *in vitro,* in the treated animals and also achieved other improvements regarding amyloid markers [346]. The neuroprotector effect of this class of compounds, in addition to its own anti-microbacterial properties, was described in several other disease models including cerebral ischemia, spinal cord injury, Parkinson´s disease (PD), Huntington´s disease (HD), Amyotrophic lateral sclerosis (ALS), Multiple Sclerosis (MS), and AD.

Combination of Doxy with Tauroursodeoxycholic Acid (TUDCA)

is already in phase II of clinical trials. TUDCA is a biliary acid with antiapoptotic and antioxidant activity. In recent studies combined doxycycline and TUDCA administration to mice with amyloid deposition using two different concentrations of both drugs, was more effective when compared with either parent drugs. Significantly lowering of TTR deposition and associated tissue markers was observed. The observed synergistic effect of doxy/TUDCA in the range of human tolerable quantities, in the transgenic TTR mice models prompts their application in FAP, particularly in the early stages of disease. During this study, it was suggested that a possible mechanism for TTR extracellular aggregation is the influence of secreted metabolites generated by oxidative stress and apoptosis on TTR [330].

I. 4. 6 NOVEL TARGET FOR FAP TREATMENT AND POLYMER-DRUG CONJUGATES APPROACH

TTR has been proposed to trigger neurodegeneration through its engagement to the Receptor for Advanced Glycation End products (RAGE). This receptor is a member of the immunoglobulin superfamily of cell surface molecules and has been described as a receptor for advanced glycation end products (AGEs). RAGE is expressed at low basal levels in most adult tissues, except in lungs where is present in higher ratio in healthy and elderly adults. At cellular level, RAGE is expressed in most of cell types: endothelial, monocytes-macrophages, epithelial or neurons [369]. Between its functions, it represents an important factor in innate immunity against pathogens, but it also interacts with endogenous ligands resulting in chronic inflammation. Recent therapeutic strategies highlights RAGE as an important target to treat RAGE activation-associated diseases [370].

RAGE signalling has been implicated in multiple human illnesses such as AD, diabetes or aging associated diseases among others. This receptor is also up-regulated in tissues from FAP patients [349]. The secreted RAGE form, named soluble RAGE (sRAGE), acts as a decoy to trap ligands and prevent interaction with cell surface

receptors. sRAGE was shown to have important inhibitory effects in several cell culture and transgenic mouse models, in which it prevented or reversed full-length RAGE signalling. Following these results, the possibility of using a RAGE peptide to prevent toxicity triggered by TTR toxic aggregates was investigated. Saraiva et al. showed that a human RAGE peptide, corresponding to the 102–118 amino acid region of the RAGE V-domain, was able to bind TTR and abolish TTR-induced toxicity in cell culture [371] and transgenic mouse models (unpublished data), in which it prevented or reversed full-length RAGE signalling. As it has been previously referred, TTR-aggregate species appear in early disease development stages and coexist with fibril deposits in later phases; therefore, RAGE peptide constitutes a versatile tool for FAP treatment.

Because the major drawback that hinders peptides/proteins application in therapies is their variable solubility, low bioavailability and limited stability, one purpose of the present thesis is to move a step further this therapy enhancing the activity already found with doxy and RAGE peptide in FAP with polymer-drug conjugates, increasing their specificity and diminishing their systemic toxicity. These vehicles present advantages not just for peptides but also for small chemical compounds, allowing a controlled drug release at the desired site.

Moreover, the property of polymer multivalency allows the conjugation of several active compounds within the same polymeric carrier, the combination of doxy and RAGE peptide could synergistically enhance the therapeutic value of these prodrugs [228]. This concept has been already detailed in section II.5.2. Due to the molecular complexity of FAP it is expected to achieve better therapeutic output if more than one molecular pathway of disease is targeted.

BIBLIOGRAPHY

1. Duncan, R. and R. Gaspar, *Nanomedicine(s) under the microscope.* Mol Pharm, 2011. **8**(6): p. 2101-41.
2. Ringsdorf, H., *Structure and properties of pharmacologically active polymers.* J Polym Sci, 1975. **51**: p. 135-153.
3. C. de Duve, et al., *Lysosomotropic agents.* Biochem Pharmacol, 1974. **23**(18): p. 2495-531.
4. R. Duncan, *Development of HPMA copolymer-anticancer conjugates: Clinical experience and lessons learnt.* Adv Drug Deliv Rev, 2009. **61**(13): p. 1131-1148.
5. M.J. Vicent and R. Duncan, *Polymer conjugates: nanosized medicines for treating cancer.* Trends Biotechnol, 2006. **24**(1): p. 39-47.
6. M. J. Vicent, H. Ringsdorf, and R. Duncan, *Polymer therapeutics: Clinical applications and challenges for development.* Adv Drug Deliv Rev., 2009. **61**(13): p. 1117.
7. Duncan, R., *Polymer therapeutics as nanomedicines: new perspectives.* Curr Opin Biotech, 2011. **22**(4): p. 492-501.
8. F. Canal, J. Sanchis, and M.J. Vicent, *Polymer-drug conjugates as nano-sized medicines.* Curr opin Biotech, 2011. **22**(894-900).
9. http://www.who.int/mental_health/neurology/en/.
10. Kabanov, A.V. and H.E. Gendelman, *Nanomedicine in the diagnosis and therapy of neurodegenerative disorders.* Prog. Polym. Sci., 2007. **32**(8-9): p. 1054-1082.
11. K. Christensen, et al., *Ageing populations: the challenges ahead.* Lancet, 2009. **374**(9696): p. 1196-208.
12. A. M. Palmer, *The role of the blood-CNS barrier in CNS disorders and their treatment.* Neurobiol Dis, 2009. **37**(1): p. 3-12.
13. www.un.org.
14. T. M. Barchet and M. M. Amiji, *Challenges and opportunities in CNS delivery of therapeutics for neurodegenerative diseases.* Expert Opin Drug Deliv, 2009. **6**(3): p. 211-25.

15. A. J. Robichaud, *Approaches to palliative therapies for Alzheimer's disease.* Curr Top Med Chem, 2006. **6**(6): p. 553-68.
16. L. B. Elman, et al., *Palliative care in amyotrophic lateral sclerosis, Parkinson's disease, and multiple sclerosis.* J Palliat Med, 2007. **10**(2): p. 433-57.
17. Fernandes, C., U. Soni, and V. Patravale, *Nano-interventions for neurodegenerative disorders.* Pharmacol Res, 2010. **62**(2): p. 166-78.
18. Chiras, D.D., *Human biology.* Jones & Barlett Learning, 7th edition, 2011. **Chapter 10**.
19. S. C. Zhang, *Defining glial cells during CNS development.* Nat Rev Neurosci, 2001. **2**(11): p. 840-3.
20. F. L. Cardoso, D. Brites, and M. A. Brito, *Looking at the blood-brain barrier: molecular anatomy and possible investigation approaches.* Brain Res Rev, 2010. **64**(2): p. 328-63.
21. S. Brady, et al., *Basic Neurochemistry: Principles of Molecular, Cellular, and Medical Neurobiology*2011: Elsevier Science.
22. K. K. Wang, et al., *Hyaluronic acid enhances peripheral nerve regeneration in vivo.* Microsurgery, 1998. **18**(4): p. 270-5.
23. N. J. Abbott, L. Ronnback, and E. Hansson, *Astrocyte-endothelial interactions at the blood-brain barrier.* Nat Rev Neurosci, 2006. **7**(1): p. 41-53.
24. K. Kristensson, *Microbes' roadmap to neurons.* Nat Rev Neurosci, 2011. **12**(6): p. 345-357.
25. J. Lichota, et al., *Macromolecular drug transport into the brain using targeted therapy.* J Neurochem, 2009. **113**(1): p. 1-13.
26. Ehrlich, P., *Das Sauerstoff-Beürfniss des Organismus; eine farbenanalytische Studie.* Hirschwald, Berlin, 1885.
27. Pardridge, W.M., *Blood-brain barrier drug targeting: the future of brain drug development.* Mol Interv, 2003. **3**(2): p. 90-105, 51.
28. P. M. Carvey, B. Hendey, and A. J. Monahan, *The blood-brain barrier in neurodegenerative disease: a rhetorical perspective.*

J Neurochem, 2009. **111**(2): p. 291-314.

29. Su, Y. and P.J. Sinko, *Drug delivery across the blood-brain barrier: why is it difficult? how to measure and improve it?* Expert Opin Drug Deliv, 2006. **3**(3): p. 419-35.
30. I. Brasnjevic, et al., *Delivery of peptide and protein drugs over the blood-brain barrier.* Prog Neurobiol, 2009. **87**(4): p. 212-51.
31. V. Katyshev and P. Dore-Duffy, *Perycyte coculture models to study astrocyte, pericyte and endothelial cell interactions.* Methods Mol Biol, 2012. **814**(4): p. 467-481.
32. A. Armulik, et al., *Pericytes regulate the blood-brain barrier.* Nature, 2010. **468**(7323): p. 557-61.
33. O. O. Ogunshola, *In vitro modeling of the blood-brain barrier: simplicity versus complexity.* Curr Pharm Des, 2011. **17**(26): p. 2755-61.
34. R. D. Bell, et al., *Pericytes control key neurovascular functions and neuronal phenotype in the adult brain and during brain aging.* Neuron, 2010. **68**(3): p. 409-27.
35. S. Nag, *Blood-brain barrier: biology and research.* Springer, Berlin, 2003.
36. K. Francis, et al., *Innate immunity and brain inflammation: the key role of complement.* Expert Rev Mol Med, 2003. **5**(15): p. 1-19.
37. R. S. el-Bacha and A. Minn, *Drug metabolizing enzymes in cerebrovascular endothelial cells afford a metabolic protection to the brain.* Cell Mol Biol (Noisy-le-grand), 1999. **45**(1): p. 15-23.
38. K. A. Witt, et al., *Peptide drug modifications to enhance bioavailability and blood-brain barrier permeability.* Peptides, 2001. **22**(12): p. 2329-43.
39. M. I. Alam, et al., *Strategy for effective brain drug delivery.* Eur J Pharm Sci, 2010. **40**(5): p. 385-403.
40. A. K. Kumagai, K. J. Dwyer, and W.M. Pardridge, *Differential glycosylation of the GLUT1 glucose transporter in brain capillaries and choroid plexus.* Biochim Biophys Acta, 1994.

1193(1): p. 24-30.

41. W. M. Pardridge, *Blood-brain barrier drug targeting: the future of brain drug development.* Mol Interv, 2003. **3**(2): p. 90-105, 51.
42. L. Descamps, et al., *Receptor-mediated transcytosis of transferrin through blood-brain barrier endothelial cells.* Am J Physiol, 1996. **270**(4 Pt 2): p. H1149-58.
43. F. Herve, N. Ghinea, and J. M. Scherrmann, *CNS delivery via adsorptive transcytosis.* AAPS J, 2008. **10**(3): p. 455-72.
44. N. K. Gonatas, et al., *Endosomes and Golgi vesicles in adsorptive and fluid phase endocytosis.* J Cell Biol, 1984. **99**(4): p. 1379-90.
45. A.H. Schinkel, *P-Glycoprotein, a gatekeeper in the blood-brain barrier.* Adv Drug Deliv Rev, 1999. **36**(2-3): p. 179-194.
46. L. Wolfgang and P. Heidrun, *Role of drug efflux transporters in the brain fro drug disposition and treatment of brain diseases.* Prog Neurobiol, 2005. **76**: p. 22-76.
47. Y. Chen and L.Liu, *Modern methods for delivery of drugs across the blood-brain barrier.* Adv Drug Deliv Rev, 2011. **64**(7): p. 640-665.
48. J. Rip, J., G. J. Schenk, and A. G. de Boer, *Differential receptor-mediated drug targeting to the diseased brain.* Expert Opin Drug Deliv, 2009. **6**(3): p. 227-37.
49. S. Sato, et al., *Effect of barrier opening on brain edema in human brain tumors.* Acta Neurochir Suppl (Wien), 1994. **60**: p. 116-8.
50. A. Reichel, D. J. Begley, and N. J. Abbott, *An overview of in vitro techniques for blood-brain barrier studies.* Methods Mol Med, 2003. **89**: p. 307-24.
51. V. Katyshev and P. Dore-Duffy, *Pericyte coculture models to study astrocyte, pericyte, and endothelial cell interactions.* Methods Mol Biol, 2011. **814**: p. 467-481.
52. S. Man, et al., *alpha4 Integrin/FN-CS1 mediated leukocyte adhesion to brain microvascular endothelial cells under flow*

conditions. J Neuroimmunol, 2009. **210**(1-2): p. 92-9.

53. V. Siddharthan, et al., *Human astrocytes/astrocyte-conditioned medium and shear stress enhance the barrier properties of human brain microvascular endothelial cells.* Brain Res, 2007. **1147**: p. 39-50.
54. O. Steiner, et al., *Differential roles for endothelial ICAM-1, ICAM-2, and VCAM-1 in shear-resistant T cell arrest, polarization, and directed crawling on blood-brain barrier endothelium.* J Immunol, 2010. **185**(8): p. 4846-4855.
55. R. Montesano, L. Orci, and P. Vassalli, *In vitro rapid organization of endothelial cells into capillary-like networks is promoted by collagen matrices.* J Cell Biol, 1983. **97**(5 Pt 1): p. 1648-52.
56. L. R. Ment, et al., *An in vitro three-dimensional coculture model of cerebral microvascular angiogenesis and differentiation.* In Vitro Cell Dev Biol Anim, 1997. **33**(9): p. 684-91.
57. A. Al Ahmad, et al., *Astrocytes and pericytes differentially modulate blood-brain barrier characteristics during development and hypoxic insult.* J Cereb Blood Flow Metab, 2010. **31**(2): p. 693-705.
58. van Rooy, I., et al., *Comparison of five different targeting ligands to enhance accumulation of liposomes into the brain.* J Control Release, 2011. **150**(1): p. 30-6.
59. Gajbhiye, V. and N.K. Jain, *The treatment of Glioblastoma Xenografts by surfactant conjugated dendritic nanoconjugates.* Biomaterials, 2011. **32**(26): p. 6213-25.
60. C. Zhan, et al., *Micelle-based brain-targeted drug delivery enabled by a nicotine acetylcholine receptor ligand.* Angew Chem Int Ed, 2011. **50**(24): p. 5482-5.
61. Qin, Y., et al., *Liposome formulated with TAT-modified cholesterol for enhancing the brain delivery.* Int J Pharm, 2011. **419**(1-2): p. 85-95.
62. Ding, H., et al., *Inhibition of brain tumor growth by intravenous poly (beta-L-malic acid) nanobioconjugate with pH-dependent*

drug release [corrected]. Proc Natl Acad Sci U S A, 2010. **107**(42): p. 18143-8.

63. A.Regina, et al., *Antitumour activity of ANG1005, a conjugate between paclitaxel and the new brain delivery vector Angiopep-2.* Br J Pharmacol, 2008. **155**(2): p. 185-97.
64. J. K. Atwal, et al., *A therapeutic antibody targeting BACE1 inhibits amyloid-beta production in vivo.* Sci Transl Med, 2011. **3**(84).
65. X. Zhang, et al., *Analytical methods for brain targeted delivery system in vivo: perspectives on imaging modalities and microdialysis.* J Pharm Biomed Anal, 2012. **59**: p. 1-12.
66. A. R. Menjoge, R. M. Kannan, and D.A. Tomalia, *Dendrimer-based drug and imaging conjugates: design considerations for nanomedical applications.* Drug Discov Today, 2010. **15**(5-6): p. 171-85.
67. S. Aime and P. Caravan, *Biodistribution of gadolinium-based contrast agents, including gadolinium deposition.* J Magn Reson Imaging, 2009. **30**(6): p. 1259-67.
68. F .Ye, et al., *Noninvasive visualization of in vivo drug delivery of poly(L-glutamic acid) using contrast-enhanced MRI.* Mol Pharm, 2006. **3**(5): p. 507-15.
69. R. Saito, et al., *Gadolinium-loaded liposomes allow for real-time magnetic resonance imaging of convection-enhanced delivery in the primate brain.* Exp Neurol, 2005. **196**(2): p. 381-9.
70. Hornak, J.P., *The basis of MRI.* http://www.cis.rit.edu/htbooks/mri/, 2011.
71. B. P. Eliceiri, A. M. Gonzalez, and A. Baird, *Zebrafish model of the blood-brain barrier: morphological and permeability studies.* Methods Mol Biol, 2010. **686**: p. 371-378.
72. M. H. Turner, J. F. Ullmann, and A.R. Kay, *A method for detecting molecular transport within the cerebral ventricles of live zebrafish (Danio rerio) larvae.* J Physiol, 2012. **15**(2233-2240).

73. Rihel, J. and A.F. Schier, *Behavioral screening for neuroactive drugs in zebrafish.* Dev Neurobiol, 2012. **72**(3): p. 373.
74. E. Markovsky, et al., *Administration, distribution, metabolism and elimination of polymer therapeutics.* J Control Release, 2012. **161**(2): p. 446-460.
75. G. H.Huynh, D.F. Deen, and F.C. Szoka, Jr., *Barriers to carrier mediated drug and gene delivery to brain tumors.* J Control Release, 2006. **110**(2): p. 236-59.
76. A.J. Halliday and M.J. Cook, *Polymer-based drug delivery devices for neurological disorders.* CNS & Neurological disorders- Drug targets, 2009. **8**(3): p. 205-221.
77. M. T. Krauze, et al., *Safety of real-time convection-enhanced delivery of liposomes to primate brain: a long-term retrospective.* Exp Neurol, 2008. **210**(2): p. 638-44.
78. M. M. Patel, et al., *Getting into the brain: approaches to enhance brain drug delivery.* CNS Drugs, 2009. **23**(1): p. 35-58.
79. T. Inoue, et al., *Therapeutic efficacy of a polymeric micellar doxorubicin infused by convection-enhanced delivery against intracranial 9L brain tumor models.* Neuro Oncol, 2009. **11**(2): p. 151-7.
80. Yang, H., *Nanoparticle-mediated brain-specific drug delivery, imaging, and diagnosis.* Pharm Res, 2010. **27**(9): p. 1759-71.
81. Gabathuler, R., *Approaches to transport therapeutic drugs across the blood-brain barrier to treat brain diseases.* Neurobiol Dis, 2010. **37**(1): p. 48-57.
82. H. Brem and P. Gabikian, *Biodegradable polymer implants to treat brain tumors.* J Control Release, 2001. **74**(1-3): p. 63-7.
83. M.Pardridge, W., *Blood-brain barrier delivery.* Drug Discov Today, 2007. **12**(1-2): p. 54-61.
84. T. S. Salahuddin, et al., *Observations on exudation of fibronectin, fibrinogen and albumin in the brain after carotid infusion of hyperosmolar solutions.* Acta Neuropathol., 1998. **77**: p. 5-13.
85. N. J.Abbott, L.Ronnback, and E.Hansson, *Astrocyte-endothelial*

interactions at the blood-brain barrier. Nat Rev Neurosci, 2006. **7**(1): p. 41-53.

86. P. Debbage, *Targeted drugs and nanomedicine: present and future.* Curr Pharm Des, 2009. **15**(2): p. 153-72.
87. K. Arumugam, et al., *A study of rivastigmine liposomes for delivery into the brain through intranasal route.* Acta Pharm, 2008. **58**(3): p. 287-97.
88. M. M. Migliore, et al., *Brain delivery of proteins by the intranasal route of administration: a comparison of cationic liposomes versus aqueous solution formulations.* J Pharm Sci, 2009. **99**(4): p. 1745-61.
89. C. A. Lipinski, et al., *Experimental and computational approaches to estimate solubility and permeability in drug discovery and development settings.* Adv Drug Deliv Rev, 2001. **46**(1-3): p. 3-26.
90. W. H. Oldendorf, *Brain uptake of radiolabeled amino acids, amines, and hexoses after arterial injection.* Am J Physiol, 1971. **221**(6): p. 1629-1639.
91. C. Rousselle, et al., *New advances in the transport of doxorubicin through the blood-brain barrier by a peptide vector-mediated strategy.* Mol Pharmacol, 2000. **57**(4): p. 679-686.
92. Wang, H., et al., *The efficacy of self-assembled cationic antimicrobial peptide nanoparticles against Cryptococcus neoformans for the treatment of meningitis.* Biomaterials, 2010. **31**(10): p. 2874-81.
93. W. Lu, et al., *Brain delivery property and accelerated blood clearance of cationic albumin conjugated pegylated nanoparticle.* J Control Release, 2007. **118**(1): p. 38-53.
94. A. R. Jones and E. V. Shusta, *Blood-brain barrier transport of therapeutics via receptor-mediation.* Pharm Res, 2007. **24**(9): p. 1759-71.
95. Pardridge, W.M., *Drug and gene targeting to the brain with molecular Trojan horses.* Nat Rev Drug Discov, 2002. **1**(2): p.

131-9.

96. C. F. Xia, R. J. Boado, and W.M. Pardridge, *Antibody-mediated targeting of siRNA via the human insulin receptor using avidin-biotin technology.* Mol Pharm, 2009. **6**(3): p. 747-51.
97. Y. Zhang, R. J. Boado, and W.M. Pardridge, *Marked enhancement in gene expression by targeting the human insulin receptor.* J Gene Med, 2003. **5**(2): p. 157-63.
98. M. J. Coloma, et al., *Transport across the primate blood-brain barrier of a genetically engineered chimeric monoclonal antibody to the human insulin receptor.* Pharm Res, 2000. **17**(3): p. 266-74.
99. W. M. Pardridge, et al., *Human insulin receptor monoclonal antibody undergoes high affinity binding to human brain capillaries in vitro and rapid transcytosis through the blood-brain barrier in vivo in the primate.* Pharm Res, 1995. **12**(6): p. 807-16.
100. W. M. Pardridge, J. Eisenberg, and J. Yang, *Human blood-brain barrier insulin receptor.* J Neurochem, 1985. **44**(6): p. 1771-8.
101. A. G. de Boer and P.J. Gaillard, *Strategies to improve drug delivery across the blood-brain barrier.* Clin Pharmacokinet, 2007. **46**(7): p. 553-76.
102. Gaillard, P.J., *Crossing barriers from blood-to-brain and academia-to-industry.* Ther Deliv, 2010. **1**(4): p. 495-500.
103. P. J. Gaillard, et al., *Abstract 5687: Development of glutathione pegylated liposomal doxorubicin (2B3-101) for the treatment of brain cancer.* Cancer Res, 2012. **15**(72 (8 Supplement)): p. 5687.
104. P. J. Gaillard, et al., *Enhanced brain delivery of liposomal methylprednisolone improved therapeutic efficacy in a model of neuroinflammation.* J Control Release, 2012. **164**(3): p. 364-369.
105. A. Beduneau, P.S. and J.P. Benoit, *Active targeting of brain tumors using nanocarriers.* Biomaterials, 2007. **28**(33): p. 4947-67.

106. T. Bansal, et al., *Novel formulation approaches for optimising delivery of anticancer drugs based on P-glycoprotein modulation.* Drug Discov Today, 2009. **14**(21-22): p. 1067-74.
107. E. H. Morgan, *Iron metabolism and transport.* Hepatology. A text book of liver disease, 1996. **1**(D.Zakin and T.D. Boyer, eds.): p. 526-554.
108. J. R. Burdo and J. R. Connor, *Brain iron uptake and homeostatic mechanisms: an overview.* Biometals, 2003. **16**(1): p. 63-75.
109. P. Ponka and C. N. Lok, *The transferrin receptor: role in health and disease.* Int J Biochem Cell Biol, 1999. **31**(10): p. 1111-37.
110. T. Moos and E.H. Morgan, *Transferrin and transferrin receptor function in brain barrier systems.* Cell Mol Neurobiol, 2000. **20**(1): p. 77-95.
111. T. Moos and E. H. Morgan, *The significance of the mutated divalent metal transporter (DMT1) on iron transport into the Belgrade rat brain.* J Neurochem, 2004. **88**(1): p. 233-45.
112. Y. Zhang and W.M. Pardridge, *Rapid transferrin efflux from brain to blood across the blood-brain barrier.* J Neurochem, 2001. **76**(5): p. 1597-600.
113. T. R. Daniels, et al., *The transferrin receptor part II: targeted delivery of therapeutic agents into cancer cells.* Clin Immunol, 2006. **121**(2): p. 159-76.
114. Y. Aktas, et al., *Development and brain delivery of chitosan-PEG nanoparticles functionalized with the monoclonal antibody OX26.* Bioconjug Chem, 2005. **16**(6): p. 1503-11.
115. W. A. Jefferies, et al., *Transferrin receptor on endothelium of brain capillaries.* Nature, 1984. **312**(5990): p. 162-3.
116. H. J. Lee, et al., *Targeting rat anti-mouse transferrin receptor monoclonal antibodies through blood-brain barrier in mouse.* J Pharmacol Exp Ther, 2000. **292**(3): p. 1048-52.
117. H. Karatas, et al., *A nanomedicine transports a peptide caspase-3 inhibitor across the blood-brain barrier and provides neuroprotection.* J Neurosci, 2009. **29**(44): p. 13761-9.
118. M. Willis and E. Forssen, *Ligand-targeted liposomes.* Adv Drug

Deliv Rev, 1998. **29**(3): p. 249-271.

119. D. B. Fenske, I. MacLachlan, and P. R. Cullis, *Long-circulating vectors for the systemic delivery of genes.* Curr Opin Mol Ther, 2001. **3**(2): p. 153-8.
120. G. Storm and J.A. Crommelin, *Liposomes: quo vadis?* PSTT, 1998. **1**: p. 19-31.
121. I. S. Zuhorn and D. Hoekstra, *On the mechanism of cationic amphiphile-mediated transfection. To fuse or not to fuse: is that the question?* J Membr Biol, 2002. **189**(3): p. 167-79.
122. K. Ulbrich, et al., *Transferrin- and transferrin-receptor-antibody-modified nanoparticles enable drug delivery across the blood-brain barrier (BBB).* Eur J Pharm Biopharm, 2009. **71**(2): p. 251-6.
123. D. Wu and W.M. Pardridge, *Pharmacokinetics and blood-brain barrier transport of an anti-transferrin receptor monoclonal antibody (OX26) in rats after chronic treatment with the antibody.* Drug Metab Dispos, 1998. **26**(9): p. 937-9.
124. Paul, S.M., *Therapeutic antibodies for brain disorders.* Sci Transl Med, 2011. **3**(84).
125. L. Juillerat-Jeanneret and F. Schmitt, *Chemical modification of therapeutic drugs or drug vector systems to achieve targeted therapy: looking for the grail.* Med Res Reviews, 2007. **27**(4): p. 574-590.
126. Duncan, R., *The dawning era of Polymer Therapeutics.* Nature Rev Drug Discov, 2003. **2**(5): p. 347-360.
127. Donaruma, L.G., *Synthetic biologically active polymers.* Prog Polym Sci, 1975. **4**: p. 1-25.
128. Seymour, L., *Review: synthetic polymers with intrinsinc anticancer activity.* J Bioac Comp Polym, 1991. **6**(2): p. 178.
129. A. V. Kabanov, P. L. Felgner, and L.W. Seymour, *Self-assembling complexes for gene delivery. From laboratory to clinical trials.* Wiley, Chichester, 1998.
130. D. W. Pack, et al., *Design and development of polymers for gene delivery.* Nat Rev Drug Discov, 2005. **4**(7): p. 581-93.

131. M. Yokoyama, et al., *Polymer micelles as novel drug carrier: adriamycin-conjugated poly(ethylene glycol)-(poly(aspartic acid) block copolymer.* J Control Release, 1990. **11**(1-3): p. 269-278.
132. Y. Matsumura and K. Kataoka, *Preclinical and clinical studies of anticancer agent-incorporating polymer micelles.* Cancer Sci, 2009. **100**(4): p. 572-9.
133. W.B. Liechty, et al., *Polymers for drug delivery systems.* Annu Rev Chem Biomol Eng, 2010. **1**: p. 149.
134. R. M. England, I. Conejos-Sánchez, and M.J. Vicent, *Drug delivery strategies: Polymer Therapeutics.* 2012. **Chapter 8.2**(RSC publishing): p. 456-482.
135. Y. Matsumura and H. Maeda, *A new concept for macromolecular therapeutics in cancer chemotherapy: mechanism of tumoritropic accumulation of proteins and the antitumor agent smancs.* Cancer Res, 1986. **46**(12 Pt 1): p. 6387-92.
136. H. Maeda, et al., *Vascular permeability enhancement in solid tumor: various factors, mechanisms involved and its implications.* Int Immunopharmacol, 2003. **3**(3): p. 319-28.
137. K. Greish, et al., *Macromolecular therapeutics: advantages and prospects with special emphasis on solid tumour targeting.* Clin Pharmacokinet, 2003. **42**(13): p. 1089-105.
138. L. W. Seymour, et al., *Influence of molecular weight on passive tumour accumulation of a soluble macromolecular drug carrier.* Eur J Cancer, 1995. **31A**(5): p. 766-70.
139. D. Peer, et al., *Nanocarriers as an emerging platform for cancer therapy.* Nat Nanotechnol, 2007. **2**(12): p. 751-60.
140. T. Lammers, et al., *Drug targeting to tumors: principles, pitfalls and (pre-)clinical progress.* J Control Release, 2011. **161**(2): p. 175-187.
141. R. Duncan, *Polymer conjugates as anticancer nanomedicines.* Nature Reviews Cancer, 2006. **6**(9): p. 688-701.
142. M. K. Danquah, X. A. Zhang, and R. I.Mahato, *Extravasation of*

polymeric nanomedicines across tumor vasculature. Adv Drug Deliv Rev, 2011. **63**(8): p. 623-39.

143. N. A. Stasko, et al., *Cytotoxicity of polypropylenimine dendrimer conjugates on cultured endothelial cells.* Biomacromolecules, 2007. **8**(12): p. 3853-3859.
144. M. E. H. El-Sayed, A. S. Hoffman, and P. S. Stayton, *Smart polymeric carriers for enhanced intracellular delivery of therapeutic macromolecule.* Expert Opin. Biol. Ther., 2005. **5**(1): p. 23-32.
145. Juliano, R.L., X. Ming, and O. Nakagawa, *Cellular uptake and intracellular trafficking of antisense and siRNA oligonucleotides.* Bioconjug Chem, 2012. **23**(2): p. 147-157.
146. Canton, I. and G. Battaglia, *Endocytosis at the nanoscale.* Chem Soc Rev, 2012. **41**(7): p. 2718-39.
147. P. Sabbatini, et al., *A phase II trial of paclitaxel poliglumex in recurrent or persistent ovarian or primary peritoneal cancer (EOC): a Gynecologic Oncology Group Study.* Gynecol Oncol, 2008. **111**(3): p. 455-60.
148. S. D. Chipman, et al., *Biological and clinical characterization of paclitaxel poliglumex (PPX, CT-2103), a macromolecular polymer-drug conjugate.* Int J Nanomedicine, 2006. **1**(4): p. 375-83.
149. F. P. Seib, A. T. Jones, and R. Duncan, *Comparison of the endocytic properties of linear and branched PEIs, and cationic PAMAM dendrimers in B16f10 melanoma cells.* Journal of Controlled Release, 2007. **117**(3): p. 291-300.
150. M. E. Davis, *The first targeted delivery of siRNA in humans via a self-assembling, cyclodextrin polymer-based nanoparticle: from concept to clinic.* Mol Pharm, 2009. **6**(3): p. 659-68.
151. http://www.calandopharma.com/.
152. Y. Bae, et al., *Preparation and biological characterization of polymeric micelle drug carriers with intracellular pH-triggered drug release property: tumor permeability, controlled subcellular drug distribution, and enhanced in vivo antitumor*

efficacy. Bioconjug Chem, 2005. **16**(1): p. 122-30.

153. C. L. Duvall, et al., *Intracellular Delivery of a Proapoptotic Peptide via Conjugation to a RAFT Synthesized Endosomolytic Polymer.* Molecular Pharmaceutics, 2010. **7**(2): p. 468-476.
154. N. M. Moore, C. L. Sheppard, and S. E. Sakiyama-Elbert, *Characterization of a multifunctional PEG-based gene delivery system containing nuclear localization signals and endosomal escape peptides.* Acta Biomaterialia, 2009. **5**(3): p. 854-864.
155. T. Skovsgaard and N. I. Nissen, *Membrane transport of anthracyclines.* Pharmacology & Therapeutics, 1982. **18**(3): p. 293-311.
156. M. J. Vicent and R. Duncan, *Polymer conjugates: nanosized medicines for treating cancer.* Trends Biotechnol, 2006. **24**(1): p. 39-47.
157. R. Duncan, H. Ringsdorf, and R. Satchi-Fainaro, *Polymer therapeutics--polymers as drugs, drug and protein conjugates and gene delivery systems: past, present and future opportunities.* Adv Polym Sci, 2006. **192**: p. 1-8.
158. H. Maeda and T. Konno, *Metamorphosis of neocarzinostatin to SMANCS:chemistry, biology, pharmacology and clinical effect of the first prototype anticancer polymer in Neocarzinostatin: the past, present and future of an anticancer drug.* Springer, Berlin, 1997((eds Maeda, Edo & Ishida)): p. 227-267.
159. Y. Levy, et al., *Adenosine deaminase deficiency with late onset of recurrent infections: response to treatment with polyethylene glycol-modified adenosine deaminase.* J Pediatr, 1988. **113**(2): p. 312-7.
160. F. Fuertges and A. Abuchowski, *The clinical efficacy of poly(ethylene glycol) modified proteins.* J Control Release, 1990. **11**(1-3): p. 139-148.
161. F. F. Davis, *The origin of pegnology.* Adv Drug Deliv Rev, 2002. **54**(4): p. 457-8.
162. Knop, K., et al., *Poly(ethylene glycol) in drug delivery: pros and cons as well as potential alternatives.* Angew Chem Int Ed,

2010. **49**(36): p. 6288-308.

163. S. Tamborero and M.J. Vicent, *Conjugados poliméricos y su utilización como nanomedicinas anticancerígenas.* www.biojournal.net, 2006(March).
164. S. N. S.Alconcel, A. S. Baas, and H. D. Maynard, *FDA-approved poly(ethylene glycol)-protein conjugate drugs.* Polymer Chemistry, 2011. **2**(7): p. 1442-1448.
165. M. Barz, et al., *Overcoming the PEG-addiction: well-defined alternatives to PEG, from structure-property relationships to better defined therapeutics.* Polymer Chemistry, 2011. **2**: p. 1900-1918.
166. E. Segal and R. Satchi-Fainaro, *Design and development of polymer conjugates as anti-angiogenic agents.* Advanced Drug Delivery Reviews, 2009. **61**(13): p. 1159-1176.
167. P. Caliceti and F. M. Veronese, *Pharmacokinetic and biodistribution properties of poly(ethylene glycol)-protein conjugates.* Adv Drug Deliv Rev, 2003. **55**(10): p. 1261-77.
168. C. S. Fishburn, *The pharmacology of PEGylation: balancing PD with PK to generate novel therapeutics.* J Pharm Sci, 2008. **97**(10): p. 4167-83.
169. S.N.S. Alconce, A.S. Baas, and H.D. Maynard, *FDA-approved poly(ethylene glycol)-protein conjugate drugs.* Polymer Chemistry, 2011. **2**: p. 1442-1448.
170. F. M. Veronese and A. Mero, *The impact of PEGylation on biological therapies.* BioDrugs, 2008. **22**(5): p. 315-29.
171. Bontempo, D. and H.D. Maynard, *Streptavidin as a macroinitiator for polymerization: in situ protein-polymer conjugate formation.* J Am Chem Soc, 2005. **127**(18): p. 6508-9.
172. J. Liu, et al., *In situ formation of protein-polymer conjugates through reversible addition fragmentation chain transfer polymerization.* Angew Chem Int Ed, 2007. **46**(17): p. 3099-103.
173. B. Le Droumaguet and J. Nicolas, *Recent advances in the*

design of bioconjugates from controlled/living radical polymerization Polym Chem, 2010. **1**: p. 37-54.

174. F. Alexis, et al., *Factors affecting the clearance and biodistribution of polymeric nanoparticles.* Mol Pharm, 2008. **5**(4): p. 505-15.
175. J. V. Jokerst, et al., *Nanoparticle PEGylation for imaging and therapy.* Nanomedicine (Lond), 2011. **6**(4): p. 715-28.
176. R. Webster, et al., *PEG and PEG conjugates toxicity: towards an understanding of the toxicity of PEG and its relevance to PEGylated biologicals. PEGylated Protein Drugs: Basic Science and Clinical Applications.*, 2009, Birkhäuser Basel. p. 127-146.
177. Hinds, K.D., *Biomaterials for Delivery and Targeting of Proteins and Nucleic Acids.* CRC, Boca Raton, FL, 2005. **2005**.
178. R. Duncan, et al., *Polymer-drug conjugates: towards a novel approach for the treatment of endrocine-related cancer.* Endocr Relat Cancer, 2005. **12 Suppl 1**: p. S189-99.
179. J. Sanchis, et al., *Polymer-drug conjugates for novel molecular targets.* Nanomedicine, 2010. **5**(6): p. 915-935.
180. Iyer, A.K., et al., *Exploiting the enhanced permeability and retention effect for tumor targeting.* Drug. Discov. Today, 2006. **11**(17-18): p. 812-818.
181. Duncan, R., *Designing polymer conjugates as lysosomotropic nanomedicines.* Biochem. Soc. Trans., 2007. **35**: p. 56-60.
182. M.J. Vicent, et al., *Polymer conjugates as therapeutics: future trends, challenges and opportunities.* Exp Opin Drug Rev, 2008. **61**: p. 1220-1231.
183. M. J. Vicent, et al., *Polyacetal-diethylstilboestrol: A polymeric drug designed for pH-triggered activation.* J Drug Target, 2004. **12**(8): p. 491-501.
184. R. Tomlinson, et al., *Polyacetal-doxorubicin conjugates designed for pH-dependent degradation.* Bioconjug Chem, 2003. **14**(6): p. 1096-1106.
185. V. Gimenez, et al., *Demonstrating the importance of polymer-conjugate conformation in solution on its therapeutic output:*

Diethylstilbestrol (DES)-polyacetals as prostate cancer treatment. J Control Release, 2012. **159 (2)**: p. 290-301.

186. J. Hardwicke, et al., *Bioresponsive dextrin-rhEGF conjugates: in vitro evaluation in models relevant to its proposed used as treatment for chronic wounds.* Mol Pharm, 2010. **7**: p. 699-707.
187. M. Baker, *Whole-animal imaging: The whole picture.* Nature, 2010. **463**(7283): p. 977-80.
188. M. M. Herth, et al., *72/74As-labeling of HPMA based polymers for long-term in vivo PET imaging.* Bioorg Med Chem Lett, 2010. **20**(18): p. 5454-8.
189. M. M. Herth, et al., *Radioactive labeling of defined HPMA-based polymeric structures using [18F]FETos for in vivo imaging by positron emission tomography.* Biomacromolecules, 2009. **10**(7): p. 1697-703.
190. M. Longmire, P. L. Choyke, and H. Kobayashi, *Dendrimer-based contrast agents for molecular imaging.* Curr Top Med Chem, 2008. **8**(14): p. 1180-6.
191. Kobayashi, H., et al., *New strategies for fluorescent probe design in medical diagnostic imaging.* Chem Rev, 2010. **110**(5): p. 2620-40.
192. S.C. Richardson, et al., *The use of fluorescence microscopy to define polymer localisation to the late endocytic compartments in cells that are targets for drug delivery.* J Control Release, 2008. **127**(1): p. 1-11.
193. S. Bhaskar, et al., *Multifunctional Nanocarriers for diagnostics, drug delivery and targeted treatment across blood-brain barrier: perspectives on tracking and neuroimaging.* Part Fibre Toxicol, 2010. **7**(3).
194. X. Chen, P. S. Conti, and R. A. Moats, *In vivo near-infrared fluorescence imaging of integrin alphavbeta3 in brain tumor xenografts.* Cancer Res, 2004. **64**(21): p. 8009-14.
195. Jaspers, K., et al., *MR angiography of collateral arteries in a hind limb ischemia model: comparison between blood pool*

agent Gadomer and small contrast agent Gd-DTPA. PLoS One, 2011. **6**(1): p. e16159.

196. L. W. Seymour, et al., *Phase II studies of polymer-doxorubicin (PK1, FCE28068) in the treatment of breast, lung and colorectal cancer.* Int J Oncol, 2009. **34**(6): p. 1629-36.
197. Scheinberg, D.A., et al., *Conscripts of the infinite armada: systemic cancer therapy using nanomaterials.* Nat Rev Clin Oncol, 2010. **7**(5): p. 266-76.
198. M. E. Gindy and R. K. Prud'homme, *Multifunctional nanoparticles for imaging, delivery and targeting in cancer therapy.* Expert Opin Drug Deliv, 2009. **6**(8): p. 865-78.
199. R. Gaspar and R. Duncan, *Polymeric carriers: preclinical safety and the regulatory implications for design and development of polymer therapeutics.* Adv Drug Deliv Rev, 2009. **61**(13): p. 1220-1231.
200. Sakamoto, J.H., et al., *Enabling individualized therapy through nanotechnology.* Pharmacol. Res., 2010. **62**(2): p. 57-89.
201. S. A. Shaffer, et al., *In vitro and in vivo metabolism of paclitaxel poliglumex: identification of metabolites and active proteases.* Cancer Chemother Pharmacol, 2007. **59**(4): p. 537-48.
202. C. M. Thomas and J. F. Lutz, *Precision synthesis of biodegradable polymers.* Angew Chem Int Ed, 2011. **50**(40): p. 9244-6.
203. L. Y. Qiu and Y.H. Bae, *Polymer architecture and drug delivery.* Pharm Res, 2006. **23**: p. 1-30.
204. L. Izzo, et al., *Impact of polymer tacticity on the physico-chemical behaviour of polymers proposed as therapeutics.* Int J Pharm, 2011. **408**(1-2): p. 213-222.
205. Liu, J., et al., *Endocytic uptake of a large array of HPMA copolymers: Elucidation into the dependence on the physicochemical characteristics.* J Control Release, 2010. **143**(1): p. 71-9.
206. Vaidya, A., et al., *Bioconjugation of polymers: a novel platform for targeted drug delivery.* Curr Pharm Des, 2011. **17**(11): p.

1108-25.

207. M. van Dijk, et al., *Synthesis and applications of biomedical and pharmaceutical polymers via click chemistry methodologies.* Bioconjug Chem, 2009. **20**(11): p. 2001-16.

208. C.Boyer, et al., *Bioapplications of RAFT polymerization.* Chem Rev, 2009. **109**(11): p. 5402-36.

209. G. Moad, E. Rizzardo, and S. H. Thang, *Toward living radical polymerization.* Acc Chem Res, 2008. **41**(9): p. 1133-42.

210. N. V. Tsarevsky and K. Matyjaszewski, *"Green" atom transfer radical polymerization: from process design to preparation of well-defined environmentally friendly polymeric materials.* Chem Rev, 2007. **107**(6): p. 2270-99.

211. N. Hadjichristidis, et al., *Synthesis of well-defined polypeptide-based materials via the ring-opening polymerization of alpha-amino acid N-carboxyanhydrides.* Chem Rev, 2009. **109**(11): p. 5528-78.

212. M. Mammen, S. Choi, and G.M. Whitesides, *Polyvalent interactions in biological systems: implications for design and use of multivalent ligands and inhibitors.* Angew Chem Int Ed, 1998. **37**: p. 2754-2794.

213. P. Ferruti, et al., *A novel modification of poly(L-lysine) leading to a soluble cationic polymer with reduced toxicity and with potential as a transfection agent.* Macromol Chem Phys, 1998. **199**(11): p. 2565-2575.

214. H. Dautzenberg and A. Zintchenko, *Polycationic Graft Copolymers as Carriers for Oligonucleotide Delivery. Complexes of Oligonucleotides with Polycationic Graft Copolymers.* Langmuir, 2001. **17**(10): p. 3096-3102.

215. M. Pechar, et al., *Hydrolytically and reductively degradable carriers of biologically active molecules based on multiblock polymers of poly(ethylene glycol).* J Control Release, 2006. **116**(2): p. e8-10.

216. Montero de Espinosa, L. and M.A. Meier, *Synthesis of star- and block-copolymers using ADMET: head-to-tail selectivity during*

step-growth polymerization. Chem Commun (Camb), 2011. **47**(6): p. 1908-10.

217. M. K. Mirhra and S. Kobayashi, *Star and hyperbranched polymers.* Marcel Dekker, 1999.
218. S. E. Stiriba, H. Kautz, and H. Frey, *Hyperbranched molecular nanocapsules: comparison of the hyperbranched architecture with the perfect linear analogue.* J Am Chem Soc, 2002. **124**(33): p. 9698-9.
219. Carlmark, A., et al., *New methodologies in the construction of dendritic materials.* Chem Soc Rev, 2009. **38**(2): p. 352-62.
220. J. M. J. Fréchet, et al., *Dendrimers and Hyperbranched Polymers: Two Families of Three-Dimensional Macromolecules with Similar but Clearly Distinct Properties.* J Macromol Scie Part A, 1996. **33**(10): p. 1399-1425.
221. E. R. Gillies and J.M. Frechet, *Dendrimers and dendritic polymers in drug delivery.* Drug Discov Today, 2005. **10**(1): p. 35-43.
222. A. Samad, M. I. Alam, and K. Saxena, *Dendrimers: a class of polymers in the nanotechnology for the delivery of active pharmaceuticals.* Curr Pharm Des, 2009. **15**(25): p. 2958-69.
223. A. Paul, et al., *Drug mimic induced conformational changes in polymer-drug conjugates characterized by Small Angle Neutron Scattering.* Biomacromolecules, 2010. **11**: p. 1978-1982.
224. A. Paul, M. J. Vicent, and R. Duncan, *Using small-angle neutron scattering to study the solution conformation of N-(2-hydroxypropyl)methacrylamide copollymer-doxorubicin conjugates.* Biomacromolecules, 2007. **8**: p. 1573-1579.
225. M. Barz, et al., *Synthesis and in vitro evaluation of defined HPMA folate conjugates: influence of aggregation on folate receptor (FR) mediated cellular uptake.* Biomacromolecules, 2010. **11**: p. 2274-2282.
226. M. Fujita, et al., *Brain tumor tandem targeting using a combination of monoclonal antibodies attached to*

biopoly(beta-L-malic acid). J Control Release, 2007. **122**(3): p. 356-63.

227. C. Chariton, et al., *TIRF microscopy as a screening method for non-specific binding on surfaces.* J. Colloid Interface Sci, 2011. **354**: p. 405-409.
228. F. Greco and M.J. Vicent, *Combination therapy: opportunities and challenges for polymer-drug conjugates as anticancer nanomedicines.* Adv Drug Deliv Rev, 2009. **61**(13): p. 1203-13.
229. http://www.celator.ca.
230. M. P. Borgman, et al., *Biodistribution of HPMA copolymer-aminohexylgeldanamycin-RGDfK conjugates for prostate cancer drug delivery.* Mol Pharm, 2009. **6**(6): p. 1836-47.
231. S. C. Ghosh, et al., *N,N-Dimethylsphingosine conjugates of poly-L-glutamic acid: synthesis, characterization, and initial biological evaluation.* Bioorg Med Chem Lett, 2009. **19**(3): p. 1012-7.
232. Eldar-Boock, A., et al., *Integrin-assisted drug delivery of nano-scaled polymer therapeutics bearing paclitaxel.* Biomaterials, 2011. **32**(15): p. 3862-74.
233. K. Miller, et al., *Targeting bone metastases with a bispecific anticancer and antiangiogenic polymer-alendronate-taxane conjugate.* Angew Chem Int Ed, 2009. **48**(16): p. 2949-54.
234. E. Segal, et al., *Targeting angiogenesis-dependent calcified neoplasms using combined polymer therapeutics.* PLoS One, 2009. **4**(4): p. e5233.
235. T. Lammers, et al., *Effect of intratumoral injection on the biodistribution and the therapeutic potential of HPMA copolymer-based drug delivery systems.* Neoplasia, 2006. **8**(10): p. 788-95.
236. Cuchelkar, V., P. Kopeckova, and J. Kopecek, *Synthesis and biological evaluation of disulfide-linked HPMA copolymer-mesochlorin e6 conjugates.* Macromol Biosci, 2008. **8**(5): p. 375-83.
237. J. Li, et al., *Polyethylene glycosylated curcumin conjugate*

inhibits pancreatic cancer cell growth through inactivation of Jab1. Mol Pharmacol, 2009. **76**(1): p. 81-90.

238. M. Oman, J. H. Liu, and J. Chen, *Using N-(2-hydroxypropyl)methacrylamide copolymer drug bioconjugate as a novel approach to deliver a Bcl-2-targeting compound HA14-1 in vivo.* Gen Ther Mol Biol, 2006. **10A**(113-122).
239. F. Greco, et al., *HPMA copolymer-aminoglutethimide conjugates inhibit aromatase in MCF-7 cell lines.* J Drug Target, 2005. **13**(8-9): p. 459-470.
240. T. Lammers, et al., *Simultaneous delivery of doxorubicin and gemcitabine to tumors in vivo using prototypic polymeric drug carriers.* Biomaterials, 2009. **30**(20): p. 3466-75.
241. L. Santucci, et al., *Cardiac safety and antitumoral activity of a new nitric oxide derivative of pegylated epirubicin in mice.* Anticancer Drugs, 2007. **18**(9): p. 1081-91.
242. S. Wadhwa and R.J. Mumper, *Polypeptide conjugates of d-penicillamine and idarubicin for anticancer therapy.* J Control Release, 2012. **158**: p. 215-223.
243. Vicent, M.J., *Polymer-drug conjugates as modulators of cellular apoptosis.* AAPS J, 2007. **9**(2): p. E200-7.
244. Jiang, P., et al., *Effective targeting of the tumor microenvironment for cancer therapy.* Anticancer Res, 2012. **32**(4): p. 1203-12.
245. Thompson, C.B., et al., *Enzymatic depletion of tumor hyaluronan induces antitumor responses in preclinical animal models.* Mol Cancer Ther, 2010. **9**(11): p. 3052-64.
246. Vicent, M.J. and E. Perez-Paya, *Poly-L-glutamic acid (PGA) aided inhibitors of apoptotic protease activating factor 1 (Apaf-1): an antiapoptotic polymeric nanomedicine.* J Med Chem, 2006. **49**(13): p. 3763-5.
247. B. Santamaria, et al., *A nanoconjugate Apaf-1 inhibitor protects mesothelial cells from cytokine-induced injury.* PLoS One, 2009. **4**(8): p. e6634.
248. J. Hardwicke, et al., *Investigation of the potential of polymer*

therapeutics in corneal re-epithelialisation. Br J Ophthalmol, 2010. **94**(12): p. 1566-70.

249. J. Dernedde, et al., *Dendritic polyglycerol sulfates as multivalent inhibitors of inflammation.* Proc Natl Acad Sci USA, 2010. **107**(46): p. 19679-84.
250. M. J. Vicent, et al., *Nanoconjugates as intracorporeal neutralizers of bacterial endotoxins.* J Control Release, 2009. **142**(2): p. 277-85.
251. Low, S.A. and J. Kopecek, *Targeting polymer therapeutics to bone.* Adv Drug Deliv Rev, 2012.
252. S.Sakuma, et al., *Stabilization of enzyme-susceptible glucoside bonds of phloridzin through conjugation with poly(gamma-glutamic acid).* J Control Release, 2009. **133**(2): p. 125-31.
253. J. Fang, et al., *SMA-copolymer conjugate of AHPP: a polymeric inhibitor of xanthine oxidase with potential antihypertensive effect.* J Control Release, 2009. **135**(3): p. 211-7.
254. L. Wan, et al., *Novel multi-component nanopharmaceuticals derived from poly(ethylene) glycol, retro-inverso-Tat nonapeptide and saquinavir demonstrate combined anti-HIV effects.* AIDS Res Ther, 2006. **3**: p. 12.
255. Y. Gao, K. Katsuraya, and e. al., *Synthesis of azidothymidine-bound sulfated alkyl oligosaccharides and their inhibitory effects on AIDS virus infection in vitro.* Polym J., 1998. **30**: p. 243-248.
256. P. Vlieghe, et al., *Synthesis of new covalently bound kappa-carrageenan-AZT conjugates with improved anti-HIV activities.* J Med Chem, 2002. **45**(6): p. 1275-83.
257. S. Wannachaiyasit, P. Chanvorachote, and U. Nimmannit, *A novel anti-HIV dextrin-zidovudine conjugate improving the pharmacokinetics of zidovudine in rats.* AAPS PharmSciTech, 2008. **9**(3): p. 840-50.
258. G. Giammona, G. Cavallaro, and G. Pitarresi, *Studies of macromolecular prodrugs of zidovudine.* Adv Drug Deliv Rev, 1999. **39**(1-3): p. 153-164.

259. K. C. Chimalakonda, et al., *Synthesis, analysis, in vitro characterization, and in vivo disposition of a lamivudine-dextran conjugate for selective antiviral delivery to the liver.* Bioconjug Chem, 2007. **18**(6): p. 2097-108.
260. M. Sedlak, *Amphotericin B: from derivatives to covalent targeted conjugates.* Mini Rev Med Chem, 2009. **9**(11): p. 1306-16.
261. J. Golenser and A. Domb, *New formulations and derivatives of amphotericin B for treatment of leishmaniasis.* Mini Rev Med Chem, 2006. **6**(2): p. 153-62.
262. J. Golenser, et al., *Efficacious treatment of experimental leishmaniasis with amphotericin B-arabinogalactan water-soluble derivatives.* Antimicrob Agents Chemother, 1999. **43**(9): p. 2209-14.
263. S. Nicoletti, K. Seifert, and I. H. Gilbert, *N-(2-hydroxypropyl)methacrylamide-amphotericin B (HPMA-AmB) copolymer conjugates as antileishmanial agents.* Int J Antimicrob Agents, 2009. **33**(5): p. 441-8.
264. A. Nan, et al., *Targetable water-soluble polymer-drug conjugates for the treatment of visceral leishmaniasis.* J Control Release, 2004. **94**(1): p. 115-27.
265. G. Pasut and F. M. Veronese, *PEG conjugates in clinical development or use as anticancer agents: an overview.* Adv Drug Deliv Rev, 2009. **61**(13): p. 1177-88.
266. Varshosaz, J., et al., *Preparation of budesonide-dextran conjugates using glutarate spacer as a colon-targeted drug delivery system: in vitro/in vivo evaluation in induced ulcerative colitis.* J Drug Target, 2010. **19**(2): p. 140-53.
267. J. Varshosaz, et al., *Synthesis and evaluation of dextran-budesonide conjugates as colon specific prodrugs for treatment of ulcerative colitis.* Int J Pharm, 2009. **365**(1-2): p. 69-76.
268. S. Keely, et al., *Dexamethasone-pDMAEMA polymeric conjugates reduce inflammatory biomarkers in human*

intestinal epithelial monolayers. J Control Release, 2009. **135**(1): p. 35-43.

269. Liu, X.M., S.C. Miller, and D. Wang, *Beyond oncology--application of HPMA copolymers in non-cancerous diseases.* Adv Drug Deliv Rev, 2010. **62**(2): p. 258-71.
270. J. Hwang, et al., *Alpha-methylprednisolone conjugated cyclodextrin polymer-based nanoparticles for rheumatoid arthritis therapy.* Int J Nanomedicine, 2008. **3**(3): p. 359-71.
271. S. Shaunak, et al., *Polyvalent dendrimer glucosamine conjugates prevent scar tissue formation.* Nat Biotechnol, 2004. **22**(8): p. 977-84.
272. L. Mondragon, et al., *Modulation of cellular apoptosis with apoptotic protease-activating factor 1 (Apaf-1) inhibitors.* J Med Chem, 2008. **51**(3): p. 521-9.
273. M.Orzaez, et al., *Conjugation of a novel Apaf-1 inhibitor to peptide-based cell-membrane transporters: effective methods to improve inhibition of mitochondria-mediated apoptosis.* Peptides, 2007. **28**(5): p. 958-68.
274. Fang, J., et al., *Tissue protective effect of xanthine oxidase inhibitor, polymer conjugate of (styrene-maleic acid copolymer) and (4-amino-6-hydroxypyrazolo[3,4-d]pyrimidine), on hepatic ischemia-reperfusion injury.* Exp Biol Med (Maywood), 2010. **235**(4): p. 487-96.
275. A. Rodriguez-Hernandez, et al., *Intraluminal-restricted 17 beta-estradiol exerts the same myocardial protection against ischemia/reperfusion injury in vivo as free 17 beta-estradiol.* Steroids, 2008. **73**(5): p. 528-38.
276. S. Bertuglia, F. M. Veronese, and G. Pasut, *Polyethylene glycol and a novel developed polyethylene glycol-nitric oxide normalize arteriolar response and oxidative stress in ischemia-reperfusion.* Am J Physiol Heart Circ Physiol, 2006. **291**(4): p. H1536-44.
277. B. Kateb, et al., *Nanoplatforms for constructing new approaches to cancer treatment, imaging, and drug delivery:*

what should be the policy? Neuroimage, 2010. **54 Suppl 1**: p. S106-24.

278. A. Beduneau, P. Saulnier, and J.P. Benoit, *Active targeting of brain tumors using nanocarriers.* Biomaterials, 2007. **28**(33): p. 4947-67.
279. J. Kreuter, *Nanoparticulate systems for brain delivery of drugs.* Adv Drug Deliv Rev, 2001. **47**(1): p. 65-81.
280. A. Regina, et al., *Antitumour activity of ANG1005, a conjugate between paclitaxel and the new brain delivery vector Angiopep-2.* Br J Pharmacol, 2008. **155**(2): p. 185-97.
281. Pardridge, W.M., *Molecular Trojan horses for blood-brain barrier drug delivery.* Discov. Med., 2006. **6**(34): p. 139-43.
282. Kabanov, A.V., et al., *A new class of drug carriers: micelles of poly(oxyethylene)-poly(oxypropylene) block copolymers as microcontainers for drug targeting from blood in brain.* J. Control. Release, 1992. **22**(2): p. 141-157.
283. Batrakova, E.V., et al., *Anthracycline antibiotics non-covalently incorporated into the block copolymer micelles: in vivo evaluation of anti-cancer activity.* Br. J. Cancer, 1996. **74**(10): p. 1545-52.
284. M. Yokoyama, et al., *Characterization and anticancer activity of the micelle-forming polymeric anticancer drug adriamycin-conjugated poly(ethylene glycol)-poly(aspartic acid) block copolymer.* Cancer Res., 1990. **50**(6): p. 1693-700.
285. Batrakova, E.V. and A.V. Kabanov, *Pluronic block copolymers: evolution of drug delivery concept from inert nanocarriers to biological response modifiers.* J. Control. Release, 2008. **130**(2): p. 98-106.
286. Kabanov, A.V. and V.Y. Alakhov, *Pluronic block copolymers in drug delivery: from micellar nanocontainers to biological response modifiers.* Crit. Rev. Ther. Drug Carrier Syst., 2002. **19**(1): p. 1-72.
287. Sahay, G., D.Y. Alakhova, and A.V. Kabanov, *Endocytosis of nanomedicines.* J. Control. Release, 2010. **145**(3): p. 182-95.

288. Witt, K.A., et al., *Pluronic p85 block copolymer enhances opioid peptide analgesia.* J. Pharmacol. Exp. Ther., 2002. **303**(2): p. 760-7.
289. Batrakova, E.V., et al., *Polypeptide point modifications with fatty acid and amphiphilic block copolymers for enhanced brain delivery.* Bioconjug. Chem., 2005. **16**(4): p. 793-802.
290. Price, T.O., et al., *Transport across the blood-brain barrier of pluronic leptin.* J. Pharmacol. Exp. Ther., 2010. **333**(1): p. 253-63.
291. Banks, W.A., et al., *Principles of strategic drug delivery to the brain (SDDB): development of anorectic and orexigenic analogs of leptin.* Physiol Behav, 2011. **105**(1): p. 145-9.
292. Sharma, A.K., et al., *Prevention of MDR development in leukemia cells by micelle-forming polymeric surfactant.* J. Control. Release, 2008. **131**(3): p. 220-7.
293. M. Fujita, et al., *Brain tumor tandem targeting using a combination of monoclonal antibodies attached to biopoly(beta-L-malic acid).* J. Control. Release, 2007. **122**(3): p. 356-63.
294. Ljubimova, J.Y., et al., *Poly(malic acid) nanoconjugates containing various antibodies and oligonucleotides for multitargeting drug delivery.* Nanomedicine, 2008. **3**(2): p. 247-65.
295. Ding, H., et al., *Inhibition of brain tumor growth by intravenous poly (beta-L-malic acid) nanobioconjugate with pH-dependent drug release [corrected].* Proc. Natl. Acad. Sci. USA, 2010. **107**(42): p. 18143-8.
296. J. A. Portilla-Arias, et al., *Biodegradable nanoparticles of partially methylated fungal poly(beta-L-malic acid) as a novel protein delivery carrier.* Macromol. Biosci., 2008. **8**(6): p. 551-9.
297. K. A. Witt, et al., *Pharmacodynamic and pharmacokinetic characterization of poly(ethylene glycol) conjugation to met-enkephalin analog [D-Pen2, D-Pen5]-enkephalin (DPDPE).* J

Pharmacol Exp Ther, 2001. **298**(2): p. 848-56.

298. I. Gozes, *Neuroprotective peptide drug delivery and development: potential new therapeutics.* Trends Neurosci, 2001. **24**(12): p. 700-705.
299. R. G. Soderquist, et al., *PEGylation of brain-derived neurotrophic factor for preserved biological activity and enhanced spinal cord distribution.* J Biomed Mater Res A, 2009. **91**(3): p. 719-29.
300. Wang, Y., et al., *Transport of epidermal growth factor in the stroke-injured brain.* J Control Release, 2010. **149**(3): p. 225-35.
301. M. Stroh, et al., *Multiphoton microscopy guides neurotrophin modification with poly(ethylene glycol) to enhance interstitial diffusion.* Nat Mater, 2004. **3**(7): p. 489-94.
302. D. Wu and W.M. Pardridge, *Neuroprotection with noninvasive neurotrophin delivery to the brain.* Proc Natl Acad Sci U S A, 1999. **96**(1): p. 254-9.
303. T. Sakane and W.M. Pardridge, *Carboxyl-directed pegylation of brain-derived neurotrophic factor markedly reduces systemic clearance with minimal loss of biologic activity.* Pharm Res, 1997. **14**(8): p. 1085-91.
304. Y. Zhang and W.M. Pardridge, *Conjugation of brain-derived neurotrophic factor to a blood-brain barrier drug targeting system enables neuroprotection in regional brain ischemia following intravenous injection of the neurotrophin.* Brain Res, 2001. **889**(1-2): p. 49-56.
305. G. S. Liao, et al., *Pharmacological actions of nerve growth factor-transferrin conjugate on the central nervous system.* J Nat Toxins, 2001. **10**(4): p. 291-7.
306. Frank, T., et al., *Pegylated granulocyte colony-stimulating factor conveys long-term neuroprotection and improves functional outcome in a model of Parkinson's disease.* Brain, 2012.
307. Sarin, H., et al., *Effective transvascular delivery of*

nanoparticles across the blood-brain tumor barrier into malignant glioma cells. J. Transl. Med., 2008. **6**: p. 80.

308. G. Wu, et al., *Targeted delivery of methotrexate to epidermal growth factor receptor-positive brain tumors by means of cetuximab (IMC-C225) dendrimer bioconjugates.* Mol Cancer Ther, 2006. **5**(1): p. 52-9.
309. Li, Y., et al., *A dual-targeting nanocarrier based on poly(amidoamine) dendrimers conjugated with transferrin and tamoxifen for treating brain gliomas.* Biomaterials, 2012. **33**(15): p. 3899-908.
310. Y. E. Kurtoglu, et al., *Poly(amidoamine) dendrimer-drug conjugates with disulfide linkages for intracellular drug delivery.* Biomaterials, 2009. **30**(11): p. 2112-21.
311. G. Wu, et al., *Molecular targeting and treatment of an epidermal growth factor receptor-positive glioma using boronated cetuximab.* Clin Cancer Res, 2007. **13**(4): p. 1260-8.
312. Dai, H., et al., *Intrinsic targeting of inflammatory cells in the brain by polyamidoamine dendrimers upon subarachnoid administration.* Nanomedicine (Lond), 2010. **5**(9): p. 1317-29.
313. R. S. Navath, et al., *Stimuli-responsive star poly(ethylene glycol) drug conjugates for improved intracellular delivery of the drug in neuroinflammation.* J Control Release, 2009. **142**(3): p. 447-56.
314. S. Kannan, et al., *Microglial activation in perinatal rabbit brain induced by intrauterine inflammation: detection with 11C-(R)-PK11195 and small-animal PET.* J Nucl Med, 2007. **48**(6): p. 946-54.
315. J.M. Oliveira, et al., *Dendrimers and derivatives as a potential therapeutic tool in regenerative medicine strategies-a review.* Progress in Polym Sci, 2010. **35**: p. 1163-1194.
316. R. J. Christie, N. Nishiyama, and K. Kataoka, *Delivering the code: polyplex carriers for deoxyribonucleic acid and ribonucleic acid interference therapies.* Endocrinology, 2009. **151**(2): p. 466-73.

317. Yu, H. and E. Wagner, *Bioresponsive polymers for nonviral gene delivery.* Curr. Opin. Mol. Ther., 2009. **11**(2): p. 165-78.
318. Kichler, A., *Gene transfer with modified polyethylenimines.* J. Gene. Med., 2004. **6 Suppl 1**: p. S3-10.
319. Zhang, H. and S.V. Vinogradov, *Short biodegradable polyamines for gene delivery and transfection of brain capillary endothelial cells.* J. Control. Release, 2010. **143**(3): p. 359-66.
320. Perez, A.P., et al., *Increased brain radioactivity by intranasal P-labeled siRNA dendriplexes within in situ-forming mucoadhesive gels.* Int J Nanomedicine, 2012. **7**: p. 1373-85.
321. W. Ke, et al., *Gene delivery targeted to the brain using an Angiopep-conjugated polyethyleneglycol-modified polyamidoamine dendrimer.* Biomaterials, 2009. **30**(36): p. 6976-85.
322. Huang, R.Q., et al., *Efficient gene delivery targeted to the brain using a transferrin-conjugated polyethyleneglycol-modified polyamidoamine dendrimer.* FASEB J., 2007. **21**(4): p. 1117-25.
323. www.angiochem.com.
324. F. I. Staquicini, et al., *Systemic combinatorial peptide selection yields a non-canonical iron-mimicry mechanism for targeting tumors in a mouse model of human glioblastoma.* J Clin Invest, 2011. **121**(1): p. 161-73.
325. Batrakova, E.V., et al., *A macrophage-nanozyme delivery system for Parkinson's disease.* Bioconjug. Chem., 2007. **18**(5): p. 1498-506.
326. Klyachko, N.L., et al., *Cross-linked antioxidant nanozymes for improved delivery to CNS.* Nanomedicine, 2012. **8**(1): p. 119-29.
327. Saraiva, M.J., *Transthyretin mutations in health and disease.* Hum. Mutat., 1995. **5**: p. 191-196.
328. Y. Ando, M. Nakamura, and S. Araki, *Transtyretin-related familial amyloidotic polyneuropathy.* Arch Neurol, 2005. **62**(7): p. 1057-1062.
329. C. Andrade, *A peculiar form of peripheral neuropathy. Familial*

atypical generalized amyloidosis with special involvement of the peripheral nerves. Brain, 1952. **75**: p. 408-427.

330. I. Cardoso, et al., *Synergy of combined Doxycycline/TUDCA tretment in loweing Transthyretin deposition and associated biomarkers: studies in FAP mouse models.* Journal of Translational Medicine, 2010. **8**(74): p. 1-11.
331. L. Gales, et al., *Iodination of salicylic acid improves its binding to transthyretin.* Biochim Biophys Acta, 2008. **1784**(3): p. 512-7.
332. fau.pearlashes.com/anatomy, *Chapter17: Histology of nervous tissue.*
333. Ando Y., N.M., Araki S., *Transtyretin-Related Familial Amyloidotic Polyneuropathy.* Arch. Neurol., 2005. **62**: p. 1057-1062.
334. http://www.iupui.edu/~amyloid/.
335. Zeldenrust, S.R., *ATTR: diagnosis, prognosis and treatment.* Amyloidosis, Contemporary Hematology, 2010(Book chapter): p. 191-204.
336. Y. Ando, et al., *A different amyloid formation mechanism: de novo oculoleptomeningeal amyloid deposits after liver transplantation.* Transplantation, 2004. **77**(3): p. 345-9.
337. L. Lladó, et al., *Risk of transmission of systemic transthyretin amyloidosis after domino liver transplantation.* Liver Transpl, 2010. **16**: p. 1386.
338. J.A. Hamilton and M.D. Benson, *Transthyretin: a review from a structural perspective.* Cell Mol Life Sci, 2001. **58**(10): p. 1491-1521.
339. Munar-Qués, M., *Actualización de la amiloidosis. Amiloidosis hereditarias.* Med Clin (Barc), 1994. **103**: p. 109-115.
340. M. J. Saraiva, *Hereditary transthyretin amyloidosis: molecular basis and therapeutical strategies.* Expert Rev Mol Med, 2002. **4**(12): p. 1-11.
341. J. Buxbaum, J. Koziol, and L.H. Connors, *Serum transthyretin levels in senile systemic amyloidosis: effects of age, gender and*

ethnicity. Amyloid, 2008. **15**(4): p. 255-61.

342. I. Cardoso, M. Brito, and M.J. Saraiva, *Extracellular matrix markers for disease progression and follow-up of therapies in familial amyloid polyneuropathy V30M TTR-related.* Disease Markers, 2008. **25**(1): p. 37-47.
343. A. Quintas, et al., *Tetramer dissociation and monomer partial unfolding precedes protofibril formation in amyloidogenic transthyretin variants.* J. Biol. Chem., 2001. **276**(29): p. 27207-27213.
344. I. Cardoso, et al., *Transthyretin fibrillogenesis entails the assembly of monomers: a molecular model for in vitro assembled transthyretin amyloid-like fibrils.* J. Mol. Biol., 2002. **317**(5): p. 683-695.
345. A. M. Damas and M.J. Saraiva, *TTR Amyloidosis-structural features leading to protein aggregation and their implications on therapeutic strategies.* J. Structural Biology, 2000. **130**: p. 290-299.
346. I. Cardoso and M.J. Saraiva, *Doxycycline disrupts transthyretin amyloid: evidence from studies in a FAP transgenic mice model.* The FASEB Journal, 2006. **20**: p. 234-239.
347. M. M. Sousa, et al., *Deposition of transthyretin in early stages of familial amiloidotic polyneuropathy: evidence for toxicity of nonfibrillar aggregates.* Am J Pathol, 2001. **159**(1993-2000).
348. M.M. Sousa, et al., *Interaction of the Receptor for Advanced Glycation End Products (RAGE) with Transthyrein Triggers Nuclear Transcription Factor kB (NF-kB) Activation.* Laboratory Investigation, 2000. **80**(7): p. 1101-1111.
349. M.M. Sousa, et al., *Familial amyloid polyneuropathy: receptor for advanced glycation end products-dependent triggering of neuronal inflammatory and apoptotic pathways.* J Neurosci., 2001. **21**: p. 7576-7586.
350. I. Cardoso, et al., *Comparative in vitro and ex vivo activities of selected inhibitors of transthyretin aggregation: relevance in drug design.* Biochem J, 2007. **408**(1): p. 131-8.

351. I. Cardoso, G. Merlini, and M. J. Saraiva, *4'-iodo-4'-deoxydoxorubicin and tetracyclines disrupt transthyretin amyloid fibrils in vitro producing noncytotoxic species: screening for TTR fibril disrupters.* FASEB J, 2003. **17**(8): p. 803-9.
352. H. Puchtler and F. Sweat, *Congo Red as a stain for fluorescence microscopy of amyloid.* J Histochem Cytochem, 1965. **13**(8): p. 693-694.
353. A. Tosoni, G.B., M. Nebuloni, *Electron microscopy in the diagnosis of amyloidosis.* In Tech, 2011. http://www.intechopen.com/books/amyloidosis-mechanisms-and-prospects-for-therapy/electron-microscopy-in-the-diagnosis-of-amyloidosis.
354. H. Sakaki, et al., *Diagnosis of familial amyloidotic polyneuropathy by recombinant DNA tecniques.* Biochem Biophys Res Commun, 1984. **125**: p. 636-642.
355. B. Bonaiti, et al., *TTR familial amyloid polyneuropathy: does a mitochondrial polymorphism entirely explain the parent-of-origin difference in penetrance?* Eur J Hum Genet, 2010. **18**(8): p. 948-52.
356. B. Macedo, et al., *Biomarkers in the assesment of thereapies in Familial Amyloidotic Polyneuropathy.* Mol Med, 2007. **13**(11-12): p. 584-591.
357. www.amyloidosis.org.
358. K. Misu, et al., *Late-onset familial amyloid polyneuropathy type I (transthyretin Met30-associated familial amyloid polyneuropathy) unrelated to endemic focus in Japan. Clinicopathological and genetic features.* Brain, 1999. **122**: p. 1951-1962.
359. O. B. Suhr, et al., *Liver transplantation for hereditary transthyretin amyloidosis.* Liver Transpl 2000. **6**: p. 263-276.
360. M. Nakamura, et al., *Gene therapy: lessons learned from liver transplantation for transthyretin-amyloidosis.* Gen Ther, 2004. **11**: p. 838-846.

361. M. D. Benson, et al., *Targeted suppresion of an amyloidogenic transthyretin with antisense oligonucleotides.* Muscle Nerve, 2006. **33**: p. 609-618.
362. T. Kurosawa, et al., *Selective silencing of a mutant transthyretin allele by small interfeing RNAs.* Biochem Biophys Res Commun, 2005. **337**: p. 1012-1018.
363. http://www.alnylam.com/capella/tag/ttr/.
364. T. Klabunde, et al., *Rational design of potent human transthyretin amyloid disease inhibitors.* Nat Struct Biol, 2000. **7**(4): p. 312-21.
365. K. Tojo, et al., *Diflunisal stabilizes familial amyloid polyneuropathy-associated transthyretin variant tetramers in serum against dissociation required for amyloidogenesis.* Neurosci Res, 2006. **56**(4): p. 441-9.
366. S. M. Johnson, et al., *Biochemical and structural evaluation of highly selective 2-arylbenzoxazole-based transthyretin amyloidogenesis inhibitors.* J Med Chem, 2008. **51**(2): p. 260-70.
367. Johnson, S.M., et al., *The transthyretin amyloidoses: from delineating the molecular mechanism of aggregation linked to pathology to a regulatory-agency-approved drug.* J Mol Biol, 2012. **421**(2-3): p. 185-203.
368. S. E. Kolstoe, et al., *Trapping of palindromic ligands within native transthyretin prevents amyloid formation.* Proc Natl Acad Sci U S A, 2010. **107**(47): p. 20483-8.
369. J. Brett, et al., *Survey of the distribution of a newly characterized receptor for advanced glycation end products in tissues.* Am J Pathol, 1993. **143**(6): p. 1699-712.
370. J. A. Mosquera, *Role of the receptor for advanced glycation end products (RAGE) in inflammation.* Invest Clin, 2010. **51**(2): p. 257-268.
371. F. A. Monteiro, et al., *In vitro inhibition of transthyretin aggregate-induced cytotoxicity by full and peptide derived forms of the soluble receptor for advanced glycation end*

products (RAGE). FEBS Lett, 2006. **580**(14): p. 3451-6.

372. Johnson, K.P., *Glatiramer acetate for treatment of relapsing–remitting multiple sclerosis.* Exp Rev Neurotherapeutics, 2012. **12**(4): p. 371-384.
373. Singer, J.W., *Paclitaxel poliglumex (XYOTAX™, CT-2103), a macromolecular taxane.* J Control Release, 2005. **109**(1-3): p. 120-126.
374. M. P. Melacon, C.L., *Multifunctional synthetic poly(L-glutamic acid)-based cancer therapeutic and imaging agents.* Molecular Imaging, 2011. **10**(1): p. 28-42.
375. J. Cheng and T.J. Deming, *Synthesis of polypeptides by ring-opening polymerization of alpha-amino acid N-carboxyanhydrides.* Top Curr Chem, 2012. **310**: p. 1-26.
376. Deming, T.J., *Methodologies for preparation of synthetic block copolypeptides: materials with future promise in drug delivery.* Adv Drug Deliv Rev, 2002. **54**: p. 1145-1155.
377. Deming, T.J., *Synthetic Polypeptides for Biomedical Applications. Progress in Polymer Science **32**, 858-875.* Prog Polym Sci, 2007. **32**(858-875).
378. W. Vayaboury, et al., *Synthesis of N-protected-L-lysine and alpha-benzyl-L-glutamate N-carboxyanhydrides (NCA) by carbamoylation and nitrosation.* Amino Acids, 2004. **27**(2): p. 161-167.
379. H. Leuchs, *Fiber die Glycin-carbonsauren* Dtsch Chem Ges, 1906. **39**: p. 857.
380. H. Leuchs and W. Manasse, Dtsch Chem Ges, 1907. **40**: p. 3235.
381. H. Leuchs and W.Geiger, Dtsch Chem Ges, 1908. **41**: p. 1721.
382. E. Peggion, et al., *Polymerization of gamma-benzyl-L-glutamate N-carboxyanhydride: effects of conditions of polymer precipitation on the molecular weight distribution.* Biopolymers, 1966. **4**(6): p. 695-704.
383. M. Goodman and J. Hutchison, *The mechanisms of polymerization of N-unsubstituted N-Carboxyanhydrides.* J Am

Chem Soc, 1966. **88**(15): p. 3627-3630.

384. D. Baillard and C. Bamford, *Reactions of N-Carboxy-alpha-anhydrides catalysed by tertiary bases.* J Chem Soc, 1956. **381**.
385. H. Kricheldorf, *alpha-amino acid-N-carboxyanhydrides ans related heterocycles. .* Springer, New York, 1987.
386. H. Kricheldorf, *Polypeptides and 100 years of chemistry of alpha-amino acid N-carboxyanhydrides.* Angew Chem Int Ed, 2006. **45**(35): p. 5752-84.
387. H. Kricheldorf, *Polypeptides. Models of biopolymers by ring opening polymerization.* In: Pencze S (ed) . CRC, Boca Raton, 1990: p. 1-132.
388. T. Aliferis, H. Iatrou, and N. Hadjichristidis, Biomacromolecules, 2004. **5**: p. 1653-1656.
389. T. Aliferis, H. Iatrou, and N. Hadjichristidis, *Well-defined linear multiblock and branched polypeptides by linking chemistry* J. Polym Sci Part A: Polym Chem, 2005. **43**: p. 4670-4673.
390. I. Dimitrov and H. Schlaad, *Synthesis of nearly monodisperse polystyrene-polypeptide block copolymers via polymerisation of N-carboxyanhydrides.* Chem Commun (Camb), 2003(23): p. 2944-2945.
391. Deming, T.J., *Facile synthesis of block copolypeptides of defined architecture.* Nature, 1997. **390**(6658): p. 386-9.
392. H. Lu and J. Cheng, *Hexamethyldisilazane-mediated controlled polymerization of alpha-amino acid N-carboxyanhydrides.* J Am Chem Soc, 2007. **129**(46): p. 14114-5.
393. Y. Knobbler, S. Bittner, and M. Frankel, *Reaction of N-carboxy-alpha-aminoacid anhydrides with hydrochlorides of hydroxylamine, O-alkylhydroxylamines and amines.* J Chem Soc, 1964. **3941**.
394. Y. Knobbler, et al., *alpha-aminoacyl derivatives of aminobenzoic acid and amino-oxy-acids by reaction of their hydrochlorides with amino-acid N-carboxyanhydrides.* J Chem Soc, 1969. **1969**: p. 1821-1824.
395. A. C. Farthing and R.J. Reynolds, *Anhydro-N-carboxy-DL-*

phenyl-alanine. Nature, 1950. **165**(4199): p. 647.

396. D. Coleman and A.C. Farthing, *628. Synthetic polypeptides. Part II. Properties of oxazolid-2 : 5-diones and an initial study of the preparation of polypeptides there-from.* J Chem Soc, 1950: p. 3218-3222

397. Habraken, G.J.M., et al., *Optimization of N-carboxyanhydride (NCA) polymerization by variation of reaction temperature and pressure.* Polymer Chemistry, 2011. **2**(6): p. 1322-1330.
398. F. Fuchs, *Über N-Carbonsäure-anhydride.* Berichte der deutschen chemischen Gesellschaft (A and B Series), 1922. **55**(9): p. 2943-2943.
399. W.H. Daly and D. Poche, *The preparation of N-carboxyanhydrides of α-amino acids using bis(trichloromethyl)carbonate.* Tetrahedron letters, 1988. **29**(46): p. 5859-5862.
400. A. Karatzas, et al., *Complex macromolecular chimeras.* Biomacromolecules, 2008. **9**(7): p. 2072-80.
401. M.J. Vicent, et al., "*Síntesis controlada de poliglutamatos con baja polidispersidad y arquitecturas versátiles*" N. de solicitud: P201131713, 2012.
402. I. Conejos-Sánchez*, et al., *A Controlled and versatile NCA polymerization method for the synthesis of polypeptides.* Polym Chem, 2013.
403. C.L. Chang, M.K. Leung, and M.H. Yang, *Alkyl and dialkylammonium tetrafluoroborate catalyzed cis–trans isomerization of 1,3,5-trimethyl-1,3,5-triphenylcyclotrisiloxane.* Tetrahedron, 2004. **60**(41): p. 9205-9212.
404. R. M. Macholz, *W. Kliegel: Bor in Biologie, Medizin und Pharmazie. Physiologische Wirkung und Anwendung von Borverbindungen. Tab. .* Springer-Verlag, Berlin, Heidelberg, New York 1980. , 1981. **25**(7): p. 701-701.
405. E. Bernhardt, et al., *Die Reaktionen von M[BF4] (M = Li, K) und (C2H5)2O·BF3 mit (CH3)3SiCN. Bildung von M[BFx>(CN)4—x]*

(M = Li, K; x = 1, 2) und (CH3)3SiNCBFx(CN)3—x, (x = 0, 1). Z Anorg Allg Chem, 2003. **629**(4): p. 677-685.

406. V. J.Gerber and H. G. Elias, *Multimerisation: Assoziation und aggregation. VII. Poly-γ-benzyl-L-glutamat in reinen lösungsmitteln.* Die Makromolekulare Chemie, 1968. **112**(1): p. 142-159.
407. E. R. Blout and M. Idelson, *Polypeptides VI. Poly-alpha-glutamic acid: preparation and helix-coil conversions.* J Am Chem Soc, 1956. **78**(497-498).
408. Deming, T.J., *Polypeptide-based materials.* Topics in Current Chemistry. Springer, 2012. **310**.
409. W. E. Hanby, S. G. Waley, and J. Watson, *Synthetic polyglutamic acid.* Nature, 1956. **161**(132).
410. Günay, K.A., P. Theato, and H.-A. Klok, *Standing on the shoulders of Hermann Staudinger: Post-polymerization modification from past to present.* Journal of Polymer Science Part A: Polymer Chemistry, 2013. **51**(1): p. 1-28.
411. M. A. Gauthier, M. I. Gibson, and H. A. Klok, *Synthesis of Functional Polymers by Post-Polymerization Modification.* Angew Chem Int Ed, 2009. **48**(1): p. 48-58.
412. K. Thompson and S. Michielsen, *Novel synthesis of N-substituted polyacrylamides: Derivatization of poly(acrylic acid) with amines using a triazine-based condensing reagent.* Journal of Polymer Science Part A: Polymer Chemistry, 2006. **44**(126-136).
413. C. Woghiren, B. Sharma, and S. Stein, *Protected thiol-polyethylene glycol: a new activated polymer for reversible protein modification.* Bioconjug Chem, 1993. **4**(5): p. 314-8.
414. D. R. Grassetti and J. F. Jr. Murray, *Determination of sulfhydryl groups with 2,2'- or 4,4'-dithiodipyridine.* Arch Biochem Biophys, 1967. **119**(1): p. 41-9.
415. S. L. Snyder and P. Z. Sobocinski, *An improved 2,4,6-trinitrobenzenesulfonic acid method for the determination of amines.* Anal Biochem, 1975. **64**(1): p. 284-8.

416. N. M. B. Smeets, e.a., *A Scalable synthesis of L-Leucine-N-carboxyanhydre.* Org Process Research & Development, 2005. **9**: p. 757-763.

AIMS OF THE RESEARCH

AIMS OF THE RESEARCH

The present thesis aims at developing novel polymer conjugates for the treatment of neurodegenerative diseases. This principal objective is divided in specific tasks:

- ***Development of novel polymer carriers based on poly-L-glutamic acid (PGA): a biodegradable, multifunctional and versatile polymer.***

  Chapter II covers the synthesis of novel polyglutamates by means of ring-opening polymerisation (ROP) of α-N-carboxyanhydrides (NCA) making use of tetrafluoroborate ammonium salts, a novel approach with this type of polymerisation. Deprotection optimisation and post-polymerisation processes are included in this chapter.

- ***Exhaustive physico-chemical characterisation of these novel entities for a better understanding of their biological behaviour as well as in vitro and in vivo evaluation to validate them as adequate drug delivery systems.***

  In Chapters II, III and IV all the characterisation of the synthesised polyglutamates is described. Chapters II and III contain the routine characterisation for polymers as well as the synthetic routes for their conjugation with different labelling moieties and targeting ligands. Chapter IV is focused on the experimentation in cellular models in order to evaluate conjugate cytotoxicity and cellular internalisation pathways. In this chapter also conjugate biodistribution is studied in animal models where special attention is taken on brain accumulation and secretion routes.

- ***Their application to novel therapeutic targets in the polymer therapeutics area, such as neurodegenerative disorders. Within this topic, two aims were pursued:***

  1. ***To cross Blood-Brain Barrier (BBB) by means of receptor-mediated endocytosis through covalent binding of targeting ligands,***

Chapter III comprises polyglutamate labelling with targeting moieties such as transferrin, mAbOX26, Angiopep-2 and cPEP. The *in vivo* evaluation of their efficacy as brain homing vectors is described in Chapter IV.

2. ***To build novel polymer-drug conjugates (PDCs) for the treatment of an amyloidotic disease where the peripheral nervous system (PNS) is mainly involved and therefore BBB passage was not a prerequisite.***
   In Chapter V, Familial Amyloidotic Polyneuropathy (FAP) constituted the therapeutical approach for novel PDCs in the present thesis. Two bioactive molecules: a low MW drug (doxycycline) and a peptidic sequence (RAGEpep), were conjugated to PGA and PEG used as carriers building a family of conjugates which were rationally designed, characterised and evaluated *in vitro.* A preliminary study *in vivo* has been also performed in a FAP animal model.

- ***The use of combination therapy as a useful tool able to design conjugates with enhanced therapeutic value.***
  Due to the different targets and the possible synergism in the treatment, doxy and RAGEpep conjugates were proposed for combination therapy in FAP treatment. A preliminary study *in vivo* utilising this concept is described in Chapter V
  .

CHAPTER II.

SYNTHESIS AND CHARACTERISATION OF NOVEL POLY-L-GLUTAMIC ACID-BASED BLOCK COPOLYMERS AS POLYMERIC CARRIERS

CHAPTER II. SYNTHESIS AND CHARACTERISATION OF NOVEL POLY-L-GLUTAMIC ACID-BASED BLOCK COPOLYMERS AS POLYMERIC CARRIERS

As stated in the introduction, the pursuit for novel drug delivery carriers more defined and better characterised is currently on first line of investigation in the polymer therapeutics field. On the other hand, routine clinical use of copaxone [7, 372] and the promising phase III clinical results including the recent designation as orphan drug of the polymer drug conjugate Opaxio® (polyglutamic acid (PGA) paclitaxel conjugate, formerly Xyotax, PPX, CT-2103) [201, 373] have underlined the high potential of synthetic polypeptides within nanomedicine, in particular polyglutamates (PGA) [374]. Following these guidelines, in the present work a family of controlled and versatile polyglutamates has been developed by means of an improved methodology of ring-opening polymerisation of α-N-carboxyanhydrides (ROP-NCA).

II. 1 ANTECEDENTS: Ring-Opening Polymerisation (ROP) of α-Amino acid N-Carboxyanhydrides (NCAs)

The vast group of polypeptide copolymers include countless classes of different materials. They are composed by one of the main building blocks used in nature- the amino acids (AAs) constitutive of natural proteins. Precisely controlled AA sequences and compositions confer unique protein properties. Their versatility allows different roles, such as the possibility to catalyse chemical reactions in organisms, trigger specific physiological processes or determine cell and tissue structural features; evolving with a complete array of useful properties for life processes. Since many decades ago, there is a growing interest in developing synthetic routes for the preparation of these natural polymers in biotechnology applications. To reproduce self-assembling of these precise and well-defined structures is considered one of the main requirements to this respect [375]. Chemical synthesis has made possible the access to complex

polypeptide sequences of controlled molecular weight (MW) whose regular secondary structures obtainable by introducing different blocks provides a wide panel of opportunities. Among all synthetic procedures, the Ring Opening Polymerisation (ROP) of α-amino acid-N-carboxyanhydrides (NCAs) is the most accepted technique to obtain polypeptides and polypeptide-based block copolymers with remarkable good yields and on multigram scale, with no detectable racemisation at the chiral centers. These synthetic systems had been already applied in a wide variety of fields including drug delivery, molecular imaging or surface coating materials [211, 376-378].

Historically, first NCA polymerisation data was reported in the very beginning of the 20th century by Leuchs [379-381] and almost 50 years later, synthesis reproducibility remained nearly unfeasible, as well as the construction of more complex architectures or defined polymers. Apart from the typical difficulties in monomer stability, excessive purification requirements or the need of fractionation techniques to reach pure well-defined copolymers, the main problem relied on the co-existence of alternative reaction mechanisms during polymerisation: several interchangeable pathways can occur giving rise to broad dispersities[6] unpredictable molecular weights, and poor controlled chain termini and length [165].

Every NCA can be polymerised by a nucleophile or a base. Both initiation steps lead to a different propagation mechanism. Therefore, the ROP of NCAs can follow the nucleophile initiated “normal amine” (NA), as well as the base initiated “activated monomer” (AM) mechanism. The NA mechanism (NAM) is based on the nucleophilic attack of the initiator, therefore, the use of primary amines (more nucleophilic than basic character) will mainly lead to this pathway. This

[6] Dispersity or polidispersity index (Đ): Dispersity is an inherent property of polymers. It is calculated with the expression:

$$Đ = \frac{Mw}{Mn}, Mw = \frac{\sum n_i M_i}{\sum n_i}, Mn = \frac{\sum n_{ii}}{\sum (n_i / M_i)},$$

where Mw is the mass-average molar mass and Mn is the number-average molar mass.

mechanism promotes a linear correlation among ring-opening chain growth process with monomer conversion. Furthermore, the incorporation of the initiator fragment in the final polymer is expected if side-initiating reactions are absent (FIGURE II. 1). This mechanism was proved independently by Peggion *et al* [382] and Goodman *et al*. [383].

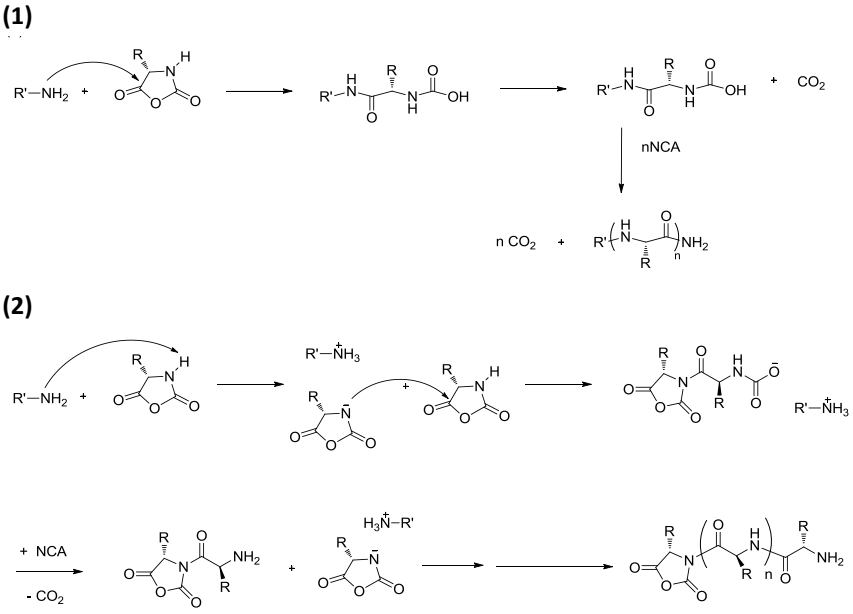

FIGURE II. 1. ROP-NCA polymerisation schemes of (1) Normal Amine Mechanism (NAM) and (2) Activated Monomer Mechanism (AMM).

In contrast, the AMM is triggered by the deprotonation of an NCA due to the basicity of the initiator. For that reason this latter mechanism is attributed to tertiary amines or metal alkoxide, with stronger basicity than nucleophilicity[384]. In the cases of tertiary and secondary amine, as well as the alkali halide-initiated polymerisations, it is believe that AMM and NAM coexist. Thus, in the AMM, it is the deprotonated NCA that becomes the nucleophile initiating chain growth (FIGURE II. 1). In the NAM, the initiation rate is faster than the propagation. A fast initiation is one of the key requirements to achieve a controlled polymerisation, leading to polypeptides with controlled Mw and low Mw/Mn as every initiator starts a polymer chain.

As AMM mechanism proceeds via anion, it is expected a faster propagation rate than the NAM ending in higher Mws, although, since AMM initiation is slower than the propagation stage polypeptides with high polydispersity indexes are obtained. This justifies the tendency to diminish the AM mechanism trying to overcome uncontrolled polymerisations. It should be emphasised that since amines can act as nucleophiles as well as bases, a given system can switch back and forth between the NA and AM mechanisms many times during a polymerisation: a propagation step for one pathway is a side reaction for the other, and viceversa. Hence, this is the reason why preparation of block co-polypeptides and hybrid block copolymers synthesised from amine initiators may have homopolymer contamination. Moreover, the existence of these interchangeable mechanisms leads to the lost of the control of the chain-end functionality which is crucial for the synthesis of hybrid copolymers starting from the polypeptide block. Apart from that, undesired termination processes, such as NCA anion rearranging into an α-isocyanatocarboxylate and carbamate mechanisms, could also exists (futher details in ref. [165]**)**.

Not only due to the initiators but also because of a number of factors, polymerisation process could end in uncontrolled reactions ruining the living nature of NCA-ROPs. For instance, factors which must be taken seriously into account are NCA monomers and solvent purity, presence of water moisture, CO_2 pressure, temperature, presence of salts or cleavability of the protecting groups, undesired terminating processes, etc [211, 385, 386].

In order to solve all the associated problems to NCA polymerisation, many researchers have developed new techniques and mechanisms for NCA-ROP [211, 385-388]. So far the most promising approaches rendering well defined polypeptides are based on initiation of highly purified NCAs with primary amines through high vacuum techniques (HTV) [389], amine hydrochloride salts [390], heavy metal catalysts [391], hexamethyldisilazanes (HMDS) [392] as well as optimisation of reaction conditions (pressure, temperature etc.) [378, 388]. Limitations of these techniques are found for example

in the complex equipment needed for HVT set up and do not touch the chemical reactivity of the initiating amine, the sensitiveness of the HMDS amines to hydrolytic reactions or the side effects of the heavy metal catalysts in biomedical applications if exhaustive purification is not performed.

Deming *et al* developed a new class of NCA-initiators based in zero valence nickel and cobalt complexes [391], achieving living polymerisation of NCAs with high Mw polypeptides via an unprecedented activation of the NCAs into covalent propagating species. They managed to obtain homo and block co-polypeptides with narrow Mw distributions (<1.2), controlled molecular weight (500-500.000Da), preserving the original chirality of the NCA monomer. This protocol was found useful for a wide range of NCAs [375]. Main drawbacks rely on complete removal of the metal from the final product, the initiating complex synthesis and the requirement of a hydrogen atom at the 3-N of the NCA.

Schlaad *et al*. reported the use of primary amine hydrochloride salts as macroinitiators in order to avoid the AMM mechanism [390]. Similar to controlled radical polymerisation techniques, the nucleophilic amine terminus is transferred into a dormant (i.e. protonated) state. The reactivity of primary amine hydrochlorides toward NCAs was first investigated by Knobler *et al*.[393, 394]. In particular, interesting about this method is the researcher efforts on emphasising for decades that removal of HCl, the most common impurity from Fuchs–Farthing NCA synthesis, is crucial for successful NCA polymerisation, also because chloride has been described as an initiator of NCA polymerisation [395, 396]. The main drawbacks are that the polymerisation time increases due to the reduced reactivity of the active sites leading to incomplete monomer conversion. Therefore, remaining monomer has to be removed before a second block can be synthesised. In their work Schlaad and co-workers reported polydispersities below 1.1 and Mn not higher than 22 KDa. For the normal initiation with a primary amine methodology, control over polymerisation process is often lost and consequently, to achieve high

degree of polymerisation (DP) or more complex architectures (graft, dendritic, stars, branched,..) turns to be complicated due to interference of side reactions.

In general polyglutamates synthesised in a controlled manner (NAM mechanism) and in the absence of heavy metals having a molecular weight average ranging from some thousands up to 80 kg mol-1 and polydispersity (Đ) of 1.2 to 1.5 are reported in literature. However the products described are synthesised either at small scale or with low Đ, both characteristics have never been reported together [378, 385, 388, 389, 397]. This fact emphasises the necessity of obtaining well-defined synthetic polypeptides and highlights the interest in finding methodologies to enhance polymer Mw giving birth to biodegradable and versatile systems to be implemented in the different clinical needs.

In this context, a synthetic pathway to a plethora of functional polyglutamates (homopolymers, diblock and triblock co-polymers) with well-defined structures, tuneable Mws and low dispersities (Đ=Mw/Mn <1.2) by means of NCA-ROP has been developed and optimised within this thesis.

II. 2 RESULTS AND DISCUSSIONS

II. 2. 1 NCA MONOMER SYNTHESIS. SYNTHESIS OF α-BENZYL L-GLUTAMATE N-CARBOXYANHYDRIDE (NCA) (2).

The synthesis of N-α-carboxyanhydrides (NCAs) constitutes a key stage for the later polypeptide synthesis. For this reason, acceptable yields and the use of monomers of extremely high purity are required in this first step. Historically, there are two methods described in literature for the NCA synthesis: *Leuchs* methodology [379], based on the cyclation of the N-alkoxycarbonyl amino acid halides forming the α-amino acid NCA (FIGURE II. 2(A)) and the modified method so called *Fuchs-Farthing* (FIGURE II. 2(B)) when process involves the direct phosgenation of unprotected α-amino acids [395, 398].

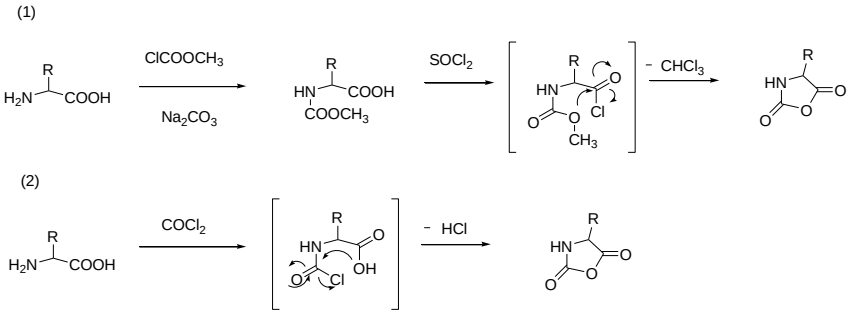

FIGURE II. 2 Scheme of N-α-carboxyanhydrides synthesis described by (1) *Leuchs* and (2) *Fuchs*.

Phosgene was the initial reagent in this latter protocol, which is a highly toxic gas. Triphosgene was suggested as alternative [399], it is economically viable, robust, and as a solid material easier to manipulate. Importantly, one of the main problems linked to the use of phosgene is the fact that by-products can be formed due to an excess of the starting reagent and HCl (FIGURE II. 3) leading to broad or multimodal molecular weight distribution of the final polypeptide.

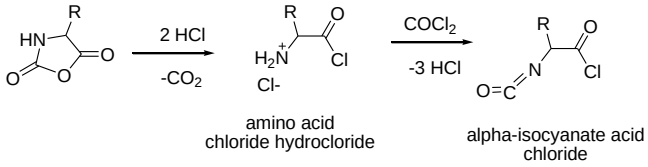

FIGURE II. 3 Byproduct formation in presence of HCl and phosgene in excess.

NCA formation mechanism is depicted in FIGURE II.4. In this thesis, the synthesis of NCA monomer has been significantly improved. The starting protocol chosen from Fuchs-Farthing method was carried out with triphosgene, which is transformed to diphosgene that decomposes by temperature giving phosgene thus, the stoichiometric control is achieved. Once that was solved, the main objective was to ensure the complete removal of any HCl traces due to their capability to promote NCA self-degradation (FIGURE **II. 4**).

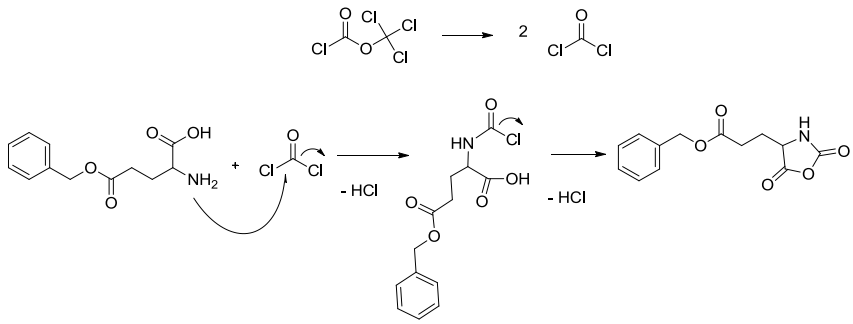

FIGURE II. 4 γ-Benzyl-L-glutamate N-Carboxyanhydride synthesis. The mechanism involving the direct phosgenation of the unprotected α-amino acid. Cyclation proceeds through the formation of N-chloroformyl amino acid intermediates and the loss of a second HCl molecule completes the NCA.

In order to remove HCl, herein basification was not possible as amines or other commonly used strong bases would attack the formed NCA decomposing it. For this reason, different changes were included into the former protocol: (i) limonene was added due to its non-nucleophilic/-basic HCl-scavenger ability (

FIGURE II. 5 II. 5) and (ii) bubbling an inert gas into the reaction solution pushing HCl out. As an additional step, the solid obtained was precipitated and recrystallised several times to remove last traces of HCl and any possible remaining impurities.

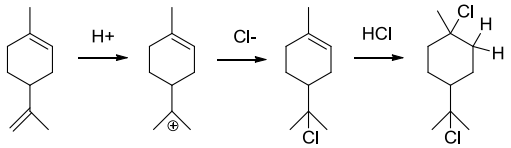

FIGURE II. 5 HCl capture mechanism by limonene.

Monomer identity was achieved by NMR analysis as well as with the melting point. Examples of the results obtained are summarised In TABLE II. 1 and FIGURE II. 6. The NMR spectra in $CDCl_3$ showed the correspondent signals of the compound. Both synthetic methodologies drove to similar results. The only difference was the larger monomer storability achieved with the second method due to a better purification procedure. In all cases, once the NCA monomer was obtained its usage was immediate. Even though, storability of the pure

product was feasible, the monomer was recrystallysed before use to avoid any possible impurities derived from auto-polymerisation processes. The melting points were in good agreement with the values reported in literature [385], the light deviation corresponds to the difference in solvent for the recrystalisation.

(A)

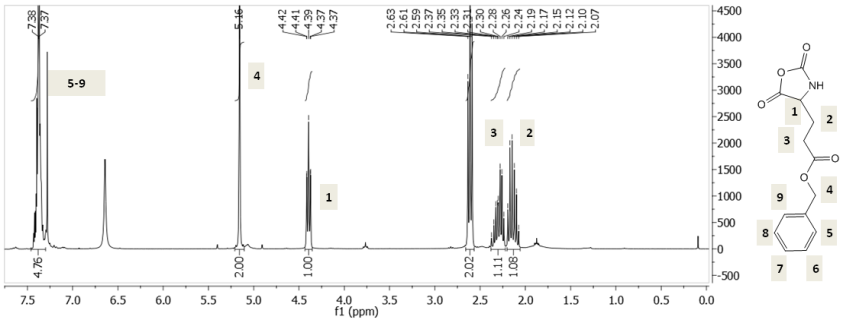

(B)

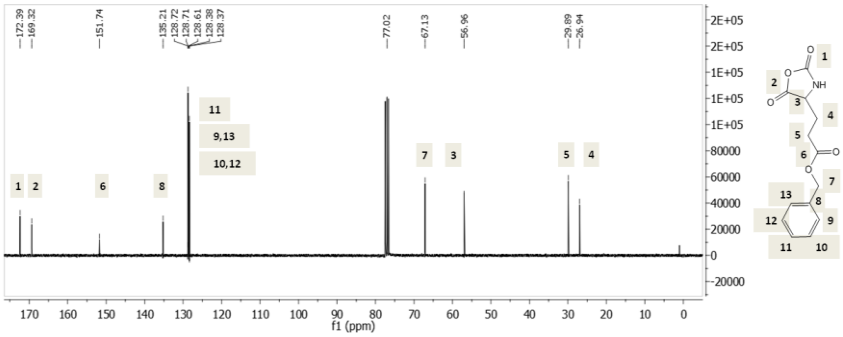

FIGURE II. 6 ^{1}H-NMR (A) and ^{13}C-NMR (B) spectrums of the γ-benzyl-L-glutamate N-carboxyanhydride (**2**).

	Yield (%)	Melting point (˚C)	Melting point lit. (˚C)
Method 1	87	92.5-94	97
Method 2	90	93-94	97

TABLE II. 1. γ-Benzyl-L-Glutamate N-Carboxyanhydride (**2**) synthesis.

II. 2. 2 GENERAL PROCEDURE FOR NCA POLYMERISATION. SYNTHESIS OF POLY-ɤ-BENZYL L-GLUTAMATE.

II. 2. 2. 1 Initiators

Initiators not only trigger the polymerisation process but also they can be used to (i) introduce an ending group into the polypeptide either as a specific linkage point for further conjugation or (ii) as a reference group to determine the degree of polymerisation (DP) and/or (iii) to introduce other polymeric block. In this work, initiators fulfil some of the previously described roles acting as a reference to quantify the glutamic acid (GA) units via NMR and more importantly as a linear polymer block in specific cases.

Initially, n-butylamine was used but it was substituted by neo-pentylamine to obtain a better signal-to-noise ratio in ^{1}H NMR measurements. This amine has 9 instead of the 3 terminal protons, which facilitates DP determination by ^{1}H-NMR.

Moreover, in the present work the polymer polyethylene glycol (PEG) was used as a macroinitiator aiming to built diblock co-polymers. The mixture of polymers with different hydrophilic character may result in conferred amphiphilic properties to the final system. Therefore, PEG was employed as macroinitiator constituting the most polar unit in the block copolymer system. Tailoring the number of PEG blocks as well as the length of the polypeptide chain, our aim was to obtain a family of polypeptides with a variety of conformation in solution and consequently with different biological properties regarding cellular membrane transport.

Using the previously described initiators, ROP of-NCAs provided two different polymer platforms: the homopolymer polybenzyl-L-glutamate (PBLG) by means of n-butylamine (**3**) or neopentyl amine (**4**), and the diblock copolymer PEG-*b*-PBLG (**6**) thanks to the PEG initiator. General schemes of their synthesis are shown in FIGURE II. 7, (A) and (B), respectively.

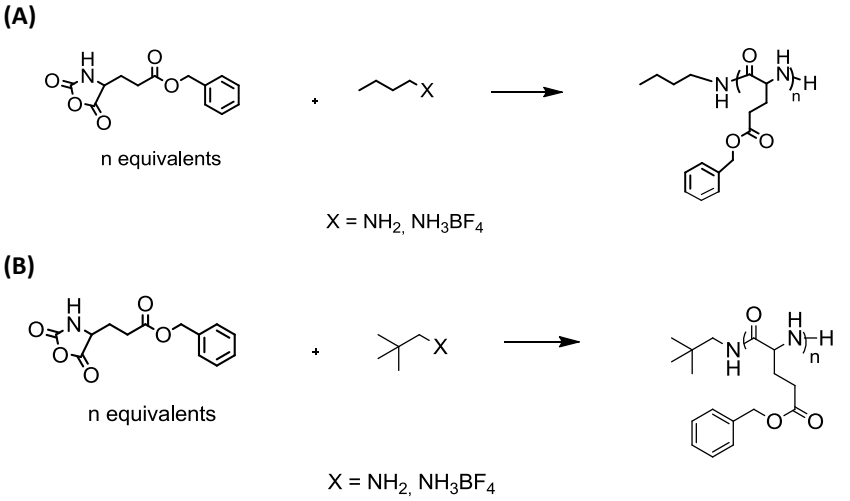

FIGURE II. 7 PGA homopolymer synthesis. General scheme for polymerisation (A) using n-butylamine (nBu) or its ammonium tetrafluoroborate salt. (B) utilising neopentyl amine (npt) or its ammonium tetrafluoroborate salt.

II. 2. 2. 2. Optimisation of NCA polymerisation conditions

The wide range of reaction pathways available make the controlled polymerisation of NCAs a challenging task. The first method used in this work (section II.4.1) consisted on Glu(Bz)-NCA polymerisation in a low polar solvent under less controlled conditions. In the second method (section II.4.2) the process was improved by the implementation of more sophisticated equipment and strict inert conditions, well-dried reagents and solvents. Studies carried out in our group pointed DMF as the most appropriate solvent for the polymerisations leading to acceptable yields, controlled Mw with narrow polydispersities. In DMF it is possible to avoid the formation of the salt between the intermediate of the carbamic acid and the amino groups of the propagating chains, restoring the normal first order kinetic of the polymerisation [211, 400, 401]. The conditions used in each method are summarised in TABLE II. 1.

	Material and reagents	Reaction conditions		
		T (°C)	Reaction time	NCA initiator
Method 1	Inert atmosphere, anhydrous solvent (CH_2Cl_2, $CHCl_3$)	25°C	3d	normal amine
Method 2	Inert atmosphere, CO_2 exit, anhydrous solvent (DMF), well-dried reagents, Schlenk tubes	0, 25, 40°C	Optimal	normal amine/ BF_4 salt

TABLE II. 2 Conditions used for ROP-NCA polymerisation.

In the table below (TABLE II. 3) characteristics of the diblock (DB) co-polymers synthesised through the first and the second methods using primary amine as initiator are described. FIGURE II. 8 shows the general scheme for this polymerisation. The initiator and the ratio [monomer]/[initiator] ([M]/[I]) was varied in order to synthesise a polyglutamate family with wide ranges of Mw (TABLE II. 3).

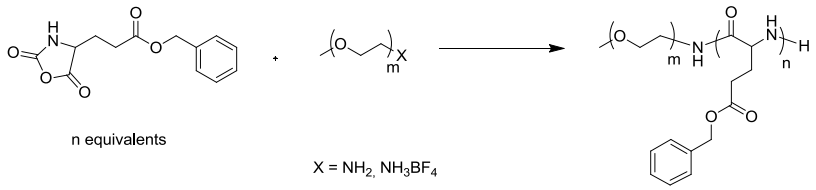

FIGURE II. 8 Diblock co-polymer synthesis. General scheme for polymerisation using methyl-PEG-amine or its ammonium tetrafluoroborate salt as initiator.

The first methodology did not allow achieving high Mw polymers due to the lack of a controlled environment that yielded to a poor performance when polymers with DP 400 or 800 were seek. Polymer polydispersities obtained were also broader than expected (TABLE II. 3). Second methodology gave rise to more homogeneous systems with lower dispersities (1.05-1.20), reproducibility batch-to-batch and scalability (from 100mg to 10g synthesis). In any case, DB with more than 200 units was not obtained with the conditions tested

					GPC (DMF 0,1%LiBr)			
Method	**Initiator**	**[M]/[I]**	**t_R (d)**	**Yield (%)**	**DP**	**Mn (g/mol)**	**Đ**	
1	N-Butyl-NH_2	200	3	82	184	40296	1.391	
		400	3	87	154	33726	1.388	*
		800	3	87	110	24090	1.312	
	mPEG-NH_2	200	3	95	208	47501	1.333	
		400	3	66	149	34578	1.247	*
		800	3	59	92	22152	1.295	*
2	mPEG-NH_2	200	14	48	134	31175	1.146	
		400	14	54	207	47298	1.051	

TABLE II. 3 NCA polymerisation through method 1 (at 25°C) and 2 (at 4°C) using amine initiators. Đ=polydispersity index, (*)=bimodal distribution.

In addition, method 1 showed bimodal distributions in the GPC analysis which confirmed the co-existence of other chains apart from the expected PEG-*b*-PBLG. As already explained, any impurity or the non-removed humidity (H_2O) could have started the polymerisation ending in mixtures of homopolymers with diblocks. Thus, conditions of method 2 were selected for NCA-ROP and were established as the starting point in the next studies.

Exploring of NCA polymerisation using tetrafuoroborate ammonium salts

To circumvent the mentioned challenges regarding NCA polymerisation, in this work novel initiators are proposed to enable controlled multigram synthesis of well-defined polyglutamates covering a wide Mw range. This novel synthetic approach involves the use of ammonium salts such as the non-nucleophilic anion tetrafluoroborate (BF_4^-) [401, 402]. These salts combine (i) the advantages of the primary amine hydrochloride salts avoiding the AMM mechanism and reducing the reactivity of the amine (lower

nucleophilicity but much lower basic character); and (ii) a counter ion lacked of nucleophilic character, overcoming the main drawback of the Schlaad methodology. Its inert character is based on the symmetry of the ion leading to an equal charge distribution and its composition of high electronegative fluorine atoms, which diminish the basicity of the anion. Thus, side reactions based on the nucleophilic character of the counter ion have been effectively suppressed. Based on these advantages, a more controlled polymerisation was expected with these initiators.

a) Methodology for BF_4^- ammonium salts preparation.

These salts were easily prepared by the reaction of the corresponding amine with the HBF_4 diethylether complex [403] and purified by recrystallisation. Schemes of the synthesis are depicted in FIGURE II. 9. Although BF_4 salts have been reported to be safe[404], it is important to note that, salt traces have never been detected in ^{19}F NMR after removal of the protection groups and workup (FIGURE II. 10).

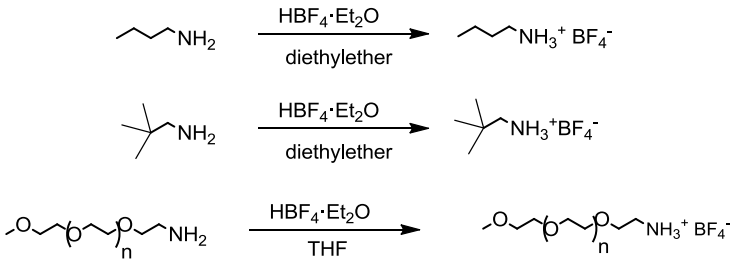

FIGURE II. 9 Synthetic route for BF4 salts obtaining.

In order to prove all mentioned assumptions and to demonstrate the versatility of the presented method, BF_4 salts of neopentyl amine, butylamine as well as polyethylene glycol mono-methylether amine were prepared. The three salt conversions were quantitative and NMR analysis (FIGURE II. 11, FIGURE II. 12 and FIGURE II. 13) confirmed their identity

(A)

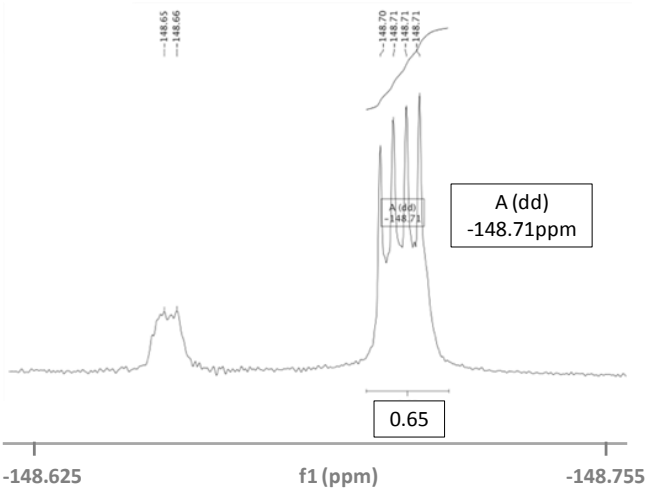

(B)

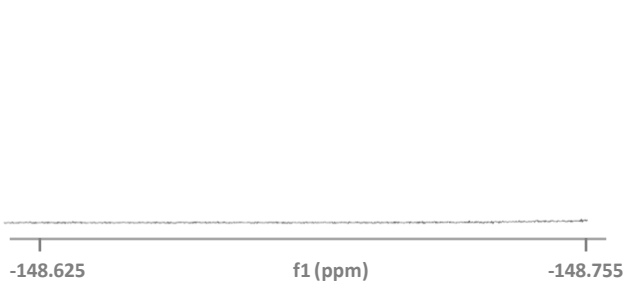

FIGURE II. 10 (A) ^{19}F–NMR of PBLG before benzyl deprotection. (B)^{19}F–NMR of PGA, after benzyl deprotection[7] (see ref.[405]).

[7] Explanation of chemical shifts: B has two isotopes with spin > ½ and because the ion is symmetric one can observed quadrupole splitting rather than quadrupole broadening. For [(^{10}B)F_4]- ^{10}B (19.58% abundance) has spin (I) 3 so (2nI +1), n =1 the resonance will be split into seven lines of equal intensity (19.58/7). On top of this (chemical shift probably but not necessarily the same) [(^{11}B)F_4] ^{11}B (80.42% abundant) has spin 3/2 so (2nI +1) the resonance will be split into 4 lines of equal intensity so about 20% (80/4) with a different B-F coupling.

(A)

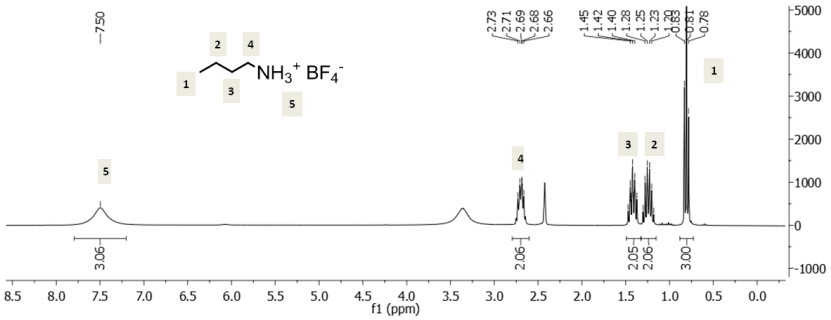

(B)

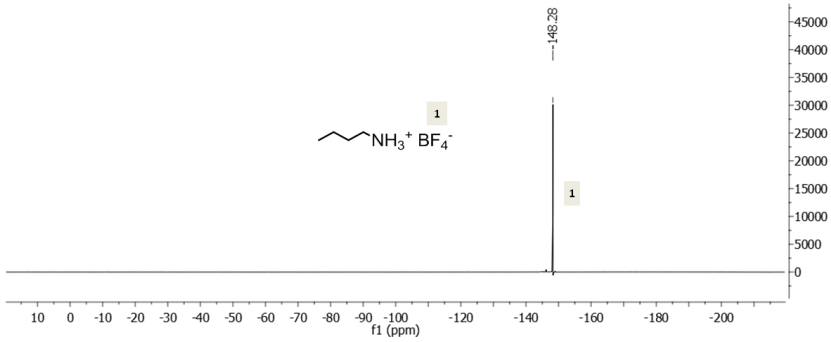

FIGURE II. 11 NMR spectra of nBu-NH_3BF_4 (**14**) (A) ^{1}H and (b) ^{19}F.

(A)

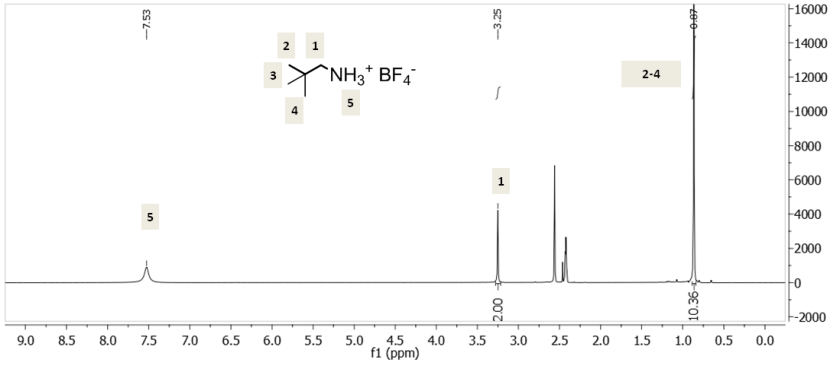

(B)

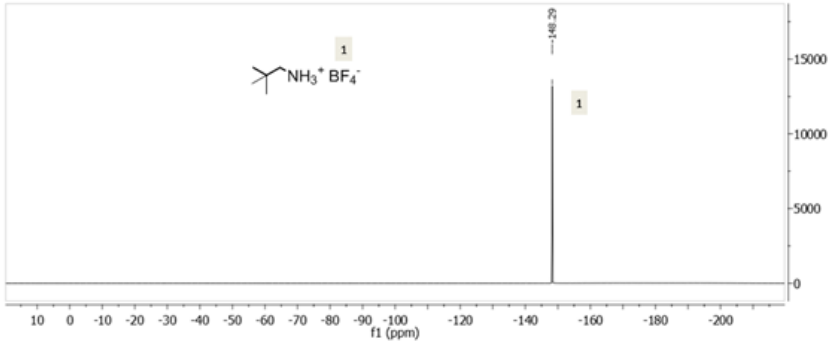

FIGURE II. 12 NMR spectra of npt-NH_3BF_4 (**15**) (A) ^{1}H and (b) ^{19}F.

(A)

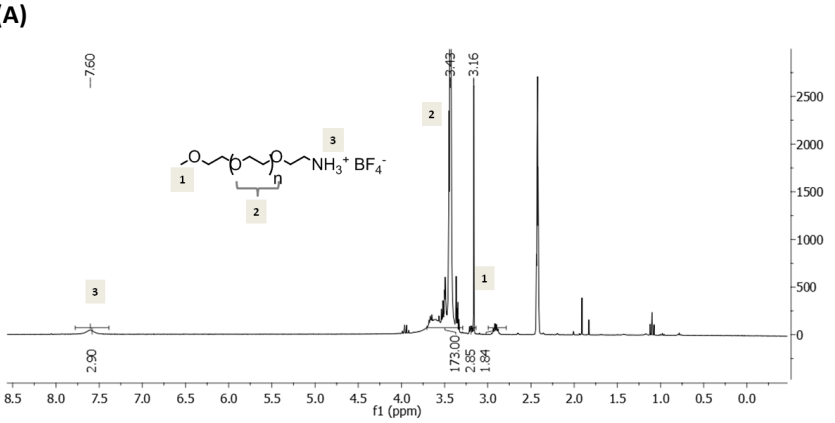

(B)

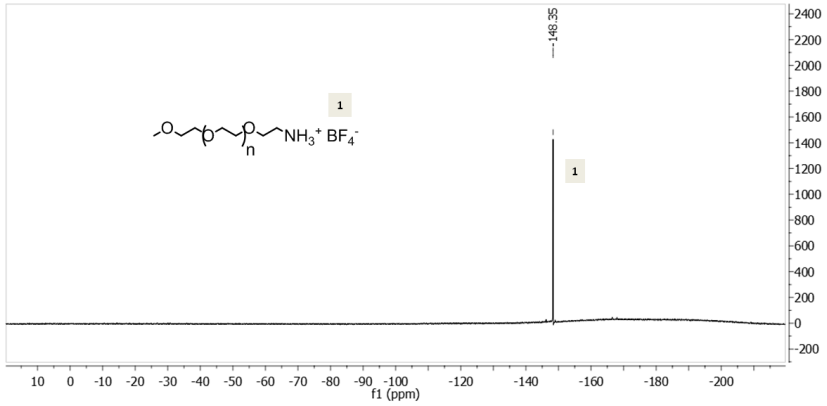

FIGURE II. 13 NMR spectra of mPEG-NH_3BF_4 (**16**) (A) ^{1}H and (B) ^{19}F.

b) NCA polymerisation studies with BF_4 salts

Firstly, PGA homopolymer synthesis was carried out. A comparison study among the BF_4 salts and the normal amine initiators was performed with the neopentyl initiator. Reaction conditions and polymer characteristics determined are displayed in

TABLE II. 4. GPC analysis as well as IR were used to monitor reaction progression. FIGURE II. 14 shows an example of these analyses.

The ratio [M]/[I] was previously investigated [401] as clearly influenced NCA polymerisations. The study showed that a higher dilution leads to less defined polymers that may be attributed to secondary structure formation, which is dependent on polypeptide concentration in solution. For a ratio [M]/[I]=200, the best yield and DP was reach with 0.1g/mL monomer concentration. Therefore, polymerisations presented in this work maintained this value.

Temperature was varied from 4°C to 40°C in all cases. As expected, due to the equilibrium among the ammonium salt/dormant amine, it was confirmed that the reaction rate was slower for BF_4 salts and for high Mw PGAs, longer time or higher temperature was

required. Therefore, 4°C was discharge for BF_4 salts initiation. In the same way, reactions carried out at 40°C showed higher dispersity indexes and lower DPs than expected. These facts could be attributed to DMF decomposition to dimethylamine (DMA) at high temperature. DMA could also initiate NCA polymerisation, leading to more polydisperse systems and consequently smaller chain length due to the monomer consumption.

In all synthesis, final products identity was done by ^{1}H-NMR ($CDCl_3$) and GPC analysis. Some examples of the results obtained are shown in FIGURE II. 16 and FIGURE II. 15.

(A)

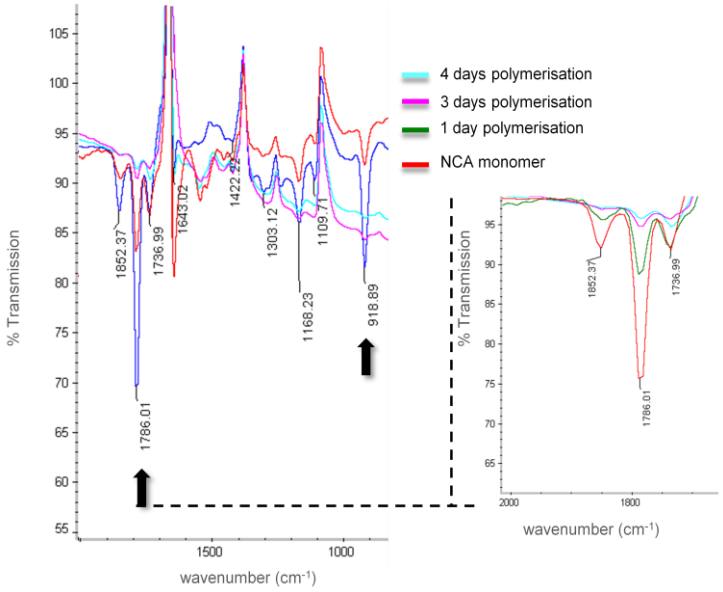

(B)

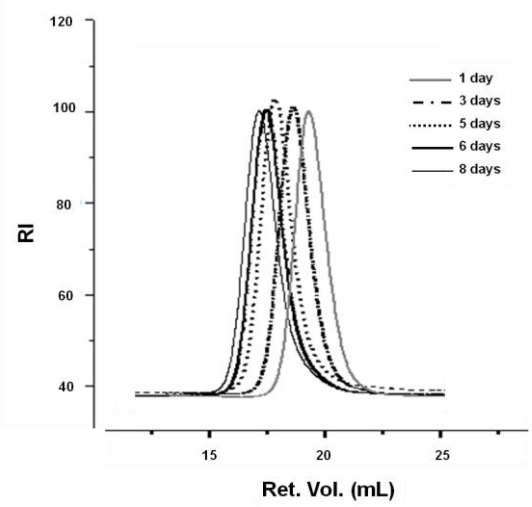

FIGURE II. 14 Polymerisation reaction monitored through: (A) FTIR technique: IR spectra of poly(L-Glu(Bzl)) in DMF solution over time reaction[8]. (B) GPC analysis: GPC traces of the polymerisation reaction to obtain PBLG DP=100 (DMF).

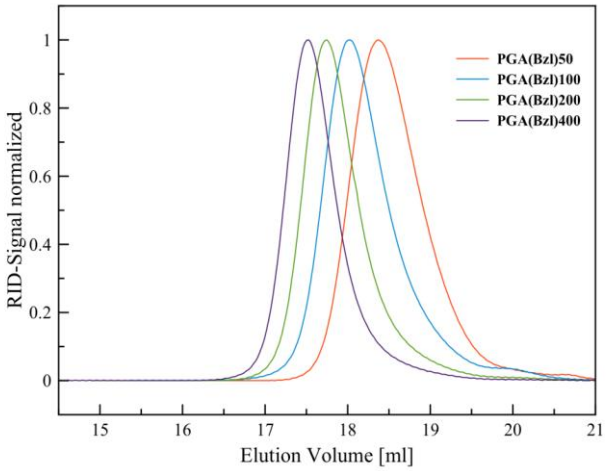

FIGURE II. 15 GPC traces in DMF of the npt-PBLG with DP=50, 100, 200, 400.

[8] NCA monomer related peaks are found at 1785 and 920cm-1 (*red line*). They were used to monitor the reaction (peak at 1857 cm^{-1} also belongs to the NCA monomer but can be hidden by DMF absorption).

As a conclusion of the study with NH_2 and BF_4 neopentyl initiators it could be said that, polymer MW was precisely controlled up to a DP of 200 with NH_2 at low temperature or BF_4 at 25°C. When higher Mw were required, only BF_4 salt initiators achieved the desired DP (FIGURE II. 17). Even DP=800 was achieved without the need of complex initiators or demanding experimental setup [401]. The polymers had low dispersities indexes (1.05-1.20) indicating living character of the polymerisation itself (see TABLE II. 4). Our novel initiators provided reproducibility batch-to-batch as well as enabled the scalability of the synthesis, from 100mg to 10g of starting NCA monomer.

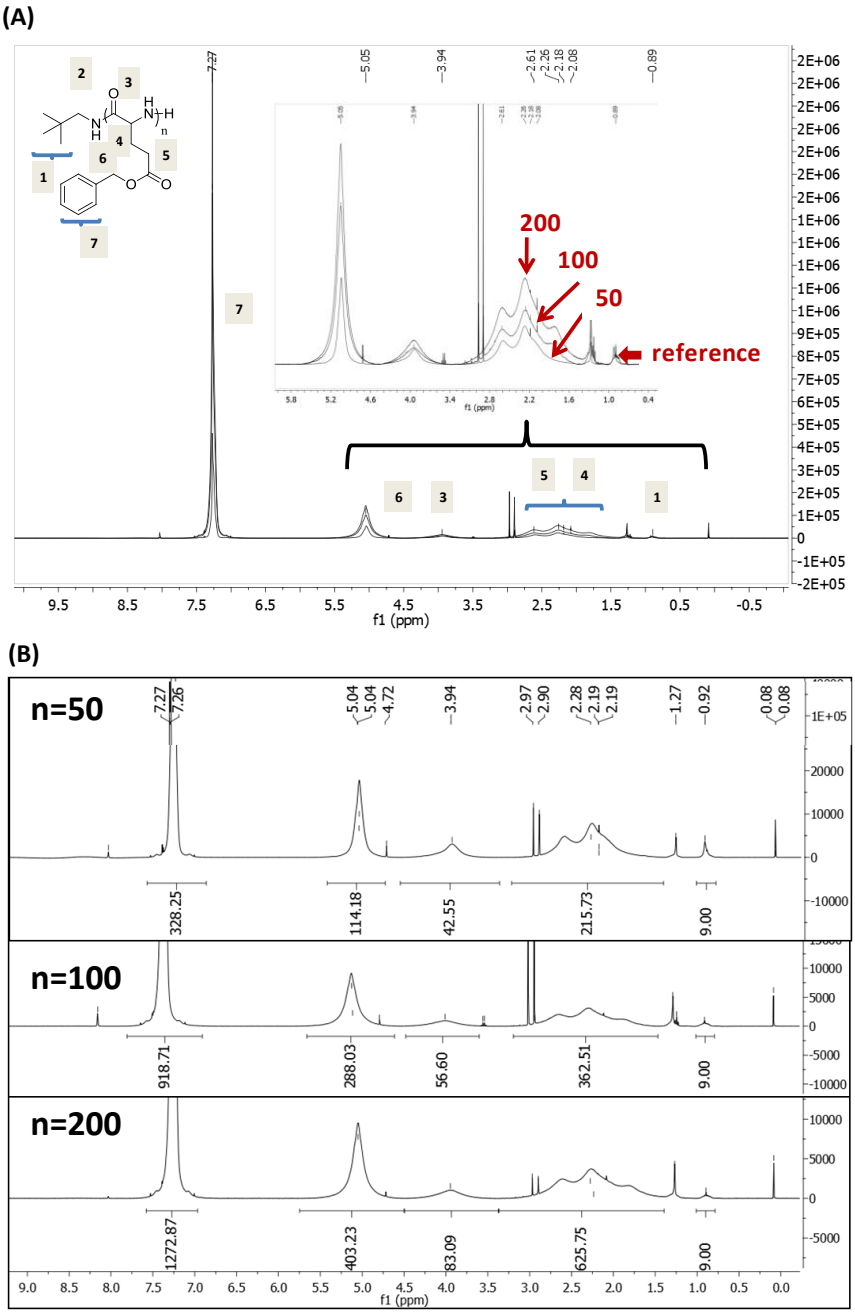

FIGURE II. 16 ^{1}H-NMR spectra of npt-PBLG$_n$ (**10**; n=50, 100, 200). (A) Overlay spectra where differences among the different DP polyglutamates can be observe having the initiator peak as reference. (B) Individual integration of each PBLG specie.

					GPC data (DMF 0,1%LiBr)			GPC data (HFIP)		NMR data
Initiator	**DP_{th}**	**T (°C)**	**t_R (d)**	**Yield (%)**	**Mn**	**Đ**	**GA units**	**Mn**	**Đ**	**GA units**
npt-NH_2	50	4	5	74	9365	1.134	43	9275	1.16	57
	100		8	64	27806	1.064	127	22169	1.113	144
	200		11	68	28675	1.100	131	23609	1.138	202
	400		16	90	15675	1.140	72	29499	1.108	190
npt-NH_2	50	25	5	74	9581	1.210	44	9316	1.11	47
	100		7	80	11876	1.170	54	10984	1.140	78
	200		10	79	13914	1.138	64	12084	1.158	114
	400		15	78	16365	1.160	75	12475	1.155	121
npt-BF_4	50	25	5	73	10612	1.151	48	7891	1.221	40
	100		8	62	16390	1.104	75	15108	1.17	73
	200		11	75	22545	1.133	103	20399	1.150	197
	400		16	85	44182	1.079	202	35806	1.160	405
npt-BF_4	50	40	3	64	6700	1.100	32	-	-	-
	100		10	76	23186	1.203	106	-	-	-
	200		11	83	26024	1.226	119	-	-	-
	400		11	84	17103	1.26	78	-	-	-

DP=degree of polymerisation, npt=neopentylamine, GA=glutamic acid, Đ=polydispersity, -=measurement not performed

TABLE II. 4 PBLG synthesis through ROP-NCA polymerisation by means of different initiators and reaction conditions. Number of glutamic acid (GA) units was calculated in two solvents (N,N' -dimethylformamide (DMF) and 1,1,1,3,3,3- Hexafluoro-2-propanol (HFIP) and by $_1$H-NMR ($CDCl_3$) .

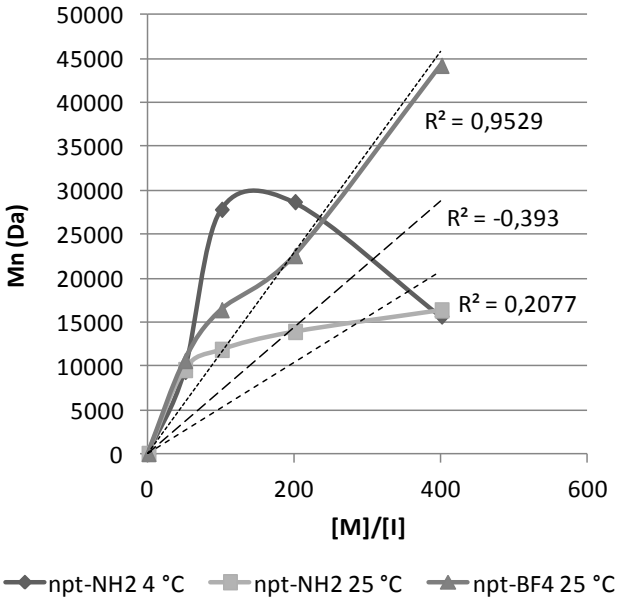

FIGURE II. 17 Representation of the theoretical DP ([M]/[I]) vs. Mn (kg/mol) from GPC (HFIP) data. Legend: ( ) npt-BF_4 at 25°C, ( ) npt-NH_2 at 25°C, ( ) npt-NH_2 at 4°C.

As it is specified in TABLE II. 4, the final polymers were analysed by GPC in two different solvents: DMF and HFIP (FIGURE II. 15). GPC measurements should be carried out in the absence of secondary structures for a proper Mw, and Đ data determination. Even DMF, which is usually effective enough in disrupting hydrogen bonds, is not able to completely disrupt polypeptide secondary structures. HFIP was used as alternative solvent to DMF to ratify an adequate Mw, and Đ data determination [401]. Comparison of the polymer Mw obtained showed not significant differences for both solvents (TABLE II. 4). Looking at the GPC traces, slight tailing can be observed for 50 and 100 unit PGAs since in this range a small amount of polymers are too short to form helical structures and therefore a mixture of random coils and helical structures is present within the same polymer sample (FIGURE II. 15). This can be confirmed by CD spectroscopy (FIGURE II. 18) and NMR (4.8 ppm). This means that secondary structures cannot be neglected in GPC measurements. As in nature, low MW PGAs

display a more pronounced contribution of random coil structures. However, those effects are absent for higher MW PGAs and therefore are not attributed to undefined polypeptides but to the nature of the polypeptide itself (FIGURE II. 15 and FIGURE II. 18) [406].

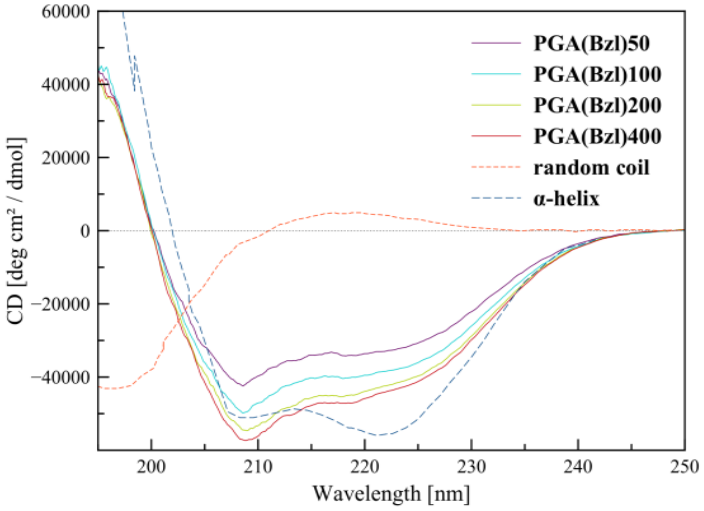

FIGURE II. 18 CD spectra in HFIP at 20°C.

Using amino terminated PEG initiators, PEG-PGA block copolymers (**6**) were synthesised with the two versions of initiator: $mPEG_{2000}$-NH_2 and $mPEG_{2000}$-NH_3BF_4. The study included temperature modulation (4, 25 and 40°C) (see TABLE II. 1). Diblock copolymers with the expected Mw (DP100 or 200) and low Đs (1.1-1.2) were obtained at low temperatures, using either the NH_2 or the BF_4 form of the $mPEG_{2000}$ as initiator. Hence, T=4°C with or without BF_4 salts as initiator were selected for diblock copolymers. When high Mw DB would be desired, BF_4 salts would be probably required.

In the next figure (FIGURE II. 19), it is exemplified the characterisation guidelines used for DB.

					GPC (DMF 0,1%LiBr)		
Initiator	DP_{th}	T (°C)	t(d)	Yield (%)	Mn	Đ	GA units
PEG-NH_3BF_4	200	4	21	91	27005	1.27	115
	200	25	21	86	21264	1.35	88
	200	40	21	79	17856	1.32	73
PEG-NH_2	200	4	15	90	25882	1.23	109
	200	25	12	68	12208	1.13	47
	200	40	21	74	11456	1.32	44

TABLE II. 5 DB_{200} copolymer synthesis. NCA polymerisation in DMF with methyl-PEG-amine and its tetrafluoroborate salt at different temperatures (4, 25 and 40°C).

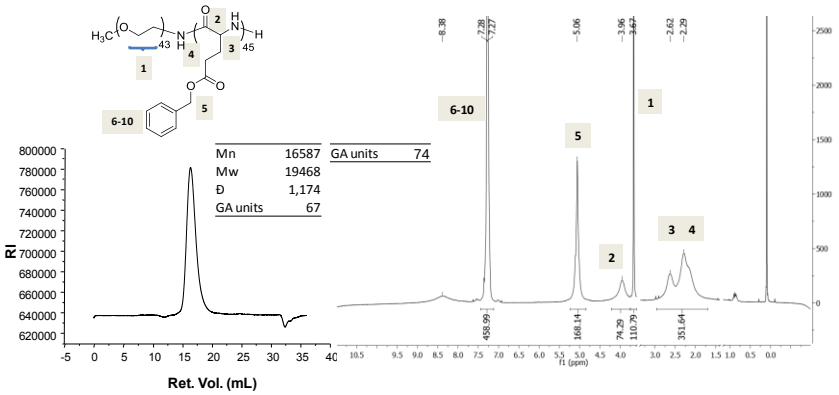

FIGURE II. 19 Diblock copolymer characterisation through GPC (left) and NMR (^{1}H, CDCl3) (right) techniques.

The results showed up to now demonstrate that, using our optimised NCA approach, the control over polymer end groups could be enhanced enabling the synthesis of well-defined homo and diblock polypeptides of a variety of MW [401]. As an example of the versatility of our novel technique, the polymers obtained are summarised in the TABLE II. 6, specifying the DP variation and all the BF_4 initiators tested.

Initiator	DP_{th}	Yield (%)	Mn (Da)^A	Đ^A	DP^A	DP^B
Neopentyl-NH_3BF_4	50	73	10512	1.1	48	40
	100	70	16425	1.1	75	73
	200	75	22557	1.1	103	197
	400	85	44238	1.1	202	405
	1200	80	156585	1.2	715	-
n-Butyl-NH_3BF_4	50	64	6789	1.1	31	29
	100	64	13797	1.1	63	60
	200	63	16206	1.1	74	107
	400	72	31536	1.2	144	212
	800	53	48399	1.2	221	-
	1200	51	94389	1.2	431	-
PEG(2000)-NH_3BF_4	50	73	6947	1.2	23	38
	100	81	13955	1.2	55	79
	200	80	17678	1.2	72	149

A=Data obtained by SEC in DMF, B=Data obtained by ^{1}H-NMR, DP=degree of polymerisation, Đ=polydispersity, -=Values below the detection limit.

TABLE II. 6 NCA polymerisation in DMF with BF_4 salts as initiators.

II. 2. 2. 3 Synthesis of the diblock PGA_n-PEG through N-terminus conjugation to the synthesised polypeptides

Another pathway to obtain diblock copolymers could be achieved by conjugation of end-chain amino group of the PGA to a PEG block with the adequate terminal group. This reaction was carried out from two different starting points: PEG conjugation on (i) protected PBLG and (ii) deprotected PGA. Both synthetic schemes are depicted in FIGURE II. 20. The main drawbacks encountered with this strategy

were the availability/exposure of the end-chain amino group for reaction and the complete removal of unreacted PEG chains. Aqueous conditions were used for the deprotected PGA and organic solvent for the protected one. HFIP was selected in order to avoid secondary structure formation and therefore, to enhance NH_2- group availability for further reaction.

(A) Method 1

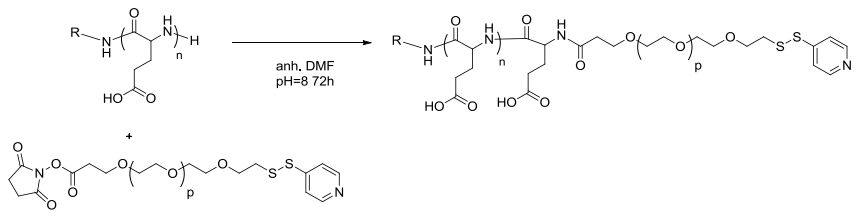

(B) Method 2

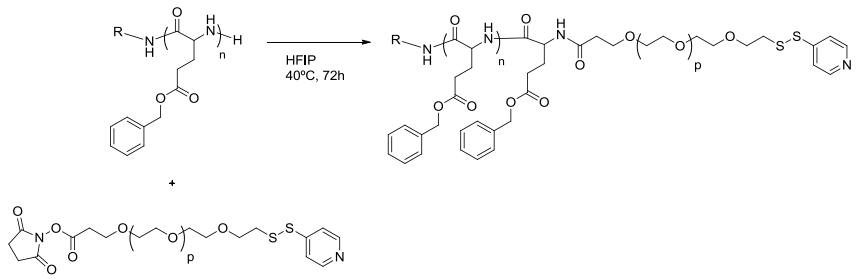

FIGURE II. 20 Alternative synthesis schemes for the obtention of DBs (**5**).

Yields of HFIP reactions were markedly higher (90%) than those obtained from the aqueous one (40-60%). This methodology was selected as the best alternative. Both explained methodologies provide a novel pathway for DB synthesis. However, comparing this approach with the use of NCA polymerisation through PEG initiator, the latest one offers more homogeneous final diblocks, whereas PEG posterior linkage could give mixtures of PGA and PEG-*b*-PGA as well as lower yields. On the other side, the proposed post-polymerisation PEG linkage endows the system with a specific semitelechelic point of conjugation.

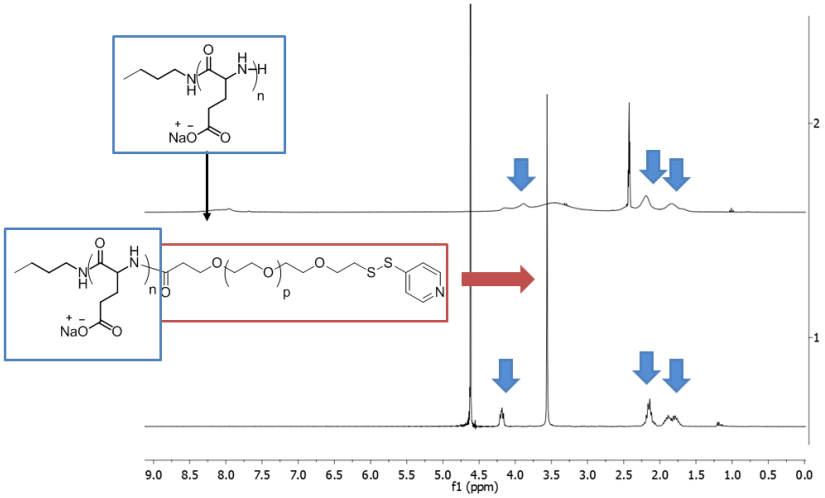

FIGURE II. 21 Alternative diblock copolymer synthesis through method 1. NMR characterisation, before and after the reaction.

II. 2. 2. 4 Poly-benzyl-L-glutamate (PBLG) deprotection

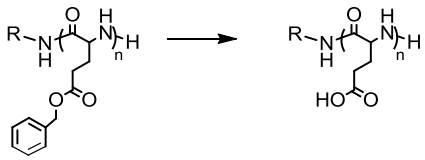

FIGURE II. 22 General scheme for PBLG deprotection. Benzyl group removal.

The final PGA polymers must be obtained using a deprotection method that ensures full removal of protecting groups without racemisation; an issue, which is often not considered carefully and could induce important changes in nanomedicine behaviour in a clinical setting. Changes in secondary structure due to polypeptide racemisation will alter immunological properties, degradation profile, and secondary structure. Consequently drug release, the PK profile and biodistribution maybe unpredictable upon polypeptide-drug conjugation.

Deprotection using TFA/HBr or acetic acid/HBr is known to lead to deprotection in the absence of racemisation [407, 408], but may lead to chain cleavage from protonation of side-chain ester groups which react with the amide backbone basic environment avoid

it but racemisation can occur unless base equivalents are controlled and hydrogenation is ineffective for Mw superior to 10kDa (larger chains keep helical conformation impeding access to the catalyst) [409]. However, these conditions are not suitable for sensitive functional end groups derived from functional initiators, e.g. alkyne or biotin moieties as well as PEG based block copolymers (i.e. PEG is rapidly degraded under those conditions, see FIGURE II. 25). In respect to those needs we have developed a basic deprotection protocol avoiding racemisation. Importantly, longer reaction times (up to 16 h) are required when undertaking large scale deprotection at acidic as well as basic conditions to ensure full benzyl group removal and polypeptide stability including secondary structure conformation.

Deprotection under acid conditions: HBr/TFA

The use of the mixture of HBr/TFA leaded to complete removal of the benzyl group through simple reaction conditions. Along the optimisation procedure, it was proposed to diminish the harsh conditions were PBLG was exposed. Initially, 4eq of HBr per benzyl group were used and reaction was carried out for 16h, yielding 100% of deprotection (calculated by proton NMR analysis in DMSO-d_6). Then, equivalents were decreased to 2 with good results. Final reaction time to achieve full deprotection was also reduced from 16h to 5h. For big scale deprotection of PBLG (>600mg), 16h were still requierd to accomplish complete deprotection. Yields were considered quantitative under the named optimal conditions. The polymers were characterised by ^{1}H-NMR analysis ($CDCl_3$ or DMSO-d_6).

In the next figure (FIGURE II. 24) it is shown the characteristic spectra PGA before and after DB deprotection.

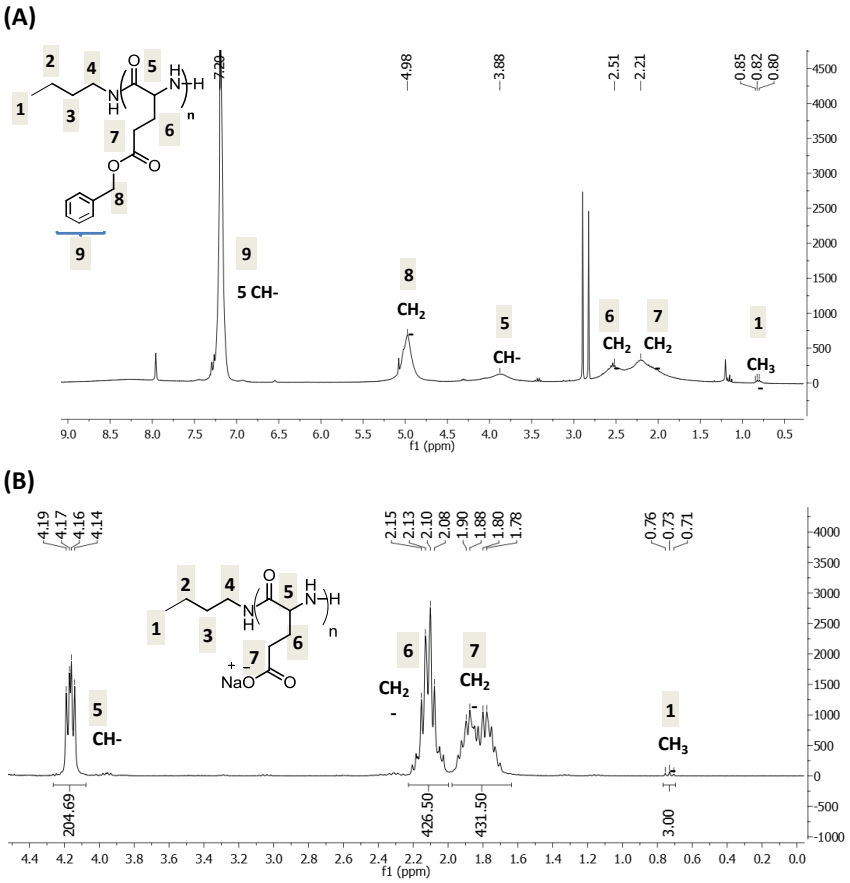

FIGURE II. 23 ^{1}H-NMR spectra of nBu-PGA$_{200}$ (A) protected (3) and (B) deprotected (**4**).

Regarding the PEG-*b*-PGA copolymer (FIGURE II. 24), more careful set up was sorely required. Acid deprotection led to complete removal of the benzyl groups. However, when protected and deprotected block-copolymers were evaluated for size in solution measurement by DLS technique it was observed a pronounced size reduction after deprotection (data not shown). Therefore, integrity of PEG blocks was considered to be damaged within the deprotection process.

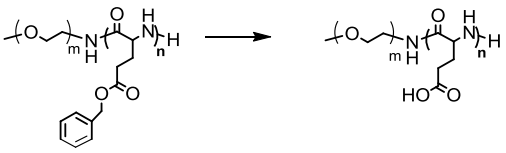

FIGURE II. 24 General scheme for DB deprotection (**7**). Benzyl group removal.

HBr is a common reagent used for ethers cleavage and further studies confirmed that PEG was being degraded under the deprotection conditions used. PEG stability studies under acidic and basic conditions were performed obtaining the GPC profiles overlaid in FIGURE II. 25. This confirmed that HBr/TFA deprotection was not suitable for PEG block copolymers.

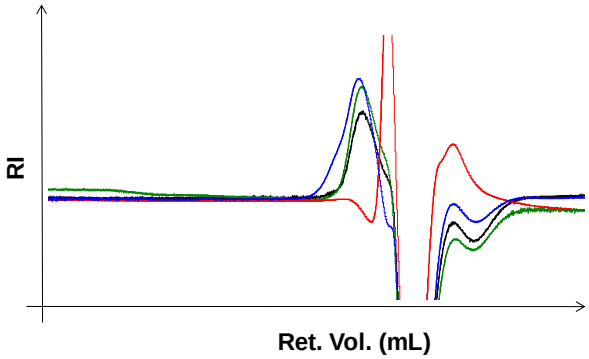

FIGURE II. 25 PEG exposure to deprotection conditions:
(black: non-treated, red: HBr/TFA treatment, blue: Pd/C, green: LiOH)

Deprotection by catalytic hydrogenation

Hydrogenation process was suggested as an alternative for HBr/TFA deprotection. Bz removal was completely achieved for both species (homo- and diblock), however it presented the handicap of charcoal removal afterwards, which ended up with marked low yields (10-30%) and non-pure final products. Several methods were exploited trying to (i) remove the carbon without success (e.g. filtration through celite, centrifugation, ultrafiltration, size exclusion chromatography, etc.) or (ii) revert the probably adsorption of the polymer to the charcoal, that could not be reversed even with

repeated washing steps with AcOH and DMSO. Then, this deprotection method was rejected.

Deprotection under basic conditions: NaOH aq./THF

Hence, we were aiming for a dual purpose with the use of this alternative methodology: to find the suitable mildest basic conditions of benzyl removal that at the same time could maintain PEG integrity. Basic deprotections using LiOH and NaOH were evaluated by subjecting PEG to the selected conditions (see TABLE II. 7). NMR and GPC analysis of the PEG after the exposition were carried out. PEG signals and size were not altered after 5h in NaOH solution (with the theoretical 2 equivalents per Bz group). Under the same conditions, PEG-*b*-PBLG was fully deprotected. From this preliminary study, it was concluded that basic deprotection was an adequate candidate because deprotection was reached and PEG did not resulted damaged.

Searching for the mildest conditions, Kataoka's protocol for PEG-poly(b-benzylaspartate) deprotection [131] was proposed as a model in which the benzyl groups are easily removed by using a solution of NaOH at 0°C during ten minutes. The protocol needs a mixture of organic/aqueous solvents to solubilise either the polymer or the NaOH. For our systems, a ratio of THF/H_2O 8:1 was able to solubilise the reagents. Ten minutes of reaction gave an insoluble product whose ^{1}H-NMR analysis concluded that the deprotection did not occur. For that reason, longer reaction times were evaluated.

In our previous studies (TABLE II. 7), 2eq of NaOH and 5h at 25°C raised to full deprotection in DBs, therefore same parameters were tested decreasing temperature to 4°C. The product was left to react for 5h, the reaction was acidified with acetic acid (glacial) and purified by ultracentrifugation.

Compound	Method	eq. per Bz group	t_R (h)	Bz removal	PEG Integrity[A]	PEG integrity[B]
PEG_{2000}-PGA_{71}	LiOH	4	24	yes	Lower PEG signal	-
PEG_{2000}-PGA_{71}	NaOH	4	24	yes	Lower PEG signal	-
$mPEG_{2000}$	LiOH	4	24	-	New signals	-
$mPEG_{2000}$	NaOH	4	24	-	New signals	-
$mPEG_{2000}$	LiOH	2	7	-	Lower intensity of the new signals	
$mPEG_{2000}$	NaOH	2	7	-	Almost no new signals	-
$mPEG_{20000}$	NaOH	2	5	-	-	Comparable to non treated
PEG_{2000}-PGA_{71}	NaOH	2	5	yes	Comparable PEG signal	-

A=^{1}H-NMR data, B=GPC data

TABLE II. 7 Conditions evaluated for studying PEG integrity under PBLG deprotection.

The product obtained was completely deprotected according to its ^{1}H-NMR. In addition, after comparison of PEG signal before and after deprotection (see FIGURE II. 26), differences were considered no significant. Then, it was concluded that PEG may be not damage under this conditions.

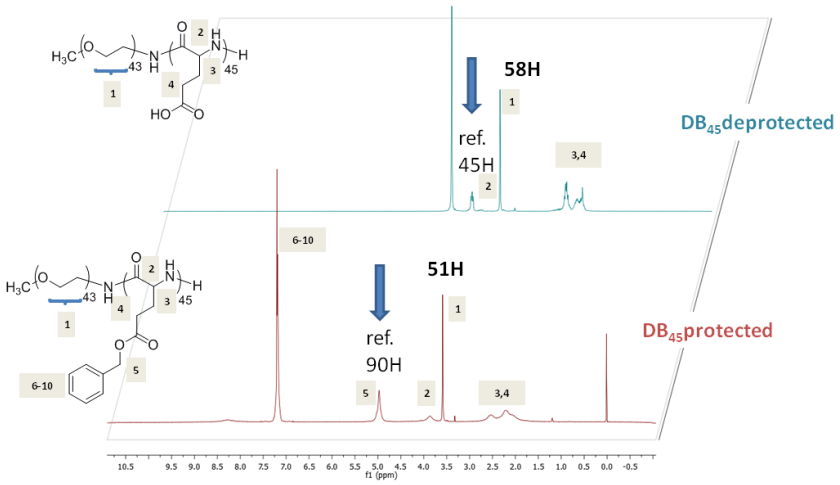

FIGURE II. 26 Evaluation by ^{1}H-NMR of DB deprotection under basic conditions.

a) Optimisation of the basic conditions for Bz removal

(i) Use of homopolymers as starting point

The effectiveness of the basic deprotection was preliminary studied with PGA homopolymers to optimise conditions for Bz removal.

After the studies enumerated in TABLE II. 7, the protocol was modified to find milder conditions. Equivalents of NaOH were decreased and consequently reaction time enhanced (TABLE II. 8). In parallel, this study tried to reveal if under these novel conditions the stereochemistry of the Cα of the polypeptides by deprotonation/protonation equilibrium and isomerisation processes was affected in the final product. It is well reported that the strong basic conditions can influence in the stereochemistry [375, 408]. For that purpose, each deprotected polymer was evaluated to determine its specific rotation ($[\alpha]^{T}_{\lambda}$) value, that was calculated according to the literature with the formula in FIGURE II. 27.

$$[\alpha]^{T}_{\lambda} = \frac{\alpha \cdot 100}{L \cdot c}$$

FIGURE II. 27 Formula for determining the specific rotation [α] of the polypeptide chain. α=observed rotation, L=polarimeter cell length (dm), c=concentration (g/100mL), T=temperature.

Amino acids α-carbon is chiral which confers optical activity. All natural amino acids have an L configuration, which is related to the rotation of the plane of polarised light to the left giving negative alpha values. The rotation degree of polarised light depends on the number of chiral molecules that it encounters through the polarimeter cell. For biocompatibility of our systems, L configuration is desired.

	eq. GA units	**eq. NaOH**	**THF:$H_2$0 ratio (v/v)**	**t (h)**	**α (average)**	**SD**	**%s^2 coeff**	**$[\alpha]^{25}_{\lambda}$**
PBLG	1	1.2	4:1	24	-0.146	0.001	-0.727	-1.46
(45units)	1	1.2	5.3:1	24	-0.283	0.001	-0.473	-2.83
	1	**1.2**	**8:1**	**24**	**-0.311**	**0.001**	**-0.428**	**-3.11**

TABLE II. 8 Optimisation of the THF:H_2O ratio and concentration with 1.2 eq, 24h. SD=standard deviation, coeff=coefficient.

Negative values were assigned to L conformation. In this preliminary study, the most negative value was considered as the best result taking into account the previous statement. Therefore, the ratio 8:1 THF:$H_2$0 was selected for the next study.

Aiming to reduce the reaction time, 16h was evaluated repeating the same conditions than TABLE II. 9. However deprotection was not achieved with 1.2eq of NaOH. For that reason, the equivalents were increased to 1.5 and 16h was maintained this time. The experiments done let us to conclude that deprotection depended on the THF:H_2O ratio, being optimal under 8:1 ratio.

	eq. GA units	eq. NaOH	THF:H_20 ratio (v/v)	t (h)	α (average)	SD	$\%s^2$ coeff	$[\alpha]^{25}_{\lambda}$
PBLG (45units)	1	1.5	64:1	16	*			
	1	1.5	32:1	16	*			
	1	1.5	16:1	16	-0.466	0.002	-0.330	-4.66
	1	**1.5**	**8:1**	**16**	**-0.479**	**0.002**	**-0.345**	**-4.79**
	1	1.5	4:1	16	-0.237	0.001	-0.598	-2.37

*deprotection not achieved.

TABLE II. 9 Optimisation of the THF:H_2O ratio and concentration with 1.5 eq, 16h.

The next study was focused on diminishing the reaction time with 1.5eq of NaOH, once THF:H_2O ratio was fixed. Results are summarised in TABLE II. 10 and 8h were at least needed to achieve PBLG deprotection. However, a more negative alpha value was obtained for 16h reaction.

	eq. GA units	eq. NaOH	THF:H_20 ratio (v/v)	t (h)	α (average)	SD	$\%s^2$ coeff	$[\alpha]^{25}_{\lambda}$
PBLG (45 units)	1	1.5	8:1	2	*			
	1	1.5	8:1	4	*			
	1	1.5	8:1	6	*			
	1	1.5	8:1	8	-0.484	0.003	-0.7586	-4.84
	1	**1.5**	**8:1**	**16**	**-0.615**	**0.002**	**-0.2877**	**-6.15**

*deprotection not achieved.

TABLE II. 10 Time optimising using 8:1 THF:H_2O ratio and 1.5 eq. NaOH.

Therefore, this first study using the homopolymer, let us to conclude that 1.5eq, 16h and the THF:H_20 ratio 8:1 parameters were able to deprotect the polybenzylglutamate, with the highest negative alpha value that we could obtained being around -0,6.

With the purpose of proving that the found conditions were correct regarding non-stereochemical changes along the deprotection, α values of comparable polymers were studied. The selected species were:

(i) A commercial deprotected PGA_n with different GA units (n=100, 200 and 300).

(ii) L-polyglutamates obtained by solid phase peptide synthesis (SPPS). SPPS provide a defined stereochemistry in the polypeptide chain, e.g. L-peptide. Our comparison with these polymers was centered on proving that racemisation did not occur either during polymerisation. The number of linked glutamic acid units obtained through this technique is limited, overall if protected side chains are necessary in the final polypeptide.

(iii) HBr deprotected polyglutamates. As named before, acid deprotection has been demonstrated not to affect to stereochemistry of the initial polymer. This procedure was carried out with our polyglutamates as well as with the SPPS commercial one.

The collected data from each species is compiled in the table below (TABLE II. 11). [α] values from commercial PGA (-5.67, -5.45, -4.85), SPPS PGA (-5.12) and HBr deprotection (-5.55, -5.50) are in the same range that those achieved with our optimised basic deprotection products (-6.15). In addition, it was demonstrated that strong basic conditions affect optical activity as PGA_{15} after treatment with concentrated NaOH gave positive [α] value (0.07).

	α coefficient	SD	%s2 coeff.	$[\alpha]^{25}_{\lambda}$
Other commercial PGAn (n=100units)	-0.567	0.001	-0.2242	-5.67
Other commercial PGAn (n=200units)	-0.545	0.001	-0.243	-5.45
Other commercial PGAn (n=300units)	-0.485	0.002	-0.315	-4.85
PGA_{20} HBr deprotected	-0.555	0.001	-0.210	-5.55
PGA_{15} (SPPS)	-0.512	0.002	-0.357	-5.12
PGA_{15} (SPPS) treated with NaOH 2M, 16h	0.007	0.001	18.470	0.07

TABLE II. 11 Observed rotation for several commercial PGAs in comparison with ROP-NCA synthesised PGA.

As a final corroboration of the basic deprotection versatility, the influence outcome of the polyglutamate Mw was studied. TABLE II. 12 shows the rotation angle coefficient values obtained which confirm that under these conditions polypeptide is fully deprotected independently of the chain length and optical activity remains untouched.

$PBLG_n$	α (average)	SD	$\%s^2$ coeff.	$[\alpha]^{25}_{\lambda}$
n=100	-0.6545	0.0022	-0.3314	-6.55
n=200	-0.6594	0.0019	-0.2868	-6.59
n=400	-0.6643	0.0019	-0.285	-6.64

TABLE II. 12 Comparison of the observed rotation from PGAs with different DP after deprotection with the optimal basic protocol.

Summarising, in all cases yields were quantitative under the named optimal conditions (1.5eq NaOH in 8:1 THF/H_2O ratio, 16h) with complete deprotection without deviations in the specific rotation ($[\alpha]^{T}_{\lambda}$) value of deprotected PGA (TABLE II. 12). Moreover, the $[\alpha]^{T}_{\lambda}$ values were identical to PGA 15mers prepared by SPPS independent from the optimised acidic or basic methodology (FIGURE II. 29).

(ii) Protocol adaptation to diblock copolymers

After establishing deprotection conditions with homopolymers, diblock systems were evaluated with the same protocol. However, the use of 1.5eq of NaOH lead to uncomplete deprotections forcing to start a novel optimisation process.

Using 16h and the ratio 8:1 THF:H_2O settle parameters from homopolymer studies, the equivalents of NaOH were varied. TABLE II. 13 shows how 2, 3 or 4 equivalents managed to deprotect the PGA block giving acceptable [α] values. Therefore, following with the minimal harsh path the lowest value was chosen: 2 eq, even if deprotection yield had to be forfeit.

	eq. NaOH	[NaOH]	α (average)	SD	$\%s^2$ coeff.	$[\alpha]^{25}_{\lambda}$
PEG-*b*-PGA$_n$ (n=45units)	**2**	**0.02**	**-0.551**	**0.002**	**-0.29**	**-5.51**
	3	0.031	-0.51	0.001	-0.292	-5.10
	4	0.041	-0.44	0.005	-0.325	-4.40

TABLE II. 13 Optimisation of the NaOH equivalents for DB deprotection using the same conditions of time and THF/H_2O ratio (16h, 8:1).

In addition when reaction time was increased, the same trend on [α] values was observed (TABLE II. 14).

	eq. NaOH	t (h)	α (average)	SD	$\%s^2$ coeff.	$[\alpha]^{25}_{\lambda}$
PEG-*b*-PGA$_n$ (n=45units)	**2**	**16**	**-0.535**	**0.003**	**-0.468**	**-5.35**
	2	21	-0.517	0.001	-0.283	-5.17
	2	24	-0.494	0.003	-0.648	-4.94

TABLE II. 14 Optimisation of the reaction time for DB deprotection.

Summarising, 2 equivalents of NaOH per carboxyl group, 8:1 THF/H_2O ratio and 16h handled PEG integrity whereas deprotection was successful. As an example, in FIGURE II. 28 the NMR spectrum of DB_{100} deprotected it is shown.

HBr/TFA was selected as simple and effective methodology for homopolymers deprotection, adjustable to the starting amount of polymer. With the procedure described above it was demonstrated that basic deprotection is also affordable with same successful results: avoiding racemisation (FIGURE II. 29(A)), full benzyl group removal (FIGURE II. 29(B)) with quantitative yields and polypeptide stability including secondary structure conformation (FIGURE II. 29(C)). Concerning the diblock co-polymer systems, basic deprotection solved the substantial drawbacks observed in the HBr/TFA protocol enabling to address jointly PEG integrity and benzyl removal.

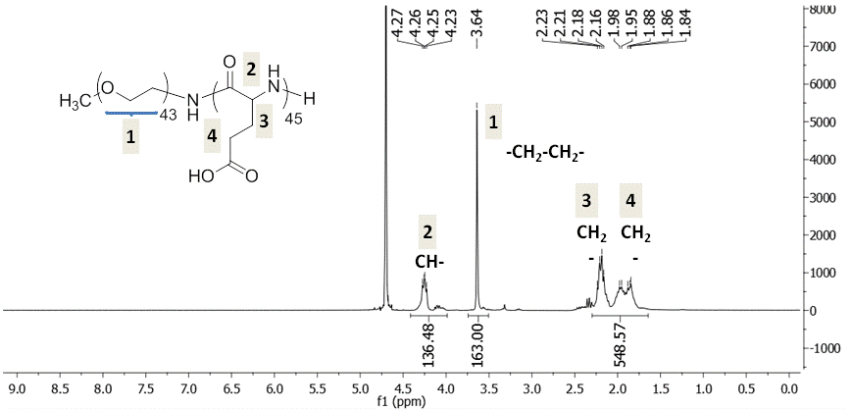

FIGURE II. 28 ^{1}H-NMR (D_2O) spectra of DB_{100} deprotected.

(A)

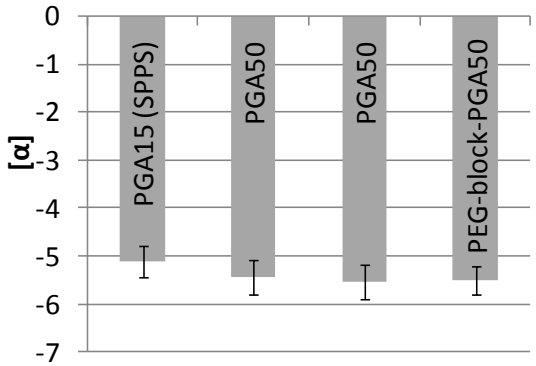

(B)

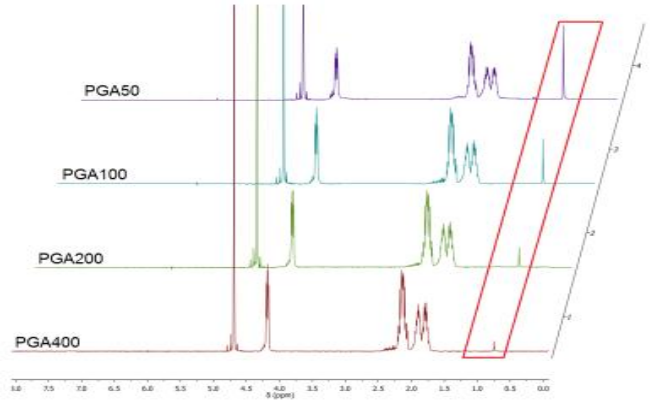

(C)

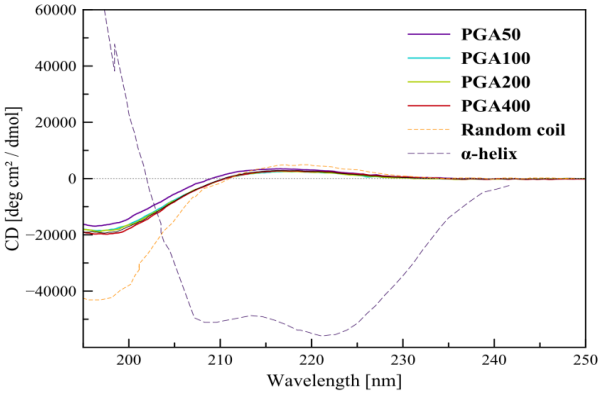

FIGURE II. 29 Deprotection methodology optimised for homopolymers and diblock co-polymers for complete benzyl group removal. (A) Schematic conditions of acidic (1) and basic (2) deprotection methodologies. R represents Neopentyl-, nButyl- or PEG- initiators, *n* is the number of repeating units of the glutamic block. The deprotection methodology was optimised for homopolymers and diblock co-polymers for complete benzyl group removal and non-stereochemical changes. For this last purpose, comparison between the observed rotation [α] was performed analysing a PGA_{15} synthesised by SPPS, PGA_{50} after acidic and basic deprotection and PEG-*b*-PGA_{50} after basic deprotection as it is reflected in the diagram. The formula used for determining the specific rotation of the polypeptide chain was $[\alpha]^{T}_{\lambda} = (\alpha)\cdot 100 / L\cdot c$ where L is the polarimeter cell length (dm), c the sample concentration (g/100 mL) and T the temperature, which was 25 °C. (B) ^{1}H-NMR (D_2O) analysis after deprotection of PBLG with different DP (50, 100, 200 and 400).

In red is pointed out the signal of the initiator used, neopentyl, indicating polymer integrity after deprotection. (C) Circular dichroism (CD) spectra in ddH_2O at 20 °C.

II. 2. 2. 4 Synthesis of the triblock copolymer PEG_1-b-PGA_n-PEG_2 (TB)

With the purpose to synthesise a versatile polymer carrier able to allow a site-specific conjugation for peptide/protein (semitelechelic PGA) together with a multifunctional part for drug linkage to be transported to the brain, a novel system was proposed: an amphiphilic block-copolymer based on PGA and PEG.

The designed versatility and multifunctionality of the proposed polymeric platform could allow the conjugation in the same polymer carrier of (i) a targeting residue (e.g. transferring, monoclonal antibodies, peptides) which habilitates receptor-mediated transport to the brain, (ii) bioactive agent(s) for the selected disease and/or (iii) imaging probes to monitor the *in vitro* or *in vivo* studies.

Following with the chemical part, for the synthesis of this carrier ROP-NCA polymerisation was applied through a PEG initiator as detailed in section II.2.2.1. Once the diblock copolymer was obtained (PEG_{2000}-*b*-PGA_n), a third block consisting on a bifunctional PEG was bound to the amino terminal group of the polypeptide block.

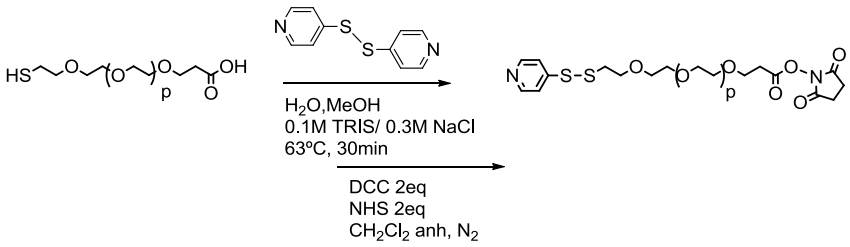

FIGURE II. 30 Derivatisation of the bi-functionalised PEG: SH-PEG-COOH. Scheme of sulfhydryl activation of the followed by NHS activation of the carboxyl group.

PEG derivatisation is shown in FIGURE II. 30. Firstly, PEG vector was deactivated in the present work. On one side, the carboxyl

group was activated with N-hydroxisuccinimide (NHS). This group will favoured amide bond formation with the PGA block. On the other side, PEG presented a sulfhydryl group aiming to confer specificity and selectivity required for the linkage with the targeting ligand/biomolecule through a disulphide bond. To avoid crosslinking and enhance triblock reactivity, 4-thiopyridine (4TP) group was used. Scheme of both activations are pictured in FIGURE II. 30.

COOH-PEG-S-S-4TP was successfully obtained and its identity was confirmed by ^{1}H NMR- signals characteristics from the introduced 4TP group, although Ellman assay (indirect calculation of the existent free SH- groups) and the 4TP test (direct quantification of the released 4TP) were the most appropriated methodologies to verify the activation of the sulfhydryl group. Both assays determined an 85-96% of activation in the final product.

To accomplish the amide bond, reactivity of the PEG carboxyl group was enhanced. This step involved carboxyl group activation with a well established protocol. NHS activation was effectively achieved and the Snyder test gave the percentage of activation which ranged from 80-90%. Once NHS-PEG-S-S-4TP (**13**) was synthesised and characterised, the next step was its conjugation to the PEG-*b*-PGA copolymer (**7**). The methodology used started with the deprotected DBs with different polypeptide block lengths aiming to construct a family of amphiphilic block-copolymers. The general synthetic scheme for triblock (**9**) obtaining is shown in FIGURE II. 31.

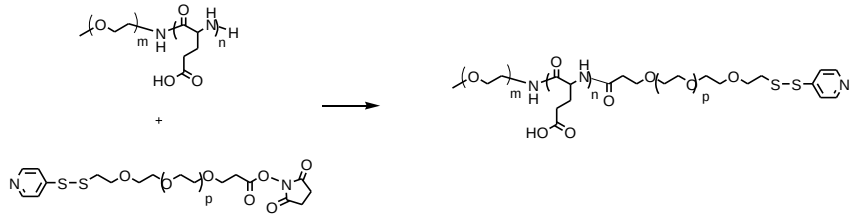

FIGURE II. 31 General scheme for triblock (TB, **9**) copolymer synthesis.

Coupling reaction was carried out in DMF at basic pH as any of the described amide bond formation carried out within this work. For purification, un-reacted PEG was removed by ultrafiltration after

converting the TB to its sodium salt form. Then, the resulting product was passed through a size exclusion column (Sephadex G25) using ddH_2O as eluent. After lyophilising the fractions, identity of each of them was verified by NMR analysis. To determine the degree of PEG introduced, 4TP assay was also performed.

In FIGURE II. 32, ^{1}H-NMR (D_2O) examples of the different TBs synthesised and the percentage of 4TP activation achieved are shown. When comparison among the starting deprotected DB and the obtained TB was done, PEG signal was found out to increase and 4TP presence confirmed the coupling among both polymers. Therefore, TBs (PEG_{200}-PGA_n-PEG_{3400}, **9**) were successfully synthesised and a family of amphiphilic block copolymers (n=100, 150,200) based on PEG and PGA was achieved.

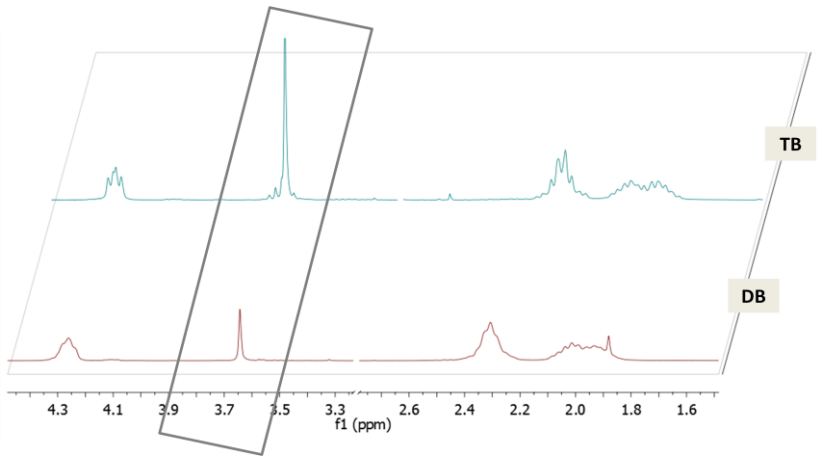

FIGURE II. 32 ^{1}H NMR characterisation of TBs. 1H-NMR comparison of db dep (**7**) and TB (**9**).

Purification steps and unreacted PEG-*b*-*PGA* lead to low yields (30-40%). After the DB synthesis through alternative methods (section II.2.2.3), it was concluded that reaction between protected PGA and PEG in the organic solvent HFIP allowed the coupling of both polymers with high yields. Hence this methodology was proposed as a viable option to increase the yield of the reaction.

II. 2. 2. 5 Other post-polymerisation approaches: incorporation of alkyne and amide functionalities

Polypeptide block allows further functionalisation of the polymer offering multiple options for a unique system. This process is called post-polymerisation and constitutes a useful approach for the synthesis of functional polymers overcoming the limited functional group tolerance of most of the controlled polymerisation techniques [410, 411]. Due to all the advantages of the above described methodology of NCA polymerisation, the post-polymerisation modification of well-defined polyglutamates was only explored focused on the incorporation of functionalities for site-specific conjugation.

With the synthesised homo- and block-copolymers, several modifications have been successfully performed as its reflected in reference [401]. In this process, the carboxyl groups are point of linkage to different molecules which offers a novel pendant group like e.g. alkyne, amino, azide, sulfhydryl group or even act as a spacer among the polymer and the selected moiety, e.g. PEG, a biological responsive peptidic sequence, etc.

In the present thesis, only incorporation of alkyne and amine groups into the PGA chain are described due to their use for fluorescence probe (section III.1.1.1), tracing agent (section III.1.1.2) or peptide ligand (section III.3.2.3) conjugation (note: sulfhydryl groups have been also introduced in this work although from a different starting compound, see section III.3.2.3). Both modifications were chosen to have suitable moieties for a click-chemistry attachment or amide bonding of the corresponding compound with all the benefits that this kind of reactions lead as pointed out in the introduction.

Alkyne modification: Post-polymerisation modification with propargylamine.

PGA post-polymerisation modification with propargylamine was performed as reported by Thompson *et al.*[412] (FIGURE II. 33). The activation of the carboxylic acids within the polymer backbone of PGA was carried out by using 4-(4,6-Dimethoxy-1,3,5-triazin-2-yl)-4-methyl morpholinium chloride (DMTMM·Cl^-).

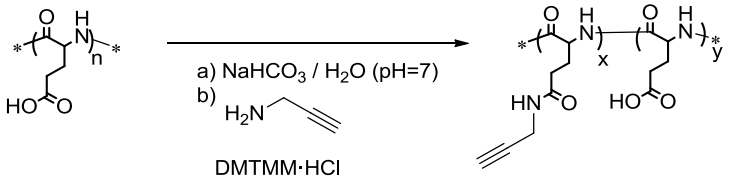

FIGURE II. 33 General scheme of PGA block post-polymerisation modification with propargylamine (**21**).

Afterwards, propargylamine was added into the reaction mixture leading to the corresponding alkyne modified polymer. The mechanism of action of DMTMM·Cl^- is shown in section III.1.1.1, and consists in the formation of the corresponding activated ester with the release of 4-methylmorpholine in a first step. This activated ester reacts with the corresponding amine compound by adjusting the pH of the reacting mixture to 8 in order to favour the amine form of the compound instead of the protonated one that coexist in equilibrium, with non nucleophilic character (FIGURE III. 37, Chapter III). Alkyne content was determined by ^{1}H-NMR analysis. Specifically, the peak at 3.81 ppm corresponds with the two protons of the CH2 of the propargyl residue, and the signal at 2.48 ppm corresponds with the acetylenic proton of the propargyl residue. Thus, in comparison with the protons of PGA, the % of substitution of each polymer was calculated. The usual yield of this reaction gave approximately half of desired percentage. This was taken into account in order obtain the desired percentage in the final polymer. Results are summarised in TABLE II. 15. The resulting Mw of the polymer was calculated taking into account the percentage of modified GA units.

PGA_n	Alkyne Content (calc.)	Alkyne Content (^{1}H-NMR)
n=100	50 %	31 %
n=100	20%	11%

TABLE II. 15 Alkyne modified polyglutamates (**21**).

Amine modification: Post-polymerisation modification with a monoprotected diamine.

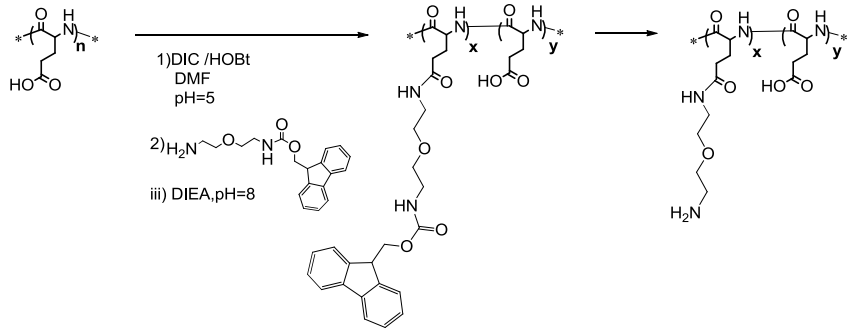

FIGURE II. 34 General scheme of PGA block post-polymerisation modification with amine groups.

The interchange of a carboxylic pendant group by an amine was with a monoprotected diamine: 2-(2(Fmoc-amino)ethoxy)ethylamine. First, COOH groups were preactivated by DIC/HOBt to later coupling of the non protected amine of the diamine. The mechanism of DIC/HOBt coupling is shown in section III.1.1.1. After the reaction time, solvent was evaporated and the residue was washed in a mixture of acetone:chroloform were the polymer remained insoluble but the non-reacted monoprotected diamine was able to be recovered. From this solution, Fmoc absorbance (290nm) was measured and therefore, indirectly calculation of the coupled diamine. An additional estimation was performed after Fmoc deprotection, repeating the operation after the deprotection time. Free Fmoc was again dissolved in the same solvent mixture and

quantified, giving a direct percentage of the inserted amines. TABLE II. 16 shows a compilation of results obtained for TB_{200} (**9**) amine modification.

	%free Fmoc-diamine	**%Fmoc (=diamine grafted)**
TB_{200}	94	6
TB_{200}	70	30

TABLE II. 16 Amine modified polyglutamates (**24**).

An alternative of amine modification is detailed in chapter III section III.3.2.3 (using Boc-diamine) due to the required labelling of the polymer carrier to be used in PET experiments.

II. 3 CONCLUSIONS

The main aim of this first chapter was to develop a robust methodology for synthesising a family of polymers to be used as carriers in the form of polymer-drug conjugates. The biodegradable and biocompatible poly-glutamic acid was the polymeric platform chosen and the ring-opening polymerisation of α-amino acid N-carboxyanhydrides (ROP-NCA) the methodology selected.

This family was constituted by three systems depending on the polymerisation initiator used and the subsequent post-polymerisation process performed: homopolymers (PGA_n), diblock copolymers (PEG-*b*-PGA_n), and triblock copolymers (PEG-PGA_n-PEG). Then within each system the length of the polypeptide block was varied from n=100 to n=800. The reason for this variation was to either observe differences concerning the hydrophilic/hydrophobic ratio among PEG and PGA blocks directly related with conformation in solution and *in vitro/in vivo* properties and/or exploiting the major or minor capacity of loading for drugs/probes.

First, NCA monomer synthesis of y-benzylglutamic acid by means of Fuchs-Farthing method resulted in the obtention of highly pure monomers. Like any impurity as humidity, acid or basic traces could start undesired side reactions, special emphasis was done in their avoidance or removal either in the synthesis or in the purification. Specifically, limonene was used as scavenger agent for the removal of the HCl produced in the monomer system in combination with a bubbling process using an inert gas. Precipitation as well as repeated recrystallisation steps were performed and finally several test (e.g. THF solubility, the melting point and ^{1}H-NMR analysis) were done to identify possible polymerisation. The obtained monomer was well dried and stored under inert atmosphere. In any case, monomer was either freshly synthesised or recrystallised before use to finally ensure a controlled NCA ring opening polymerisation.

Initial polymerisation methodology involved the use of amine initiators and fixed reaction conditions (anh. $CHCl_3$, 25°C, t_R=3days)

while the degree of polymerisation (DP) was varied (200, 400, 800). As result from this, final n=200 was the higher DP achieved and polydispersities ranged between 1.2-1.4. Thus, a new strategy was developed. On one hand, improvement of the technique was optimised by polymerisation under Schlenk conditions, including exhaustively dried reagents, solvents and material together with optimal settings with respect to temperature and reaction time. In order to monitor the NCA conversion, FTIR spectroscopy and GPC were used. With these conditions, control over the reaction was achieved and narrow Mw distribution (Đ=1.01-1.2) were obtained. On the other hand, novel initiators based on ammonium tetrafluoroborates were synthesised and for the first time investigated for polyglutamates obtaining [401]. The comparison study between NH_2 and BF_4 neopentyl initiators concluded that, Mw of polymers were precisely controlled up to a DP of 200 with NH_2 at low temperature or BF_4 at 25°C. When higher Mw was required, only tetrafluoroborate salt initiators achieved the desired DP. Summarising, with BF_4 initiators homopolymers with DP800 and with low dispersity were able to be achieved [401].

The results had shown clearly the benefits of this new developed strategy, consolidated as a very simple methodology. Our novel synthetic approach overcame most of the inherent drawbacks of ROP of NCAs leading to a controlled polymerisation with living nature: control over Mw was achieved as well as over the amino terminal group, like demonstrated latter conjugations with high yields on this site. Additionally, the synthesis was scaled up from milligrams to gram, conserving the control on the Mw and the low polydispersities [401]. As an extra advantage, these novel initiators as nBuBF4 and nptBF4 are obtained as solids (in contrast to their amine form which is liquid) and it facilitates their precise use and consequently a more controlled and predictable degree of polymerisation.

Using PEG as macroinitiator for diblock synthesis: PEG-*b*-PGA_n, low temperatures for the diblock polymers were the best option, with or without BF_4 salts for DP 100 or 200. Probably, when high Mw

diblocks are desired BF_4 salts will be required.

The next step involved the deprotection of the y-benzylpolyglutamates leading to PGA. In the case of homopolymers, acidic deprotection in HBr/TFA as well as basic conditions with the mixture NaOH aq. /THF resulted in successful benzyl group removal without compromising the chiral properties of the chain independently of the length. For simplicity in the protocol and the almost quantitative yields obtained with the HBr/TFA method, it was finally chosen for the deprotection of the homopolymers. Concerning the diblocks, optimisation was successful finding out the most adequate reaction conditions. Acidic deprotection compromised PEG integrity and basic conditions solved this problem achieving full deprotection with acceptable yields. Parameters were optimised with caution and with the main aim of determining the less dangerous conditions for the polymers in terms of sodium hydroxide equivalents and reaction times. Thus, diblocks were safely deprotected without PEG degradation. Along the deprotections, the specific rotation value ($[\alpha]^T_\lambda$) of each polymer was calculated by means of the observed rotation measurement (α). The study pursued the obtaining of the highest negative alpha values, which should correspond to the L conformation of the amino acids. To use them as a reference, several commercial PGAs and acidic PBLG deprotections gave similar values and therefore this parameter was considered as a control and served us to claim the L conformation maintenance after deprotection.

After diblock synthesis and deprotection, a third block was coupled through an amide bond in the N-terminal extreme of the PGA building block giving rise to the triblock copolymer PEG-*b*-PGA-*b*-PEG-S-S-4TP. This PEG played a double function. First and more importantly providing to the whole system a specific point of linkage for probe/targeting ligand conjugation through a disulphide bond. The main problems of the synthesis were the purification steps where diblock, unreacted PEG and final triblock had to be separated. Thus, reaction yields where very low. Secondly these type of polymer structures featuring two PEG blocks with the biodegradable PGA

segment could offer different morphologies and alternative structures respect to the homopolymer or the diblock. Their study may reveal new avenues for drug delivery and different or combined cellular pathway mechanisms.

In parallel, it has been investigated an alternative strategy for the synthesis of DB copolymers based on the incorporation of the PEG block on the already synthesised peptidic block. In this case, the terminal amino group of PGA was used for coupling a PEG block via amide bond, giving the construct PBLG-*b*-PEG-S-S-4TP. The synthesis was performed in aqueous and organic media, achieving higher yields in the latter one. The diblock was successfully deprotected using the optimised basic methodology. The main purpose of the synthesis of these hybrid diblock copolymers was to compare them in terms of *in vitro* and *in vivo* behaviour with the TB (PEG-*b*-PGA-*b*-PEG-S-S-4TP), given that both have the same capacity for conjugation in the polypeptide block and a specific point of linkage in the chain end of the PEG block. The main differences expected from these systems belonged to the conformational point of view, regarding conformation in solution as well as spatial distribution of the linked ligands/probes to the PEG chain-end. These structural characteristics should be reflected in the general in *vitro/in vivo* behaviour of the final compounds.

Finally as it was demonstrated that the use of organic media for DB synthesis succeeded, it is proposed that the TB synthesis from protected DB and using HFIP in order to couple the other PEG chain, could enhance the reaction yield and efficiency, therefore improving the methodology for its obtaining.

After deprotection, post-polymerisation modification approaches with carboxyl pendant groups of the PGA backbone can be performed. This strategy enables to build polymers with different functional groups for specific and orthogonal conjugations. Alkyne, amine and sulfhydryl groups had been easily introduced through carboxyl group activation either with DIC/HOBt or DMTMM coupling

methodologies. These groups were latter used for labeling or targeting ligand specific conjugation (CHAPTER III).

In summary, a novel NCA-ROP methodology through ammonium tetrafluoroborate salts and an optimised deprotection procedure had leaded to the development of a versatile polymeric platform based on the clinically approved PGA, enabling the synthesis of future polymer conjugates.

II. 4 MATERIALS AND METHODS

II. 4. 1 RING-OPENING POLYMERISATION (ROP) OF α-AMINO ACID N-CARBOXYANHYDRIDES (NCAS). FIRST METHODOLOGY.

II. 4. 1. 1 NCA monomer synthesis. Synthesis of ɤ-Benzyl L-Glutamate N-Carboxyanhydride (NCA) (2).

Monomer synthesis protocol was reproduced from reference [399] and reproduced with some modifications detailed below. The general synthesis of NCA monomer (**2**) is depicted in

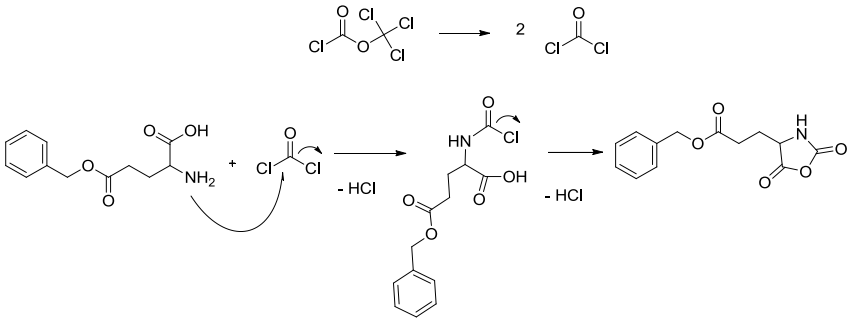

FIGURE II. 4FIGURE II. 4.

H-L-Glu(OBzl)-OH (**1**) (8.43mmol, 1eq, 237.26 g/mol) was placed in a 2-neck 25mL round bottom flask and anhydrous THF freshly distilled was added (25mL). A reflux column was placed and the mixture was stirred and heated up to 50°C under a N_2 atm. Then, 0.5eq of trisphosgene (4.2mmol, 296.75 g/mol) was weighted and dissolved in anh. THF freshly distilled (3mL). Once dissolved, it was added under a N_2 atm with a glassware syringe. The reaction was left stirring for 3 h at 50°C under a N_2 atm. (completed solution was observed after 1 h of reaction). Afterwards, reaction solvent was evaporated under vacuum to the fourth of its initial volume and obtained residue was diluted with anhydrous ethyl acetate (16mL). The filtrate was then precipitated from THF/ ethyl acetate into fresh hexane (120mL) and filtered under vacuum. The white solid was precipitated following the described protocol twice more. Finally, the white solid obtained was dried under N_2 flow and used immediately.

Yield: 87%, m.p.: 92.5-94°C, ^{1}H-NMR (DMSO-d_6):δ (ppm) 2.01 (2H, m), 3.31 (2H, s), 4.48 (1H, t), 5.10 (2H, s), 7.37 (5H, s) 9.10 (1H, s).

II. 4. 1. 2 General procedure for NCA polymerisation. Synthesis of poly-ɤ-Benzyl L-Glutamate.

HOMOPOLYMER (nBuPBLG$_n$)

The general synthesis of nBu-PGA homopolymer (**3**) is depicted in FIGURE II. 7.

2g of NCA monomer (**2**) (7.5 mmol, 264 g/mol) were placed in a 100mL round bottom flask. After purging with N_2 flow, monomer was dissolved under agitation with anh. CH_2Cl_2 (30mL). Then, a stock solution of the initiator in anh. CH_2Cl_2 (n-butylamine (0.738g/cm^3, 73.14g/mol) was prepared and calculated equivalents were added into the monomer solution. Reaction was maintained in an inert atmosphere with an outlet for CO_2 escape. After 3days in agitation at 25°C, the content was poured into fresh diethyl ether (400mL) and white solid obtained was collected after centrifugation ((2600rpm, 4°C, 10min). Product was dried at 40°C under vacuum for 16h. The product obtained was analysed by GPC (DMF, 0.1%LiBr) (FIGURE II. 15) and by ^{1}H-NMR ($CDCl_3$) (FIGURE II. 16).

Yield: 85-92 %, ^{1}H-NMR (300 MHz, $CDCl_3$) δ 7.19 (d, *J*=3.3 Hz, 5H), 4.98 (s, 2H), 3.88 (s, 1H), 2.95 – 1.38 (m, 4H), 0.81 (d, *J*=7.3 Hz).

e.g. nBu initiated PBLG$_{100}$: ^{1}H NMR (300 MHz, $CDCl_3$), δ 7.19 (d, *J*=3.3 Hz, 5H), 4.98 (s, 2H), 3.88 (s, 1H), 2.95 – 1.38 (m, 4H), 0.81 (d, *J*=7.3 Hz, 0.03H).

DIBLOCK (DB$_n$, PEG-b-PGA$_n$)

The general synthesis of DB (**6**) is depicted in FIGURE II. 8.

1g of NCA monomer (**2**) (3.8 mmol, 264 g/mol) were placed in a 25mL round bottom flask. After purging with N_2 flow, monomer was dissolved under agitation with anh. $CHCl_3$ (20mL). Then, a stock solution of the initiator in anh. $CHCl_3$ (MeO-PEG-NH_2, 1892g/mol) was prepared and calculated equivalents were added into the monomer solution. Then contents were preserved in an inert atmosphere with an outlet for CO_2 escape. After 3days in agitation at 25°C, solution was

precipitated into fresh diethyl ether (200mL) and white solid obtained was collected after centrifugation ((2600rpm, 4°C, 10min). Solid was washed several times with ddH_2O and afterwards dried at 40°C under vacuum for 16h. The product obtained was analysed by GPC (DMF, 0.1%LiBr) and by ^{1}H-NMR ($CDCl_3$).

Yield: 53-91%, ^{1}H-NMR (300 MHz, DMF) δ 8.62 (s, 1H), 7.47 (s, 5H), 5.23 (dd, *J*=21.8, 12.5 Hz, 2H), 4.24 (s, 1H), 3.56 (s, xH), 2.43 (d, *J*=52.9 Hz, 4H).

II. 4. 1. 3 Deprotection of poly(ɤ-benzyl-L-glutamate). Hydrogen bromide in TFA.

HOMOPOYMER ($nBuPGA_n$)

The general deprotection of PBLG is depicted in FIGURE II. 22.

In a round bottom flask, poly(*γ*-benzyl-L-glutamate (1.25g, 5.69mmol Glu units, average MW unit=219g/mol) was dissolved in TFA under agitation at 25°C. After product dissolving, 4eq (per benzyl group) of HBr (33%v/v, 1.49g/mol,81g/mol) were added drop by drop. Once glass stopper was placed, yellow mixture was left stirring for 16h. Afterwards, solution was precipitated in a large excess of diethyl ether and white solid in suspension was recovered by centrifugation (2600rpm, 4°C, 10min). Solid was washed per triplicate with fresh diethyl ether. Finally, the product was dried under high vacuum and deprotection success was checked by ^{1}H-NMR ($CDCl_3$, DMSO-d^6).

If product was needed in its sodium salt, ddH_2O was added together with $NaHCO_3$ and vortexed until complete solution was observed. For salt excess removal, product was purified by dialysis or ultrafiltration (MWCO=1000-3000Da) with ddH_2O. ^{1}H-NMR (D_2O) analysis was performed. Finally, to get again the acid form if needed, the product was then precipitated by dropwise addition of HCl 6M up to a final pH equal to 3.

Yield: 80-90%, ^{1}H-NMR (300 MHz, D_2O) δ: 4.31-4.26 (m, 1H), 2.38-2.14 (m, 2H) 2.10-1.80 (m, 2H) 2.10-1.80 (m, 2H).

DIBLOCK (PEG- b-PGA$_n$)

The general deprotection of DB is depicted in FIGURE II. 24, obtaining the PEG-*b*-PGA$_n$ copolymer (**7**). Diblock deprotection was carried out as homopolymer described protocol.

Yield: 40-65%, ^{1}H NMR (300 MHz, D_2O) δ (ppm) 4.16 (1H, t), 1.76-1.89 (2H, m), 2.13 (2H, m), 3.45 (xH, s), i.e. DB_{100} δ (ppm) 1.76-1.89 (200H, m), 2.13 (200H, m), 3.45 (172H, s), 4.16 (100H, t).

II. 4. 1. 4 Synthesis of the diblock PGA$_n$-PEG

The alternative diblock PGA$_n$-PEG (**5**) synthesis is depicted in FIGURE II. 20.

Method A

In a round bottom flask, 100 mg of PGA as its carboxylic form (14.6mmol, 1eq, 13674g/mol) were dissolved in anh. DMF under agitation and N_2 flow. In a vial, NHS-PEG-SS-4TP (**13**) (11mmol, 1.5eq, 3357g/mol) was dissolved in minimum amount of anh DMF under N_2 flow and added to main solution. pH was adjusted to 8 with DIEA. Reaction was allowed to proceed stirring for 72h under inert atmosphere at 25°C. Solvent was removed under vacuum and the obtained residue was dissolved in $NaHCO_3$ for purification. Firstly, crude was ultrafiltrated (Vivaspin®, MWCO=3000Da, 60mL ddH_2O), and after concentrate the upper part, this was purified through a size exclusion column (Sephadex G25). 50 fractions of 2mL were collected and lyophilised. For product identification, 4TP assay and ^{1}H-NMR analysis of the resultant products was performed. For complete unreacted PEG removal, ultrafiltration was carried out with the appropriate MW cut off.

Yield: 40-60%, 4TP activation: 94%, ^{1}H-NMR (300 MHz, D_2O): δ (ppm) 1.76-1.89 (2H, m), 2.13 (2H, m), 3.45 (xH, s), 4.16 (1H, t), 7.60 (zH, d) 8.40 (zH, s).

(PEG proton signals (x and z) depended on DP of the PGA block and the

yield of the coupling reaction, i.e. DB_{100} (PGA_{100}-PEG-S-S-4TP) with 60% third block coupling: δ (ppm) 1.76-1.89 (2H, m), 2.13 (2H, m), 3.45 (1.69H, s), 4.16 (1H, t), 7.60 (0.012H, d) 8.40 (0.012H, s).

Method B

In a round bottom flask, 100 mg of PBLG (92 GA units, 0.005mmol, 1eq, 20200g/mol) were dissolved in hexafluoro-2-propanol HFIP (10mL) under agitation. In a vial, NHS-PEG-SS-4TP (0.006mmol, 1.3eq, 3219g/mol) was dissolved in 2mL of HFIP and added to main solution. Reaction was left to proceed for 72h under inert atmosphere at 40°C (oil bath). Then, volume of reaction was precipitated into cold diethylether and washed twice. For product identification, ^{1}H-NMR analysis of the resultant products was performed.

Yield: 90%, ^{1}H-NMR (300 MHz, DMF) δ 8.62 (s, 1H), 7.47 (s, 5H), 5.23 (dd, *J*=21.8, 12.5 Hz, 2H), 4.24 (s, 1H), 3.56 (s, xH), 2.43 (d, *J*=52.9 Hz, 4H).

Note: This protocol required further deprotection of the PBLG block. The process was carried out under the optimised NaOH aq/THF conditions explained in section II.4.2.5. Yield: 85%

II. 4. 1. 5 Synthesis of the copolymer PEG_1-b-PGA_n-PEG_2 (TB)

The general synthesis of TB (**7**) is depicted in FIGURE II. 31.

After obtaining the amphiphilic diblock-*co*-polymers constituted by polyethylenglycol (PEG) and polyglutamic acid (PGA), N-terminal end of the polypeptide block allows the conjugation of a third block. In this project, this opportunity has been used by coupling a third PEG block with a specific terminal group: an activated sulfhydryl, 4TP. It confers the system a determined linking point for antibody, protein or peptide as targeting moiety through a disulfide bound.

Methodology for derivation of the third PEG block.

The general procedure of PEG derivation is depicted in FIGURE II. 30.

a) Sulfhydryl group activation of SH-PEG-COOH: 4TP-PEG-COOH (12)

In a 25mL round bottom flask, COOH-PEG-SH (0.158mol, 1eq, 3163g/mol) was dissolved in 2mL of ddH_2O. 4,4'-dipyridyl-disulfide (3.16mol, 20eq, 222.73g/mol) was also dissolved in 2mL of MeOH and added dropwised into the main solution. Then, 3mL of TRIS buffer 0.1M / NaCl 0.3M (pH=10) were added and the reaction was stirred at 65°C for 30min under a reflux column. The product was purified through a Sephadex G-25 column using acetic acid 0.1N as eluent. 50 aliquots of 2mL each were collected and freeze-dried. Product identity was confirmed by ^{1}H-NMR, by an indirect Ellman's assay looking at unreacted SH groups and a direct test through 4TP release.

Yield: 57%, 4TP activation: 85-96%

b) Characterisation of the activated SH group: 4TP

Ellman's assay

Ellman test determines the number or concentration of free thiols in a sample. Ellman's reagent, 5,5´-dithiobis(2-nitrobenzoic acid) (DTNB), rapidly reacts by means of a estequiometric interchange thiol-disulphide in presence of free thiol in media. Thiols react with DTNB by cleaving its disulphide bond and releasing 2-nitro-5-thiobenzoate (NTB^-), which ionizes to the NTB^{2-} dianion in water at neutral and alkaline pH. This NTB^{2-} ion has a yellow color (λ=412nm). Reaction is highly sensitive to pH conditions, oxygen and temperature. Consequently, this test is performed with an excess of DTNB at neutral pH and fixed T. To carry the experiment, two stock solutions were prepared and placed on ice: (i) DTNB solution: 3mM DTNB, 50mM in sodium acetate (ddH_2O) and (ii) TRIS solution 1M pH=8.

Firstly, a calibration curve was done using as standard 2-aminoethanethiol (FIGURE II. 35), ranging concentrations from 10 to 100µM.

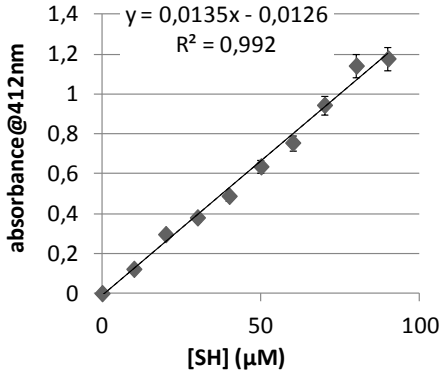

FIGURE II. 35 Calibration curve for the Ellman test.

In a quartz cuvette, 50µL DTNB stock, 100µL TRIS stock, 840µL ddH_2O and 10µL of the sample in solution were well homogenised. After 30min incubation, absorbance at 412nm was acquired. Concentration of thiol groups was calculated by means of the calibration curve of the standard and the stechiometry of the reaction.

4TP release content measurement

The 4TP group was found to react readily in the presence of free thiols [413] under mild conditions at neutral pH. The reaction can be monitored by the absorbance at 323nm, corresponding to the 4-thiopyridone leaving group.

For carrying out the test, a sample stock 2mM in ddH_2O was prepared. As –SH reagent, 2-aminoethanethiol was selected and a stock 91mM in ddH_2O was set.

In a quartz cuvette it was added: 200µL of sample stock, 200µL of the –SH reagent sock and 1.2mL of potassium phosphate buffer 0.1M pH=7. Absorbance at 323nm was measured. $\varepsilon_{4TP}=1.98x10^4 M^{-1}cm^{-1}$ [414] .

c) NHS activation of the carboxyl group. Obtaining of 4TP-PEG-NHS (13)

In a 25mL round bottom flask, COOH-PEG-SS-4TP (**13**) (0.086mol, 1eq, 3273g/mol) was added and purged under N_2 flow. Then, it was dissolved in 6mL of anh. CH_2Cl_2 under inert atmosphere at 25°C. DCC (0.18mol, 2eq, 203.33g/mol) was added under N_2 flow. The reaction was left to proceed for 10min. After that time, NHS (0.179mol, 2eq, 115.09g/mol) was dissolved in 4mL of anh. CH_2Cl_2 in a purged vial. When NHS solution was incorporated into the main reaction, turbidity appeared due to the formation of the urea derivative. The reaction was left stirring for 5h at rt. Afterwards, the solution was filtered out and poured in cold diethyl ether to remove DCC excess. A pale yellow product was obtained and dried under high vacuum. TNBS assay was used to determine activation degree of the desired NHS-PEG-SS-4TP.

Yield: 84%, activation: 87%.

d) Quantification of carboxyl group activation by TNBS assay

TNBS test according to the Snyder and Sabocinsky assay [415] was performed to measured the degree of activation of the carboxyl end groups of PEG.

As amine-bearing regent, a solution 10X of the dipeptide Gly-Gly in borate buffer 0.1M pH=8 (0.0216mmol/mL, 132.12g/mol) was prepared. Solution 1X was obtained by a dilution 1:10 in borate buffer, achieving the 0.00215mmol/mL desired solution. An equimolar mass of the sample (NHS-PEG-SS-4TP, 3357g/mol) was prepared. For that, 7.2mg of bifunctionalised PEG were dissolved in 1m of the Gly-Gly stock. The reaction was left to proceed for 30min (*reaction solution*). TNBS (5% m/v, 293.17g/mol) solution was also prepared in a concentration of 7.34mg/mL in ddH_2O.

In plastic cuvettes, the following solutions (TABLE II. 17) were prepared per duplicate. After homogenisation, they were left 30min protected from light. Finally, absorbance in UV at 420nm was measured. The degree of activation was calculated as:

$$\%activation = 100 - \left(abs_{(SAMPLE)} \cdot \frac{100}{abs_{(REF)}} \right)$$

where $abs_{(SAMPLE)}$ is the absorbance of the reaction mixture and $abs_{(REF)}$ is the absorbance of the Gly-Gly stock solution.

	Buffer (µL)	TNBS solution (µL)	Gly-Gly solution 1X (µL)	*Reaction Solution*(µL)
Blank	975	25	0	0
Sample	950	25	0	25
Reference	950	25	25	0

TABLE II. 17 Reagent and buffer amounts for each sample in the TNBS test.

Third PEG block conjugation. Methodology for triblock (TB) synthesis.

The general synthesis of TB (**9**) is depicted in FIGURE II. 31.

In a 50mL round bottom flask is placed 1eq of diblock previously deprotected (**6**) (0.031mmol, mPEG-PGA_n, e.g. n=109 GA units, 15953g/mol), dissolved in anh. DMF (10 mL) and purged with N_2. In parallel, 1.3eq of NHS-PEG-SS-4TP (**13**) (0.041mmol, 3357g/mol) was dissolved in anh. DMF and under N_2 flow before being added to the reaction mixture. The pH was adjusted to 8 with DIEA. The reaction was allowed to proceed under inert atmosphere at 25°C for 3 days. Thereafter, the flask was placed under high vacuum to remove the solvent. The solid residue was dissolved with the minimum amount of $NaHCO_3$ 1M and ultrafiltered (Vivaspin®, MWCO=5000Dal) with ddH_2O for PEG excess removal and purified with a G-25 Sephadex™ column (eluent: ddH_2O). The fractions were freeze-dried and product identity was performed by NMR analysis as well as the 4TP release assay.

Yield: 35%, ^{1}H-NMR (300 MHz, D_2O): δ (ppm) 1.76-1.89 (2H, m), 2.13 (2H, m), 3.45 (xH, s), 4.16 (1H, t), 7.60 (zH, d) 8.40 (zH, s).

(PEG proton signals (x and z) were related to the each single specie, i.e. TB_{200} with 100% third block coupling: δ (ppm) 1.76-1.89 (400H, m), 2.13 (400H, m), 3.45 (455H, s), 4.16 (200H, t), 7.60 (2H, d) 8.40 (2H, s),

activation: 85-96%.

II. 4. 2 RING-OPENING POLYMERISATION (ROP) OF α-AMINO ACID N-CARBOXYANHYDRIDES (NCAs). SECOND METHODOLOGY

II. 4. 2. 1 NCA monomer synthesis. Synthesis of ɤ-Benzyl L-Glutamate N-Carboxyanhydride (NCA).

The general synthesis of NCA monomer (**2**) is depicted in FIGURE II. 4.

Protocol from N.M.B Smeets *et al*. [416] was used as template, although several modifications were performed with the aim of increasing the purity and stability of the monomer, critical parameter for NCA polymerisation. The product was analysed by ^{1}H-NMR, IR and melting point which confirms its identity and purity.

H-L-Glu(OBzl)-OH (**1**)(71.7mmol, 1eq, 237.26g/mol) was added to a 2-neck 500mL round bottom flask fitted with a reflux column and a dropping funnel under nitrogen flow. System was purged and then freshly distilled anh. THF (150mL) was added and the contents were heated to 50^{o}C under constant agitation. Limonene (71.5mmol, 1eq, 0.84g/cm^{3},136.24g/mol) was added to the stirring suspension. Afterwards, diphosgene (0.043mmol, 0.6eq, 1.6525g/cm^{3}, 197.83g/mol) diluted in anh. THF (10mL) was added dropwise via an addition funnel. The reaction was left stirring for 2h at 50^{o}C whilst purging with nitrogen. Afterwards, reaction mixture was bubbled with nitrogen to aid the removal of HCl for 2h whilst the nitrogen outlet was directed through a NaOH 1M solution to neutralise the gas. Then, solvent was evaporated under vacuum to the fourth of its initial volume and then ethyl acetate (16mL) was added. Mixture was precipitated into cold hexane (500mL) giving a white precipitate, which was isolated by vacuum filtration and washed with cold hexane. Solid was recrystallised from anh. toluene (60mL) and THF (30mL, anhydrous) where crystallisation was induced by the dropwise addition of hexane. When precipitation was observed the product was left overnight in an inert atmosphere at -20^{o}C. The crystals were filtered and washed with cold hexane and then dried under vacuum.

Recrystallisation was repeated twice. Absence of HCl traces was ensured by dissolving the obtained product (2-4mg) in minimum amount of THF and added dropwise to a 0.1mmol silver nitrate solution (1mL). No precipitation was observed when pure. ^{1}H-NMR and melting point analysis confirmed product identity and purity.

Note: synthesis scalable up to 34g of starting material.

Yield: 87%, m.p. 93-94^{o}C, ^{1}H-NMR: ($CDCl_3$, 300MHz, 235et): δ=2.00-2.30 (m, 2H, CH_2CH_2), 2.52-2.60 (m, 2H, $CHCH_2$), 4.30-4.34 (m, 1H, CH), 5.09 (s, 2H, OCH_2), 6.40 (s, 1H, NH), 7.30 (m, 5H, Ph), ^{13}C-NMR: (CDCl3, ppm):δ=27.5, 30.6, 57.6, 67.8, 129.2, 129.4, 129.5, 135.9, 152.4, 170.2, 173.3.

II. 4. 2. 2 Methodology for BF_4^- ammonium salts preparation.

Synthesis of tetrafluoroborate n-butylammonium salt

Synthesis scheme of nBuBF4 salt (**14**) is drawn in FIGURE II. 9.

Butylamine (2.7mmol, 73.14g/mol) was dissolved in diethyl ether (1mL), and tetrafluoroboric acid diethyl ether complex $HBF_4.Et_2O$ (2.7mmol, 1.18g/cm^3, 161.93g/mol) was added dropwise to the solution leading to the formation of a white solid salt. Product was dried under vacuum and recrystallised from ethylacetate.

Yield: 60%, ^{1}H-NMR (300 MHz, DMSO) δ 7.58 (s, 3H), 2.84 – 2.71 (m, 2H), 1.56 – 1.43 (m, 2H), 1.39 – 1.25 (m, 2H), 0.89 (t, *J*=7.3 Hz, 3H). ^{13}C-NMR (300 MHz, DMSO-d_6) δ = 38.64, 29.09, 19.08, 13.49.

Synthesis of tetrafluoroborate neopentylammonium salt

Synthesis scheme of nptBF4 salt (**15**) is drawn in FIGURE II. 9.In a 15mL vial, neopentylamine (36.74mmol, 0.745g/cm^3, 87.16g/mol) was dropwise added over 5mL of $HBF_4{\cdot}Et_2O$ (34.5mmol, 1.18g/cm^3, 161.93g/mol), resulting in a white solid formation. Solvent was evaporated and solid was recrystallised twice from ethyl acetate and washed with cold hexane after filtration. Final product was dried

under vacuum.

Yield: 42%, ^{1}H-NMR (300 MHz, DMSO-d_6) δ=7.53 (s, 3H), 3.25 (s, 2H), 0.87 (s, 9H). 13C NMR (300 MHz, DMSO) δ=49.94, 30.21, 26.78.

Synthesis of tetrafluoroborate PEG ammonium salt

Synthesis scheme of mPEGBF4 salt (**16**) is drawn in FIGURE II. 9. In a 5mL round bottom flask, MeO-PEG(2000)-amine (0.3mmol, 1910g/mol) was dissolved in THF (3mL), and $HBF_4.Et_2O$ (0.3mmol, 1.18g/cm^3, 161.93g/mol) was added to the solution leading to the formation of a pale yellow salt. Solvent was evaporated and the solid residue was washed three times with hexane (washes were repeated until pH was not acidic). The obtained solid was dried under high vacuum and NMR analysis (^{1}H and ^{19}F) were performed to achieve identify.

Yield: quantitative, ^{1}H-NMR (300 MHz, DMSO-*d*6):δ (ppm): 7.69 (s, 3H), 3.78 – 3.70 (m, 2H), 3.52 (d, *J*=5.4 Hz, 139H), 3.47 – 3.39 (m, 6H), 3.24 (s, 3H), 3.06 – 2.91 (m, 2H).

II. 4. 2. 3 General procedure for NCA polymerisation. Synthesis of poly-ɤ-Benzyl L-Glutamate.

Material used for polymerisation was exhaustively cleaned before use. All devices (Schlenk tube, stirring bar, stopper) were placed first in DMF (rinsed with acetone), then in diluted H_2O_2 and finally rinsed with ddH_2O. Afterwards, material was dried 24h at 80°C. All solvents used were recently distilled and over molecular sieve and inert atmosphere (Ar). Initiators were dried under vacuum before use and monomer was freshly distilled and well dried.

Synthesis scheme of x-PBLG (**3** and **10**) is drawn in FIGURE II. 7.

1g of NCA monomer (**2**) (3.8mmol, 264 g/mol) was added to a Schlenk tube and purged with cycles of vacuum/Ar. Then, under Ar flow, anh. DMF (freshly purified) was added (concentration: 0.1g/mL). Once dissolved, initiator was added and reaction was left stirring under Ar/N_2 atmosphere with constant pressure. Reaction was monitored with GPC by MW and with FTIR by monomer signals

disappearance. When reaction stopped, solution was precipitated in cold diethyl ether (50mL) and the obtained mixture was centrifuged (2600rpm, 4°C, 10min). Supernatant was removed and the white solid was then suspended in ddH_2O and freeze-dried. The product obtained was analysed by GPC (DMF, 0.1%LiBr) and by ^{1}H-NMR.

PBLG homopolymer: ^{1}H-NMR (300 MHz, DMF) δ 8.58 (s, 1H), 7.42 (s, 5H), 5.19 (s, 2H), 4.21 (s, 1H), 2.81 (s, 2H), 2.45 (s, 2H). ^{13}C-NMR (101 MHz, DMF) δ 175.94 (s), 172.26 (s), 162.77– 162.18 (m), 161.98 (s), 136.76 (s), 128.87 – 127.75 (m), 66.05 (s), 57.13 (s), 35.41 - 34.17 (m), 32.48 (s) , 30.84, 30.30 – 29.04 (m), 27.28 (s), 25.99 (s). Npt initiated $PBLG_{100}$: ^{1}H NMR (400 MHz, $CDCl_3$) δ 7.27 (s, 208H), 4.93 (t, *J*=65.8 Hz, 65H), 3.94 (s, 13H), 3.14 – 1.44 (m, 82H), 0.89 (s, 2H).

PEG-*b*-$PBLG_n$: ^{1}H-NMR (300 MHz, DMF) δ 8.62 (s, 1H), 7.47 (s, 5H), 5.23 (dd, *J*=21.8, 12.5 Hz, 2H), 4.24 (s, 1H), 3.56 (s, xH), 2.43 (d, *J*=52.9 Hz, 4H).

II. 4. 2. 4 Optimisation study for diblock PEG-b-PGA_n synthesis. Comparison between NH_2- and BF_4-.

In order to establish the best conditions for the synthesis of PEG-*b*-PGA diblock, an optimisation study was performed. TABLE II. 5 describes the variety of conditions tested, which included: initiators, temperature and solvent. The synthetic steps followed have been already described in section II.4.2.3.

II. 4. 2. 5 Deprotection of poly(ɤ-benzyl-L-glutamate).

The general deprotection of x-PBLG is depicted in FIGURE II. 22.

Deprotection of poly(ɤ-benzyl-L-glutamate) with HBr in trifluoroacetic acid. Optimal conditions

100mg of poly-ɤ-benzyl-L-glutamate (**3**, **10**) were dissolved in 3mL TFA (TFA volume should be enough to dissolve the polymer and not precipitate after HBr addition) in a round bottom flask. Once dissolved, 2eq of HBr (48%v/v, 1.49g/cm^3, 81g/mol) per carboxylic

group were added dropwise. Then, a glass stopper was placed and yellow mixture was left stirring for 5h. Note: For large scale deprotection of PBLG (>600mg), 16h were needed to achieve full deprotection. Then, the solution was poured into a large excess of cold diethyl ether leading to a white solid that was recovered after centrifugation (2600rpm, 4°C, 10min). The product (**4** or **11**) was washed (3x) with diethyl ether and dried over high vacuum. After that, the product was then purified by acid-base precipitation ($NaHCO_3$ /HCl 6M). Dialysis or ultrafiltration was done leading to the sodium salt form.

Yield: 75-86%, ^{1}H-NMR (300 MHz, D_2O) δ: 4.31-4.26 (m, 1H), 2.38-2.14 (m, 2H) 2.10-1.80 (m, 2H) 2.10-1.80 (m, 2H).

Deprotection by reduction with Palladium/charcoal

Poly(*γ*-benzyl-L-glutamate) or DB (100-200mg) was dissolved in DMF dist. (6mg/mL) under inert conditions (N_2 flow). The, catalytic amount of palladium on charcoal was added and the flask was again purged. The solution was placed in a hydrogen atmosphere and left under agitation for 24h at 25°C. The charcoal was removed by filtration through Celite®. Solution obtained was concentrated under high vacuum and after ddH_2O addition freeze-dried.

Yield: 10-30%, PGA homopolymer: ^{1}H-NMR (300 MHz, D_2O) δ: 4.31-4.26 (m, 1H), 2.38-2.14 (m, 2H) 2.10-1.80 (m, 2H) 2.10-1.80 (m, 2H).

Basic deprotection with NaOH aq./THF mixture. Optimal conditions

HOMOPOLYMER

In a round bottom flask, PGA (5.1µmol, 9761g/mol, n=45 GA units) was dissolved in THF (16mL) at room temperature. Then, the solution was cool down up to 4°C and maintained in agitation. In a vial, 1.5eq of NaOH per carboxylic group (7.7µmol, 40g/mol) were dissolved in 2mL of ddH_2O and then added dropwise to the main solution. Turbidity was found after NaOH addition. The solutions were left under vigorous stirring for 16h. Afterwards, THF was evaporated and the residue was diluted with ddH_2O, purified and concentrated by

ultrafiltration (Vivaspin®, 3000Da). Upper part of the tube was freeze-dried yielding a white solid that was analysed by NMR (D_2O).

Yield: 40-60%, PGA homopolymer: ^{1}H-NMR (300 MHz, D_2O) δ: 4.31-4.26 (m, 1H), 2.38-2.14 (m, 2H) 2.10-1.80 (m, 2H) 2.10-1.80 (m, 2H)

DIBLOCK

In a 50mL round bottom flask, protected diblock (0.184mmol, 12208 g/mol, n=47 GA units) was dissolved in 16mL of THF at room temperature. Then, the solution was cool down up to 4°C and stirred. In a vial, 2eq of NaOH per carboxylic group of the polypeptide block (0.369mol, 40g/mol) were dissolved in 2mL of ddH_2O and then added dropwise to the main solution. Turbidity was found after NaOH addition. The solutions were left under vigorous stirring for 16h. Afterwards, THF was evaporated and the residue was diluted with ddH_2O, purified and concentrated by ultrafiltration (Vivaspin®, 3000Da). Upper part of the tube was freeze-dried yielding a white solid that was analysed by NMR (D_2O).

Yield: 40-70%, ^{1}H NMR (300 MHz, D_2O) δ (ppm) 4.16 (1H, t), 1.76-1.89 (2H, m), 2.13 (2H, m), 3.45 (xH, s), i.e. DB_{50} δ (ppm) 1.76-1.89 (100H, m), 2.13 (100H, m), 3.45 (172H, s), 4.16 (50H, t).

Optimisation for NaOH aq/ THF deprotection study

50mg of polymer (PGA or PEG-*b*-PGA, TABLE II. 18) was dissolved in THF at room temperature. Then, solution was cool down and maintained in agitation at 4°C. Finally the NaOH solution was added dropwise. Turbidity was found in all the cases once the NaOH was added. The solutions were left under vigorous stirring the desire time. All conditions exploited (reaction time, NaOH equivalents and addH_2O/THF ratio) are detailed in TABLE II. 8, TABLE II. 9,TABLE II. 10, TABLE II. 13 and TABLE II. 14. The organic solvent was removed under vacuum, and the aqueous phase was purified by ultracentrifugation using a Vivaspin® (MWCO=3000Da). The samples were concentrated, filtered (0.2µm) and freeze-dried.

Study was monitored by polarimeter measurements for evaluating the coefficient of deviation of polarised light [α]. Each sample was dissolved in ddH_2O at 10mg/mL concentration and average data was obtained after 20 measurements. The obtained products were analysed by ^{1}H-NMR- to prove complete deprotection.

	initiator	Mn	Mw	PDI	GA units
PGA_{50}	npt-	9761	11752	1.2	45
PEG-*b*-PGA_{50}	PEG-	12208	13731	1.1	47

TABLE II. 18 Protected polymers information

.

II. 4. 3 POST-POLYMERISATION TECHNIQUES: INCORPORATION OF ALKYNE AND AMIDE FUNCTIONALITIES

II. 4. 3. 1 Alkyne modification for click-chemistry (21)

Synthesis scheme of alkyne coupling to TB (**21**) is depicted in FIGURE II. 33.

For 25%mol modification: in one round bottom flask, 100mg of PGA (0.78mmol, GA units, 1eq) were suspended in 10mL of ddH_2O. In a vial, DMTMM·Cl^- (0,39mmol, 0.5eq, 276.7g/mol) was dissolved in 5mL of ddH_2O and then added to the main solution. After 10 minutes in agitation, propargylamine (0.78mmol, 1eq, 0.86g/cm^3, 55.04g/mol) were added and the pH was checked to 8 (if pH was lower, it was adjusted with $NaHCO_3$ 1M solution). The reaction was allowed to proceed stirring at 25°C for 16h. Product purification was carried out by ultrafiltration (Vivaspin®, MWCO=3000Da) and after concentration, upper part of the tube was freeze-dried. White solid obtained was analysed by ^{1}H-NMR (D_2O) to determine the degree of modification.

Note: Ultrafiltration was preferred in case of large amount of starting material. For small amounts, size exclusion chromatography (Sephadex™ G25, PD-10) reduced the lost of material. Acid/base precipitation of the modified PGA was also tested since PGA is

insoluble in aqueous media in it is as carboxylic acid form and soluble in its sodium salt form. In addition, all by-products were water soluble. Precipitation was carried out by acidification of the reaction solution (adding dropwise HCl 1M) until pH 3 to 4 and resolution by basification with sodium bicarbonate. The process was repeated three times to yield white polymers after freeze-drying of the soluble form.

Yield: 80-90%, ^{1}H-NMR (300 MHz, D_2O) δ: 4.30 – 4.02 (m, 1H), 3.81 (s)*, 2.48 (s)*, 2.35 –2.02 (m, 2H), 2.01- 1.65 (m, 2H).

*The number of corresponding hydrogens depends on the percentage of functionalisation of the polymer backbone.

II. 4. 3. 2 Amine modification

First of all, as the TB was obtained in its sodium salt form it had to be acidified to become soluble in DMF. Acidification was carried out by dissolving the polymer in the minimum volume of ddH_2O and HCl 6M was dropwise added while pH was controlled. At pH around 4-3, precipitation was observed. After centrifugation, pellet and supernatant were freeze-dried and ^{1}H-NMR analysis (DMF-d_7) of both was performed.

Method for 100% amine insertion.

Synthesis scheme of diamine coupling to TB (**24**) is depicted in FIGURE II. 34.

In a round bottom flask, 34.5mg of TB_{200} (0.19mmol GA units, 1eq, average MW unit of glutamic acid=102.4g/mol, 56.63% COOH) were dissolved in 5mL of anhydrous DMF at 25°C under N_2 flow. After dissolution, 1.5eq of DIC (0.806g/mL, 126.2g/mol) were added and, after 5 min, 1.5eq of HOBt (135.13 g/mol). After 10min stirring, the mono protected Fmoc-diamine ((2-(2(Fmoc-amino)ethoxy)ethylamine hydrochloride, 0.095mmol, 1eq 362.85 g/mL)was added in the reaction. The pH was adjusted to 8 with DIEA and the reaction was left to proceed for 24 h and monitored by TLC. The solvent was evaporated under vacuum and non-reacted Fmoc-diamine was

removed washing the residue with 8-10mL $CHCl_3$: acetone (4:1 ratio). The washing mixture was collected, evaporated and redissolved in a known volume of MeOH. Absorbance (λ=290nm) was evaluated for non-reacted Fmoc-diamine quantification. The solid residue was dried under high vacuum. The next step was to deprotect the Fmoc-diamine coupled to the polymer. Deprotection was performed with a mixture of DMF:piperidine (20% v/v) at 25°C under inert atmosphere. The reaction was left in agitation 1 h. Then, the solvent was again removed under evaporation. Again, the solid residue was washed with a $CHCl_3$: acetone mixture (4:1 ratio, v/v) for dissolving the Fmoc group and quantify it as described. The solid residue was dried under vacuum and kept at -20°C until next reaction. For grafting efficiency calculation, absorbance measurements of non-reacted Fmoc-diamine and released Fmoc- were used to calculate their concentration. By subtraction, percentage of diamine coupled was obtained.

Yield: 80%, % amine coupling: 30%mol.

Note: Other post-polymerisation procedures for sulfhydryl group introduction or an alternative method for amine insertion using a Boc-monoprotected diamine had been performed in this thesis. Protocols are detailed in section III.2.3 because of their use as linkers for targeting ligand conjugation.

II. 4. 4 ROUTINE TECHNIQUES IN POLYMER CHARACTERISATION

In polymer chemistry synthesis routine techniques like NMR spectroscopy or GPC provide essential information as compound identity, MW or Đ determination. Both techniques have different background basis and apart from their inherent advantages and disadvantages, they represent the accepted standard methodology for polymer characterisation. FT-IR was utilised in this work as an extra-tool for polymerisation monitoring technique in parallel with GPC. In addition, circular dicroism (CD) provides information on the secondary structure of the analysed sample, which remains important in our synthesised polypeptides for future clinical applications.

II. 4. 4. 1 Sample characterisation by NMR Spectroscopy

NMR analysis provided and confirmed the identity of the analysed compound. ^{1}H and ^{13}C-NMR analysis of all obtained compounds were done at least with approx. 20mg of compound and dissolved in 0.5-0.6mL of the appropriate deuterated solvent. The PGA protected form was dissolved in $CDCl_3$, DMSO-d_6 or DMF-d_7; the PGA deprotected form o in DMSO-d_6 or DMF-d_7 and the sodium salts form in D_2O.

For the determination of the Mw by this methodology, characteristic peaks of the repeating unit (GA) were compared to the initiator peak (also to peaks of a different block such as PEG, to determine block ratios in block copolymers). Accuracy of MW determination depended on [M]/[I] ratio, being decreased in larger polymers. It has to be remarked that polymer chains not containing the added initiator could lead to an overestimation of the MW (polymerisation initiated by impurities,..).For the protected samples the 2 benzylic protons (-CH_2-C_6H_5) were used and the average of the values obtained for α-proton and side group-protons (-CH_2-CH_2-) was used for the chain length determination of deprotected samples.

Bidimensional experiments as COSY or diffusion studies by 2D-DOSY were also carried out with the synthesised polymer conjugates.

All the experiments were done at 25°C. NMR analysis was operating in frequencies of 300 MHz or 500MHz. All data processed and analysed using the TopSpin® 2.0 software.

II. 4. 4. 2 GPC analysis of protected polymers

Gel permeation chromatography (GPC) is an established method to determine true MW distributions of polymers that follows size exclusion chromatography (SEC) principles. Molecules are separated according to their hydrodynamic volume. Mw is determined from the measured retention volume (R_V) by means of a calibration curve. It is important to remark that calibration curve also depends on

the polymer used, thus calibration standards and the samples have to be of the same or similar nature. The signals obtained by all detectors (refractive index, viscosity, light scattering) depend solely on concentration what requires a careful control on injected sample concentration.

GPC analysis of polypeptides using PMMA (polymethyl methacrylate)standards for calibration may lead to errors in Mw determination. The structures are not completely comparable and same hydrodynamic radius in solution may not have the same Mw.

In this project, GPC measurements were performed in organic solvent: DMF (0.1%LiBr) as mobile phase, 0.8-1mL/min at 70°C. Samples were carefully weighted and diluted (to a known concentration, usually 6 to 8mg/mL) using the same mobile phase and filtered (0.2µm) before injection. 100µL of the dilution was injected and analysed for 45min. Standards use for calibration were poly(methyl methacrylate) (PMMA**)/**DMF standards. They allow a relative comparison of the MW and polydispersity of the injected samples. Exact determination of Mw by GPC for polymers corresponds to those with random coil conformation. In our case, polypeptides are often organised in stable secondary or tertiary structures like parallel β-sheet, anti-parallel β-sheet or α-helix. To solve this, mobile phases with effective hydrogen bonds disruption ability are suitable. DMF posses this characteristic although do not fully disrupt secondary structures of homo-polypeptides. As solution, parallel measurements in a better solvent able to diminish formation of suprastructures: hexafluoro-2-propanol (HFIP) as solvent, were carried out in order to compare results (experiments carried out in Mainz, Germany), as well as CD to ensure absence of secondary structures of the synthesised polypeptides. Therefore, GPC was also performed with HFIP containing 3g/L potassium trifluoroacetate as eluent at 40°C. The columns were packed with Modified silica (PFG columns particle size: 7µm, porosity: 100 & 1000Å, PSS). A refractive index detector (G 1362A RID) was used to detect the polymer. MWs were calculated using a calibration performed with PMMA standards (Polymer Standards Services GmbH)

and Toluene as internal standard.

II. 4. 4. 3 Circular dicroism (CD) analysis

As mentioned above, CD analysis was carried out in Mainz (Germany). The protected polymers were dissolved in hexafluoro-2-propanol (containing 3g/L trifluoroacetate) at a concentration of 1mg/mL and diluted to 0.25mg/mL. The deprotected samples were dissolved in water and diluted to a concentration of 0.25 mg/mL.

The UV Absorption at 205nm of all subsequently measured samples (same desired concentration of 0.25mg/mL) was averaged, and the CD spectra were corrected by dividing all values by the value of absorption of the sample at 205nm and then multiplying it by the averaged value. This was done to even small concentration variations during sampling). The measured ellipticity was converted to molar ellipticity per amino acid (concentration, MW of the amino acid and path length in the sample were calculated out of the ellipticity resulting in [deg cm² $dmol^{-1}$]).

$$\theta_m(\lambda) = \frac{\theta(\lambda) \times M}{10 \times c \times l}$$

II. 4. 4. 4 Infrared (IR) spectroscopy analysis for polymerisation monitoring

To get information about the kinetics of the polymerisation process, the reaction solution was analysed by infrared (IR) spectroscopy performing a time course experiment. IR permits to identify the bonds existing in the analysed molecule. The transformation of monomer into polymer can be easily identified through the disappearing of specific bands from monomer bonds.

Polymerisation reactions were carried out in DMF media, therefore a cell for liquids was used. All samples analysed were under solution or previously dissolved in DMF. Analysis was carried out at 25˚C.

DMF strongly absorbs in the IR region, therefore suitable peaks to follow the reaction had to be found. FIGURE II. 14 shows the IR spectra of pure DMF, Glu(Bz)NCA dissolved in DMF and p-L-Glu(Bz) in DMF. Discarding peaks obscured by DMF and those matching with the polymer, peaks corresponding only to the NCA monomer were localised at 1857, 1785 cm^{-1} and 920$cm^{-1.}$. Peaks at 1785 and 920cm^{-1} were selected due to their lower signal-to-noise ratio.

BIBLIOGRAPHY

1. Duncan, R., *Polymer therapeutics as nanomedicines: new perspectives.* Curr Opin Biotech, 2011. **22**(4): p. 492-501.
2. Johnson, K.P., *Glatiramer acetate for treatment of relapsing–remitting multiple sclerosis.* Exp Rev Neurotherapeutics, 2012. **12**(4): p. 371-384.
3. Singer, J.W., *Paclitaxel poliglumex (XYOTAX™, CT-2103), a macromolecular taxane.* J Control Release, 2005. **109**(1-3): p. 120-126.
4. S. A. Shaffer, et al., *In vitro and in vivo metabolism of paclitaxel poliglumex: identification of metabolites and active proteases.* Cancer Chemother Pharmacol, 2007. **59**(4): p. 537-48.
5. M. P. Melacon, C.L., *Multifunctional synthetic poly(L-glutamic acid)-based cancer therapeutic and imaging agents.* Molecular Imaging, 2011. **10**(1): p. 28-42.
6. J. Cheng and T.J. Deming, *Synthesis of polypeptides by ring-opening polymerization of alpha-amino acid N-carboxyanhydrides.* Top Curr Chem, 2012. **310**: p. 1-26.
7. N. Hadjichristidis, et al., *Synthesis of well-defined polypeptide-based materials via the ring-opening polymerization of alpha-amino acid N-carboxyanhydrides.* Chem Rev, 2009. **109**(11): p. 5528-78.
8. Deming, T.J., *Methodologies for preparation of synthetic block copolypeptides: materials with future promise in drug delivery.* Adv Drug Deliv Rev, 2002. **54**: p. 1145-1155.
9. Deming, T.J., *Synthetic Polypeptides for Biomedical Applications. Progress in Polymer Science **32**, 858-875.* Prog Polym Sci, 2007. **32**(858-875).
10. W. Vayaboury, et al., *Synthesis of N-protected-L-lysine and alpha-benzyl-L-glutamate N-carboxyanhydrides (NCA) by carbamoylation and nitrosation.* Amino Acids, 2004. **27**(2): p. 161-167.
11. H. Leuchs, *Fiber die Glycin-carbonsauren* Dtsch Chem Ges,

1906. **39**: p. 857.

12. H. Leuchs and W. Manasse, Dtsch Chem Ges, 1907. **40**: p. 3235.
13. H. Leuchs and W.Geiger, Dtsch Chem Ges, 1908. **41**: p. 1721.
14. M. Barz, et al., *Overcoming the PEG-addiction: well-defined alternatives to PEG, from structure-property relationships to better defined therapeutics.* Polymer Chemistry, 2011. **2**: p. 1900-1918.
15. E. Peggion, et al., *Polymerization of gamma-benzyl-L-glutamate N-carboxyanhydride: effects of conditions of polymer precipitation on the molecular weight distribution.* Biopolymers, 1966. **4**(6): p. 695-704.
16. M. Goodman and J. Hutchison, *The mechanisms of polymerization of N-unsubstituted N-Carboxyanhydrides.* J Am Chem Soc, 1966. **88**(15): p. 3627-3630.
17. D. Baillard and C. Bamford, *Reactions of N-Carboxy-alpha-anhydrides catalysed by tertiary bases.* J Chem Soc, 1956. **381**.
18. H. Kricheldorf, *alpha-amino acid-N-carboxyanhydrides ans related heterocycles.* . Springer, New York, 1987.
19. H. Kricheldorf, *Polypeptides and 100 years of chemistry of alpha-amino acid N-carboxyanhydrides.* Angew Chem Int Ed, 2006. **45**(35): p. 5752-84.
20. H. Kricheldorf, *Polypeptides. Models of biopolymers by ring opening polymerization.* In: Pencze S (ed) . CRC, Boca Raton, 1990: p. 1-132.
21. T. Aliferis, H. Iatrou, and N. Hadjichristidis, Biomacromolecules, 2004. **5**: p. 1653-1656.
22. T. Aliferis, H. Iatrou, and N. Hadjichristidis, *Well-defined linear multiblock and branched polypeptides by linking chemistry* J. Polym Sci Part A: Polym Chem, 2005. **43**: p. 4670-4673.
23. I. Dimitrov and H. Schlaad, *Synthesis of nearly monodisperse polystyrene-polypeptide block copolymers via polymerisation of N-carboxyanhydrides.* Chem Commun (Camb), 2003(23): p. 2944-2945.

24. Deming, T.J., *Facile synthesis of block copolypeptides of defined architecture.* Nature, 1997. **390**(6658): p. 386-9.

25. H. Lu and J. Cheng, *Hexamethyldisilazane-mediated controlled polymerization of alpha-amino acid N-carboxyanhydrides.* J Am Chem Soc, 2007. **129**(46): p. 14114-5.

26. Y. Knobbler, S. Bittner, and M. Frankel, *Reaction of N-carboxy-alpha-aminoacid anhydrides with hydrochlorides of hydroxylamine, O-alkylhydroxylamines and amines.* J Chem Soc, 1964. **3941**.

27. Y. Knobbler, et al., *alpha-aminoacyl derivatives of aminobenzoic acid and amino-oxy-acids by reaction of their hydrochlorides with amino-acid N-carboxyanhydrides.* J Chem Soc, 1969. **1969**: p. 1821-1824.

28. A. C. Farthing and R.J. Reynolds, *Anhydro-N-carboxy-DL-phenyl-alanine.* Nature, 1950. **165**(4199): p. 647.

29. D. Coleman and A.C. Farthing, *628. Synthetic polypeptides. Part II. Properties of oxazolid-2 : 5-diones and an initial study of the preparation of polypeptides there-from.* J Chem Soc, 1950: p. 3218-3222

30. Habraken, G.J.M., et al., *Optimization of N-carboxyanhydride (NCA) polymerization by variation of reaction temperature and pressure.* Polymer Chemistry, 2011. **2**(6): p. 1322-1330.

31. F. Fuchs, *Über N-Carbonsäure-anhydride.* Berichte der deutschen chemischen Gesellschaft (A and B Series), 1922. **55**(9): p. 2943-2943.

32. W.H. Daly and D. Poche, *The preparation of N-carboxyanhydrides of α-amino acids using bis(trichloromethyl)carbonate.* Tetrahedron letters, 1988. **29**(46): p. 5859-5862.

33. A. Karatzas, et al., *Complex macromolecular chimeras.* Biomacromolecules, 2008. **9**(7): p. 2072-80.

34. M.J. Vicent, et al., *"Síntesis controlada de poliglutamatos con baja polidispersidad y arquitecturas versátiles"* N. de solicitud: P201131713, 2012.

35. I. Conejos-Sánchez*, et al., *A Controlled and versatile NCA polymerization method for the synthesis of polypeptides.* Polym Chem, 2013.

36. C.L. Chang, M.K. Leung, and M.H. Yang, *Alkyl and dialkylammonium tetrafluoroborate catalyzed cis–trans isomerization of 1,3,5-trimethyl-1,3,5-triphenylcyclotrisiloxane.* Tetrahedron, 2004. **60**(41): p. 9205-9212.

37. R. M. Macholz, *W. Kliegel: Bor in Biologie, Medizin und Pharmazie. Physiologische Wirkung und Anwendung von Borverbindungen. Tab. .* Springer-Verlag, Berlin, Heidelberg, New York 1980. , 1981. **25**(7): p. 701-701.

38. E. Bernhardt, et al., *Die Reaktionen von M[BF4] (M = Li, K) und (C2H5)2O·BF3 mit (CH3)3SiCN. Bildung von M[BFx>(CN)4—x] (M = Li, K; x = 1, 2) und (CH3)3SiNCBFx(CN)3—x, (x = 0, 1).* Z Anorg Allg Chem, 2003. **629**(4): p. 677-685.

39. V. J.Gerber and H. G. Elias, *Multimerisation: Assoziation und aggregation. VII. Poly-γ-benzyl-L-glutamat in reinen lösungsmitteln.* Die Makromolekulare Chemie, 1968. **112**(1): p. 142-159.

40. E. R. Blout and M. Idelson, *Polypeptides VI. Poly-alpha-glutamic acid: preparation and helix-coil conversions.* J Am Chem Soc, 1956. **78**(497-498).

41. Deming, T.J., *Polypeptide-based materials.* Topics in Current Chemistry. Springer, 2012. **310**.

42. W. E. Hanby, S. G. Waley, and J. Watson, *Synthetic polyglutamic acid.* Nature, 1956. **161**(132).

43. M. Yokoyama, et al., *Polymer micelles as novel drug carrier: adriamycin-conjugated poly(ethylene glycol)-(poly(aspartic acid) block copolymer.* J Control Release, 1990. **11**(1-3): p. 269-278.

44. Günay, K.A., P. Theato, and H.-A. Klok, *Standing on the shoulders of Hermann Staudinger: Post-polymerization modification from past to present.* Journal of Polymer Science Part A: Polymer Chemistry, 2013. **51**(1): p. 1-28.

45. M. A. Gauthier, M. I. Gibson, and H. A. Klok, *Synthesis of*

Functional Polymers by Post-Polymerization Modification. Angew Chem Int Ed, 2009. **48**(1): p. 48-58.

46. K. Thompson and S. Michielsen, *Novel synthesis of N-substituted polyacrylamides: Derivatization of poly(acrylic acid) with amines using a triazine-based condensing reagent.* Journal of Polymer Science Part A: Polymer Chemistry, 2006. **44**(126-136).
47. C. Woghiren, B. Sharma, and S. Stein, *Protected thiol-polyethylene glycol: a new activated polymer for reversible protein modification.* Bioconjug Chem, 1993. **4**(5): p. 314-8.
48. D. R. Grassetti and J. F. Jr. Murray, *Determination of sulfhydryl groups with 2,2'- or 4,4'-dithiodipyridine.* Arch Biochem Biophys, 1967. **119**(1): p. 41-9.
49. S. L. Snyder and P. Z. Sobocinski, *An improved 2,4,6-trinitrobenzenesulfonic acid method for the determination of amines.* Anal Biochem, 1975. **64**(1): p. 284-8.
50. N. M. B. Smeets, e.a., *A Scalable synthesis of L-Leucine-N-carboxyanhydre.* Org Process Research & Development, 2005. **9**: p. 757-763.

CHAPTER III

LABELLED AND TARGETED POLYGLUTAMATES

CHAPTER III. LABELLED AND TARGETED POLYGLUTAMATES

In order to biologically evaluate the potential of the polyglutamates synthesised and described in chapter 1 as drug carriers and to understand polymer *in vitro*/*in vivo* fate, two complementary approaches were followed.

First, carriers can exploit not only their inherent passive targeting (by the EPR effect, see introduction chapter) but also a specific active targeting to an organ, cell or even an intracellular organelle [1]. This could be achieved by the conjugation of targeting ligands. In this project, active targeted conjugates by the linkage of protein (transferrin), antibody (mAbOX26) or peptidic sequences (Angiopep-2 and cPEP) have been designed to surpass the blood-brain barrier (BBB) by means of transcytosis (section I.1.4). With this aim, the preferred type of covalent bond to be used was the disulphide bond as this bioreversible linkage allows the ligands to be released in presence of a reductive environment or by disulfide reductases encountered in the brain following transcytosis [2]. *In vivo* proof of concept of this fact was demonstrated with a peptide inducing enhanced cerebral flow [3]. The chemical steps done towards this aim were based on ligand derivatisation in order to add sulfhydryl groups for later conjugation or to use/expose those already present in their structure.

Second, their polyvalent character given by the multifunctionality enables to exploit labelling approaches by probe conjugation to investigate their *in vivo* biodistribution, pharmacokinetics (PK), cell trafficking or cell localisation. The effectiveness of the administered nanomedicine as well as disease progression and therapeutic response could be literally observed. On this basis, conjugate monitoring, with or without drug/targeting ligand, was carried out in this thesis by means of several non-invasive imaging modalities either *in vitro* or *in vivo* (see Chapter IV). Different tracers or probes named in TABLE III. 19 have been covalently bound to allow monitoring of the synthesised polyglutamates.

Labelling moiety		Technique	Labelled systems	REF	Type of bond
Rhodamine	Fluorophore	Fluorescence *in vitro*	TB		amide
Oregon green	Fluorophore	Fluorescence *in vitro*	TB		amide
		Fluorescence *in vivo*	TB		amide
Cyane 5.5	NRI dye	Optical imaging in *vivo*	PGA		click
			PGA-Doxy		amide
			DB		amide
			DB-Tf		amide
DTPA/Gd	Contrast agent	MRI	TB		amide
			TB-mAbOX26		amide
Tyramine/^{18}F		PET	TB		amide
DOTA/^{68}Ga		PET	PGA		amide
			PGA-Doxy		amide
			DB		amide

TABLE III. 19 Imaging probes utilised for polyglutamate labelling.

III. 1 RESULTS AND DISCUSSION

III. 1. 1 GENERAL SYNTHETIC METHODOLOGIES FOR POLYMER LABELLING

PGA multivalency can be exploited not only for tailoring drug loading but also for dye labelling. Labelled-PGA can be readily detected in biological fluids and tissues when a fluorescent dye or a radioactive tracer is conjugated to its backbone. Derivatisation of the carboxylic acid pendant groups offers a vast number of possibilities for probe conjugation, from a highly selective linkage through click chemistry (triazol) to a simple amide bond [4].

An essential step for validation of a novel polymeric carrier is the exploration of its trafficking properties *in vitro* as well as its biodistribution and fate *in vivo*. The synthesised polyglutamates presented distinct levels of complexity featured by their variations in size (MW) and composition (presence of one or two PEG blocks) which lead to differences in conformation. These characteristics offer the opportunity of setting carriers with different purposes depending on the cell internalisation pathway followed, facility for crossing any biological barrier, body distribution as well as secretion route exploited. This information could be gain by the introduction of labelling moieties into the polymer chain. Furthermore, labelling combined with drug conjugation could be included under the concept named ´theranostics´ [5, 6].

PGA pendant groups enable probe conjugation, which can be modulated thanks to its number of GA units. In the present project, several probes have been tested covering two different approaches: molecular imaging (optical imaging and magnetic resonance imaging (MRI)) and radionuclide imaging (positron emission tomography, PET). Polyglutamates have been tagged using fluorescent molecules such as Oregon Green (OG), Rhodamine (Rho) or the near-infrared (NIR) dye Cyane5.5; imaging contrast agents as diethylenetriaminepenta-acetic acid dianhydride (DTPA)/Gd and PET tracers as 1,4,7,10-tetraazacyclododecane-N,N'',N''',N''''-tetraacetic acid (DOTA)/^{68}Ga or Tyramine/^{18}F. Bioimaging of the CNS encompasses techniques involving nuclear medicine studies such PET and single photon emission computed tomography (SPECT). Morphological studies include MRI and computed tomography (CT). Nowadays, combination of this neuroimaging tests are essential to provide diagnostic support and provide the advantage to identify underlying neurological processes involved in disease progression [7].

In order to obtain the selected type of bond between the probe and the polymer post-polymerisation modification approaches were followed. In many cases, not only for labelling, these strategies were used to attach targeting moieties (section III.3.2.3) or to allow drug conjugation (section V.3.1.3). Post-polymerisation modification

constitutes an attractive approach for the synthesis of functional polymers overcoming the limited functional group tolerance of many controlled polymerisation techniques. Due to all the advantages of the above-described methodology of NCA polymerisation, the exploration of the post-polymerisation modification of the well-defined polyglutamates was studied with a view to the incorporation of functionalities for site specific conjugation.

With this objective in mind, carboxyl pendant groups of the PGA block were modified in order to obtain different ending functionalities (-NH_2,-SH, -C≡CH,…) allowing conjugation of targeting ligands, drugs through spacers and/or fluorescence or radioactive probes.

III. 1. 1 .1 Fluorescence labelling

The conjugation of fluorescent probes to PGA enabled to study the cellular uptake and trafficking in an endothelial cell line and to investigate *in vivo* biodistribution of the novel synthesised triblocks. Optical imaging is a traditional and well established tool in biomedicine. Use of light for imaging has the advantages of simplicity, low-cost and uncomplicated equipment. It is a non-invasive and non-ionising technique, which allows repeated doses without damaging the animal. It also permits multicolour fluorescence detection and therefore resolution of multiple targets using fluorescent labels able to be spectrally resolved. In addition, the use of fluorescent optical agents enables visualisation of otherwise invisible cellular and sub-cellular processes.

Limitations of the technique are related to the scattering. For *in vivo* monitoring, thick tissues diffuse and absorb light reducing significantly the resolution, therefore, the low penetration capabilities cannot provide depth and size information. Moreover the use of fluorescence probes that show concentration and/or pH-dependent quenching and that are released from the carrier following internalisation lead to misinterpretation of images [8, 9].

For macromolecular therapeutics and nano-sized drug delivery systems, fluorescent labelling uses are focused on determining intracellular trafficking, conjugate cell-specific localisation and/or *in vivo* fate and PK. Epifluorescence and fluorescence laser scanning confocal microscopy can be used to study the intracellular fate of delivery systems. In particular, live cell confocal imaging allows visualising trafficking between multiple compartments within individual living cells over time avoiding any possible artefact derived from fixation protocols [10].

Regarding *in vivo* optical imaging, many novel fluorophores have been developed to fluoresce in the NIR optical window (700-1000nm), where optical absorption is negligible and light can penetrate deeply. Traditionally, PK and biodistribution studies were based on quantifying the therapeutic agent by HPLC, mass spectroscopy or measuring radioactivity. Today, optical imaging using NIR fluorescent or luminescent tools facilitates this task. It involves the injection of fluorescent probes, transgenic cells or species able to express fluorescent proteins when activated in a particular manner. Fluorescence imaging has been successfully translated from microscopy level to small animal imaging and even to the clinics [11]. NIR fluorescent dye Cy5.5 has proved to be a promising agent for *in vivo* demarcation, highly exploited in tumour studies such gliomas [12, 13].

In the present thesis, the fluorophore OG was chosen for *in vitro* studies (cell internalisation) and the NIR dye cyane5.5 (Cy5.5) for *in vivo* biodistribution studies. Conjugation was performed (i) through amide bonds between amino derivatised fluorophores and the PGA block (or PEG terminal group in case of blocks) or (ii) through click-chemistry involving a prior post-polymerisation modification of the PGA carboxyl groups with an azide derivative of the fluorophore. Common protocols developed in this thesis involved the activation of the carboxyl groups of the polypeptide block. For this purpose, different methods had been used: (i) activation by carbodiimides (DIC, DCC), (ii) NHS activation and (ii) 4-(4,6-dimethoxy-1,3,5-triazin-2-yl)-4-

methylmorpholiniuym chloride (DMTMM) coupling reagent [4]. Carbodiimides are common acylating agents used in amino acid coupling procedures either in organic or aqueous media. 1,3-dicyclohexylcarbodiimide (DCC) and 1,3-diisopropilcarbodiimide are the most used reagents towards amide or ester formation. Main drawback is the generation of insoluble byproducts (dicyclohexylurea or diisopropylurea) during activation/acylation, but this can be prevented by the addition of HOBt (1-hydroxybenzotriazole). This reagent increases the reactivity of the intermediate, improving the carboxyl activation [14](FIGURE III. 36).

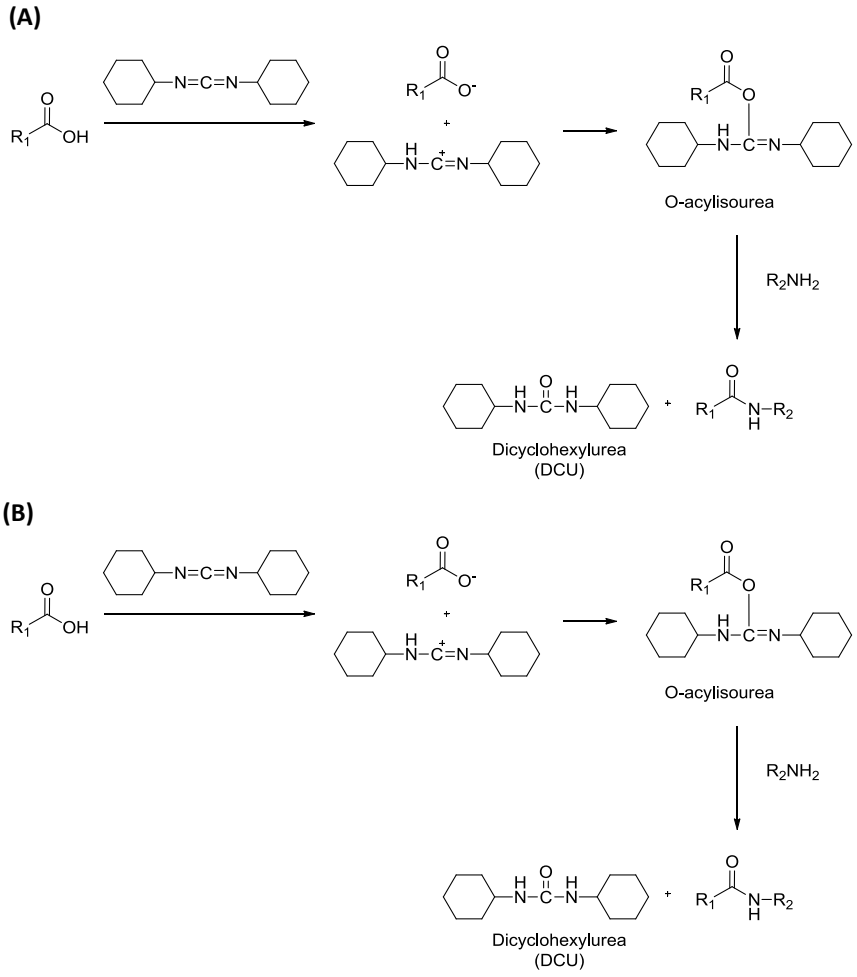

FIGURE III. 36 Carbodiimide coupling scheme (example with DCC). (A) Mechanism for amide formation. A side product is observed when DCC is

used alone (transition O to N-acylurea, path A), (B) HOBt addition suppresses *N*-acylurea formation by protonation of the *O*-acylisourea (Path B).

In aqueous media, N-(3-dimethylaminopropyl)-N-ethylcarbodiimide (EDC or EDAC) is also a popular condensing agent[15]. NHS or sulfo-NHS are moieties coupled to carboxylic acids after its activation. In organic or aqueous media (respectively), these groups increase coupling efficiently or create a stable amine-reactive product. DMAP (dimethylamino pyridine) is often used as catalyst in the amino- or alcohol- later coupling (sulpho-NHS is detailed in Chapter V). On the other hand, DMTMM enables an efficient one-step condensation and byproducts or reagents in excess are easily removed (Scheme in FIGURE III. 37). Furthermore, it is compatible with many solvents including water, alcohols, THF, DMF, etc. and no rigorous pH control is necessary [16, 17].

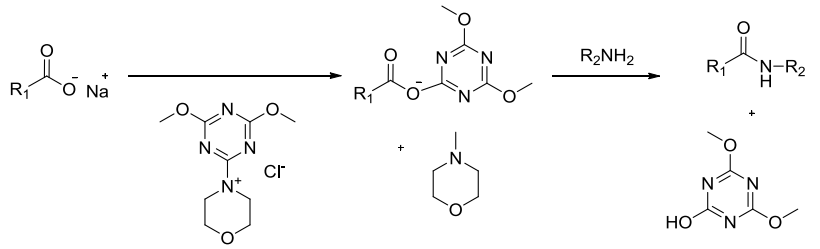

FIGURE III. 37 DMTMM coupling scheme to form an amide bond.

Methodology for labelling with Rhodamine (Rho)

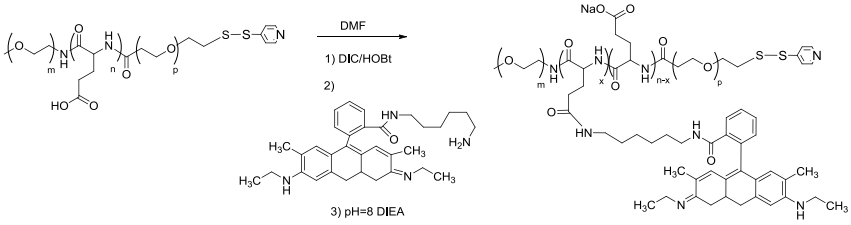

FIGURE III. 38 Scheme of Rhodamine labelling.

Rhodamine (N-(6-Aminohexyl)rhodamine 6G-amide bis(trifluoroacetate)) is a widely used dye for multiple cell assays. In this case, the amino group of the Rho derivative was conjugated to the

TB_{200} (**9**) through the carboxylic groups of PGA block by means of a DIC-coupling mediated reaction (FIGURE III. 38) (0.5 %mol Rho, 24.5% yield (FIGURE III. 39)) giving the conjugate TB-Rho (**17**). However, the fluorescence detection after conjugation resulted unsatisfactory both via fluorometer and even by HPLC analysis: its emission was not easily detected. This low output could difficult future *in vivo* assays. As a result, Oregon Green cadaverine (OG) was chosen as alternative.

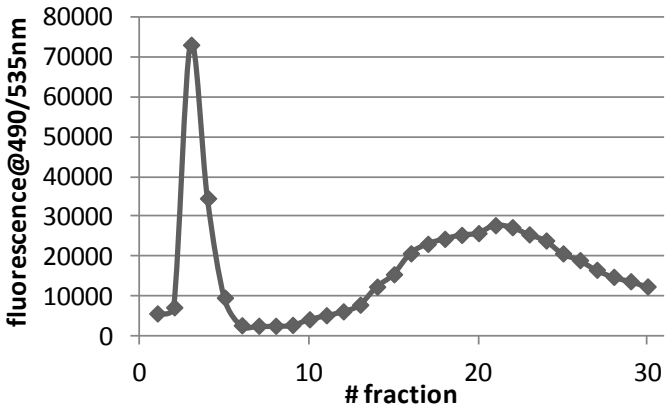

FIGURE III. 39 Representative images of the elution profile of TB-Rho (**17**) used to quantify Rho polymer loading.

Methodology for labelling with Oregon Green (OG) cadaverine.

OG labelling was a successful methodology independently of the selected PGA derivative: homopolymer, diblock or triblock (Scheme in FIGURE III. 40). Conjugation yields ranged from 80 to 90%. In FIGURE III. 41 an elution profile of a triblock labelling is shown and TABLE III. 20 compiles an example of the species labelled with this fluorophore.

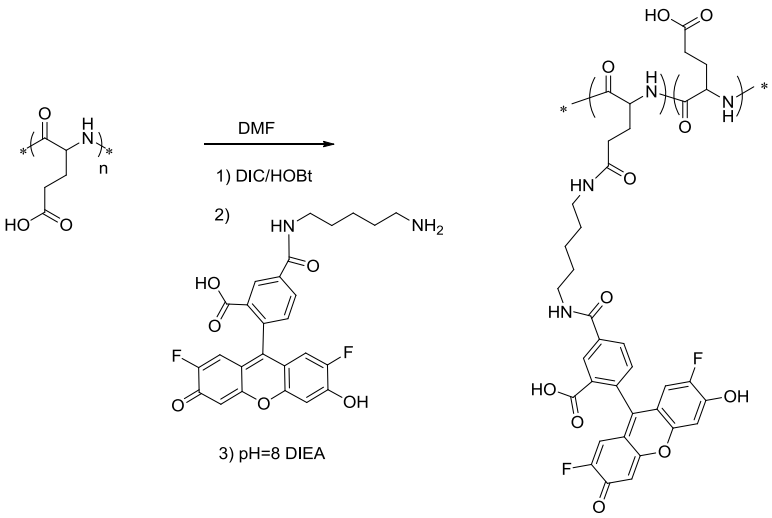

FIGURE III. 40 Scheme of OG-cadaverine labelling.

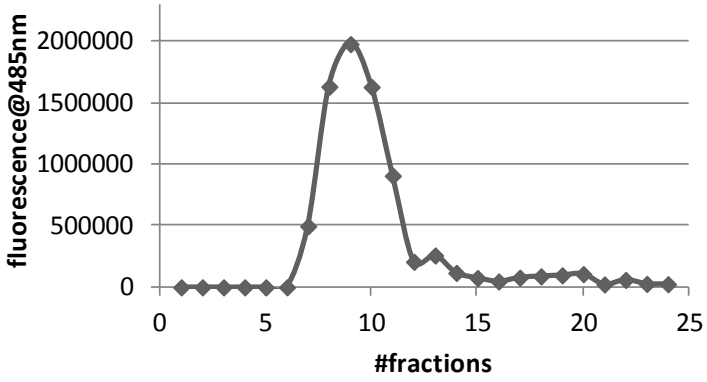

FIGURE III. 41 Elution profile after purification of triblock labelling with Oregon green moiety. Fluorescent measurement of each fraction after dilution.

Polymeric carrier	DP	%OG mol
TB	200	0.90
	200	0.6
	200	1.3
	200	0.6
	200	1.7
	200	1.6
	150	0.72
	150	0.78
	100	0.83
	100	0.80
	100	0.76
	100	0.45

TABLE III. 20 Examples of triblocks (**9**) labelled with Oregon green.

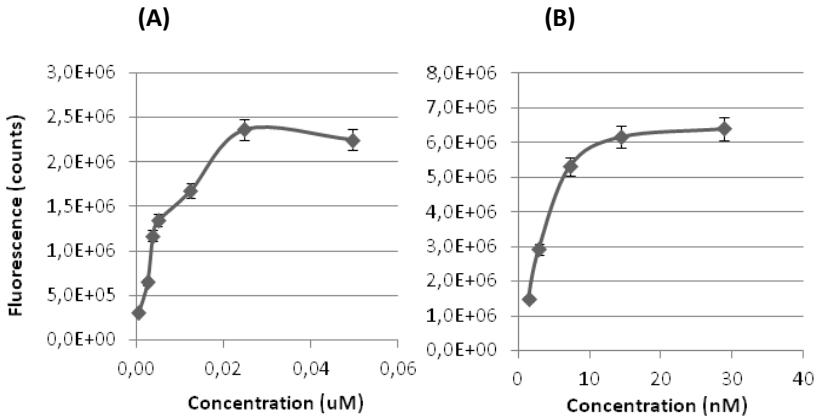

FIGURE III. 42 Quenching phenomena of OG and TBO.(A) Oregon green and (B) TBO.

This probe has been reported to be stable against changes in pH [10]A proof was performed to test this statement trying to mimic later polymer extraction of *in vivo* experiments, resulting in reduced signal under acidic conditions and not affected by basic environment. Same behaviour was found for TBO (**20**) (FIGURE III. 43). In order to transfer this knowledge to our *in vivo* studies, fluorescent

measurements considered the pH of the media as well as sample dilutions to identify possible false measurements due to quenching effect.

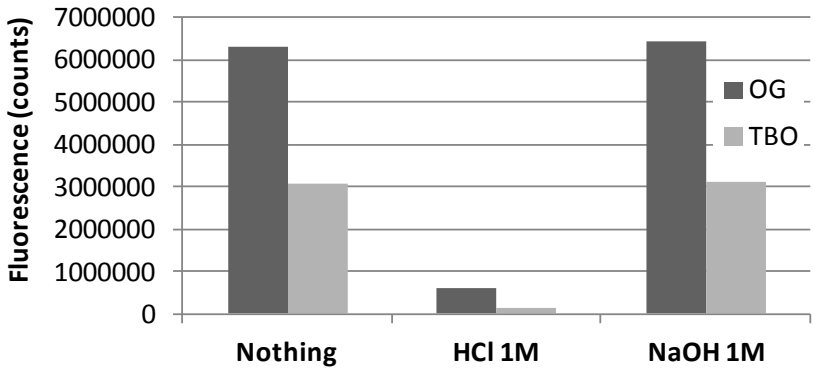

FIGURE III. 43 pH sensitivity of OG probe and TBO under acidic or basic conditions.

Methodology for labelling with Cyane5.5 (Cy5.5)

Two derivates of Cy5.5 were selected for labelling PGA homopolymer and DB, both with an average of 100 GA units. On one hand, PGA homopolymer modified with alkyne moieties (**21**) was conjugated to Cy5.5-azide (**22**) (see FIGURE III. 44(A)). As expected, click chemistry reaction showed a high chemoselectivity under mild reaction conditions and enabled us to obtain a non biodegradable linker. In organic solvents, CuBr/N,N,N',N',N''-pentamethyldiethylenetriamine (PMDTA) are the most common reagents. The active specie is Copper (I), which can be readily oxidised to Copper (II) in presence of water. For this reason, the systems were always carefully degassed before and after catalyst addition. PMDTA function is to stabilise Cu(I) in solution thanks to its tridentate structure.

DB_{100} (**5**) labelling was performed with Cy5.5-NH_2 (**34**), via an amide bond. The synthetic scheme is depicted in FIGURE III. 44 (B). Dye loading was calculated after analysing the fractions obtained from a PD10 column in a fluorometer (see experimental section for details)

(FIGURE III. 45 (A,B)). The results obtained are summarised in TABLE III. 21.

(A)

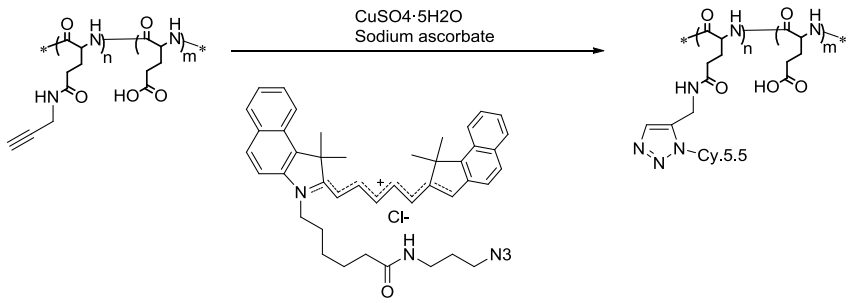

(B)

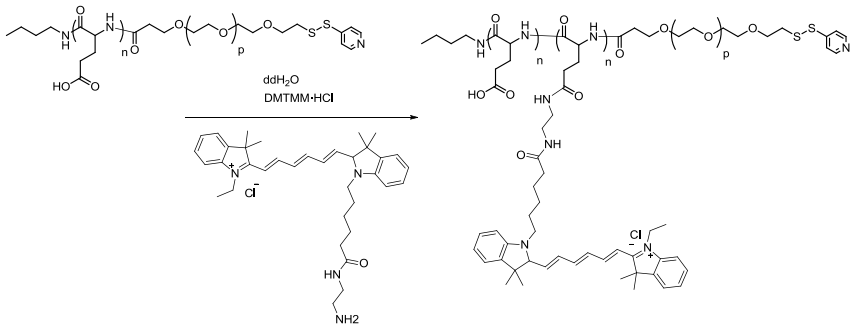

FIGURE III. 44 Cyane5.5 labelling (A) PGA through click-chemistry (**22**), (B) DB through amide bonding (**34**).

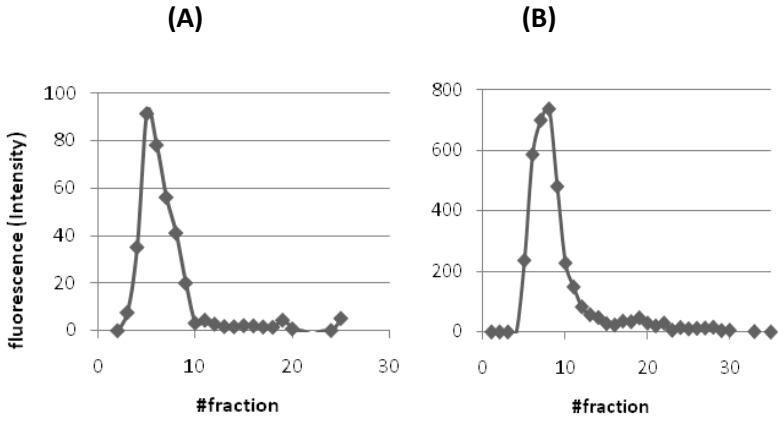

FIGURE III. 45 Fluorescent measurement of fractions from purification of (A) PGA-Cy5. (**22**), (B) DB-Cy5.5 (**34**).

REF	%mol Cy5.5	%labelling yield	REF

PGA_{100}	**4, 11**	1.80	87	**22**
DB_{100}	**7**	1.63	91	**34**

TABLE III. 21 Results of Cy5.5 polymer labelling.

III. 1. 1 .2 Contrast agents labelling. DTPA/Gd complex.

Magnetic resonance imaging (MRI) is a non-invasive technique commonly used in medical imaging to produce high quality images of the inside body. It does not use ionising radiation and provides 3D images of anatomic structures with high spatial resolution [18].

Briefly, MRI process basis relies on creating images from the manipulation of hydrogen atoms under magnetic fields. Atoms with and odd number of protons and neutrons such as hydrogen possess a specific quantum property called ´spin angular momentum´. Spin is where an atom rotates about its own axis, atoms are charged particles and therefore they create small magnetic fields. The atoms are able to occupy multiple different states of spin, but are normally randomly distributed between them. However, in presence of an external magnetic field (B_0) the atoms will align either with (lower energy level) or against (high energy level) the field, the difference between the two energy levels being proportional to B_0 [19]. This phenomenon results in giving the object inside the magnetic field a very weak magnetic charge described by what is known as the net magnetisation vector (NMV). Hydrogen atoms dominate the NMV caused by placing a body (human body is primarily fat and water, both have many hydrogen atoms, approx 63%) in an external magnetic field. The image creation is based on measuring of the return of the NMV back to its original orientation. This is defined as relaxation. Each tissue differs from other due to velocity of this relaxation, then, MRI allows differentiating between body tissues. MRI contemplates two types of relaxation constants: T1, which is the time constant for the NMR to return to their equilibrium state with the external magnetic field (longitudinal) and T2, which is the time constant for the NMV to leave the plane perpendicular to the external magnetic field (transverse) [20]. These constants specifically depend on the water content of the material. For

instance, tightly packed solid tissues with close interaction between hydrogen nucleus relax more quickly than loosely structured liquids, so tissues such as skeletal muscle have a shorter T2s while e.g. cerebrospinal fluid possess a longer T2. Relaxation emits energy, which is detected by a scanner and mathematically converted into an image.

In order to extract more information from imaging, contrast agents have been employed. These compounds are used to improve the MRI visibility of internal body structures by altering the relaxation times of the tissue atoms. Paramagnetic metals used for enhance MRI signal (Gd(III) [21], Fe(III), Cr(III), Mn(II)) have permanent magnetic fields, although the magnetic moments of individual domains are unaligned. After exposure to an external magnetic field, individual domain moments become aligned, generating a strong local field. Paramagnetic metal ions interact with water molecules increasing relaxation of the water molecules due to the water-metal complex, decreasing remarkably the T1 value from the water molecules and enhancing the signal of the proton [19]. MRI contrast agents can be classified by their administration route, chemical composition, magnetic properties, effect on the image, metal centre nature or biodistribution and applications (e.g. extracellular fluid agents, blood pool agents, organ specific agents, active targeting/cell labelling agents,…).

Scientific research utilises MRI as a useful tool for non-invasive and real-time evaluation for drug delivery. Contrast agents enhance the signal in target tissue for accurate diagnosis or detection. MRI is among the modalities which require a certain quantity of reporter groups to accumulate in the area under observation, as occurred in optical imaging technique. To reach the needed local concentration of the contrast agent, conjugation to polymer vehicles, such as poly-L-glutamic acid, has been already advocated since ability to carry multiple reporter moieties increase efficiency of the agents [18, 22].

Nowadays, almost 30% of all MRI scans today use some type of non-specific gadolinium-based contrast agent [21, 23]. The administered contrast agent typically makes diseased tissue appear

brighter (or in determined cases darker) than the surrounding tissue. The first approved contrast agent, Gd-DTPA (gadopentetate dimeglumine, Magnevist®) appeared in 1988 and several other compounds have followed it. Usually, gadolinium-based agents are administered i.v. As mentioned in the Chapter I, an intravascular contrast agent based on a large dendrimer containing 24 gadolinium ions (Gadomer-17, MW 30-35kDa)was transferred to the clinics although recently it has been retired due to a non-adequate PK profile [24].

The purpose of utilising MRI in this project was to monitor BBB crossing. MRI technique has achieved greater advances in this body area, providing accurate information about changes in cerebral function in brain *in vivo*. It should be remarked that Gd(III) chelates do not pass by itself the BBB because their hydrophilic character.

Methodology for labelling for MRI analysis by DTPA/Gd conjugation

Aiming at complexing Gd(III), carboxylic groups of the PGA block previously functionalised with a di-amine (2-[2(Fmoc-amino)ethoxy]cethylamine hydrochloride) by DIC-coupling (section II.2.2.5) provided a free amine group for DTPA conjugation The monoprotected di-amine avoids cross-linking reactions. The synthetic scheme is shown in FIGURE III. 46. The degree of DTPA substitution was determined by titration with a solution of $GdCl_3$ later evaluated with 4-(2-pyridylazo)resorcinol as Gd(III) indication, observing a clear variation from yellow (complexed Gd) to orange (free Gd). Results are summarised in TABLE III. 22.

For *in vivo* studies, gadolinium chelation was performed adding dropwise a solution of $GdCl_3$ in water to an aqueous solution of TB-diamine-DTPA (**25**), giving the complex TB-diamine-DTPA/Gd (**26**). Then purification was carried out to remove free Gd using the resorcinol indicator described above until absence of Gd. Mass percentage of complexed Gd is detailed for all the TB tested in TABLE III. 22. Taking into account that length of PGA block can be varied

during the polymerisation, percentage of complexed Gd(III)could be also customised.

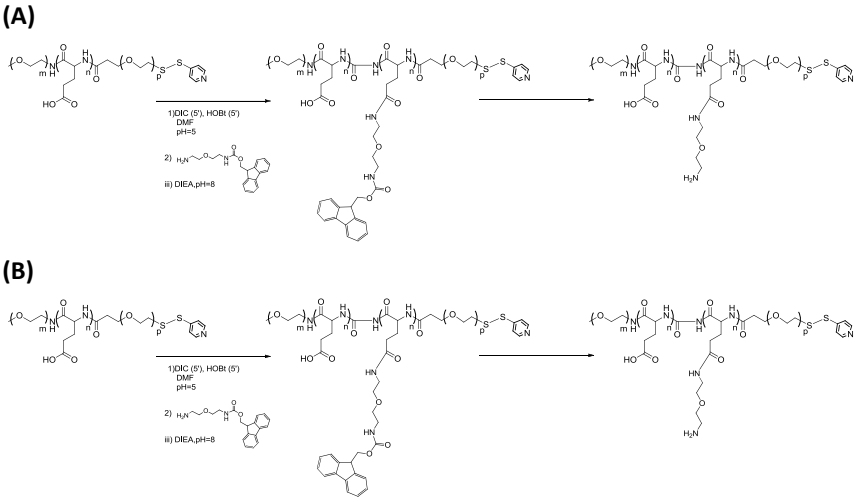

FIGURE III. 46 Scheme of synthesis for DTPA / Gd labelling procedure.

Compound	DP	Degree of diamine substitution (mol/mol of COOH)	1eq DTPA:1eq Gd Gd content (%w/w)
TB-diamine	200	6	5.7
TB-diamine	200	30	25.2
TB-diamine	100	8	8.9
TB-diamine	100	30	29.0

TABLE III. 22 Results for TB-diamine-DTPA labelling.

III. 1. 1 .3 Labelling with radionuclides

Radionuclide imaging techniques are non-invasive, highly sensitive, quantitative and enable whole body scanning. Oppositely, poor spatial and temporal resolution or limited half-life of the radioactive compounds count as their main disadvantages. Focusing on patients treatment, this ionising radiation limit their repeated use [25]. PET application in diagnosis and biomedical research is

outstanding. In particular, its use for brain study and heart functions has become essential. It allows monitoring through positron emitter-labelled compounds and it has been proved to be more sensitive than MRI or computed tomography (CT) although high costs and required equipment limit its applicability [11].

In brief, a chemical compound labelled with a short-lived positron-emitting radionuclide of carbon, oxygen, nitrogen, or fluorine is injected into the body. The activity of such a radiopharmaceutical is quantitatively measured by means of photomultiplier-scintillator detectors. As the radionuclide decays, positrons are annihilated by electrons, giving rise to gamma rays that are detected simultaneously. While fluorescence emission is limited by a low penetration depth, PET ability to detect organ accumulation is highly accurate, regardless of tissue depth [26].

In this work, positron emitters (^{18}F, ^{68}Ga) were incorporated into the PGAs through covalent or complexation chemistry. This strategy is tedious and lengthy although in most cases it does not significantly alter the platform structure. Usually, a non-metal PET nuclide like ^{18}F is incorporated by means of covalent attachment, but a metal radioisotope such as ^{68}Ga needs a chelator, which usually provides high yields. For stable complexation, chelating agents based on polyamine carboxylic acids e.g. DTPA, DOTA or 1,4,7-triazacyclododecane-N,N'',N'''-tetraacetic acid (NOTA). Thus far, complex ^{68}Ga-DOTA is one of the most widely used and therefore, it was the selected for our purposes.

Methodology for labelling with Tyramine for PET monitoring after ^{18}F conjugation

First step involved the coupling of tyramine to the PGAs (scheme in FIGURE III. 47). The phenolic compound named tyramine was covalently linked to the triblocks (**27**) of different length: 100, 150, 200, achieving percentages detailed in TABLE III. 23.

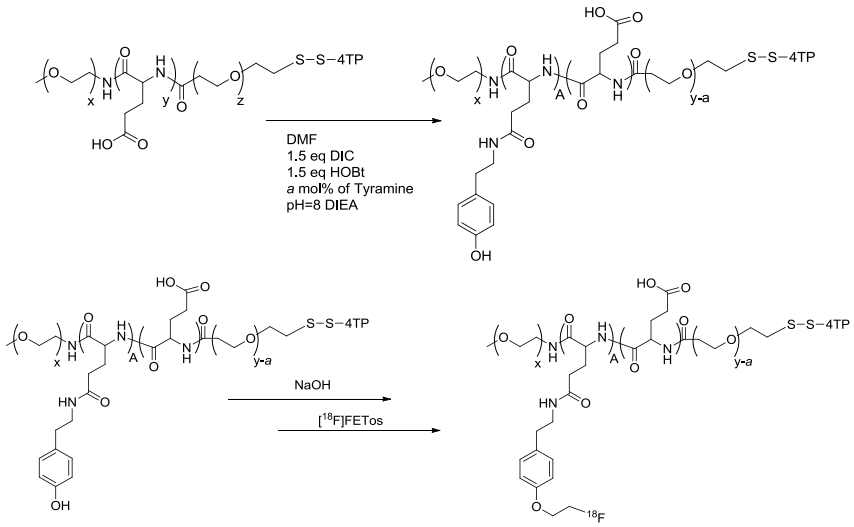

FIGURE III. 47 Tyramine labelling synthetic scheme.

Compound	Theoretical %mol Tyramine	Experimental %mol Tyramine
TB_{150}	5	3
TB_{150}	12	0.3
TB_{200}	20	16

TABLE III. 23 Total tyramine content in the TBs-Ty (**27**).

Tyramine conjugation aim was to later coupling a [^{18}F]fluoralkyl synthon[9]. The synthon used was the 2-[^{18}F]fluoroethyl-1-tosylate ([^{18}F]FETos) which allows for site-specific radiofluorination at phenolic groups, and should not influence the structural properties of the self-assembled nanosystems itself. Labelling protocol is described in reference [27] and the fluorination step was performed in the Institute of Nuclear Chemistry, Johannes Gutenberg-University Mainz, Germany by Dorothea Moderegger.

[9] SYNTHONS are prosthetic groups.

Fluorination process yielded low ^{18}F content. In order to create the needed nucleophile, products were dissolved in DMF and NaOH was added to get the O^- nucleophile from the tyramine units. In our products, carboxyl groups from the PGA were firstly deprotonated instead the hydroxyl benzyl ones. To solve the problem, solubility of the systems in organic aprotic solvents had to be achieved. Calcium, ammonium and lithium salts of PGA were synthesised by cation exchange with the sodium PGA salt and later desalted by SEC. Ion exchange was successfully achieved and the resulting calcium and lithium salts were soluble in DMSO. Lithium salt was selected to continue with the experiments although the labelling percentage achieved was again not sufficient to perform biodistribution experiments. Therefore, this labelling methodology was dismissed.

Methodology for labelling with DOTA/ Ga for PET monitoring

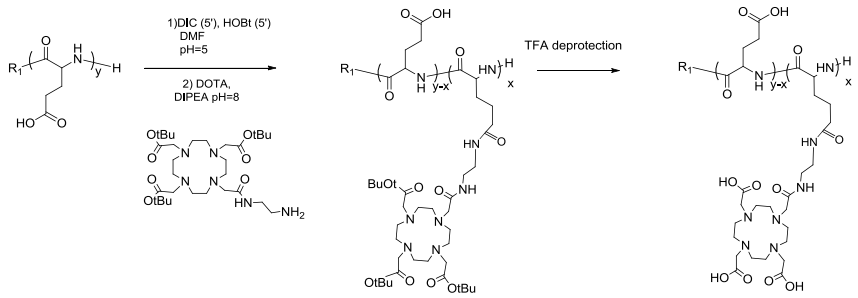

FIGURE III. 48 Synthetic approach followed for DOTA labelling.

R_1=nBu, PEG.

DOTA is one of the most popular chelators used for radiolabelling purposes due to its capability to form stable complexes with various M^{2+} and M^{3+} ions, e.g. ^{68}Ga, ^{90}Y, ^{111}In, and ^{177}Lu. Our strategy consisted on the linkage of a DOTA amino derivative through an amide bond to the PGAs: homopolymer and DB both with 100 GA units (scheme in FIGURE III. 48). Varying the initial equivalents of DOTA, several coupling percentages were achieved (TABLE III. 24). Reactions proceeded quantitatively giving labellings of 2 to 11%mol of DOTA, calculated after ^1H-NMR analysis (FIGURE III. 49).

	DP	Theoretical %mol DOTA	eq. DOTA (x)	Real %mol DOTA*	% mass yield
PGA_{100}	106	5	0.05	2	94
	106	10	0.1	9.8	80
DB_{100}	94	11.5	0.115	11	71

*calculated by ^{1}H-NMR.

TABLE III. 24 Results for DOTA polymer labelling: PGA-DOTA (**28**) and DB-DOTA (**29**).

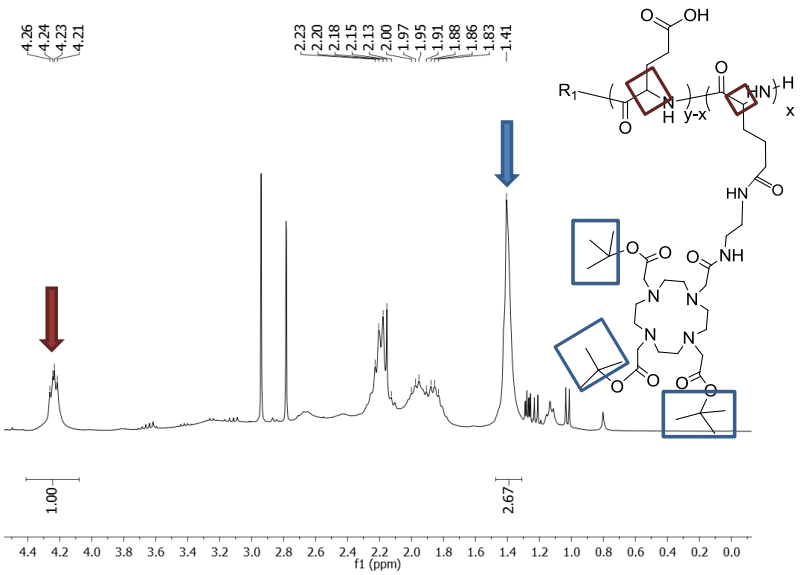

FIGURE III. 49 ^{1}H-NMR of PGA-DOTA 10% labelled. Example of molar percentage calculation.

DOTA protecting groups allow solubility in most organic solvents, and the tert-butyl ester removal procedures do not need strong conditions, which could affect the polypeptide chain. Deprotection conditions used in this work were optimised to achieve an optimal result in the shortest time without damaging the carrier either systems where ligands are already coupled (peptidic sequences owning disulphide bonds). Initial protocol involved 15h in agitation in TFA although 3h in a mixture TFA/H_2O/TIPS (95:2.5:2.5) enabled a

satisfactory result, being profitable for other purposes (FIGURE III. 50).

(A)

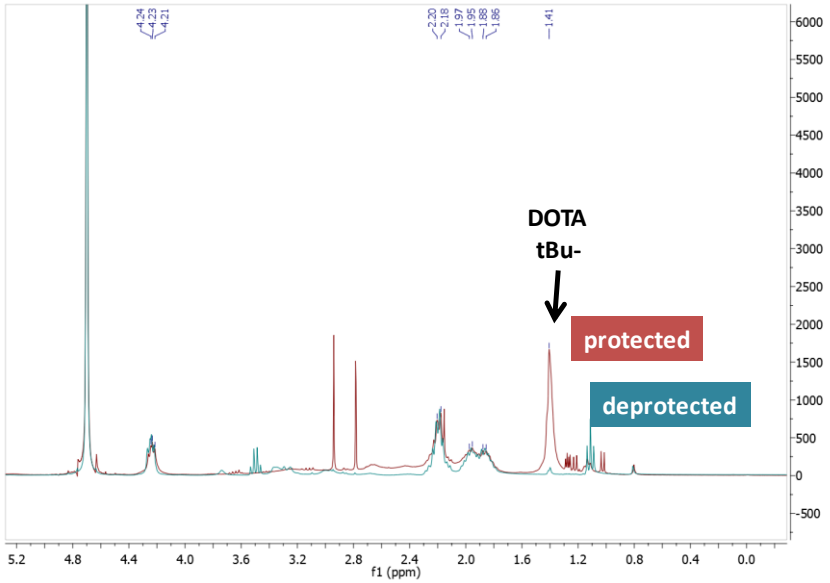

(B)

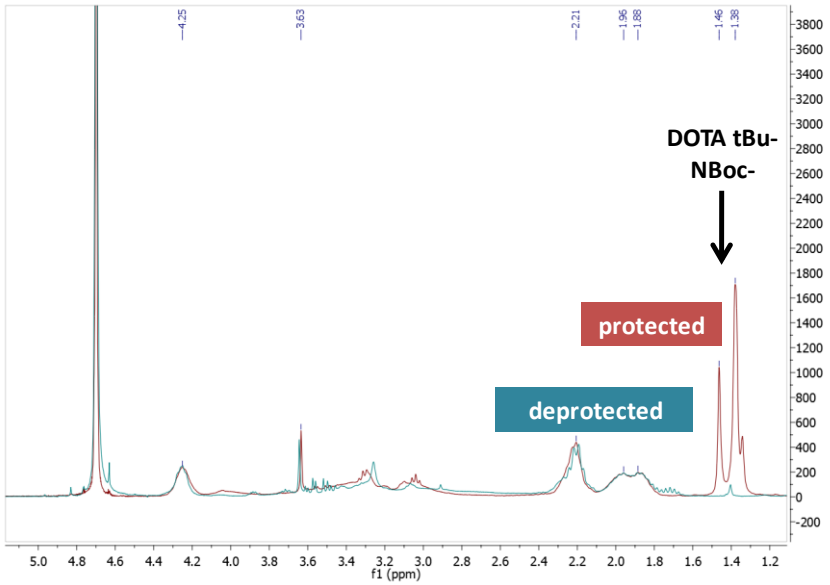

FIGURE III. 50 DOTA deprotection ^{1}H-NMR spectra: (A) PGA-DOTA (**43**), (B) DB-DOTA-diamine-N-Boc (**45**) deprotection.

Gallium labelling was performed at the CIEMAT (Madrid).

Radiochemical yields were in all cases 86.3%±3.4 (n=5). Radionuclide purity was calculated as the ratio activities of 68Ge versus 68Ga in the eluate, corrected for decay expressed in %. The RNP was $<3.4\cdot10^{-4}$ %± $0.4\cdot10^{-4}$ in all cases.

III. 1. 2 TARGETING LIGAND CONJUGATION FOR BBB CROSSING THROUGH ACTIVE TRANSPORT

For the purpose of blood-brain barrier crossing, the PGA family presented in this project has been designed to gather multiple possibilities exploiting active targeting strategies through covalent binding of ligands for brain receptors: (i) availability of different regions in the polymer backbone (which serve for site-specific conjugation together with the option of post-polymerisation modifications) and (ii) insertion of cleavable linkers in specific environmental situations. Insertion of PEG blocks as well as modulation of the PGA block length block were also proposed with the aim of obtaining conjugates with different solution conformation, which could help BBB crossing.

As mentioned in the introduction, the selected strategy to achieve this goal has been active transport: drug delivery systems conjugated to ligands capable of binding receptors overexpressed in BBB (sections I.1.4 and I.1.7). In particular, the transferrin receptor (TfR) and the low-density lipoprotein receptor-related protein-1 (LRP1) were selected as target. In the case of TfR, not only the natural ligand but also a monoclonal antibody (mAbOX26) [3, 28, 29] or an iron-mimicking cyclic peptide [30] were evaluated. For LRP1, Angiopep-2 peptide was chosen due to its recent progress in clinical trials [31, 32].

Regarding type of linkage, the use of disulphide bonds guaranties site-specific conjugation in the different block copolymers synthesised, either achieved by the introduction of –SH groups in the terminal PEG block or through post-polymerisation modification of the PGA side-chains. As an alternative, the use of amide linkers has been also explored e.g. with the cyclic peptide.

On the other hand, the selected ligand (protein, antibody or

peptide) should also bear the adequate functionality (-SH) and this group should not be linked to bioactive roles, if not, it should be chemically introduced to allow conjugation without compromising their inherent biological activity. Introduction of extra cysteine (Cys) residues or small molecules with sulfhydryl groups is commonly used to achieve chemoselective derivatisation. In contrast, those ligand disulfide bridges not implicated in essential roles, can be mildly reduced to gain–SH anchoring points for polymer conjugation [33-35].

For instance, in the present work Tf was thiolated with 2-iminothiolane and mAbOX26 was exposed to mild reductive conditions to cleave S-S bridge. Angiopep-2 was derivatised with an extra cysteine at C- terminal.

III. 1. 2. 1 Transferrin (Tf)

As stated in the introduction, TfR is expressed in the BBB and its function relies on iron transcytosis pathway. On this basis, Tf was coupled to the synthesised polyglutamates to evaluate their future potential as drug delivery systems across the BBB.

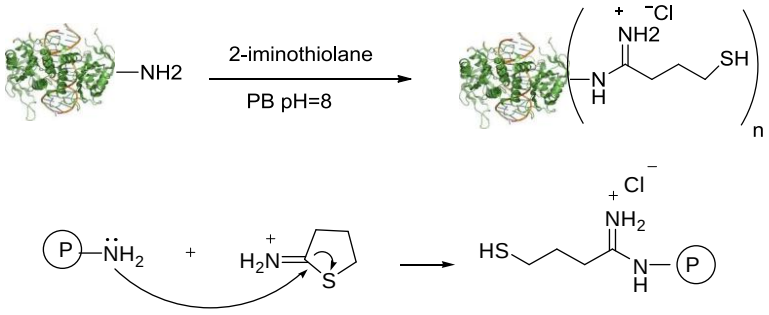

FIGURE III. 51 Transferrin (Tf) thiolation procedure.

First, Tf thiolation process was successfully achieved by means of different concentrations of 2-iminothiolane (FIGURE III. 51) and (TABLE III. 25). The purification procedure was monitored by absorbance (Tf (280nm) and 2-iminothiolane (240nm)) (FIGURE III. 52). The number of SH groups was calculated by MS MALDI TOF (Tf MW=78KDa) (FIGURE III. 53).

[Tf] mmol	% excess	[2-iminothiolane] mmol	Yield	-SH groups introduced
58	76.2	44	80	24-46
64	30.0	19	68	9-15

TABLE III. 25 Results for Tf thiolation (Tf_{thio}).

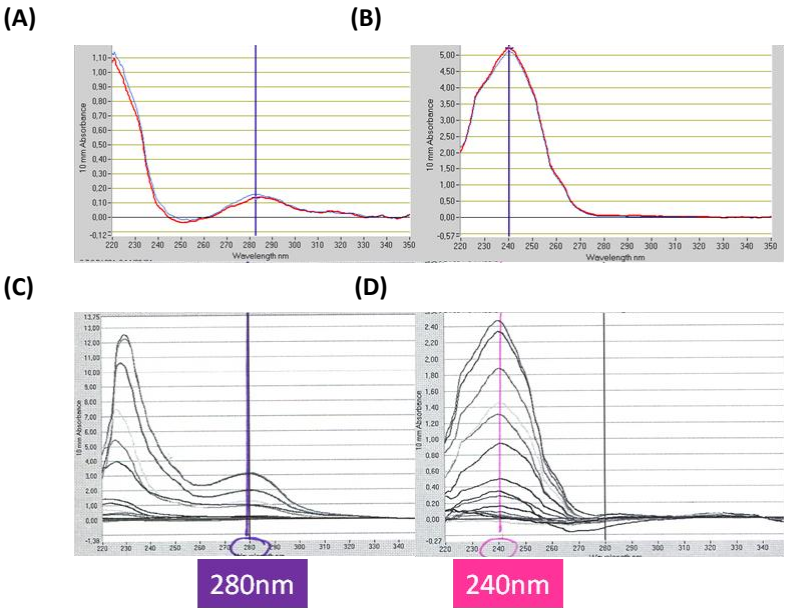

FIGURE III. 52 Tf_{thio} purification through PD10 column. Detection of protein fraction location by means of absorbance (Nanodrop®). (a) Spectra of Tf, detection at 220 and 280nm. (b) Spectra of 2-iminothiolane, maximum at 240nm (c) Overlay of spectra from fractions 8 to 19. (d) Overlay of spectra from fractions 20 to 40.

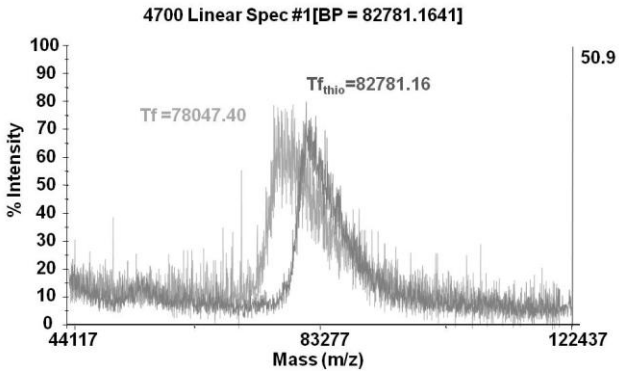

FIGURE III. 53 Comparison of MS MALDI TOF spectra from Tf and thiolated Tf.

For later conjugation, thiolated transferrin was synthesised and used immediately after its purification and quantification. To establish the most suitable ratio between carrier and protein, Tf conjugation to block copolymers was firstly optimised (FIGURE III. 54 and TABLE III. 26).

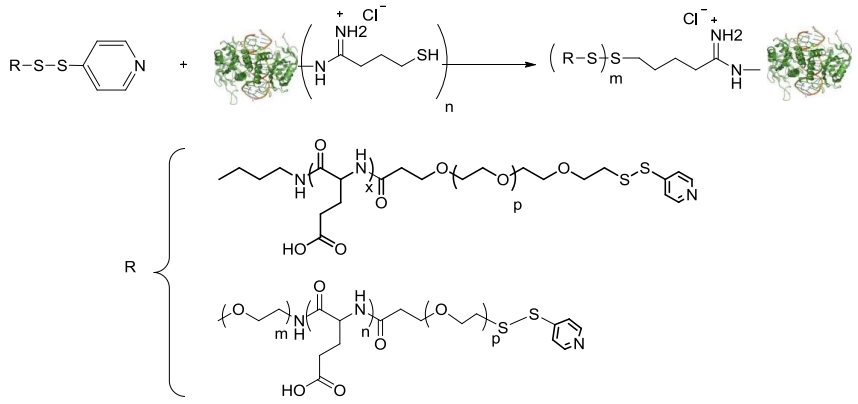

FIGURE III. 54 Tf conjugation to polyglutamate systems.

In the first attempts, Tf conjugation was monitored through Bradford assay. With the equivalent ratio 1:1, coupling efficiency was not 100% and free protein was observed (FIGURE III. 55). Subsequently, polymer equivalents were increased from 1 to 6, achieving better results (FIGURE III. 56 and FIGURE III. 57). From all polymers tested (100, 150 and 200), 200 unit PGA gave the best results with better conjugation efficiency and absence of unreacted protein (FIGURE III. 56).

POLYMER	DP	eq.	eq. Tf_{thio}
TB	200	1	1
	200	1.5	1
	200	6	1
	200	6	1
	150	1.5	1
	150	3	1

	100	0.4	1
	100	2.5	1
TBO	200	0.7	1
	200	2.5	1
	200	6	1
DB-Cy5.5	100	1	6

TABLE III. 26 Tf polymer conjugation to TB (**5**), TBO (**20**) and DB-Cy5.5 (**34**). DP=degree of polymerisation.

(A)

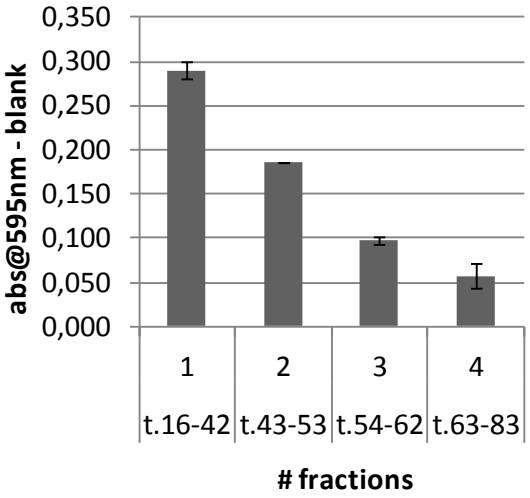

(B)

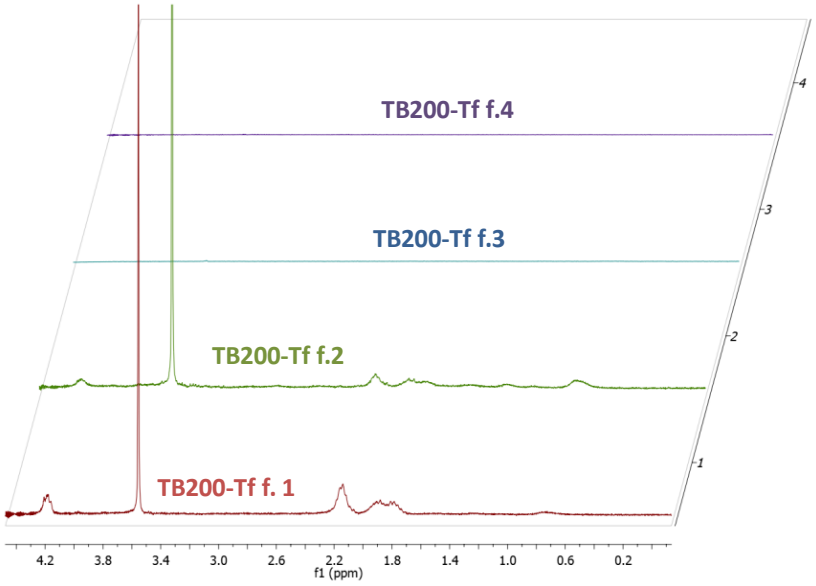

(C)

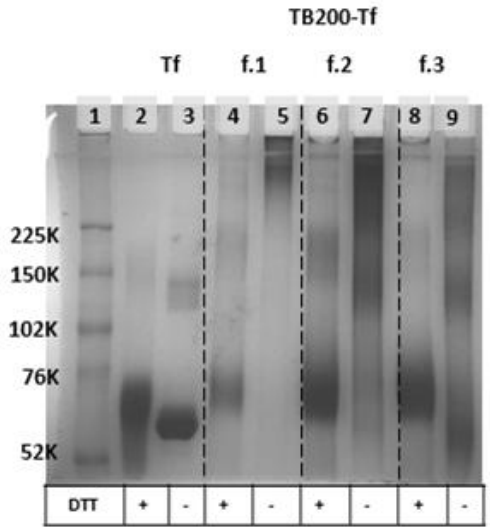

FIGURE III. 55 Tf conjugation to $TB_{200.}$ Analysis of the fractions after FPLC purification of the reaction. (A)Bradford measurement for Tf quantification of each fraction. (B) ^{1}H-NMR analysis for TB detection of each fraction. (C) SDS-PAGE gel analysis of the fractions 1, 2 and 3.

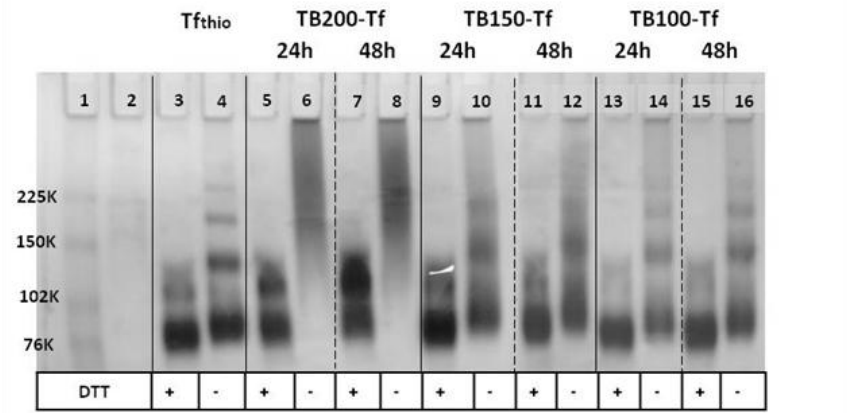

FIGURE III. 56. Tf-thio conjugation to different TBs. Reaction monitoring through SDS-PAGE analysis.

This result was reproducible for OG labelled TB_{200} (FIGURE III. 57), although purification was needed to remove unreacted protein. Unfortunately, initial fluorescence decreased after Tf conjugation by half. Therefore, use of Oregon green was discharged, changing to Cy5.5. This NRI dye proved to provide a better and more stable fluorescent output.

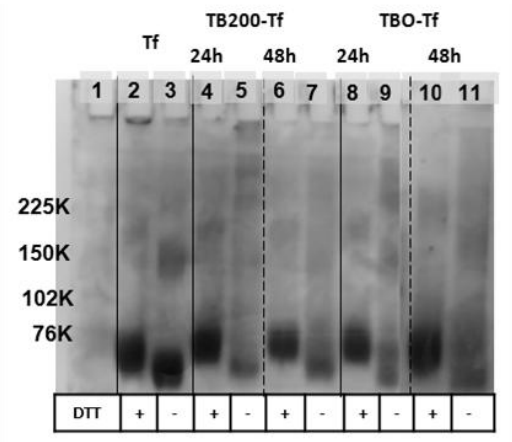

FIGURE III. 57 Tf-thio conjugation to OG labelled TB (**33**) and TB_{200} (**32**). Reaction monitoring through SDS-PAGE analysis.

Cyane labelled DB was conjugated to Tf using the optimised protocol (1eq DB: 6eq Tf_{thio}). As it can be seen in the SDS-PAGE gel showed in FIGURE III. 58, a successful protein conjugation was

achieved. Purification by FPLC and quantification of protein content by Nanodrop® yielded a 65% Tf conjugation.

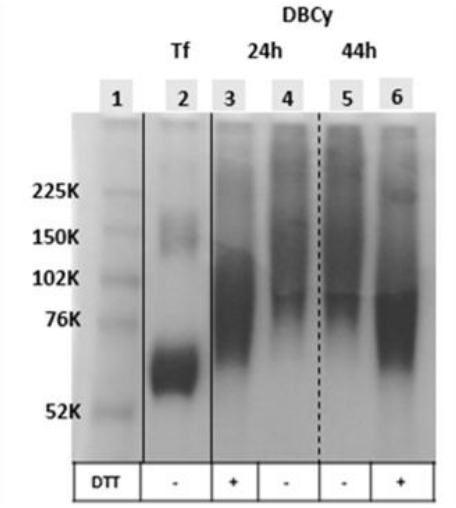

FIGURE III. 58 Tf_{thio} conjugation to Cy5.5 labelled DB (DB-Tf-Cy5.5, **35**). Reaction monitoring through SDS-PAGE analysis.

III. 1. 2. 2 Monoclonal antibody OX26 (mAbOX26)

Ligand-mediated drug delivery to the brain has also exploited the chimeric peptide technology, wherein a non-transportable drug is conjugated to a BBB transport vector [29]. An example is a receptor-specific monoclonal antibody that undergoes receptor-mediated transcytosis through the BBB *in vivo*. Transferrin is limited as a brain targeted vector since its receptors are almost saturated under physiologic conditions due to high endogenous Tf plasma concentration. However, antibodies directed to TfR have been shown selective BBB endothelium binding due to the high expression levels of TfR in these cells. Therefore, these antibodies can be considered potential carriers for the delivery of therapeutic agents to the CNS. Intense work with mAbs against the TfR (e.g. mAbOX26) demonstrated preclinical efficacy in animal models, although a translation into clinical applications met with far less effective results. On this basis, mAbOX26 was selected as an alternative to the Tf protein [28, 29, 36].

mAbOX26 was reduced under mild conditions with

dithiothreitol (DTT) in order to expose its own reactive sulfhydryl groups (scheme in FIGURE III. 59). The reduced antibody purification was successfully achieved as demonstrated by the absorbance analysis (280nm) of the obtained fractions (FIGURE III. 60).

Immediately after reduction, antibody was conjugated to the polymeric platform (FIGURE III. 61). In this case, platform selected was TB_{200}-di-DTPA/Gd (**26**) (68% yield) to allow further MRI analysis *in vivo*. OX26-conjugates were maintained in solution (PBS pH=7.4) prior to its use to avoid reconstitution problems after lyophilisation.

FIGURE III. 59 Mild reduction of the mAbOX26.

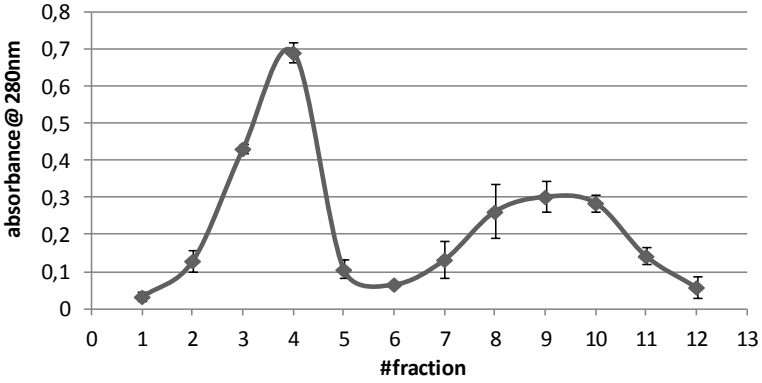

FIGURE III. 60 Fractions absorbance (280nm) of mAbOX26 reduction purification.

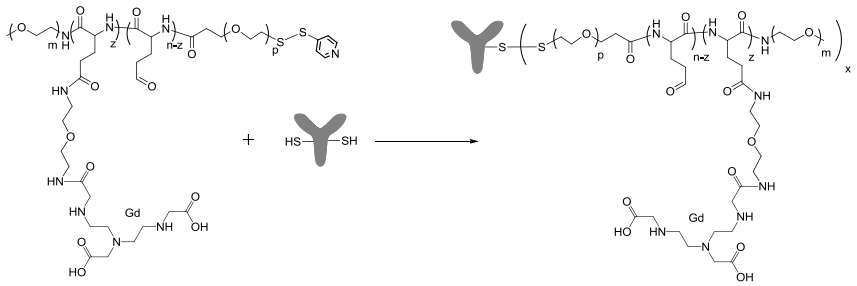

FIGURE III. 61 Reduced mAbOX26 conjugation to TB-diamine-DTPA/Gd.

III. 1. 2. 3 Peptidic sequences

Active transport is an upward trend and introduction of peptide-based strategies provide an alternative platform capable of breaching the BBB. Hence, we proposed two peptide sequences with demonstrated potential for this goal by means of targeted polymer-drug conjugates: the Angiopep-2 peptide [31, 32]and the iron-mimicking cyclic peptide [30].

In this first attempt, both peptides have been conjugated to the PGA_n and PEG-*b*-PGA_n diblock (both with n=100) by means of a small spacer linked to the pendant carboxyl groups, able to provide the desired ending point for their covalent coupling: a disulphide bond for the derivate Angiopep-2 (FIGURE III. 62(A)) and an amide linkage for the cyclic peptide (FIGURE III. 62(B)).

- **Angiopep-2**

To provide sulfhydryl pendant groups, 3-aminopropane-1-thiol was coupled to the COOH from PGA side-chains. The post-polymerisation modifications were performed successfully, achieving 6 and 10%mol functionalisation for PGA homopolymer and DB, respectively (calculation by NMR, FIGURE III. 50). Do to the presence of disulphide bridges, DOTA deprotection methodology was optimised to avoid disulphide breakage and therefore 4TP group maintenance. Basic deprotection by means of tBuOK was not successful due to

solubility issues. Finally, acidic deprotection was carried out with excellent results after careful optimisation (reaction time) (detailed protocol in Section III.3.2.3) to yield to quantitative deprotections.

Angiopep-2 derivative was successfully conjugated to PGA (**41**) and DB (**42**) through disulphide bonds. The purification of the conjugate was monitored by absorbance in Nanodrop® (FIGURE III. 63). Peptide loading was estimated by ^{1}H-NMR and confirmed by amino acid analysis. Total peptide loadings achieved are detailed in TABLE III. 27.

(A)

(B)

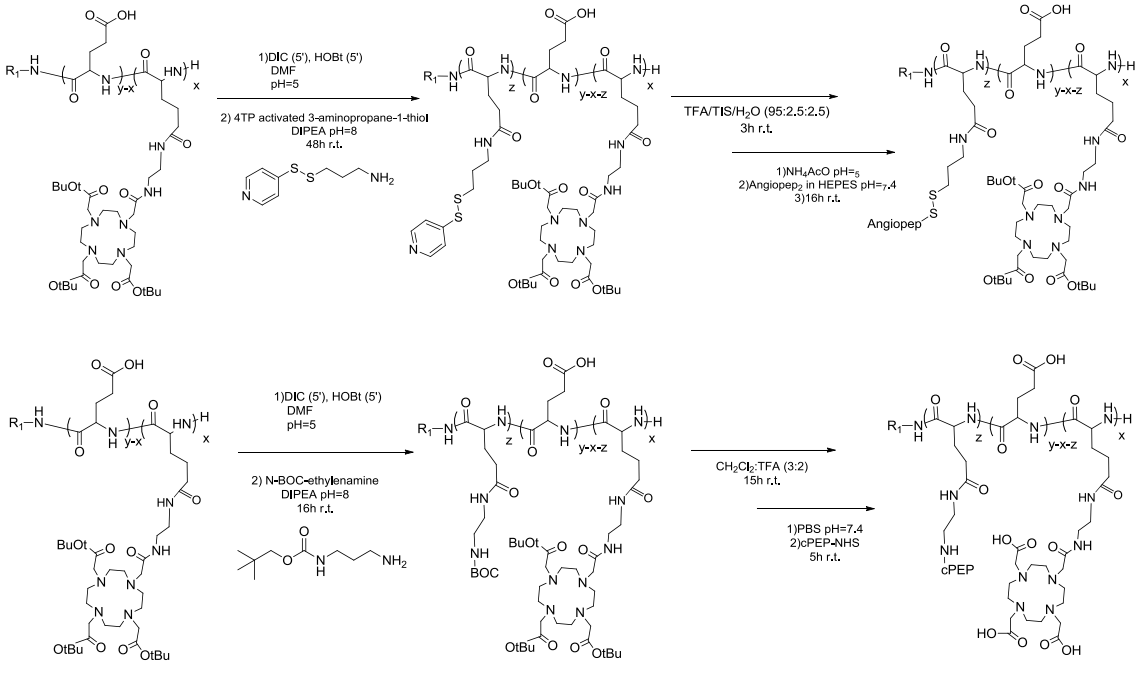

FIGURE III. 62 Synthesis scheme of peptide conjugation: (A) Angiopep-2, (B) cPEP.

(A)

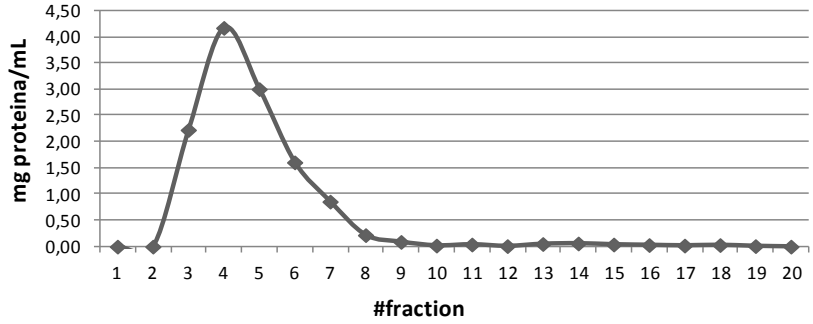

(B)

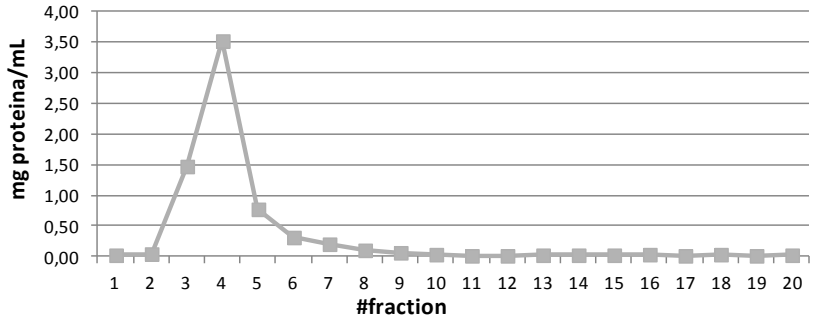

FIGURE III. 63 Absorbance analysis of PGA-Angiopep2 / DB-Angiopep2 fractions after purification: (A) PGA (**41**), (B) DB (**42**).

(A)

Conjugate	REF	mmol conj	MW unit (g/mol)	eq. Angiopep2	mmol eq
PGA-DOTA$_{10\%}$-Cys4TP$_{6\%}$	**39**	0.225	200.41	0.05	0.011
DB-DOTA$_{11\%}$-Cys4TP$_{10\%}$	**40**	0.106	230.63	0.05	0.005

(B)

Conjugate	REF	mmol conj	MW unit (g/mol)	eq. cPEP	mmol eq
PGA-DOTA$_{2\%}$-ethylenediamine$_{9\%}$	**45**	0.1398	160.94	0.09	0.0126
DB-DOTA$_{11\%}$-ethylenediamine$_{11\%}$	**46**	0.1145	218.24	0.11	0.0126

(C)

Conjugate	REF	%mol DOTA	% mol linker	%mol peptide	
				^{1}H-NMR	AA analysis
PGA-DOTA-Ang	**41**	11	9	4.7	3.9
DB-DOTA-Ang	**42**	11	10	4.5	3.5
PGA-DOTA-cPEP	**47**	2	9	2.75	n.d.
DB-DOTA-cPEP	**48**	11	11	3.4	2.8

AA=amino acid, n.d.=not determined

TABLE III. 27. Peptide conjugation to DOTA labelled PGA and DB. (A) Cys4TP linker conjugation. (B) Boc-ethylendiamine linker conjugation. (C) Angiopep-2 or cPEP conjugation.

- **Iron-mimicking cyclic peptide (cPEP)**

In order to introduce amino pendant groups into PGA side-chains N-Boc-ethylenamine was employed. The post-polymerisation modification was performed successfully either in PGA or DB (11% mol funcionalisation) (calculation by NMR, FIGURE III. 50).

Deprotection conditions of the diamine were optimised in order to remove at once the Boc protecting group and the DOTA t-butyl groups. The protocol described above was used either for homo-PGA or PEG-*b*-PGA block. cPEP coupling point to the polymeric carrier was a carboxylic acid of one of its amino acids. With the aim of enhancing the success of the reaction, NHS activation was performed previous to the conjugation step. Full activation was accomplished as detected by ^{1}H-NMR (DMSO-d_6) and then cPEP was conjugated to PGA homopolymer and DB. Peptide loading was estimated by ^{1}H-NMR and confirmed by amino acid analysis (TABLE III. 27).

III. 2 CONCLUSIONS

The forthcoming aim for the synthesised polyglutamates (homopolymer, diblocks and triblocks) was their evaluation as polymer drug carriers. First requisite was to label them with molecular probes to allow monitoring in future *in vitro* and *in vivo* studies. Furthermore, polyglutames were conjugated to different targeting ligands aiming to use them as drug delivery carriers able to cross the brain protecting barrier.

In this chapter, optimisation of the conjugation conditions for probes as well as targeting moieties to targeted and non-targeted systems has been performed. Depending on the monitoring technique expected to be used, the most appropriate label moiety was selected. In all cases, the chemistry approach was based in a covalent linkage, either an amine or a triazole bond. Both unions remain stable under the biological conditions for the required time of study, which is necessary to monitor the conjugate and not the free probe. Furthermore, all the processes were always done trying to link the minimum amount of probe able to produce the adequate signal for detection. This rational design enables to extrapolate the results to the polymer carriers themselves.

For optical imaging studies the fluorophores Rhodamine (Rh), Oregon Green (OG) and Cyane5.5 (Cy5.5) were chosen. Initial conjugation of an amine derivative of Rh did not result in enough fluorescence output of the conjugate complicating its latter detection in cells or animals. Therefore, an amine derivative of OG (OG-cadaverine) replaced it giving good labelling yields with TB (DP=100, 150, 200). This probe was linked via amide bond to the PGA block. Purification of the conjugates was performed by SEC columns and the percentage of conjugated OG was easily calculated after fluorescence measurement of the recovered fractions. These labelled systems were tested to reveal if future exposure to different pHs and concentration will mask real fluorescence and consequently the result. Studies of pH stability showed that fluorescence of the free or conjugated OG decreased in acidic media while not in basic environment, contrarily to

that reported [10].This consequence was taken into account regarding the organ extraction procedures, in order to recover the fluorescence signal. Investigation of quenching properties also demonstrated differences between the limits of detection from OG and TBO. To incorporate this result in future studies, the dilution of the obtained samples was always performed to determine and confirm the real concentration.

Aiming to perform biodistribution studies of the novel obtained polymeric platforms, Cy5.5 was conjugated to PGA homopolymer and diblock copolymer. Post-polymerisation modifications increase the options for probe conjugation. Therefore in the first case, a previous derivation was done by introducing alkyne groups for further conjugation with an azide-cy5.5 derivative. Due to the high selectivity of this click chemistry reaction, conjugation process resulted very simple and with good labelling yields. The diblock labelling was carried out through the amide bonding with an amino derivative of this dye. Again synthesis gave good degree of probe conjugation for later studies.

To explore other monitoring techniques and in parallel searching for the most appropriate to observe BBB crossing, other probes were conjugated to our polymers. MRI fulfilled both statements and therefore the chelator DTPA was conjugated to TB systems (DP=100,200) for Gd complexion. The selected DTPA was an anhydride derivative in order to avoid crosslinking reactions with our polymers. Again a post-polymerisation modification was performed to introduce amine groups for DTPA linkage. Final Gd(III) addition was monitored by titration with an indicator (4-(2-pyridylazo)resorcinol. TB-diamine-DTPA/Gd was successfully obtained, varying the gadolinium content thanks to the different GA units of each starting TB used.

Another leading technique in the named area is PET. The labels used to take profit of this methodology were the radionuclides ^{18}F and ^{68}Ga. A previous step needed before labelling with both elements was

the conjugation of moieties such as tyramine and DOTA, respectively. In the first case, tyramine conjugation to TB was performed via amidic bond and TBs with DP 100 and 200 were used. Different percentages of modification were achieved to be able to tune ^{18}F labelling for appropriate detection. Unfortunately, fluorination process did not succeed due to the need of tyramine units deprotonation. PGA carboxylic groups complicated this process due to their favoured deprotonation instead of the hydroxyl benzyl ones. Thus, this labelling procedure was dismissed.

In the case of gallium, an amino derivative of DOTA was initially coupled to the carboxyl groups of PGA_{100} and DB_{100}. Reactions rendered high yields and deprotection protocols were successfully carried out as demonstrated by their ^{1}H-NMR analysis.

PGAs were designed aiming to display different behaviour for crossing biological barriers due to its conformation in solution, presenting mixed mechanisms of internalisation. In any case, to enhance future drug delivery into the brain, targeting ligand conjugation was performed. All the employed moieties presented the property of being internalised by receptor-mediated endocytosis. The chemical approahc developed in this work was mainly based on (i) the specific point of linkage of the ligand (in the PEG block of the TBs or DBs or in the PGA chain) and (ii) the use of a biodegradable bond which allowed the separation from the polymer-drug conjugate once the target was reached avoiding its recycling outside the brain.

TfR was the first attempt in the project and for it, its natural ligand Tf was conjugated. The protein was first derivatised with 2-aminothiolane to introduce SH- groups for disulphide bonding achieving the best conjugation with the TB_{200} (PEG-*b*-PGA_{200}-*b*-PEG-SS-4TP) with 1:6 equivalent ratio (TB:Tf_{thio}), where no free protein was observed by Western blot analysis. Same protocol was used for linking the thiolated protein to the OG labelled TB (TBO), although fluorescence of the final conjugate decreased significantly making difficult its use in animal/cell studies in order to compare the data with

the non-targeted carrier. Two alternatives were proposed: first the use of Cy5.5 and therefore, DB_{100}-Cy5.5 was successfully conjugated to thiolated Tf using the same chemical scheme. Secondly the substitution of the ligand by a more selective one without problems of receptor saturation like Tf. The mAbOX26 was proposed and to follow within the same chemistry strategy its -SH were exposed for conjugation by means of a mild reduction. The antibody was later conjugated to TB_{200}-DTPA/Gd for comparing biodistribution with the non-targeted TB. mAb conjugation was easily detected by absorbance measurement. Working with this type of ligands could come into solubility problems due to it should be kept the biomolecule structure. Denaturation may promote non-recognition by the receptor and other problems. Therefore, the final product had to be maintained in solution to avoid precipitation which was not able to be redissolved.

Finally as a simpler strategy, we chose peptides targeting the TfR with an iron-mimicking cyclic peptide or the low-density lipoprotein receptor-related protein-1 (LRP1) with the Angiopep-2. These molecules offer higher manageability along the chemical modifications and are not subjected to structural conformations essential for the recognition by the receptor. They were effectively conjugated to PGA_{100} and DB_{100}. Both platforms were previously modified after polymerisation to introduce -SH groups to conjugate the Angiopep-2 and with amine groups for the cyclic peptide. In the last one, disulphide bond was not used because of the presence of an internal disulphide bond in the peptide to simplify the conjugation chemistry. For this approach, the chelator moiety DOTA was initially coupled to the polymer platforms for PET analysis. All the chemistry used rendered good yields along the whole process.

Summing up, several labelling techniques were accomplished and different targeting moieties were successfully conjugated to the homopolymers, diblocks and triblocks. Next step was to evaluate (i) internalisation pathway in cells and (ii) their respective biodistribution (specially for BBB crossing) between targeted and non-targeted PGAs as well as among the homo- and the block copolymers.

III. 3 MATERIALS AND METHODS

III. 3. 1 GENERAL SYNTHETIC METHODOLOGIES FOR POLYMER LABELLING

III. 3. 1. 1 Synthesis of fluorescently-labelled conjugates

Methodology for labelling with Rhodamine (Rho)

Scheme of TB-Rho (**17**) synthesis is depicted in FIGURE III. 38.

Under nitrogen flow, TB_{200} (0.277mmol, 1eq, average Mw unit=102.4 g/mol, 56.63%COOH groups) was dissolved in anh. DMF (10mL). Then, DIC (1.5eq per carboxyl group, 0.86g/mL, 126.2 g/mol) was added and after 5 min, the same equivalents of HOBT (135.13 g/mol). In order to achieve a 2% molar of conjugated Rho, 0.055mmol of Rhodamine (740.73 g/mol) were added after 10 minutes. DIEA was added to increase the pH up to 8. The reaction was left stirring 18h under inter conditions and at RT. After removal of DMF under high vacuum, the residue was re-suspended in the minimum amount of $NaHCO_3$ 1. Solution was purified through a PD-10 column packed with Sephadex^{TM} G-25M in order to remove the un-conjugated Rho. Fluorescence of the collected fractions was monitored with a spectrofluorometer Victor (λ_{Ex}=528 nm, λ_{Em}=553nm).

Yield: 73%. Labelling efficiency: 25% (0.05mol% labelling)

Methodology for labelling with Oregon Green (OG) cadaverine.

Synthesis scheme of OG labelling is depicted in FIGURE III. 40.

*HOMOPOLYMER (**18**)*

In a two neck round bottom flask, 29mg of polyglutamic acid (0.22mmol GA units, 1eq, 129g/mol) was weighted and dissolved in 1mL of anh. DMF under N_2 flow. Then, DIC (0.00674mmol, 0.03eq, 0.806g/mL, 126.13g/mol) was added and the reaction was left to proceed for 5 minutes. After that, HOBt (6.74µmol, 0.03eq, 135.13g/mol) was added in solid form. 10min later, Oregon Green (OG) cadaverine (2.01µmol, 0.009eq, 496.47g/mol) of Oregon Green Cadaverine was added. The pH was adjusted to 8 with DIEA. The

mixture was left stirring for 16-18h protected from light. Finally, the solvent was removed under high vacuum. The obtained residue was dissolved in the minimum amount of $NaHCO_3$ 1M and purified with a PD-10 column packed with Sephadex™ G-25M using ddH_2O as eluent. OG loading was calculated by fluorescence spectroscopy by registration of the fluorescence in all the fractions collected from the column.

Yield: 80-85%. Labelling efficiency: 80-90 %.

*TRIBLOCK (TBO)(**20**)*

In a two neck round bottom flask, 14.4mg of TB_{200} (0.08mmol GA units, 1eq, average MW unit of glutamic acid=102.4g/mol, 56.63%COOH) was weighted and dissolved in 1mL of anh. DMF under N_2 flow. Then, DIC (0.24mmol, 3eq, 0.806g/cm^3, 126.13g/mol) was added and the reaction was left to proceed for 5 minutes. Afterwards, HOBt (0.24mmol, 3eq, 135.1 g/mol) was added directly as solid. 10min later, OG cadaverine ($1.6 \cdot 10^{-3}$mmol, 2%mol theoretical, 496.47g/mol) was added. The pH was adjusted to 8 with DIEA. The mixture was left stirring for 24h protected from light. Solvent was removed under high vacuum. The obtained residue was dissolved in the minimum amount of $NaHCO_3$ 1M and purified with a PD-10 column packed with Sephadex™ G-25M using ddH_2O as eluent. OG loading was calculated by fluorescence spectroscopy by registration of the fluorescence in all the fractions collected from the column.

Yield: 80-85%. Labelling efficiency: 84%

Oregon Green pH stability study and quenching properties

For pH study, OG and TB_{200}-OG (0.72%mol OG) solutions were mixed with solutions 1M of NaOH aq. and 1M HCl. Fluorescence measurement was done at wavelengths λ_{em}=535nm, λ_{ex}=485nm.

In case of observation of fluorescence quenching, independent solutions of OG and TB200-OG in DMSO were prepared and different concentrations. Dilutions fluorescence was measured as explained

previously.

Methodology for labelling with Cyane5.5

Synthesis scheme of Cy5.5 labelling is depicted in FIGURE III. 44.

*HOMOPOLYMER: PGA-click-Cy (**22**)*

Cy5.5 azide derivative conjugation. Copper catalysed alkyne-azide coupling (CuACC).

In a Schlenk tube, 1eq of copolymer (PGA-propargylamine, 0.5µmol, 20000g/mol) was dissolved in anh. DMF. Reactor was purged with N_2 flow and degassed by performing two freeze-pump-thaw cycles. In a vial, a solution of CuBr and PMDTA was prepared by dissolving both reagents in anh. DMF (CuBr: 1eq, 143.45g/mol; PMDTA: 1eq, 173.3g/mol), bubbling nitrogen through the solution for 20min to prevent oxidation of Cu(I). Once the CuPMDTA complex was dissolved, it was added to the solution and after that, the probe Cy5.5-azide derivate (3eq, 743.42g/mol). The mixture was deoxygenated by freeze-pump-thaw cycles. The resulting mixture was stirred at 40°C under a nitrogen atmosphere for 48h, protected from light. The solvent was removed under evaporation at high vacuum and the residue was redissolved with the minimum amount of $NaHCO_3$ 1M. Solution was purified through a PD-10 column packed with Sephadex™ G-25M. Fractions were analysed by fluorometer device to evaluate the percentage of Cy5.5 conjugated and those containing the conjugate signal were joined and freeze dried.

Max ex/em wavelength of the labelled PGA=629/692nm.

Labelling efficiency: 87% (1.8%molCy5.5).

*DIBLOCK-Cy5.5 (**34**)*

In one round bottom flask, 100mg of DB_{200} (PGA_{100}–PEG-SS-4TP, 0.72mmol, 1eq, average MW unit of glutamic acid (sodium salt form)=160.5g/mol) were suspended in 8mL of ddH_2O. For a 2%mol labelling, next steps were followed: in a vial, DMTMM·Cl^-

(0.0217mmol, 0.03eq, 276.7g/mol) was dissolved in 1mL of ddH_2O and then added to the main solution. After 10 minutes in agitation, Cyane5.5-NH_2 derivate (0.0144mmol, 0.02eq, 589.25g/mol) previously dissolved in 7mL ddH_2O was added to the main solution. Finally, pH was checked to 8 (if pH was lower, it was adjusted with $NaHCO_3$ 1M solution). The reaction was monitored by TLC (MeOH) and it was left under agitation at RT for 40h. The mixture was freezed-dried and the blue powder obtained was redissolved in ddH_2O and purified through a PD-10 column packed with Sephadex™ G-25M using ddH_2O as eluent. Fractions collected were analysed by fluorometer device.

In addition, 4TP release assay was performed to ensure its stability after the reaction.

Max ex/em wavelength of the labelled PGA=598/655nm.

Labelling efficiency: 90.86% (1.63%molCy5.5), 4TP assay: positive.

III. 3. 1. 2 Contrast agents labelling. DTPA/Gd complex.

Methodology for labelling for MRI analysis by DTPA/Gd conjugation

DTPA conjugation to TB-diamine.

Synthesis scheme of DTPA conjugation to TB is depicted in FIGURE III. 46. 35mg of TB_{200}-$diamine_{30\%}$ (**24**) (0.19mmol GA units, 1eq, average MW unit=188g/mol) were weighted and dissolved in 4mL of anh. DMF under N_2 flow. Amino pendant groups were activated with DIC (0.08mmol, 0.45eq, 0.806g/cm^3, 126.13g/mol) as the coupling reagent for 5 minutes. After that time, HOBt (0.08mmol, 0.45eq, 135.1 g/mol) was added directly in solid form. The reaction was then left to proceed for 10minutes more. Afterwards, DTPA anhydride (0.056mmol, 0.3eq, 357.32g/mol) was added. The pH was adjusted to 8 with DIEA. At the end of the reaction, solvent was removed under evaporation and product was dissolved in $NaHCO_3$ 1M for further purification by ultrafiltration (Vivaspin® MWCO3000) or PD-10 column. Then, the fractions were lyophilised and product was collected. The degree of DTPA substitution was determined by titrating DTPA with

$GdCl_3$ solution using 4-(2-pyridylazoi)-resorcinol as Gd(III) indicator.

Gd(III) chelation

Complexation scheme of Gd(III) is depicted in FIGURE III. 46.

For Gd(III) chelation, the ratio 1:1eq DTPA:$GdCl_3$ was considered. TB_{200}-diamine-DTPA (as sodium salt) (**24**) (was dissolved in PBS 0.1M pH=7.4, while $GdCl_3$ (0.001mmol, stock: 100mg/mL, 263.61g/mol) was dissolved in ddH_2O and dropped into the main solution. During this procedure, pH was monitored and remained constant to 8. In parallel, the degree of Gd(III) complexation was determined by titrating aliquots using 4-(2-pyridylazo)resorcinol (which turns from yellow to orange in presence of free Gd). After 4.5h of reaction, no free Gd was detected and the reaction was stopped by freeze-drying the reaction mixture [37]. The white powder obtained was purified through a PD-10 column for desalting.

Yield: 100%

III. 3. 1. 3 Labelling with radionuclides

Methodology for labelling with Tyramine for PET monitoring after ^{18}F conjugation

Synthesis scheme of tyramine labelling to TB is depicted in FIGURE III. 47.

In a round bottom flask, triblock PEG-*b*-PGA_n-*b*-PEG-SS-4TP (**9**) (1eq, 0.15mmol of GA unit) was placed and the system was purged with nitrogen flow. Then, it was dissolved in 15mL of anh. DMF under stirring at 35°C in an oil bath under inert atmosphere. Then, DIC (1.5eq, 0.22mmol, 0.806g/mL, 126.2g/mol) was added and after 5min, the same equivalents of HOBT (1.5eq, 0.22mmol, 135.13 g/mol) as solid. Ten minutes later, tyramine (for 20%mol: 0.028mmol, 137.18 g/mol) were added to the reaction. The pH was adjusted to 8 with DIEA. The reaction was left under constant agitation at 35°C protected from light, under N_2 atm. After 24h, DMF was evaporated under vacuum. The residue was perfectly re-suspended in 1mL of DMF and it

was purified through LH20 column (using DMF as eluent). 30 fractions of 1mL were collected and afterwards each fraction was evaporated under vacuum individually. Then, ddH_2O was added to freeze-dry the tubes and dry them properly. ^{1}H-NMR and COSY analysis (DMF-d_7)) were done of each product obtained. TABLE III. 23 shows the different TBs labelled with tyramine.

Yield: 85%. ^{1}H-NMR (300 MHz, DMF-d_7) δ (ppm) 1.76-1.89 (2H, m), 2.13 (2H, m), 3.45 (xH, s), 4.16 (1H, t), 6.97 (d, nH), 6.70 (*n*H), 7.60 (d) 8.40 (zH, s).

(PEG proton signals (x and z) were related to DP of the PGA block and tyramine signals (n) depended on the percentage coupled (when conjugated, tyramine benzyl signals are broader and doublet is not recognisable, i.e. TB_{100}-16%mol tyramine: δ (ppm) 1.76-1.89 (200H, m), 2.13 (200H, m), 3.45 (455H, s), 4.16 (100H, t), 6.97 (d, 32H), 6.70 (d, 32H), 7.60 (2H, d) 8.40 (2H, s).

Methodology for labelling with DOTA/Ga for PET monitoring

DOTA conjugation

General procedure for DOTA/Ga conjugation is depicted in FIGURE III. 48.

*HOMOPOLYMER (PGA-DOTAtBu) (**28**)*

In a round bottom flask, PGA_{100} (**11**) 2.32mmol, 1eq, average MW GA unit=129g/mol) was placed and system was purged under constant nitrogen flow. Product was dissolved with 20mL of anh. DMF. Then, 1.5eq of DIC (0.35mmol, 0.836g/cm^3, 126.20g/mol) was added to the reaction and after 5min, 1.5eq of HOBt (0.35mmol, 135.10g/mol) was incorporated as a solid. 10min later, DOTA-NH_2 derivate (tert-butyl 2,2´,2´´-(10-(2-(2aminoethylamino)-2oxoethyl)-1,4,7-tetrazacyclododecane-1,4,7-triyl)triacetate (for 10%mol: 0.23mmol, 0.1eq, 614.82/mol) dissolved in anhydrous DMF was dropped to the reaction. Depending on the degree of conjugation desired, DOTA equivalents were modified (TABLE III. 24). The pH was

adjusted to 8 with DIEA. After 48h stirring at RT, solution was concentrated under high vacuum. Purification was performed by precipitation of the concentrated solution in an excess of cold acetone. Pale yellow precipitate was recovered after centrifugation (2600rpm, 4°C, 10min) and dried under vacuum. Percentage of DOTA conjugation was calculated by ^{1}H-NMR analysis (D_2O).

Yield: 88%. %mol DOTA: 9.8, ^{1}H-NMR (300 MHz, D_2O) (9.8%mol DOTA): δ 4.24 (1H), 2.31 – 1.76 (m, 4H), 1.41 (s, 2.7H).

*DIBLOCK (DB-DOTAtBu) (**29**)*

In a round bottom flask, diblock mPEG-*b*-PGA_n (**7**) (n=100, 0.7166mmol, 1eq, average MW GA unit (salt form)=171.31g/mol) was placed and then dissolved with 5mL ddH_2O. Then, DMTMM·Cl (0.0717mmol, 0.115eq, 0.836g/cm^3, 126.20g/mol) was added to the reaction and after 10min, DOTA-NH_2 derivate (for 11.5%mol: 0.0717mmol, 0.115eq, 614.82/mol) previously dissolved in anh. DMF (1mL) was dropped to the reaction. pH was adjusted to 8 with DIEA. After 48h stirring at RT, solution was concentrated under high vacuum. Purification was performed by precipitation of the concentrated solution in an excess of cold acetone. Pale yellow precipitate was recovered after centrifugation (2600rpm, 4°C, 10min) and dried under vacuum. Percentage of DOTA conjugation was calculated by ^{1}H-NMR analysis (D_2O).

Yield: 71%. %mol DOTA: 10.8. ^{1}H-NMR: (300 MHz, D_2O)(10.8%mol DOTA): δ 4.24 (1H), 3.6 (s), 2.31 – 1.76 (m, 4H), 1.41 (s, 2.9H).

DOTA deprotection

Deprotection scheme of tBu groups from conjugated DOTA moiety is depicted in FIGURE III. 48.

To avoid crosslinking reactions, carboxyl groups of DOTA moiety are usually protected. In the present derivative, ending groups were protected by t-butyl groups. Carboxyl groups were deprotected with the protocol described below, before ^{68}Ga complexation.

(A) The PGA-DOTAtBu conjugate was dissolved in CH_2Cl_2 /TFA (3:2, v/v) mixture and left under agitation 15h at room temperature. Afterwards, solution was precipitated into an excess of cold diethyl ether. Yellow solid obtained was collected, washed with fresh ether and dried over vacuum. Full deprotection was checked by ^{1}H-NMR analysis.

Yield: 91%. Deprotection yield: 100%

(B) The PGA-DOTAtBu conjugate was dissolved in TFA/H_2O/TIS (95:2.5:2.5 v/v) mixture and left under agitation 3h at room temperature. Afterwards, solution was precipitated into an excess of cold diethyl ether. Yellow solid obtained was collected, washed with fresh ether and dried over vacuum. Full deprotection was checked by ^{1}H-NMR analysis.

Yield: 89%. Deprotection yield: 100%

Gallium labelling

For ^{68}Ga labelling, first this radionuclide was eluted, purified and concentrated. Then, the obtained ^{68}Ga was transferred into microwave tube and the pH was adjusted to 3.5-4 by adding HEPES buffer. Immediately, the DOTA labelled system (e.g. PGA-DOTA (8.61mg) in aqueous solution was added 500µL. The mixture reaction was heated at 90°C for 5min by a microwave laboratory with monomodal radiation (Discover Benchmate, CEM). Then, purification was performed with a exclusion molecular chromatography cartridge (Bio Gel P-6 Bio Rad) using PB pH=7 as eluent. The elution profile was determined by fractionating and measuring the fractions with an activimeter (VDC 405 Veenstra). Radiochemical yield (RY) was calculated as percentage of the activity in each fraction eluated from the molecular exclusion cartridge of the total activity purified, corrected for the decay.

Radionuclide purity (RNP) was assessed by γ-spectrometry (HPBGe detector) immediately and after 24-48h in order to determine the ^{68}Ga breakthrough.

III. 3. 2 Targeting ligands conjugation for BBB crossing through active transport

III. 3. 2. 1 Transferrin

Firstly, sulfhydryl groups were introduced in the protein by the reaction of its own amino groups with 2-iminothiolane. These –SH groups are the specific linkage point to conjugate the PEG-SS-4TP block of diblock or triblock systems.

Methodology for Tf thiolation

Synthetic scheme of thiolated Tf is depicted in FIGURE III. 51.

The protocol from Ulbrich *et al*. detailed in ref [38] was used with few modifications. In a round bottom flask, human holo-transferrin (0.58mmol, 1eq, 78KDa) was dissolved at a concentration of 10mg/mL in phosphate buffer pH=8.0 and incubated with a solution 6.9mg/mL of 2-iminothiolane (76.2molar excess, 44mmol, 137.63g/mol) in the dark for 1.5h at RT and constant shaking. Purification was performed with two methodologies described below.

(i) The thiolated Tf was purified directly through a Sephadex G25 column using PB pH=8 as eluent. In each fraction, protein amount was checked twice by absorbance measurement with Nanodrop® (λ_{max}=220, 280nm, Ɛ=82.74 mM^{-1} cm^{-1}) measurement and Bradford assay (protocol detailed in appendix III). Fractions were joined and total amount of protein was measured with the named methodologies and percentage of SH-groups introduced was calculated after MS MALDI-TOF analysis.

(ii) The mixture was purified by Ultrafiltration (Vivaspin® MWCO=10000Da) and using PB pH=8 as eluent. Washes were performed until no absorbance signal of 2-iminothiolane (λ_{max}=240nm, Nanodrop® measurement) was detected. Finally, protein concentration was determined by Nanodrop® (λ_{max}=220, 280nm) and MW by MS MALDI TOF analysis.

Protein was used in solution for next reaction immediately after its synthesis.

Thiolated transferrin conjugation to polyglutamates systems

Synthetic scheme of conjugate TB-Tf (**33**) is depicted in FIGURE III. 54.

Thio-Tf conjugation to TB-OG

Synthetic scheme of OG labelling of TB-Tf (**33**) is depicted in FIGURE III. 40.

In a 10mL round bottom flask, 6.8mg of TBO (n=200, 1.6%mol OG, 6eq) were dissolved in 2mL of PB pH=8 and 1eq of thiolated Tf (in solution, 81KDa) was added under agitation. The reaction was purged with nitrogen flow, protected from light and left under constant agitation at RT. After 24, reaction was placed at 4°C for 24h. Aliquots (20µL) from the solution were taken at different time points for SDS-PAGE gel analysis (protocol detailed in appendix III), with and without reduction conditions. Then, the reaction volume was reduced by Ultrafiltration (Vivaspin® MWCO=2000Da) and purified through FPLC equipped with a size exclusion column (Sephacryl S300 column, flow rate=1mL/min, solvent A: PB pH=8; isocratic method, wavelength=215, 254, 280nm). Collected fractions were analysed by Nanodrop® for protein detection and quantification; and OG presence was detected visually and confirmed by fluorescence measurement by Victor® spectrophotometer.

Thio-Tf conjugation to DB-Cy5.5

Synthetic scheme of Cy5.5 labelling of DB-Tf (**35**) is depicted in FIGURE III. 44.

In a round bottom flask, DB_{100}-Cy5.5 (**34**)(1.63%mol Cy5.5, 8.4eq) was dissolved in 2mL of ddH_2O and 1eq of thiolated Tf (in solution) was added. The reaction was purged with nitrogen flow, protected from light and left under constant agitation at RT. After 24, reaction was placed at 4°C for 48h. Aliquots (20µL) from the solution were taken at different time points for SDS-PAGE gel analysis (protocol detailed in appendix III) with and without reduction conditions.

When reaction progress had stopped, the volume was reduced by Ultrafiltration (Vivaspin® MWCO=2000Da) and purified through FPLC

equipped with a size exclusion column (Sephacryl S300 column, flow rate=1mL/min, solvent A: PB pH=8; isocratic method, wavelength=215, 254, 280nm). Collected fractions were analysed by Nanodrop® for protein detection and quantification; and Cy5.5 presence was detected visually and confirmed by fluorometer measurement.

III. 3. 2. 2 mAbOX26

Protocol for mild reduction of the mAbOX26

Reduction scheme of mAb is depicted in FIGURE III. 59.

In a 50mL round bottom flask, mAbOX26 (0.19mmol, 95kDa aprox.) was reduced under inert atmosphere (N_2 flow) with DTT (final concentration in reaction: 50µM, 154.3g/mol) in 18mL of PBS 0.1M, for 30min under stirring at RT. Then, reaction solution was purified through a PD-10 column packed with Sephadex™ G-25M and absorbance of the fractions collected was analysed by Nanodrop® measurement (alternative purification was done by ultracentrifugation (Vivaspin®, MWCO=10000Da) at 4°C, until DTT absorbance in the low part of the tube disappeared). Bradford assay was also performed in order to confirm Ab presence in the purified solution. Once all fractions were joined, Ab concentration was determined by Nanodrop® (λ=280nm).

Reduced antibody remained always in solution to avoid difficulties in re-dissolution and it was added immediately to the selected PGAs for further reaction.

Reduced antibody conjugation

Synthetic scheme of mAb conjugation to TB-DTPA/Gd is depicted in FIGURE III. 61.

The concentrated solution of the reduced antibody (0.74mmol, 1eq, 95KDa) was added dropwise to the reaction flask with the labelled TB-DTPA/Gd (**26**) (1eq) already dissolved in PBS 0.1M pH=7.4. Reaction was left stirring for 24 h at RT under N_2 atmosphere. To concentrate the volume of the reaction for further purification,

mixture was ultracentrifugated (MWCO=10000Da) at 8000rpm and 4°C. Upper part of the ultracentrifugation was analysed to test the Ab presence and concentration by means of Bradford assay and absorbance measurement with Nanodrop®. Purification was carried out by means of FPLC equipped with a size exclusion column (Sephacryl S300 column, flow rate=1mL/min, solvent A: PBS pH=7.4, isocratic method, wavelength =215, 254, 280nm). Fractions were the antibody conjugate were found, were mixed and concentrated again by ultracentrifugation. Product was storage in solution until further use at 4°C.

III. 3. 2. 3 Peptidic sequences

Angiopep-2

4TP activated 3-aminopropane-1-thiol coupling. Spacer between peptide and polymer.

Protocol described below was calculated for achieving a theoretical 10%mol introduction of -SH groups onto the main polymeric chain.

In a round bottom flask, PGA_{100}-DOTAtBu (**28**) (1.06mmol, 1eq, 10%mol DOTA, average MW unit=188.7g/mol) was dissolved in 6mL of anh. DMF under N_2 flow. DIC-coupling of the 4TP activated 3-aminopropane-1-thiol was performed as follows: DIC (0.159mmol, 0.075eq, 0.815g/cm^3, 126g/mol) was incorporated to the reaction and 5min after, HOBt as solid form (0.159mmol, 0.075eq, 135.13g/mol). 10min later, 4TP activated 3-aminopropane-1-thiol (0.106mmol, 0.1eq, 1.012g/cm^3, 186.03g/mol) was added to the reaction solution. The pH was adjusted to 8 with DIEA. The reaction was left to proceed stirring at RT and inert atmosphere for 48h. Product purification was done by precipitating in cold acetone the reaction volume, which was placed afterwards at -20°C to facilitate complete precipitation. The obtained light brown solid was recovered by centrifugation and supernatant was discharged. Solid was dried under high vacuum and characterised by ^{1}H-NMR analysis (D_2O).

Yield: 96%. % coupling: 6%mol (homopolymer), 11% mol (DB)

^{1}H-NMR:

Homopolymer (6%mol Cys-4TP) ^{1}H NMR (300 MHz, D_2O) δ 8.32 (s, 0.6H), 7.60 (d, 0.6H), 7.34 (d, 0.6H), 7.19 (s, 0.6H), 4.23 (s, 1H), 1.26 (s).

DB (PEG-*b*-PGA) (10%mol Cys-4TP) ^{1}H NMR (300 MHz, D_2O) δ 8.31 (s, 0.10H), 7.72 (s, 0.26H), 7.18 (s, 0.10H), 3.63 (s, xH), 2.13 (d, 3.73H), 1.36 (s, 2.98H).Note: protons at 3.63ppm correspond to PEG chain.

Labelled DOTA deprotection. t-butyl removal.

Protocol described below was used either for homopolymer (PGA) or PEG-*b*-PGA block copolymer.

PGA-DOTAtBu-Cys-4TP (**37**) (0.083mmol, average MW per unit=217.24g/mol) was dissolved in TFA/TIPS/ddH_2O (95:2.5:2.5 v/v) and left 3h under constant agitation at RT. Then, solution was precipitated into an excess of cold diethyl ether. The yellow solid obtained was collected, washed with fresh ether and dried over vacuum. Complete deprotection was checked by ^{1}H-NMR analysis.

Yield: 100%. Deprotection: 100%

Conjugation of derivative Angiopep-2 to the polymer platform by disulphide bond formation

For Angiopep-2 conjugation either to PGA or DB, same equivalents of peptide than the introduced linker were used (TABLE III. 27). E.g. PGA conjugation: 45mg of PGA-$DOTA_{11\%}$-$Cys4TP_{6\%}$ (**39**) (0.225mmol, 1eq, MW unit=200.41g/mol) were dissolved in ammonium acetate 150mM pH=5 (4mL). At the same time, the peptide (0.011mmol, 0.05eq, 2300g/mol) was dissolved in 3mL HEPES 10mM pH=7.4 buffer. The two solutions were mixed up reaching a pH of 6. The reaction was left to proceed for 16h under agitation. Afterwards, product was purified through a PD-10 column and fractions were analysed by absorbance measurement (Nanodrop®) (FIGURE III. 63) and ^{1}H-NMR (D_2O). Peptide quantification was performed by amino acid analysis performed in the University of Barcelona (*Unitat de Tècniques Separatives i Síntesi de Pèptids Centres*

Científics I Tecnològics).

Yield: 68%(homopolymer), 70 % (diblock)

Molar % peptide coupling:

		% Angiopep-2	
	REF	**^{1}H-NMR (ppm)**	**AA content (%mol)**
PGA-DOTA-SS-Cys-Angiopep2	**41**	4.7	3.9
DB-DOTA-SS-Cys-Angiopep2	**42**	4.5	3.5

AA=amino acid

Iron-mimicking cyclic peptide

Di-amine monoprotected coupling. Spacer between peptide and polymer.

*HOMOPOLYMER (PGA-DOTAtBu-BOCdiamine) (**43**)*

Protocol described below was calculated for achieving a theoretical 5%mol introduction of -NH_2 groups onto the main polymeric chain.

In a round bottom flask, PGA-DOTAtBu (**28**) (0.53mmol, 1eq, 10%mol DOTA, average MW unit=188.7g/mol) was dissolved in 3mL of anh. DMF under nitrogen flow. Once dissolved, DIC-coupling of the N-Boc-ethylenamine was performed as follows: DIC (0.0397mmol, 0.075eq, 0.815g/cm^3, 126g/mol) was incorporated to the reaction and 5min after, HOBt as solid form (0.0397mmol, 0.075eq, 135.13g/mol). 10min later, N-Boc-ethylamine (0.0265mmol, 0.05eq, 1.012g/cm^3, 160.21g/mol) was added to the reaction solution. pH was adjusted to 8 with DIEA. Afterwards, reaction was left to proceed under constant agitation at RT and inert atmosphere for 48h.

Product purification was done by precipitating in cold acetone the reaction volume, which was placed afterwards at -20°C to facilitate complete precipitation. Pale yellow product was recovered by

centrifugation and supernatant was discharged. Solid was dried under high vacuum and characterised by ^{1}H-NMR analysis (D_2O).

Yield: 100%. % diamine content: 9% (determined by ^{1}H NMR (300 MHz, D_2O): δ 4.23 (1H), 1.37 (d, 3.76H)).

*DIBLOCK (DB-DOTAtBu-BOCdiamine) (**44**)*

Protocol described below was calculated for achieving a theoretical 5%mol introduction of -NH_2 groups onto the main polymeric chain.

In a round bottom flask, mPEG-*b*-PGA_n-DOTAtBu (**29**) (0.17mmol, 1eq, 11%mol DOTA, average MW unit (salt form)=234.6g/mol) was suspended in 3mL of ddH_2O. Once dissolved, DMTMM-coupling of the n-Boc-ethylenamine was performed as follows: 2.4mg of DMTMM·Cl (0.0085mmol, 0.05 eq, 276.77g/mol) was added dissolved in 1mL of ddH_2O. After 10 minutes, N-Boc-ethylendiamine (0.0085mmol, 0.5eq, 1.012g/cm^3, 160.21g/mol) was added. The pH of the mixture was 8. The reaction was allowed to proceed over 48h at room temperature.

Then, the reaction solution was purified by ultrafiltration (Vivaspin®, MWCO=3000Da) using ddH_2O. Once the volume was concentrated, solution in the upper part of the tube was freeze-dried. The obtained white solid was dried under high vacuum and characterised by ^{1}H-NMR analysis (D_2O).

Yield: 78%

% diamine content: 11%mol (determined by ^{1}H-NMR (300 MHz, D_2O): δ 4.25 (s, 1H), 3.63(s, xH), 2.21 (s, 2H), 1.96 (s, 2H), 1.42 (d, *J*=25.1 Hz, 4H)). Note: protons at 3.63ppm correspond to PEG chain.

Di-amine deprotection. N-Boc group removal.

PGA-DOTAtBu-n-Boc-ethylenediamine (**43**) (0.43mmol, average MW per unit=161.69g/mol) was dissolved in CH_2Cl_2:TFA (6:4, v/v) and left 15h under constant agitation at room temperature. Then, solution was precipitated into an excess of cold diethyl ether. The

yellow solid obtained was collected, washed with fresh ether and dried over vacuum. Complete deprotection was checked by ^{1}H-NMR analysis.

Yield: 90%. Deprotection: 100%

NHS activation of the cyclic peptide (cPEP).

Under inert environment, 30mg of cPEP (0.032mmol, 1eq, 940g/mol) were dissolved in anh. DMSO (0,5mL). After complete dissolution, DCC (0.042mmol, 1.3eq, 206.33g/mol) was added. After 5min, NHS (0.042mol, 1.3eq, 115.09g/mol) was incorporated to the reaction mixture and it was left to proceed for 16h at RT and N_2 atm. After that time, reaction was precipitated into cold ether and pellet was freeze-dried. Percentage of activation was obtained after NMR signals integration.

Yield: 30mg. %NHS activation: 100% (determined by ^{1}H-NMR, peak at 2.6ppm).

Conjugation of the cyclic peptide to the polymer platform

For conjugation to the polymeric platform, same equivalents of peptide than the introduced linker were used (TABLE III. 27). E.g. PGA conjugation: 22.25mg of PGA-DOTA$_{2\%}$-ethylendieamine$_{9\%}$ (**45**) (0.1398mmol, 1eq, MW unit=160.94g/mol) were dissolved in PBS buffer pH=7.4 (4mL). Then, 13mg of cPEP-NHS (0.0126mmol, 0.09eq, 1033g/mol) were added. Reaction was left under agitation for 5h. Afterwards, product was purified through a PD-10 column and fractions were analysed by ^{1}H-NMR (D_2O). Peptide quantification was performed by amino acid analysis in the University of Barcelona (*Unitat de Tècniques Separatives i Síntesi de Pèptids Centres Científics I Tecnològics*).

Yield: 80% (homopolymer), 75%(diblock)

Molar % peptide coupling:

		% cPEP	
	REF	**^{1}H-NMR (ppm)**	**AA content (%mol)**
PGA-DOTA-cPEP	**47**	2.75	n.d.
DB-DOTA-cPEP	**48**	3.40	2.8

AA=amino acid, n.d.=not determined

BIBLIOGRAPHY

1. Duncan, R., *The dawning era of Polymer Therapeutics.* Nature Rev Drug Discov, 2003. **2**(5): p. 347-360.
2. Pardridge, W.M., *Vector-mediated drug delivery to the brain.* Adv Drug Deliv Rev, 1999. **36**(2-3): p. 299-321.
3. U. Bickel, et al., *Pharmacologic effects in vivo in brain by vector-mediated peptide drug delivery.* Proc Natl Acad Sci U S A, 1993. **90**(7): p. 2618-22.
4. M. Barz, A. Duro-Castano, and M.J. Vicent, *A versatile post-polymerization modification method for polyglutamic acid: Synthesis of orthogonal reactive polyglutamates and their use in "click chemistry".* Polymer Chemistry, 2013.
5. Duncan, R. and R. Gaspar, *Nanomedicine(s) under the microscope.* Mol Pharm, 2011. **8**(6): p. 2101-41.
6. Duncan, R., *Polymer therapeutics as nanomedicines: new perspectives.* Curr Opin Biotech, 2011. **22**(4): p. 492-501.
7. Kabanov, A.V. and H.E. Gendelman, *Nanomedicine in the diagnosis and therapy of neurodegenerative disorders.* Prog. Polym. Sci., 2007. **32**(8-9): p. 1054-1082.
8. S.C. Richardson, et al., *The use of fluorescence microscopy to define polymer localisation to the late endocytic compartments in cells that are targets for drug delivery.* J Control Release, 2008. **127**(1): p. 1-11.
9. Baker, W.D. and N.J. Mansfield, *Effects of horizontal whole-body vibration and standing posture on activity interference.* Ergonomics, 2010. **53**(3): p. 365-74.
10. F. P. Seib, A. T. Jones, and R. Duncan, *Comparison of the endocytic properties of linear and branched PEIs, and cationic PAMAM dendrimers in B16f10 melanoma cells.* Journal of Controlled Release, 2007. **117**(3): p. 291-300.
11. S. Bhaskar, et al., *Multifunctional Nanocarriers for diagnostics, drug delivery and targeted treatment across blood-brain barrier: perspectives on tracking and neuroimaging.* Part Fibre

Toxicol, 2010. **7**(3).

12. X. Chen, P. S. Conti, and R. A. Moats, *In vivo near-infrared fluorescence imaging of integrin alphavbeta3 in brain tumor xenografts.* Cancer Res, 2004. **64**(21): p. 8009-14.
13. L. L. Muldoon, et al., *Imaging and nanomedicine for diagnosis and therapy in the central nervous system: report of the eleventh annual Blood-Brain Barrier Disruption Consortium meeting.* AJNR Am J Neuroradiol, 2006. **27**(3): p. 715-21.
14. G. B. Fields and R. L. Noble, *Solid phase peptide synthesis utilizing 9-fluorenylmethoxycarbonyl amino acids.* Int J Pept Protein Res, 1990. **35**(3): p. 161-214.
15. N. Nakajima and Y. Ikada, *Mechanism of amide formation by carbodiimide for bioconjugation in aqueous media.* Bioconjug Chem, 1995. **6**(1): p. 123-30.
16. M. Kunishima, C.K., J. Morita, K. Terao, F. Iwasaki, S. Tani, *4-(4,6-Dimethoxy-1,3,5-triazin-2-yl)-4-methylmorpholinium Chloride: An Efficient Condensing Agent Leading to the Formation of Amides and Esters.* Tetrahedron letters, 1999. **55**: p. 13159-13170.
17. Pelet, J.M. and D. Putnam, *An in-depth analysis of polymer-analogous conjugation using DMTMM.* Bioconjug Chem, 2011. **22**(3): p. 329-37.
18. F .Ye, et al., *Noninvasive visualization of in vivo drug delivery of poly(L-glutamic acid) using contrast-enhanced MRI.* Mol Pharm, 2006. **3**(5): p. 507-15.
19. S.C. Lee, et al., *Therapeutic nanodevices.* Nanotechnology Encyclopedy, Bharat Bhushan, 2004(ed. Springer Verlag).
20. *Auckland MRI research group. What is MRI?* www.atlas.scmr.org/mri.html, 2012.
21. S. Aime and P. Caravan, *Biodistribution of gadolinium-based contrast agents, including gadolinium deposition.* J Magn Reson Imaging, 2009. **30**(6): p. 1259-67.
22. E. F. Jackson, et al., *Magnetic resonance imaging of therapy-induced necrosis using gadolinium-chelated polyglutamic*

acids. Int J Radiat Oncol Biol Phys, 2007. **68**(3): p. 830-8.

23. P. Caravan and R.B. Lauffer, *Contrast agents: basic principles.* Clinical Magnetic Resonance Imaging, In: Edelmann RR, Hessenlink, JR, Zlatkin MB, Crues JC, editors. Philadelphia, Saunders, 2005. **1**.
24. Jaspers, K., et al., *MR angiography of collateral arteries in a hind limb ischemia model: comparison between blood pool agent Gadomer and small contrast agent Gd-DTPA.* PLoS One, 2011. **6**(1): p. e16159.
25. Kobayashi, H., et al., *New strategies for fluorescent probe design in medical diagnostic imaging.* Chem Rev, 2010. **110**(5): p. 2620-40.
26. Inc., E.B., *Positron Emission Tomography (PET).* Encyclopædia Britannica Online Academic Edition, 2012.
27. M. M. Herth, et al., *Radioactive labeling of defined HPMA-based polymeric structures using [18F]FETos for in vivo imaging by positron emission tomography.* Biomacromolecules, 2009. **10**(7): p. 1697-703.
28. H. J. Lee, et al., *Targeting rat anti-mouse transferrin receptor monoclonal antibodies through blood-brain barrier in mouse.* J Pharmacol Exp Ther, 2000. **292**(3): p. 1048-52.
29. D. Wu and W.M. Pardridge, *Pharmacokinetics and blood-brain barrier transport of an anti-transferrin receptor monoclonal antibody (OX26) in rats after chronic treatment with the antibody.* Drug Metab Dispos, 1998. **26**(9): p. 937-9.
30. F. I. Staquicini, et al., *Systemic combinatorial peptide selection yields a non-canonical iron-mimicry mechanism for targeting tumors in a mouse model of human glioblastoma.* J Clin Invest, 2011. **121**(1): p. 161-73.
31. C. Che, et al., *New Angiopep-modified doxorubicin (ANG1007) and etoposide (ANG1009) chemotherapeutics with increased brain penetration.* J Med Chem, 2010. **53**(7): p. 2814-24.
32. A. Regina, et al., *Antitumour activity of ANG1005, a conjugate between paclitaxel and the new brain delivery vector Angiopep-2.* Br J Pharmacol, 2008. **155**(2): p. 185-97.

33. T. Etrych, et al., *HPMA copolymer conjugates with reduced anti-CD20 antibody for cell-specific drug targeting. I. Synthesis and in vitro evaluation of binding efficacy and cytostatic activity.* J Control Release, 2009. **140**(1): p. 18-26.

34. T. Etrych, et al., *Star-shaped immunoglobulin-containing HPMA-based conjugates with doxorubicin for cancer therapy.* J Control Release, 2007. **122**(1): p. 31-8.

35. D. Willner, et al., *(6-Maleimidocaproyl)hydrazone of doxorubicin--a new derivative for the preparation of immunoconjugates of doxorubicin.* Bioconjug Chem, 1993. **4**(6): p. 521-7.

36. D. Wu and W.M. Pardridge, *Neuroprotection with noninvasive neurotrophin delivery to the brain.* Proc Natl Acad Sci U S A, 1999. **96**(1): p. 254-9.

37. E. F. Jackson, et al., *Magnetic Resonance Imaging of Therapy-Induced Necrosis Using Gadolinium-Chelated Polyglutamic Acids.* International journal of radiation oncology, biology, physics, 2007. **68**(3): p. 830-838.

38. K. Ulbrich, et al., *Transferrin- and transferrin-receptor-antibody-modified nanoparticles enable drug delivery across the blood-brain barrier (BBB).* Eur J Pharm Biopharm, 2009. **71**(2): p. 251-6.

CHAPTER IV

BIOLOGICAL CHARACTERISATION OF POLYGLUTAMATES

CHAPTER IV. BIOLOGICAL CHARACTERISATION OF POLYGLUTAMATES

Biological evaluation in cell models, i*n vitro* tests, usually precede *in vivo* evaluation of every therapeutic. The objectives include the evaluation of toxicity, the determination of the cell internalisation pathway and cell trafficking, proof of efficient targeting and activity studies. Besides, selection of the appropriated cell line will facilitate data extrapolation to posterior *in vivo* assays.

BBB physiology and pathology has capture scientific and industrial interest, leading to a massive number of in *vitro* BBB models, from which those based on cells of non-cerebral origin have been significantly reported [1]. Endothelial and epithelial cells of non-cerebral origin have been deeply used to study different aspects of BBB function. Specifically, endothelial cells are the most important cell types of the BBB as they form a continuous sheet covering the inner surface of the capillaries. As stated in the introduction section I.1.3.1, these cells are interconnected by tight junctions (TJs) which form a belt-like structure at the apical side, constructing the physical feature of the barrier.

Herein, the cell line HUVEC (human umbilical vein endothelial cell line) was chosen due to their endothelial origin for carrying out preliminary cell viability studies as well as to explore the possible internalisation mechanisms followed by the synthesised polyglutamates. HUVEC cells are a non-cerebral cell type of human origin, which are able to be isolated from the umbilical cord. They are one of the most widely used endothelial cells [1, 2]. As it has been already mentioned, the use of cell models in co-culture rather than monoculture represents better the BBB [3] and the introduction of flow systems even go a step further [4]. It is planned to use these more advanced models as future work in order to evaluate the capacity of targeted PGAs to cross the BBB. In addition, HeLa cells were exploited in toxicity and internalisation studies as an extra cell line with non-endothelial origin to compare the behaviour of our

PGAs. This cell type is an immortal cell line derived from cervical cancer cells; the oldest and most commonly used human cell line in research [5].

Next step in the evaluation of PDCs involves its *in vivo* study, including biodistribution and pharmacokinetics (PK) studies as well as the proof of the therapeutic activity in the adequate animal model. Characteristics such as PK, biodistribution and metabolic clearance are important parameters directly related with the overall effectiveness of novel macromolecular delivery vectors (FIGURE IV. 1). The determination of conjugates distribution into the body after systemic administration has been catalogued as a top priority [6] and the polymeric carrier together with the bioresponsive polymer-drug linker used clearly determine drug distribution *in vivo* and drug fate.

There are required factors to achieve an adequate biodistribution, i.e. non-specific accumulation, non-alteration of the immune system, blood circulation extravasation to reach the site of action (i.e. diseased organ, inflammation or tumourogenic area, etc…) and binding to a molecular target and/or undergoing cellular internalisation. Physicochemical properties of the polymeric backbone such as chemical composition, size, MW, polydispersity, conformation in solution (shape), charge or hydrophobic-hydrophilic blocks ratio (among others) could significantly modify all these parameters. Size, along with chemical composition, influences in hepatic filtration tissue extravasation, tissue diffusion and kidney excretion. Charge could induce different patterns of behaviour e.g. higher uptake by phagocytosis, shorter blood circulation half-life due to positive charges. It is well recognised that neutral or negatively charged systems have a reduced plasma protein adsorption and low rate of non-specific cellular uptake, decreasing side-effects of unexpected toxicity. Moreover, aggregation processes derived from these characteristics may also influence the final distribution [7]. Solution conformation (shape and size) adopted after polymer conjugate administration is a key feature that determine conjugate biodistribution [8]. In this context, one of the hypotheses from the

present work was that the length of the inner polypeptide block as well as the presence of one or two PEG terminal blocks will be translated onto a different biodistribution and PK profile due to the different solution conformation adopted.

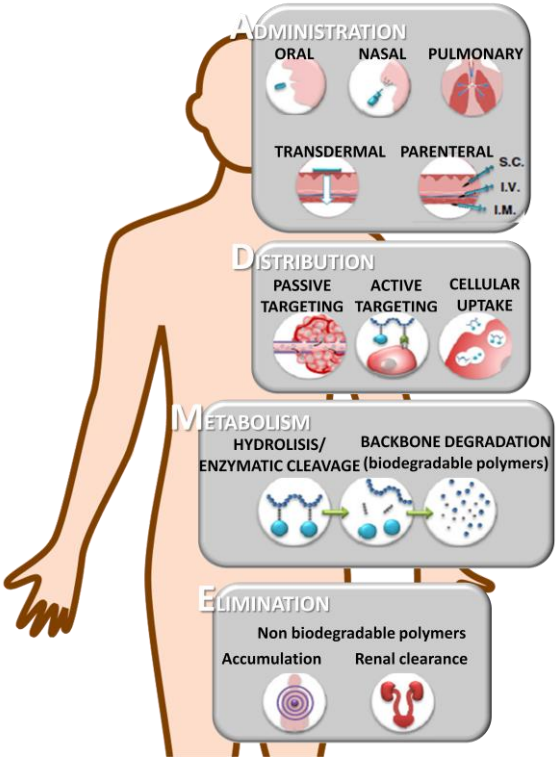

FIGURE IV. 1 Drug ADME routes in the human body. Redrawn from ref. [8].

The purpose of the experiments carried out in this chapter was to validate *in vivo* the synthesised family of amphiphilic block copolymers as polymer carriers for targeted drug delivery. Biodistribution studies allowed monitoring the compound of interest into the body after i.v. administration, identifying organ distribution and the ultimate routes of metabolism and clearance (FIGURE IV. 2).

Different techniques available for conjugate monitoring have been already tested with PT, being able to quantitate the free and bound drug in biological fluids and tissues by means of radioactivity, HPLC, atomic absorption spectroscopy (AAS), and in the clinics using

probes for gamma camera imaging [10, 11], MRI and PET [12]. Lately, the use of near infra-red (NIR) fluorescent and luminescent tools to visualise nanomaterials had become popular in preclinical models although proper quantitation is difficult due to the problems associated with signal tissue penetration and artefacts [13, 14].

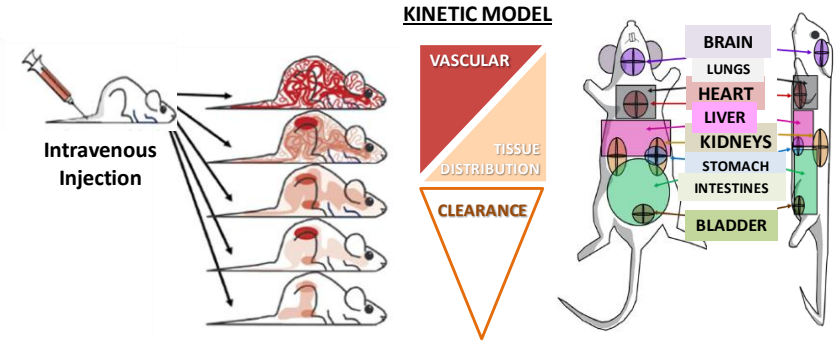

FIGURE IV. 2 Diagrammatic representation of the mice biodistribution model and organ region model. Adapted from ref.[9].

Independent biodistribution studies with non-targeted and targeted systems were performed. Non-invasive imaging techniques were selected for our purpose, namely: fluorescence labelling for optical imaging, MRI and PET. It has to be considered the impact of the labelling probe on the size, shape and physicochemical properties of the final conjugate; in case of high MW conjugates modifications will be always milder than in low MW. Regardless, the intrinsic nature of the probe itself (hydrophobicity, charges) as in the case of some Cy5.5 derivates could significantly alter the real biodistribution of the labelled polymer if not carefully controlled.

IV. 1 RESULTS AND DISCUSSIONS

IV. 1. 1 *IN VITRO* EVALUATION IN AN ENDOTHELIAL CELL LINE

IV. 1. 1. 1 Evaluation of polymer cell viability by MTT assay

The MTT (3-(4,5-dimethylthiazolyl-2)-2,5-diphenyltetrazolium bromide) assay is a colorimetric assay that measures cell proliferation as well as reduction in cell viability when metabolic events lead to cell death (apoptosis and/or necrosis). It can also be used to assess the rate of survival of a given cell line when it is incubated in the presence of xenobiotics and in the derivation of cell growth curves. The reduction of tetrazolium salts is accepted as a reliable process to analyse cell proliferation as the yellow tetrazolium MTT is only reduced when mitochondrial reductase enzymes are active, and therefore conversion can be directly related to the number of viable (living) cells. Reduction results in the intracellular formation of purple formazan crystals that are insoluble in aqueous media, which are spectrophotometrically measured after solubilisation with DMSO (see FIGURE IV. 3). The effectiveness or toxicity of the agent in causing cell death is determined through a dose-response curve.

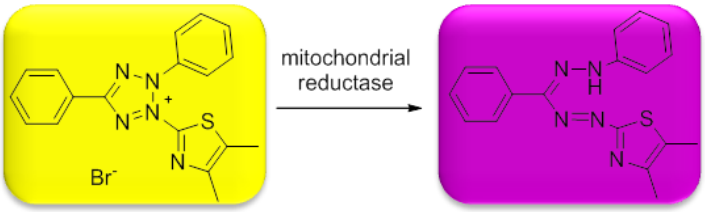

FIGURE IV. 3 Chemical structure of MTT (yellow colour) and its reduced formazan product (violet). This transformation is performed by mitochondrial reductases in live cells.

The MTT test compares favourably to other methods, such as trypan blue which only evaluates cell membrane integrity and only qualitative, or the [^{3}H]-thymidine incorporation assays which requires handling of radioactive substances, is time-consuming and involves cell

harvesting or medium changes. MTT provides a linear relationship between cell activity and absorbance based in the cellular metabolic activity. In addition, it is a quantitative method adaptable for high-throughput screening.

The MTT assay was used in the present work to assess the cell viability of the synthesised family of PGAs, including the novel triblock *co*-polymers (TBs) against HeLa and HUVEC cell lines at different concentrations up to 72 h incubation. Results are summarised in FIGURE IV. 4. Cell viability was calculated as a percentage of the viable untreated control cells.

The graphs below revealed the absence of cell toxicity with TB100 and TB150 against HUVEC cells up to 72h. A slight decrease in cell viability was observed after 72h with TB200 possibly due to a different solution conformation (FIGURE IV. 4). Rest of compounds (PGA homopolymers and DB systems) showed cell viability higher than 80% above 2mg/mL concentrations at both time periods in both cell lines.

(A)

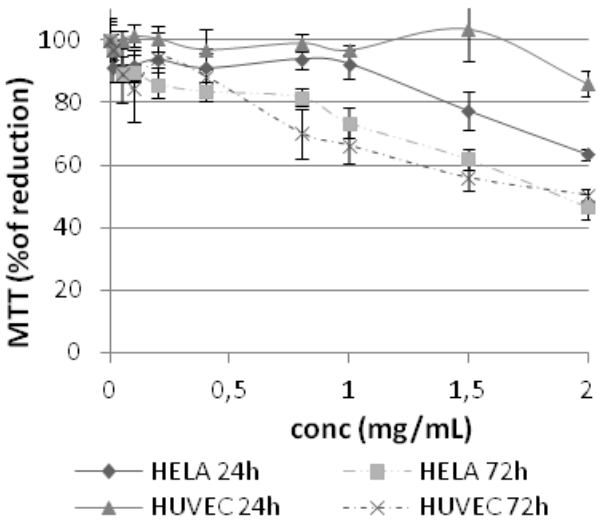

(B)

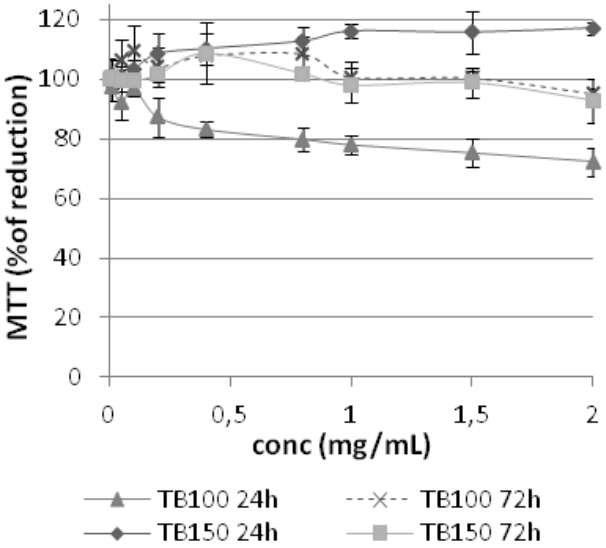

FIGURE IV. 4 Dose-response curves for cell viability in HUVEC (A,B) and HeLa (A) cells treated with TB_{200} (A) or TB_{100}, TB_{150} (B). Error bars correspond to standard deviation from five independent measurements.

IV. 1. 1. 2 Cellular internalisation studies of triblock co-polymers by flow cytometry and confocal fluorescent microscopy

Fluorescent technology has greatly facilitated the study of biological processes [15, 16]. Through fluorescent probe bioconjugation onto polymeric nanosystems it has been evidenced the possibility of investigate their internalisation pathways.

Probes such as the fluorophore OG have been extensively reviewed for cellular studies to determine cell trafficking [16-19] and for *in vivo* studies although in a minor extent [20]. In this type of experiments it is recommended to use of non-toxic polymer concentrations, to ensure the absence of free dye and to define potential artefacts resulting from pH and/or concentration-dependant fluorescent quenching phenomena. In theory, minimal probe loading is desirable to avoid data misinterpretation as explained above,

fluorescent probes could drive conjugate cellular and in vivo fate (charge, modification of original solution conformation of the vehicle,…). Moreover, linkage with the fluorophore as well as the fluorophore itself should be biologically stable to ensure adequate carrier monitoring. Herein, polymers labelled with the fluorescent probe OG (OG labelled triblock *co*-polymers (PEG-*b*-PGA_n-*b*-PEG, n=100, 150 and 200) were used for cell internalisation studies. Explanation on internalisation pathways is given in sections I.2.3 and I.2.4.

Well known techniques, such as, flow cytometry (FACS) (cell uptake) together with live-cell confocal microscopy analysis (subcellular fate and pathway) in HUVEC cells, were used aiming to study cellular trafficking of the labelled polyglutamates. By FACS, experiments were also carried out at different temperatures, 37°C (total uptake) and 4°C (cell binding) to determine the presence of energy dependent or non-dependent internalisation mechanisms, such as endocytosis or diffusion, respectively (FIGURE IV. 6). It is noteworthy to remark that all experiments were done in the presence of leupeptine (a protease inhibitor), to avoid lysosomal degradation of PGA along the incubation periods.

Previous studies carried out in our laboratory in HeLa cells showed that TB100-OMe-OG (non published data) was internalised by a mixed mechanism combining endocytosis and diffusion but an absence of cell binding (FIGURE IV. 5). This was the starting point to think that this carrier could be applied to cross BBB.

Unfortunately, this result was not that evident in HUVEC cells for any of the novel systems and mostly endocytic uptake mechanisms were observed although in specific example similar results were again encountered (FIGURE IV. 6 and FIGURE IV. 7) (see detailed explanation below).

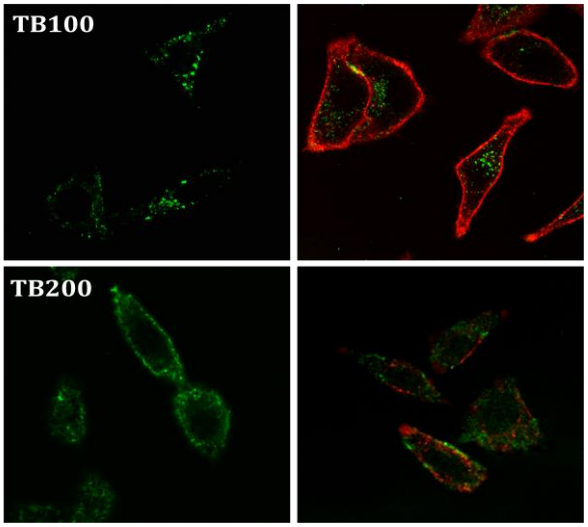

FIGURE IV. 5 Confocal microscopy study with TB100-OMe and TB200-OMe labelled with OG (green fluorescence) in HeLa cells. Red fluorescence corresponds to the membrane marker FM 4-64**.**

The main difference encountered with the tested triblocks was the length of the polypeptide block, which was expected to play a role in solution conformation influencing cell uptake kinetics. The time dependent profiles of all TB showed an energy dependent uptake mechanism as indicated the decreased internalisation at low temperature (FIGURE IV. 6). It is important to note that, after careful physicochemical analysis of the different TB, the theoretical DP (200, 400 and 800) was determined as 200, 150 and 100, respectively due to the experimental issues described in chapter 1 with the first methodology of polymerisation (section II.2.2.2). Taking into account that equivalents of OG were equal for all TBs (0.0125mgOG/mL) it could be conclude that theoretically higher DP polymers were faster internalised at short times (15,30min) than those with lower DP, reaching also a greater uptake after 5h. TB200 reached a plateau after 2h whereas TB100 and TB150 continued their internalisation in a time-dependent manner. TB150 was the only system with a different profile (similar to that observed previously in HeLa cells with TB100-OMe-OG, FIGURE IV. 5), which could indicate a complementary internalisation mechanism at short incubation times (passive diffusion). This fact was

not corroborated by live-cell confocal microscopy study.

Due to differences in the osmotic pressure, it has been already reported that bigger compounds can be endocytosed more rapidly increasing their accumulation inside the cell. Analysing our results, higher MW carrier displayed the higher internalisation which can be explained that by the different solution conformation adopted, with a greater size vesicle-like formation in the case of TB150 due to self-assembling rearrangements. Conformation in solution plays a role in cell internalisation and therefore DLS studies are going to be carried out to confirm this hypothesis.

(A) **TB_{100}**

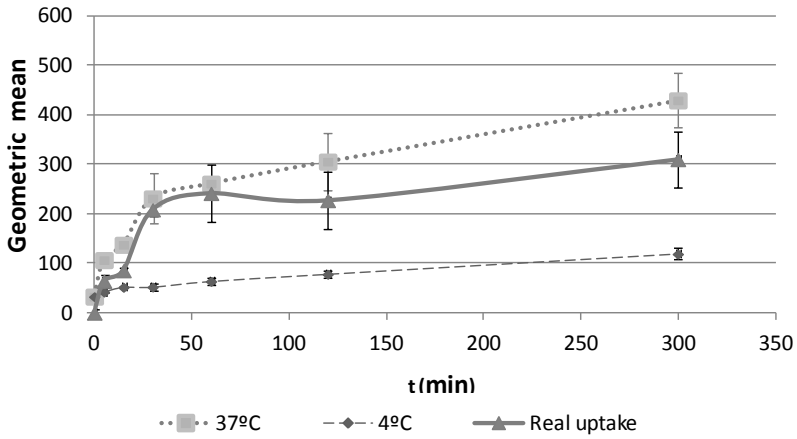

(B) **TB_{150}**

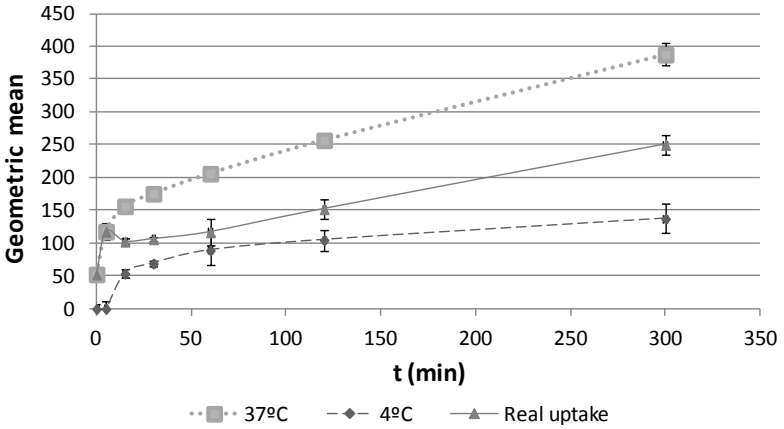

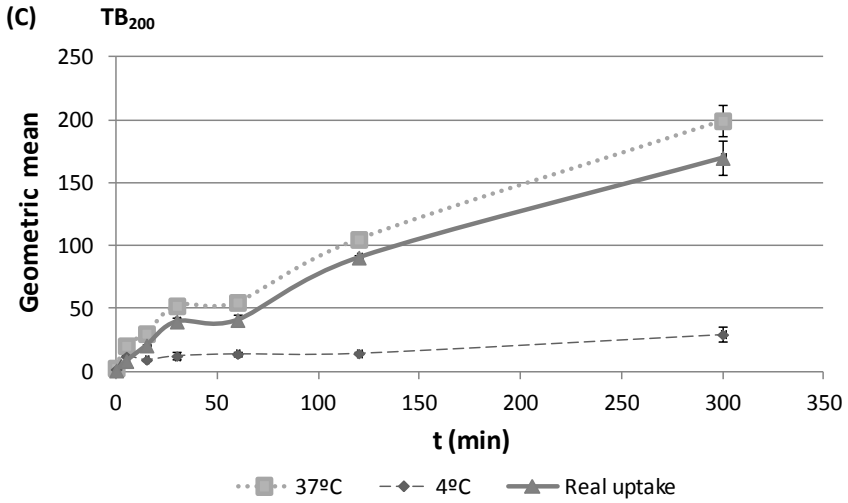

FIGURE IV. 6 Time dependent cell-association of OG-labelled triblocks with HUVEC cells at 37 and 4 °C, by flow cytometry. Panel A, B and C shows the time-dependent association at 37°C, 4 °C and the real uptake (A)TB100, (B)TB150, (C)TB200. The values represent mean ± S.E.M.; n > 3. TB_{200}-OG, TB_{150}-OG, TB_{100}-OG.

TB200-OG was more deeply studied due to the more controlled synthetic aspects. As expected, a vesicular labelling and co-localisation with lysosomal marker was observed (FIGURE IV. 7, TB_{200}) demonstrating a lysosomotropic delivery mechanism of TB_{200}-OG. Green fluorescence (TBO signal) increased over time inside cells, importantly, co-localisation with the red fluorescent signal of the lysosomal marker Texas Red-dextran (TRD) was also achieved.

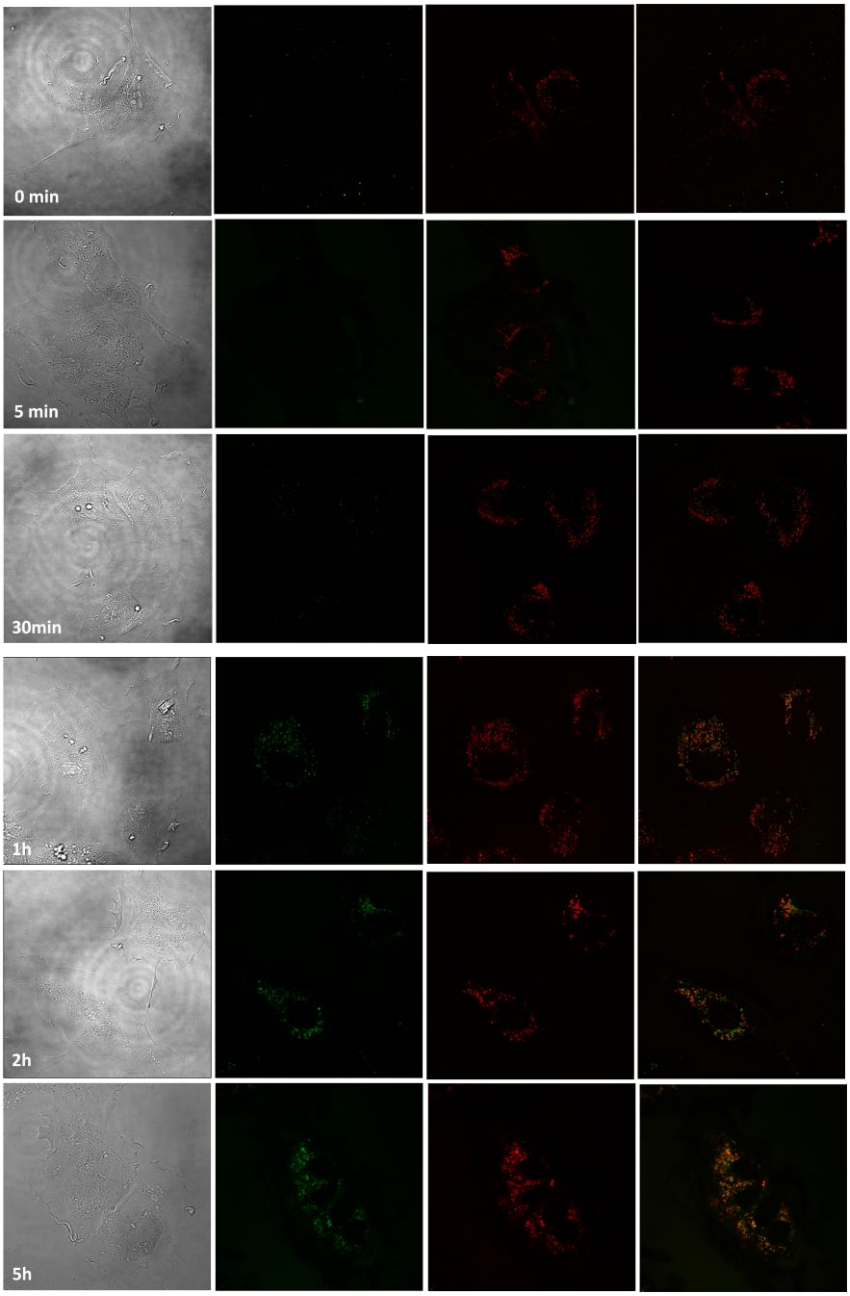

FIGURE IV. 7 Confocal microscopy live cell images of HUVEC cells incubated at 37°C with TB_{200}-OG at 0, 5, 30min and 1, 2, 5h.

In a parallel experiment, TB (PEG-*b*-PGA_n-*b*-PEG-X) with n=100,150 and 200 and X=PEG-SS-4TP or PEG-OMe were evaluated after 1h incubation in HUVEC cell lines. This incubation time was selected due as explained for FIGURE IV. 5. An example of the images obtained is illustrated in FIGURE IV. 8. Fluorescence output of each compound was different depending on the species, showing lower signal the methylated TBs. This is an important issue to consider, in order to correctly interpret the obtained data. Both TB_{150} showed again a possible mixed mechanism, combining endocytosis (energy dependent) and passive diffusion (non-energy dependent). This is assumed due to the observation of the green vesicular forms plus the cytosolic diffused green. This behaviour is more remarked in the methylated TB although TB-OMe were determined to have lower MW than the one expected due to problems in the PGA block deprotection (HBr affected to PEG blocks promoting their degradation).

It is important to note that, these TBs are complex dynamic systems with conformation highly dependent on concentration used. Deeper studies on solution conformation are being carried out by means of SANS in order to understand the above-described cell uptake differences between TBs.

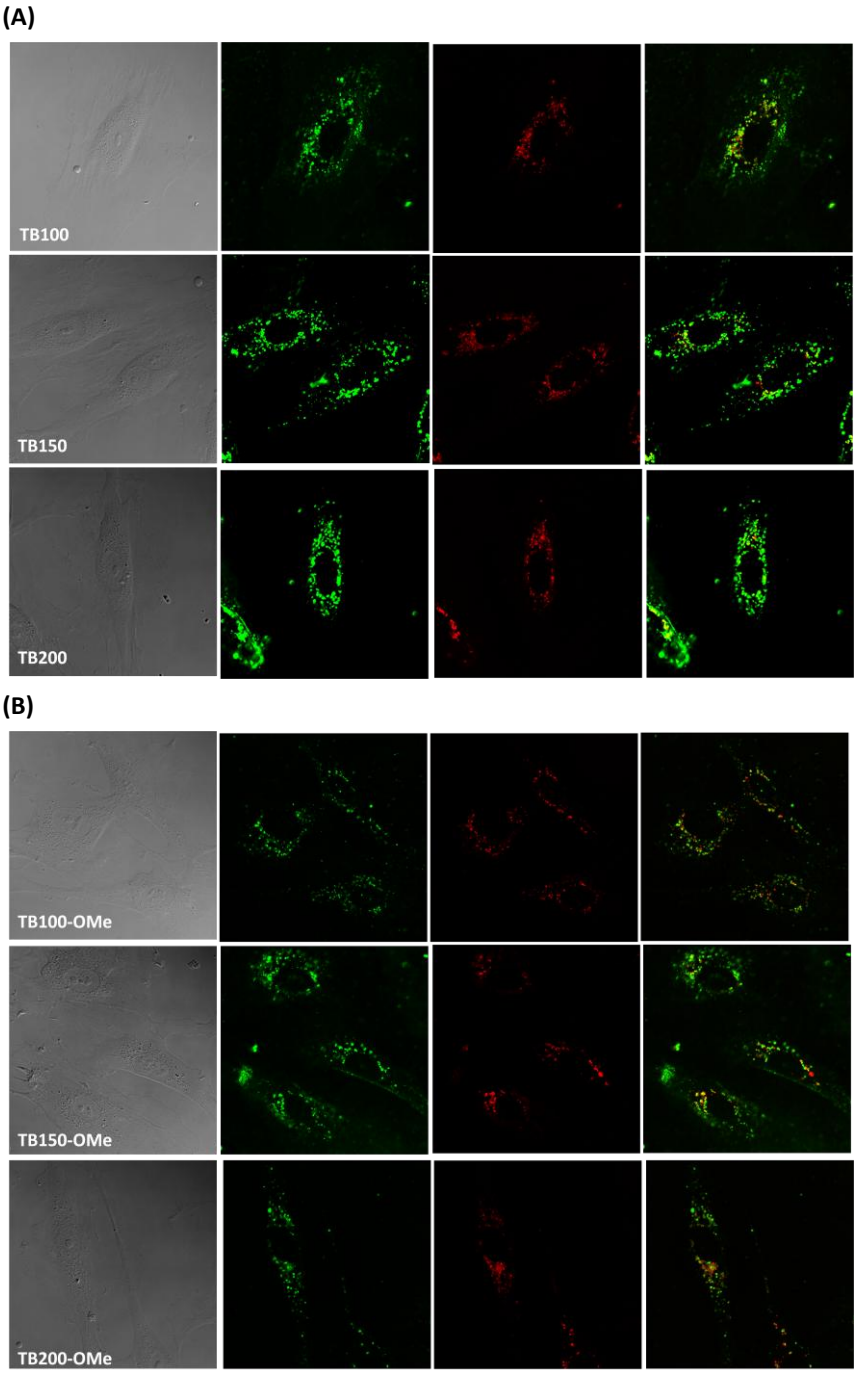

FIGURE IV. 8 Confocal microscopy live cell images of HUVEC cells incubated at 37°C at 1h with OG labelled (A) TB_{200}, TB_{150}, TB_{100} and (B) TB_{200}-OMe, TB_{150}-OMe, TB_{100}-OMe.

IV. 1. 2 IN VIVO STUDIES. BIODISTRIBUTION EXPERIMENTS

In vivo imaging modalities. Brief introduction.

In vivo imaging methodologies are gaining fast acceptance in biomedical research. These techniques have improved *in vitro* analyses of tissue samples collected from cohorts of treatment groups. These technologies are non-invasive and non-traumatic over a time. Their differences rely on sensitivity, specificity, resolution, ease of use and cost (FIGURE IV. 9). In this work, starting experiments were done with fluorescence optical imaging. This technique allows easy labelling of the polymers and a variety of fluorescent probes (wavelengths) to work with. In addition, spatial resolution is good and it is a non ionising radiation. Main limitation comes from their limited tissue penetration, poor anatomical resolution (1mm) and difficulties in quantification. However, for whole body distribution detection, fluorescence optical imaging is still considered an efficient tool.

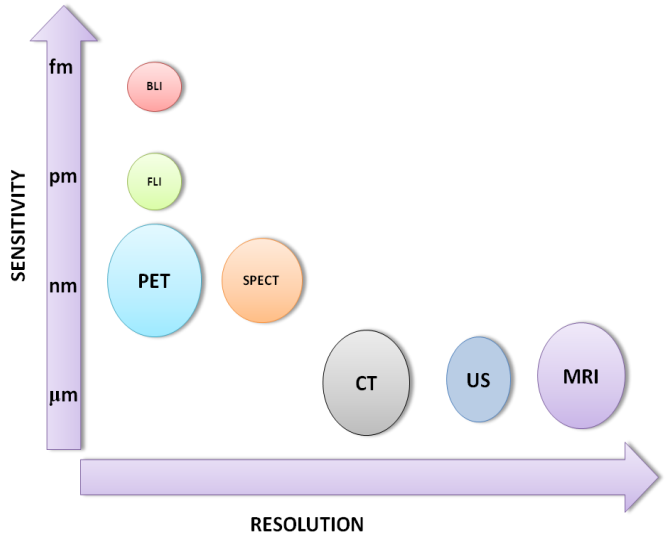

FIGURE IV. 9 *In vivo* imaging modalities. BLI=bioluminescence imaging, MRI=magnetic resonance imaging, PET=positron emission tomography, FLI=fluorescence imaging, CT=computed tomography, US=ultrasounds, SPECT=Single Photon Emission Computed Tomography.

MRI is able to overcome fluorescence limitations providing higher spatial resolution. This fact provides better assessment of polymer detection in specific areas like the brain. In contrast, MRI has low sensitivity. Finally, PET also improves fluorescence output related with spatial resolution and tissue penetration. However, PET limitations lies on relatively short half-lives of some radionuclides and the need of the adequate facilities to perform the experiments.

IV. 1. 2. 1 Biodistribution studies of non-targeted polyglutamates

Before moving towards biodistribution studies of the targeted systems, a technique validation proof of concept was performed. Non-targeted PGA homopolymer (**4**, **11**), diblock PGA-*b*-PEG (**5**, **7**) and triblock (PEG-*b*-PGA-*b*-PEG-SS-4TP, (**9**) structures were evaluated *in vivo* to test the possible toxicity, routes of clearance and to determine polymer circulation half-life time ($t_{1/2}$).

IV. 1. 2. 1. 1 Ex vivo biodistribution of TB_{200}-OG in rats

OG labelled TB_{200} (**20**) was i.v. administrated to healthy male Wistar rats (0.005mg OG/kg). As a control groups, non-labelled TB_{200} and free OG were i.v. administrated in equal equivalents. First group of animals were sacrificed 4h post administration; second after 24h. In this experiment, it was only collected *ex-vivo* data through homogenisation of the blood and extracted organs by fluorescence quantification. The results are shown in FIGURE IV. 10.

(A)

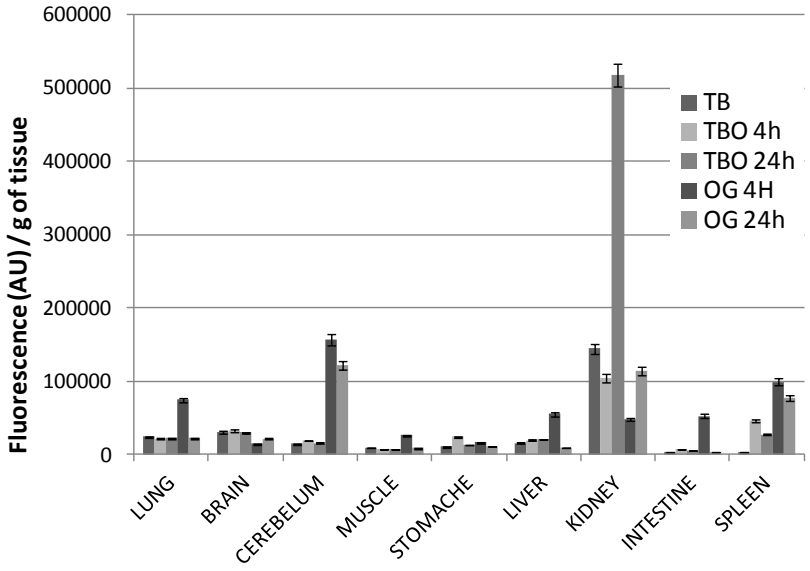

(B)

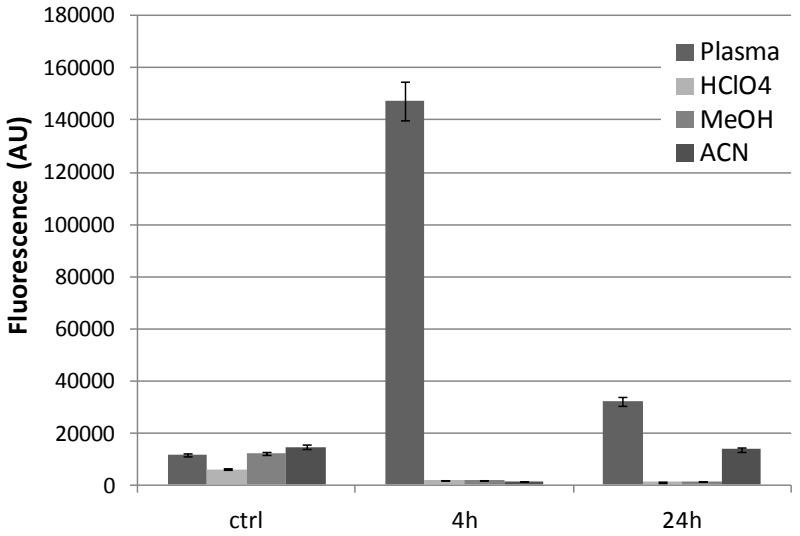

FIGURE IV. 10 TBO (TB_{200}-OG) biodistribution (A) organs analysis (fluorescence per gram of tissue) and (B) plasma under different treatments.

Plasma fluorescence output was determined in the spectrofluorometer to optimise conjugate extraction from tissues as

well as to estimate $t_{1/2}$ of the TB (FIGURE IV. 10 (B)). Plasma signal was measured directly (bar ■), after $HClO_4$ solution addition (bar ■), after washing with MeOH the pellet of the latest treatment (bar ■) and after pellet washed with ACN (bar ■). It was observed that serum fluorescence decreased dramatically after $HClO_4$ treatment. This reduction was possibly produced by TB_{200}-OG precipitation together with plasmatic proteins. Due to this fact, the extraction protocol was modified. $NaHCO_3$ washed of the pellet was performed in the homogenated tissues in order to obtain the sodium salt of the TB and solubilise it to the aqueous phase for its subsequent fluorescence measuring. Regarding the $t_{1/2}$, due to practical issues, t=0min group was omitted therefore a proper calculation was not able to be performed. Despite of it, fluorescence at 4h indicates that compound was still detected in blood circulation and after 24h detected fluorescence triplicated the control measurements. These experiments were corroborated by means of other technique as described below.

In FIGURE IV. 10 (A) it is represented the normalised data of homogenated tissue. For fluorescence total quantification, data from $HClO_4$ and $NaHCO_3$ treatments were combined. Non-specific accumulation of TBO was observed in any analysed organ. The higher fluorescence intensities were detected in the liver for OG and in the kidneys for TBO, suggesting the respective preferred secretion routes.

IV. 1. 2. 1. 2 In vivo biodistribution of TB_{200}-DY787 and DB-Cy5.5

To carry out *in vivo* monitoring, dye properties should include good tissue penetration. In this respect, NIR dyes overtake other fluorescence probes. Main reasons for changing the methodology as well as the animal model were (i) diminishing the amount of conjugate needed for administration and (ii) a NIR dye to obtain better signal output continuing with low molar percentage of conjugated labelling probe. To carry out *in vivo* monitoring, NIR properties of the dyes Cy5.5 or DY787 allow better tissue penetration than OG and mice need lower doses than rats for a proper detection. First, in order to corroborate the ex vivo results described above, TB_{200} (**9**) was labelled

with the NIR dye DY-781 (Dyomics, GmbH) and in vivo biodistribution studies were carried out in Halle, Germany by Prof. Mäder group. TB_{200}-DY781 was i.v. administered to 4 nude mice instead of rats due to FLI penetration limitations. The labelled TB was monitored *in vivo* and also *ex vivo* (FIGURE IV. 11). *In vivo* images were taken by *Maestro*™ in vivo fluorescence imaging system and fluorescence intensities of the unmixed DY781 images were quantified using Maestro software (FIGURE IV. 11(C)). In the first hours after injection the fluorescence intensity increased due to conjugate invasion in tissues, whereas immediately after injection it is circulating in large blood vessels. Later, fluorescence intensity decreased to 10% of the initial fluorescence after 66h. Possible degradation processes could co-exist and after long periods fluorescence could be assigned to free dye and not to the conjugate. One important observation to note is the strong kidney signal obtained even after 22 hours (FIGURE IV. 11(A, B)). A closer analysis seemed to showed accumulation of the fluorescence probe in the renal tubules (nephrons). Further analyses are being performed in order to explain this unexpected result.

In parallel, at *CIPF*, Cy5.5 labelled diblock *co*-polymer DB_{200} (PGA_n-PEG, **5**) biodistribution assay was monitored by FLI and organ fluorescence quantification was determined by fluorometer analysis. Athymic nude mice were injected via the tail vein with a single dose of 2mg Cy5.5/kg of DB_{200}-Cy5.5. At 2, 4, 6 and 24h post administration, the mice were anesthetised and fluorescence images were acquired by IVIS®Spectrum imaging system to track in vivo whole-body biodistribution of the diblock *co*-polymer. After i.v. injection, labelled DB was distributed in the blood and transiently directed to the excretory organs. As observed in the FIGURE IV. 19, fluorescence signal is localised in the kidneys (dorsal view) and bladder (ventral view) which confirms the renal secretion of the polymer carrier. To further corroborate this result, after 4h, animals were euthanized and blood, liver, spleen, kidneys, heart and spleen were collected. All tissues were analysed by *ex vivo* FLI (FIGURE IV. 20) and fluorescence was quantified by spectrofluorometer after homogenising the organs (FIGURE IV. 22). *In vivo, ex vivo* and quantitation data confirmed the

renal excretion route as well as the absence of non-specific accumulation in any other organ.

(A)

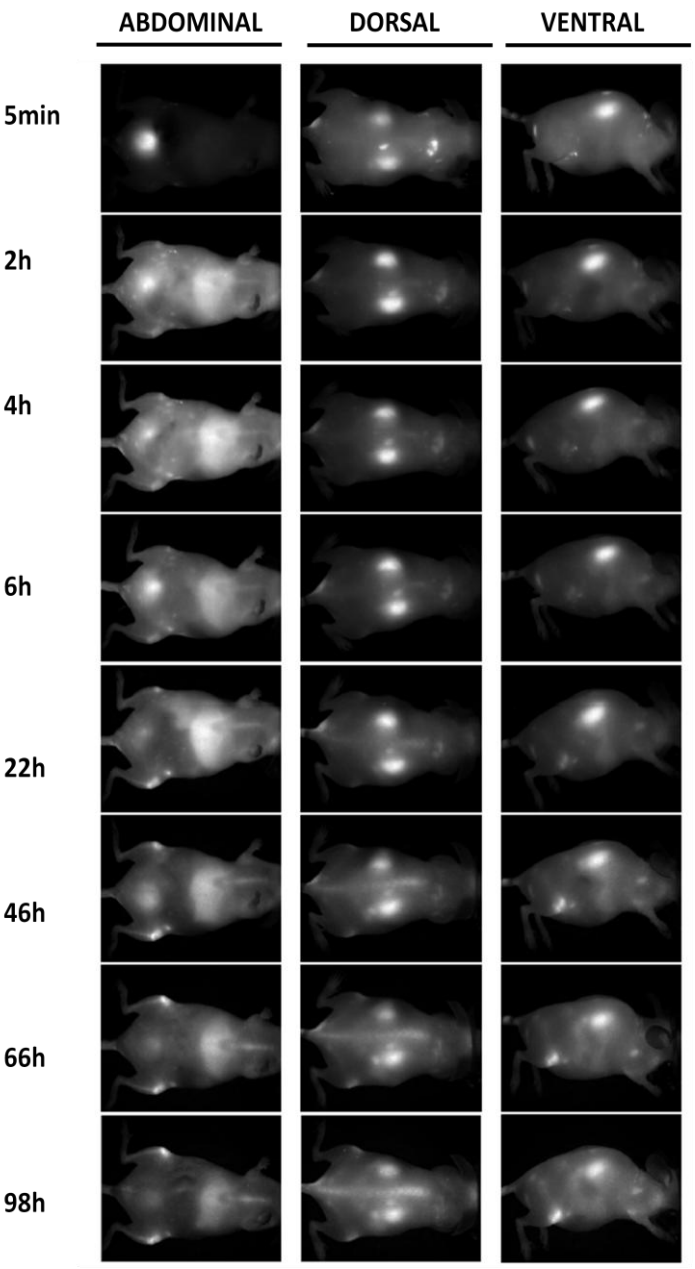

(B)

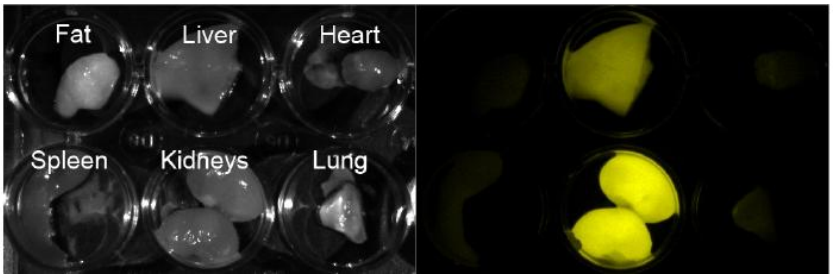

(C)

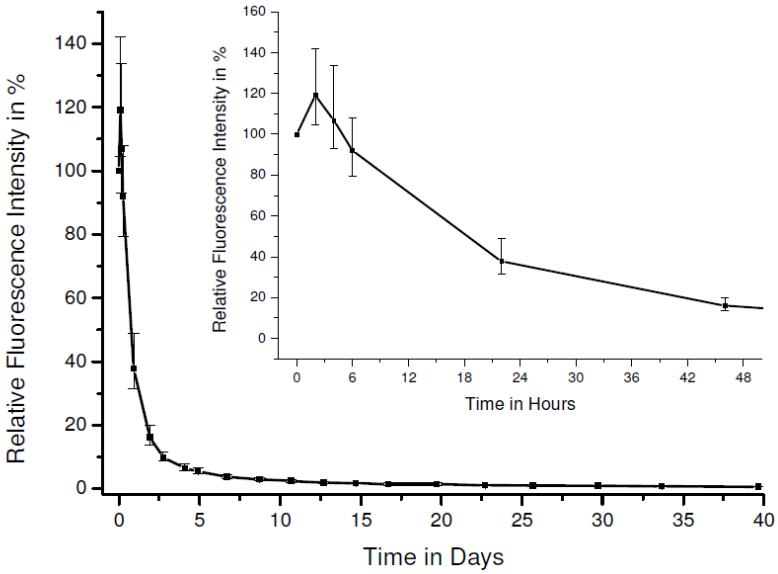

FIGURE IV. 11 TB_{200} biodistribution monitoring through FLI. (a) Unmixed DY-781 gray scale fluorescence images. Fluorescence intensities are white. (b) Organs 22 hours after injection of 1 mg TB_{200}-DY781 conjugate. Photo (left) and fluorescence image (right). (c) Decrease of fluorescence intensity from abdominal mice images over time.

These preliminary data on biodistribution based on fluorescent studies comparing triblock and diblock systems (DP=200) could be summarised in a clear renal secretion of both systems with a non-specific accumulation in the other studied organs. Further studies with a greater number of animals are being carried out in Halle to allow a better comparison between TB and DB pharmacokinetic parameters by FLI.

IV. 1. 2. 1. 3 TB biodistribution: use of contrast agents (DTPA/Gd) for MRI

Our final aim in this project was to ensure whether our novel amphiphilic carriers were capable of crossing the blood-brain barrier by their inherent properties. Taking into account that percentage of the total administered dose accumulated inside the brain would be very small (as reported max. 4% of administered dose [21-25]), sensitivity of the monitoring technique has to be greater than that offered by fluorescence approaches. Therefore, MRI was proposed and selected as an appropriate technique for *in vivo* brain imaging. This imaging methodology stands out because of its precision and accuracy. Its spatial resolution among similar but not identical tissues is particularly useful for lesion or tumour detection, perceiving abnormalities earlier than with other imaging tools. The methodological aspects and the full technique description have been already detailed in section IV.3.2.1.3 and IV.1.2, respectively. MRI in vivo studies were performed in collaboration with O. Cauli and V. Felipo from the Neurobiology Laboratory of the Centro de Investigación Príncipe Felipe (Valencia) and experiments were carried out in Madrid at Instituto de Investigaciones Biomédicas "Alberto Sols" (CSIC/UAM).

The MRI contrast enhancement for the TB-DTPA/Gd conjugates was preliminary evaluated in healthy male Wistar rats. Animals were anesthetised and control parameters were fixed before starting the experiment. The labelled triblock co-polymers (PEG-*b*-PGA_n-*b*-PEG) with n=100 and 200 were injected i.v. in a tail vein at a dose of 0.2mmol Gd/kg (TABLE IV. 1). FIGURE IV. 12 shows the images of the rat head before contrast and after the injection of the polymer conjugate TB_{100}-DTPA/Gd. Animals were monitored *in vivo* looking for brain detection (0, 1, 6 and 24h post-administration), investigating if the carrier owned inherent properties which allowed BBB crossing. In all cases studied, signal of the triblock *co*-polymers produced significant contrast enhancement in the blood vessels, (red arrows in FIGURE IV. 12) even in the brain ventricles. As expected with non-targeted conjugates, no signal was observed at any time point in the

rat brain. Same results were observed for both triblock *co*-polymers with different polypeptide block length (TB100 and TB200). Therefore, it was clear the need of a targeting vector to promote active transport of the conjugates across BBB.

Product name	Total mass (g)	$GdCl_3$ amount (aprox.) mmol of Gd^{3+}	mmol OX26
TB_{100}-DTPA/Gd	0,044	0,055	-
TB_{200}-DTPA/Gd	0,053	0,042	-
TB_{100}-OX26-DTPA/Gd	0,066	0,057	$1 \cdot 10^{-5}$
TB_{200}-OX26-DTPA/Gd	0,036	0,084	$5 \cdot 10^{-5}$

TABLE IV. 1 Targeted /non-targeted gadolinium labelled triblock *co*-polymers for MRI biodistribution studies.

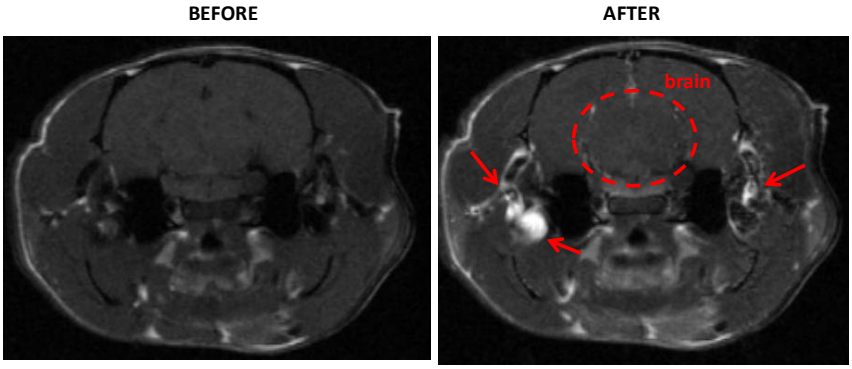

FIGURE IV. 12 Magnetic resonance image of TB_{200}-DTPA/Gd (**26**): T1-weighted image of the rat head (left) after and (right) before the injection. Arrows indicate signal observed from the conjugated complexed agent.

IV. 1. 2. 1. 4 PGA-homopolymer biodistribution: radio-tracer conjugation of DOTA/Ga for PET

PET is a good alternative to MRI with greater sensibility and therefore resolution. Therefore it was also studied to complement previous data. Once PGA derivatives were conjugated with DOTA, gallium labelling and animal experiments were carried out by the Unit of Biomedical Applications of Radioisotopes and Pharmacokinetics at the *CIEMAT* (Madrid).

In the case of PGA_n homopolymer (**11**) evaluation, FVB/NJ mice (n=25) were injected PGA_{100}-DOTA/Ga i.v. a dose between 0.2 and 1.4 MBq of PGA-[^{68}Ga]-DOTA (21± 4 µg compound/g body weight). Animals were monitored up to 3h (FIGURE IV. 13) and 5 mice per time were sacrificed (0.25, 0.5, 1, 2 and 3h) extracting the organs for radioactivity measurement (FIGURE IV. 14). The biodistribution study clearly revealed the expected renal excretion route (signal in bladder and kidneys) of the homopolymer which is confirmed in the *ex vivo* analysis data. The highest percentage of the injected dose was found in the kidney, along compound secretion. The results only covered 3h after administration due to gallium decay. PK analysis was performed considering a compartmental model. Half life time estimation of the conjugate was 0.59h. This value was in good agreement with data obtained in studies carried out with PGA-Cy5.5 and other PGA-drug conjugates in our laboratory (data non published) using the same protocol detailed for fluorescence analysis agreed with the biodistribution profile found out after PET studies with PGA-DOTA/Ga and also with the estimated $t_{1/2.}$

Reviewing the presented data in mice biodistribution of the non-targeted polyglutamates (homopolymer, DB and TB), all of them had in common similar PK profiles, with a clear renal elimination and non-accumulation in any other specific tissue. Differences in size (PGA_{100}, DB_{200} and TB_{200}) showed a prolonged $t_{1/2}$ in bigger MW species. None of the tested polyglutamates demonstrated a significant accumulation in the brain, therefore BBB crossing without targeting was not achieved.

(A)

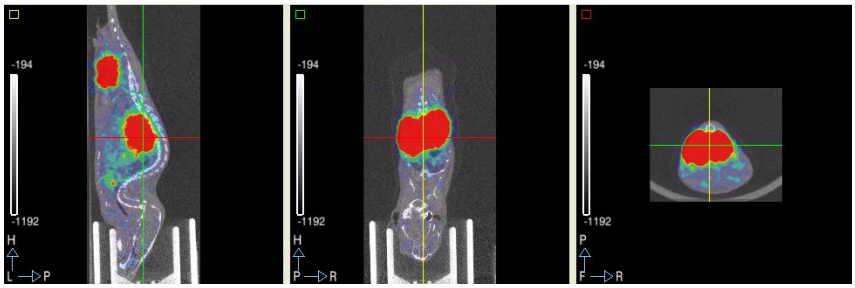

(B)

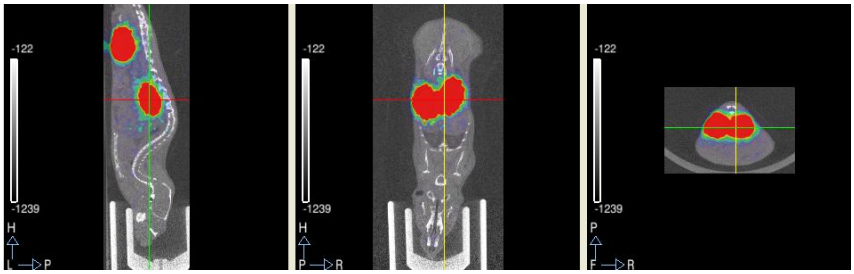

(C)

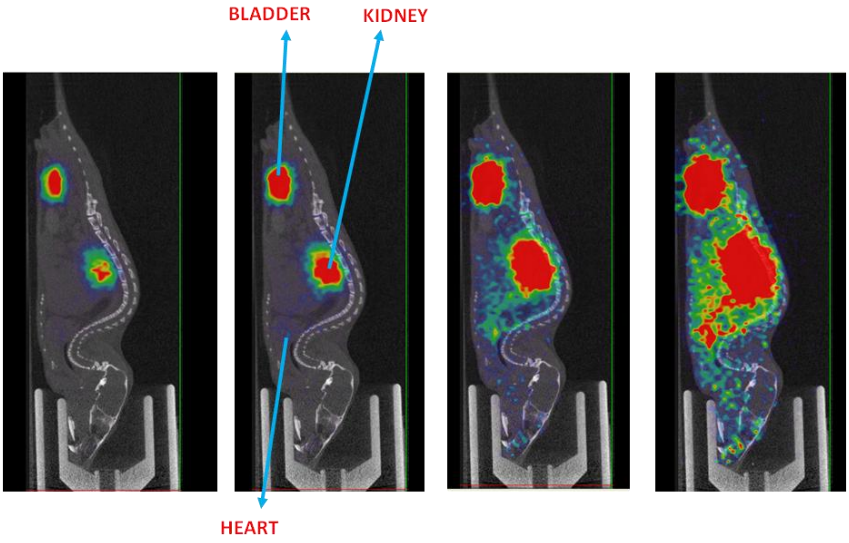

FIGURE IV. 13 PET imaging of PGA-DOTA/^{68}Ga (50,5 µCi) in healthy mice. (A) Sagittal, coronal and transverse images captured 18minutes post-administration, (B) 160min. (C) sagittal planes with different saturation degrees.

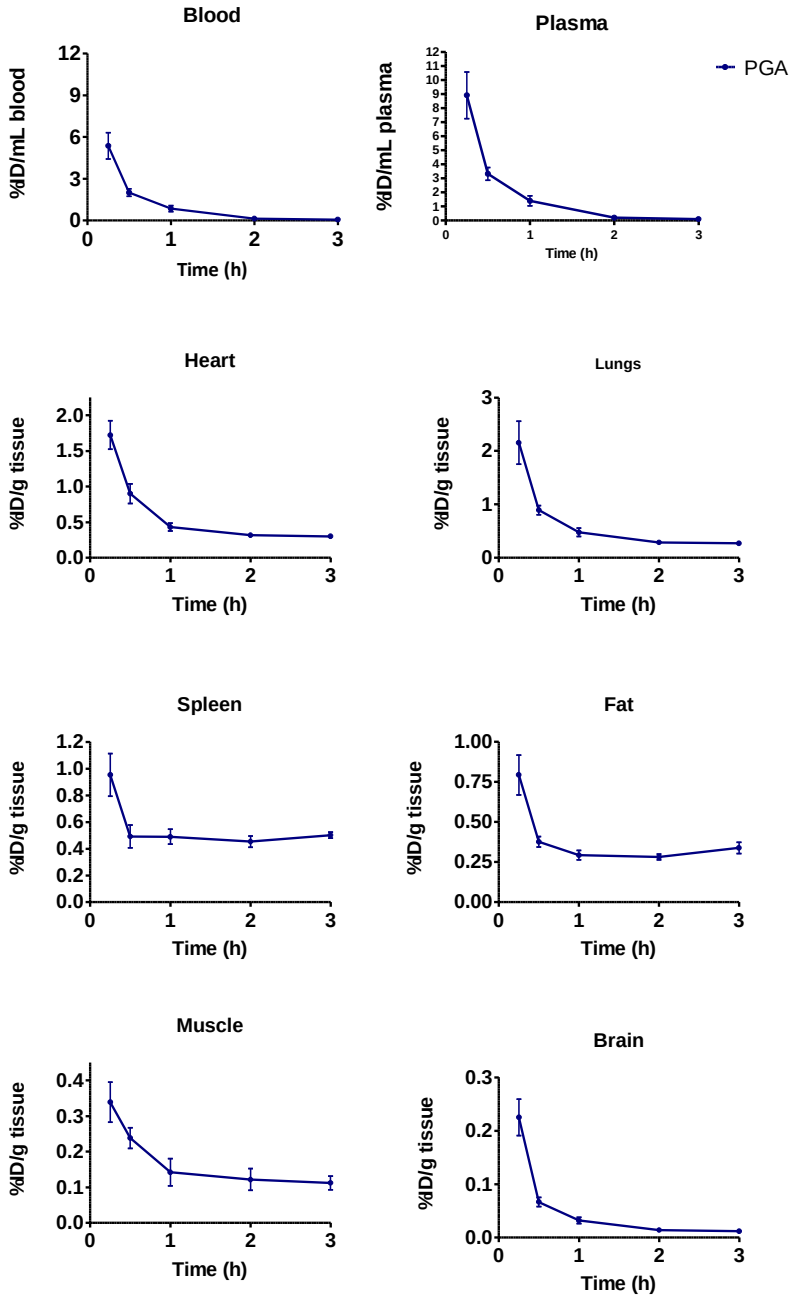

FIGURE IV. 14 PGA_{100} labelled with DOTA/Ga biodistribution. Data expressed as normalised %ID vs. time.

IV. 1. 2. 2 Biodistribution studies of targeted polyglutamates

Active targeting can be implemented additionally to the inherent passive targeting of polymeric nanocarriers with the possibility of overcoming critical biological barriers such as the BBB. This approach is expected to lead to higher and faster accumulation in the targeted organ increasing drug concentration. Design bases is once more a critical point because chemical properties of the additional ligand may have important effects on the entire conjugate by influencing on the cellular uptake [26] or resulting in lower efficiency [27]. Although BBB *in vitro* models are under constant evolution trying to accurately reproduce the complex features of this biological barrier, there is still no fully effective system reported. Undoubtedly, and even with prior in vitro evaluation, the evaluation of the constructs *in vivo* is a mandatory examination to confirm their success or failure as transporters across BBB and drug delivery carriers into the brain. Therefore and due to the absence of the optimal *in vitro* models to date, in the present work we have only used *in vivo* models to evaluate BBB crossing. Methodology to examine effectiveness of our targeted polyglutamates vehicles cover the techniques explained in sections I.1.6.2, I.2.5 and IV.1.2.

IV. 1. 2. 2. 1 Brain detection by immunohistochemistry. Transferrin-TB conjugate

With the purpose of detecting if Tf conjugates were able to cross the BBB, Western Blot technique (protocol detailed in appendix III) was selected to detect endogenous Tf from brain homogenate samples. Human Tf covalently conjugated to TB carrier was administrated i.v. in rats and after 4h post-injection, animal was sacrificed and brain harvested and preserved for the proposed study.

Previous to the *in vivo* analysis, anti-Tf antibody binding affinity and limit of detection for free and conjugated human Tf were examined. Samples numbered in FIGURE IV. 15were analysed first by electrophoresis and then by immunobloting. Proteins were isolated from fresh-frozen brain and cerebellum tissues homogenates.

(A)

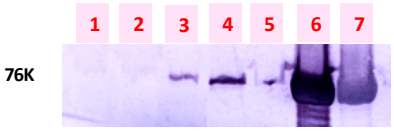

1	Homogenated rat brain
2	Homogenated rat brain
3	Tf $0.3 \cdot 10^{-3}$ mg/mL
4	Tf $0.3 \cdot 10^{-3}$ mg/mL
5	Tf $1,6 \cdot 10^{-3}$ mg/mL
6	Tf_{thio} $1,6 \cdot 10^{-3}$ mg/mL
7	Tf 0,5mg/mL
8	Tf_{thio} 0,5mg/mL

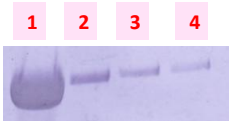

1	Tf_{thio} 0.5mg/mL
2	Tf_{thio} $5 \cdot 10^{-3}$ mg/mL
3	TB200-Tf $5 \cdot 10^{-3}$ mg/mL
4	TB200-Tf $2.4 \cdot 10^{-3}$ mg/mL

(B)

1	Mw marker
2	Cerebellum ctrl
3	Cerebellum Tf
4	Cerebellum TB-Tf
5	-
6	Brain ctrl
7	BrainTf
8	BrainTB-Tf

FIGURE IV. 15 Immunohistochemical analysis of (A) human Tf, thiolated Tf and TB_{200}-Tf and homogenated rat brain without treatment and (B) treated rats with TB_{200}-Tf and Tf.

A preliminary test on the biodistribution of the Tf targeted triblock *co*-polymer TB_{200} (**33**) was performed in healthy Wistar 4h post-injection. Free Tf and TB_{200}-Tf were administered to rats intravenously at a dose of 16mgTf/kg in a single bolus of 0.5mL. In this case, non-labelled conjugate was used aiming to detect the Tf through immunohistochemistry analysis.

Preliminary data showed that Human Tf was recognised in the brain by the anti-Tf monoclonal antibody even after its thiolation (FIGURE IV. 15 (A)). Besides, after Tf conjugation detection was still possible allowing us to identify in a qualitative manner our conjugate in the brain mass (FIGURE IV. 15(A)). The lowest concentrations tested were 0.0024mgTf/mL for TB and 0.0003mgTf/mL for Tf. As control, brain homogenates of non-injected animals were exposed to anti-Tf antibody to explore crossed reactivity with the own rat Tf. As it can be appreciated in FIGURE IV. 15(A), cross reactivity was not significant . Results are compiled in FIGURE IV. 15(B). Even though equivalent amount of protein was administrated to the animals, higher detection in both organs was achieved for the free protein. As conclusion it is possible to say that, TB_{200}-Tf was able to cross the BBB although remarkably less than free Tf.

IV. 1. 2. 2. 2 Biodistribution study by Optical Imaging. Transferrin-DB-Cy5.5 conjugate

As described in section IV.1.2.1.2, FLI using IVIS® Spectrum was performed for the DB_{200}-Cy5.5 (**34**) in order to validate this polymer as a drug delivery platform. In parallel, the same vector was covalently conjugated to Tf (**35**) and its capacity for BBB crossing *in vivo* was evaluated under the same technique. This study was performed in the Molecular Biology and Biochemistry Research Centre for Nanomedicine (*CIBBIM-Nanomedicine,* Vall d'Hebron Hospital, Barcelona). Following the same protocol (section IV.1.2.1.2), DB_{200}-Tf-Cy5.5 (**35**) was given through i.v. injection at a dose of 0.3mg Cy5.5/mL in athymic nude mice. Compounds and schedule are detailed in TABLE IV. 2.

COMPOUND	number of animals	End time points (h)
CTRL	3	4 / 24
Cy5.5	2	4 / 24
DB-Cy5.5	1	4
DB-Tf-Cy5.5	5	4 / 24

TABLE IV. 2. Fluorescent labelled systems for biodistribution experiments by fluorescence imaging. Number of animals and sacrificing time schedule.

Analysis of whole body imaging datasets for the targeted DB represented in FIGURE IV. 16 yielded temporal information on organ distribution. Free Cy5.5 was spread into the whole body, observing accumulation in kidneys, liver (dorsal view, FIGURE IV. 16 (A)), intestines, salivary glands (ventral view, FIGURE IV. 16(B)) and brain (FIGURE IV. 16 (C)). Comparing the fluorescence output with the labelled conjugate, free cy5.5 is not an appropriate control due to the different signal obtained. The tissue uptake of free Cy5.5 was highly pronounced compared with the uptake of DB-Tf-Cy5.5, even though the Cy5.5 administered concentration was 1/7 times less than the present in the DB. It is clear that original fluorescence of the dye is dramatically diminished after polymer conjugation In the case of DB-Tf-Cy5.5 fluorescence signal was observed in the kidneys and the bladder indicating renal secretion. Concerning the brain, *in vivo* monitoring could be attributed to the conjugate presence in blood vessels surrounding the brain. Accumulation in this organ along the time was not observed.

After *ex vivo* analysis, free dye showed its presence in all organs analysed (FIGURE IV. 17, FIGURE IV. 18, FIGURE IV. 19, FIGURE IV. 20) 4h post-administration with clear disappearance after 24h except in the kidneys. On the contrary, DB_{200}-Tf-Cy was again only localised in kidney, liver and in less extent in the spleen. As expected, polymer conjugation significantly alters PK and biodistribution of low MW molecules such as the NIR dye used. Results were compared with the non-targeted DB-Cy5.5 (**34**). Although in *ex vivo* images a higher signal was identified in the liver for DB-Tf (FIGURE IV. 20), quantification by fluorimetry did not show any significant difference between the targeted (Tf-DB-Cy5.5) and non-targeted carrier (DB-Cy5.5) (FIGURE IV. 22). Renal secretion was again the predominant secretion pathway for the targeted diblock. Unfortunately, non-significant differences were found between treated and control mice after spectrofluorometer analysis. After 24h, DB-Tf-Cy5.5 conjugate was not longer detected in the blood stream as shown in fluorescence

measurement arriving to basal levels (FIGURE IV. 21).

(A) Dorsal view

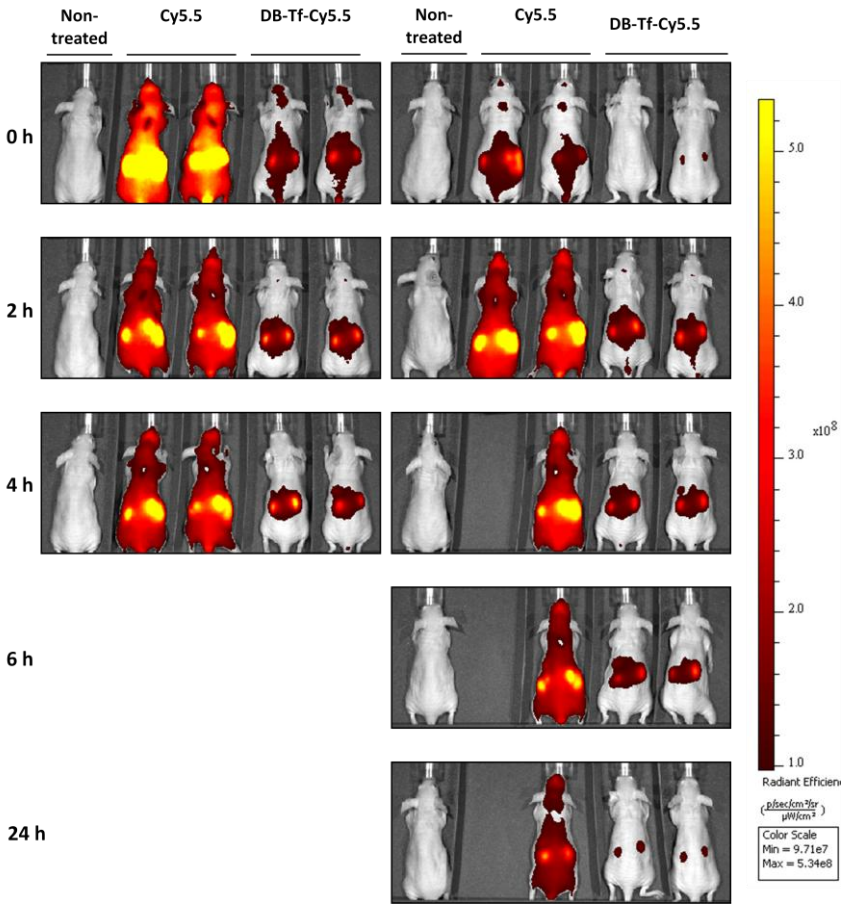

(B) Ventral view

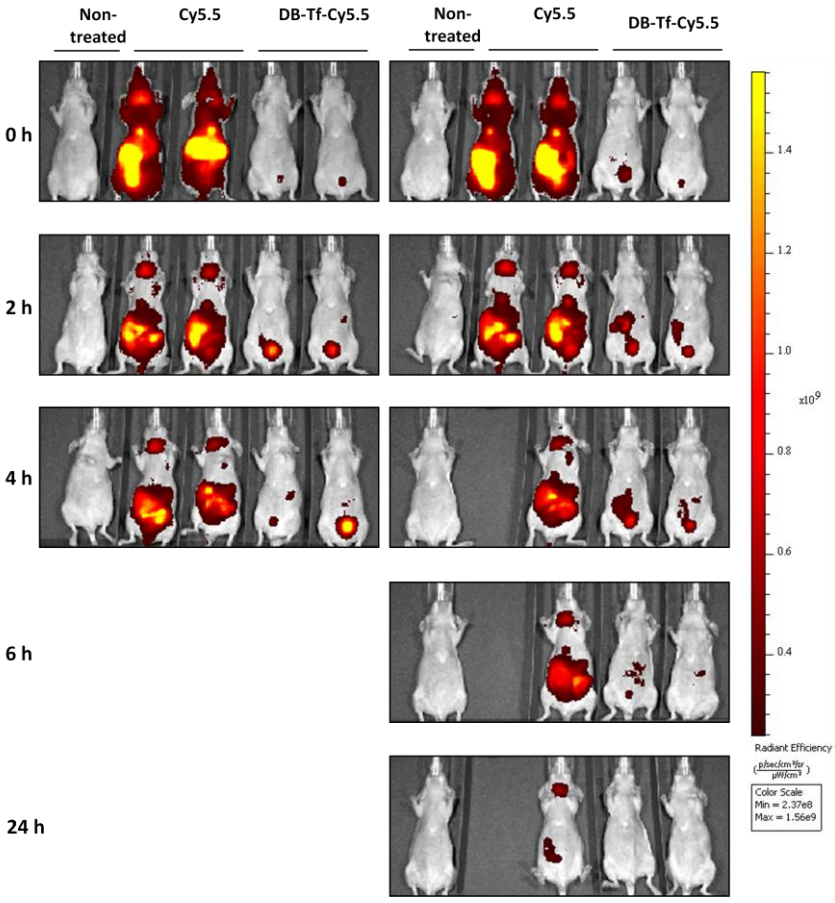

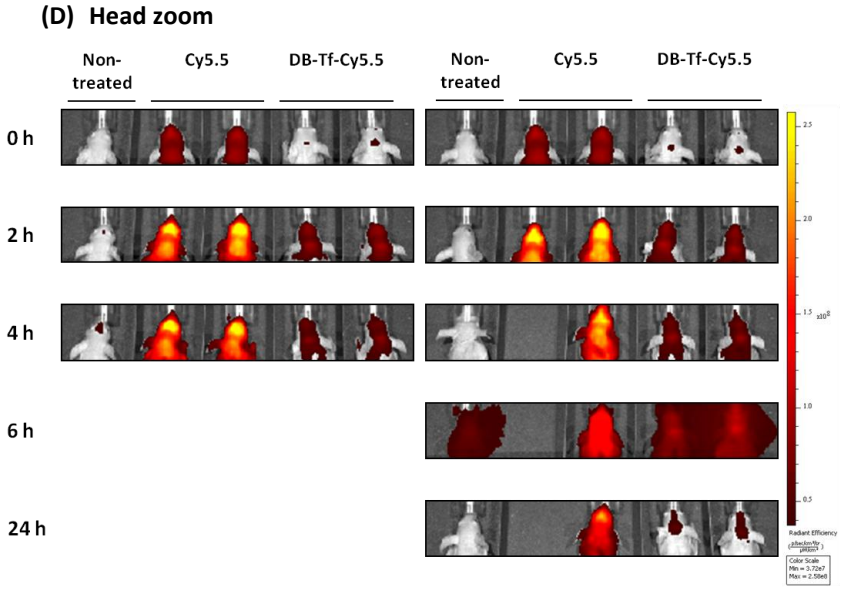

FIGURE IV. 16 Non-invasive monitoring of the Cy5.5 labelled DB_{200}-Tf (**35**) and the free dye overtime after i.v. administration at 4 and 24h post-injection: (A) dorsal view (B) ventral view (c) head zoom.

In conclusion, through FLI technique renal secretion was demonstrated for DB-Tf conjugate as well as non-specific accumulation in any analysed organ, however, this technique did not show any brain uptake. It is believed optical imaging techniques are not adequate to study transport to the brain due to the limit of detection as this technique is not sensitive enough and the evaluation of the images was not a simple due to the low fluorescence registered in the organ (FIGURE IV. 20).

(A) Brain

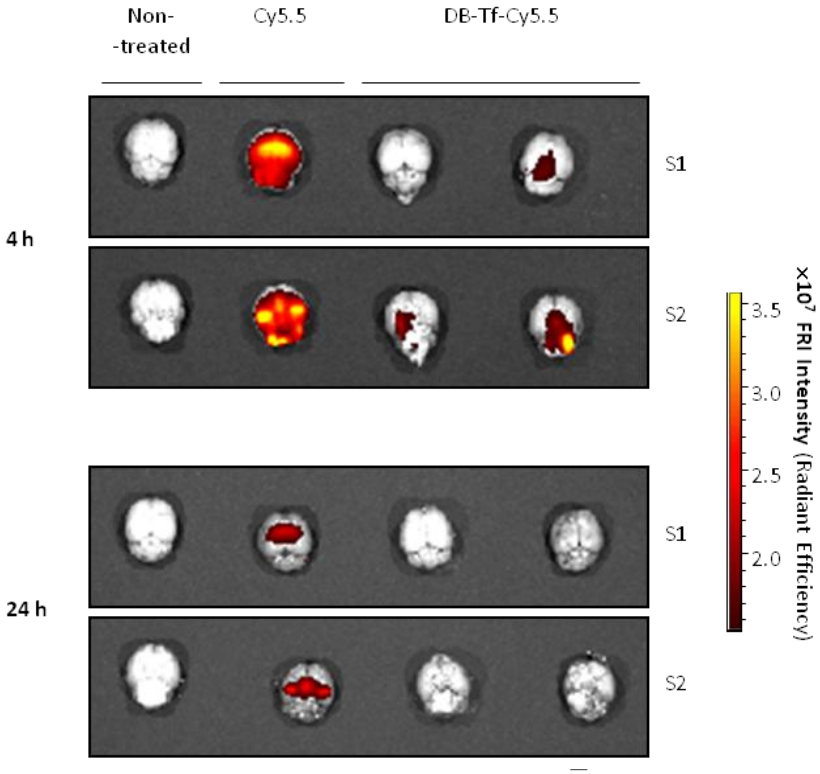
Non-
-treated
Cy5.5
DB-Tf-Cy5.5
4 h
24 h
S1
S2
S1
S2
×10⁷ FRI Intensity (Radiant Efficiency)
3.5
3.0
2.5
2.0

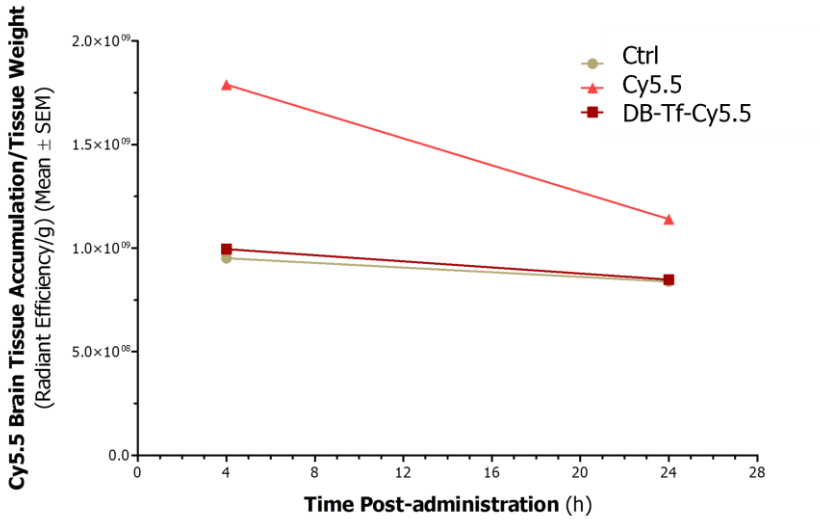
Cy5.5 Brain Tissue Accumulation/Tissue Weight
(Radiant Efficiency/g) (Mean ± SEM)
2.0×10⁰⁹
1.5×10⁰⁹
1.0×10⁰⁹
5.0×10⁰⁸
0.0
0
4
8
12
16
20
24
28
Time Post-administration (h)
Ctrl
Cy5.5
DB-Tf-Cy5.5

(B) Liver

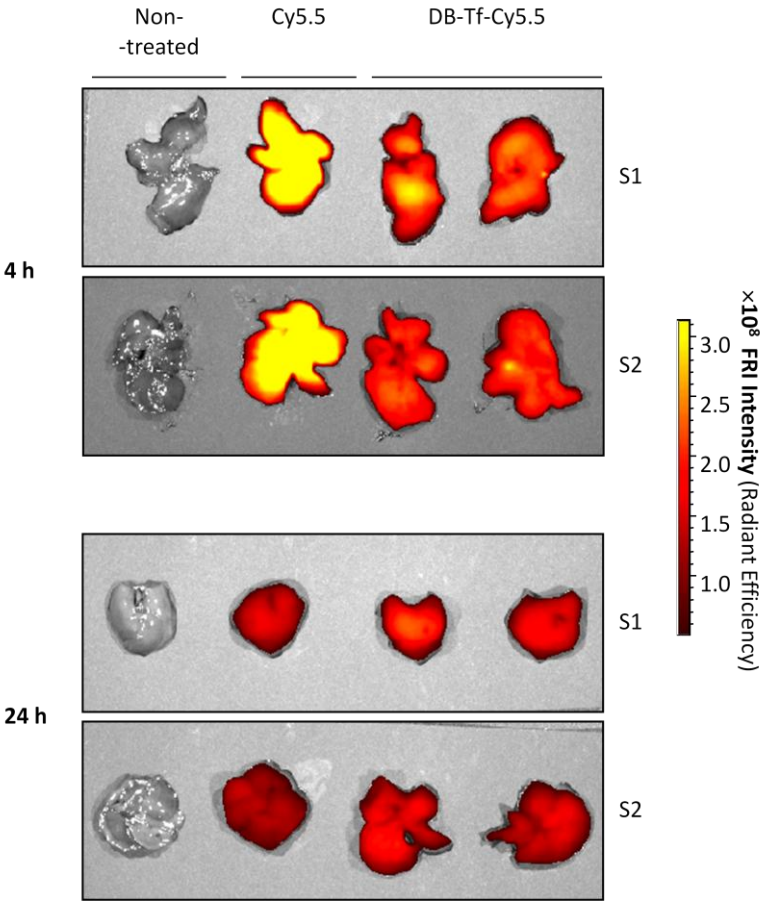
Non-
-treated
Cy5.5
DB-Tf-Cy5.5
4 h
24 h
S1
S2
S1
S2
×10⁸ FRI Intensity (Radiant Efficiency)
3.0
2.5
2.0
1.5
1.0

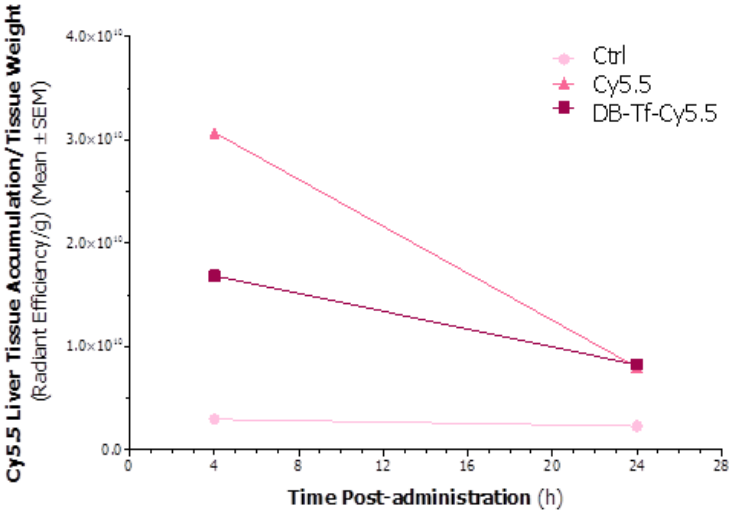
Cy5.5 Liver Tissue Accumulation/Tissue Weight
(Radiant Efficiency/g) (Mean ± SEM)
4.0×10¹⁰
3.0×10¹⁰
2.0×10¹⁰
1.0×10¹⁰
0.0
0
4
8
12
16
20
24
28
Time Post-administration (h)
Ctrl
Cy5.5
DB-Tf-Cy5.5

(C) Kidneys

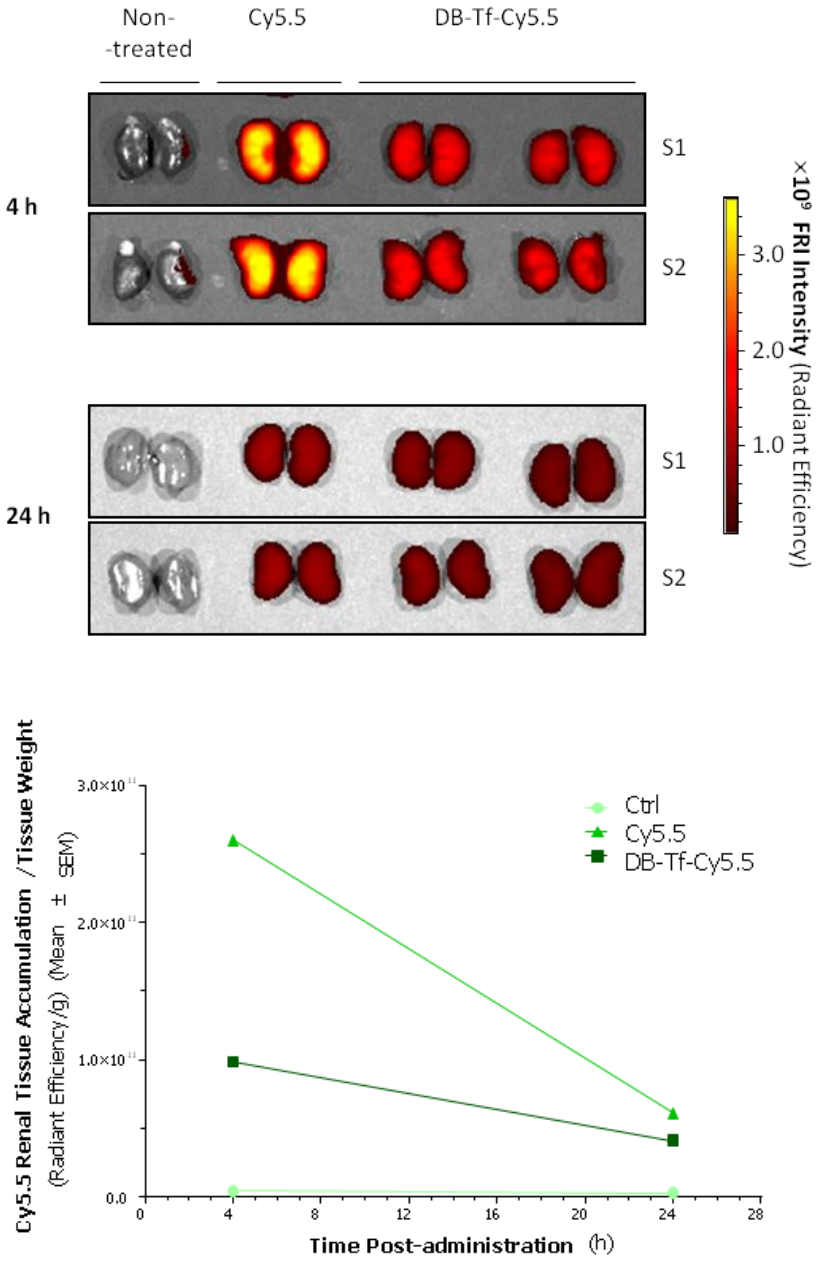

FIGURE IV. 17 *Ex vivo* fluorescence images of organs retrieved from the mice after i.v. injection of Cy5.5-labeled DB_{200}-Tf and free dye: (A) brain, (B) liver and (C) kidneys.

(A)

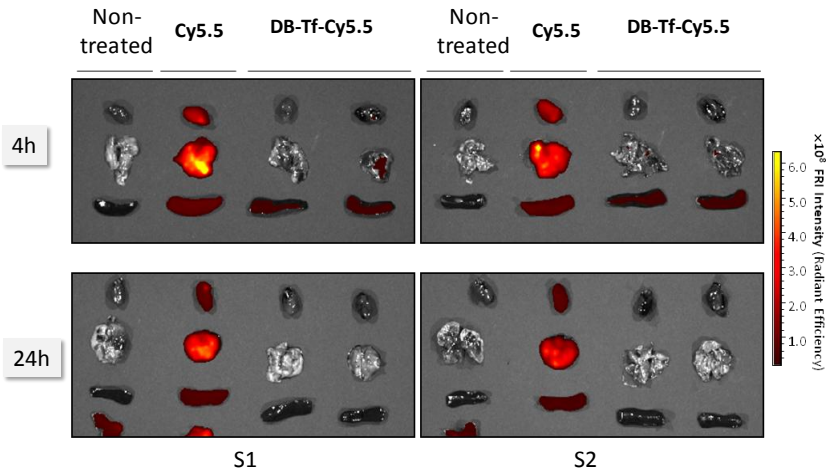

(B)

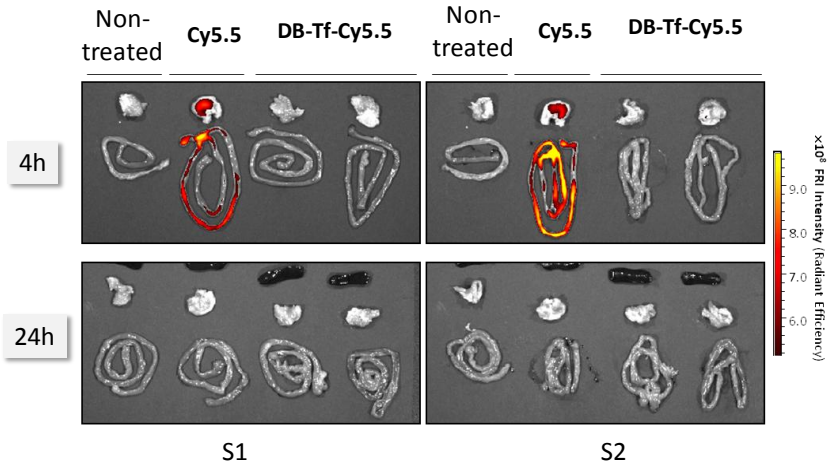

FIGURE IV. 18 *Ex vivo* fluorescence images of organs retrieved from the mice after i.v. injection of Cy5.5-labeled DB_{200}-Tf and free dye at 4 and 24h post-injection. (A) Heart, lungs and spleen. (B) Stomach and intestines.

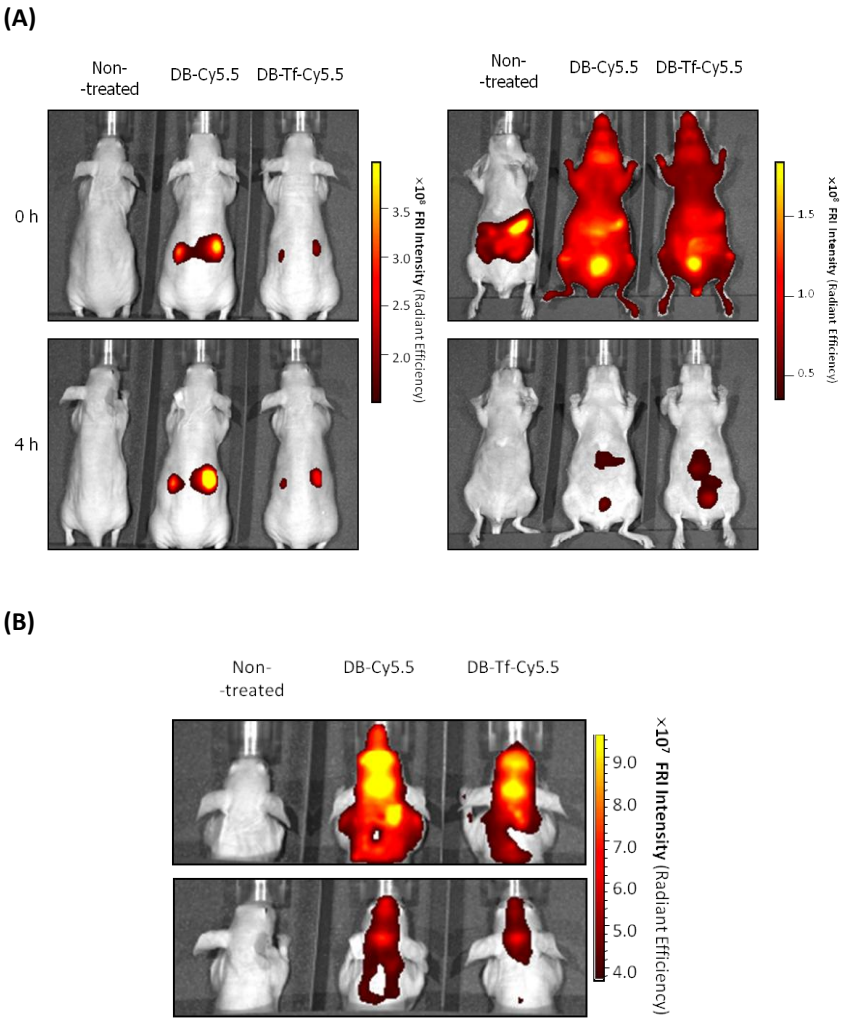

FIGURE IV. 19. Comparison study among the targeted and non-targeted DB_{200}. In vivo monitoring images: (A) dorsal view (left) and ventral view (right). (B) Head image zoom.

(A) Brain

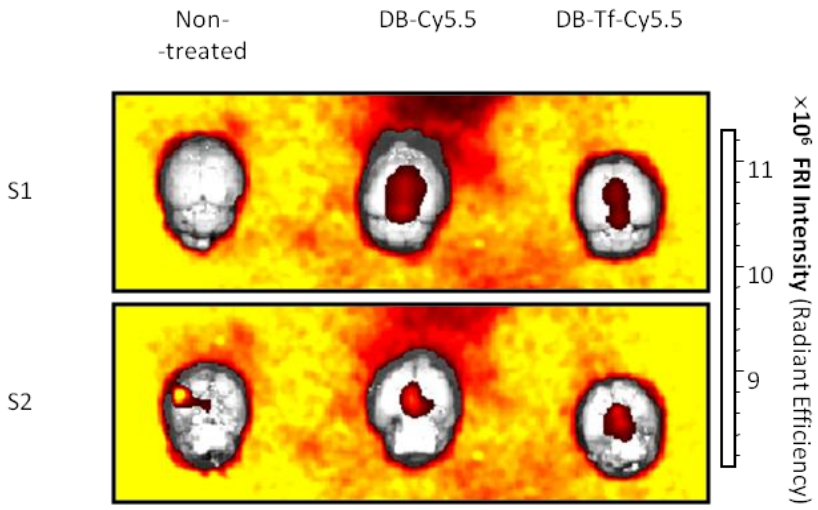

(B) Liver

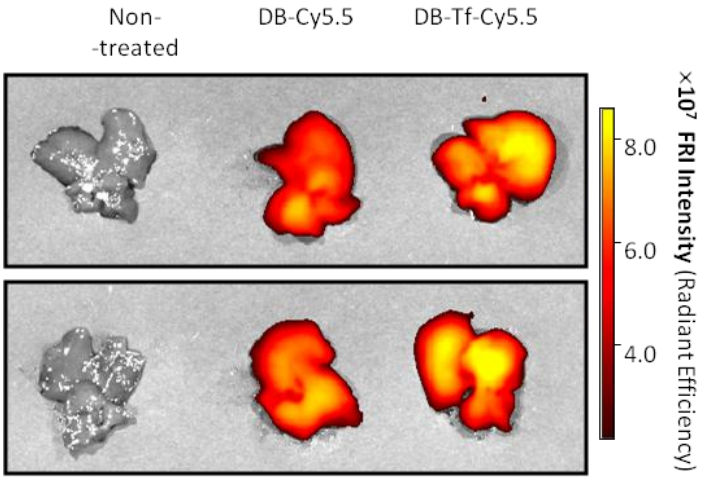

(C) Kidneys

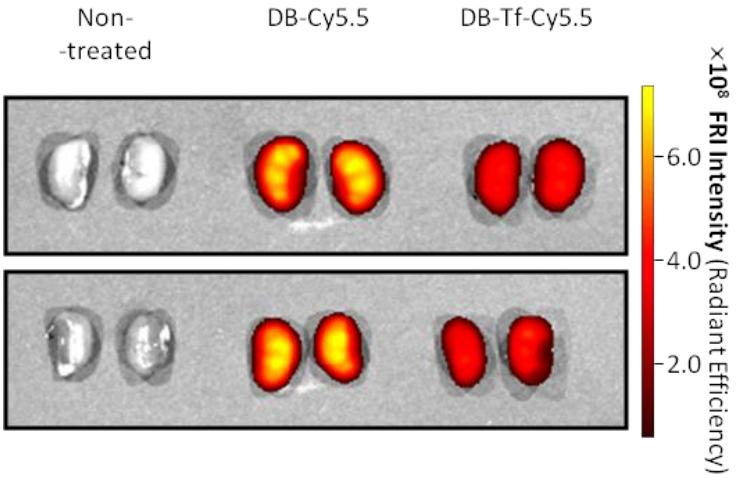
Non-
-treated
DB-Cy5.5
DB-Tf-Cy5.5
×10⁸ FRI Intensity (Radiant Efficiency)
6.0
4.0
2.0

(D)

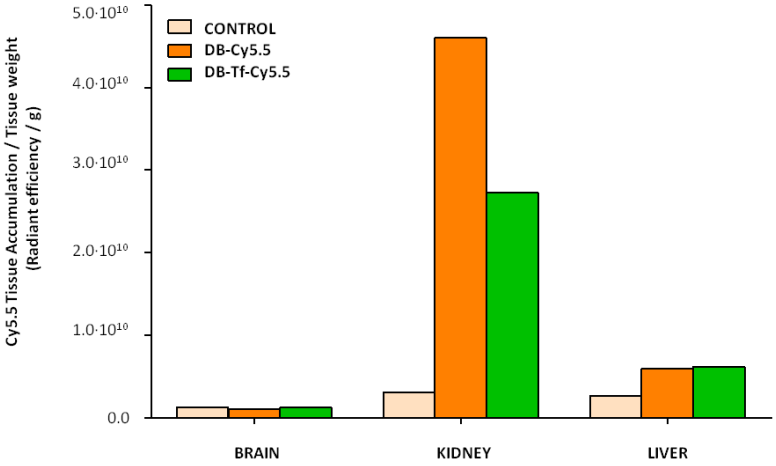
Cy5.5 Tissue Accumulation / Tissue weight
(Radiant efficiency / g)
5.0·10¹⁰
4.0·10¹⁰
3.0·10¹⁰
2.0·10¹⁰
1.0·10¹⁰
0.0
CONTROL
DB-Cy5.5
DB-Tf-Cy5.5
BRAIN
KIDNEY
LIVER

(E)

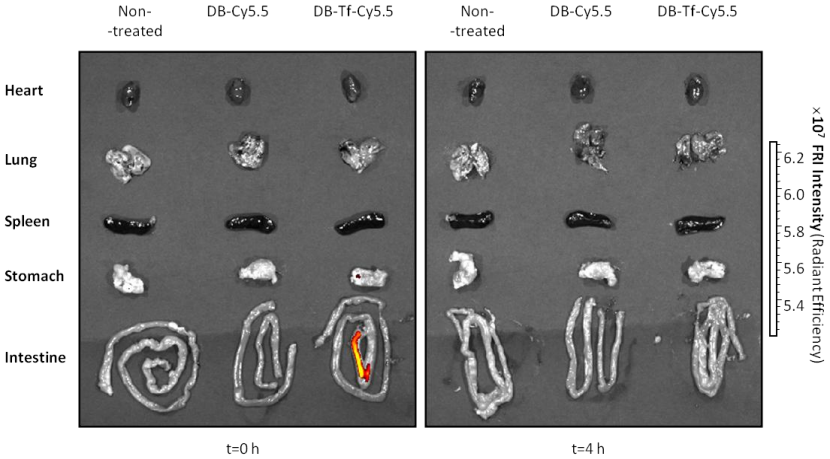

FIGURE IV. 20 *Ex vivo* fluorescence images of organs retrieved from the mice 4h after i.v. injection of the cyane labelled DB_{200} and DB_{200}-Tf systems: (A) brain, (B) liver and (C) kidney. In all images, both side of each organs were captured, upper photo is side 1 (S1) and lower photo is the other (S2). (D) Quantification of the labelled triblocks (targeted/non-targeted) in brain, liver and kidneys compared with non-injected animals. Relative fluorescence intensities were normalised with tissue weight.(E) *Ex vivo* monitoring of heart, lungs, spleen, stomach and intestines.

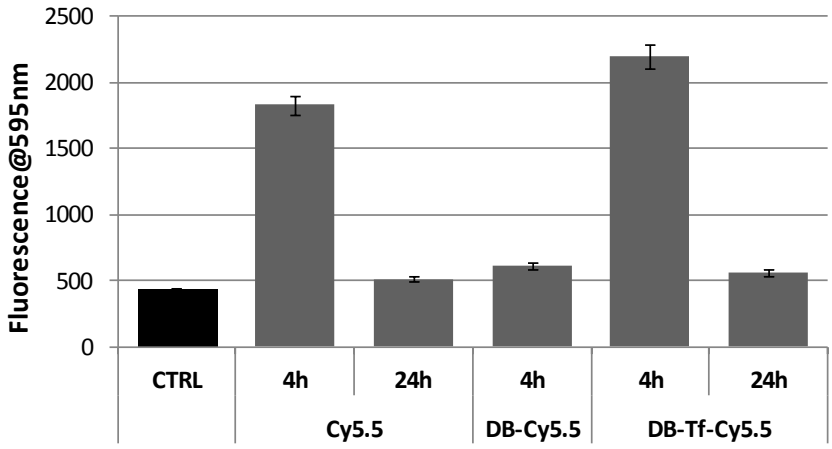

FIGURE IV. 21 Fluorescence analysis of plasma from Cy5.5, DB_{200}-Cy5.5 and DB_{200}-Tf-Cy5.5 injected animals after 4 and 24h.

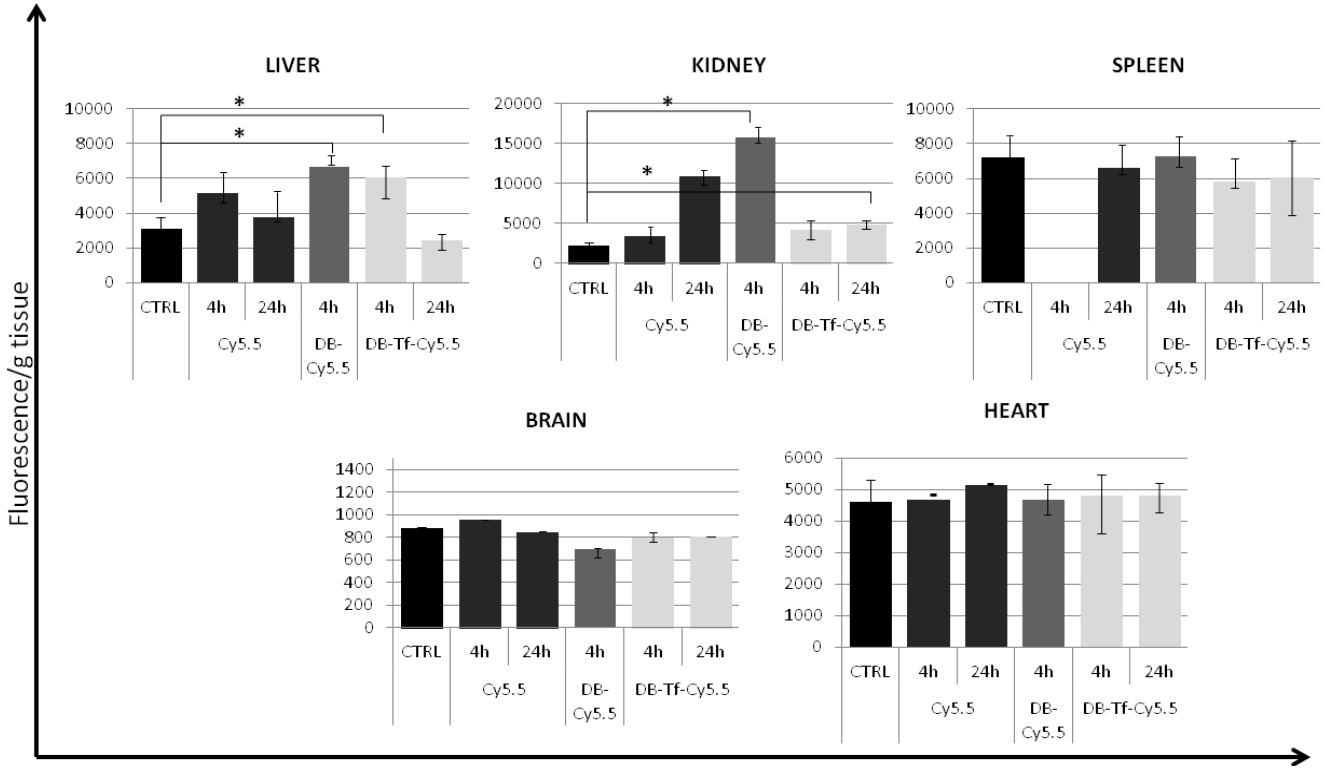

FIGURE IV. 22 Quantification of fluorescence signal from the excised organs normalised per gram of tissue. Data correspond to Cy5.5, DB_{200}-Cy5.5 and DB_{200}-Tf-Cy5.5 treated mice.

IV. 1. 2. 2. 3 Biodistribution study by MRI. Monoclonal antibody OX26 (mAb OX26)-TB-DTPA/Gd conjugate

A strategy to circumvent endogenous competition of Tf while targeting the TfR, is by means of antibodies against this receptor. The mAbOX26 does not bind the natural ligand site but another epitope. Pardridge *et al.* reported that mAbOX26 has approximately fourfold greater BBB permeability than cationised albumin [25]. With this targeting motif, several compounds have been successfully targeted to the brain (section I.1.8). For this reason, mAb OX26 was conjugated to our carriers (TB). After the discouraging results obtained with optical imaging approaches, it was decided to use MRI as detection technique aiming to detect a conjugate brain accumulation; this was achieved by labelling the carriers with DTPA/Gd complexes. Preliminary *in vivo* experiments were performed with TB_{100}-DTPA/Gd-OX26 (**26**), although gadolinium signal was not detectable. Therefore, a higher MW TB was use in order to increase DTPA functionalisation and consequently Gd^{3+} loading in the conjugate. However, the increase of DTPA/Gd loading significantly decrease the solubility of the carrier and consequently limitation of the administered dose to the animals were encountered.

TB_{200}-DTPA/Gd-OX26 (**26**) was administrated i.v. at a dose of 0.2mmol Gd/kg (TABLE IV. 1). Due to solubility problems, the conjugate was highly diluted and 2mL had to be injected by perfusion during 1min. Unfortunately, after 24h no signal was observed either in the blood circulation or in the brain. It should be considered that Gd content was lower than that required to achieve a good MRI signal. Usually, percentage of the total dose injected able to cross the BBB is between 1-4% which depending on the sensitivity of the employed technique could be undetectable. *Ex-vivo* analysis was not performed and should be considered to finally determine if conjugates crossed or not.

COMPOUND	REF	%DOTA[A]	%pep [A]	%pep [B]	MW unit (g/mol)[A]	GA units[C]
PGA-Angiopep2-DOTA	**41**	10	4.7	3.95	301,98	106
DB-Angiopep2-DOTA	**42**	11	4.5	3.54	323,25	94
PGA-cPEP-DOTA	**47**	2	2.75	n.d.	207,61	106
DB-cPEP-DOTA	**48**	11	3.4	2.81	261,61	94

pep=peptide, A=determined by ^{1}H-NMR, B=determined by amino acid analysis, C=determined by GPC, n.d.=not determined

TABLE IV. 3. DOTA labelled systems (PGA_{100} and PEG-*b*-PGA_{100}) for biodistribution experiments with PET technique. Quantification of DOTA and peptide loading.

This methodology was finally discarded due to its low sensitivity and the solubility problems presented when antibody was conjugated with the labelled polymeric systems with the Gd^{3+} complexation.

IV. 1. 2. 2. 4 Biodistribution studies by PET. Targeting peptides conjugated to PGA-DOTA and DB-DOTA

Work performed with Tf and the mAb OX26 set up the chemical basis for conjugation to the polymer carrier as well as directed the study towards a more suitable brain monitoring technique, such as PET. After all results obtained, peptidic targeting residues instead of protein or antibodies were considered to be a more feasible approach towards the design of carrier capable to cross BBB due to experimental and possible future industrial issues (scalability, costs, etc). It is important to remind that, three polymeric platforms were evaluated with and/or without targeting motif: PGA homopolymer, triblock and diblock *co*-polymers.

For these reasons, two peptides were selected to move forward with our aim. In first place and to continue the exploitation of the Tf receptor, an iron-mimic peptide was proposed: cyclic peptide

cPEP. This peptide can recognise the Tf as demonstrated *in vivo* studies in healthy mice and into xenografts of human malignant gliomas [28]. Peptide chemical structure homes an internal disulphide bond that can trigger cross-linking problems if disulphide bond is used as conjugation strategy. Therefore, an amide bond was used as linker. The second peptide chosen was the Angiopep-2 derivatised with a cysteine group in the C-terminal. This peptide is the most advanced motif in clinical trials for treatment of brain gliomas [29]. However, Tf is not its target receptor. Angiopep-2 is endocytosed by the low-density lipoprotein receptor-related protein (LRP-1). Disulphide-bridge chemistry was applied for this peptide in its conjugation to the polymeric carrier.

Regarding all the monitoring techniques so far used, PET was selected as offered (i) the appropriate sensitivity to detect brain accumulation, (ii) the need of a low percentage of tracer, which makes the results resemble to the real outcome of the non-labelled conjugate and (iii) an easy work-out to quantitate the signal of single organs in *ex vivo* experiments, avoiding extraction procedures.

As a pilot study, PGA homopolymer (**11**) and diblock co-polymer (n=100) (**7**) were used due to the simple chemistry required in their polymerisations and as a starting point. Once DOTA labelling was optimised (section III.1.1.3), polymer post-polymerisation steps were done prior to the conjugation of any of the peptides. With this strategy, higher loadings of the targeting molecules were obtained. In summary, four systems labelled with DOTA/^{68}Ga were evaluated in an in vivo preliminary experiment to be used as screening to select the best carrier/vector (carried out at *CIEMAT*, Madrid): PGA-angiopep2, DB-Angiopep2, PGA-cPEP and DB-cPEP (TABLE IV. 3). FVB/NJ mice were injected intravenously with a dose between 0.2 and 1.4MBq of the labelled [^{68}Ga]-DOTA compounds (21± 4 µg compound/g body weight) and monitored up to 3h (FIGURE IV. 13). Then, at specific time points (0.25, 0.5, 1, 2 and 3h) a mouse was sacrificed and the extracted organs used for radioactivity measurements (FIGURE IV. 14).

Biodistribution studies corroborated the renal excretion route as the elimination pathway for all the analysed compounds (signal in bladder and kidneys, (FIGURE IV. 23 to FIGURE IV. 26). Organs were excised and radioactivity signals was measured and normalised with the grams of tissue. The collected data is represented in FIGURE IV. 27. Again, a major signal was identified in the kidneys. Biodistribution assay had to be concluded after 3h post-injection, before a complete clearance from the blood stream occurred, due to the short half-life of the radio-nuclei, 68 min. It is important to mention that, with other imaging techniques (optical fluorescence imaging), DB or PGA clearance from the kidneys was demonstrated (image of FIGURE IV. 13(PGA) and FIGURE IV. 16 (DB)).

(A)

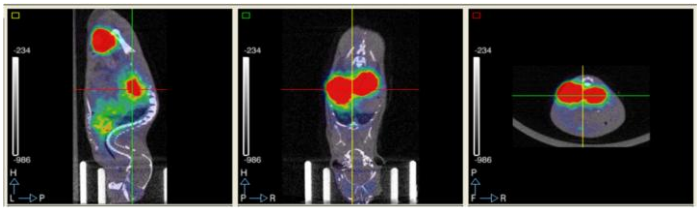

(B)

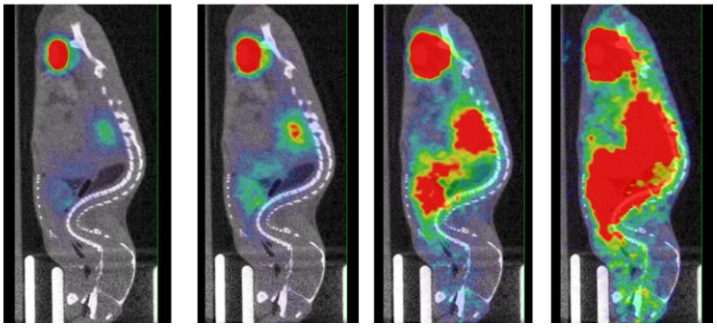

FIGURE IV. 23 PET imaging of DB_{100}-Angiopep2-DOTA/^{68}Ga (**42**) in healthy mice. Sagittal, coronal and transverse images captured immediately after administration (superior), sagittal planes with different saturation degrees (inferior).

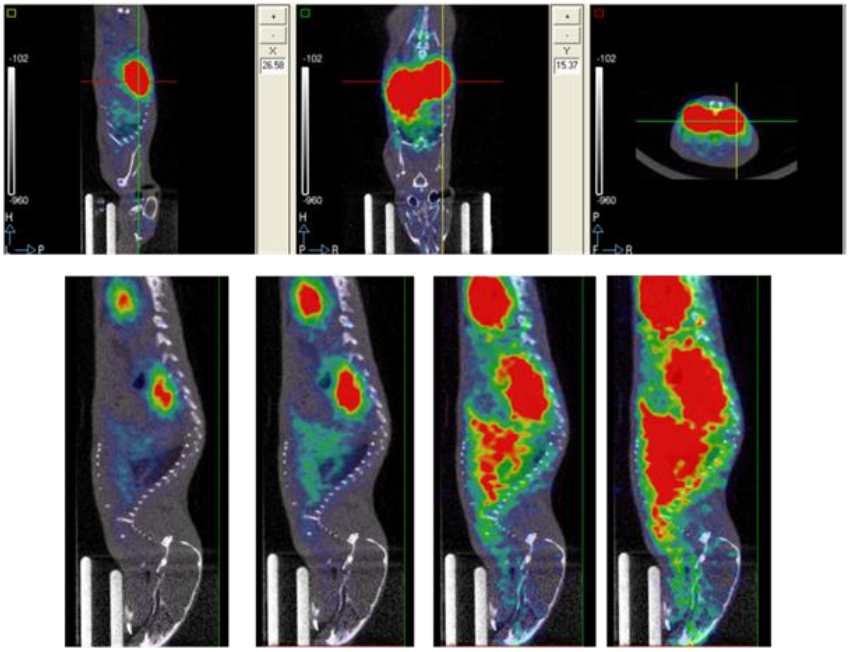

FIGURE IV. 24 PET imaging of PGA_{100}-Angiopep2-DOTA/^{68}Ga (**41**) in healthy mice. Sagittal, coronal and transverse images captured immediately after administration (superior), sagittal planes with different saturation degrees (inferior).

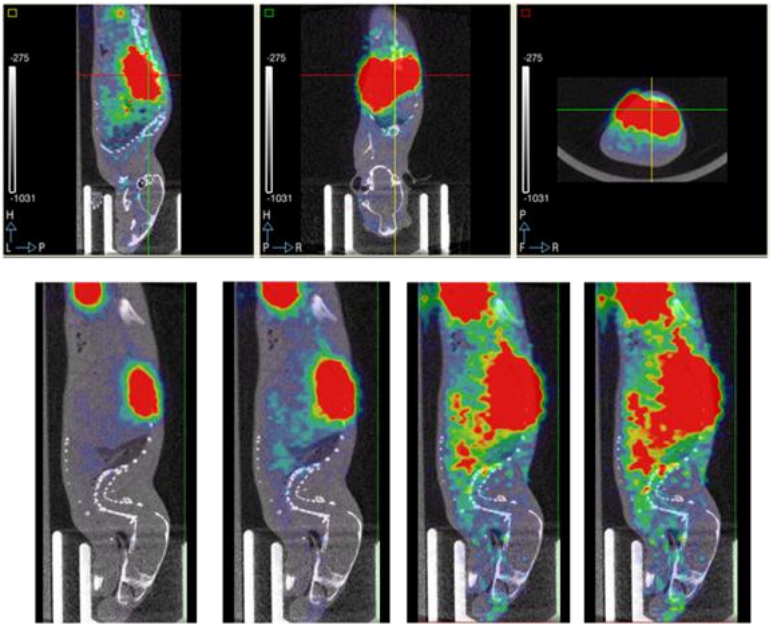

FIGURE IV. 25. PET imaging of DB_{100}-cPEP-DOTA/^{68}Ga (**47**) in healthy mice.

Sagittal, coronal and transverse images captured immediately after administration (superior), sagittal planes with different saturation degrees (inferior).

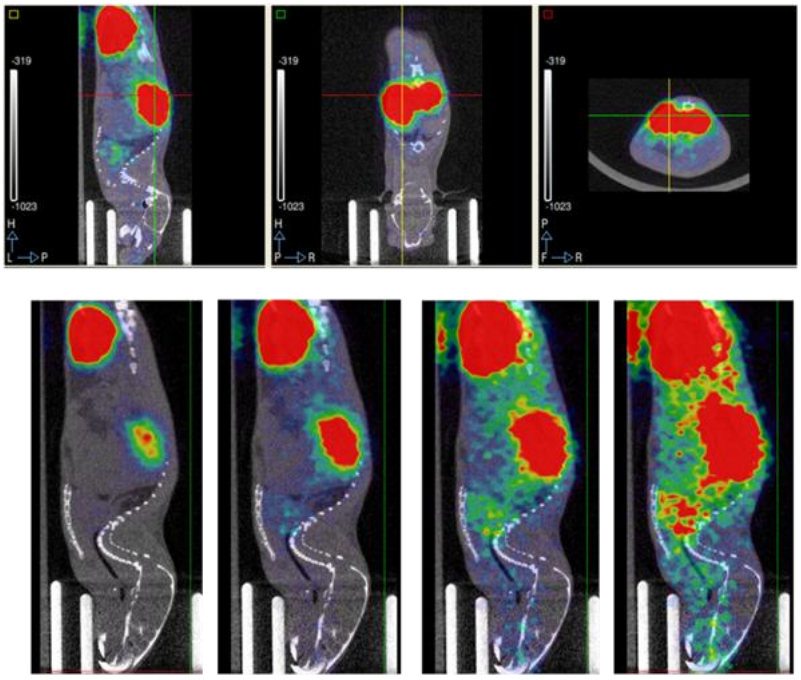

FIGURE IV. 26 PET imaging of DB_{100}-cPEP-DOTA/^{68}Ga (**48**) in healthy mice. Sagittal, coronal and transverse images captured immediately after administration (superior), sagittal planes with different saturation degrees (inferior).

Concerning the brain, our main interest in this biodistribution experiment, the highest radioactive signal was detected for the Angiopep-2 conjugates. Angiopep-2 labelled systems showed the major accumulation in brain at 30min post administration and cPEP at 1h. Signal reduction could be attributed either to conjugates pump-out of the brain by efflux systems or that signal observed belongs to blood vessels surrounding the brain. The low levels of internalisation could be explained to low exposure of the peptide ligands to the receptors due to polymer solution conformation as conjugation through side-chains were used as first approach.

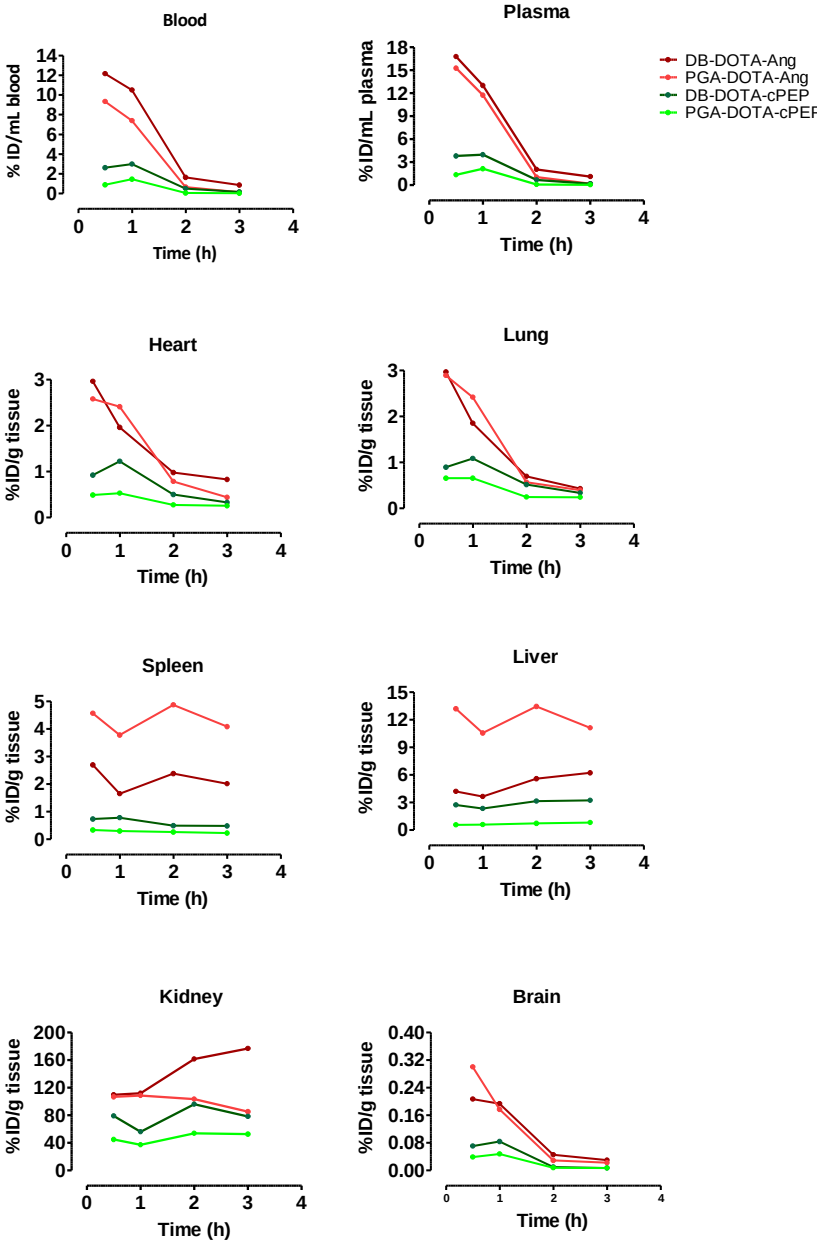

FIGURE IV. 27 Normalised data of radioactivity signal of each organ respect the injected dose (ID). Time course experiment. All polyglutamates had DP=100.

With both peptides, diblocks achieved lower percentages than homopolymers. The proposed reason was a lower peptide recognition due to PEG blocks forming an outershell hiding peptide molecules attached in the polypeptide block.

Currently, new studies are ongoing trying to solve this issue. For that, PEG has been use as a semitelechelic block providing a unique conjugation point for the targeting moiety. Meanwhile TB synthesis is still under optimisation, these studies are being performed with DB-4TP (**5**) and PGA homopolymer with a star-like architecture, aiming to improve the BBB crossing.

Main advantage will rely on a better control of ligand conjugation and a better exposure in solution of the peptides for receptor recognition.

IV. 2 CONCLUSIONS

After optimising the polymerisation process (chapter II) and labelling/targeting steps (chapter III), the obtained PGA-based polymeric carriers were evaluated *in vitro* and *in vivo*. The novel polyglutamate system: the triblock PEG-*b*-PGA_n-*b*-PEG-4TP was firstly evaluated to test its cell viability. With n=100, 150 and 200 Glu units, preliminary assays were carried out in the human endothelial cell line HUVEC. This assay validated the TBs as acceptable drug carriers.

Then, identification of the internalisation mechanism studies through flow cytometry and confocal microscopy techniques were carried out. In this study, several samples were incubated in presence of the lysosomal marker Texas Red-dextran (TRD) to identify possible co-localisation with the labelled polymers and therefore establish a lysosomotropic intracellular pathway. These studies demonstrated that all members of the TB family entered in the cells via an energy dependent pathway, endocytosis. Higher DP TBs were faster internalised as expected for bigger systems. Solution conformation studies by SANS are ongoing to corroborate these results.

Previous studies in our laboratory showed a mixed internalisation pathway of the TB_{200}-OG (PEG-*b*-PGA_{200}-*b*-PEG-OMe), combining endocytosis with diffusion. An extra study was performed aiming to compare two terminal groups: methyl and activated disulphide group. However, the observed diffusion behaviour was not reproduced in any of the analysed TB. This fact dismissed the possibility of exploiting inherent properties of TB conformation for diffusion through biological barriers. Therefore, the conjugation of targeting moieties came to the fore instead of its supplementary role.

After *in vitro* evaluation, the different systems (PGA, DB and TB) were subjected to *in vivo* studies. On one side, each member by itself had to prove their biocompatibility, safety, non accumulation in any specific organ and adequate secretion. On the second hand, our systems were proposed as candidates for BBB drug delivery systems.

After discard diffusion processes and considering the difficulty of the barrier, active targeting was required to reach our goal. Hence, biodistribution experiments were performed with targeted systems for comparing advantages of the selected ligands and the parent polyglutamates.

Several techniques were evaluated, ranging from optical imaging with a fluorescent probe or a NIR dye, MRI with a contrast agent or PET with a radionuclide. Regarding the non-targeted systems, PGA (PGA-DOTA), DB (DB-Cy5.5) and TB (TBO) showed renal secretion, non specific accumulation and none of them presented inherent properties for BBB crossing. Accumulation in liver was also observed but significantly less than that observed in the kidney. The experiments performed with all the different imaging techniques pointed out that for brain crossing detection PET were the best. The percentage of the injected dose able to cross BBB is usually very low (< 4% of the injected dose) so the most sensitive technique is required for brain detection.

Among the BBB ligands evaluated, TB-Tf was detected in rat brain after i.v. injection after WB analysis. However, comparison with the same administered dose of free Tf showed a significant reduction on the internalised amount. DB and DB-Tf biodistributions were compared by means of fluorescence imaging and no differences were detected at brain region. As at normal levels Tf receptor remains saturated and possibilities for BBB crossing by means of the endogenous Tf are reduced, the mAbOX26 was suggested as an alternative ligand. By means of MRI, TB-OX26-DTPA/Gd was not detected in the mouse brain after i.v. Problems on solubility of the final conjugate resulted in highly diluted doses, which possibly hindered the compound detection. Finally, with the objective of simplify the whole procedure, peptidic sequences were chosen as targeting moieties. Angiopep-2 is the most advanced peptide ligand in clinical trials [29, 30], this and a cyclic peptide mimicking the iron molecule [28]were studied. At this stage, we had already decided that DB output concerning biodistribution was similar to TB, presenting

also an easier synthetic pathway with better yields. Therefore, PGA homopolymer and DB were selected for comparison with these two novel targeting vectors. Preliminary studies evidenced higher radioactivity for the angiopep-2 conjugates than for the cPEP in the brain although concentration was not maintained. Either conjugates were pumped out or not internalised due to a failed exposure of the peptides for receptor recognition. The results observed could be attributed to low exposure of the peptide ligands to the receptors due to polymer conformation. DB systems gave in both cases lower percentages perhaps because PEG blocks formed an outershell hiding the peptide molecules attached in the polypeptide block. The suggested solution was to use PEG as semitelechelic block providing a unique conjugation point for targeting moiety, which probably will be more accessible for receptor recognition. DB-4TP synthesis was optimised and, while TB is ongoing, this system will be tested *in vivo* as well as branched PGAs (star). Main advantage will rely on a better control of ligand conjugation and availability in solution of the peptides for receptor recognition. BBB crossing is still a goal to achieve. However, many steps on the right direction had been set up the most optimal technique for visualising and quantifying BBB crossing of our conjugates. PET, as well as all of our novel systems had been evaluated and with the last conjugates synthesised better results are expected due to a better exposure of the peptidic residues.

IV. 3 MATERIALS AND METHODS

IV. 3. 1 *IN VITRO* EVALUATION IN AN ENDOTHELIAL CELL LINE

IV. 3. 1. 1 Cell culture protocol

HUVEC cells were cultured in Medium 200 supplemented with Low Serum Growth Supplement (LSGS). Once split, cells were maintained at 37°C in an atmosphere of 5% CO_2 and 95% air. After 24h, cells were already adhered. Medium was replaced each 2-3 days and underwent passage once weekly when 80% of cell confluence was reached [31].

IV. 3. 1. 2 Evaluation of polymer toxicity and cell recovery through the MTT assay

MTT assay conditions

The cytotoxicity of the triblocks (TB_{100}, TB_{150} and TB_{200}) was evaluated using the MTT cell viability assay (24 and 72 h incubation) with HUVEC and HeLa cells. Both cell lines were seeded into sterile 96-well microtitre plates (density (cell/cm^2) in TABLE IV. 4) in their correspondent medium (TABLE IV. 4). They were incubated for 1 day before the test compounds (0.2µm filter-sterilised) were added to give a final concentration in the range of 0 - 2 mg/mL drug-equiv. After further 67 h incubation, MTT (20µL of a 5 mg/mL solution in PBS) was added to each well, and the cells were incubated for 4h. After removal of the medium, the precipitated formazan crystals were dissolved in optical grade DMSO (100µL), and the plates were read spectrophotometrically at 570 nm after 30 min using a microtitre plate reader. Cell viability was expressed as a percentage of the viability of untreated control cells. FIGURE IV. 28 shows the map followed in the assay. The absorbance values were represented as the percentage of cell viability having as reference (100% cell viability) the non-treated cells.

	cell density (cells/cm^2)	cell media
HUVEC	20000	Medium200 + 2% (v/v) LSGS
HeLa	15000	DMEM + 10% (v/v) FBS

FBS=fetal bovine serum, LSGS=low serum growth supplement, HUVEC=human umbilical vein endothelial cells, HeLa= human cervix

TABLE IV. 4 Cell lines exploited for cytotoxicity experiments of the polyglutamates.

	1	2	3	4	5	6	7	8	9	10	11	12
A												
B		0	0,01	0,05	0,1	0,02	0,4	0,8	1	1,5	2	
C		0	0,01	0,05	0,1	0,02	0,4	0,8	1	1,5	2	
D		0	0,01	0,05	0,1	0,02	0,4	0,8	1	1,5	2	
E		0	0,01	0,05	0,1	0,02	0,4	0,8	1	1,5	2	
F		0	0,01	0,05	0,1	0,02	0,4	0,8	1	1,5	2	
G												

FIGURE IV. 28 Example of a map of MTT assay in a 96 well plate. Concentrations units: mg/mL.

Note: For MTT assay optimisation, growth curves of the named cell lines were done at different cell concentrations for finding proper cell density to carry out the experiment. A cell growth study could be follow during 7days. Each day, 20µL MTT solution was added to each well of the plate and the cells were incubated for 4h. Then, the medium from the wells in this row (n=6) was removed and replaced with optical grade DMSO (100 µL/well) to solubilise the formazan crystals. Once dissolved, absorbance was determined as explained before. Then, the formazan-DMSO mixture was removed from the wells and replaced with PBS (100µL/well). Plates were placed back into the incubator and same process was continued daily over 7 days.

IV. 3. 1. 3 Evaluation studies of the mechanism of the cellular entry

Confocal fluorescent microscopy: Live-cell imaging

For live-cell imaging, HUVEC cells were seeded in glass bottom culture dishes (10000cell/cm^2) and left to adhere to the coverslips for > 12 h. To assess the subcellular localisation of the polymers, cells were incubated for either 15 min or 1 h at 37°C in complete medium (1 mL) containing OG-labelled conjugates (10µL of 0.01mg/mL OG-equiv. stock) and leupeptine (10µL of 10mM stock). Before visualisation, medium containing the polymers was removed from the cells by aspiration, and the cells were washed three times with fresh medium (37°C). Finally, clear complete media was added and cells were subsequently viewed for a maximum of 30 min. Pulse and chase experiments were performed (TABLE IV. 5).

In some studies, previous to polymer incubation or in parallel, 5µL of a TRD solution (50mg/mL in sterile PBS) were added to the cells. After 1h of incubation, medium was removed and replaced with fresh one. Cells were incubated 5h at 37°C. After chase time cells were washed trice with PBS supplemented with 10%(v/v) of FBS (3mL) and the glass was removed and set on the microscope chamber.

Samples were analysed under the microscope and images were captured after excitation of the fluorophore. Images were captured with an inverted DM IRE2 microscope equipped with a λ-blue 60 x oil immersion objective and handled with a TCS SP2 system, equipped with an Acoustic Optical Beam Splitter (AOBS). Excitation was performed with an argon laser ((OG 496nm) and HeNe laser (Texas Red-dextran 594nm). Images were captured at an 8-bit grey scale and processed with LCS software (version 2.5.1347a, Leica Germany) containing multicolour, macro and 3D components.

Time point	Pulse time	Chase time
0min	0min	0min
5min	5min	5min
30min	15min	30min
1h	1h	1h
2h	1h	2h
5h	1h	5h

TABLE IV. 5 Confocal microscopy study time points. Pulse and chase times exploited for the internalisation *in vitro* studies.

Cellular uptake by fluorescent activated cell sorting (FACS)

Binding and uptake of OG-labelled triblocks by HUVEC cells

HUVEC cells were seeded in 6-well plates at a density of 15000cel/cm^2 (1 mL cell suspension per well) and allowed to adhere for 24 h. In the binding experiments conducted at 4°C, the cells were pre-incubated at this temperature for 30 min prior to addition of conjugate. 10µL of OG-labelled polymers (0.01mg OG/mL) and 10µL of leupeptine 10mM were added and the cells incubated for 0 to 300 min either at 37°C or 4°C. At each sample time, cells were placed on ice, then washed three times with ice-chilled PBS (5 mL), and PBS (1 mL) was added before the cells were scraped from the plate with a rubber policeman and collected in falcon tubes. The cell suspension was centrifuged at 4°C (600 x g for 10 min). The cell pellet was re-suspended in ice-chilled PBS (200 µL). Cell-associated fluorescence was then analysed using a Becton Dickinson FACSCalibur cytometer (California, USA) equipped with an argon laser (488 nm) and emission filter for 550 nm. Data collection involved 25,000 counts per sample, and the data were analysed using CELLQuestTM version 3.3 software. Data are expressed by plotting the shift in geometric mean of the entire population (i.e. geometric mean after incubation with the polymer-geometric mean in absence of polymer). Cells incubated without polymer conjugate were used to account for the background fluorescence.

IV. 3. 2 BIODISTRIBUTION EXPERIMENTS

IV. 3. 2. 1 Biodistribution studies of non-targeted polyglutamates

IV. 3. 2. 1. 1 Triblock biodistribution by *ex vivo* Optical Imaging Analysis

OG labelled triblock (TB_{200}-OG, 0.72%mol OG) was dissolved in serum saline at 14mg/mL, injected intravenously (i.v.) as a single dose in male Wistar rats (n=3) and sacrificed 4h post-injection. A second group (n=3) was injected with the same dose and sacrificed 24h later. As control, mice (n=3) were injected equivalent dose of the polymer without labelling (TB_{200}).

Immediately after sacrificing, the blood was collected in heparinised eppendorfs and placed on ice. Blood was centrifuged (4000rpm, 10min, 4°C) and serum (supernatant) was collected and frozen for later analysis. Organs (brain, cerebellum, heart, spleen, liver, bladder, stomach, gut, muscle and fat) were excised, weighted, frozen in liquid nitrogen and stored at -80°C for following examination. Each organ was treated individually with a cold solution composed of $HClO_4$ 6% / EtOH 40% at a proportion 1g tissue/4mL and placed in ice. Then, samples were homogenised using an Ultraturrax® Homogenizer. Also serum samples were treated with the same protocol but adding the same sample volume of perchloric acid solution. The suspension was centrifuged (60min, 4000rpm, 4°C) and the supernatant stored for analysis (*sup1*). In order to improve the extraction of the labelled polymer, pellets were sonicated for 60min in 1mL of $NaHCO_3$ 1M / 2mL of H_2O, centrifuged in the same conditions as described above and the supernatant stored for further analysis (*sup2*). As it was found that OG is pH sensitive (the fluorescence is inhibited by acidic pH), the $HClO_4$ supernatants (*sup1*) were neutralised with NaOH, freeze-dried and resuspended in 1mL of PBS at pH 7.4 (*sup3*) for further analysis. All the samples (*sup1, sup2, sup3*) were analysed with a spectrofluorometer (λ_{ex}=485nm, λ_{em}=535nm). Serum fluorescence was also directly measured before any treatment. Final data was normalised by dividing fluorescence signal per organ mass.

IV. 3. 2. 1. 2 DB-Cy5.5 biodistribution: *in vivo* and *ex vivo* monitoring by fluorescence imaging

Cy5.5 labelled DB_{200} (**34**) (1.63%molCy5.5) biodistribution was conducted in nude mice in order to determine organ distribution as well as conjugate $t_{1/2}$ in blood. As control, free Cy5.5 was injected. Compounds distribution *in vivo* as well as *ex vivo* was monitored by means of tissue fluorescence imaging (FLI) using the IVIS® Spectrum.

Athymic nude mice (Harlam, 8 weeks) were treated intravenously with a single dose of 2mg Cy5.5/Kg of DB-Cy5.5 resuspended in serum saline. Animals were anesthetised using 1-3% isoflurane. The whole-body biodistribution of the labelled diblock was monitored non-invasively by FLI using the IVIS® Spectrum Imaging System with excitation and emission wavelengths of 675/720nm, respectively. Five mice were imaged at a time and imaging settings of the experiment (exposure time, binning, field of view, f/stop, field of view) were set during the experiment to capture optimal fluorescent output. Time course experiment was carried out (0, 2h, 4h, 24h). The light emitted from the fluorescent DB-Cy5.5 was detected, digitalised and electronically displayed as a pseudocolor overlay onto a gray scale animal image. Regions of interest (ROI) from displayed images were drawn manually selecting the fluorescent signals and quantified as Efficiency. Mice were euthanized at 4 and 24h post administration. Blood was collected individually by cardiac puncture and processed for plasma obtaining by centrifugation (4000rmg, 10min, 4°C) and placed in ice or frost until evaluation. Organs of interest (heart, lungs, spleen, kidneys, liver and brain) were dissected from mice, and fluorescence images of excised tissues were obtained by ex vivo FLI. Tissue samples were also stored at -80°C to quantify fluorescence after compound extraction from the organ.

<u>Blood and organ analysis</u>

Cy5.5 detection in excised organs was optimised for fluorescence quantification. Protocol for organ homogenation described in section IV.3.2.1.1 was reproduced. Once all the supernatants were collected (*sup1, sup2, sup3*), they were analysed

with a spectrofluorometer (λ_{ex}=595nm, λ_{em}=680). Serum fluorescence was also measured directly before any treatment. Final data was normalised by dividing fluorescence signal by the organ mass.

IV. 3. 2. 1. 3 TB biodistribution: use of contrast agents (DTPA/Gd) for MRI

For this experiment, triblock systems (PEG-*b*-PGA_n-PEG, n=100 and n=200) covalently conjugated to DTPA/Gd were resuspended in serum saline in a concentration 0.2mmol Gd^{3+}/Kg animal. Male Wistar rats (m=220±5g) were used. Anaesthesia was initiated by inhalation of oxygen (1 L/min) containing 3% isofluorane and maintained during the experiment employing a mask and 2% isofluorane in O_2. Animal temperature was maintained at approx. 37°C with a heated probe. The physiological state of the rats was monitored using a Biotrig physiological monitor (Bruker, Germany) that controlled the respiratory rate and body temperature.

For anatomical reference, a multi-slice rapid acquisition and relaxation enhancement (RARE) sequence was performed with the following parameters: RARE factor=8, time of repetition (TR) = 3000 ms, effective echo time (TE)=60ms, averages=2, 6 coronal slices, slice thickness 1.2 mm, field of view (FOV)=3.8 cm, matrix=256 x 256. Then, regional contrast agent uptake was assessed. A series of T1- weighted spin echo images were sequentially acquired over one hour following the injection of the contrast agent. The acquisition parameters were: number of repetitions 30, TR=300ms, TE=9.5ms, averages=6, slice thickness 1.5 mm and number of sections with axial orientation=20, FOV=3.8 cm x 3.8cm, matrix=256 x 256 which corresponds with a resolution of 148 x 148m^2. The compounds were administered intravenously through the vein tail as a bolus 9min after initiate the acquisition. Animals were monitored immediately after administration and at 1, 6 and 24h.

In each MRI experiment, T1-weighted (T1-W) spin-echo anatomical images were acquired with a multi slice multi echo (MSME) sequence in axial orientations. In all animals, the same five coronal slices were imaged to obtain parametric maps generated on a pixel by

pixel basis. As explained, Gd is a paramagnetic metal that increase T1 relaxation time of water protons. This phenomenon is detected in MRI images with an increased hyperintensity quantified by ImageJ software that analyses grey intensities in selected brain areas.

IV. 3. 2. 1. 4 PGA homopolymer biodistribution by PET

FVB/NJ mice (CIEMAT Laboratory Animals Facility, Madrid) were housed on a 12-hour light and 12-hour dark cycle. Free access to food and water was allowed at all times. All animal protocols were approved by the Institutional Animal Care and Use Committee at *CIEMAT* (Madrid). Mice weight was 25±4g.

For the pharmacokinetics and biodistribution study, 50 mice (n = 5 per group and time point) were anesthetised with 1.5% isofluorane, and between 0.2 and 1.4MBq PGA-[^{68}Ga]-DOTA (21±4µg compound/g body weight) per mouse was injected intravenously through the tail vein. At 0.25, 0.5, 1, 2, and 3 hours post-injection, blood samples were obtained from mice by terminal bleeding via cardiac puncture following isoflurane anaesthesia; organs (lungs, heart, spleen, kidneys, liver and brain) and some tissues (muscle, fat) were isolated, rinsed with normal saline, weighted, and the radioactivity was measured using the Cobra II auto-gamma counter. The blood samples were centrifuged (3000rpm, 10min, 25°C) and the supernatant of plasma was collected. The %ID (injected dose) and the %ID/g were calculated by comparison with standards taken from the injected solution for each animal. The data were expressed as the mean ± SD.

IV. 3. 2. 2 Biodistribution studies of targeted polyglutamates

Note: Except especified cases, experiments detailed below were done with healthy Balb/c mice (9-12month old), which were used as mouse model for the *in vivo* biodistribution studies. For *in vivo* FLI experiments, animals were first anesthetised and shaved to remove hair interference with fluorescence signal.

IV. 3. 2. 2. 1 TB-Tf detection in brain through immunohistochemistry

Tissue Preparation

TB_{200}-Tf was dissolved in serum saline (1.75mg Tf/mL) as well as human Tf (1.75mg Tf/mL). Compounds were administered individually by i.v. route (0.5mL, tail vein) to Wistar rats which were sacrificed 4h after injection, together with a non-injected rat as control. Brain and cerebellum were removed and immediately frozen at -80°C until analysis. Organs were homogenised (10%w/v) in ice-cold Tris saline buffer (20mM Tris-HCl pH=7.5, EDTA 10mM, PMSF 0.2mM) supplemented with a cocktail of proteinase inhibitors (Complete, Roche Diagnostics GmbH, Germany). Then, the homogenates were sonicated and protein concentration was measured with the BCA (bicinchoninic acid) protein test (Thermo Fisher Sci.). All process was performed at 4˚C and samples were stored at 80˚ until further analysis.

SDS-PAGE and western blotting

Polyacrylamide gel (8%) was prepared. Tissue proteins were suspended in LB 2X buffer (with or without DTT) and heated at 95°C for 7min (appendix III). Together with molecular weight marker, samples were loaded into the gel wells and electrophoresis was performed. Proteins were transferred electrophoretically from the gels to a PVDF membrane, which afterwards was incubated with 10% skim milk in PBS Tween20 for blocking. Subsequently, membrane was incubated with the mouse anti-Tf antibody (1:5000). After overnight incubation at 4°C, membrane was washed and incubated with the

HRP-conjugated secondary antibody anti-mouse. After washing, staining was developed with the HRP-conjugated substrate kit.

IV. 3. 2. 2. 2 DB-Tf-Cy5.5 biodistribution: i*n vivo* and *ex vivo* monitoring by fluorescence imaging

The biodistribution of transferrin (Tf) conjugated DB was evaluated by FLI using the IVIS®Spectrum Imaging System, following the protocol described in section IV.3.2.1.2 100µL of a solution of 2mg Cy5.5/mL of Tf-DB-Cy5.5 (1.86%mol Cy.5) was intravenously administrated to each mouse (n=5). Imaging time points were done at 0, 2, 4 and 24h while end time points at 4 and 24h.

IV. 3. 2. 2. 3 Monoclonal antibody OX26 conjugated to TB-DTPA/Gd

Same methodology explained in section IV.3.2.1.3 was used for biodistribution of the targeted TB_{100} with the reduced mAbOX26.

IV. 3. 2. 2. 4 Targeting peptides conjugated to PGA-DOTA and DB-DOTA

Experimental protocol as described in section IV.3.2.1.4.

BIBLIOGRAPHY

1. Wilhelm, I., C. Fazakas, and I.A. Krizbai, *In vitro models of the blood-brain barrier.* Acta Neurobiol Exp (Wars), 2011. **71**(1): p. 113-28.
2. D. Langford, et al., *Signalling crosstalk in FGF2-mediated protection of endothelial cells from HIV-gp120.* BMC Neurosci, 2005. **6**: p. 8.
3. R.D. Hurst and I.B. Fritz, *Properties of an immortalised vascular endothelial/glioma cell co-culture model of the blood-brain barrier.* J Cell Physiol, 1996. **167**(1): p. 81-88.
4. O. O. Ogunshola, *In vitro modeling of the blood-brain barrier: simplicity versus complexity.* Curr Pharm Des, 2011. **17**(26): p. 2755-61.
5. J. R. Masters, *HeLa cells 50 years on: the good, the bad and the ugly.* Nat Rev Cancer, 2002. **2**(4): p. 315-9.
6. W. R. Sanhai, et al., *Seven challenges for nanomedicine.* Nat Nanotechnol, 2008. **3**(5): p. 242-4.
7. F. Alexis, et al., *Factors affecting the clearance and biodistribution of polymeric nanoparticles.* Mol Pharm, 2008. **5**(4): p. 505-15.
8. E. Markovsky, et al., *Administration, distribution, metabolism and elimination of polymer therapeutics.* J Control Release, 2012. **161**(2): p. 446-460.
9. Vasquez, K.O., C. Casavant, and J.D. Peterson, *Quantitative whole body biodistribution of fluorescent-labeled agents by non-invasive tomographic imaging.* PLoS One, 2012. **6**(6): p. e20594.
10. L. W. Seymour, et al., *Hepatic drug targeting: Phase I evaluation of polymer-bound doxorubicin.* Journal of Clinical Oncology, 2002. **20**(6): p. 1668-1676.
11. P. A. Vasey, et al., *Phase I clinical and pharmacokinetic study of PK1 [N-(2-hydroxypropyl)methacrylamide copolymer doxorubicin]: first member of a new class of chemotherapeutic*

agents-drug-polymer conjugates. Cancer Research Campaign Phase I/II Committee. Clin Cancer Res, 1999. **5**(1): p. 83-94.

12. Duncan, R. and R. Gaspar, *Nanomedicine(s) under the microscope.* Mol Pharm, 2011. **8**(6): p. 2101-41.
13. H. Pearson, *The good, the bad and the ugly.* Nature, 2007. **447**(7141): p. 138-40.
14. M. Baker, *Whole-animal imaging: The whole picture.* Nature, 2010. **463**(7283): p. 977-80.
15. P. Watson, A. T. Jones, and D. J. Stephens, *Intracellular trafficking pathways and drug delivery: fluorescence imaging of living and fixed cells.* Adv Drug Deliv Rev, 2005. **57**(1): p. 43-61.
16. S.C. Richardson, et al., *The use of fluorescence microscopy to define polymer localisation to the late endocytic compartments in cells that are targets for drug delivery.* J Control Release, 2008. **127**(1): p. 1-11.
17. S. C. Richardson, et al., *Intracellular fate of bioresponsive poly(amidoamine)s in vitro and in vivo.* J Control Release, 2010. **142**(1): p. 78-88.
18. F. P. Seib, A. T. Jones, and R. Duncan, *Comparison of the endocytic properties of linear and branched PEIs, and cationic PAMAM dendrimers in B16f10 melanoma cells.* Journal of Controlled Release, 2007. **117**(3): p. 291-300.
19. S. C. Richardson, et al., *Intracellular fate of bioresponsive poly(amidoamine)s in vitro and in vivo.* J Control Release, 2009. **142**(1): p. 78-88.
20. Eldar-Boock, A., et al., *Integrin-assisted drug delivery of nano-scaled polymer therapeutics bearing paclitaxel.* Biomaterials, 2011. **32**(15): p. 3862-74.
21. H. J. Lee, et al., *Targeting rat anti-mouse transferrin receptor monoclonal antibodies through blood-brain barrier in mouse.* J Pharmacol Exp Ther, 2000. **292**(3): p. 1048-52.
22. C. F. Xia, R. J. Boado, and W.M. Pardridge, *Antibody-mediated targeting of siRNA via the human insulin receptor using avidin-*

biotin technology. Mol Pharm, 2009. **6**(3): p. 747-51.

23. Y. Zhang, R. J. Boado, and W.M. Pardridge, *Marked enhancement in gene expression by targeting the human insulin receptor.* J Gene Med, 2003. **5**(2): p. 157-63.
24. M. J. Coloma, et al., *Transport across the primate blood-brain barrier of a genetically engineered chimeric monoclonal antibody to the human insulin receptor.* Pharm Res, 2000. **17**(3): p. 266-74.
25. W. M. Pardridge, R. J. Boado, and Y.S. Kang, *Vector-mediated delivery of a polyamide ("peptide") nucleic acid analogue through the blood-brain barrier in vivo.* Proc Natl Acad Sci U S A, 1995. **92**(12): p. 5592-6.
26. M. Barz, et al., *Synthesis and in vitro evaluation of defined HPMA folate conjugates: influence of aggregation on folate receptor (FR) mediated cellular uptake.* Biomacromolecules, 2010. **11**: p. 2274-2282.
27. P.A. Flanagan, et al., *Evaluation of protein-N-(2-hydroxypropyl)methacrylamide copolymer conjugates as targetable drug carriers. 1. Binding, pinocytic uptake and intracellular distribution of transferrin and anti-transferrin receptor antibody conjugates.* Biochim Biophys Acta, 1989. **993**(1): p. 83-91.
28. F. I. Staquicini, et al., *Systemic combinatorial peptide selection yields a non-canonical iron-mimicry mechanism for targeting tumors in a mouse model of human glioblastoma.* J Clin Invest, 2011. **121**(1): p. 161-73.
29. A. Regina, et al., *Antitumour activity of ANG1005, a conjugate between paclitaxel and the new brain delivery vector Angiopep-2.* Br J Pharmacol, 2008. **155**(2): p. 185-97.
30. C. Che, et al., *New Angiopep-modified doxorubicin (ANG1007) and etoposide (ANG1009) chemotherapeutics with increased brain penetration.* J Med Chem, 2010. **53**(7): p. 2814-24.
31. M. C. Phelan, *Basic techniques in mammalian cell tissue culture.* Curr Protoc Cell Biol, 2007. **Chapter 1**: p. Unit 1 1.

CHAPTER V.

THERAPEUTICAL APPLICATION APPROACH: FAMILIAL AMYLOIDOTIC POLYNEUROPATHY

CHAPTER V. THERAPEUTICAL APPLICATION APPROACH: POLYMER DRUG CONJUGATES FOR THE TREATMENT OF FAMILIAL AMYLOIDOTIC POLYNEUROPATHY

After achieving clinical arena, a second generation of polymer conjugates is now focused on improved polymer structures, to implement polymer-based combination therapies and to design conjugates towards novel molecular targets which will further progress this platform technology [1-3]. Second generation conjugates has undertaken the challenge of targeting diseases other than cancer. Therefore, innovation in polymer conjugates application is also driving new areas such as the regenerative medicine and other chronic and debilitating diseases. Although industrialisation framework is slowly evolving regarding these scenarios these novel chemical entities have already shown promising data [4-7].

As coined in the introduction (sections I.1 and I.4), amongst the different types of amyloidosis Alzheimer's (AD) and Parkinson's (PD) diseases are renowned examples. Familial amyloid polyneuropathies (FAP) also constitute a group of inherited amyloidosis [8]. One of the most common FAP is caused by a mutated protein called transthyretin (TTR), which forms amyloid deposits mainly in the peripheral nervous system. TTR has been proposed to trigger neurodegeneration through engagement with the RAGE receptor. Prof. M.J. Saraiva *et al.* have discovered a specific peptidic sequence named RAGE peptide able to suppress TTR aggregate-induced cytotoxicity in cell culture [9]. A reduced version of that peptide containing six amino acids (aa) (RAGEpep) was showed to maintain the activity and the affinity of the initial peptide (unpublished sequence). The same laboratory proved that doxycycline (doxy) acts as a TTR fibril disrupter *in vitro* and *in vivo* [10, 11]. Based on both statements, avoidance of TTR aggregates (TTRagg) cytotoxicity and breaking up TTR fibrils are promising targets for therapeutic proposes, and even more their combination.

In this chapter, the design of polymer drug conjugates for the

treatment of a rare amyloidotic diseased named Familial Amyloidotic Polyneuropathy (FAP) (section I.4) is described. Conjugation to polymers of two bioactive molecules for FAP treatment was proposed in order to confer the unique properties of PDCs to exhibit higher therapeutic effect than the corresponding therapeutics alone. For both bioactives, a rational for design was implemented selecting the appropriate polymeric vehicle and suitable linkers with/without bioresponsiveness under the extracellular scenario where their activity should be displayed.

As already described, polymer conjugation promotes changes in the biodistribution compared to the parent drug, avoiding undesired accumulation in non-affected organs and diminishing the administered dose and/or its frequency. In the case of doxy, poly-L-glutamic acid (PGA) has been chosen due its multivalence, biodegradability and biocompatibility. Thanks to the side-chain functionalities of the carrier, drug loading has been tailored through different linkers yielding conjugates ranging from 2 to 60ωt% total doxy content (FIGURE V. 1).

For RAGEpep, polyethylene glycol (PEG) derivatives have been selected to covalently link the peptide through two different types of linkages: disulphide and peptidic bond (FIGURE V. 2). PEG is a well-known polymeric carrier characterised by its semi-telechelic properties ideal for peptide and protein conjugation. PEG is FDA approved and has already demonstrated in the clinics its capacity of increasing compound stability and reduce its immunogenicity; thus increasing its therapeutic index [12].

Both conjugate families have been synthesised, characterised through several physico-chemical techniques, tested *in vitro*, evaluated in healthy animals for biodistribution studies and finally, preliminary activity experiments in a FAP *in vivo* model have been also carried out.

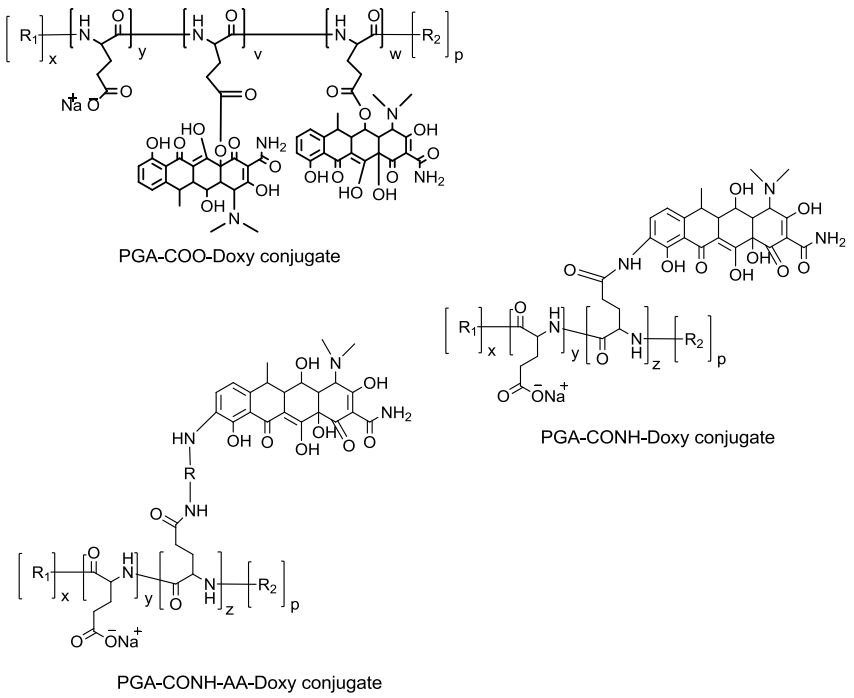

FIGURE V. 1 Synthesised family of PGA-X-Doxy conjugates.

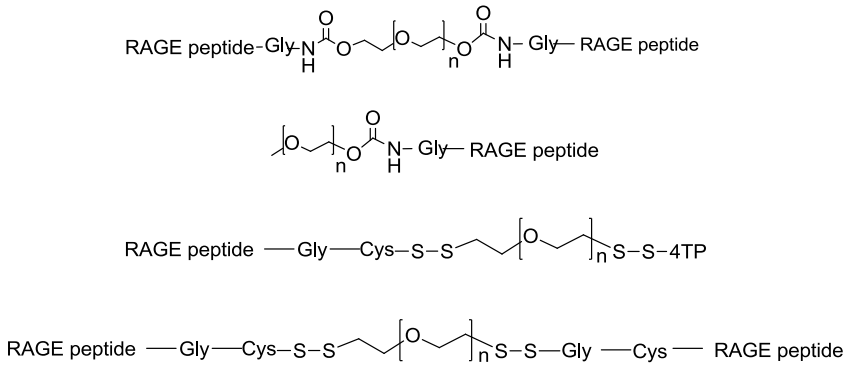

FIGURE V. 2 Synthesised family of PEG-RAGEpep conjugates.

As a final remark, the concept of polymer-based combination therapy [3] has been introduced in this project by combining both single conjugates (PGA-Doxy + PEG-RAGEpep). A first approach selecting the best polymer conjugate candidate from each bioactive molecule has been drive towards preliminary *in vitro* and *in vivo* test.

Further experiments are ongoing in order to design the best possible combinations.

The aim of this study relied on obtaining novel polymer drug conjugates for treating FAP, for the first time in the field, being able to use those systems as single agents or in combination therapy.

V. 1 RESULTS AND DISCUSSIONS

V. 1. 1 SYNTHESIS AND CHARACTERISATION OF THE POLYMER-DRUG CONJUGATES

V. 1. 1. 1 PGA-X-Doxy conjugates

In FAP, fibril deposits are localised extracellularly. Consequently, doxy must act extracellularly and intracellular release and excretion was not considered an issue as PGA is a biodegradable polymer. Areas of TTR deposition are characterised by the surrounding inflammation [13, 14]. This fact constitutes an advantage for polymer conjugate accumulation due to the passive targeting by the EPR effect (section I.2.2).

Taking this into consideration, two different linkages were exploited to investigate if drug release was a requirement for an effective response: a biodegradable (ester) and a non biodegradable bond (amide). For this goal, the drug was conjugated to PGA either (i) *directly* (by its own alcohol groups) or (ii) after its derivatisation by introducing an amine group in its benzyl group (FIGURE V. 3) or (iii) indirectly through peptidic sequences used as linkers (Gly-Gly and Leu-Gly,(FIGURE V. 3). Previous to conjugation of doxy-NH_2 derivative (**49**), its own activity was tested in vitro finding out comparable results to the parent drug (FIGURE V. 30). Chemistry strategy was based on post-polymerisation modification of PGA side chains by activation through NHS, DIC/HOBt or DMTMM (section III.1.1.1) [15]. Several examples of the different conjugates obtained together with their reaction conditions are shown in TABLE V. 1.

A family of conjugates with different total drug loading was achieved in order to determine the most efficient conjugates. Parameters such as, drug availability due to solution conformation or kinetics of drug release can be directly correlated with drug loading. Total drug content (ωt%) was determined by UV (273nm) [16] taken a doxy calibration curve as reference (FIGURE V. 4).

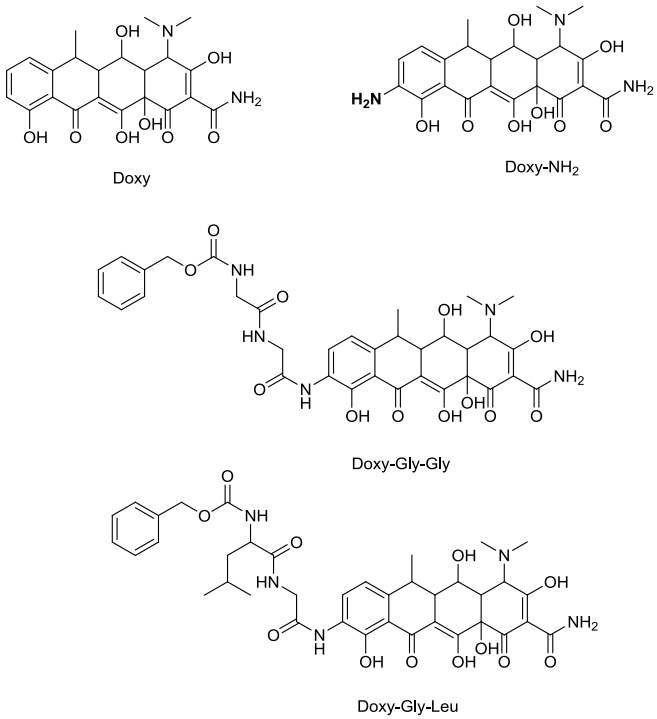

FIGURE V. 3 Doxycycline chemical structure and their derivatives.

Free drug content in the conjugates synthesised was determined by LCMS and HPLC. In LCMS analysis, doxy and doxy-NH_2 were detected (MW=444g/mol, [M+1]=445g/mol; and MW=459g/mol, [M+1]=460g/mol, respectively) at retention time around 10min (FIGURE V. 5). Direct evaluation of PBS aliquots of PGA-X-Doxy conjugates did not detect free doxy (detection limit <0.012mg/mL). Second attempt in which samples were lyophilised and extracted with MeOH confirmed the result (FIGURE V. 5(C)). Again, in all cases drug signals were undetectable concluding that free drug was under the accepted limit for clinical development. In parallel, free drug content was also measured by HPLC (see flow conditions in experimental methods) (FIGURE V. 6). The absence of any signal determined a free drug concentration under the limit of detection of the used technique (0.01mg/mL).

	Reaction conditions	Total drug content (ωt%)[A]	Free drug content (ωt% of total drug)[B]
PGA-COO-DOXY conj.	PGA-NHS/DMAP	26	<0.04
	PGA-NHS/DMAP	2	<0.50
	PGA-NHS/DMAP	26	<0.04
	PGA-NHS/DMAP	22	<0.05
	PGA-NHS/DMAP	33	<0.03
PGA-LG-NH-DOXY conj.	DMTMM·Cl/DMF	9	<0.11
	DMTMM·Cl/DMF	9	<0.11
PGA-GG-NH-DOXY conj.	DMTMM·Cl/DMF	6	<0.17
	DMTMM·Cl/DMF	14	<0.07
PGA-NH-DOXY conj.	DIC/HOBt	15	<0.07
	DIC/HOBt	22	<0.05
	DIC/HOBt	26	<0.04
	DIC/HOBt	33	<0.03
	DIC/HOBt	35	<0.03
	DMTMM·Cl/DMF	18	<0.06
	DMTMM·BF_4/H_2O	20	<0.05
	DMTMM·BF_4/H_2O	51	<0.02
	PGA-NHS/DMAP	14	<0.07
	PGA-NHS/DMAP	17	<0.06
	PGA-NHS/DMAP	30	<0.03
	PGA-NHS/DMAP	43	<0.02
	PGA-NHS/DMAP	59	<0.02

A=data obtained by UV, B=data obtained by HPLC or LCMS

TABLE V. 1 Examples of the synthesised PGA-X-Doxy conjugates. Reaction conditions used, total drug loading and free drug content.

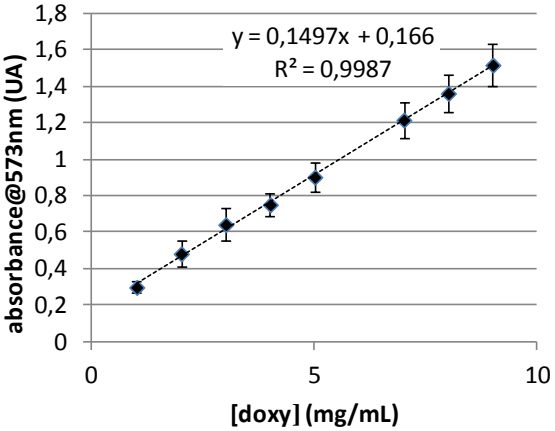

FIGURE V. 4 Calibration curve of doxycycline in water. Absorbance measured at 273nm.

(A)

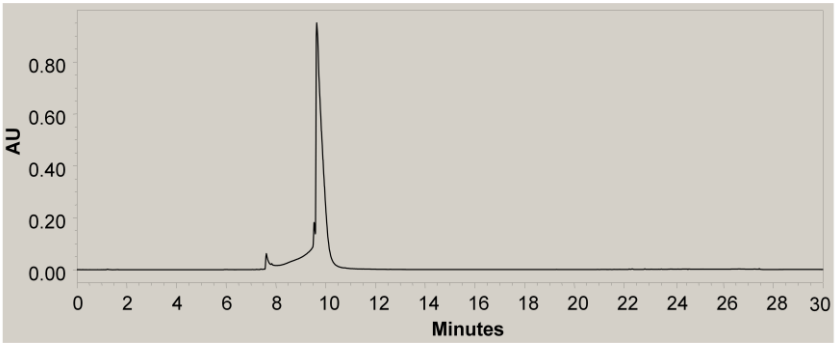

(B)

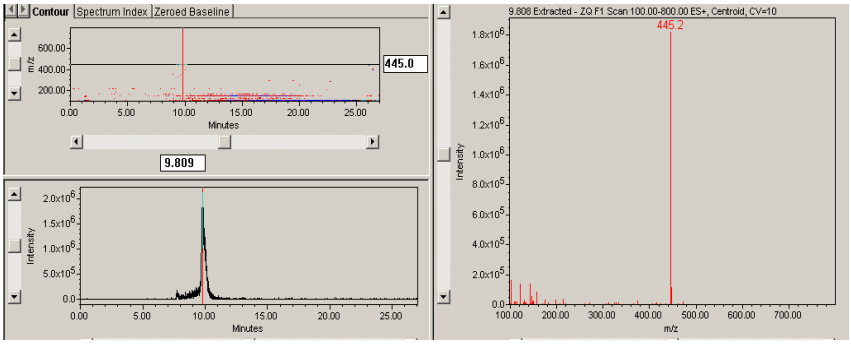

(C)

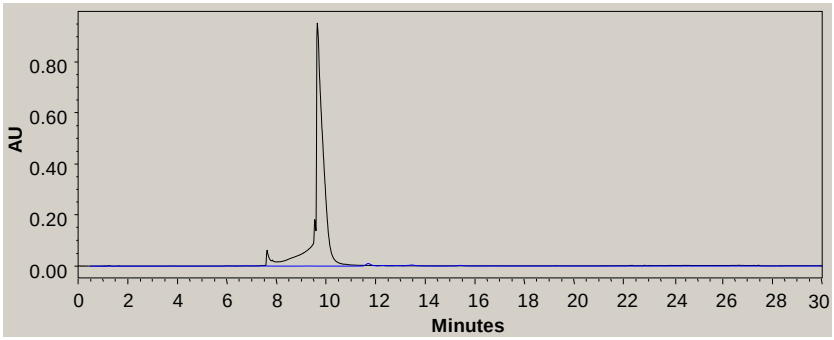

FIGURE V. 5 Doxycycline (D1) analysis by LCMS. (A) UPLC spectra (B) MS spectra (C) Free drug test (black line=doxy, blue line=PGA-CONH-doxy 15ωt%).

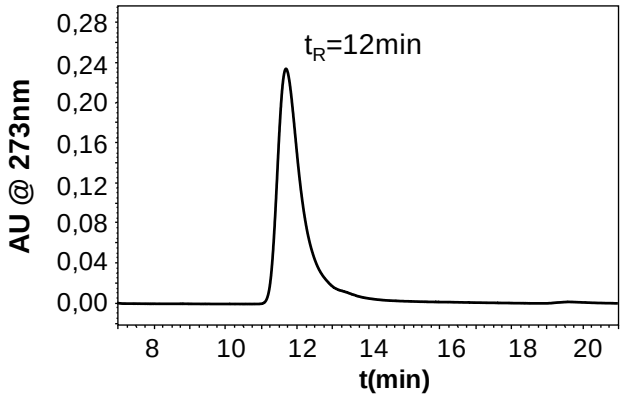

FIGURE V. 6 Example of a PGA-Doxy GPC trace (absorbance at 273nm, mobile phase: PBS pH7.4, t_R=12min)

V. 1. 1. 2 Synthesis of RAGEpep derivates including PEG-RAGEpep conjugates

Peptide therapeutics themselves display well known challenges for *in vivo* use, e.g. low stability, poor PK and potential immunogenicity [17]. PEGylation emerged as a robust alternative for p/p delivery (section I.2.4.1) achieving the clinical arena and with many conjugates under development. This technique has evolved over time not only varying MW of the polymer carrier as well as its architecture but also covering all type of linkages such as disulphide,

hydrazone, triazole, etc [18-20]. Currently, PEG also plays a relevant role in combination with other polymeric carriers in many different structures contributing with their inherent properties.

Our bioactive molecule in this case was a 6aa peptide sequence named RAGE peptide (unpublished sequence), a truncated sequence derived from and with similar properties as the originally reported RAGE peptide[9]. Due to its semitelechelic properties, in a first stage PEG was selected as carrier for its delivery. Peptide function is base on the recognition of the TTRagg in order to bind them. This union avoids interaction between TTRagg and the RAGE receptor. When TTRagg-RAGE receptor binding is inhibited, the apoptosis cascade is stopped and, therefore it could be said that, RAGEpep is able to diminish cell toxicity triggered by the TTR aggregates. RAGE peptide and its derivatives (RAGE peptide-Gly, PEP1 and RAGE peptide-Gly-Cys, PEP2, FIGURE V. 7) were obtained by Fmoc-based solid phase peptide synthesis (SPPS) (section V.3.1.3).

FIGURE V. 8 shows yield, purity and MW of the final products. Figure X shows an example of the obtained results.

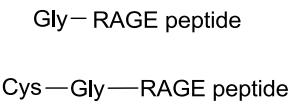

FIGURE V. 7 RAGE peptide derivatives.

Within the same scope than that explained above for PGA-doxy conjugates, RAGEpep was linked through biodegradable and non-biodegradable linkers in order to study if its release was required for activity. In addition, mono- and bifunctional PEG was used as carrier in order to better understand the importance of solution conformation and drug loading on binding affinity, an consequently, in the final therapeutic output.

(A)

Peptide	Nomemclature	Purity (%)[A]	MW (g/mol)[B]
RAGE peptide		94.5	855
RAGE peptide-Gly	PEP1	97.8	912
RAGE peptide-Gly-Cys	PEP2	96.3	1015

A=calculated by HPLC, B=calculated by MS

(B)

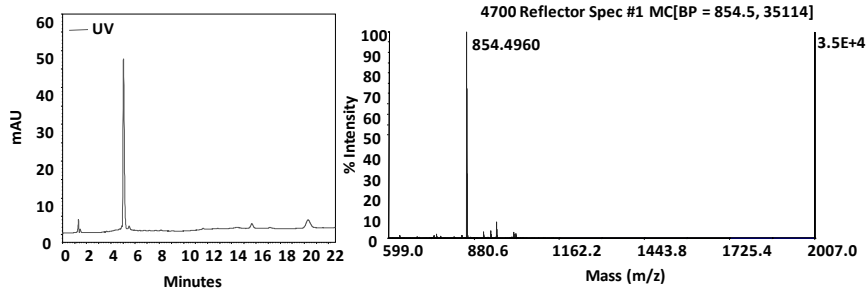

FIGURE V. 8 (A) Purity and molecular weight of the RAGE peptide derivatives synthesised by Fmoc-SPPS (B) HPLC trace and MS-MALDI TOF analysis of the RAGE peptide.

First attempt of conjugation was done with a di-carboxyl activated PEG (NHS-PEG-NHS) using the RAGE peptide sequence, although low conjugation yields were obtained. Possibly, this was due to steric hindrance or to the reduced nucleophilicity of the amino group from the N-terminal fragment. Therefore, a spacer was placed. This led to increased conjugation efficiency but also conferred greater mobility to the peptide in order to enhance TTRagg recognition. The simplest amino acid was selected: glycine (Gly). Mono- and bi-functional conjugates (C1P1 and C2P1, respectively) were then synthesised (schemes in FIGURE V. 9) and purified.

In parallel, conjugates where peptide could be released in presence of a reductive environment (such inflammation areas or in cytosol) were also synthesised. For that, the spacer glycine-cysteine (Gly-Cys) was coupled to the RAGEpep using the same methodology. In this case, the PEG derivative used was OPSS-PEG-OPSS (FIGURE V. 10).

(A)

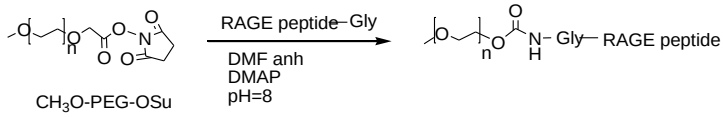

(B)

FIGURE V. 9 Synthesis of the RAGE peptide conjugates (A) C1P1 (**61**) and (B) C2P1 (**60**).

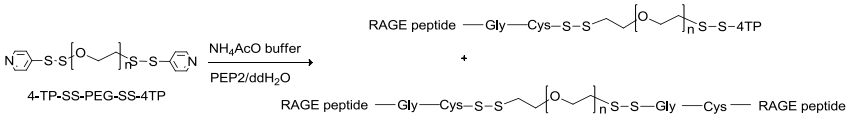

FIGURE V. 10 Synthesis of the RAGE peptide conjugates C1P2 (**63**) and C2P2 (**64**).

Successful separation of unconjugated reagents was performed by means of FPLC (see appendix III for details) using a cationic exchange column (Macrocap SP) (FIGURE V. 11, FIGURE V. 12). Using a fraction collector, tubes containing the product were joined, desalted and lyophilised.

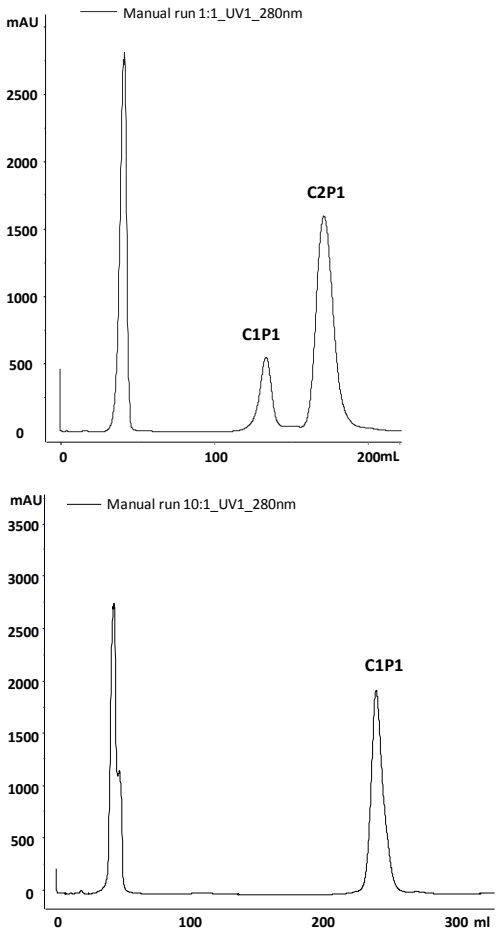

FIGURE V. 11 FPLC chromatogram of C2P1 and C1P1 purification. (absorbance=280nm)

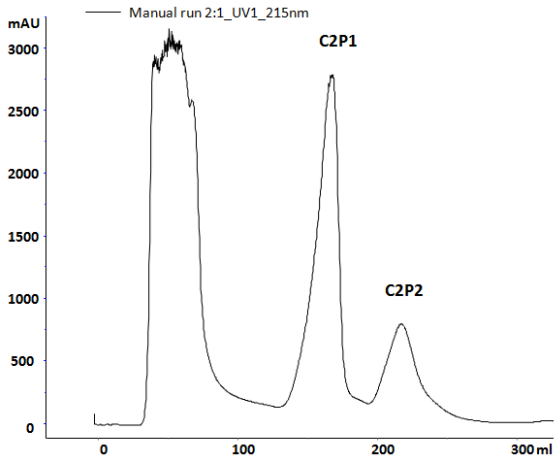

FIGURE V. 12 FPLC chromatogram of C1P2 and C2P2 purification. (absorbance=215nm)

V. 1. 1. 3 Synthesis of fluorescently labelled conjugates

As explained in Chapter IV, the conjugation of NIR dye Cy5.5 was selected as strategy to perform *in vivo* biodistribution analysis of the novel PDCs. For this aim, an amino derivative of this fluorophore (FIGURE V. 13) was used in order to react with the carboxylic acid pendant groups of the PGA or the activated carboxyl terminal group of the bi-functionalised PEG.

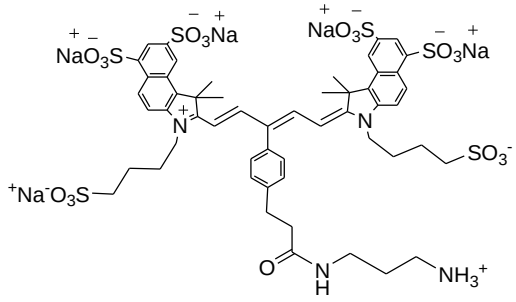

FIGURE V. 13 Cyane5.5 derivative with an amino group (6S-IDCC).

V. 1. 1. 3. 1 PGA-CONH-Doxy conjugate fluorescence labelling

PGA-Doxy conjugate was obtained as sodium salt, then this conjugate was only soluble in aqueous solutions. Consequently, the activation of carboxyl groups for conjugation of the fluorophore was

carried out in buffer media. Sulfo-NHS esters are identical to NHS except for the sulfonate (-SO_3) group on the ring that confers water solubility allowing the reaction in aqueous media. The mechanism of the reaction is shown in the figure below (FIGURE V. 14).

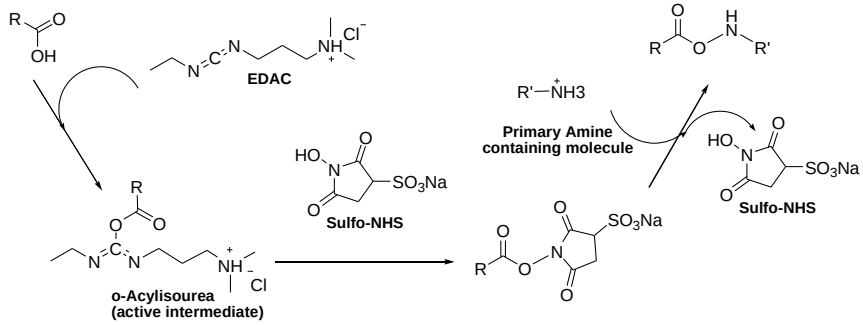

FIGURE V. 14 EDC-mediated reaction through the formation of a sulfo-NHS ester intermediate. Using the water-soluble carbodiimide EDC, a carboxylate-containing molecule can be transformed into an active ester by reaction in sulfo—NHS esters. This hydrophilic active groups couple rapidly with amines [21].

Conditions were obtained from reference [22]. Labelling was only performed on that conjugate showing the best *in vitro* activity and therefore chosen for *in vivo* activity studies (**51**, 17ωt%). The scheme of the reaction is depicted in FIGURE V. 15. Labelled conjugate was purified with a PD-10 column packed with Sephadex™ G-25 and the total fluorescence of each aliquot was quantified with a fluorescence spectrometer (λ_{em}=595, $\lambda_{exc:}$=680). Labelling efficiency yielded a 1.07%mol Cy5.5, i.e. 0.007mg Cy5.5 in 9mg of final conjugate.

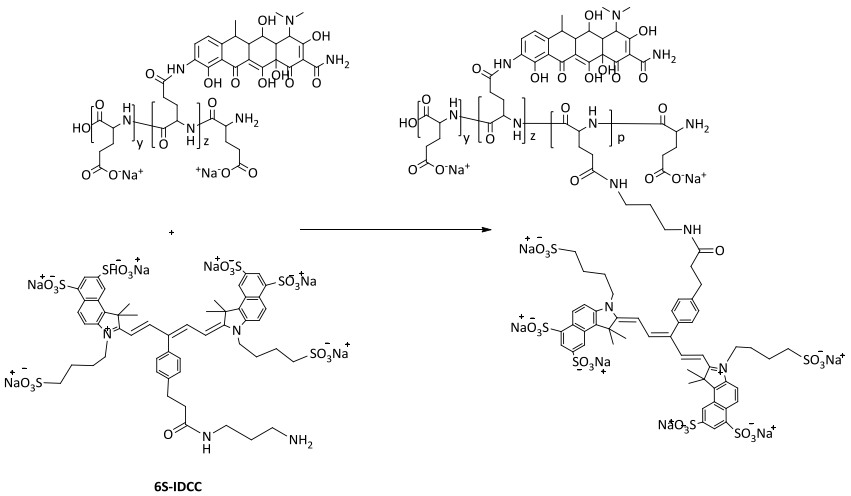

FIGURE V. 15 PGA-CONH-Doxy labelled with the fluorescence probe Cy5.5.

V. 1. 1. 3. 2 PEG-PEP1 conjugate fluorescence labelling

The PEG carrier used for RAGEpep conjugation was mono- or bi-functionalised. Consequently, one of the two extremes had to be linked to the fluorophore and the other to the bioactive molecule (scheme in FIGURE V. 16). Then, C1P1 was selected to carry out the biodistribution assay. Labelled conjugate (**67**) was purified by SEC (a PD-10 column packed with Sephadex^{TM} G-25) and the total fluorescence of each aliquot was quantified with a fluorescence spectrometer (λ_{em}: 595, $\lambda_{exc:}$ 680). Labelling efficiency 0.11%mol Cy5.5, i.e. 0.005mg Cy5.5 in 16mg of final conjugate.

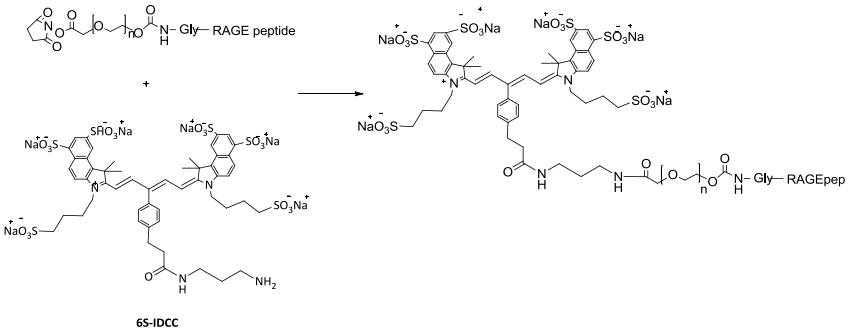

FIGURE V. 16 C1P1 fluorescence labelling synthesis.

V. 1. 1. 4 Synthesis of radioactive labelled PGA-Doxy conjugate

As a comparative methodology for biodistribution studies, PGA-CONH-Doxy was labelled with the chelating-agent DOTA for ^{68} Ga complexation and subsequent PET analysis (scheme in FIGURE V. 17).

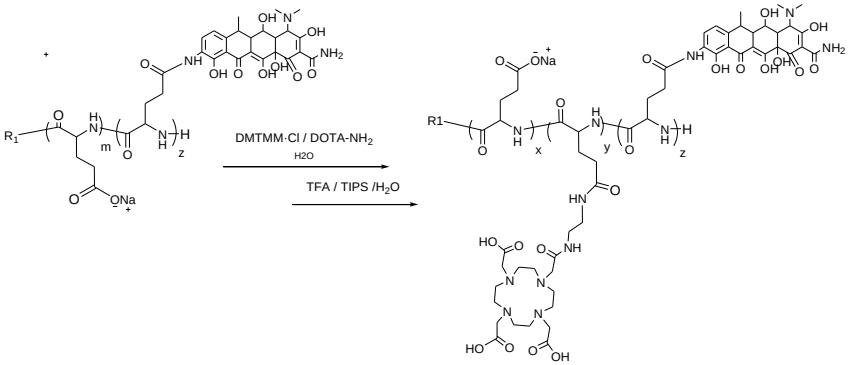

FIGURE V. 17 DOTA labelling of the conjugate PGA-Doxy.

Polymer drug conjugate was first linked to tBu-DOTA achieving an 8%mol functionalisation as calculated by ^{1}H-NMR (D_2O) (FIGURE V. 18). Previous studies demonstrated doxy stability in acidic media thus DOTA deprotection under the optimised conditions (section III.1.1.3 and III.3.2.3) was performed with satisfactory results, obtaining the PGA-Doxy-DOTA (**65**). Then, ^{68}Ga complexation was carried out by the Unit of Biomedical Applications of Radioisotopes and Pharmacokinetics at the CIEMAT (Madrid) in order to perform *in vivo* biodistribution experiments. Radiochemical yield was 86.3%±3.4. Radionuclide purity was calculated as the ratio activities of ^{68}Ge versus ^{68}Ga in the eluate, corrected for decay expressed in %. The RNP was $<3.4\cdot10^{-4}\%\pm0.4\cdot10^{-4}$.

(A)

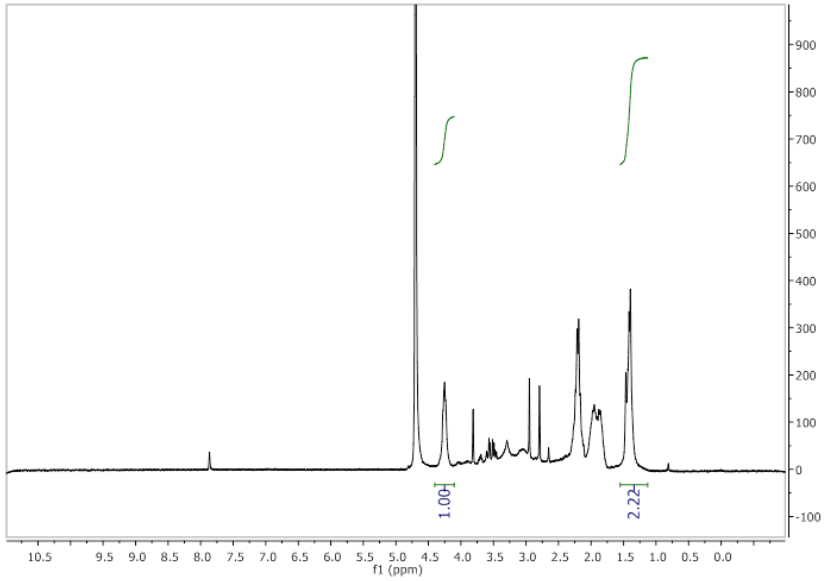

(B)

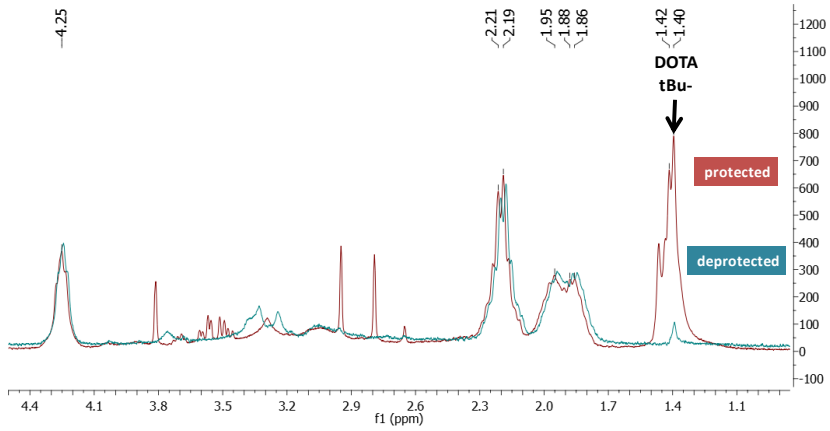

FIGURE V. 18 (A) ^{1}H-NMR spectrum of PGA-DOTAtBu-Doxy for %mol DOTA calculation. (B) ^{1}H-NMR comparison before and after deprotection.

V. 1. 2 PHYSICO-CHEMICAL CHARACTERISATION OF THE POLYMER-DRUG CONJUGATES

It has become evident that careful physico–chemical characterisation of polymer conjugates is essential to understand biological behaviour *in vitro* and *in vivo*, and to aid the prediction of optimum structure for development of a clinical candidate e.g. comparison between HPMA copolymer-Dox (PK1) and HPMA copolymer-Dox-galactosamine (PK2) both in phase I/II clinical trials [7, 17, 23, 24]. Innovative and validated methodologies use is increasing due to their usefulness to ensure optimisation of properties relevant to finally achieve the clinical setting [2, 7, 23, 25]. As it has been emphasised in the introduction (section I.2.5.2), it is important to report key conjugate properties, such as, the conformation adopted in solution or the stability of the bonds between drug and carrier in the different scenarios they will undergo once injected into the body. These characteristics include, among others, MW and polydispersity, size, hydrophilicity and hydrophobicity, solution conformation as well as stability or degradation profiles within biological settings.

In this thesis, all these parameters had been set up though the techniques explained below. A general example of the properties analysed and usual techniques for polymer-drug conjugates characterisation is summarised in TABLE V. 2 and further detailed in appendix III

PDC property	Technique
Covalent drug conjugation	NMR, FT-IR, MS
Total and free drug content	HPLC, UV, NMR
MW, PDI	GPC, MS, Light Scattering
Size, conformation in solution	SANS, SAXS, DLS, TEM, SEM, PGSE-NMR
Formation of supramolecular assemblies	SAXS, NMR, DLS

TABLE V. 2 Routine techniques for polymer-drug conjugates physicochemical characterisation. From ref [26].

V. 1. 2. 1 Conformation in solution, plasma stability and pH degradation studies of PGA-X-Doxy conjugates

Conjugate solution conformation. Determination of the Hydrodynamic Radius (R_h)

Conformation in solution is a useful tool to explain conjugate activity either *in vitro* or *in vivo*. Drug availability in the adopted conformation could be directly related with the observed activity.

Size distribution and hydrodynamic diameter of our polydispersed population of PGA-X-Doxy conjugates with different drug loading was measured by DLS (appendix III). The conjugates were dissolved in PBS at 10mg/mL. Similar hydrodynamic diameter was demonstrated for PGA-CONH-Doxy (**51**) with different drug loadings,(i. e. 15 and 43ωt%, with 6.2±1.3nm and 7.5±0.7nm) (FIGURE V. 19).

(A) PGA-CONH-Doxy 15ωt%

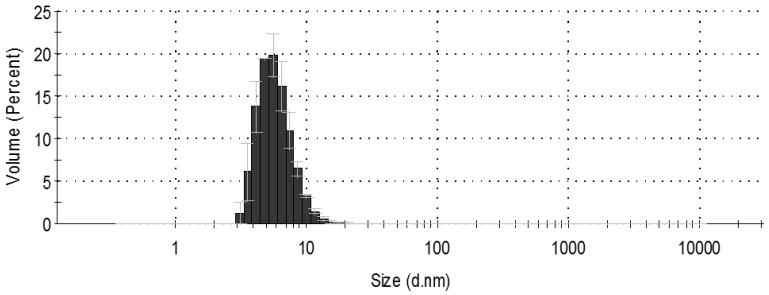

(B) PGA-CONH-Doxy 43ωt%

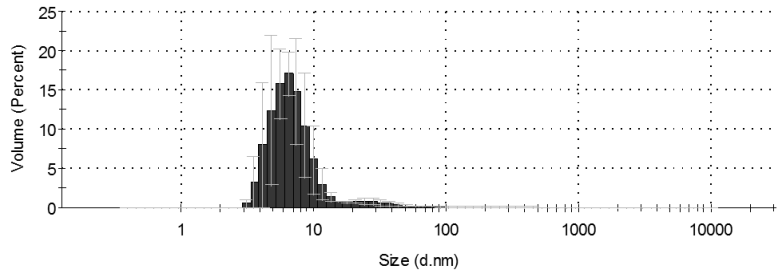

FIGURE V. 19 DLS profiles for (1) PGA-CONH-Doxy 15ωt% and (B) PGA-CONH-Doxy 43ωt% in PBS.

In order to further elucidate if drug loading differences triggered different size and/or shape of the doxy conjugates, SANS studies (appendix III) were performed with the same conjugates. These studies were done at the Institute Laue-Langevin in Grenoble (France) with our collaborators from the School of Chemistry in the Cardiff University (Cardiff, UK). PGA-CONH-Doxy 15ωt% and PGA-CONH-Doxy 43ωt% were dissolved at 10mg/mL in deuterated PBS at 37°C to mimic biological conditions. All assays were performed in 2mm quartz cells performing measurements of 1h per sample.

The scattering data for the PGA conjugates was fitted to form factors for polydiperse Gaussian coils, spherical and rods and the values obtained are presented in TABLE V. 3 (graphics are depicted in FIGURE V. 20). The scattering data was corrected for the scattering and transmission of the solvent and quartz cell and normalised by placing on an absolute intensity scale with a well characterised standard.

		DLS	SANS
	% ωt	**Volume (d, nm)**	**r / L**
PGA-CONH-Doxy	15	6.2±1.3	40 / 400
			32 / 8.5
PGA-CONH-Doxy	43	7.5±0.7	36 / 95
			23 / 13.5

TABLE V. 3 Conformation in solution data of PGA-CONH-Doxy conjugates analysed by DLS and SANS. r=radius, L=length.

After analysing the data obtained from SANS, the structures present do not fit to simple models such as coils or spheres, but in any case, it could be concluded that even if the conjugate with greater loading (43ωt%) seemed to have a larger hydrodynamic radius, there were not significant changes in the solution conformation when both conjugates were compared.

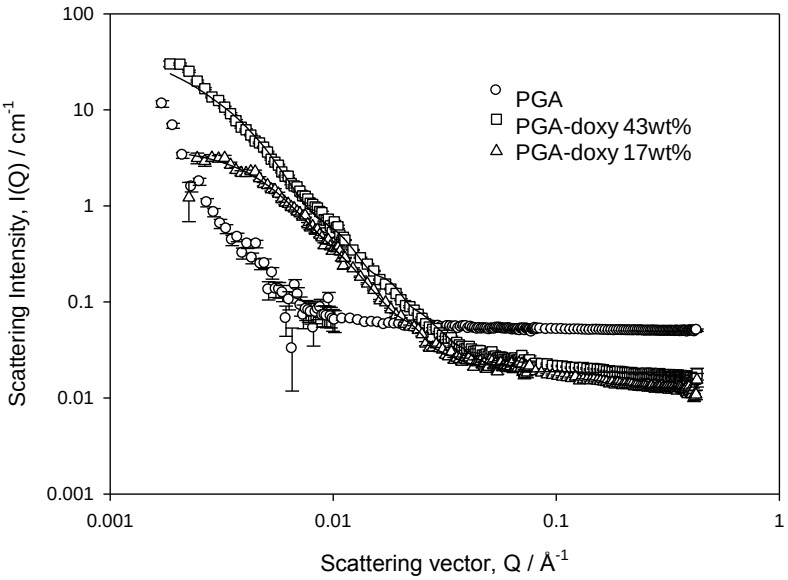

FIGURE V. 20 SANS diagram of conjugates solutions in deuterated PBS (10mg/mL). PGA-CONH-Doxy 43ωt% (squares), PGA-CONH-Doxy 17ωt% (triangles), PGA (circles).

DLS and SANS analysis were in good agreement showing that conformation in solution is not major difference between the PGA-Doxy conjugates synthesised. Importantly, SANS analysis demonstrated that doxy conjugation significantly changes the original PGA conformation (circles in FIGURE V. 20).

.

Drug release studies under hydrolytical conditions

Polymer conjugates are designed aiming to achieve a stable system in the blood stream and after reaching the desired target trigger drug release under a specific physiological scenario. For example, inflammation reduces local pH to 5.5 or even lower, therefore sensitive pH-labile linkers (acetal, hydrazone, ester, etc) will be susceptible to be hydrolysed. Besides, controlled drug release could be achieved for a prolonged period of time.

Concerning this thesis, the aim of the drug release studies performed was to observe the stability of the synthesised PGA-Doxy conjugates under physiological conditions encountered in cell and *in vivo* experiments.

First, analysis of conjugates' stability in plasma revealed non-significant doxy release after 24h (FIGURE V. 21).

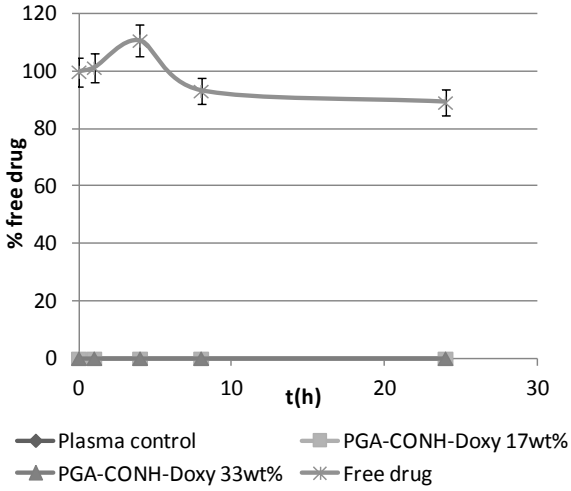

FIGURE V. 21 Plasma stability of PGA-Doxy conjugates. HPLC detection of drug release.

Mimicking the *in vitro* conditions as well as the acidic pH expected in the drug site of action, PGA-Doxy conjugates families were incubated up to 17 days at 37°C in PBS at different pHs 5.5 and 7.4. Sample analysis was done by directly analysis of the conjugates monitoring the absorbance of the whole conjugate after its injection through a GPC column (appendix III). Results here were difficult to interpret and further analyses are ongoing in order to better understand the behaviour of the conjugates under hydrolytical conditions.

In parallel, drug release in *in vitro* conditions (PBS, pH=7.4, 37°C, 17days) was also evaluated. By means of LCMS (appendix III), it was proved that in the case of the amide conjugates no release was

observed after 22days of incubation (detection limit under 0.012mg/mL). However, 1.9% of total ester conjugate drug was released (FIGURE V. 22(B1-B3)). Same result was observed for the HPLC analysis (FIGURE V. 22(A)), where the area under the curve (AUC) of the total conjugate decreased while remained almost constant for the rest of the PGA-Doxy families.

(A)

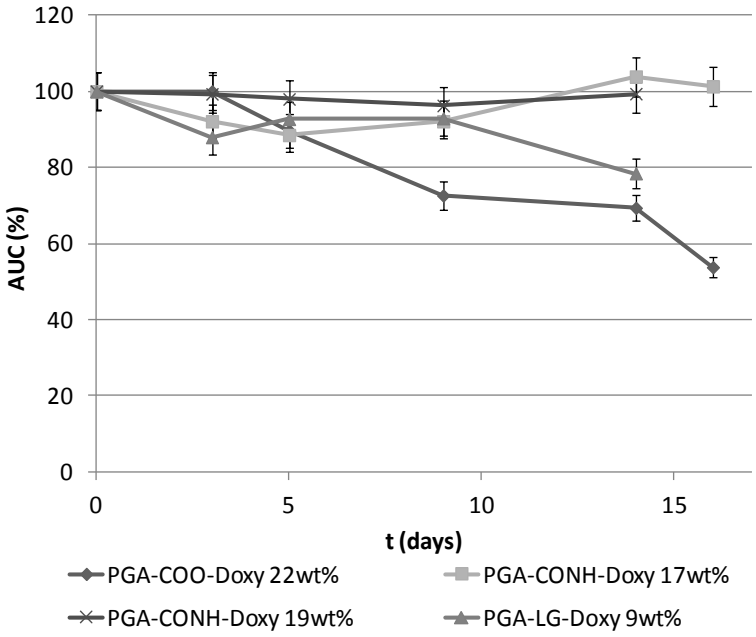

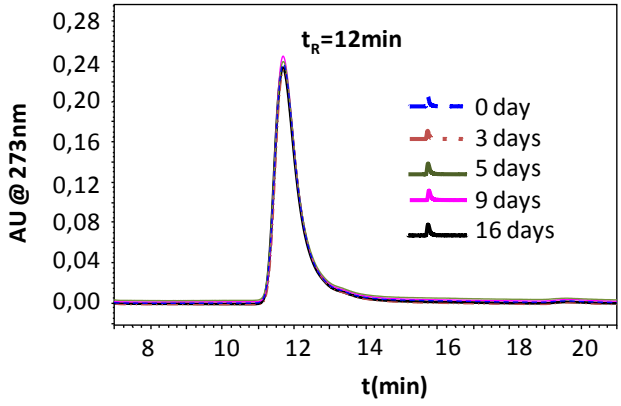

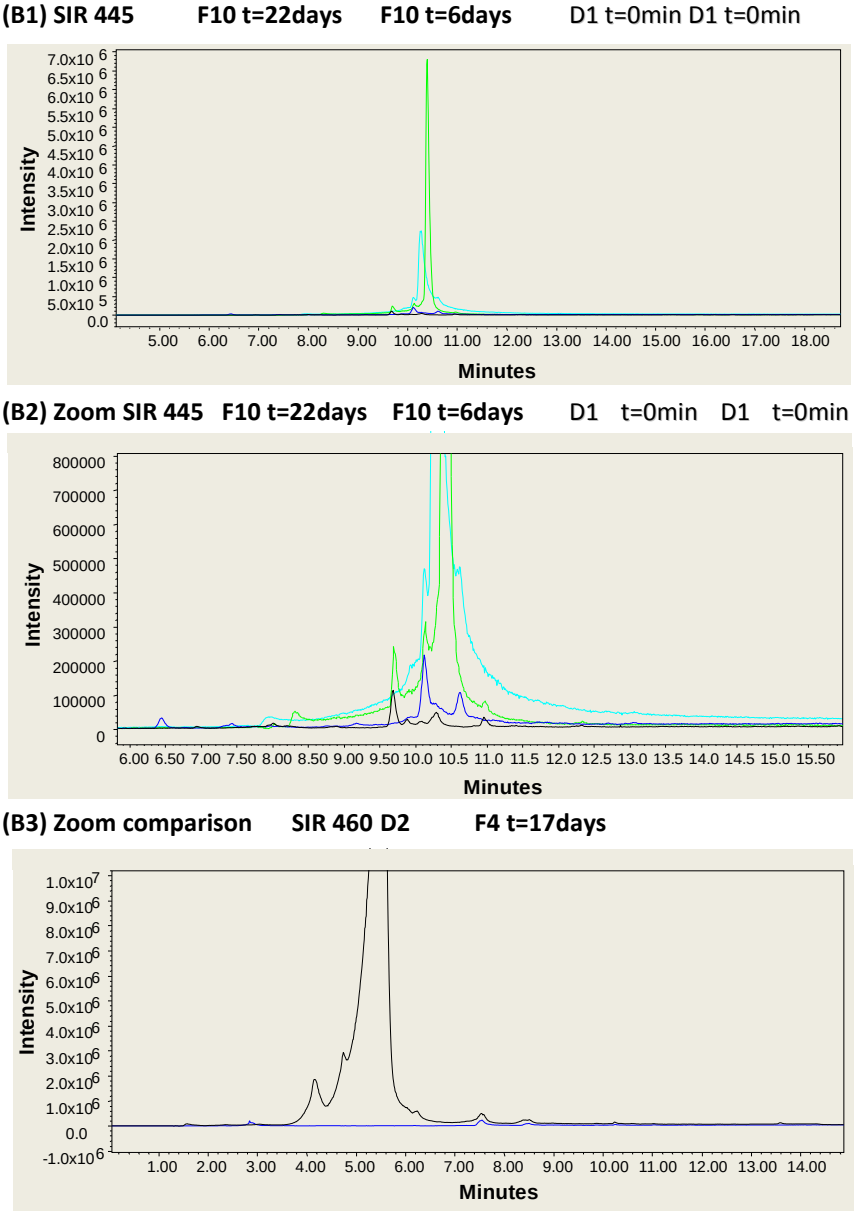

FIGURE V. 22 Stability of PGA-X-Doxy conjugates in *in vitro* conditions. (A) HPLC representation of the percentage of area under the curve (AUC) vs the incubation time (days) in PBS at 37°C; and HPLC chromatograms of PGA-CONH-Doxy 15ωt% along the time course analysis, (B) LCMS analysis of the aliquots to detect the released drug: (B1) Data from PGA-COO-Doxy 22ωt% (F10) compared with doxy (D1) ; (B2) Zoom of (B1); (B3) Data from PGA-CONH-Doxy 15ωt% (F4) compared with doxy-NH_2 (D2).

V. 1. 2. 2 Characterisation of RAGE peptide conjugates: stability in different conditions, conformation in solution and TTR affinity studies

Molecular weight determination

Techniques like NMR and MS spectroscopy were used to achieve identity of the PEG conjugate synthesised (appendix III) (FIGURE V. 23(A). FIGURE V. 23(B) shows the MS MALDI-TOF results of the PEGylated peptides. The polydispersity of PEG is reflected into the polydispersity of the conjugate. Integration of peptide ^{1}H-NMR signals (aromatic H) clearly identified the number of peptide molecules per PEG chain (FIGURE V. 24).

(A)

	Type of bond	Ratio PEG:pep	MW^{A} (Da)	Đ
C1P1	non bio-degradable	1:1	3933	1.02
C2P1	non bio-degradable	1:2	4971	1.02
C1P2	degradable	1:1	4899	1.05
C2P2	degradable	1:2	5873	1.05

(B)

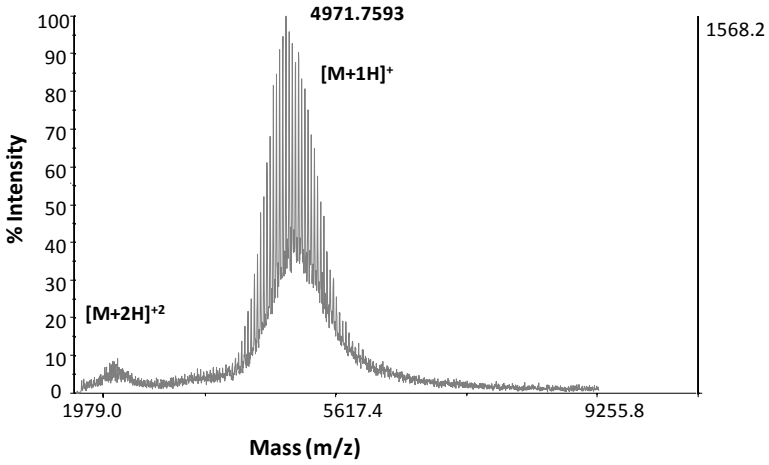

FIGURE V. 23 Characterisation data of the CXPX conjugates. (A) Table with measurement of MW by MS MALDI-TOF and PEG:PEP ratio by NMR-^{1}H (D_2O), (B) example of the characterisation of C2P1 with a MS spectra.

(A) C1P1

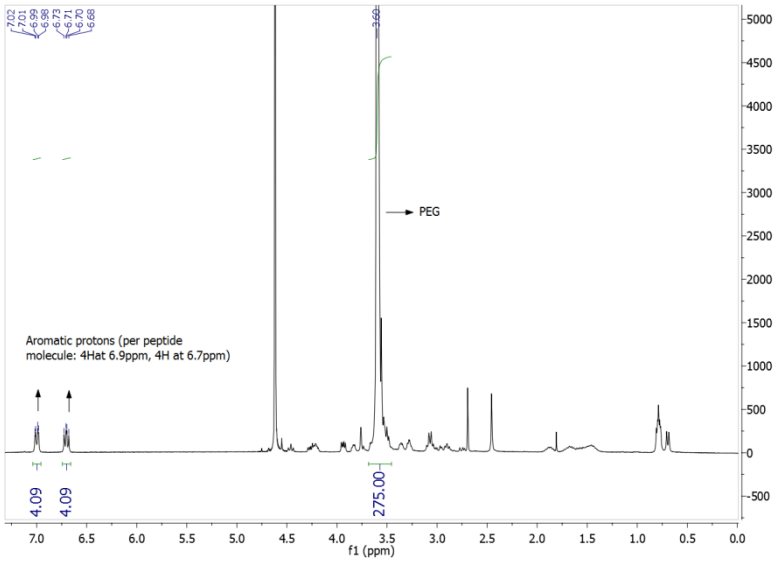
7.02
7.01
6.99
6.98
6.73
6.71
6.70
6.68
3.60
PEG
Aromatic protons (per peptide molecule: 4Hat 6.9ppm, 4H at 6.7ppm)
4.09
4.09
275.00
f1 (ppm)

(B) C2P1

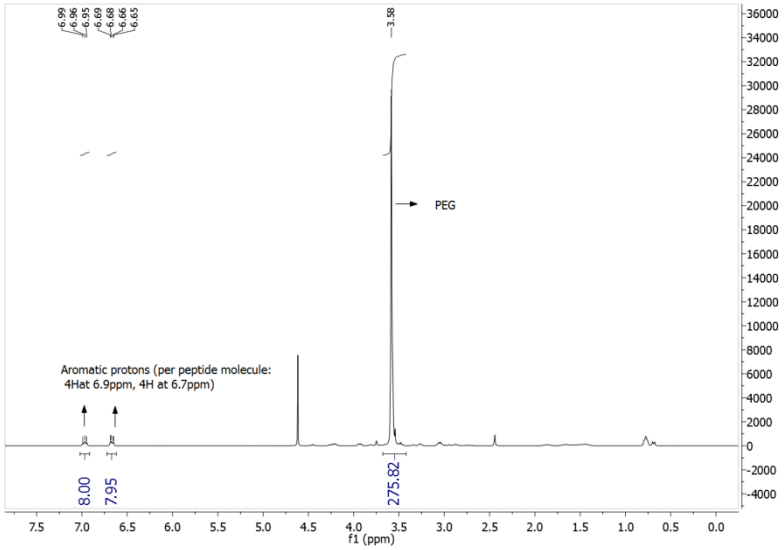
6.99
6.96
6.95
6.69
6.68
6.66
6.65
3.58
PEG
Aromatic protons (per peptide molecule: 4Hat 6.9ppm, 4H at 6.7ppm)
8.00
7.95
275.82
f1 (ppm)

(C) C1P2

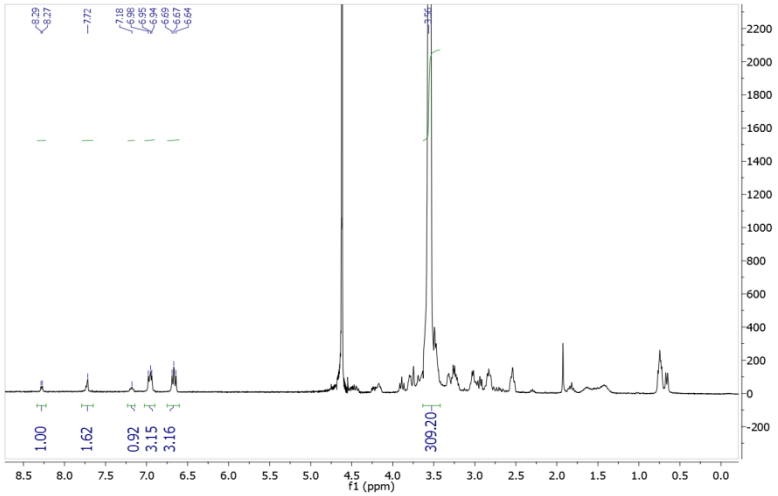

(D) C2P2

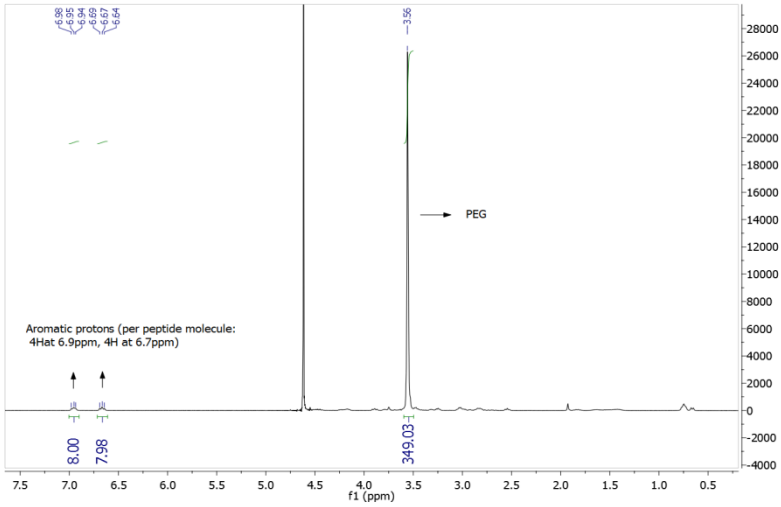

FIGURE V. 24 ^{1}H –NMR spectrums of the CXPX conjugates in D_2O: (A) C1P1: mPEG-PEP1, (B) PEP1-PEG-PEP1, (C) PEG-PEP2, (D) PEP2-PEG-PEP2.

Stability studies

Next step on characterisation was to evaluate their stability under different physiological conditions: in cell media for *in vitro* tests and in plasma for *in vivo* studies. The conjugates were dissolved in cell media or plasma and incubated at 37°C. A time course experiment was

performed by extracting aliquots which were analysed by HPLC (FIGURE V. 25) and MS spectroscopy (TABLE V. 4), respectively.

(A)

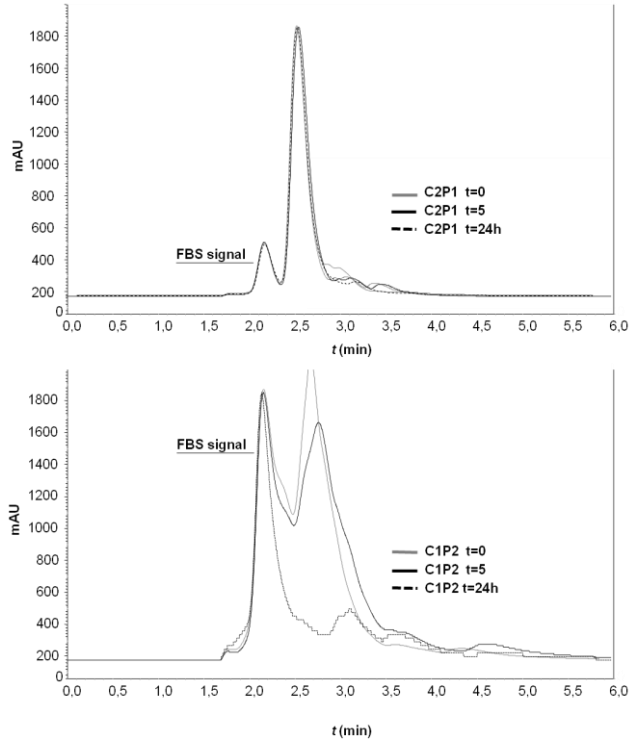

(B)

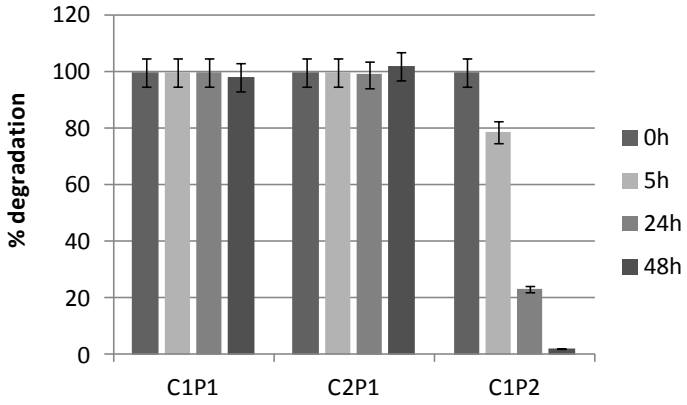

FIGURE V. 25 Stability studies of the conjugates synthesised in presence of cell media. (A) Chromatograms of conjugates C2P1 and C1P2, (B) representation of the percentage of degradation (area under the curve (AUC)

vs. time for conjugates C1P1, C2P2 and C1P2.

t (h)	MW C1P1 (g/mol)	%MW loss	MW C2P1 (g/mol)	%MW loss
0	4019,8	100.0	5024.5	100.0
5	3701	92.1	4907.0	97.7
24	3618,3	90.0	4409.7	87.8

TABLE V. 4 Plasma stability studies of (a) C2P1 and (b) C1P1, MW determined by MS-MALDI TOF analysis.

As FIGURE V. 25(A) shows, conjugates with peptidic linkage were more stable than conjugates with disulphide bond in cell media after 48h of incubation. Free peptide was not dissolving in cell media; therefore, PEG confers a major advantage in this scenario allowing the RAGEpep to become a possible FAP treatment. In plasma, same behaviour was observed due to the lack of peptide solubility while all conjugates did solubilise. After 48h, conjugates were not still fully degraded and at least a molecule of peptide remained attached as shown by MW calculation. Summarising, PEG as carrier greatly enhanced RAGE peptide solubility and significantly diminished fast peptide degradation.

Conjugate Solution Conformation

It has been already demonstrated that conjugate solution conformation is critical on its therapeutic output [27-33]. Although in the present study polymer must protect peptide from protease degradation once in the body, peptide inhibitory activity also requires certain grade of exposition to be able to be recognised by and bind to the RAGE receptor. PEG conjugates were analysed by DLS in PBS media at neutral pH finding differences depending on the number of peptide molecules attached and the type of bond used.

From FIGURE V. 26(A) it can be concluded that only C2P2 exhibits differences in solution conformation, displaying the highest hydrodynamic ratio (nm) of the conjugate family as well as the most irreproducible behaviour compared to C1P1, C2P1 and C1P2.

(A)

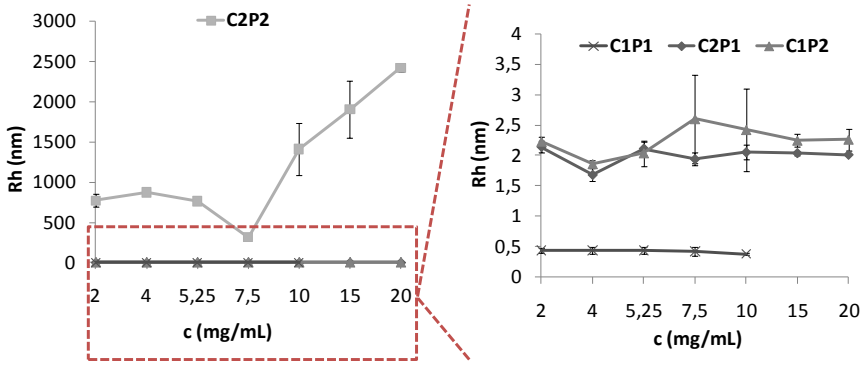

(B)

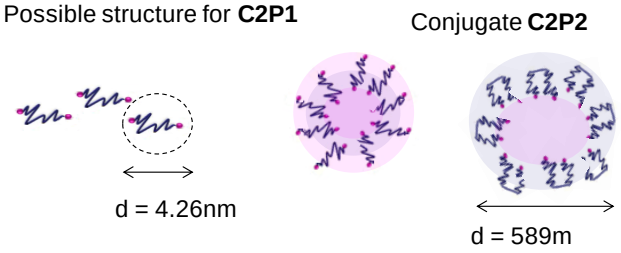

FIGURE V. 26 (A) Hydrodynamic radius (nm) measurement by DLS of the CXPX conjugates in PBS 0.020M media (B) Conformation in solution proposed based on the results obtained.

To explore if this behaviour was concentration dependent, a second study was performed. DLS is able to determine the critical micelle concentration (CMC) [34], finding out if aggregation relied on micelle formation. Below the CMC the intensity of scattered light detected from each concentration is similar to that obtained from the media. However, once the CMC is reached this intensity increases due to the presence of micelles and the intercepts obtained in the correlation functions are much higher (see an example in FIGURE V. 27).

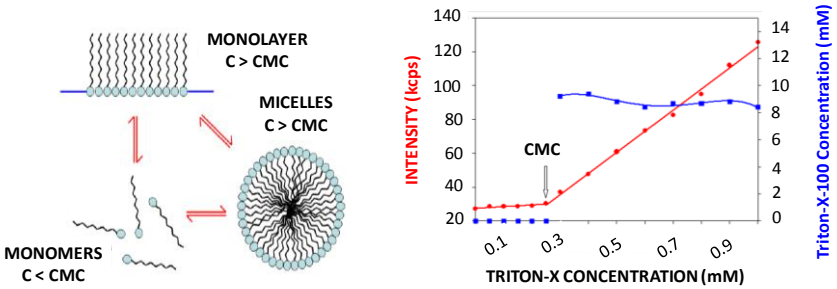

FIGURE V. 27 A compound can exist as different phases depending upon the concentration of the sample. At low concentrations macromolecules may be unassociated monomers. As concentration increases, the hydrophilic/hydrophobic forces may cause self-aggregation resulting in the formation of monolayers or micelles [34].

Comparing this with our data (FIGURE V. 28), size (blue line) remains constant in C1P1, C1P2, C1P2 (R_h=0.6-3nm) while concentration varied. PEG of 5000g/mol has been reported to be around 2nm [35], which is in god agreement with our DLS data. On the contrary, C2P2 presented variations together with fluctuating intensity data. A possible CMC could be assigned around 7.5mg/mL, a relatively high concentration for these type of systems. In FIGURE V. 26(B), there is a cartoon with the possible structures that could be encountered in solution for the different conjugates according to the obtained sizes. It was also confirmed that the type of linkage use could influence the final conformation adopted by the conjugate. Consequently, the existence of unimers is proposed for conjugate C2P1 whereas the formation of dynamic micelle–like structures are expected from conjugate C2P2.

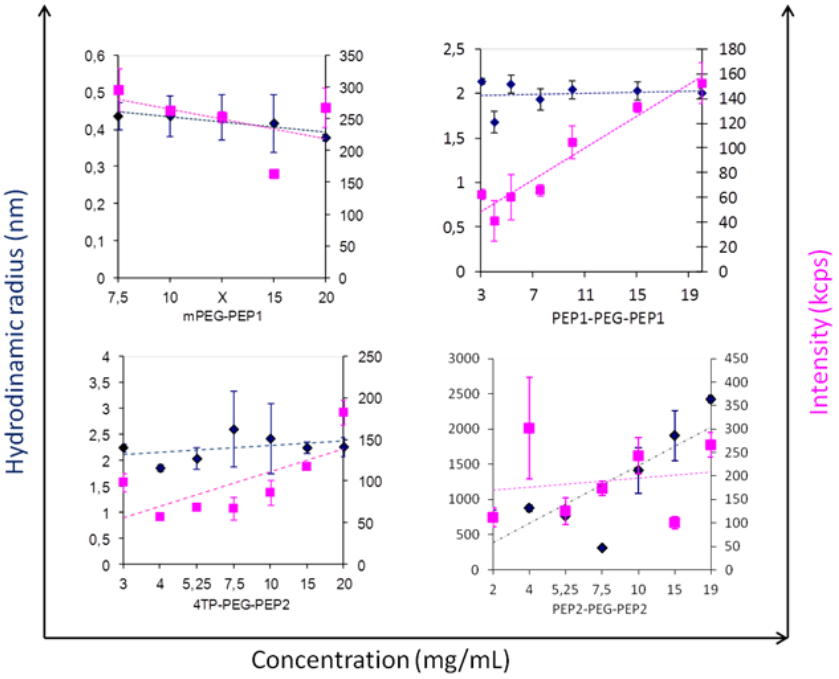

FIGURE V. 28 A plot of the intensity of scattered light (in kilo counts per second, kps) and hydrodynamic diameter (in nm) obtained for various concentrations of the PEG conjugates (CXPX) prepared in PBS 0.02M pH7.4. The intersection of the two lines may corresponds to the critical micelle concentration (CMC).

TTR aggregates binding assays

The interaction of RAGEpep with TTRagg was firstly studied by competition binding assays using ^{125}I-labelled TTR. The peptide and its conjugates were adsorbed to the plate wells at a constant concentration of 5µg RAGE/well. Unlabelled TTR was tested for its ability to compete with the labelled protein for binding to the adsorbed peptide or the PEGylated forms. However, in any of the four experiments performed results were conclusive. Positive and negative controls together with the compounds exhibited rare behaviours which were difficult to interpret. For that reason, an alternative methodology for binding experiments was proposed. Surface plasmon resonance (SPR) method was used in order to find out if the affinity of the peptides for the TTRagg was maintained after PEGylation. BIAcore® device utilise the natural phenomenon of SPR to find out the

affinity of the interaction between the compounds tested. In our study, TTRagg were immobilised on a chip and its affinity with RAGE peptide conjugates was tested.

SPR or Biacore, is a standard technology for interactional study of biomolecules. This technology has the advantage of being able to work with biomolecules in their native forms, without the need of introduction of a label or tag. The SPR-based technology continuously monitors the changes of mass deposition on the detector surface, and allows sensitive and reliable characterisation of biomolecular interactions and provides information such as association/dissociation rate and affinity.

The sensor chip selected was a CM5. Its matrix was a carboxymethylated dextran covalently attached to a gold surface. Molecules were covalently coupled to the sensor surface via amine, thiol, aldehyde or carboxyl groups. Selected via for TTR attaching to this chip was the amine coupling. Amine coupling makes use of the N-terminus and ε-amino groups of lysine residues of the ligand. Below a typical sensorgram of the immobilisation of a ligand to a CM5 sensor chip using this procedure is shown (FIGURE V. 29). The numbered points refer to the different theoretical stages in the immobilisation procedure.

In this experiment, TTR aggregates were covalently immobilised on the sensor chip surface while the peptides/conjugates were injected across the sensor surface, using cell media as vehicle and 37°C to mimic *in vitro* conditions. The interaction found between TTR and PEP1 or amide conjugates (C1P1, C2P1) was reversible and regeneration step after the run was not needed, while with PEP2 or disulphide conjugates (C1P2, C2P2) was irreversible and chip regeneration was carried out injecting Gly 10mM pH=2.5.

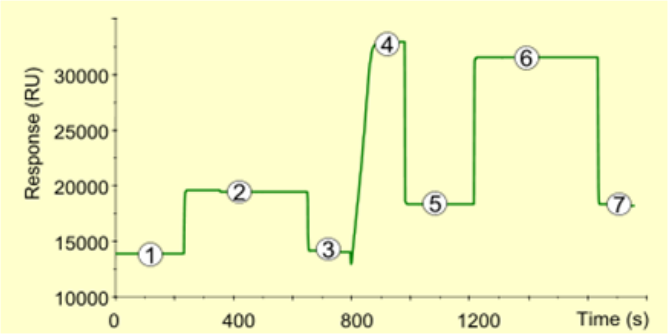

FIGURE V. 29 Amine coupling of a protein onto the sensor chip. Steps: (1) Baseline for the unmodified sensor chip surface with continuous flow. (2) Injection of NHS/EDC to activate the surface by modification of the carboxymethyl groups to N-Hydroxysuccinimide esters. (3) Baseline after activation. Activation of the surface has only a very slight effect on the SPR signal. (4) Injection of ligand leads to electrostatic attraction and coupling to the surface matrix. At this point, the ligand solution is still in contact with the sensor surface, and response includes both immobilised and non-covalently bound ligand. The NHS esters react spontaneously with the amines on the ligand to form covalent links. (5) Immobilised ligand before deactivation. The ligand has passed the sensor surface and most of the protein that is not covalently bound is eluted. (6) Deactivation of unreacted NHS-esters using ethanolamine hydrochlorid 1M adjusted to pH 8.5 with NaOH. The increased SPR signal is due to a change in the bulk refractive index. The deactivation process also removes any remaining electrostatically bound ligand. (7) Point 7 minus Point 3 gives the amount of immobilised ligand after deactivation.

Results recorded are compiled in TABLE V. 5. All peptides and conjugates, except C2P2, bind TTR with different K_D values, therefore recognising the protein. C2P2 data were not reproducible and statistical parameter χ^2 was not in the acceptable range. Summarising, in general it could be said that PEGylation was not affecting to the capability of binding of the original peptide to TTRagg, its molecular target.

Conjugate		K_D (M)	χ^2 (average*)
RAGEpep		0.0016	1.43
PEP1		0.0017	0.13
PEP2		n.r.	> 10
PEG–pep1	**C1P1**	0.0028	0.78
pep1–PEG–pep1	**C2P1**	0.0065	4.16
PEG–pep2	**C1P2**	0.001	3.17
pep2–PEG–pep2	**C2P2**	n.r.	>10

n.r.=non reproducible data, *n=10

TABLE V. 5 BIAcore® data. Binding constant between TTR protein and the CXPX conjugates.

V. 1. 3 *IN VITRO* ACTIVITY STUDIES OF THE POLYMER-DRUG CONJUGATES

Once both novel polymer conjugate families were fully characterised and batch-to-batch reproducibility was achieved, their *in vitro* evaluation was performed. Activity assays reproducing those performed with the parent drugs were carried out to asses that conjugation was not decreasing their inherent properties.

Doxy disrupting action *in vitro* was demonstrated after its incubation with TTR fibrils. These fibrils were produced with the variant TTR Leu55Pro, which is described as one of the most aggressive mutations in the FAP disease and tends to form fibrils *in vitro* under physiological conditions (PBS pH=7.4) [36]. In the case of RAGE peptide conjugates, RAGE peptide protecting effect was evaluated in a established *in vitro* FAP model with the RN22 cells [9]. RN22 cells are a rat Schwannoma cell line characterised by their Schwann cell like phenotype. Schwan cells are the principal glia of the peripheral nervous system (PNS). TTR amyloid deposits can be found in any part of the PNS, including the nerve trunks, plexuses and sensory and autonomic ganglia. In peripheral nerve, deposition occurs extracellularly, mainly in the endoneurium close to Schwann cells and

to collagen fibrils. In FAP, TTR mature fibrils have been described as the causative agent of disease but the protein is not toxic in this state while initial aggregates are [36].

V. 1. 3. 1 TTR fibril disruption studies of the PGA-X-Doxy conjugates

Assessment of fibril formation was monitored by Transmission Electron Microscopy (TEM). Examples of the obtained images are shown in FIGURE V. 30. Before starting conjugate incubation with the fibrils, a homogenous batch of fibrils with similar length was prepared.

Screening for TTR fibril disrupters

Tetracyclines have already demonstrated anti-amyloidogenic properties toward Aβ-amyloid not only in the inhibition of fibril formation but also to disaggregate the already formed fibrils [37]. In the case of doxycycline, previous findings revealed that it acts as a TTR fibril disrupter *in vitro* and *in vivo,* in fact this drug is currently in clinical trials for AD [10, 11, 38]. Prior to the *in vivo* assays, a selection of PGA-X-Doxy conjugates (TABLE V. 6) was evaluated for its capability to break the TTR formed fibrils in order to select the most active candidate.

Visualisation of samples by TEM revealed that, at a drug concentration of 180μM/100μg fibrils, many conjugates were able to disrupt the fibrils after 3days (PGA-CONH-Doxy 15ωt%) or 6 days (PGA-CONH-Doxy 30ωt%, PGA-GG-Doxy 6ωt%), as can be observed in FIGURE V. 30. This fact was determined due to the appearance of fibrils of smaller extension or a complete disaggregation. Named conjugates demonstrated higher activity than parent drug at equal drug concentration (FIGURE V. 30) Hence, PGA conjugation demonstrated not only to maintain original activity after its linkage but also to enhance it. This property has been found very interesting. From this experiment it was also discovered that PGA conceals activity as itself (FIGURE V. 30).Fibrils were disrupted after 6 days of incubation although at higher lengths than conjugates. Disaggregating effect could be attributed to a possible polymer intercalation where negative charges of the carboxyl groups promote fibril disruption. In nature,

other polyanions such as gycosaminoglycans or proteoglycans have been described to be involved in the formation of amyloid deposits. Comparable promoting effects have been attributed to polycations like PEI, polyLys or polyArg [39]. Thus, further studies to elucidate PGA behavior will be carried out in order to determine its possible inherent capability for fibril disaggregation as polymeric drug. Overall, the highest activity observed at shorter time belonged to a member of the amide linkage family: PGA-CONH-Doxy 15ωt%.

Conjugate	% ωt Doxy	3.6mM Doxy
PGA-NH-DOXY conj.	51.29	3.61 mg / mL
	15.00	12.33 mg / mL
PGA-COO-DOXY conj.	26.00	7.12 mg / mL
	21.50	8.60 mg / mL
	33.00	5.61 mg / mL
	30.05	6.16 mg / mL
PGA-LG-NH-DOXY conj.	9.00	20.56 mg / mL
	8.50	21.76 mg / mL
PGA-GG-NH-DOXY conj.	13.60	13.60 mg / mL
	6.10	30.33 mg / mL
DOXY		1.85 mg / mL
DOXY-NH_2		2.01 mg / mL

TABLE V. 6 PGA-X-Doxy conjugates tested *in vitro.*

After compiling the results of solution conformation and bond stability studies, it could be concluded that doxy release is not a requirement for activity (see FIGURE V. 22 where no release was detected in the PBS stability study after 3days or where LCMS data revealed no free doxy existence even after 17days). Conjugate solution

conformation looking at different drug loading did not reveal any significant differences (see section V.1.2.1), which could indicate that drug exposure is either not an issue for activity.

Regarding DLS analysis, aliquots were taken at the same moment and time point than TEM samples. Results are depicted in FIGURE V. 31. Vast majority of the treated fibril samples were significantly different ($p<0.05$) from the control fibrils after 6 days of incubation. It was observed that the progression in particle size (radius, r (nm)) with time differed according to whether drug or conjugate was present or not. Control TTR showed a heterogeneous preparation with species with radii of around 700nm. The incubated fibrils for 6 days with conjugates resulted in smaller particle sizes, ranging from 300-530nm.

Control fibrils t=0

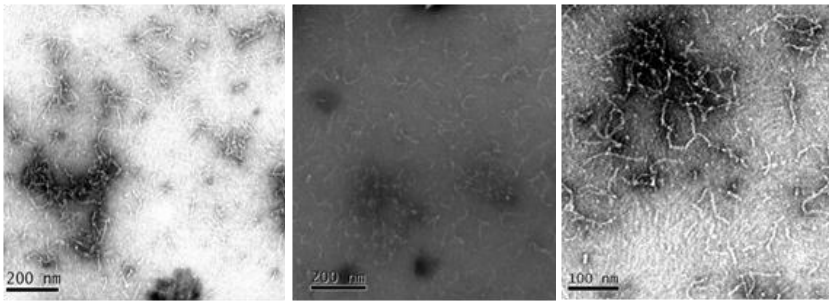

PGA-CONH-Doxy 15ωt%, t=6d

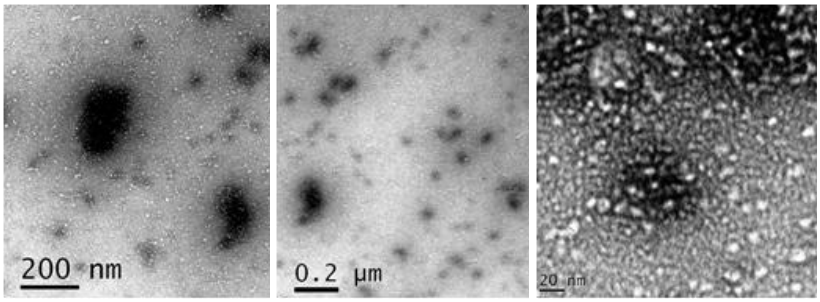

PGA-CONH-Doxy 30ωt%, t=6d

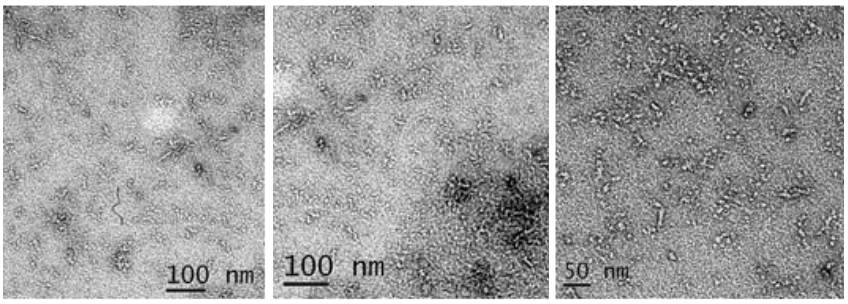

PGA-CONH-gly-gly-Doxy 14ωt%, t=6d

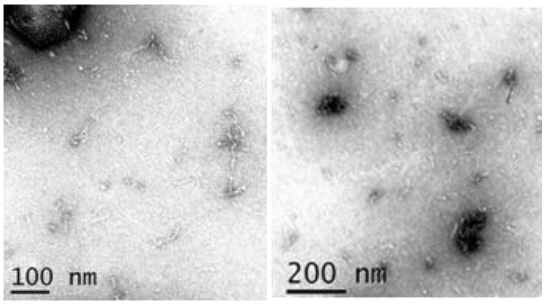

(B) Doxycycline, t=10d **(C) Doxy-NH_2, t=10d**

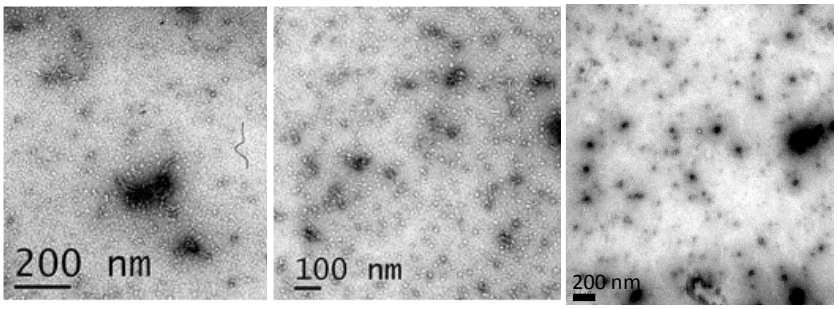

(D) PGA, t=6d

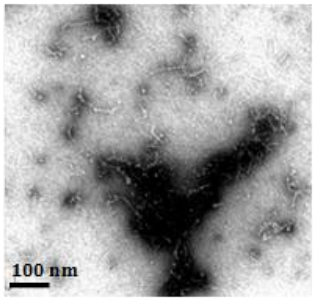

FIGURE V. 30 Effect of Doxycycline conjugates was tested on the *in vitro* assembly of TTR L55P fibrils followed by TEM. In the control situation, after 13 days incubation at 37°C, TTR initial aggregates are organised into mature fibrils.(A) When doxy conjugates were active (i.e.. PGA-CONH-Doxy 15ωt%, PGA-CONH-Doxy 30ωt%, PGA-GG-Doxy 14ωt%), fibrils were disrupted producing small round particles and shorter fibrils. (B) When doxy concentration was increased, activity was observed. (C) Doxy-NH_2 showed comparable activity to the original parent drug. (D) Unexpectedly, PGA (added as a negative control) produced fibril reduction and round particles were observed.

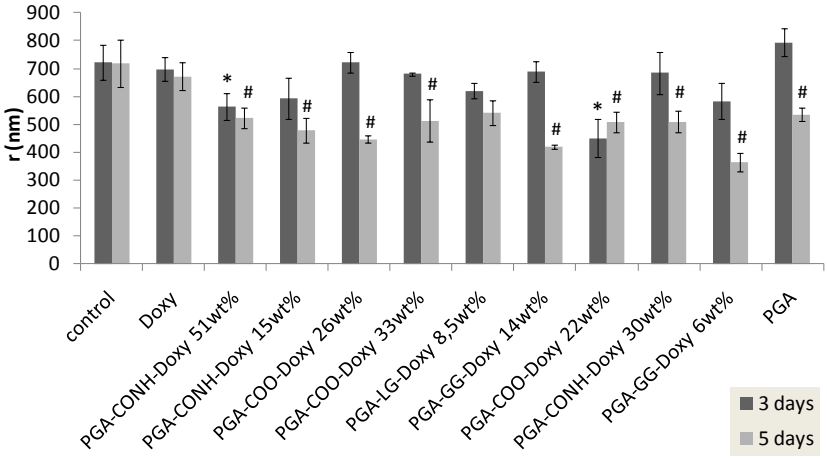

FIGURE V. 31 Particle size (hydrodynamic radius (nm)) measured by DLS. (*=significant data respect control (t=3days), #=significant data respect control (t=6days), $p<0.05$).

Sizes obtained by DLS cannot be comparable with those lengths measured by TEM. It is important to remark that, both techniques underwent in different scenarios and therefore, final data could not be interpreted in the same manner. In the case of TEM, fibrils are adsorbed onto the grid and after the staining, they remain dry. Single fibrils are observed. On the other hand, DLS measurements are carried out in solution. Sizes given were a result of a theoretical spherical particle. Most probably, radius data was directly related with the size of fibrils and reduction in fibril size entailed a reduction in the radius of the fibril aggregate particle.

Considering the results obtained, it has been clearly ratified that PGA-X-Doxy conjugates act as fibril disruptors at lower drug equivalent concentrations than the parent drug. PGA-CONH-Doxy 15ωt% was selected for further studies.

V. 1. 3. 2 Cytotoxicity of the species resulting from the action of PGA-X-Doxy

In FAP, TTRagg have been identified as the cytotoxic species

oppositely to the mature fibrils that although they could be considered as non-toxic, they could instead trigger apoptosis after their deposition[36]. This assay was proposed trying to understand if structures resulting from fibril disruption were able to promote cell death mechanisms. Using the RN22 cell line, cytotoxicity of the species resulting from fibril disruption by the most active doxy conjugates was evaluated and compared with the fibrils and the aggregates. Conjugates selected for this study were PGA-CONH-Doxy 15ωt% (**51**), 30ωt% and PGA-GG-Doxy 6ωt% (**52**).

A first study (FIGURE V. 32(A)) concluded that toxicity of the sub-products were similar than that for mature fibrils and not higher than that obtained for the aggregates. TEM images revealed a non-homogenous population after the treatment in the control sample (data not shown) probably due to non-mature enough samples. A second experiment did not arise either any concluding results as no significant differences were obtained, toxicity of the fibrils treated with the conjugates were similar to the fibrils (FIGURE V. 32(B)).

From the experiments it was concluded that toxicity of the fragments were not significantly different to fibrils. However, free doxy did not improve cell bioavailability while the conjugate PGA-CONH-Doxy 15ωt% showed better output. Repetition of the assay and further evaluation *in vivo* would confirm if these fragments could induced any other effect.

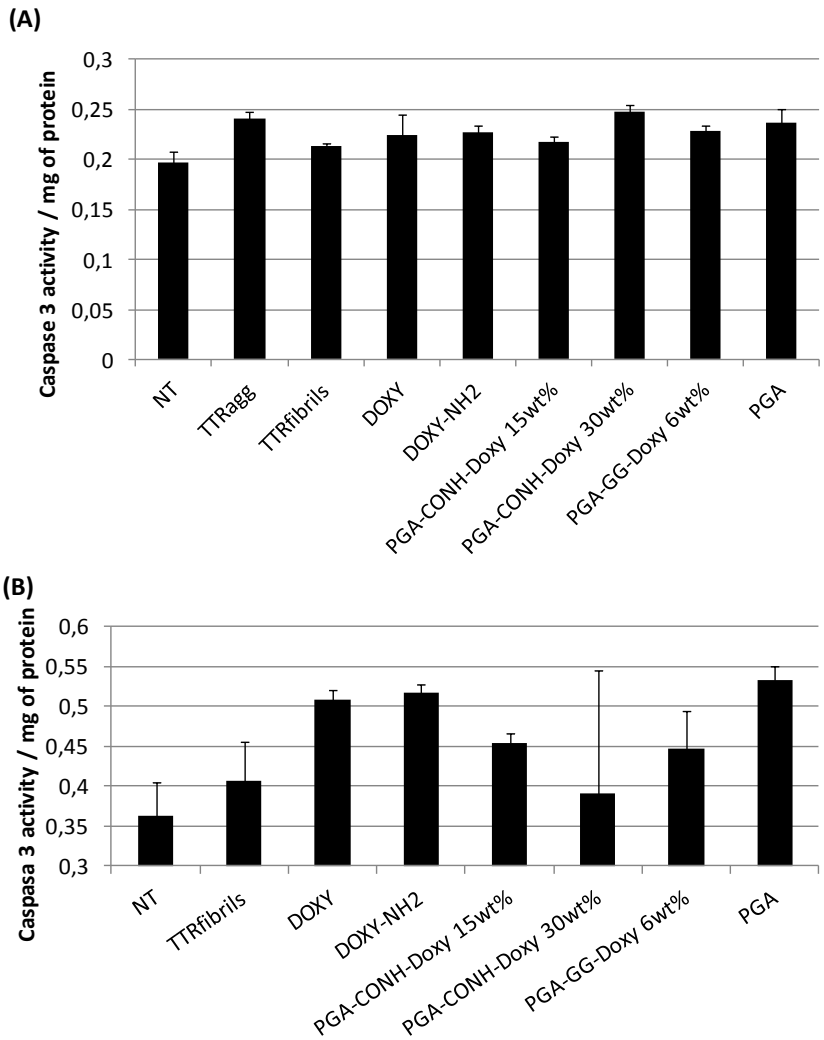

FIGURE V. 32 (A) First trial of caspases-3 test after fibril incubation with PGA conjugates (B) Second trial of caspase-3 test after fibril incubation with PGA conjugates.

V. 1. 3. 3 Activity of the RAGE peptide conjugates as inhibitors of TTRagg induced toxicity. Caspase-3 assay

To investigate the pharmacological activity of the PEG-RAGE peptide conjugates they were first incubated with TTRaggs before incubating with RN22 cells for 24h or 48h. Apoptotic cell death was then quantified using a caspase–3 activity fluorometric assay based on

the hydrolysis of the peptidic substrate acetyl–Asp–Glu–Val–Asp–7–amido–4–methylcoumarin (A–DEVD–AMC) resulting in the release of 7–amino–4–methylcoumarin (AMC) fluorescent moiety. In order to normalise the data, the protein content of the RN22 cells was determined using Bradford assay (appendix III).

The PEG-RAGEpep conjugates retained RAGE peptide activity (FIGURE V. 33). In all the experiments performed, the conjugate C2P1 (PEP1-PEG-PEP1) was the best inhibitor of TTR-agg induced cytotoxicity in Schwann cells at 24h. Those conjugates containing disulphide linkers produced less reproducible data and lower activity, therefore, it could be concluded that PEG-RAGE conjugates with the amide linker are more effective in preventing cytotoxicity induced by the TTRagg at 24h. It is important to note that addition of the PEG polymer alone appears to promote growth after 24h PEG could act as 'nutrient' (assay is carried out at 1% serum to avoid confluence during the incubation period) balancing the effect of toxicity caused by TTRagg. However, this effect disappears after 48h.

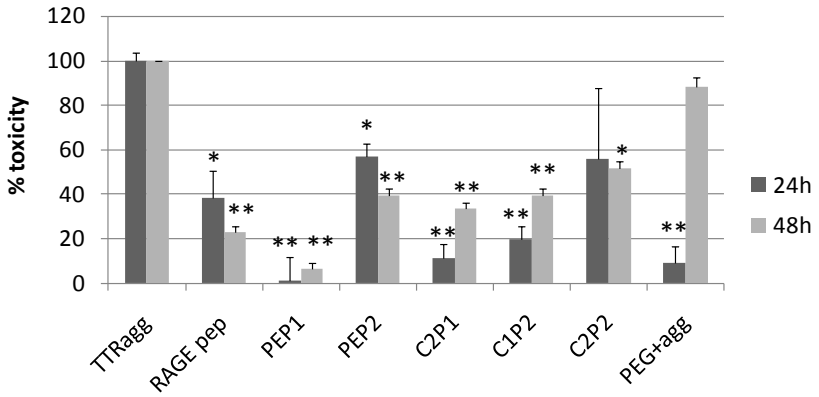

FIGURE V. 33 Activation of caspase-3 in RN22 cells exposed 24 and 48h to 10µM of RAGE peptide after incubation alone, with their derivatives or with the RAGE peptide conjugates. PEG was used as control. *Significantly different from aggregates (*, $p<0.05$; **, $p<0.005$).

Conformation in solution may explain activity *in vitro* where C2P2 activity resulted in the lowest of the group. Rest of conjugates

demonstrated to have a stable conformation in solution (R_h=0.6-3nm) non-concentration dependent where possibly peptide availability is better for TTRagg interaction therefore improving conjugate activity.

In conclusion, the data relating to TTR binding affinity, conjugate linker stability and the solution conformation of PEG-RAGE peptide conjugates indicate that the PEG RAGE peptide conjugates containing amide linkers have the greatest potential for future development as FAP inhibitors. Moreover, this novel conjugate has potential as a FAP therapeutic to be used alone in the early stages of the disease or as part of rationally designed combination therapy.

V. 1. 3. 4 Haemolysis assay of the synthesised polymer-drug conjugates

As PEG-RAGEpep conjugates are proposed for administration by the intravenous (i.v.) route their ability to induce red blood cell (RBC) lysis in vitro was studied as a preliminary measure of haematocompatibility [28]. PEI and dextran represented the positive and the negative control, respectively. Dextran is used as a plasma volume expander and PEI is a cationic polymer with a marked haemolytic character. Haemolytic profiles of PGA-Doxy and PEG-RAGEpep conjugates were evaluated and results are represented in FIGURE V. 34. None of the conjugates showed haemolytic properties indicating their suitability for i.v. administration.

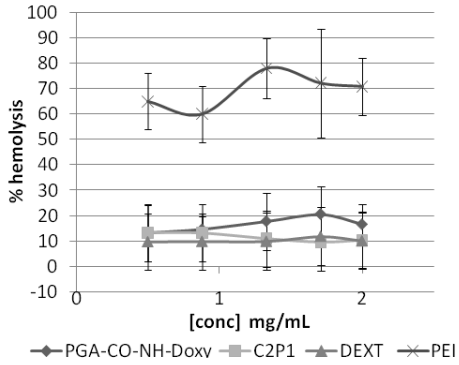

FIGURE V. 34 Haemolytic activity of PGA-CONH-Doxy (**51**) conjugate and the PEGylated RAGE peptide C2P1 (**60**) at 1h. Data expressed as mean (n=3).

V. 1. 4 *IN VIVO* EVALUATION STUDIES OF THE POLYMER-DRUG CONJUGATES

Polymer-drug conjugates evaluation continues with biodistribution studies and proof of activity *in vivo*. Efficacy of the novel conjugates lies in their PK, biodistribution and metabolic clearance. The pathway involves circulation in the blood, interaction with major organs (e.g., liver, kidneys, etc); transport to target tissue and cells ending with the effective drug action (with an appropriate release if necessary). Traditional studies were sometimes invasive and cannot accurately provide real time information on the interaction between polymers with organs and tissues, the delivery efficiency of the whole system or the therapeutic response. Nowadays, biomedical imaging technology advances provide efficient systems for non-invasive and monitoring *in vivo* drug delivery. Techniques explained in Chapter III, are some examples of how labelling the PDC allows to accomplish the reported objectives.

Concerning activity experiments, already reported PDCs' *in vivo* studies has clearly demonstrate the benefits of drug conjugation to polymer carriers [40]. Conjugation of the NIR dye Cy5.5 and the DOTA/^{68} Ga complex were the selected tags. Both strategies enabled to monitor and quantify the biodistribution and PK parameters of the conjugates *in* vivo as well as *ex vivo*. Preliminary activity studies had been performed in a FAP young mice model also evaluating the possibilities of a combination therapy. Recently, it has been proposed that therapy entailing action on signalling pathways involving RAGE or other mediators together with fibril disruption can be considered as a novel potential pharmacological approach in FAP [41].

V. 1. 4. 1 Polymer-drug conjugates biodistribution studies in mice

PGA-DOXY conjugate biodistribution

PGA-CONH-Doxy-Cy5.5

Body distribution study was carried out in healthy Balb/c mice (9-12month-old male/female). As in Chapter IV, the Cy5.5 labelled

conjugate tissue distribution was measured by means of FLI the IVIS® Spectrum imaging system. Mice were injected i.v. with 1.15mg doxy eq/kg of PGA-Doxy17ωt%-Cy5.5 (**66**). As a control, non-injected mice were used. Mice were monitored (dorsal and ventral view) after i.v. injection and a time course experiment was performed (TABLE V. **7**(A)).For this assay, mice were shaved to avoid fluorescent interference from the fur. FIGURE V. 35 shows the *in vivo* FLI images over time. The fluorescence signal was quantified in Radiant Efficiency. To further confirm the results, groups of mice for each time point were euthanised and blood, liver, kidney, spleen, brain, lungs and heart were collected. All tissues were analysed by *ex vivo* FLI (FIGURE V. 36) and total content of fluorescence was determined by VICTOR® analysis after homogenisation. Quantification data is shown as Cy5.5 fluorescence per weight of tissue at each time-point (FIGURE V. 37). As expected for a PGA conjugate, results showed no specific accumulation in any organ and renal clearance. The conjugate did not accumulate in heart, lungs, kidney or liver (FIGURE V. 38). *Ex vivo* FLI intensities and fluorescence data of the homogenated tissues showed good correlations, validating FLI intensity determinations as a good methodology to estimate non-invasively tissue-accumulations.

(A)

Time point	n (animals)
0 min	5
30 min	3
1h	4
4h	4
24h	4
96h	3
Control	4

(B)

Time point	n (animals)
0 min	4
30 min	4
4h	4
24h	4
Control	4

TABLE V. 7 Time points for fluorescent *in vivo* measuring or animal sacrificing during the biodistribution study: (A) PGA-Doxy-Cy5.5, (B) Cy5.5-PEG-PEP1.

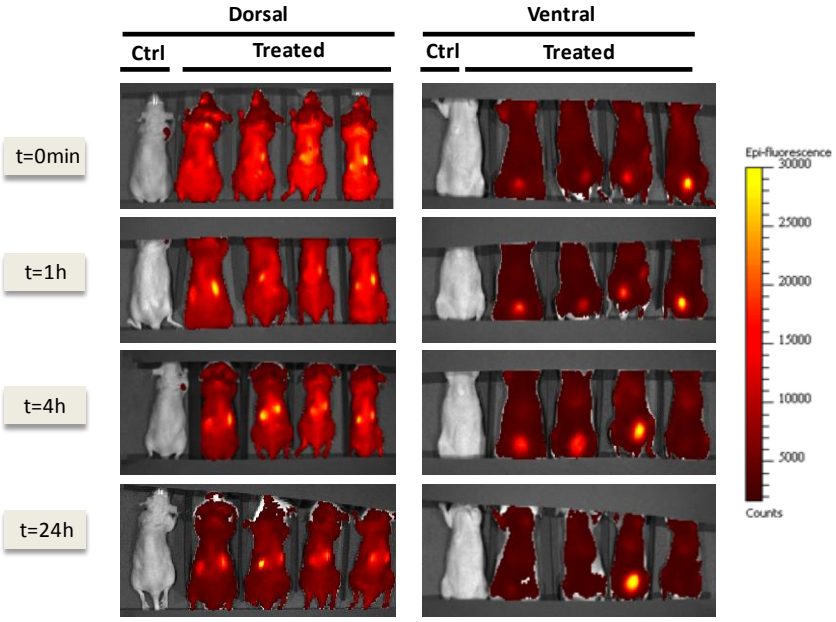

FIGURE V. 35 Whole-body biodistribution of PGA-Doxy-Cy5.5 measured by the means of *in vivo* FLI from the dorsal and ventral views using the IVIS®Spectrum.

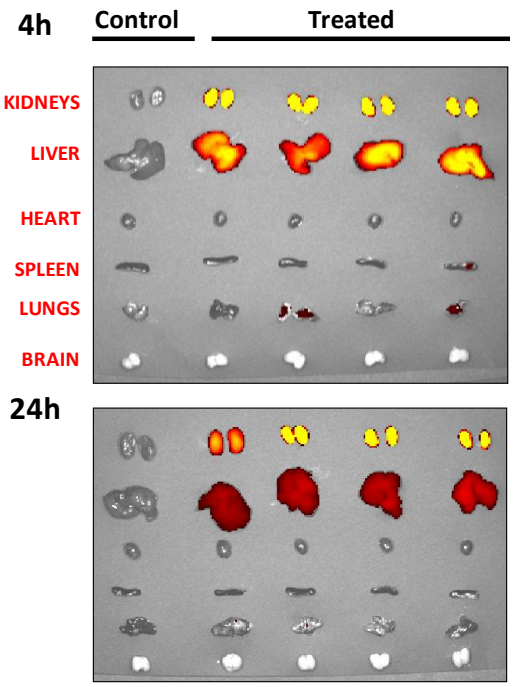

FIGURE V. 36 *Ex vivo* monitoring of PGA-Doxy-Cy5.5 overtime. Pseudocolor scale bars were consistent for all images in order to show relative changes with time.

(A)

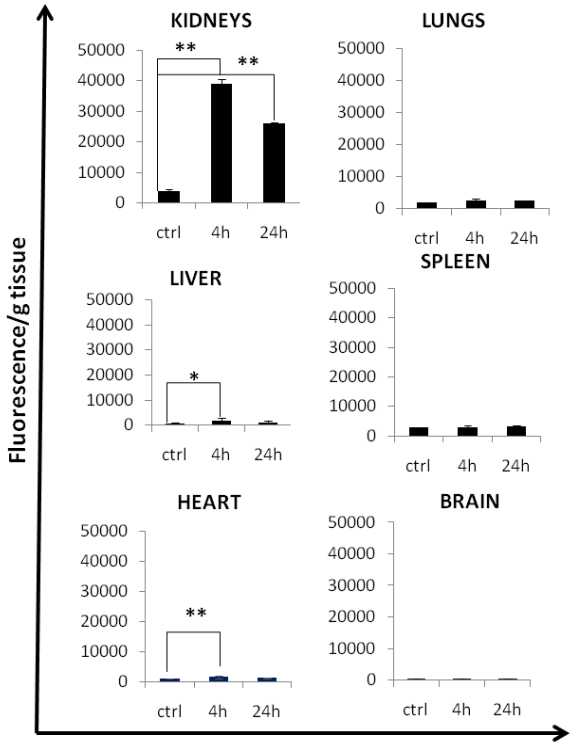

FIGURE V. 37 Normalised data of fluorescence obtained after homogenation of the excised organs from PGA-Doxy-Cy5.5 biodistribution:
(A) Same "y" axis scale
(B) Different "y" axis.

(B)

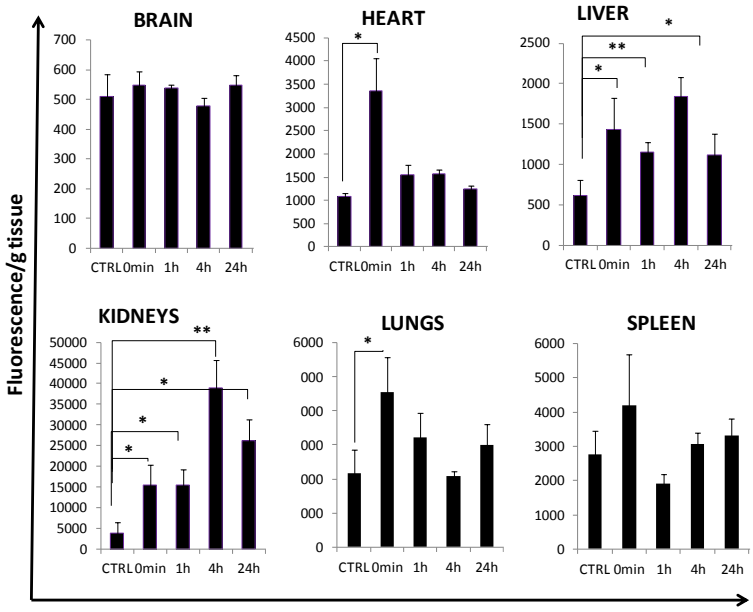

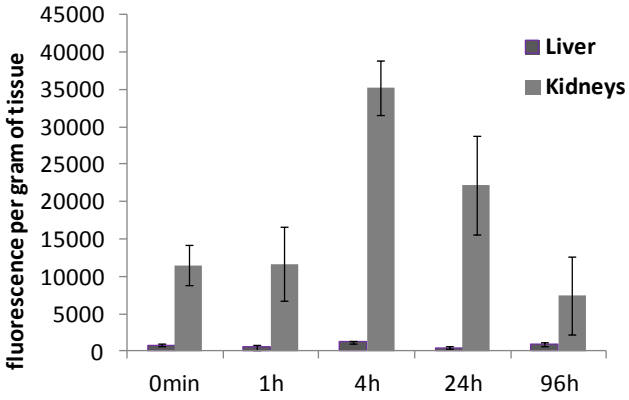

FIGURE V. 38 Comparison among kidney and liver normalised fluorescence of the in vivo distribution of PGA-CONH-Doxy-Cy5.5.

Regarding plasma analysis, fluorescence measurements were done directly without any extraction due to signal lost if treatments with organic solvents, acid or base are used. Results are graphed in FIGURE V. 39. Surprisingly, PGA-Doxy conjugate $t_{1/2}$ was found to be approximately 10min, very short $t_{1/2}$ for this type of conjugates. Reported $_{t1/2}$ for other clinically-relevant PGA conjugates are from 30 min to 5 hours [42-45]. It is believe that experimental issues could occur, such as, the binding or co-precipitation in during plasma isolation as doxy readily binds to plasma protein binding drug [46]. These experiments should be discharged as at that time pellet was not further analysed. Instead, $t_{1/2}$ was calculated by PET analysis.

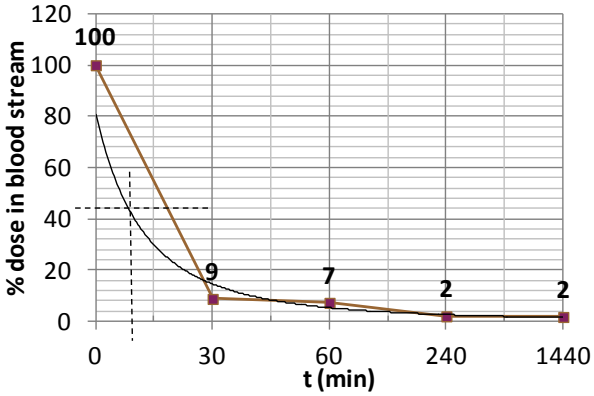

FIGURE V. 39 Half-life time ($t_{1/2}$) study of PGA-CONH-Doxy.

FVB/NJ mice were injected i.v. a dose of 21±4µg compound/g body weight of PGA-Doxy-DOTA/^{68}Ga (0.2 and 1.4MBq ^{68}Ga activity). The selected dose was adequate for a proper detection of the signal not for therapeutic proposes. Time course analysis of the radioactivity signal showed, as already seen for the control compound (PGA-DOTA), a marked signal in the kidneys (FIGURE V. 40(A)/(B)), suggesting renal secretion. However, the radioactivity levels detected in the liver or spleen of the PDC were significantly higher than the control) (FIGURE V. 40(a1)). This result suggested that drug conjugation may promote a different (probably bigger, as suggested by SANS data) solution conformation favouring liver uptake. In addition, DOTA content in the PGA-Doxy (18%) conjugate was higher than in the PGA (2%), which may also contribute to the different conformation. Slight differences were also found in the spleen and the lungs, with higher values in the labelled polymer-drug conjugate. However signal decreased indicates that compound was along the secretion process, as expected.

The PK analysis using a bicompartimental model gave key parameters to compare PGA-Doxy conjugate vs. PGA control. The volume of distribution was similar for both, approximately 5.3mL. The AUC is larger for PGA-Doxy as well as its Clearance rate (11,8mL/h vs. 7mL/h for PGA-Doxy vs. PGA, respectively). Importantly, $t_{1/2}$ of the DOTA labelled PGA-Doxy demonstrated greater value than for PGA control, 0.98h vs. 0.59h, respectively. This time, data in good agreement for that reported with PGA conjugates.

(a1)

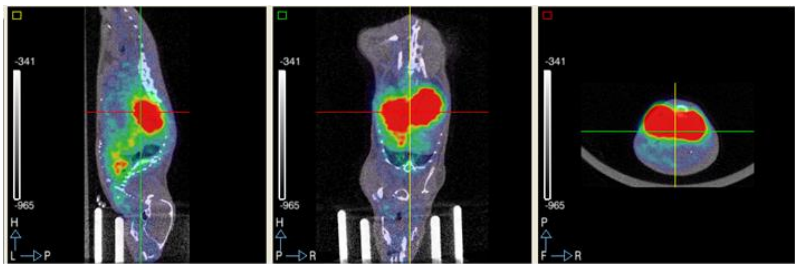

(a2)

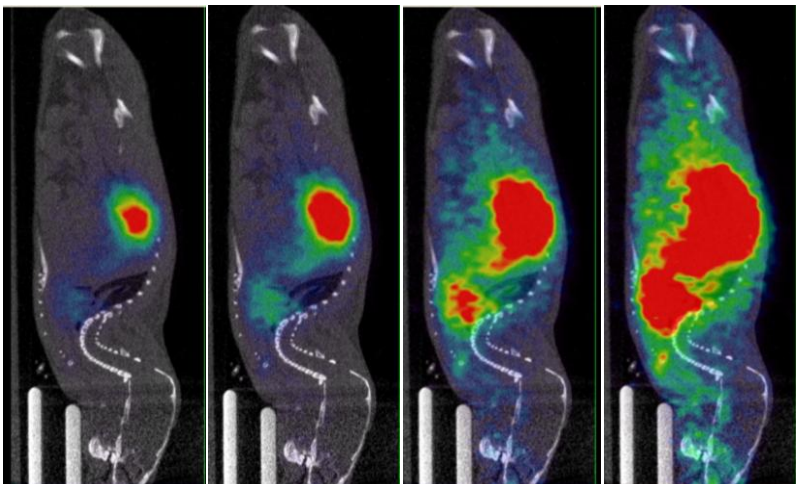

(a3)

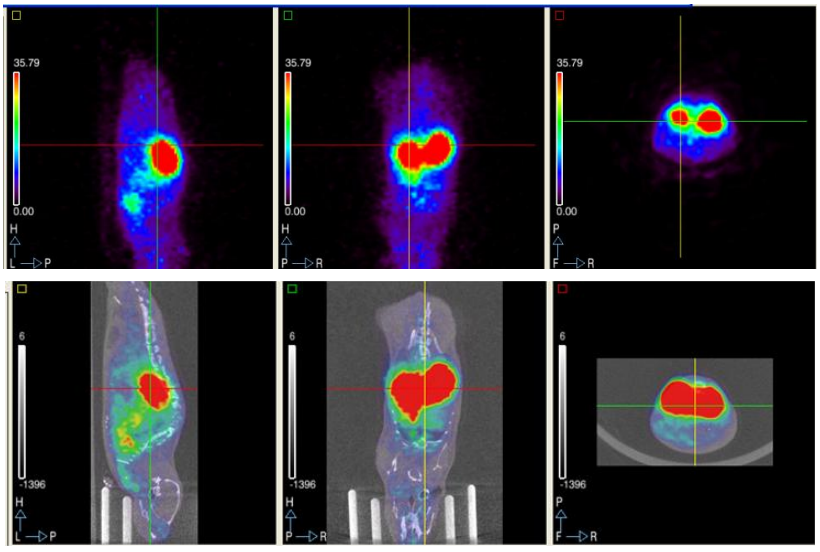
35.79
0.00
H
L
P
35.79
0.00
H
P
R
35.79
0.00
P
F
R
6
-1396
H
L
P
6
-1396
H
P
R
6
-1396
P
F
R

(B)

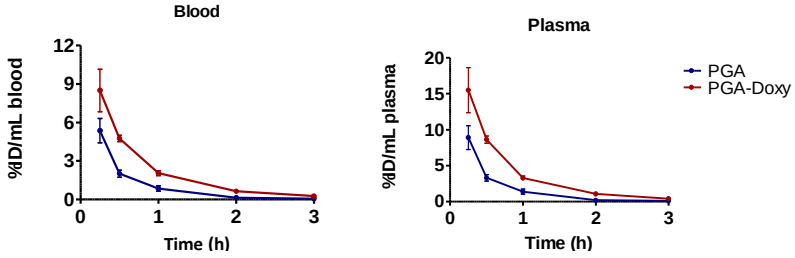
Blood
%D/mL blood
12
9
6
3
0
0
1
2
3
Time (h)
Plasma
%D/mL plasma
20
15
10
5
0
0
1
2
3
Time (h)
PGA
PGA-Doxy

(B continues)

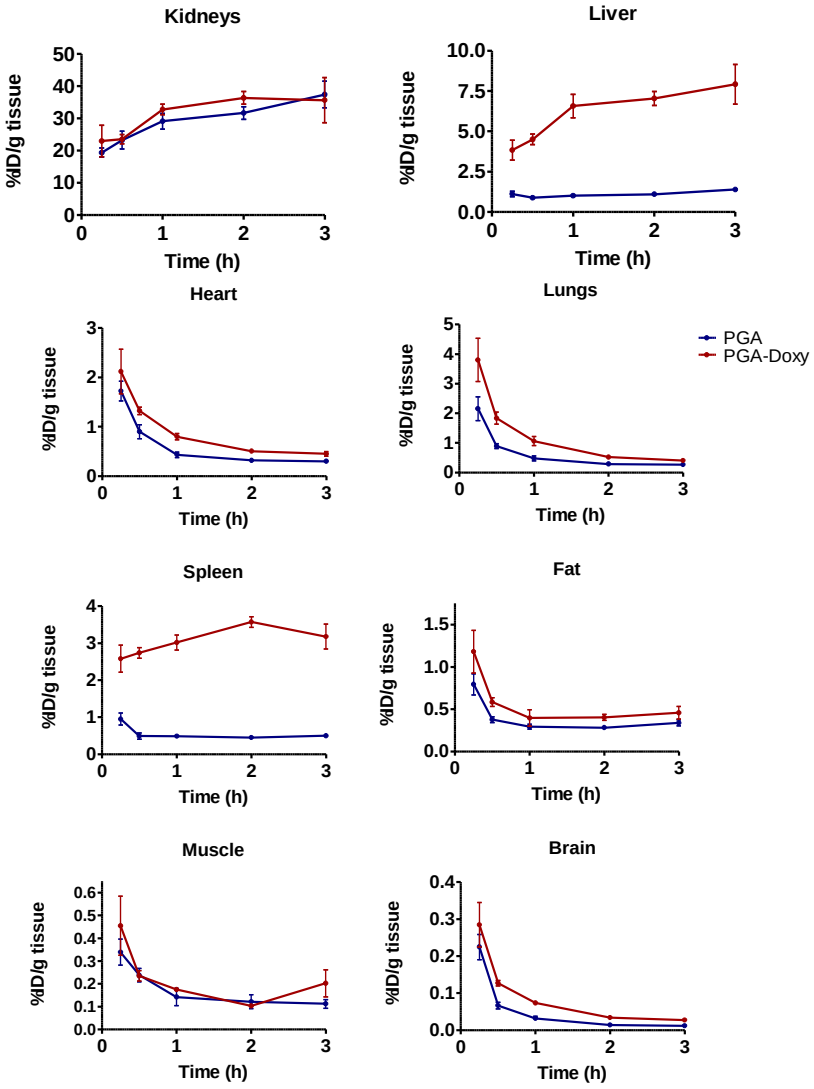

FIGURE V. 40 PET images PGA-Doxy-DOTA/^{68}Ga (46,9 µCi) (A) (a1) PET image acquired during 30min immediately after i.v. injection (a2,a3) images with different grades of signal saturation.(B) Normalised data of radioactivity signal of each organ respect the injected dose (ID). Time course experiment. All polyglutamates had DP=100.

PEP1-PEG-Cy5.5 conjugate biodistribution

Body biodistribution study was carried out in healthy Balb/c mice (6-8month-old male/female). As in Chapter IV, the Cy5.5 labelled conjugate tissue distribution was monitored by means by FLI using the IVIS® Spectrum imaging system. Mice were injected via the tail vein with 0.57mg PEP1 eq/kg of C1P1-Cy5.5 (**67**). Non-injected mice were used as control. Mice (previously shaved) were monitored *in vivo* after i.v. injection and a time course experiment was performed (TABLE V. 7(B)). FIGURE V. 43 shows the *in vivo* images taken over time. The fluorescence signal was quantified in Radiant Efficiency. In parallel, groups of mice for each time point were euthanised and blood, liver, kidney, spleen, brain, lungs and heart were collected. All tissues were analysed by *ex vivo* FLI (FIGURE V. 41) and total content of fluorescence was determined by VICTOR® analysis after homogenisation. Quantifications are shown as Cy5.5 fluorescence per weight of tissue at each corresponding time-point (FIGURE V. 42).

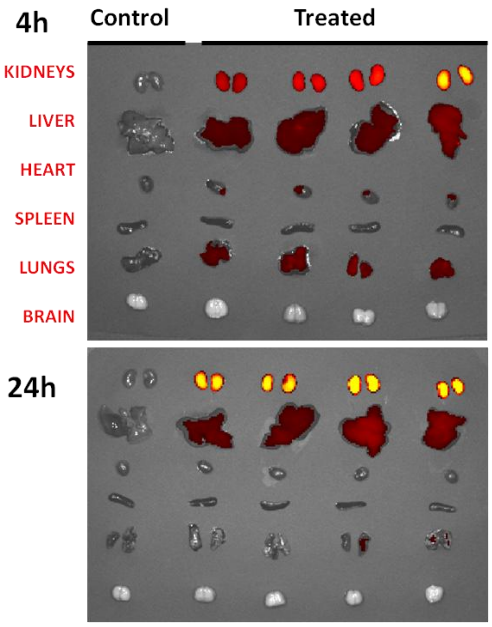

FIGURE V. 41 *Ex vivo* fluorescence of animal organs after Cy-PEG-PEP1 conjugate administration.

As named before, PEG is a non biodegradable polymer. Its amphiphilic character allows its gradual translocation from blood to peripheral compartments according the permeability of the biological barriers depending on its MW and the structural conformation. PEG is predominantly cleared in the urine, through glomerula filtration. Hepatic component in secretion increases as MW does, although urine always predominates. PEG tissue distribution has been proved to be MW dependent, in which large PEGS from 20 to 170kDa undergo slower extravasation and are retained in the peripheral organ areas for a long time. Furthermore, liver clearance requires a mass below 40-60kDa [47]. With this information and the PEGylated products currently in the market and in clinical trials (PEG 5-40kDa), the MW of the PEG selected for the RAGEpep studies was low (3000-4000g/mol).

(A)

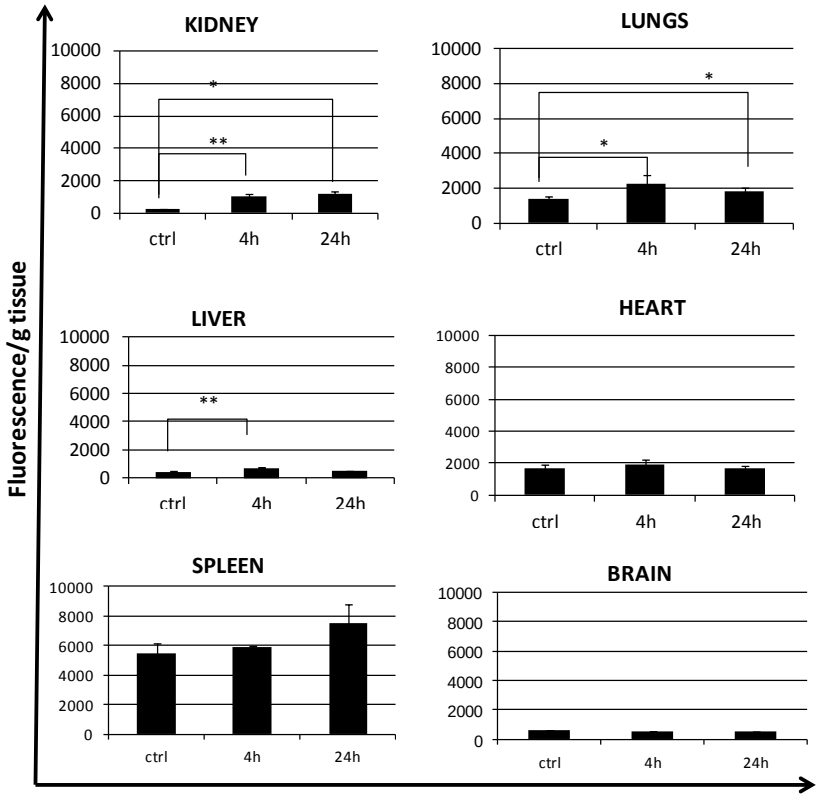

(B)

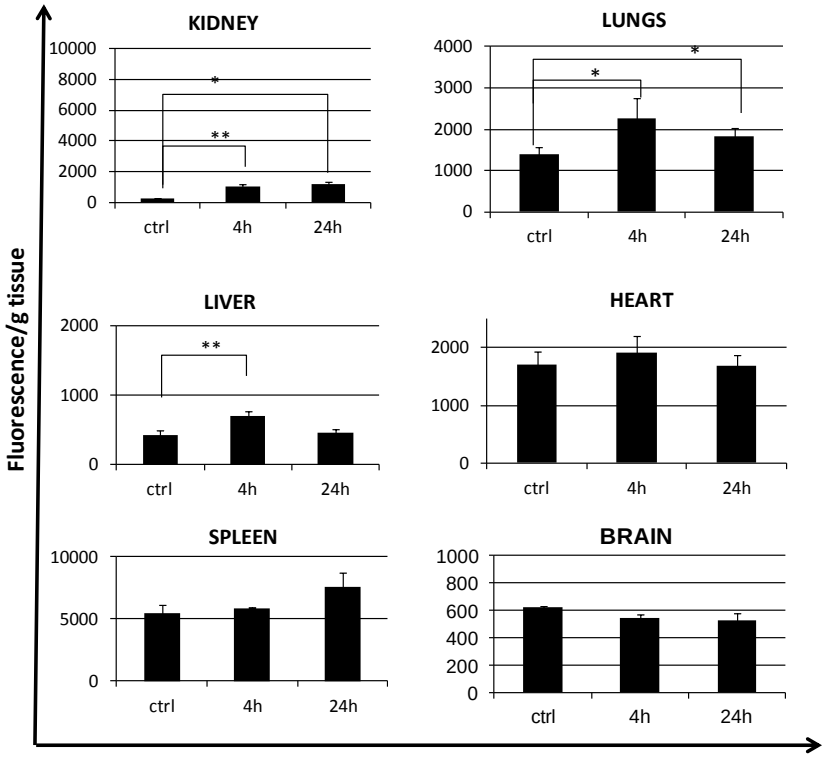

FIGURE V. 42 Normalised data of fluorescence obtained after homogenation of the excised organs from Cy-PEG-PEP1 biodistribution. (A) Same "Y"axis (B) Different "Y" axis to allow better comparison.

Images as well as fluorescence quantification showed no specific accumulation in any organ and secretion by kidney and urine. Main percentage of the administered dose was found in kidney (FIGURE V. 42) in comparison with the other organs analysed, and signal decreases over time. The signal observed in the spinal cord could be attributed to the $-SO_3^-$ groups present in the dye; this pattern corresponds to charged compounds captured by macrophages and therefore observed in this part of the body. PEG does not follow this behaviour. As conclusion, these images were not considered as a reality because Cy5.5 significantly modified the conjugate biodistribution. Biodistribution studies through PET or radioactivity (^{14}C or ^{3}H labelling) have been proposed as alternatives for this PEG

conjugate.

For $t_{1/2}$ calculation of the PEG conjugate, blood was also collected at the 0 min, 30min, 4h and 24h. After centrifugation, fluorescence measurement of the plasma was done directly without any extraction. Results are represented in FIGURE V. 44. $t_{1/2}$ corresponded approximately to 10min, lower than expected. The reported $t_{1/2}$ for PEG conjugates range from 18min to 24h as the MW goes from 3 to 190kDa [48, 49]. This fact could be probably explained as the peptide sequence used is quite small and the size of the selected conjugates are around 2 nm, smaller than those reported with larger peptides or proteins. It is also important to note the presence of negative charges of the sulphate groups from the NIR dye structure (FIGURE V. 13) that could alter the real in vivo fate of this small PEG conjugates as these negatively charged compounds have been described to be captured by macrophages. When C1P1-Cy5.5 was monitored in vivo, this pattern was found (FIGURE V. 43). Therefore, PET imaging would be a better alternative and these studies are ongoing.

To sum up, biodistribution in healthy mice of Cy5.5 labelled PEG-RAGEpep conjugate showed a favourable body distribution with no specific accumulation in any organ and renal excretion. In addition, the major achievement of this conjugate is the enhanced solubility, stability and availability of the peptide.

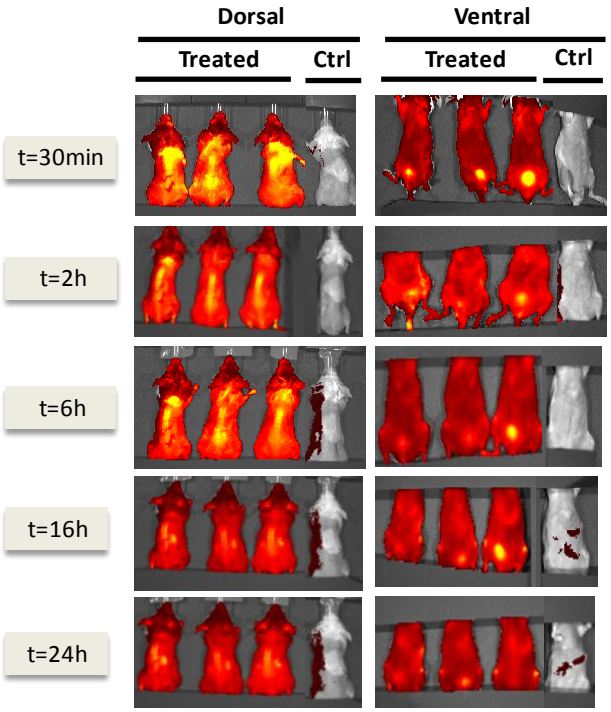

FIGURE V. 43 Whole-body biodistribution of Cy-PEG-PEP1 measured by the means of *in vivo* FLI from the dorsal and ventral views using the IVIS® Spectrum.

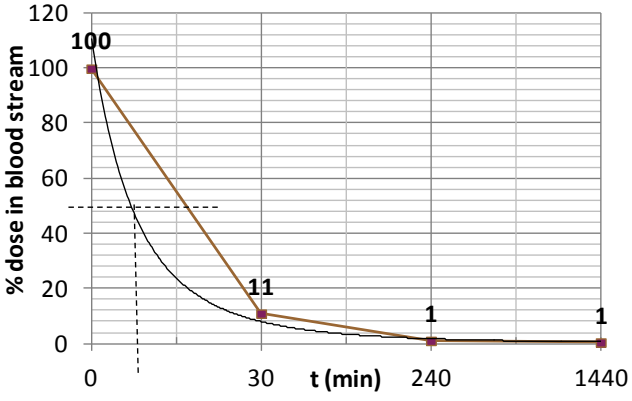

FIGURE V. 44 Half-life time ($t_{1/2}$) study of C1P1-Cy5.5.

V. 1. 4. 2 Preliminary activity studies in FAP mice model

Majority of FAP *in vivo* models are based on transgenic mice carrying human mutations on the TTR protein, being the TTRVal30Met the most common one. In this model, it was discovered that non-fibrillar amyloid TTR evolved to amyloid deposits with time thus mimicking the human pathological characteristics, although non depositions in peripheral nerves were found [11]. In humans, FAP patients can be classified according to the degree and type of deposition in nerves and fibber degeneration [50]: FAP 0, no fibber degeneration, no amyloid but non-fibrillar TTR deposition; FAP 1, mild degeneration, discrete TTR fibrils; FAP 2, considerable degeneration, abundant amyloid and FAP 3, severe degeneration and extensive amyloid deposits .

In the present animal model, animals in advanced phases of the disease (16-25months) showed TTR fibril deposits [51]; in early stages (9-11months), non-fibrillar TTR deposits were detected. Main activity in the disease is detected in the gastrointestinal path: oesophagus, stomach, small and large intestines. Old mice present both non-fibrillar deposits and TTR amyloid at the same time, certifying a kinetic evolution between these two species of the aggregation cascade.

Saraiva *et al*. evaluated doxy *in vivo* activity by oral administration following different treatment schemes optimising duration of treatment, concentration and mice model. Results confirmed its ability as TTR fibril disrupter [10, 38]. On the other hand, it was unable to remove non-fibrillar TTR or diminish non-fibrillar TTR-associated markers. Concerning the RAGEpep, *in vivo* evaluation of the peptide itself has not been performed due to the limitations from peptide intrinsic properties. Its conjugation to a polymer was a required step to enable this assay. RAGEpep test should be studied in young mice were the aggregates (non-fibrillar TTR) are present and promote disease development.

Thus, a preliminary activity test *in vivo* of the synthesised and

characterised polymer-drug conjugates was carried out. Three groups of animals (9-11 month of age, n=8) were treated intravenously with the conjugates detailed in TABLE V. 8. It has to be emphasised that *in vivo* experiment was focused to mainly test the activity of the RAGEpep conjugates in young FAP mice model. As a first trial, a combination group treated with doxycycline conjugate was also incorporated. A final group to control PGA-Doxy activity was also include.

Group	Conjugates	ωt% drug loading	Drug amount per dose
1 and 2	pep1-PEG-pep1	36	0.036mg drug/Kg
2	PGA-CONH-Doxy	17	8mg drug/Kg
3	PGA-CONH-Doxy	43	8mg drug/Kg

SCHEDULE	6 weeks
	2 doses (i.v.) weeks
	8 mice per group

TABLE V. 8 In vivo experimental set up[10].

Doses were adjusted based on preliminary data (*in vitro* and *in vivo*) and literature on the topic. For doxy, previous *in vivo* studies of Saraiva et al. concluded that an oral dose of 8mg/Kg per day and a maximum of 15 days maintained fibril disaggregation. RAGEpep has never been administered *in vivo*. All conjugates were administered intravenously. Final dose and scheme of administration schedule is

[10] Animals were given 2 doses per week during 6 weeks. *Group 1* was treated with the conjugate C2P1 (**60**), *group 2* was treated with two conjugates in the same dose (combination group): C2P1 and PGA-CONH-Doxy (**51** and **60**, respectively) and *group 3* with PGA-CONH-Doxy (51). Non-treated mice with FAP disease were used as positive controls as well as healthy mice as negative ones.

detailed in TABLE V. 8. When assay was finished, mice were sacrificed and organs (TABLE V. 9) were excised and processed for further analysis.

ORGANS
skin, heart, lung, salivary glands, tongue, eye
liver, intestine (I1, I2, I3, I4), oesophagus
kidney, spleen, pancreas, muscle w/nerve, brain, testis/uterus
9 DRGs, sciatic nerve

TABLE V. 9 Organs dissected from mice in the activity study.

Immunohistochemistry (IHC) studies of the organs from the treated mice

TTR non-fibrillar deposits (lacking the characteristic of Congo red birefringence) trigger apoptosis as well as activate oxidation pathways. Several biomarkers have been associated with TTR deposition, namely ER stress markers BiP and P-eIF2α, the Fas death receptor and oxidation products such as 3-nitrotyrosine [11]. Briefly, Fas plays a key role in apoptotic cell death regulation (induced in this assay by the non-fibrillar TTR). Fas is a tumour-necrosis receptor that binds the Fas ligand resulting in death-inducing signalling complex ending in the apoptosis cascade. BiP is a molecular chaperon synthesised in higher levels when protein folding is disturbed. Then, the process is directly related to cell stress. When TTR is present, levels of these markers increase. On the contrary, a treatment reducing TTR toxic aggregates will produce a significantly reducing rate on them.

Firstly, TTR-non fibrillar deposition in the extracted tissues was evaluated by IHC analysis. FIGURE V. 45(A/B) compiles the results of the experiment. Unexpectedly, control animals presented lower amount of TTR than treated animals. Therefore, controls were discharged and comparisons between the groups receiving treatment were done.

(A)

Oesophagus

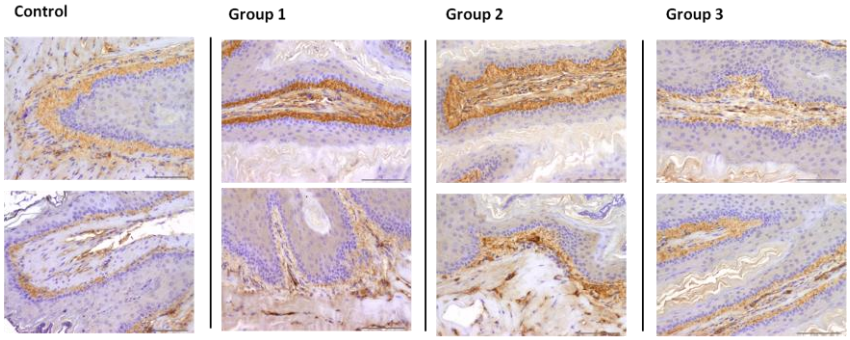

Stomach

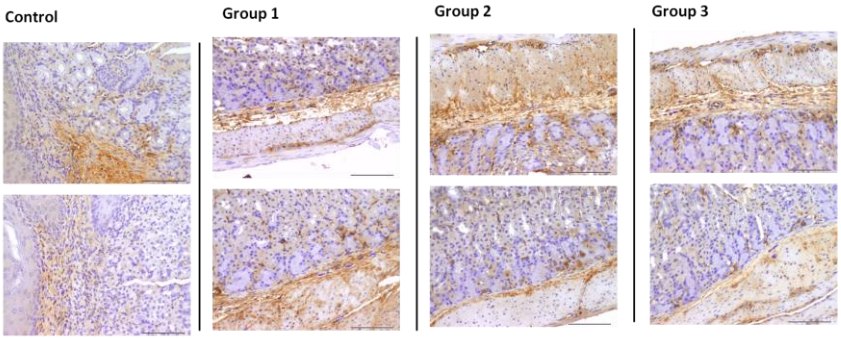

Liver

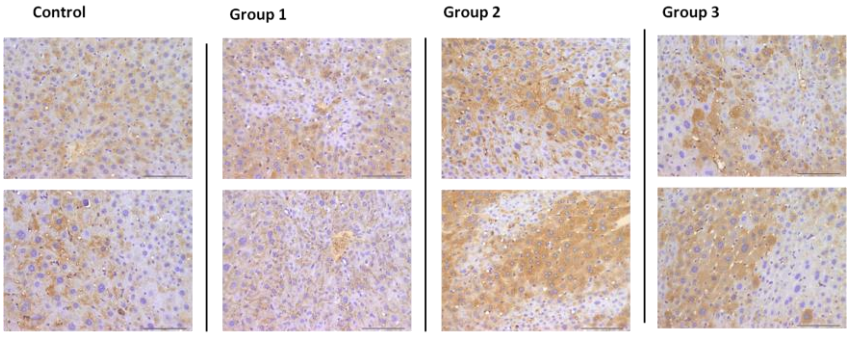

(B)

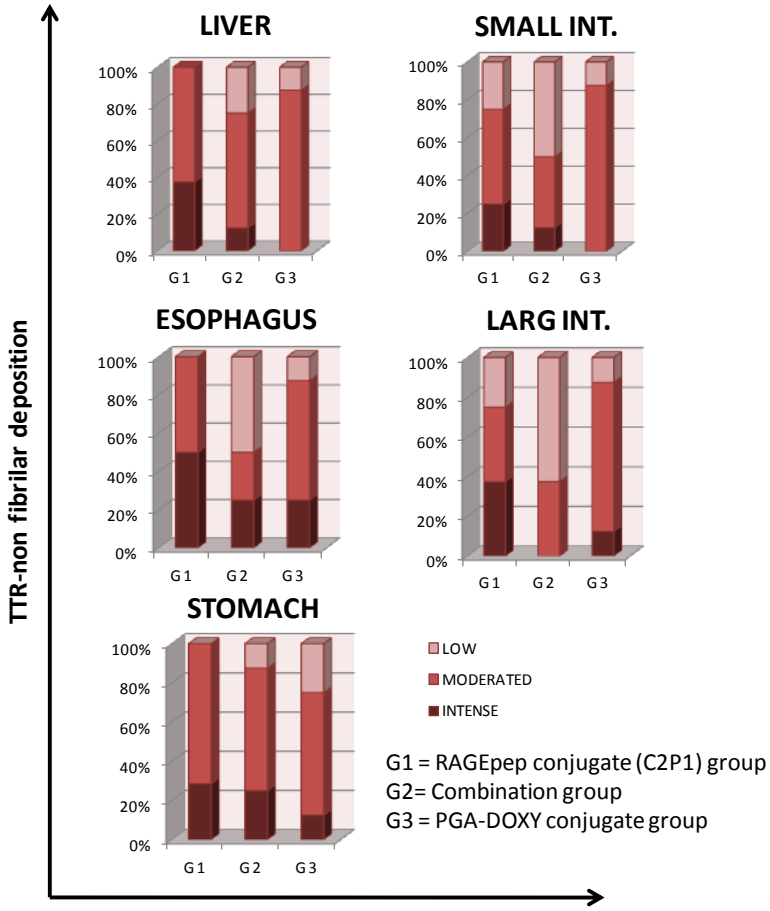

FIGURE V. 45 Non-fibrillar TTR deposition immunochemistry study in organs (oesophagus, stomach and liver) of the treated animals. (A) Representative immunohistochemistry analysis of TTR, (B) Semi-quantitative representation of the results. INT.=intestine

In the FAP animal model used, the gastrointestinal (GI) tract is the most affected organ regarding fibrillar deposition. Immunohistochemistry results (FIGURE V. 45(B)) showed similar outcomes although combination group result in lower deposition compared with C2P1 group or PGA-Doxy alone in small intestine, large intestine, and oesophagus.

IHC assays of Fas and BiP did not produce any profitable result.

All groups corresponding to treated animals had the same pattern than control animals with disease. However, representing a semi-quantitative graphic (FIGURE V. 46(B)) of BiP analysis it can be figured out that again lower amount is detected in the combination group in organs like large intestine and oesophagus. Stomach depicture was similar than PGA-Doxy group. Small intestine data cannot be used for conclusions due to the absence of good controls.

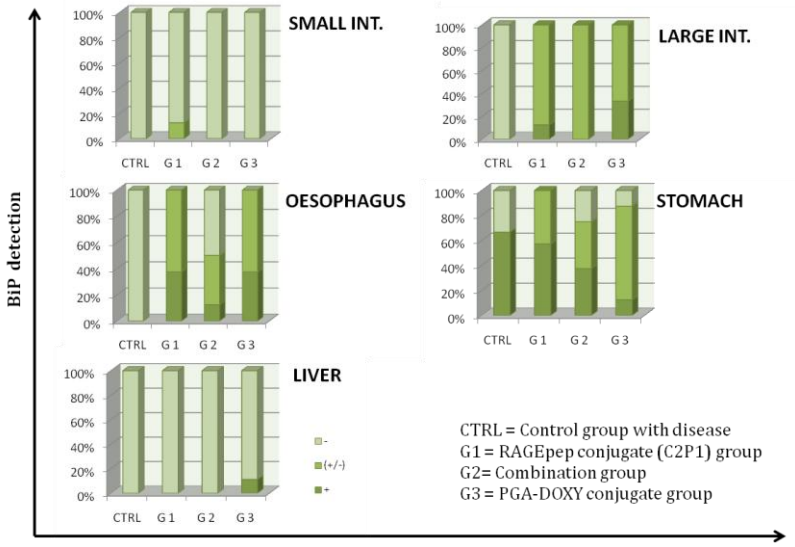

FIGURE V. 46 Immunohistochemistry analysis of BiP. Semi-quantitative representations of the antibody detection assay.

From preliminary experiment it can be deduced that possibly the dosage use for C2P1 was not sufficient to observe disease regression and a dose study should be performed. Possible synergism of PEG-RAGEpep and PGA-Doxy is not discharged, for a determinant confirmation the *in vivo* study should be performed with older mice as explained above.

Histological analysis of the organs from the treated mice

Besides IHC, organ slices were also evaluated trying to find any possible indicator of toxicity induced by these deposits in presence or absence of conjugate(s) treatment. Histological analysis enables a better assessment of severe damage. Paraffin-embedded sections were stained with haematoxylin/eosin solution (H&E). H&E-stained

slice sections were thoroughly examined under low (25× and 50×) and medium (100× and 200×) magnification. This study was performed by our collaborator Amparo Ruiz, from the Pathology Department, University of Valencia. Organs analysed were liver, small and large intestine, kidneys and liver in all animal groups (TABLE V. 10). Organs include in the gastrointestinal path were analysed due to TTR deposition and the rest due to the conjugate excretion routes.

GROUP 1	Group treated with C2P1 (PEP1-PEG-PEP1)
GROUP 2	Group treated with compound C2P1 + PGA-Doxy (17ωt%)
GROUP 3	Group treated with compound PGA-Doxy (43ωt%)
GROUP 4	Group control (with disease)
GROUP 5	Group control without disease

TABLE V. 10 Description of the animal groups used for the in vivo activity study.

Following examination, stained slices from all groups and organs showed a normal morphology with non toxic evidences due to the treatments. An exception was found for the livers from *group 4* (control group with disease), where focal necrosis, moderate inflammatory infiltrate and vascular congestion was observed. FIGURE V. 47 illustrates some of the results of the experiment. Kidney conclusions were excluded from the study because animal sacrificing methodology destroyed this tissue impeding a proper analysis.

Summarising, the findings indicate that treated animals did not show toxicity attributed to the administered conjugates, alone or in combination. Furthermore, all animals treated showed more normal patterns for liver regarding tissue morphology than the disease control animals, a possible indicator of a good performance of the conjugates as liver protectants. As mentioned above, liver is not affected by TTR deposits, however, it is the main producer of the protein.

Liver

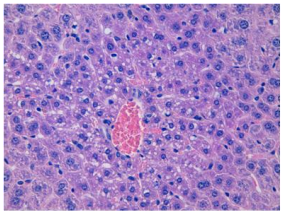

Group 1

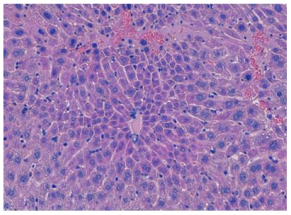

Group 2

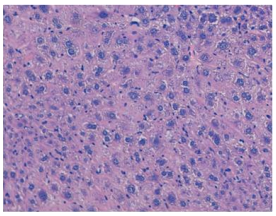

Group 3

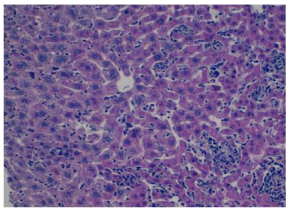

Group 4

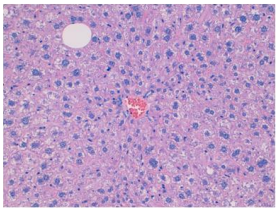

Group 5

Small intestine (I1)

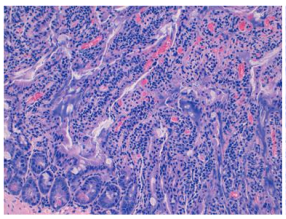

Group 1

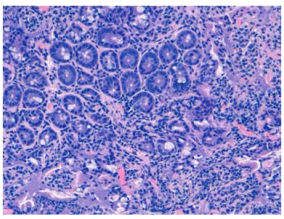

Group 2

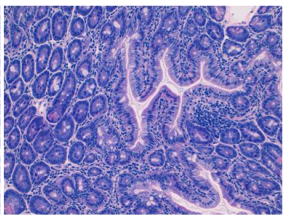

Group 3

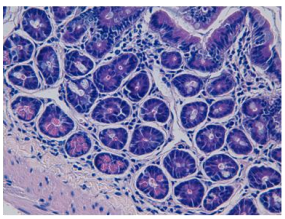

Group 4

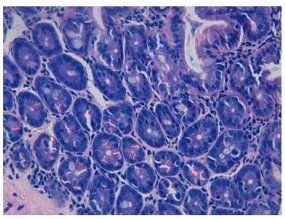

Group 5

Large Intestine (I4)

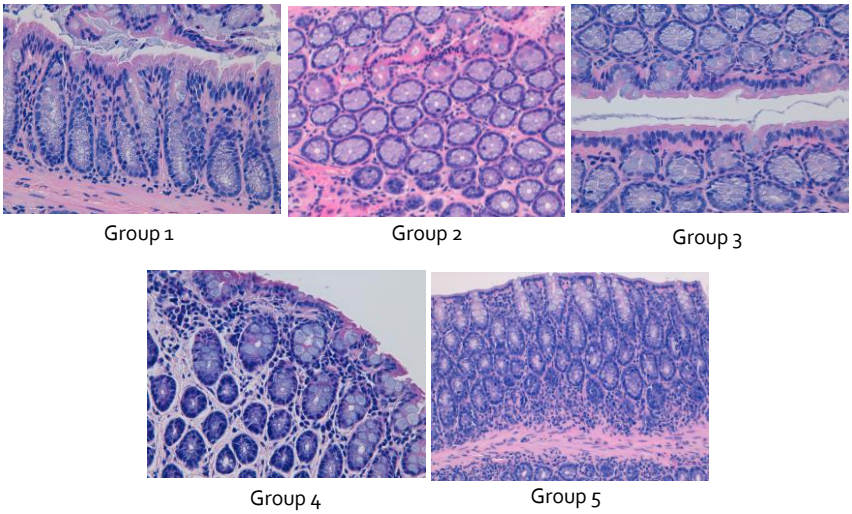

FIGURE V. 47 Examples of histology images (H&E staining) from sliced and fixed organs (liver, small and large intestine).

V. 2 CONCLUSIONS

In this chapter, polymer-drug conjugates for the treatment of FAP, an inherited rare amyloidosis, had been proposed for the first time in the area. Two bioactive molecules with recognised therapeutic properties: the low MW antibiotic drug doxycycline [10, 11, 38, 52, 53] and a novel peptide sequence derived from the original RAGE peptide [9] were conjugated to polymeric carriers. In this neuropathic disease, PNS is the main target and therefore BBB crossing was not the main issue for our PDCs although it will be an extra advantage in case this tissue was affected.

In relation to biological environment in which the PDCs will exert their action, polymer-drug linkage may confer certain capabilities for drug activity. In our case, both drugs act extracellularly therefore no intracellular internalisation was required. To investigate if drug efficacy required release from the polymer, biodegradable and non-biodegradable covalent bonds were studied.

Doxycycline conjugates

Doxycycline target are the fibrillar deposits. It disrupts these formations and decreases their associated standard markers. PGA was chosen as the polymer carrier. Besides conferring the benefits of polymer-drug conjugation (section I.2.4.2) and the well-known characteristics of the PGA itself, main purpose was to obtain a nanoconjugate capable to enhance TTRagg disruption.

A library of conjugates with 2 to 60ωt% drug loading was synthesised and characterised, linking the drug directly through ester and amide bonds or by means of a dipeptide spacer. Screening their activity as fibril disrupters, PGA-CONH-Doxy conjugates with 15 and 30ωt% demonstrated the highest response, they not only maintained the original activity but also enhanced at equal free drug concentration. This characteristic may influence in latter treatments improving the therapeutic value of the drug.

To justify the better output of a more stable linker (the amide),

physico-chemical studies were performed. Conformational studies by SANS and DLS revealed that differences on ωt% did not significantly influence the polymer conformation, which will ratify the similar activity observed *in vitro* with the named conjugates. However, significant differences were observed when compared with the parent PGA polymer.

Concerning linker stability, the designed conjugates tackle with biological surroundings as blood *(in vivo)* or cell media *(in vitro*). Covalent union between polymer and drug must remain stable until target arrival. By reproducing the conditions used for the *in vitro* test, drug release evaluation by LCMS and HPLC resulted in no drug release in the amide conjugates while ester-bearing conjugates did. Consequently, it was confirmed that for TTR fibril disruption there was no need for drug release in order to induce activity. Finally, PGA-X-Doxy conjugates were not haemolytic and were stable after plasma incubation, which confirmed the stability of the linkage and their suitability for i.v. administration.

With the selected candidate, biodistribution experiments were performed through optical imaging and PET techniques. From both studies, data showed a clear renal elimination of the conjugate and a non-specific accumulation in any organ, which confirmed the suitability of the carrier for the purposed objective. Any accumulation in an undesired organ or a marked secretion through the hepatic route will entail side effects. The radioactive labelled conjugate had a $t_{1/2}$ of 0.98h. Compared to the PGA study ($t_{1/2}$=0.59h), it can be concluded that the higher size of the conjugate in solution ends in a longer residence into the body.

RAGE peptide conjugates

In early stages of the disease, TTR aggregates trigger cell death. Then, in the advanced phase they coexists with TTR-fibrils [11]. For that reason, a drug focused on these species was proposed to be administered in combination with doxy: the RAGE peptide.

PEG is the most known polymer carrier for protein and

peptide. This semitelequelic carrier offers, among other advantages, protection against proteolytic degradation enhancing the $t_{1/2}$ in blood circulation and therefore increasing their activity.

With a parallel reasoning than in doxy conjugation, RAGEpep was derivatised for testing if drug release was required for exert its activity. Amide and disulphide linkages were selected, entailing original peptide derivatisation. A set of conjugates was synthesised and characterised. Studying their conformation in solution, DLS analysis determined critic differences among the conjugate C2P2 and the rest, confirming that linkage and number of conjugated peptide moieties could influence on conformation adopted in solution. Disulphide conjugates showed peptide release when they were subjected to *in vitro* and *in vivo* scenarios while amide ones remained stable. Additionally, amide conjugate did not show haemolytic activity. It is worthy to remark that RAGEpep or its derivatives were insoluble in plasma, even in presence of common solubilisers, pointing out that PEGylation confers the mayor advantage towards the therapeutical approach. Following with the ideal path, target recognising was the next stage. Maintenance of original peptide binding capability was tested through Surface Plasmon Resonance (SPR). All peptides and conjugates, except C2P2, bind TTR with different K_D values, therefore recognising the protein. PEGylation was not affecting to the capability of binding the TTR aggregates. .

In their *in vitro* evaluation, peptide derivatives demonstrated to retain RAGEpep activity and the conjugate C2P1 displayed the best inhibition of TTR-agg cytotoxicity at both time points. Disulphide bond conjugates results lead to less reproducible data and lower activity, remarkably in the case of C2P2. These results confirmed that a more stable polymer-peptide linker could be required in order to allow TTRagg binding and prevent cytotoxicity, as well as a stable conformation in solution where possibly exists higher peptide availability improving conjugate activity.

In conclusion, PEG-RAGEpep conjugates containing amide

linkers have greatest potential for further development as FAP inhibitors. Moreover, this novel conjugate has potential as a FAP therapeutic to be used alone in the early stages of the disease or as part of rationally designed combination therapy.

Combination therapy

One of our aims pursued the combination treatment merging the best conjugates of each family: PGA-CONH-Doxy and C2P1. As a preliminary study an *in vivo* activity experiment was carried out in an FAP mice model, in which the gastrointestinal tract is the principal system affected. Animals in early stages of the disease (9-11months) were used as the ideal model for the RAGEpep conjugates. This peptide has not been evaluated *in vivo*, mainly due to the problems associated with these small molecules which are overcome after polymer conjugation. As a complementary test, it was decided to test simultaneously the possible effects of PGA-Doxy in this model.

The animals were classified in three groups: *Group 1* was treated with the conjugate C2P1, *group 2* (combination group): C2P1 and PGA-CONH-Doxy and *group 3* with PGA-CONH-Doxy. Non-treated mice with FAP disease were used as positive controls as well as healthy mice as negative control. After the treatment period (6weeks, 2doses per week), animals were sacrificed and organs were evaluated.

First analysis was performed by immunohistochemistry, investigating known markers of the TTR deposition. TTR-non fibrillar deposition in control animals was lower than in the rest of groups, complicating results interpretation. When treated groups were compared, lower deposition was found in the combination group when compared with the individual conjugates in small and large intestine, and esophagus. Other molecular markers did not arise to profitable conclusions due to non differences among the treated groups was obtained. These outcomes can conclude that RAGEpep conjugate dose should be optimised to promote reliable activity and that possible synergism with doxy may be found in an appropriate mice model (old animals).

Secondly, organ toxicity evaluation of the administered conjugates was performed. Liver and kidneys were reviewed due to their implication in the secretion routes of PDCs; and small/large intestine for their implication in TTR deposition. By means of histological analysis, results highlighted that all groups of animals presented a typical morphology structure without toxic evidences induced by the treatments, corroborating the safety of the PDCs. The observed liver morphological recovery in treated animals suggested a possible role of the conjugates as liver protectants. As mention above, liver is not affected by TTR deposits, however, it is the main producer of the protein. Reasons for this achievement had not been clarified.

Future directions will encompass a proper test *in vivo* within an old FAP model of our conjugates with an optimisation test of the most appropriate dose. We really encourage the use of combination at this stage due to their target molecules coexist at advanced phases. Moreover, we firmly proposed the use per separate of pegylated RAGE peptide conjugate C2P1 in early stages of the disease or the PGA-CONH-Doxy alone in advanced ones. To define the best combination conjugate (both agents in the same polymer matrix or conjugated into different polymers), extra combinations studies may be carried out either *in vitro* and *in vivo*. As targets can be located in different parts of the extracellular emplacement, it can be suggested that conjugates per separate will display the best output.

V. 3 MATERIALS AND METHODS

V. 3. 1 SYNTHESIS AND CHARACTERISATION OF THE POLYMER-DRUG CONJUGATES

V. 3. 1. 1 Derivatisation procedure of doxycycline (doxy-NH_2)

The general derivation procedure of doxycycline which results in doxy-NH_2 obtaining (**49**) is depicted in FIGURE V. 48.

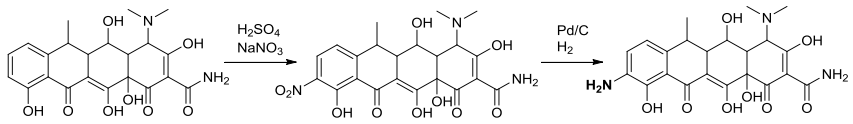

FIGURE V. 48 Synthesis of the amino derivated doxycycline (doxy-NH_2).

Doxycycline hydrochloride (0.5000g, 512.94g/mol) was slowly added to concentrated H_2SO_4 (1.75mL). After gas evolution had stopped, the orange solution was slowly precipitated into 100mL of cooled diethyl ether in an ice bath. The hydrosulphate salt was collected by filtration, washed with ether and dried under N_2 flow. The orange powder (542.12g/mol) was redissolved in H_2SO_4 (5mL), cooled to 0°C and $NaNO_3$ (1.56eq, 101mg, 84.99g/mol) was added over 10min while the reaction was stirring. After 3h at 0°C, reaction was directly precipitated into 200mL of cool diethyl ether and the mixture was filtered under vacuum. The precipitate was washed with ether and air-dried to give an orange powder which was used without further purification. ^{1}H-NMR (MeOD) analysis was carried out. Nitration can occur in two different positions (orto-(C9) and para-(C7) positions respect to the hydroxyl group. C9 is occurring preferably. Crude product (0.3634g) was dissolved in 5mL of MeOH and 10%Pd/C (25mg) was added. The system was purged with H_2 and left under H_2 pressure. Reaction was stirred for 2h. After filtration of the catalyst through celite, the solution was diluted with 7.5mL of MeOH and precipitated in 100mL of cold diethyl ether. Solvent was removed after centrifugation (8000rpm, 4°C, 5min) and pouring off the ether. Orange solid was dried under nitrogen flow and ^{1}H-NMR (MeOD) and MS-MALDI TOF analysis were carried out (FIGURE V. 49).

(A)

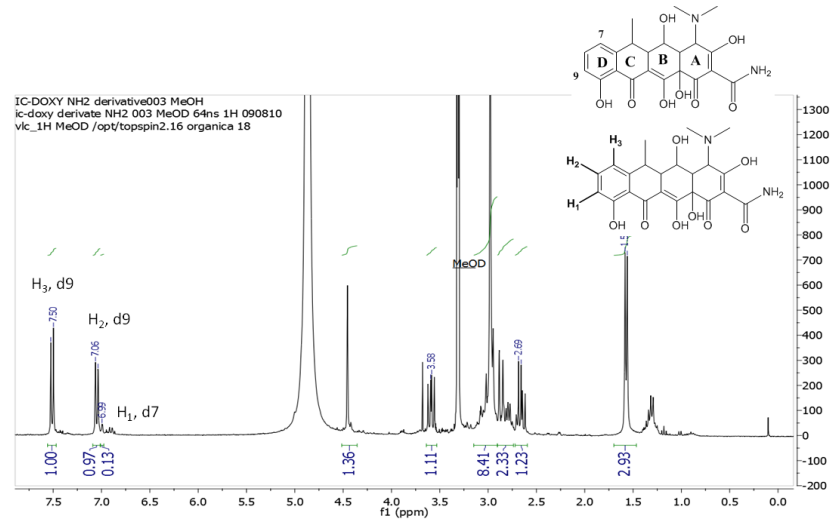

(B)

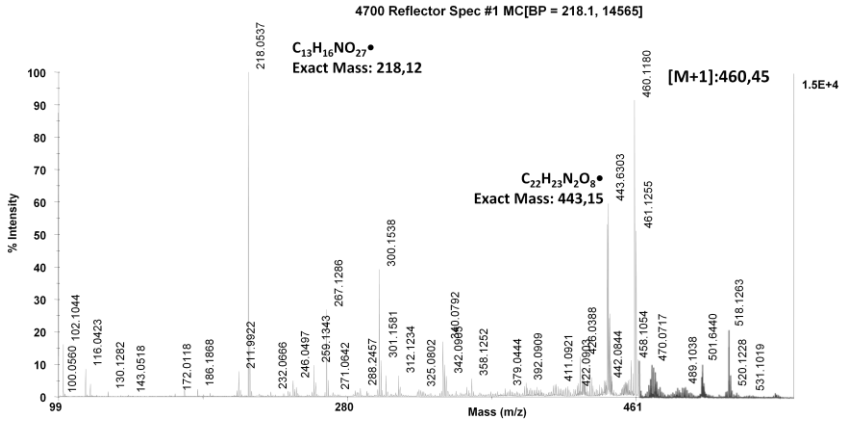

FIGURE V. 49 Characterisation of the amino-derivatised doxycycline (doxy-NH_2). by (A) NMR-^{1}H (300Hz, MeOD), (B) MS-MALDI TOF analysis.

Yield: 70% (derivate in C9 80%). ^{1}H-NMR (300 MHz, MeOD) derivate in C9 δ 7.57ppm (d, *J*=8.3 Hz, 1H), 7.06ppm (d, *J*=8.4 Hz, 1H), derivate in C7 δ 7.15ppm (s, 1H). MS analysis: [M+1]=460.1180g/mol.

V. 3. 1. 2 Doxy hydrolytical stability

15mg of doxy (0.029mmol) were dissolved in 500µL D_2O under acid (TFA) or basic (NaOH 6M) conditions. 1H-NMR analysis were performed (Bruker 300 MHz, 64ns, appendix III). Signals in acidic environment were not altered after 37h but in presence of base new

signals were observed and also yellow colour changed to dark brown.

V. 3. 1. 3 Synthesis of PGA-X-Doxy conjugates

General method for doxycycline conjugation through ester linkage (PGA-COO-Doxy)

The general synthesis of PGA-COO-Doxy conjugate (**50**) is depicted in FIGURE V. 50.

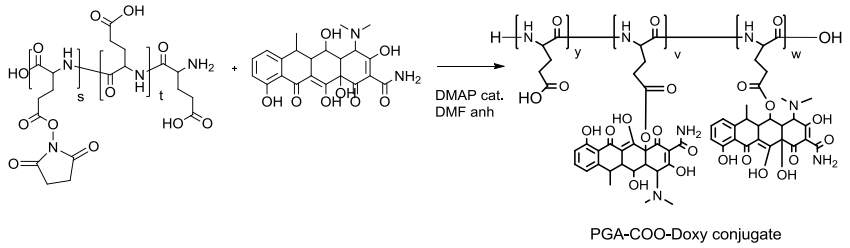

FIGURE V. 50 Synthesis of PGA-COO-Doxy conjugate.

Briefly, carboxyl groups of PGA were previously activated with N-hydroxysuccinimide. PGA-NHS (average MW unit of glutamic acid=179.6g/mol) was added to a round bottom flask and dissolved in anhydrous DMF under N_2 atmosphere. Separately, the corresponding amount for the desired molar percentage of doxy (see TABLE V. 11), 512.94g/mol) was dissolved in the same conditions and dropped in the PGA-NHS solution. Next, a catalytic amount of DMAP was incorporated and pH was adjusted to 8 with DIEA. After 12-16h under agitation at room temperature, DMF was evaporated under high vacuum until product was dried. Non-reacted drug as well as reaction organic soluble subproducts were removed by washing the crude with a mixture of $CHCl_3$:acetone (4:1) and placed in ice for 30min. Thereafter, solvent was removed by centrifugation and the solid residue was dried under vacuum. After obtaining the polymer conjugate salt form ($NaHCO_3$ 1M), crude was purified by SEC chromatography (Sephadex^{TM} G-25 / G-10; ddH_2O as eluent). Fractions were analysed by HPLC/GPC techniques (UV, λ=273nm), t_R=12min. Method: isocratic gradient with PBS 0.1M pH=7.4 as mobile phase, flow rate=1mL/min, 50min (FIGURE V. 6). Fractions containing the conjugate were mixed and after

lyophilisation, compound was characterised as detailed in section V.3.2.1.

Note: varying doxycycline equivalents, different ωt% loadings were achieved (TABLE V. 11).

	Carboxyl activation method	MW GA unit	mmol PGA	Reaction conditions	$\%mol_{theo}$ doxy	Drug	mmol	%ωt doxy	%mol*	Yield (%)
PGA-NHS	NHS/DMAP	52%mol NHS, 179.6g/mol	0.29	anh. DMF, pH=8	15	Doxy	0.044	26	9.3	90
PGA-NHS	NHS/DMAP	46.5%mol NHS, 164.4g/mol	3.86	anh. DMF, pH=8	5	Doxy-NH_2	0.193	18	6.4	92
PGA-NHS	NHS/DMAP	20%mol NHS, 148.6g/mol	0.24	anh. DMF, pH=8	22	Doxy-NH_2	0.054	35	12.5	55
PGA (acid form)	DIC/HOBt	129.1g/mol	0.23	0.35mmol DIC/HOBt, anh. DMF, pH=8	15	Doxy-NH_2	0.0345	15	5.4	50
PGA (salt form)	DMTMM·Cl	129.1g/mol	0.39	0.12mmol DMTMM (for a 30%act.), ddH_2O pH=7	10	Doxy-NH_2	0.12	10	3.5	40
PGA (acid form)	DMTMM·BF_4	129.1g/mol	0.11	0.025mmol DMTMM (for a 30%act.), anh. DMF pH=8	10	Doxy-LG-NH_2	0.008	9	3.2	51

TABLE V. 11 Representative reaction conditions for doxy conjugation. (*)=estimated.

Methodology for Doxy-NH_2 conjugation through amide linkage (PGA-CONH-Doxy)

The general synthesis of PGA-CONH-Doxy conjugate (**51**) is depicted in figure below.

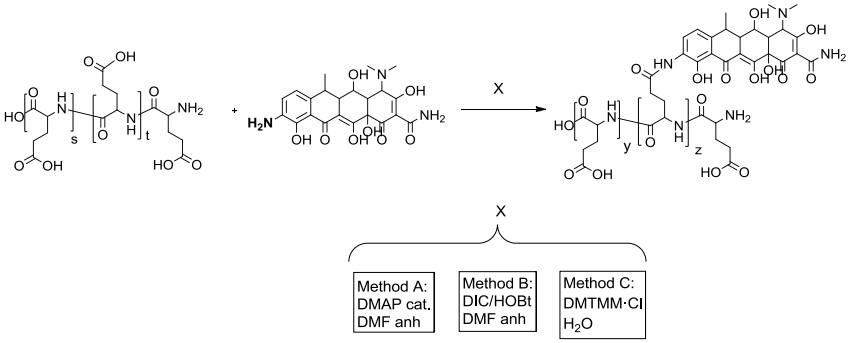

FIGURE V. 51 Synthesis of PGA-CONH-Doxy.

Method A: NHS,DMAP

Previous activated PGA (PGA-NHS, 52%mol activation, average MW unit of glutamic acid=179.6g/mol) was added to a round bottom flask and dissolved in anhydrous DMF under N_2 atmosphere. Separately, doxy-NH_2 (**49**) (see TABLE V. 11, 557.13g/mol) was dissolved in the same conditions. Once dissolved, doxy-NH_2 was dropped in the solution of PGA-NHS. Next, a catalytic amount of DMAP was added and pH was adjusted to 8 with DIEA. After 5h under agitation at room temperature, DMF was evaporated under high vacuum until product was dried. Non-reacted drug and the reaction organic soluble subproducts were removed by washing the crude with a mixture of $CHCl_3$:acetone (4:1) and placed in ice for 30min. Thereafter, solvent was removed by centrifugation and the solid residue was dried under vacuum. After obtaining the polymer conjugate salt form ($NaHCO_3$ 1M), crude was purified by SEC chromatography (Sephadex^{TM} G-25 / G-10; ddH_2O as eluent). Fractions were analysed by HPLC/GPC techniques (UV, λ=273nm), t_R=12min. Method: isocratic gradient with PBS 0.1M pH=7.4 as mobile phase, flow rate=1mL/min, 50min (FIGURE V. 6). Fractions containing the conjugate were mixed and after lyophilisation, compound was characterised as detailed in section V.3.2.1.

Note: varying doxycycline equivalents, different ωt% loadings were achieved (TABLE V. 11).

Method B: DIC/HOBt

PGA (average MW unit of glutamic acid=129.1/mol) was added to a round bottom flask and dissolved in anhydrous DMF under N_2 atmosphere. Depending on the molar percentage of drug loading, reagents amount was varied. Next protocol is detailed for 15%mol. DIC (0.035mmol, 1.5eq per carboxyl group, 0.836g/cm^3, 126.20g/mol) was added to the reaction and after 5min, HOBt (0.035mmol, 1.5eq per carboxyl group, 135.10g/mol) was incorporated as a solid. 10min later, doxy-NH_2 (**49**) (0.035mmol, 557.13g/mol) dissolved in anhydrous DMF was dropped to the reaction. pH was adjusted to 8 with DIEA. After 12-16h under agitation at room temperature, DMF was evaporated under high vacuum until product was dried. Non-reacted drug as well as reaction organic soluble subproducts were removed by washing the crude with a mixture of $CHCl_3$:acetone (4:1) and placed in ice for 30min. Thereafter, solvent was removed by centrifugation and the solid residue was dried under vacuum. After obtaining the polymer conjugate salt form ($NaHCO_3$ 1M), crude was purified by SEC chromatography (Sephadex^{TM} G-25 / G-10; ddH_2O as eluent). Fractions were analysed by HPLC/GPC techniques (UV, λ=273nm). t_R=12min. Method: isocratic gradient with PBS 0.1M pH=7.4 as mobile phase, flow rate=1mL/min, 50min (FIGURE V. 6). Fractions containing the conjugate were mixed and after lyophilisation, compound was characterised as detailed in section V.3.2.1.

Note: varying doxycycline equivalents, different ωt% loadings were achieved (TABLE V. 11).

TABLE V. 11

Method C: DMTMM coupling

Previously, sodium salt form of PGA (0.66mmol, MW unit of glutamic acid=151g/mol) was placed in a round bottom flask and dissolved in ddH_2O. For 30% carboxyl activation and 15%mol doxy loading: Separately, doxy-NH_2 (**49**) (0.2mmol, 557.53g/mol) and DMTMM·Cl (0.2mmol, 276.77g/mol)) were dissolved in also ddH_2O and then added to the flask. The reaction pH was 8. Reaction was left

under agitation 24h at room temperature and protected from light. Then, product was dried by lyophilisation and purified by SEC chromatography (Sephadex^{TM} G-25 / G-10; ddH_2O as eluent). Fractions were analysed by HPLC/GPC techniques (UV, λ=273nm), t_R=12min. Method: isocratic gradient with PBS 0.1M pH=7.4 as mobile phase, flow rate=1mL/min, 50min (FIGURE V. 6). Fractions containing the conjugate were mixed and after lyophilisation, compound was characterised as detailed in section V.3.2.1.

Note: varying doxycycline equivalents, different ωt% loadings were achieved (TABLE V. 11).

Synthesis of PGA-CONH-AA-Doxy

The general synthesis of PGA-CONH-AA-Doxy conjugates (**52**) is depicted in FIGURE V. 52.

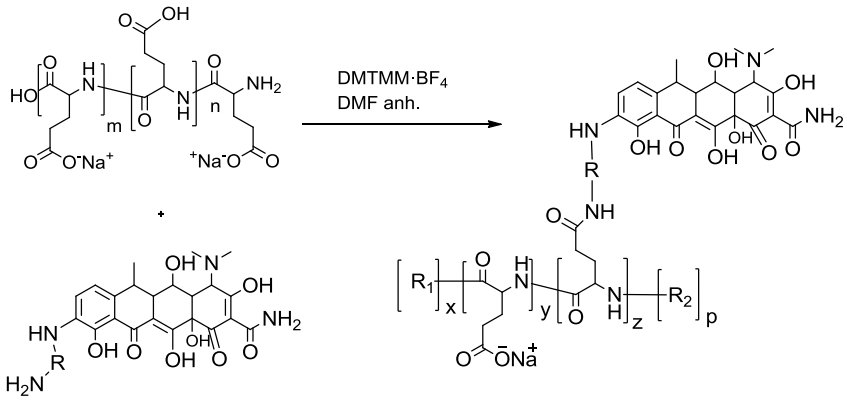

FIGURE V. 52 Synthesis scheme of PGA-CONH-AA-Doxy conjugates.

First, the amino-protected peptidil linker (Gly-Gly or Leu-Gly) was first linked to the drug, then deprotected and finally conjugated through an amide bond to the polymeric carrier.

*Synthesis of Leu-Gly-NH-Doxy (**54**)*

Z-Leu-Gly-OH (**53**) (0.064mmol, 322.36g/mol) was added to a round bottom flask and dissolved in 0.5mL anhydrous DMF under N_2 atm. and continuous agitation. Afterwards, DMTMM·BF_4 (0.07mmol, 1.1eq, 328.07g/mol) was added dissolved in 0.5mL of anhydrous DMF. After 10minutes, doxy-NH_2 (0.014mmol, 2.2eq, 557.13g/mol) was

added dissolved in 2mL of anhydrous DMF. pH was checked to be 8. The reaction was allowed to proceed for 14h stirring at room temperature and protected from light. After this, solvent was removed under vacuum and residue was washed several times with 2mL of ddH_2O through centrifugation (4°C, 4000rpm, 10min). Supernatant was collected and lyophilised. The solid obtained (28.3mg) was analysed by ^{1}H-NMR and afterwards it was dissolved in 5mL of MeOH for proceeding to remove the protecting group of the amino acid sequence. The solution was placed in a round bottom flask fitted with a septum and a stirring bar. Then, a catalytic amount of $Pd(OH)_2$ Charcoal was added and the flask was purged with N_2 to remove the air and later flask was purged with H_2. Reaction was left stirring for 12h under H_2 pressure. Afterwards, reaction was filtered though a celite column and precipitated over cold diethyl ether. Ether was removed by centrifugation and the gel obtained was dried over vacuum.

Yield: 70%. ^{1}H-NMR Doxy-NH-Gly-Leu-Z (300 MHz, MeOD) δ 7.64(m, 1H, C8 Doxy-NH-), 7.40 – 7.08 (m, 5H+1H C7 Doxy-NH-), 5.19 – 4.93 (m, 2H), 4.14 (dd, *J*=9.5, 5.3 Hz, 3H), 4.02 – 3.63 (m, 3H), 1.80 – 1.41 (m, 3H), 0.88 (t, *J*=6.5 Hz, 6H),etc. MS analysis Doxy-NH-Gly-Leu (deprotected): [M+1]=673.26g/mol

*Synthesis of Gly-Gly-Doxy (**56**)*

Z-Gly-Gly-OH (**55**) (0.079mmol, 266.25/mol) was added to a round bottom flask and dissolved in 0.5mL anhydrous DMF under N_2 atm. and continuous agitation. Afterwards, DMTMM·BF_4 (0.087mmol, 1.1eq, 328.07g/mol was added dissolved in 0.5mL of anhydrous DMF. After 10minutes, doxy-NH_2 (0.18mmol, 2.2eq, 557.13g/mol) was added dissolved in 2mL of anhydrous DMF. pH was checked to be 8. The reaction was allowed to proceed for 14h stirring at room temperature and protected from light. After this, solvent was removed under vacuum and residue was washed several times with 2mL of ddH_2O through centrifugation (4°C, 4000rpm, 10min). Supernatant was collected and lyophilised. The solid obtained (27.1mg) was analysed by ^{1}H-NMR and afterwards it was dissolved in 5mL of MeOH for proceeding to remove the protecting group of the amino acid

sequence. The solution was placed in a round bottom flask fitted with a septum and a stirring bar. Then, a catalytic amount of $Pd(OH)_2$ Charcoal was added and the flask was purged with N_2 to remove the air and later flask was purged with H_2. Reaction was left stirring for 12h under H_2 pressure. Afterwards, reaction was filtered through a celite column and precipitated over cold diethyl ether. Ether was removed by centrifugation and the gel obtained was dried over vacuum.

Yield: 70%. ^{1}H-NMR Doxy-NH-Gly-Gly-Z (300 MHz, MeOD) δ 7.64(m, 1H, C8 Doxy-NH-), 7.26 (5H+1H C7 Doxy-NH-), 4.96 (s, 2H), 3.69 (d, 2H), 3.57 (2H), etc. MS analysis Doxy-NH-Gly-Gly (deprotected): [M+1]=617.20g/mol.

Synthesis of PGA-CONH-AA-DOXY

PGA (1 eq, 0.4mmol unit of glutamic acid, 129g/mol) was placed in a round bottom flask and dissolved in anhydrous DMF (5mL) under agitation and N_2 atmosphere. Carboxyl pendant groups were activated with DMTMM·BF_4 (i.e. for a 30% activation, 0.06mmol, 328.07g/mol), which were added to main reaction previously dissolved in anh. DMF. After 10min, AA-doxy-NH_2 was added already dissolved in anh. DMF (used equivalents depended on desired molar drug percentage. In all cases, doxy derivate equivalents were double than DMTMM eq.) pH was assessed to be 8. Reaction was left under agitation for 24h protected from light at room temperature. Afterwards, solvent was removed by evaporation and residue was washed with acetone at 4°C. After remove the supernatant by centrifugation, solid product was dried. Polymer conjugate salt form was obtained ($NaHCO_3$ 1M), crude was purified by SEC chromatography (Sephadex^{TM} G-25 / G-10; ddH_2O as eluent). Fractions were analysed by HPLC/GPC techniques (UV, λ=273nm), t_R=12min. Method: isocratic gradient with PBS 0.1M pH=7.4 as mobile phase, flow rate=1mL/min, 50min. Fractions containing the conjugate were mixed and after lyophilisation, compound was characterised as detailed in section V.3.2.1.

Note: varying doxycycline equivalents, different ωt% loadings were achieved (TABLE V. 11).

Yield: 50%.

V. 3. 1. 3 Synthesis of RAGE peptide and its derivatives

General considerations about Solid Phase Peptide Synthesis (SPPS)

The solid-phase peptide synthesis (SPPS) was invented and developed by R.B. Merrifield [54], a simple and fast methodology for synthesising peptides and small protein sequences. Basically, SPPS concept is to attach covalently a growing peptide chain to an insoluble polymeric support by means of chemistry in solution. The anchored peptide is extended by serial deprotection/coupling cycles (FIGURE V. 53), which often are reproducible and result in high yields. Unlike the synthesis of peptides in solution, SPPS does not require intermediates purification since the amino acids and reagents are added in excess to drive the reactions to as to close to 100% completion as possible and the excess reagents are removed by filtration. Furthermore, reactions proceed at room temperature and only a prudent purification and characterisation is needed to verify product identity [55].

The polymeric support (resin) is selected regarding its mechanical stability, physicochemical characteristics and swollen properties and the appropriate functional groups onto which the first amino acid can be anchored. Regarding the chemistry design, attention may be paid in protection of the groups of the amino acid. Once a residue has been incorporated to the resin-bound peptide chain, it may still undergo irreversible structural modification or rearrangement during next synthetic steps.

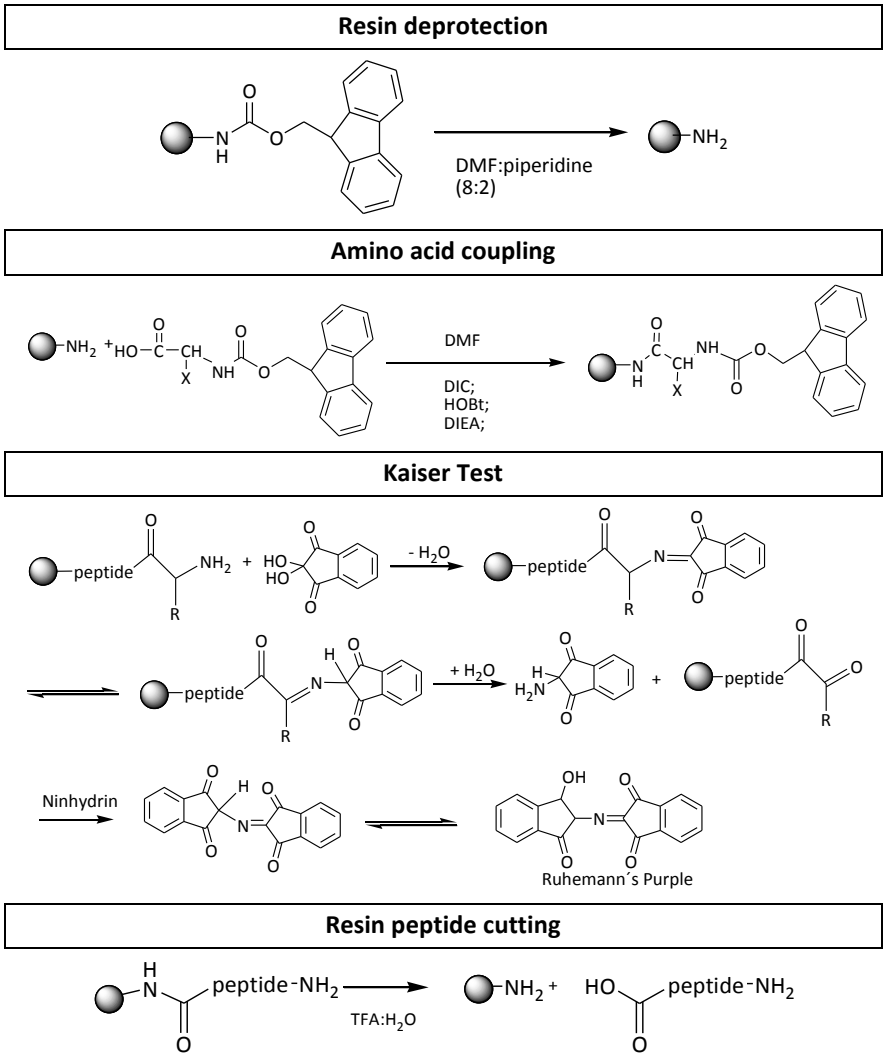

FIGURE V. 53 Synthetic scheme for Fmoc-based SPPS.

Two levels of protecting group stability are needed: groups which must remain “permanent” to prevent branching or similar problems on the side-chains and “temporary” groups able to be removed to allow for continuing the amino acid coupling. Orthogonal schemes offer the possibility of substantially milder overall conditions, because selectivity can be attained on the basis of differences in chemistry rather than in reaction rates. There are two different

protection schemes for the temporary groups of the N^{α}-amino groups: Fmoc- and Boc- based SPPS. Comparing both, Fmoc technique is by far the more common approach since it does not require treatment with hazardous HF, which requires specialised equipment and training to cleave the peptide from the resin and it does not require harsh and repeated strong acid treatments[56]. In this thesis, Fmoc-SPPS has been the selected one for peptide synthesis. Fmoc group provides single hydrogen on the β-carbon very acidic, and therefore susceptible to be removed by weak bases like piperidine or piperazine. "Permanent" protection compatible groups within this methodology are ethers, ester, and urethane derivatives based on tert-butanol. Those derivatives are cleaved at once by use of TFA at RT [57].

Protocol

A polystyrene resin was used for Fmoc-solid phase synthesis (SPPS) of the RAGE peptide and its derivatives PEP1 (**57**) and PEP2 (**58**) (FIGURE V. 7). All synthetic procedures detailed below were carried out under an inert atmosphere and after each step the excess reagents were removed by filtration.

Fmoc-Rink-amide AM polystyrene resin (100-200mesh, loading: 0.63 mmol/g) was swelled with DMF (5 mL, 1 min x 3) and CH_2Cl_2 (3 x 5 mL x 1 min), and the Fmoc group was cleaved by treating with piperidine-DMF (1:4). Several washes were performed until complete deprotection was achieved. The absorbance of the collected solutions was measured to determine the percentage of the released Fmoc (UV Vis, λ=280nm, Ɛ=4950$M^{-1}cm^{-1}$). Afterwards, resin was washed (1min, 5mL DMF x 3; 2min, 5mL MeOH x 3, and 1min, 5mL of CH_2Cl_2).

Based on the loading, the protected amino acids were incorporated as follows. In a 10mL glass vial equipped with a stopper and a stirring bar, 4 equivalents of the corresponding amino acid (Fmoc-NH-AA-COOH) were dissolved in 4mL of anhydrous DMF under N_2 flow. Once dissolved, DIC (12eq, 0.836g/cm^3, 126.20g/mol) were added to the reaction and 5 minutes later, HOBt (12eq, 135.10g/mol)

were added. Reaction was left under agitation 10min and then the whole mixture was added to the resin and pH was adjusted to 8 with DIEA. Cleavage of the Fmoc group was achieved by treatment with piperidine:DMF (1:4). Washes between couplings and deprotections were performed with the same protocol detailed before.

Completeness of the amino acid coupling was tested with the Kaiser-test [58] (FIGURE V. 53). Intensive blue colour is generated by reaction of ninhydrin with free primary amines. This test can be used to monitor the presence of free amine after not complete coupling (dark blue colour) and the complete amino acid coupling (yellow colour) after the reaction. It involves the use of three solutions: (1) phenol, 80% in ethanol, (2) KCN in H2O/ pyridine, and (3) ninhydrin, 6% in ethanol. To a few well dried resin beads, three drops of each solution were added and then the mixture was heated for 5 minutes at 80°C. Colour of the solution determined the success or incompleteness of the amino acid coupling. In case of not full conversion, reaction was repeated decreasing the equivalents of all reagents.

The resin with the coupled peptide sequence was treated with TFA:H_2O (95:5,v/v) (3mL), left under agitation at 25 °C for 10h. Then, the solution obtained from the filtration was directly precipitated in cold t-butylmethylether (40mL). The resin was washed again with 2mL of TFA:H_2O (95:5,v/v) and precipitated in the same t-butylmethylether. The suspension was centrifuged for three times (at 2000rpm, 5min), and then re-dissolved in H_2O and lyophilised. Crude peptide was re-dissolved and purified by semi–preparative HPLC (LiChrocart®250–10, LiChrospher®100 RP–18 (10 µm), flow rate = 1 mL/min, solvent A: ddH_2O 0.1 %TFA, solvent B: ACN 0.1 %TFA; method: 0 min A 90 %, 5 min A 70 %, 10 min A 70 %, 25 min A 10 %, 30 min A 90 %, 35 min A 95 %; wavelength = 220nm). The fractions containing the purified product were pooled, lyophilised and their identity was confirmed by analysis with HPLC and MS MALDI TOF. The crude peptide was re-dissolved in milli–Q water and purified by semi–preparative HPLC with a gradient of 20–100% solvent B over 40 min. Results (purity and MW of each peptide) are summarised in
FIGURE V. 8.

V. 3. 1. 5 Synthesis of RAGE peptide conjugates

V. 3. 1. 5. 1 Synthesis of PEP1-PEG-PEP1 (C2P1)

The general synthesis of PEP1-PEG-PEP1 conjugate (**60**) is depicted in FIGURE V. 9. PEP1 describes the modified RAGE peptide illustrated in FIGURE V. 7, where in N-terminal point a glycine (Gly) was incorporated.

NHS-PEG-NHS (0.014mmol, 1eq, 3023g/mol) was dissolved in 4mL of anhydrous DMSO under inert atmosphere at RT. PEP1 (**57**) (0.03mmol, 2eq, 912.05g/mol) was dissolved under the same conditions in 4mL of anhydrous DMSO and dropped into the main solution. Afterwards, catalytic amount of DMAP was added and pH was adjusted to 8 with DIEA. Reaction was left under agitation and inert atmosphere for 48h. Then the solvent was removed under vacuum, and the residue obtained was dissolved in 1mL of ddH_2O and purified by FPLC (Macrocap SP column, flow rate=1mL/min, solvent A: ddH2O, solvent B: NaCl 1M; method t=0min, A 100% 60 min, gradient: 100% solvent B in 1500min, wavelength=215, 280nm). A typical chromatogram is shown in FIGURE V. 11. The fractions were collected; lyophilised and the solid residue was desalted by Ultrafiltration (Vivaspin® MWCO 2000g/mol). The product obtained was characterised by NMR (^{1}H, ^{13}C and COSY, D_2O) and MALDI-TOF analysis (FIGURE V. 23(A)).

Yield: 60%. ^{1}H NMR (300 MHz, D_2O) δ 6.96 (s, 8H), 6.68 (s, 8H), 3.58 (s, 275H). MS MALDI-TOF analysis: 4971g/mol.

V. 3. 1. 5. 2 mPEG-PEP1 (C1P1)

The general synthesis of mPEG-PEP1 conjugate (**61**) is depicted in FIGURE V. 9. PEP1 describes the modified RAGE peptide illustrated in FIGURE V. 7, where in N-terminal point a glycine (Gly) was incorporated.

mPEG-NHS (0.017mmol, 1eq, 3023g/mol) was dissolved in anhydrous DMSO under inert atmosphere at RT. PEP1 (**57**) (0.02mmol, 1.2eq, 912.05g/mol) was dissolved under the same conditions in

anhydrous DMSO and dropped into the main solution. Total reaction volume was 5mL. Then, a catalytic amount of DMAP was added and pH was adjusted to 8 with DIEA. Reaction was left under agitation and inert atmosphere for 48h. Then the solvent was removed under vacuum and the residue obtained was dissolved in 1mL of ddH_2O and purified by FPLC (Macrocap SP column, flow rate=1mL/min, solvent A: ddH2O, solvent B: NaCl 1M; method: same as in C2P1, wavelength=215, 280nm). A typical chromatogram is depicted in FIGURE V. 11. The fractions were collected; lyophilised and the solid residue was desalted by ultrafiltration (Vivaspin® MWCO 2000g/mol). The product obtained was characterised by NMR (^{1}H, ^{13}C and COSY, D_2O) and MALDI-TOF analysis (FIGURE V. 23(A)).

Yield: 70%. ^{1}H-NMR (300 MHz, D_2O) δ 6.96 (s, 4H), 6.68 (s, 4H), 3.58 (s, 275H). MS MALDI-TOF analysis: 3933g/mol.

V. 3. 1. 5. 3 Synthesis of PEP2-PEG-PEP2 (C2P2) and PEG-PEP2 (C1P2)

The general synthesis of PEP2-PEG and PEP2-PEG-PEP2 conjugates (**63** and **64**, respectively) is depicted in FIGURE V. 10. PEP2 describes the modified RAGE peptide illustrated in FIGURE V. 7, where N-terminal point is modified by addition of the dipeptide: glycine-cysteine (Gly-Cys).

4TP-SS-PEG-SS-4TP (0.052mmol, 1eq, 3400g/mol) was dissolved under agitation in 10mL of acetate ammonium buffer 10mM pH=7 at RT. PEP2 (**58**) (0.057mmol, 1.1eq, 1057.23g/mol) was dissolved under the same conditions in 5mL of ddH_2O and dropped over 20min. The reaction was monitored by UV absorbance at 323nm, corresponding to the 4-thiopyridone leaving group [59]. Afterwards, reaction was left under agitation and inert atmosphere for 15h. Then the reaction was lyophilised. The residue obtained was dissolved in 1mL of ddH_2O and purified by FPLC (Macrocap SP column, flow rate=1mL/min, solvent A: ddH2O, solvent B: NaCl 1M; method t=0min, A 100% 60min; gradient: 100% solvent B in 2500min, wavelength=215, 280nm). A typical chromatogram is depicted in FIGURE V. 12. The fractions were collected; lyophilised and the solid residue was desalted

with a PD-10 column packed with Sephadex™ G-25 using ddH_2O as eluent. Both products were characterised by NMR (^1H, ^{13}C and COSY, D_2O) and MALDI-TOF analysis (FIGURE V. 23(A)).

C2P2. Yield: 45%. ^1H-NMR (300 MHz, D2O) δ 7.00 – 6.90 (m, 1H), 6.67 (t, *J*=7.2 Hz, 1H), 3.56 (s, 46H). MS MALDI-TOF analysis: 5873g/mol.

C1P2. Yield: 50%. ^1H-NMR (300 MHz, D2O) δ 8.28 (d, *J*=4.6 Hz, 1H), 7.72 (s, 2H), 7.18 (s, 1H), 7.03 – 6.90 (m, 4H), 6.75 – 6.60 (m, 4H), 3.56 (s, 388H). MS MALDI-TOF analysis: 4899 g/mol.

V. 3. 1. 6 Synthesis of radioactive labelled PGA-Doxy conjugate

The general derivatisation procedure of PGA-DOXY radioactive labelling (**65**) is depicted in FIGURE V. 17.

Briefly, 30mg of PGA-CONH-Doxy conjugate (**50**) (19ωt% (6.8%mol), average MW unit of glutamic acid=161.1g/mol) was added to a round bottom flask and dissolved in 1.5mL of ddH_2O. Then, DMTMM·Cl (0.1eq, 276.77g/mol)) previously dissolved in 1.5mL of ddH_2O was added and 10min later, DOTA-NH_2, 614.82g/mol, 0.011mmol) diluted in 1mL of DMF was poured into the reaction. pH was controlled and adjusted to 8 if needed. The reaction mixture was left to proceed under agitation at RT during 48h. After remove the solvent, the residue was purified by ultrafiltration (Vivaspin® MWCO 2000g/mol) and upper part of the tube was lyophilised and characterised.

Yield: 88%. Molar percentage of conjugated DOTA by NMR: 8.2%. ^1H-NMR (300 MHz, D_2O) (9.8%mol DOTA): δ 4.24 (1H), 2.31 – 1.76 (m, 4H), 1.41 (s, 2.25H).

t-Bu protecting groups of DOTA moiety were removed under acidic conditions. Labelled conjugate (50mg, MW=225.5g/mol) was dissolved in 2.85mL of TFA, 75µL ddH_2O and 75µL TIPS and left under agitation for 3h. Then, the reaction volume was precipitated into cold diethyl ether and product was collected after centrifugation. Once dried, sodium salt of the product was formed by solution in $NaHCO_3$. Salt excess was removed by ultrafiltration (Vivaspin® MWCO

3000g/mol) with ddH_2O. Final product was recovered by lyophilisation. Deprotection was proved after NMR-^{1}H (D_2O) analysis.
Yield: 94.6%. NMR-^{1}H (D_2O) in FIGURE V. 18.

For ^{68}Ga labelling, first this radionuclide was eluted, purified and concentrated. Then, the obtained ^{68}Ga was transferred into microwave tube and the pH was adjusted to 3.5-4 by adding HEPES buffer. Immediately, the DOTA labelled system (e.g. PGA-Doxy-DOTA/^{68}Ga (8.58mg) in aqueous solution was added 390µL. The mixture reaction was heated at 90°C for 5min by a microwave laboratory with monomodal radiation (Discover Benchmate, CEM). Then, purification was performed with a exclusion molecular chromatography cartridge (Bio Gel P-6 Bio Rad) using PB pH=7 as eluent. The elution profile was determined by fractionating and measuring the fractions with an activimeter (VDC 405 Veenstra). Radiochemical yield (RY) was calculated as percentage of the activity in each fraction eluated from the molecular exclusion cartridge of the total activity purified, corrected for the decay.

Radionuclide purity (RNP) was assessed by γ-spectrometry (HPBGe detector) immediately and after 24-48h in order to determine the ^{68}Ga breakthrough.

V. 3. 1. 7 Synthesis of fluorescently labelled conjugates

By means of conjugation of a near infrared dye (Cyane 5.5), conjugates were labelled for posterior biodistribution studies using optical imaging, monitoring *in vivo* as well as *ex vivo* fluorescence.

V. 3. 1. 7. 1 PGA-CONH-Doxy conjugate fluorescence labelling

The general derivatisation procedure of PGA-DOXY fluorescence labelling (**66**) is depicted in FIGURE V. 15.

Briefly, 15mg of PGA-CONH-Doxy conjugate (**50**) (17ωt% (6%mol), average MW unit of glutamic acid=161.1g/mol) was added to a round bottom flask and dissolved in 3mL of borate buffer pH=9. Then, 1-ethyl-3-(3dimethylaminopropyl)carbodiimide (EDC, 0.004

mmol, 155.24g/mol) were added and 10min later, N-hydroxysulfosuccinimide (sulfo-NHS, 0.004mmol, 217.13g/mol) was incorporated. Finally, Cy5.5 (6-SIDCC, 0.001mmol, 1362g/mol) diluted in 1mL of buffer solution was poured into the reaction. Reaction mixture was left under agitation at RT for 24h. After freeze-drying the mixture, residue was purified with a PD-10 column packed with Sephadex™ G-25 (fractions of 500µL) and fluorescence was measured (595/680nm) and fractions with the conjugate were joined. To ensure the absence of free Cy in the conjugate, final product was washed with ddH_2O with Vivaspin® MWCO 3000g/mol.

Yield: 60%. Labelling efficiency: 0.94mol%Cy5.5.

V. 3. 1. 7. 2 PEG-PEP1 conjugate fluorescence labelling

The general derivatisation procedure of PEG-PEP1 fluorescence labelling (**67**) is depicted in FIGURE V. 16.

In a 10mL round bottom flask, NHS-PEG-PEP1 (0.003mmol, 3935g/mol) was dissolved in minimum amount of borate buffer pH=9. Then, Cy5.5 (0.003mmol, 1eq, 1362g/mol) previously dissolved in same buffer, was added. A catalytic amount of DMAP was incorporated to the reaction. Final buffer volume was 6mL. Reaction was left under agitation at RT protected from light for 72h. Afterwards, reaction was lyophilised and residue was purified through a PD-10 column packed with Sephadex™ G-25. Fractions of 500µL were taken and their fluorescence was measured by Victor® spectrometer (595/680nm). Fractions corresponding to the peak signal of the labelled conjugate were joined and lyophilised. To asses that free fluorophore was not entrapped in the conjugate, final product was washed with ddH_2O with Vivaspin® MWCO 3000g/mol.

Yield: 50%. Labelling efficiency: 0.11%mol Cy5.5.

V. 3. 2 PHYSICO-CHEMICAL CHARACTERISATION OF THE POLYMER-DRUG CONJUGATES

V. 3. 2. 1 Determination of drug loading, solution conformation, plasma stability and pH degradation studies of PGA-X-Doxy conjugates

Note: PGA-X-Doxy encompasses all doxy conjugates, independently of the type of linkage/spacer between the drug and the polymeric carrier.

Determination of total drug loading by UV spectroscopy

For quantifying doxy content, drug weight percentage was determined by UV Vis. Previously, a calibration curve of the parent drug was done. A stock solution 1mg/mL of PGA-X-Doxy conjugate in ddH_2O was prepared. To obtain appropriate and reproducible absorbance measurements, samples were diluted using ddH_2O. Total drug loading of the conjugates was determined by measuring the optical density at 273nm in H_2O. PGA in the same concentration range as conjugate analysed (0-5mg/mL) in H_2O was used as blank.

Determination of free drug content by LCMS and HPLC

PGA-X-Doxy conjugates were dissolved in PBS pH=7.4. 20µL of the aliquots (100µL, 6mg/mL PGA-X-Doxy) were injected directly in the LCMS without further extraction (Kinetex column (2.6µm, C18, 100A 100x4.6mm, mobile phases ddH_2O/ACN both 0.1% formic acid). In addition, remaining volume was evaporated and solid was washed with a known volume of MeOH. After sonication and centrifugation, supernatants were also evaluated by LCMS.

In parallel, free drug detection by HPLC was carried out. PGA-X-Doxy conjugates were dissolved in PBS pH=7.4. Aliquots (100µL, 6mg/mL PGA-X-Doxy) were lyophilised and the residue was washed with 100µL of MeOH. Following centrifugation (12000rpm, 5min, 4°C), each supernatant was purified through a POROS 50R2 column to extract the free drug. 1mL fractions were collected and analysed by HPLC (RP-18 column, flow rate=1mL/min, solvent A: acetonitrile 0.1% trifluoroacetic acid, solvent B: H_2O 0.1%trifluoroacetic acid; method:

t=0 min, B 95%, t=33 min B 5%, t=35 min B 5%, t=40 min B 95%, wavelength=273nm).

Determination of mean hydrodynamic diameter of the conjugates

DLS measurements were performed at 25°C using a Malvern Zetasizer NanoZS instrument, equipped with a 532nm laser at a fixed scattering angle of 90°. Polymer conjugate solutions (10mg/mL) were prepared in PBS pH=7.4. The solutions were sonicated for 10min and filtered through a 0.20μm cellulose membrane filter. Micelle size distribution by volume was measured (diameter, nm) for each conjugate. Experiment was repeated per triplicate with n>3 measurements.

Small-angle neutron scattering (SANS) experiments were performed on the D11 instrument at the Institute Laue-Langevin in Grenoble (France) by our collaborators from the School of Chemistry in the Cardiff University (Cardiff, UK). Scattering data are expressed in terms of the scattering vector, Q, which is given by $Q=4\pi/\lambda \cdot \sin(\theta/2)$ where λ is wavelength and θ the angle at which the neutrons are scattered. The incident neutron wavelengths were 6±1Å and 12Å, giving accessible Q-ranges of 0.0017 to 0.42Å $^{-1}$ using four different sample-detector distances. Sample solutions were prepared at a conjugate concentration of 0.5-2ωt% on a 1g scale in D_2O (pH=5.5, 0.1M phosphate buffer) and placed in 2mm path length quartz cells, mounted in a sample changer thermostatted at 37°C ($\pm$ 0.2). These conditions allowed for the study of conjugates at pH, temperature and ionic strengths mimicking those experienced during drug release *in vivo*. Data were corrected for transmission intensity, electronic background and normalised against a flat scatterer according to the standard procedures for the instrument. The obtained scattering profiles I(Q) vs. Q were analysed according to $I(Q) \propto \phi Vp\ P(Q)\ S(Q) + Binc$ where ϕ is the volume fraction and Vp the particle volume. The FISH modelling suite was used for the analysis[60] . FISH incorporates parameterised form factors, P(Q) and structure factors, S(Q), to describe the dimensions of the scattering particle and inter-particle interactions .

Drug release studies under hydrolytical conditions

Stability studies under hydrolytical conditions were carried out with the PGA-X-Doxy conjugates. Conjugates (6 mg/mL) were incubated at 37°C in PBS at pH 5.5 and 7.4 for 17 days. Daily pH was checked and adjusted if necessary. 100µL of the sample solutions were taken at various time points (0, 3, 5, 9, 14, 17 days). Neutralisation of pH with ammonium phosphate buffer (1M) before MW lost analysis was performed in order to stop further degradation (t_R=12min. Method: isocratic gradient with PBS 0.1M pH=7.4 as mobile phase, flow rate=1mL/min, 50min). In parallel, free drug of samples at t=0 and 17d was evaluated to quantify drug release (conditions of plasma stability or free drug evaluation studies explained in section V.3.2.1.).

Stability of the PGA-X-Doxy conjugates in in vitro conditions

Fibril disruption studies were carried out by incubation of the conjugates with TTR fibrils in PBS media at 37°C. To test if the drug was released from the polymer platform during the in these conditions, a PBS stability-test with the same parameters was set up. Conjugates (3-6 mg/mL) in PBS 0.1M were incubated at 37°C at pH=7.4 for 17 days. Sterile conditions were used during all the experiment. 100µL of the sample solutions were taken at different time points up to 17 days. MW lost was evaluated with GPC columns in a HPLC system using methodology and parameters described before.

Furthermore, free drug extraction was performed and evaluated with LCMS system. PBS aliquots were injected directly in the LCMS without further extraction (approx. 20µL). Doxycycline was easy to detected (MW=444g/mol, [M+1]=445g/mol) at t_R=10min, as well as doxy-NH_2 (MW=459g/mol, [M+1]=460g/mol) at t_R=5min. As in PBS was not possible to observed traces of doxy in any of the degradation samples, remaining volume was evaporated and the solid was washed with MeOH to redissolved the possible free drug. After double centrifugation, supernatant was injected in LCMS.

Stability of PGA-X-Doxy conjugates in plasma

Stability in plasma was assessed by incubating each of the conjugates PGA-X-Doxy (3-6mg/mL), for 24h at 37°C in plasma freshly

extracted from rodents. Free drug was used as a positive control and plasma without doxy as negative. At several time points (0min, 1h, 4h, 8h and 24h), aliquots of 100µL were collected. To each sample, 100µL of ACN was added to precipitate the plasma proteins. After centrifugation (12000rpm, 5min, 4°C), supernatants were collected and subjected to analysis by HPLC as described above (*supernatant 1*). Pellets were washed with MeOH (100µL) to extract the free drug out of the pellets. To redissolve the free drug in MeOH, the solid was vortexed and then sonicated. Subsequent to centrifugation (12000 rpm, 5 min, 4°C), *supernatant 2* was collected and analysed by HPLC as reported below.

V. 3. 2. 2 Characteriation of RAGE peptide conjugates: stability in different conditions, solution conformation and affinity studies

PEG conjugates characterisation by NMR and MALDI-TOF

For verifying the identity and purity of each RAGE peptide conjugate, NMR studies such as ^{1}H and DOSY were carried out (D_2O), as well as MS spectra by means of MALDI-TOF. For NMR analysis, 15-20mg of conjugate were dissolved in 500µl D_2O (section NMR in the appendix III). For MS MALDI-TOF analysis, 0.5 µL of sample was spotted onto the MALDI stainless steel target plate. After droplets were air-dried at room temperature, 0.5 µL of matrix (5 mg/mL α-Cyano-4-hydroxycinnamic acid (CHCA) (Sigma) in 0.1% TFA-ACN/H2O (1:1, v/v)) was added and allowed to air-dry at room temperature. The samples were analysed with the conditions detailed in the instrumental section.

In the case of NMR analysis, aromatic peaks belonging to specific amino acids of the peptides were related with the peak of PEG (δ = 3.6ppm) as it is shown in FIGURE V. 24, determining the number of peptide molecules conjugated to the polymer. In the case of MALDI-TOF spectra (FIGURE V. 23**),** it was subtracted to the MW obtained the MW of PEG, figuring out the number of peptide molecules linked.

Stability of the PEG-X-RAGEpep conjugates in cell culture medium

Cell medium (DMEM, 10%FBS) was freshly prepared and

filtered. Under sterile conditions, the RAGE peptide conjugates were dissolved at 15mM RAGEpep equivalents. Aliquots (15µL) were taken at time 0min, 5h, 24h and 48h, immediately frozen in liquid nitrogen and stored at -80°C until evaluation. The samples were thawed, and analysed after centrifugation (4000rpm, 15min) by HPLC with a Zorbax®column (retention time conjugate CXP1: 2.6min, retention time PEP1=4.5min, reference peak of FBS=2.2min. Retention time PEP2=3.27min, retention time conjugate CXP2=2.8min. Method: isocratic gradient with PBS 0.1M pH=7.4 as mobile phase, flow rate=1mL/min, 15min).

Stability of PEG-X-RAGEpep conjugates in plasma

Stability in plasma was assessed by incubating each of the conjugates (10mg/mL), for 24h at 37°C in plasma freshly extracted from rodents. Free drug was not possible to be used as a positive control due to peptides where insoluble (either directly placed in plasma or in previously dissolved media such as water or surfactants (low MW PEG, peanut oil,…) where peptide precipitation was unavoidable even at low concentrations. Plasma without compound was used as negative control. At several time points (0min, 1h, 5h and 24h), aliquots of 100µL were collected. Samples were analysed by MS MALDI-TOF technique to monitor conjugates variation in their molecular weight (g/mol).

Conformation in solution of PEG-X-RAGEpep conjugates. DLS study.

PEG-X-RAGEpep conjugates conformation was analysed by DLS. Samples were prepared in PBS 0.20M pH=7.4 at different concentrations, ranging from 2-20mg/mL. The solutions were analysed without any other additional treatment as well as after filtration through a 0.45µm cellulose membrane filter before analysis. The size distribution by volume (%) was measured as the hydrodynamic radius (R_h, nm) for each conjugate. All measurements were made at 25 °C with a detection angle of 173°. The intensity of size distribution was obtained from the analysis of the correlation function using multiple narrow mode algorithm of the Malvern DTS software. Experiment was done per triplicate (with n≥3 measurements each).

The binding kinetics of every compound were analysed by surface plasmon resonance (SPR) measurements using a Biacore T100^{TM} instrument. A CM5 chip (carboxy-methylated dextran sensor chip) was coated by standard amine coupling chemistry (NHS/EDC) with the TTR mutant L55P **(**1.861mg/mL, ε_{280}=77660, MW=55kg/mol, isoelectric point=4.7) ([61],[46]) to a density of 10000RU. Immobilisation was performed in the channel 2 of the sensor chip and the channel 1 was used as the reference surface. HBS-EP buffer (HEPES buffered saline with EDTA and surfactant P20: 10mM HEPES, 150mM NaCl, 3mM EDTA, 0.005% Tween-20) was used as running buffer.

The device was equilibrated with cell culture medium (DMEM (low glucose), 1% P/S, 0.05 % sodium azide) and temperature set to 37°C. Stock solutions of the conjugates were dissolved in cell culture media while the RAGE peptides where dissolved in ddH_2O (10mM RAGEpep eq.). Measurements were carried out at 37°C, using a flow rate of 10µL/min with a contact time of 60s, followed by dissociation of 30s. In the case of PEP2 and its conjugates (C1P2, C2P2), the regeneration step was required, which consisted in washing with 10mM glycine pH=2.5, for 120s at the same flow. The peptides and its conjugates were injected at concentrations between 0.1 to 2.5nm. The kinetic data were obtained after the analysis of the sensograms performed with the BIAevaluation software (version 2.0). The experiment was repeated until acceptable (x^2>10) and reproducible K_D values were obtained (n>10).

V. 3. 3 *IN VITRO* ACTIVITY STUDIES OF THE POLYMER-DRUG CONJUGATES

V. 3. 3. 1 TTR-fibril disruption studies of the PGA-X-Doxy conjugates

Preparation of amyloid fibrils

TTR protein was produced in an Escherichia coli expression system (isolated, and purified as described previously [62]. After growing the bacteria, the protein was isolated and purified by preparative gel electrophoresis after ion exchange chromatography. Protein concentration was determined using the Lowry method [63].

TTR Leu55Pro was dialysed against water at pH=7.4 during 24h at 4°C. The preparation was centrifuged at 15000g for 30min at 4°C, then the pellet was washed, resuspended in sterile PBS and quantified by Lowry method [63]. Sample concentration was adjusted to 1mg/mL. Protein was later incubated at 37°C for 10-13 days until fibril formation was ratified by TEM.

Screening for TTR fibril disrupters

Stock solutions of all compounds (TABLE V. 6) (3.6mM doxy) were dissolved in sterile H_2O and filtered-sterile prior to use (0.2µm). As controls, PGA, doxy and doxy-NH_2 were tested in parallel. Aliquots of TTR L55P fibrils (1mg/mL) were prepared and the correspondent amount of every compound was added, with a final concentration of 6.7-fold molar excess of doxy (121µM/100µg fibrils). The preparations were incubated at 37°C in the dark. At given times, all aliquots were analysed by TEM and DLS to monitor fibril disruption.

Transmission electron microscopy (TEM)

For TEM analysis, sample aliquots were taken under sterile environment, vortexed and adsorbed to glow-discharged carbon-coated collodion film supported on 200-mesh copper grids. For negative staining, the grids were washed with deionised water and stained with 1% uranyl acetate solution. The grids were visualised with a Zeiss microscope operated at 60kV and exhaustively examined.

Dynamic Light Scattering (DLS)

The same samples used in TEM analysis were also analysed by DLS as a complementary technique, in order to observe variations respect to fibrils control after treatment with PGA-X-doxy conjugates. Samples were placed in sterile plastic cuvettes. The size of the generated species was measured at 633nm on a DLS instrument. All measurements were made at 25 °C with a detection angle of 173°. The intensity of size distribution was obtained from the analysis of the correlation function using multiple narrow mode algorithm of the Malvern DTS software. Values shown are the means of triplicates and the experiment was repeated three times.

V. 3. 3. 2 Cytotoxicity of the species resulting from PGA-X-Doxy incubation

Cell culture method

To optimise the cell density for the *in vitro* experiments, cell growth curves were carried out with the rat Schwannoma cell line RN22. Following the MTT protocol (Chapter IV, section IV.3.1.2), the experiment was performed with the scheme detailed. RN22 cells were seeded at a density of 4500cell/mL in cell culture medium (Dulbecco's minimal essential medium supplemented with 10% FBS and 1% P/S) into 25 cm^2 flasks maintained at 37°C in a humidified atmosphere of 95% and 5%CO_2.

Cytotoxicity study

TTR L55P fibrils were grown for 15 days (as previously described in section V.3.3.1) and then incubated for **6** days at 37°C with PGA-X-Doxy conjugates (FIGURE V. 32) (doxy 180µM /100µg fibrils). Fibril disruption was checked as detailed in the named section. Then, samples were centrifuged (15000g, 30min, 4°C) and pellet was redissolved in cell media. Each preparation was added to cells for 24h incubation. The toxicity of the species generated was assessed by caspase-3 activation (V. 3. 3. 3).

V. 3. 3. 3 Activity of the RAGE peptide conjugates as inhibitors of the TTRagg cytotocicity. Caspase-3 assay

TTR L55P aggregates were incubated with either the RAGE peptides or the PEG-RAGEpep conjugates at a RAGE peptide-equivalent concentration of 10µM found active in previous studies [61]. Under sterile conditions, the TTR L55P aggregates were dissolved in cell media (DMEM (low glucose), 1%FBS, 1%P/S) achieving 2µM concentration. Then, compounds were added from a stock solution (1mM RAGEpep eq.) achieving a final concentration of 10µM RAGEpep equivalents and incubated for 5 h at 37 °C under continuous agitation. Final volume of each solution was 3mL per compound.

The treated aggregates were then added to the RN22 cells

(1.5mL/well, 6-well plate) and the cells incubated for 24 or 48h before activation of caspases-3 was evaluated. As controls, cells without addition and cells exposed to TTR L55P aggregates were used.

Activation of caspase–3 was measured using the CaspACE colorimetric 96–well plate assay, following the manufacturer's instructions (Sigma Aldrich). Cells were trypsinised and harvested using a cell scrapper. After centrifugation (5min, 1000rpm), the cell pellet was lysed in 100µL of hypotonic lysis (Cell Lysis Buffer: 20mM HEPES, pH=7.4, 0.1% CHAPS, 50mM DTT, 2mM EDTA) by four cycles of freeze/thawing. 40 µL of each cell lysate was used (in duplicate) was used for determination of caspase–3 activation. The remaining cell lysate was used to measure total cellular protein concentration with the Bio–Rad protein assay kit, using BSA as standard. Values shown are the mean of duplicates of three independent experiments. Student's t test statistical analysis was used to determine statistical significance between cells exposed to assay media and cells exposed to different regulators and P values of less than 0.05 were considered significant (*$p<0.05$, **$p<0.005$).

V. 3. 3. 4 Haemolysis assay of the synthesised polymer-drug conjugates

Erythrocytes (RBC, red blood cells) were isolated from fresh whole rat blood, obtained by cardiac puncture after death and placed in a heparinised tube on ice[28]. Blood was diluted with PBS pH 7.4 up to 10mL and then it was centrifuged (3000 rpm, 10 min, 4 °C) three times, removing the supernatant after each centrifugation and re-suspending the cells in sterile PBS. The final RBC pellet was weighed and re-suspended at 2%(v/v) in PBS. To study the haemolytic activity of the RAGE peptides and PEG-RAGE peptide conjugates, they were dissolved in PBS stock solutions (4mg/mL) adjusted to pH 5.5 or 7.4. Then samples were added to wells (n=6, 100µL) covering the concentration range 0.8-2mg/mL of RAGE peptide equivalents. PBS was used as a control together with the reference compounds; dextran (MW=74000g/mol) as a negative control, poly(ethyleneimine) (PEI) (750,000g/mol) as a positive control and Triton X–100 1%(w/v) to

determine a 100% RBC lysis. The plates were then incubated at 37°C for 1h. To assess haemoglobin (Hb) release the plates were then centrifuged (3000rpm, 10min, 20°C) and the supernatant of each well was transferred into a new plate. The Hb released was assessed by measuring the absorbance at 570nm using a microtitre plate reader. The percentage of haemolysis of each sample was calculated relative to 100% haemolysis obtained from incubation with Triton–X 100.

V. 3. 4 *IN VIVO* EVALUATION STUDIES OF THE POLYMER-DRUG CONJUGATES

V. 3. 4. 1 Polymer-drug conjugates biodistribution studies in healthy mice

PGA-CONH-Doxy-Cy5.5 conjugate biodistribution by optical imaging technique

Healthy Balb/c mice (9-12month old) were used as mouse model for the *in vivo* distribution studies. For *in vivo* monitoring experiments, animals were first anesthetised and shaved to remove hair interference in fluorescence signal. The *in vivo* whole-body biodistribution as well as *ex vivo* monitoring of the labelled conjugate was performed through noninvasively fluorescence imaging (FLI) using the IVIS®Spectrum Imaging System. Animal care has handled in accordance to guidelines for the Care and Use of Laboratory Animals of the Centro de Investigación Príncipe Felipe, and the experimental procedures were approved by the Animal Experimentation Ethical Committee of the institution.

Biodistribution of Cy5.5 labelled PGA-CONH-Doxy conjugate (17ωt%) (**66**) was evaluated by FLI. Conjugate was dissolved in serum saline (1.40mg/mL) and animals were injected intravenously a single dose of 100μL of the solution. As controls, non-injected mice were used. Animals were anesthetised using 1-3% isofluorane. Five mice were imaged at a time and imaging settings were set depending on the fluorescence of the animals. The light emitted from the labelled conjugate was detected, digitalised and electronically displayed as a pseudocolor overlay onto a gray scale animal image. Fluorescent

signals were quantified as Efficiency. Mice were euthanised at 0, 4 and 24h post administration. Blood was collected and major organs (liver, lungs, spleen, kidneys, heart and brain) were dissected from mice and fluorescence images of excised tissues were obtained by *ex vivo* FLI. Tissues samples were harvested and stored at -80°C to quantify fluorescence.

Organs were homogenised in PBS pH=7.4 at a specific concentration by means of Ultraturrax device (approx. 1min, 13000rpm). Suspension was centrifuged (4000rpm, 1h, 4°C) and supernatants were collected for fluorescence measurement. Quantification data is shown in FIGURE V. 37. To assess conjugate total extraction, pellets were washed with ddH_2O but no significant signal was observed.

For blood samples, immediately after extraction they were centrifuge (10min, 4000rpm, 4°C) and plasma (supernatant) and pellet were frost in liquid nitrogen after analysis. Plasma was directly measured (100µL) per triplicate in 96 well-plates by fluorescence detector.

PGA-CONH-Doxy-Cy5.5 conjugate biodistribution by Positron Emission Tomography (PET)

A second biodistribution study was done by means of PET. The experiment was performed in FVB/NJ mice (25±4g). Animals were injected i.v. in the tail vein at a dose of 21±4µg PGA-Doxy-DOTA/^{68}Ga (**65**) per gram of body weight, which corresponded to a dose between 0.2 and 1.4MBq.

The mice were anesthetised with 1.5% isoflurane and monitored up to 3h. In parallel, groups of animals (n=5) were sacrificed at 25min, 50min, 1h, 2h and 3h post-injection. Blood and selected organs (heart, lungs, spleen, kidneys and liver) were collected. The radioactivity was measured and corrected for the decay in a gamma counter.

At 0.25, 0.5, 1, 2, and 3 hours following injection, blood

samples were obtained from mice by terminal bleeding via cardiac puncture following isoflurane anaesthesia; their organs (lungs, heart, spleen, kidneys, liver and brain) and some tissues (muscle, fat) were isolated, rinsed with normal saline, weighted, and radioactivity was measured using the Cobra II auto-gamma counter. The blood samples were centrifuged (10min, 3000rpm, RT) and the supernatant of plasma was transferred to a new eppendorf tube. The %ID and the %ID/g were calculated by comparison with standards taken from the injected solution for each animal. The data were expressed as the mean ± standard deviation.

PEP1-PEG-Cy5.5 conjugate biodistribution by Optical Imaging technique

Biodistribution of PEP1-PEG-Cy5.5 (**67**) was evaluated by optical imaging technique. Conjugate was dissolved in serum saline (0.66mg/mL) and animals were injected intravenously a single dose of 100µL of the solution. The in vivo whole-body biodistribution of the labelled conjugate was monitored noninvasively by FLI using the IVIS®Spectrum Imaging System. As controls, non-injected mice were used. Animals (Balb/c mice) were anesthetised using 1-3% isofluorane. Five mice were imaged at a time and imaging settings were set depending on the fluorescence of the animals. The light emitted from the labelled conjugate was detected, digitalised and electronically displayed as a pseudocolor overlay onto a gray scale animal image. Fluorescent signals were quantified as Efficiency. Mice were euthanised at 0, 4 and 24h post administration. Blood was collected (also at shorter times) and major organs (liver, lungs, spleen, kidneys, heart and brain) were dissected from mice and fluorescence images of excised tissues were obtained by ex vivo FLI. Tissues samples were harvested and stored at -80°C to quantify fluorescence.

Organs were homogenised in solution of $HClO_4$ 6% / EtOH 40% at a specific concentration by means of Ultraturrax device (approx. 1min, 13000rpm). Suspension was centrifuged for 1h at 4000g at 4°C and supernatants were collected for fluorescence measurement. To assess conjugate total extraction, pellets were washed with ddH_2O but

no significant signal was observed. For blood samples, immediately after extraction they were centrifuge (10min, 4000rpm, 4°C) and plasma (supernatant) and pellet were frost in liquid nitrogen after analysis. Plasma was directly measured (100µL) per triplicate in 96 well-plate by fluorescence detector.

V. 3. 4. 2 Preliminary activity studies of conjugates in a young FAP mice model

All animals were kept and used strictly in accordance with national rules and European Communities Council Directive (86/609/EEC), and all studies performed were approved by the Portuguese General Veterinarian Board (authorisation number 024976 from DGV-Portugal). Transgenic mice for human V30M TTR in a TTR null background were kindly provided by Professor Suichiro Maeda from Yamanashi University. In previous studies, these animals were previously analysed and ~60% of the animals over 1 year of age were found to have TTR deposition as amyloid, for instance Congo red (CR)-positive material [51] having non-fibrillar TTR deposits at younger ages.

Three groups of animals (9-11month of age, n=8) were treated intravenously with the conjugates detailed in TABLE V. 8. Animals were given 2 doses per week during 6 weeks. Group 1 was treated with the conjugate C2P1 (**60**), group 2 was treated with two conjugates in the same dose (combination group): C2P1 (**60**) and PGA-CONH-Doxy (**51**) and group 3 with PGA-CONH-Doxy (**51**). Non-treated mice were used as controls.

Animals were sacrificed after anaesthesia with ketamine/xylazine. Organs (including liver, kidney, oesophagus, stomach, small and large intestines, heart, spleen, pancreas) were immediately excised and processed. It is important to note that in this model the gastrointestinal track present the majority of fibril accumulation. Tissues were fixed in 4% neutral buffered formalin and embedded in paraffin or immediately frozen, for light microscopy or for total protein extraction, respectively.

Immunohistochemistry (IHC) studies of the organs from the treated mice

TTR-non fibrillar deposition in the extracted tissues was evaluated by immunohistochemistry as well as possible toxicity of these deposits (apoptosis).

5µm-thick sections were deparaffinised in xylol and dehydrated in a descendent alcohol series. Endogenous peroxidase activity was inhibited with 3% hydrogen peroxide/100% methanol and sections were blocked in 4% bovine serum and 1% bovine serum albumin in phosphate buffered solution (PBS). Primary antibodies used were rabbit polyclonal anti- TTR (Dako, 1:1000), rabbit polyclonal anti-Fas (St.Cruz, 1:200), and rabbit polyclonal anti-3-nitrotyrosine (Chemicon, 1:500), which were diluted in blocking solution and incubated overnight at 4°C. Antigen visualisation was performed with the biotin-extravidin-peroxidase kit (Sigma), using 3-amino-9-ethyl carbazole (Sigma) or diaminobenzidine as substrates. Immunohistochemistry analysis was carried out by two investigators unaware of the tested tissue sections.

Histological analysis of the organs from the treated mice

For evaluating conjugates toxicity, histological analysis of the tissue sections was performed. This technique enables a better assessment of severe toxicity. Paraffin-embedded sections were stained with haematoxylin/eosin solution (H&E). H&E-stained slice sections were thoroughly examined under low (25 × and 50 ×) and medium (100 × and 200×) magnification.

Statistical Analysis

All results are given as means ± SD ($n \geq 3$). When only two groups were compared, the Student's t test for small sample size was used to estimate statistical significance. If more than two groups were compared evaluation of significance was performed using one way-Analysis Of Variance (ANOVA) followed by Bonferroni post hoc test. Graph pad Instant software (Graph Pad Software Inc. CA, USA) was used. In all cases, statistical significance was set at $p < 0.05$.

BIBLIOGRAPHY

1. C. Deladriere, R. Lucas, and M.J. Vicent, *Future trends, challenges and opportunities with polymer-based combination therapy in cancer.* Drug Delivery in Oncology: from basic research to cancer therapy, 2011(Wiley-VCH Verlag GmbH & Co. KGaA): p. 805-837.
2. R. Duncan and M.J. Vicent, *Polymer therapeutics-prospects for 21st century: The end of the beginning.* Adv Drug Deliv Rev, 2013. **65**(1): p. 60-70.
3. F. Greco and M.J. Vicent, *Combination therapy: opportunities and challenges for polymer-drug conjugates as anticancer nanomedicines.* Adv Drug Deliv Rev, 2009. **61**(13): p. 1203-13.
4. Eaton, M.A., *Improving the translation in Europe of nanomedicines (a.k.a. drug delivery) from academia to industry.* J Control Release, 2012. **164**(3): p. 370-1.
5. Eaton, M., *Nanomedicine: industry-wise research.* Nat Mater, 2007. **6**(4): p. 251-3.
6. Gaspar, R. and R. Duncan, *Polymeric carriers: preclinical safety and the regulatory implications for design and development of polymer therapeutics.* Adv Drug Deliv Rev, 2009. **61**(13): p. 1220-31.
7. Duncan, R. and R. Gaspar, *Nanomedicine(s) under the microscope.* Mol Pharm, 2011. **8**(6): p. 2101-41.
8. Y. Ando, M. Nakamura, and S. Araki, *Transtyretin-related familial amyloidotic polyneuropathy.* Arch Neurol, 2005. **62**(7): p. 1057-1062.
9. F. A. Monteiro, et al., *In vitro inhibition of transthyretin aggregate-induced cytotoxicity by full and peptide derived forms of the soluble receptor for advanced glycation end products (RAGE).* FEBS Lett, 2006. **580**(14): p. 3451-6.
10. I. Cardoso and M.J. Saraiva, *Doxycycline disrupts transthyretin amyloid: evidence from studies in a FAP transgenic mice model.* The FASEB Journal, 2006. **20**: p. 234-239.

11. I. Cardoso, et al., *Synergy of combined Doxycycline/TUDCA tretment in loweing Transthyretin deposition and associated biomarkers: studies in FAP mouse models.* Journal of Translational Medicine, 2010. **8**(74): p. 1-11.

12. Webster, R., et al., *PEG and PEG conjugates toxicity: towards an understanding of the toxicity of PEG and its relevance to PEGylated biologicals. PEGylated Protein Drugs: Basic Science and Clinical Applications.*, 2009, Birkhäuser Basel. p. 127-146.

13. B. Macedo, et al., *Biomarkers in the assesment of thereapies in Familial Amyloidotic Polyneuropathy.* Mol Med, 2007. **13**(11-12): p. 584-591.

14. M.M. Sousa, et al., *Familial amyloid polyneuropathy: receptor for advanced glycation end products-dependent triggering of neuronal inflammatory and apoptotic pathways.* J Neurosci., 2001. **21**: p. 7576-7586.

15. M. Barz, A. Duro-Castano, and M.J. Vicent, *A versatile post-polymerization modification method for polyglutamic acid: Synthesis of orthogonal reactive polyglutamates and their use in "click chemistry".* Polymer Chemistry, 2013.

16. L. Wang, J. Peng, and L. Liu, *A reversed-phase high performance liquid chromatography coupled with resonance Rayleigh scattering detection for the determination of four tetracycline antibiotics.* Anal Chim Acta, 2008. **630**: p. 101-106.

17. Duncan, R., *The dawning era of Polymer Therapeutics.* Nature Rev Drug Discov, 2003. **2**(5): p. 347-360.

18. G. Pasut and F. M. Veronese, *Improvement of Drug Therapy by Covalent PEG Conjugation: An Overview From a Research Laboratory.* Israel Journal of Chemistry, 2010. **50**(2): p. 151-159.

19. Pasut, G. and F.M. Veronese, *PEG conjugates in clinical development or use as anticancer agents: an overview.* Adv Drug Deliv Rev, 2009. **61**(13): p. 1177-88.

20. F. M. Veronese and G. Pasut, *PEGylation, successful approach to drug delivery.* Drug Discovery Today, 2005. **10**(21): p. 1451-1458.

21. Hermanson, G.T., *Bioconjugate Techniques*2010: Elsevier Science.

22. Zarafshani, Z., T. Obata, and J.F. Lutz, *Smart PEGylation of trypsin.* Biomacromolecules, 2010. **11**(8): p. 2130-5.

23. M. J. Vicent, H. Ringsdorf, and R. Duncan, *Polymer therapeutics: Clinical applications and challenges for development.* Adv Drug Deliv Rev., 2009. **61**(13): p. 1117.

24. M.J. Vicent and R. Duncan, *Polymer conjugates: nanosized medicines for treating cancer.* Trends Biotechnol, 2006. **24**(1): p. 39-47.

25. Duncan, R., *Polymer therapeutics as nanomedicines: new perspectives.* Curr Opin Biotech, 2011. **22**(4): p. 492-501.

26. M.J. Vicent, et al., *Polymer conjugates as therapeutics: future trends, challenges and opportunities.* Exp Opin Drug Rev, 2008. **61**: p. 1220-1231.

27. A. Paul, et al., *Drug mimic induced conformational changes in polymer-drug conjugates characterized by Small Angle Neutron Scattering.* Biomacromolecules, 2010. **11**: p. 1978-1982.

28. V. Gimenez, et al., *Demonstrating the importance of polymer-conjugate conformation in solution on its therapeutic output: Diethylstilbestrol (DES)-polyacetals as prostate cancer treatment.* J Control Release, 2012. **159 (2)**: p. 290-301.

29. E. Markovsky, et al., *Administration, distribution, metabolism and elimination of polymer therapeutics.* J Control Release, 2012. **161**(2): p. 446-460.

30. L. Y. Qiu and Y.H. Bae, *Polymer architecture and drug delivery.* Pharm Res, 2006. **23**: p. 1-30.

31. C. M. Thomas and J. F. Lutz, *Precision synthesis of biodegradable polymers.* Angew Chem Int Ed, 2011. **50**(40): p. 9244-6.

32. Seymour, L.W., et al., *Influence of molecular weight on passive tumour accumulation of a soluble macromolecular drug carrier.* Eur J Cancer, 1995. **31A**(5): p. 766-70.

33. F. Canal, J. Sanchis, and M.J. Vicent, *Polymer-drug conjugates as nano-sized medicines.* Curr opin Biotech, 2011. **22**(894-900).

34. http://www.malvern.com.

35. P. Caliceti and F. M. Veronese, *Pharmacokinetic and biodistribution properties of poly(ethylene glycol)-protein conjugates.* Adv Drug Deliv Rev, 2003. **55**(10): p. 1261-77.

36. J. A. Palha, et al., *4'-Iodo-4'-deoxydoxorubicin disrupts the fibrillar structure of transthyretin amyloid.* Am J Pathol, 2000. **156**(6): p. 1919-25.

37. Forloni, G., et al., *Anti-amyloidogenic activity of tetracyclines: studies in vitro.* FEBS Lett, 2001. **487**(3): p. 404-7.

38. I. Cardoso, G. Merlini, and M. J. Saraiva, *4'-iodo-4'-deoxydoxorubicin and tetracyclines disrupt transthyretin amyloid fibrils in vitro producing noncytotoxic species: screening for TTR fibril disrupters.* FASEB J, 2003. **17**(8): p. 803-9.

39. Uversky, V.N. and A.L. Fink, *Protein Misfolding, Aggregation, and Conformational Diseases*2007: Springer Science+Business Media, LLC.

40. J. Sanchis, et al., *Polymer-drug conjugates for novel molecular targets.* Nanomedicine, 2010. **5**(6): p. 915-935.

41. Santos, S.D., R. Fernandes, and M.J. Saraiva, *The heat shock response modulates transthyretin deposition in the peripheral and autonomic nervous systems.* Neurobiol Aging, 2010. **31**(2): p. 280-9.

42. Li, C., et al., *Water soluble paclitaxel derivatives.* Patent, Application number US9906870, 1999.

43. Amiji, M.M., *Nanotechnology for Cancer Therapy*2006: Taylor & Francis.

44. Chipman, S.D., et al., *Biological and clinical characterization of paclitaxel poliglumex (PPX, CT-2103), a macromolecular polymer-drug conjugate.* Int J Nanomedicine, 2006. **1**(4): p. 375-83.

45. Singer, J.W., *Paclitaxel poliglumex (XYOTAX™, CT-2103), a*

macromolecular taxane. J Control Release, 2005. **109**(1-3): p. 120-126.

46. http://www.webhealthcentre.com/drugix/Doxycycline_DI0051.aspx.

47. S. N. S.Alconcel, A. S. Baas, and H. D. Maynard, *FDA-approved poly(ethylene glycol)-protein conjugate drugs.* Polymer Chemistry, 2011. **2**(7): p. 1442-1448.

48. Yamaoka, T., Y. Tabata, and Y. Ikada, *Distribution and tissue uptake of poly(ethylene glycol) with different molecular weights after intravenous administration to mice.* J Pharm Sci, 1994. **83**(4): p. 601-6.

49. Yamaoka, T., Y. Tabata, and Y. Ikada, *Fate of water-soluble polymers administered via different routes.* J Pharm Sci, 1995. **84**(3): p. 349-54.

50. M. M. Sousa, et al., *Deposition of transthyretin in early stages of familial amiloidotic polyneuropathy: evidence for toxicity of nonfibrillar aggregates.* Am J Pathol, 2001. **159**(1993-2000).

51. Sousa, M.M., et al., *Evidence for early cytotoxic aggregates in transgenic mice for human transthyretin Leu55Pro.* Am J Pathol, 2002. **161**(5): p. 1935-48.

52. Molloy, D.W., et al., *A multicenter, blinded, randomized, factorial controlled trial of doxycycline and rifampin for treatment of Alzheimer's disease: the DARAD trial.* Int J Geriatr Psychiatry, 2012.

53. R. Costa, et al., *Testing the therapeutic potential of doxycycline in a Drosophila melanogaster model of Alzheimer disease.* J Biol Chem, 2011. **286**(48): p. 41647-55.

54. Merrifield, R.B., *Solid phase peptide synthesis I. Synthesis of a tetrapeptide.* J Am Chem Soc, 1963. **85**: p. 2149.

55. Coin, I., M. Beyermann, and M. Bienert, *Solid-phase peptide synthesis: from standard procedures to the synthesis of difficult sequences.* Nat Protoc, 2007. **2**(12): p. 3247-56.

56. G. B. Fields and R. L.Noble, *Solid phase peptide synthesis*

utilizing 9-fluorenylmethoxycarbonyl amino acids. Int J Pept Protein Res, 1990. **35**(3): p. 161-214.

57. M. Cudic and G.B. Fields, *Solid-phase peptide synthesis.* Molecular Biomethods Handbook, 2008: p. 515-546.
58. Wellings, D.A. and E. Atherton, *Standard Fmoc protocols.* Methods Enzymol, 1997. **289**: p. 44-67.
59. Woghiren, C., B. Sharma, and S. Stein, *Protected thiol-polyethylene glycol: a new activated polymer for reversible protein modification.* Bioconjug Chem, 1993. **4**(5): p. 314-8.
60. Heenan, R.K., *FISH data analysis program.* Rutherford Appleton Laboratory, Didcot, U.K.
61. http://clinicaltrials.gov/ct2/show/NCT00439166.
62. Furuya, H., et al., *Production of recombinant human transthyretin with biological activities toward the understanding of the molecular basis of familial amyloidotic polyneuropathy (FAP).* Biochemistry, 1991. **30**(9): p. 2415-21.
63. Lowry, O.H., et al., *Protein measurement with the Folin phenol reagent.* J Biol Chem, 1951. **193**(1): p. 265-75.

GENERAL DISCUSSIONS

GENERAL DISCUSSIONS

Neurodegenerative disorders are considered a great challenge due to the growing incidence in advancing age population and the difficulty of their treatment beyond the palliative healing. Investigation in this area is concentrated on specific site-directed drug delivery and prompt diagnosis. The bottleneck for successful approaches lies in the difficult drug access to the brain when CNS is affected. This organ is protected by a physic and enzymatic biological barrier which confers the most unique protection existing into the human body: the blood-brain barrier (BBB) [1, 2].

Herein, polymer therapeutics (PT) had been proposed as a therapeutic alternative for the treatment of these diseases. This family of new chemical entities are well established polymeric nanomedicines with several products in the market, mainly PEGylated proteins and polymeric drugs as anticancer agents, and a growing number of polymer-drug conjugates in clinical development. Among the fourth enounced strategies for the second generation of PT, this work has encompassed most of them involving [3-7] (i) the use of biodegradable polymeric carriers, such as polyglutamates, which provide the opportunity for their use in chronic treatments and CNS disorders, (ii) utilising sophisticated methodologies for their physico-chemical characterisation allowing a better control on the final product together with the most appropriate application for our system depending on the physico-chemical behaviour observed, (iii) a novel target different than cancer and (iv) the use of combination therapy as an extra tool for enhancing the potential of our conjugates by means of synergism.

Initial efforts of the present work were directed towards the design and synthesis of polymeric platforms based in poly-L-glutamic acid (PGA). Based on the current systems able to reach the brain for drug delivery, conformation and mechanism for cellular internalisation were considered as key features for our designs. Therefore, homopolymers, diblock and triblock copolymers with different

polypeptidic block lengths as well as hydrophilic/hydrophobic character were thought to present good opportunities to achieve brain access. For this objective, NCA-ROP polymerisation was selected due to its broad acceptance to obtain polypeptides and polypeptide-based block copolymers with quantitative yields, facility to multigram scalability and avoidance of racemisation at the chiral centers [8-13]. Additionally, the option of using either molecular or macromolecular initiators provided the construction of the diblock copolymers. This polymerisation requires high purity of every component and specific reaction conditions were factors like humidity, CO_2 pressure, temperature, presence of salts or cleavability of the protecting groups, undesired terminating processes, etc., are determinant parameters to achieve successful results. Nowadays, this centenary polymerisation procedure presents promising approaches yielding well-defined polypeptides based on initiation of highly purified NCAs with primary amines under [10-13]. Unfortunately, all methods have limitations, e.g. HVT require a complex and expensive experimental setup, HMDS amines are sensitive to hydrolytic reactions, while heavy metal catalysts must be carefully removed to avoid non-specific toxicity in biomedical applications.

For the whole field of nanomedicine is vitally important to have methods that allow the large scale (from 100 g to kg) production of controlled polymeric carriers with any trace of toxic impurities. To circumvent these challenges, here we have used ammonium salts as initiators to enable controlled large scale synthesis of well-defined polyglutamates covering a wide molecular weight range. In contrast to other approaches [14-16], we have substituted the nucleophilic chloride by a non-nucleophilic tetrafluoroborate anion (BF_4^-), which is less hydrophilic and thus better soluble in a broad range of organic solvents and it has lower nucleophilicity than the related nitrate or halide salts [17-19]. Mechanistically, BF4− anion can be considered inert due to the symmetry of the ion leading to an equal charge distribution and its composition of highly electronegative fluorine atoms, which diminishes the nucleophilicity of the anion and consequently, avoiding the undesired reprotonation of the activated

monomer during the ROP of NCAs. Therefore, living nature of the polymerisation could be achieved enabling the synthesis of well-defined high molecular weight homo or block-*co*-polypeptides with preserved end group integrity.

Herein, a set of conditions suitable for the obtaining of polymers with lower dispersities, reproducibility batch-to-batch and scalability has been set up. Then, it was explored the versatility of the reported methodology by polymerisation of (OBzl)Glu-NCA with tetrafluoroborone salts of neopentyl amine, butylamine, propargyl amine, azide amine as well as polyethylene glycol mono methylether amine yielding controlled block copolymers. The presence of an end functionality allows site-specific conjugation of antibodies, proteins or imaging probes at the same time that side chain multivalency enables the design of advanced theranostics or polymer-based combination nanopharmaceutics, limelight topics in this area due to current clinical needs. MW can be precisely controlled up to a degree of polymerisation of 800 without the use of complex initiators or demanding experimental setup. The derived polymers have low dispersities indices below 1.2 indicating the well-controlled character of the polymerisation itself.

Next step after polymerisation to obtain the final PGA polymers is the deprotection, that must ensures full removal of protecting groups without racemisation; an issue, which is often not considered carefully and could induce important changes in nanomedicine behaviour in a clinical setting. Changes in secondary structure due to polypeptide racemisation will alter immunological properties, degradation profile, and secondary structure. Consequently drug release, the pharmacokinetics profile and biodistribution maybe unpredictable upon polypeptide-drug conjugation.

Deprotection using TFA/HBr or acetic acid/HBr is known to lead to deprotection in the absence of racemisation [12]; however, these conditions are not suitable for sensitive functional end groups derived from functional initiators, e.g. alkyne moieties as well as PEG

based block copolymers (i.e. PEG is rapidly degraded under those conditions). In respect to those needs a basic deprotection protocol was developed avoiding racemisation. The deprotection methodology was optimised for homopolymers and diblock co-polymers to achieve complete benzyl group removal and non-stereochemical changes.

Finally, multifunctionality of the PGA block offers the possibility of tuning the polymeric carrier introducing novel pendant groups (alkyne, amine, sulfhydryl, etc) by linking different molecules to the PGA carboxyl groups. This strategy, named post-polymerisation, contributed in the present work to enlarge the number of members of the polyglutamate family by providing site-specific conjugation points, overcoming the limited functional group tolerance of most of the controlled polymerisation techniques. In the same way, N-terminal extreme of the polypeptide block was settled up for conjugation of another polymeric block: PEG. Through this synthetic pathway, triblock copolymers were obtained as well as diblocks. The insertion of the second PEG in TBs was thought to supply a specific-linkage point by the presence of an activated sulfhydryl for further conjugation with biological ligands as targeting moieties for BBB crossing as well as to play a role in solution conformation and consequently in the cellular internalisation pathways. To corroborate our hypothesis, labelling of the novel polyglutamates as well as conjugation to targeting ligands were performed.

In the case of the labelling procedures, the best candidate was chosen depending on the monitoring technique. Amides and triazole bonds were the selected unions due to their stability under physiological conditions use. Later studies on internalisation in an endothelial cell line (HUVEC) revealed that the synthesised members of the TB family (n=100, 150, 200) were non-cytotoxic in the range of concentrations tested and their cell internalisation pathways underwent through energy dependent mechanisms: endocytosis. Co-localisation with lysosomal markers and the reduced internalisation at 4°C compared with 37°C studies corroborated this fact. In consequence, possible co-existence of mixed mechanisms of diffusion

and endocytosis (observed in previous experiments in our laboratory) were dismissed. Therefore, we proposed the use of targeting ligands conjugated to our polyglutamates to accomplish our objective of carrying drugs across the BBB. This attractive strategy does not interfere with the integrity of the barrier preventing possible brain damage.

Prior to ligand conjugation, biodistribution experiments of our novel polyglutamates (TB, DB and homopolymer) were carried out with optical imaging (DB-Cy5.5 and TBO), by MRI (TB-DTPA/Gd) or by PET (PGA-DOTA/Ga). None of the systems presented greater differences among the sizes and number of present PEG blocks. Renal excretion and non-specific accumulation in other organs were observed in all cases. Thus, our systems were validated as adequate polymeric carriers for future drug delivery applications. It is important to mention that, in vivo differences could still occur on biodistribution studies in relation to brain accumulation when different carriers varying the length of the inner polypeptidic block or the MW of the PEG blocks will be further evaluated.

Regarding active BBB targeting, disulphide bonds were preferred polymer-residue linkage due to their bioreversibility, allowing ligand release in presence of a reductive environment or by disulfide reductases encountered in the brain following transcytosis. Our approach concerns the transferrin receptor (TfR) as tool to achieve active transport of our systems trough the BBB. The conjugated moieties were the TfR natural ligand (transferrin, Tf), a monoclonal antibody (mAb) named OX26 and an iron-mimicking peptide (cPEP). Through fluorescence labelling, TB-Tf conjugation was optimised and an appropriate biodistribution with renal secretion and non-accumulation in any organ was found. Unfortunately, TB-Tf percentage encountered in the brain was insignificant if compared with the parent Tf. In order to enhance this ratio, the mAbOX26 was conjugated to TB. mAbOX26 binds TfR in an epitope different from the natural ligand site that under normal conditions remains saturated impeding the recognition of endogenous Tf. Thus, we replaced the Tf

by the antibody expecting to have better outputs. By means of MRI technique, TB-mAb OX26 biodistribution was performed. However, the chemistry used for the conjugation drove to solubility issues along the synthetic processes and polymer functionalisation did not reach an appropriate range for a detectable BBB crossing. Following reported data, rats were used as animal model [20, 21] however, in comparison o mice, higher doses of conjugates were required and the expensive cost of mAb OX26 made this approach not feasible. Moving towards mice models and searching for manageable targeting probes, short peptides were proposed as an efficient alternative. Together with the named Cpep [22], the most advanced BBB targeting vector in the field [23] was also evaluated: the Angiopep-2, which targets the low density lipoprotein receptor-related protein 1 (LRP-1).

PET was selected as the most appropriate monitoring technique after comparison with FLI or MRI due to (i) its sensitivity to detect brain accumulation, (ii) the need of a low percentage of tracer trying a better resembling with the unlabelled vehicle, and (iii) an simpler work-out to quantitate the signal of single organs in *ex vivo* experiments, avoiding extraction procedures as those required in FLI protocols. Taking profit of the synthetic approaches optimised with the previous ligands, cPEP was conjugated to DB and PGA through amide bonds and the Angiopep-2 by disulphide bridges.

In a preliminary test evaluating the differences among both peptides and both carriers, none of them achieved a significant brain accumulation in the studies performed although the obtained results showed promising results for the Angiopep-2 conjugates. Radioactive signal in the brain was higher with this vector although the observed signal decay could mean a possible pump-out of the systems or their presence in the blood surrounding the brain and not into it. With both peptides, diblocks achieved lower percentages than homopolymers. We believe that polymer conformation in solution could impede ligand recognition explaining the low internalisation. To solve this issue, we proposed to use PEG as a semitelechelic block providing a unique conjugation point for the peptide which favored its availability for

receptor recognition. Meanwhile TB-Angiopep2 conjugate synthesis is still under optimisation, PET monitoring studies are currently being performed with novel Angiopep-2 synthesised conjugates based on DB-4TP, PGA homopolymer and PGA star-like architectures, aiming to improve the BBB crossing.

As an adequate carrier for brain delivery have not been still encountered, in order to explore a neuropathological application non-fully depending on BBB crossing, a rare inherited amyloidosis named Familial Amyloidotic Polyneuropathy (FAP) was targeted. In this disease, the main affected area is the peripheral nervous system (PNS) [24]. The central nervous system (CNS) is also an amyloid-associated tissue although the incidence level is considerably lower in FAP. Therefore, crossing the BBB was not the major issue for our PDCs although it will be an extra advantage in case this tissue was affected.

One of the most common FAPs is caused by a mutated protein called transthyretin (TTR), which forms amyloid deposits, mainly in the PNS. The aggregation cascade of this mutated protein, produces a TTR aggregate (TTRagg) able to trigger neurodegeneration through engagement with the receptor-for-advanced-glycation-end-products (RAGE) receptor, which is present on peripheral neurons. In later stages of the disease, the cascade evolves up to fibril formation whose deposits promote tissue degeneration and organ failure. Saraiva *et al* discovered two biomolecules active against the named TTR species.

Firstly, a specific peptidic sequence (named RAGE peptide) able to suppress TTRagg-induced cytotoxicity in cell culture [25]. A reduced version of that peptide containing 6aa was proved to maintain the activity and the affinity of the initial peptide (unpublished sequence). Although this provides an opportunity to design novel therapeutics for FAP treatment, peptide therapeutics themselves display well known challenges for *in vivo* use, e.g. low stability, poor pharmacokinetics and potential immunogenicity. Moreover the RAGE peptide demonstrates low solubility in plasma limiting its potential for i.v. administration. Thus one of the aims of this study was the design of

an efficient polymer- RAGEpeptide FAP inhibitor.

Secondly, an antibiotic drug capable of disrupting TTR amyloid fibrils *in vitro,* in the treated animals and also achieved other improvements regarding amyloid markers [26, 27]. In this case, polymer conjugation of this low MW drug will promote changes in the biodistribution compared to the parent drug, avoidance of undesired accumulation in non-affected organs, diminution of the administered dose and/or its frequency and enhancement of the therapeutic response.

Concerning the rational design the adequateness of the polymer carrier, targeting site conditions and the labile properties of the required covalent bond were considered. As polymer platforms, PGA and PEG were again proposed, in this case for drug conjugation. Our first idea was to build individual PDCs i.e. to conjugate both drugs in independent polymers, and then to combine both drugs in the same polymer matrix. For the later, either the diblock or triblock co-polymer will accomplish our requisites. All possible combination should be evaluated looking for synergism and the best selected for FAP treatment. The fact that regions of TTR deposition in the body are characterised by a surrounding inflammation provides an additional advantage for targeted delivery our conjugates due to the potential for passive targeting due to the EPR effect that accompanies inflammation [28, 29]. Also the local reductive and slightly acidic pH environment can be used to facilitate site–specific drug release from bioresponsive linkers.

A small library of PEG-RAGE conjugates were synthesised to contain biodegradable (disulphide) and non–biodegradable (amide) linkers (to investigate if peptide release was necessary for activity) and mono- and bi-functional PEGs used to explore the importance of solution conformation. First step involved the synthesis by Fmoc-SPPS of the RAGEpep and two derivates for accomplishing the needed end-functional groups for later PEG conjugation. After confirming the identity of each conjugate by NMR and MS spectroscopy analysis,

activity studies *in vitro* in a FAP model (RN22 cell line) were performed. Results concluded that the amide conjugate carrying two molecules of RAGEpep (C2P1) showed the best inhibition of TTRagg-induced cytotoxicity in Schwann cells at 24h. Those conjugates containing disulphide linkers gave less reproducible data and lower activity. Binding affinity studies carried out by surface plasmon resonance (SPR) mimicking *in vitro* assay and the solution in conformation by DLS analysis supported this activity due to the maintenance of RAGEpep affinity for the aggregates and revealed a more stable conformation in solution which may help into RAGEpep spatial availability for the interaction. Thus, peptide release was not an requisite for its activity. In addition, C2P1 was stable after incubation 24h in plasma mimicking *in vivo* situation and did not show haemolytic properties as expected, demonstrating its suitability for i.v. administration. Biodistribution experiments performed with fluorescent derivative showed a renal secretion and non-accumulation in undesired areas.

With doxy the same rational design for polymer-drug linkage was followed and a library of PGA-Doxy conjugates with drug loading ranging from 2 to 60ωt% was synthesised and fully characterised. Selected linkages were ester and amide bonds, either directly to the polymer or through a dipeptide as linker. Screening their activity as TTR fibril disruptors, amide conjugates demonstrated higher response at equivalent parent drug dose. Specifically, conjugates with 15 and 30ωt% drug content showed the best fibril disaggregation profile. Trying to explain this fact, physico-chemical studies were performed demonstrating that drug release was not a requisite for activity. Conformation in solution was analysed by SANS and DLS techniques, determining that both conjugates presented analogous conformation, although different from unconjugated PGA. Biodistribution studies were carried out by optical imaging and PET techniques. The labelled PGA-CONH-Doxy 15ωt% was renally cleared. Half–life time value was 0.98h greater than parent PGA (0.59h) with smaller size and different solution conformation as seen by SANS. The conjugate remain stable in plasma without showing haemolytic properties indicating their

suitability for i.v. administration.

Finally, a preliminary study applying combination therapy was performed *in vivo* in a young FAP model. Best candidates of each family, C2P1 and PGA-CONH-Doxy were selected for the experiment, per separate and in combination. Animals were classified in three groups: *Group 1* was treated with the conjugate C2P1, *group 2* with C2P1 and PGA-CONH-Doxy and *group 3* with PGA-CONH-Doxy. Non-treated mice with FAP disease were used as positive as well as healthy mice as negative controls. Doses were adjusted (0.036mg RAGE pep/Kg of C2P1 and 8mg Doxy/Kg for PGA-Doxy conjugates and i.v. administered during 6 weeks with 2 doses per week). Results in non-fibrillar TTR deposition and other molecular markers were not reliable compared to the control group. However, combination group presented the best output when the three groups were compared. The studies should be repeated with a previous dose study together with trials in an older FAP model, more appropriate for doxy conjugates. Furthermore, histological analysis of key organs (gastrointestinal tract and liver) validated the safety of the conjugates. Unexpectedly, recovery of the liver morphology was observed in treated animals.

Future directions will encompass a proper *in vivo* experimental set up within an old FAP model of our conjugates with an optimisation test of the most appropriate dose. We really encourage the use of combination at this stage due to their target molecules coexist at advanced phases. Moreover, we also proposed the use per separate of pegylated RAGE peptide conjugate C2P1 in early stages of the disease or the PGA-CONH-Doxy alone in advanced phases.

To define the best combination conjugate (both agents in the same polymer matrix or conjugated into different polymers), extra combination tests may be carried out *in vitro* as well as *in vivo*. As targets can be located in different parts of the extracellular emplacement, it could be expected that conjugates per separate will display the best output.

BIBLIOGRAPHY

1. N. J. Abbott, L. Ronnback, and E. Hansson, *Astrocyte-endothelial interactions at the blood-brain barrier.* Nat Rev Neurosci, 2006. **7**(1): p. 41-53.
2. Su, Y. and P.J. Sinko, *Drug delivery across the blood-brain barrier: why is it difficult? how to measure and improve it?* Expert Opin Drug Deliv, 2006. **3**(3): p. 419-35.
3. M. J. Vicent, H. Ringsdorf, and R. Duncan, *Polymer therapeutics: Clinical applications and challenges for development.* Adv Drug Deliv Rev., 2009. **61**(13): p. 1117.
4. Duncan, R., *Polymer therapeutics as nanomedicines: new perspectives.* Curr Opin Biotech, 2011. **22**(4): p. 492-501.
5. R. Duncan and M.J. Vicent, *Polymer therapeutics-prospects for 21st century: The end of the beginning.* Adv Drug Deliv Rev, 2013. **65**(1): p. 60-70.
6. M.J. Vicent, et al., *Polymer conjugates as therapeutics: future trends, challenges and opportunities.* Exp Opin Drug Rev, 2008. **61**: p. 1220-1231.
7. F. Canal, J. Sanchis, and M.J. Vicent, *Polymer-drug conjugates as nano-sized medicines.* Curr opin Biotech, 2011. **22**(894-900).
8. Vayaboury, W., et al., *Synthesis of N-protected-L-lysine and alpha-benzyl-L-glutamate N-carboxyanhydrides (NCA) by carbamoylation and nitrosation.* Amino Acids, 2004. **27**(2): p. 161-167.
9. N. Hadjichristidis, et al., *Synthesis of well-defined polypeptide-based materials via the ring-opening polymerization of alpha-amino acid N-carboxyanhydrides.* Chem Rev, 2009. **109**(11): p. 5528-78.
10. Deming, T.J., *Methodologies for preparation of synthetic block copolypeptides: materials with future promise in drug delivery.* Adv Drug Deliv Rev, 2002. **54**: p. 1145-1155.
11. Deming, T.J., *Synthetic Polypeptides for Biomedical Applications. Progress in Polymer Science **32**, 858-875.* Prog

Polym Sci, 2007. **32**(858-875).

12. Deming, T.J., *Polypeptide-based materials.* Topics in Current Chemistry. Springer, 2012. **310**.
13. J. Cheng and T.J. Deming, *Synthesis of polypeptides by ring-opening polymerization of alpha-amino acid N-carboxyanhydrides.* Top Curr Chem, 2012. **310**: p. 1-26.
14. I. Dimitrov and H. Schlaad, *Synthesis of nearly monodisperse polystyrene-polypeptide block copolymers via polymerisation of N-carboxyanhydrides.* Chem Commun (Camb), 2003(23): p. 2944-2945.
15. Y. Knobbler, S. Bittner, and M. Frankel, *Reaction of N-carboxy-alpha-aminoacid anhydrides with hydrochlorides of hydroxylamine, O-alkylhydroxylamines and amines.* J Chem Soc, 1964. **3941**.
16. Y. Knobbler, et al., *alpha-aminoacyl derivatives of aminobenzoic acid and amino-oxy-acids by reaction of their hydrochlorides with amino-acid N-carboxyanhydrides.* J Chem Soc, 1969. **1969**: p. 1821-1824.
17. Z.J. Kamiński, et al., *N-Triazinylammonium Tetrafluoroborates. A New Generation of Efficient Coupling Reagents Useful for Peptide Synthesis.* Journal of the American Chemical Society, 2005. **127**(48): p. 16912-16920.
18. Macholz, R.M., *W. Kliegel: Bor in Biologie, Medizin und Pharmazie. Physiologische Wirkung und Anwendung von Borverbindungen. Tab.* . Springer-Verlag, Berlin, Heidelberg, New York 1980. , 1981. **25**(7): p. 701-701.
19. C.L. Chang, M.K. Leung, and M.H. Yang, *Alkyl and dialkylammonium tetrafluoroborate catalyzed cis–trans isomerization of 1,3,5-trimethyl-1,3,5-triphenylcyclotrisiloxane.* Tetrahedron, 2004. **60**(41): p. 9205-9212.
20. D. Wu and W.M. Pardridge, *Pharmacokinetics and blood-brain barrier transport of an anti-transferrin receptor monoclonal antibody (OX26) in rats after chronic treatment with the antibody.* Drug Metab Dispos, 1998. **26**(9): p. 937-9.
21. D. Wu and W.M. Pardridge, *Neuroprotection with noninvasive*

neurotrophin delivery to the brain. Proc Natl Acad Sci U S A, 1999. **96**(1): p. 254-9.

22. F. I. Staquicini, et al., *Systemic combinatorial peptide selection yields a non-canonical iron-mimicry mechanism for targeting tumors in a mouse model of human glioblastoma.* J Clin Invest, 2011. **121**(1): p. 161-73.
23. A. Regina, et al., *Antitumour activity of ANG1005, a conjugate between paclitaxel and the new brain delivery vector Angiopep-2.* Br J Pharmacol, 2008. **155**(2): p. 185-97.
24. Y. Ando, M. Nakamura, and S. Araki, *Transtyretin-related familial amyloidotic polyneuropathy.* Arch Neurol, 2005. **62**(7): p. 1057-1062.
25. F. A. Monteiro, et al., *In vitro inhibition of transthyretin aggregate-induced cytotoxicity by full and peptide derived forms of the soluble receptor for advanced glycation end products (RAGE).* FEBS Lett, 2006. **580**(14): p. 3451-6.
26. I. Cardoso, G. Merlini, and M. J. Saraiva, *4'-iodo-4'-deoxydoxorubicin and tetracyclines disrupt transthyretin amyloid fibrils in vitro producing noncytotoxic species: screening for TTR fibril disrupters.* FASEB J, 2003. **17**(8): p. 803-9.
27. I. Cardoso and M.J. Saraiva, *Doxycycline disrupts transthyretin amyloid: evidence from studies in a FAP transgenic mice model.* The FASEB Journal, 2006. **20**: p. 234-239.
28. B. Macedo, et al., *Biomarkers in the assesment of thereapies in Familial Amyloidotic Polyneuropathy.* Mol Med, 2007. **13**(11-12): p. 584-591.
29. M.M. Sousa, et al., *Familial amyloid polyneuropathy: receptor for advanced glycation end products-dependent triggering of neuronal inflammatory and apoptotic pathways.* J Neurosci., 2001. **21**: p. 7576-7586.

FINAL CONCLUSIONS

FINAL CONCLUSIONS

CHAPTER II

1. A versatile and simple methodology for the preparation of well-defined polyglutamates by means of ROP-NCA has been described. For the first time ammonium salts with non-nucleophilic tetrafluoroborate anions were used as initiators, allowing a multigram scale synthesis with defined molecular weight (up to 800 units), low polydispersity (<1.2), controlled chain end functionality and adequate stereoselectivity and absence of any trace of toxic impurity to allow biomedical applications.

2. Varying the initiators, different polyglutamate-based systems were obtained, e.g. homopolymers and diblock copolymers, with different lengths of the polypeptide block.

3. Deprotection of γ-benzylpolyglutamates under acid (TFA/HBr) as well as basic conditions (NaOH aq./THF) has been optimised in order to be exploited without compromising the integrity of PEG-based block copolymers or the incorporated sensitive functional groups.

4. Diblock copolymers (PEG-PGA_n) have been obtained either through ROP-NCA or after PGA_n post-polymerisation. In addition, this latest protocol enabled also the synthesis of triblock copolymers (PEG-PGA_n-PEG-X) in which is introduced a unique point of linkage (X) for specific anchoring of targeting ligands.

5. Post-polymerisation processes allowed the construction of polyglutamates with different functional groups than carboxylic acid for specific and orthogonal conjugation, e.g. amines, sulfhydryls or alkynes.

CHAPTER III

1. Triblock copolymers (PEG-PGA_n-PEG, n=100, 150, 200) were successfully labelled with the fluorophore Oregon green (OG) and appropriate protocols for fluorescence stability measurements were optimised. TBs (n=100, 200) were also labelled with the chelator DTPA and later complexed with Gd(III).

2. PGA homopolymer and DB systems (PGA_n, PEG-PGA_n, n=100,200) were effectively conjugated with the NIR dye Cy5.5 via click chemistry (PGA) and amide bond (DB). In addition, both systems were labelled with the radionuclide complex DOTA/^{68}Ga through amide bonds with the polymer platform.

3. Several targeting ligands for BBB crossing through receptor-mediated endocytosis were conjugated to the polyglutamates.

   a. Transferrin (Tf) was previously thiolated for latter conjugation to TBs (unlabelled or OG-labelled) and DB-Cy5.5, by means of disulphide bonds.

   b. The monoclonal antibody OX26, after a mild reduction, was successfully conjugated to TB-DTPA/Gd system again through disulphide bonds.

   c. The targeting peptides cPEP and Angiopep-2 were conjugated to PGA and DB (n=100) previously labelled with DOTA/^{68}Ga.

CHAPTER IV

1. Triblock copolymers (n=100, 150, 200) demonstrated its cell viability in a human endothelial cell line (HUVEC) and studies on cellular trafficking by means of flow cytometry and live-cell fluorescence confocal microscopy established preferentially an endocytic internalisation mechanism.

2. Targeted and non-targeted polyglutamates were subjected to biodistribution studies under different techniques: optical imaging, MRI and PET.

a. Regarding the non-targeted systems, PGA (PGA-DOTA), DB (DB-Cy5.5) and TB (TBO) showed renal secretion, non specific accumulation in any other organ and none of them presented inherent properties for BBB crossing. In these "proof of concept" studies, results demonstrated that polyglutamates were adequate carriers for drug delivery.

b. The observed sensitivity of PET experiments pointed out this technique as the preferred for conjugate brain crossing detection.

c. Among the targeted polymers, neither the Tf nor the mAbOX26 or the peptidic sequences achieved a significant accumulation in brain. Nevertheless, the peptides were selected as the best ligands due to the simplicity of their handling over the chemical process and the most advanced moieties in the field for the purposed objective. Novel architectures and PGA-based constructs are being developed allowing better exposure of the peptides and therefore, greater brain targeting results are expected.

CHAPTER V

1. For the first time in the field, novel polymer- drug conjugates for the treatment of FAP have been synthesised and characterised in this study. Two bioactive molecules, a low MW drug (doxycycline) and a 6aa peptide (RAPEpep) have been conjugated to polymeric platforms: PGA and PEG, respectively.

2. A library of PGA-Doxy conjugates with a drug loading ranging from 2 to 60ωt% was synthesised and characterised. Drug linkage was performed through ester or amide bonds, either directly to the polymer or through a dipeptide as linker. Screening their activity as TTR fibril disruptors, amide conjugates demonstrated higher response

at equivalent parent drug dose. Specifically, conjugates with 15 and 30ωt% drug content were the best. Trying to explain this fact, physico-chemical studies were performed finding out that drug release was not a requisite for activity and that conformation in solution for both conjugates was analogous, although different from unconjugated PGA. Biodistribution studies were carried out by optical imaging and PET techniques. The labelled PGA-CONH-Doxy 15ωt% was renally excreted. Half–life time value was 0.98h greater than that obtained for PGA (0.59h). All synthesised conjugates are not haemolytic remained indicating their suitability for i.v. administration.

3. RAGE peptide and two derivates (PEP1 and PEP2) with one or two amino acids extra for amide and disulphide bond linkage to the polymer were synthesised by Fmoc-solid phase peptide synthesis and characterised. A small library of RAGEpep conjugates was obtained by PEGylation and fully characterised. The amide conjugate carrying two molecules of RAGEpep (C2P1) showed the best inhibition of TTRagg-induced cytotoxicity in Schwann cells at 24h. Those conjugates containing disulphide linkers gave less reproducible data and lower activity. Binding affinity and the solution conformation studies supported this activity due to the maintenance of RAGEpep affinity for the aggregates and revealed a more stable conformation in solution, which may help into RAGEpep spatial availability for the interaction. Biodistribution experiments showed a renal secretion and non-accumulation in undesired areas.

4. A preliminary study *in vivo* in a young FAP model was carried out administering C2P1 and PGA-CONH-Doxy, per separate and in combination. Results in non-fibrillar TTR deposition and other molecular markers were not reliable compared to the control group. However, combination group presented the best output when the three groups were compared. The studies should be repeated with a previous dose study together with trials in an older FAP model, more appropriate for doxy conjugates. Furthermore, histological analysis validated the safety of the conjugates. Unexpectedly, recovery of the liver morphology was observed in treated animals.

[FINAL CONCLUSIONS]

APPENDICES

APPENDIX I. THESIS PROJECT INDEX, OBJECTIVES, METHODOLOGY AND CONCLUSIONS IN SPANISH

1. INTRODUCCION Y MARCO TEMÁTICO DE LA TESIS

Nanociencia y nanotecnología son la base de técnicas innovadoras para el transporte de fármacos con beneficios potenciales para el paciente y nuevos mercados para la industria. La obtención de nuevos sistemas de transporte de fármacos más efectivos es uno de los principales retos actuales, junto con la mejora del diagnóstico tanto *in vitro* como *in vivo* y el desarrollo de tecnologías para la ingeniería tisular y la medicina regenerativa. Además de ser necesario disponer de moléculas con actividad farmacológica para conseguir terapias efectivas se necesitan su transporte y liberación controlada para llegar a conseguir tratamientos con mayor índice terapéutico. El uso de estrategias de direccionabilidad ('targeting'), tanto activa (unión del portador a residuos dirigentes) [1, 2] como pasiva (acumulación en zonas enfermas por efecto EPR, *Enhanced and Permeability Retention effect* [3-6]) permite la acumulación del fármaco en el tejido enfermo, aumentando la actividad y reduciendo la toxicidad sistémica inherente de los fármacos. En la actualidad existen terapias muy interesantes por su actividad terapéutica o mecanismo de acción molecular pero, debido a su toxicidad, baja solubilidad del compuesto, estabilidad, capacidad de transporte intracelular o difícil farmacocinética son abandonadas antes de llegar a clínica por no disponer de un sistema de transporte celular adecuado que los solubilice, proteja o dirija a su diana molecular, ej: péptidos, proteínas o terapias basadas en ácidos nucléicos (DNA, siRNA, oligonucleótidos…).

El desarrollo multidisciplinar de la química de polímeros, la biología, la física y la medicina ha dado lugar a los primeros nanofármacos poliméricos entre los que se encuentran los 'Polímeros Terapéuticos' (PT): nanoconstrucciones híbridas que emplean polímeros hidrosolubles, tanto de forma bioactiva como parte funcional inerte de un complejo multicomponente, donde el agente bioactivo se une de forma covalente al portador polimérico mediante un enlace que responde frente a condiciones fisiológicas específicas [7, 8]. Desde un punto de vista industrial, los PT son considerados como

nuevas entidades químicas y no como simples sistemas convencionales de transporte de fármacos (‘depots’) [9]. Los sistemas de transporte tradicionales simplemente atrapan, solubilizan o liberan de forma controlada el agente bioactivo sin utilizar una conjugación química. Conceptualmente, los Polímeros Terapéuticos comparten muchas características con otros fármacos macromoleculares (como proteínas, anticuerpos u oligonucleótidos) y profármacos macromoleculares, incluyendo los inmunoconjugados. Sin embargo, poseen ventajas adicionales como la versatilidad de la química sintética, que permite confeccionar el peso molecular y adicionar características biomiméticas, o la posibilidad de incluir elementos que responden a cambios fisiológicos. El término “Polímeros Terapéuticos” engloba cinco grupos de nanoconstrucciones: fármacos poliméricos (polímeros con actividad inherente), conjugados polímero-fármaco, conjugados polímero-proteína, poliplejos con aplicación como vectores no virales en transporte génico y micelas poliméricas con el fármaco conjugado de forma covalente a un polímero anfifílico [10, 11].

Tras la salida al mercado de los primeros conjugados polímero-proteína y el creciente número de conjugados polímero-fármaco en fase clínica, los conjugados poliméricos anticancerígenos se establecen como terapia efectiva para el tratamiento del cáncer. Actualmente, esta plataforma tecnológica se centra en obtener conjugados de segunda generación que suplan las dificultades encontradas hasta el momento y propongan mejoras considerables respecto a sus características y propiedades. Se han aceptado cuatro nuevas estrategias para que esta novedosa plataforma tecnológica dé lugar a terapias más específicas y efectivas: (i) la búsqueda de nuevos soportes poliméricos (polímeros biodegradables con elevado Mw, arquitecturas poliméricas definidas y controladas), (ii) la caracterización físico-química exhaustiva de estos sistemas para una mejor comprensión de su comportamiento biológico, (iii) su aplicación a nuevas dianas terapéuticas en áreas distintas al cáncer y (iv) el uso de terapia de combinación para obtener compuestos de mayor índice terapéutico [7, 12, 13].

Siguiendo estas directrices, en la presente tesis doctoral se han

desarrollado varias de las nombradas aproximaciones: la síntesis de novedosos portadores poliméricos basados en el ácido poli-L-glutámico, caracterizado por su biodegradabilidad, multifuncionalidad y versatilidad; su utilización como base para obtener conjugados polímero-fármaco focalizados en el tratamiento de desordenes neurodegenerativos, diana novedosa y actualmente en crecimiento exponencial dentro del campo de PT y el uso de terapia de combinación como herramienta para una posible sinergia en el tratamiento.

La propuesta de la diana terapéutica elegida responde al reto actual del aumento de la expectativa de vida en nuestra sociedad, el cual ha traído consigo un incremento de las enfermedades crónicas neurodegenerativas en la población de edad avanzada. Estas enfermedades pueden subdividirse dependiendo del sistema nervioso al que afecten, el periférico (SNP) o el central (SNC). En este último la dificultad se acentúa debido a que su tratamiento requiere atravesar una barrera biológica protectora con elevada restricción al paso de fármacos al cerebro: la barrera hematoencefálica (BHE) [2, 14-16]. La estrategia propuesta en esta tesis doctoral ha sido la utilización de PT como plataforma tecnológica para el desarrollo de conjugados poliméricos multivalentes con aplicaciones para el tratamiento de la neurodegeneración, tanto a nivel periférico como central, siendo capaces de atravesar la BHE y liberar el(los) fármaco(s) conjugado(s) en el cerebro. Estos sistemas vencerían las limitaciones mostradas por agentes terapéuticos de bajo peso molecular tales como la internalización celular y aumentarían la especificidad del tratamiento. De entre las diversas metodologías existentes para cruzar la BHE, en el presente trabajo se seleccionó el transporte activo. Esta estrategia propone el uso de vehículos transportadores (sistemas de transporte de fármacos, DDS) para los nutrientes naturales, desarrollando complejos moleculares como “caballos de Troya”. Para ello, se utilizan residuos dirigentes que sean capaces de ser reconocidos por un transportador activo localizado en el área apical de la barrera hematoencefálica, como por ejemplo el receptor de transferrina (TfR).

En un primer lugar y como ejemplo de enfermedad neurodegenerativa, el trabajo se ha centrado en la obtención y estudio

de conjugados polímero-fármaco para el tratamiento de polineuropatías familiares amiloideas (PAF) que principalmente afectan a SNP, pero que parcialmente dañan al SNC, por tanto, también se han desarrollado sistemas poliméricos dirigidos para atravesar la BHE. Una vez este reto superado, el tratamiento diseñado para FAP podría explorarse en otro tipo de enfermedades amiloideas como la conocida enfermedad de Alzheimer.

Las polineuropatías amiloidóticas familiares (PAF) son enfermedades neurodegenerativas caracterizadas por una deposición sistémica extracelular de fibrillas amiloides de la proteína transtirretina (TTR) [17]. La PAF se presenta clínicamente con neuropatía periférica, sensitivo-motora y autonómica, produciendo una afectación cardíaca, ocular o renal, provocando la muerte 10-15 años tras iniciarse los primeros síntomas. Aunque con resultados variables, el trasplante hepático es la única alternativa terapéutica actualmente disponible para prevenir la progresión de la enfermedad. Por este motivo, en el presente proyecto se han desarrollado, por primera vez en el campo de la nanomedicina, nanoconjugados con potencial terapéutico como tratamiento de este tipo de enfermedades. Como agentes bioactivos para la conjugación con el portador polimérico se han utilizado la doxiciclina [18] y una secuencia peptídica específica de receptores RAGE (péptido RAGE) [19]; actividad descubierta por la colaboradora del presente proyecto M.J. Saraiva y su grupo (IBMC, Portugal).

2. OBJETIVOS DE LA INVESTIGACIÓN

El objetivo principal de la presente tesis ha sido el desarrollo de una familia de nanoconjugados de segunda generación para el tratamiento de enfermedades neurodegenerativas, creando una novedosa terapia más efectiva. Éste puede desglosarse en tres objetivos específicos: (1) la obtención de nuevos transportadores poliméricos basados en el ácido poli-L-glutámico (PGA): un polímero biodegradable, multifuncional y versátil, (2) su caracterización fisico-química exhaustiva para una mejor comprensión de su comportamiento biológico y su validación como sistemas para el transporte de fármacos, y (3) su uso para el tratamiento de nuevas dianas terapéuticas como las enfermedades degenerativas, construyendo sistemas dirigidos capaces de atravesar la barrera hematoencefálica (BHE) y, por otra parte, la obtención de conjugados polímero-fármaco para el tratamiento de PAF.

3. METODOLOGÍA

3.1 Materiales e instrumentación

Todas las reacciones descritas se han llevado a cabo bajo atmósfera inerte (nitrógeno o argón), en caso de ser necesario.

Todos los reactivos y disolventes utilizados eran de grado analítico o superior y se utilizaron sin purificación adicional (en caso de requerir purificaciones añadidas, se encuentran descritas en el correspondiente apartado).

Cromatografía por exclusión de tamaño (size exclusion chromatography, SEC). Se emplearon columnas con resina Sephadex®G25/PD10 (ddH_2O como eluyente). Para el análisis por HPLC se empleó un sistema de Waters (Milford, USA) compuesto por un muestreador automático (717), un detector fotodiodo (Z996), un sistema de tres bombas (515) y un detector de fluorescencia (modelo 2475). Para el análisis de conjugados PGA-X-Doxy se utilizaron dos columnas en serie TSK-gel (G300 y G25000 PWXL), flujo 1mL/min y PBS 0.1M como fase móvil en gradiente isocrático. Para la cromatografía en fase reversa se empleó una columna LIChroCART®, Cat.1.50943 LiChrospher®100, RP-18 (125x4mm, 5µm) de Waters Ltd. (Hertfordshire, UK) en el mismo sistema, utilizando como método gradientes de acetonitrilo 0.1%TFA (v/v) y agua 0.1%TFA (v/v). Para los conjugados PEG-péptido se utilizó una columna Zorbax®, flujo 1mL/min, PBS 0.1M pH=7.4 como fase móvil con gradiente isocrático 15min.

Cromatografía líquida (Fast Protein Liquid Chromatography, FPLC). Se utilizó un equipo AKTA PURIFIER de Amersham Biosciences el cual está formado por un sistema de bombas P900, un monitor pH/C-900, un inyector (INV-907), un detector UV (UV-900) y un recolector de fracciones (FRAC-900). Para los conjugados del péptido RAGE se utilizó una columna Macrocap SP de GE Healthcare Bio-Sciences usando como fase móvil gradientes de NaCl 1M en ddH_2O. Para los conjugados de transferrina se empleó una columna HiPrep Sephacryl S300 26/60 utilizando como fase móvil PB pH=8 en gradiente isocrático.

Espectroscopía ultravioleta-visible (UV). Los espectros de UV fueron realizados en un espectrofotómetro Jasco V-630 UV/Vis.

Cromatografía de permeación en gel (GPC). Los análisis se realizaron en un Triple Detector Array (TDA^{TM}) de Viskotek (TDA3 302) complementado con un índice de refracción (RI), detector de light scattering, detector de viscosidad y un detector UV modelo 2501. Las columnas empleadas fueron dos TSK-Gel en serie (Styragel HR3 y HR4, tamaño partícula 6um, 300x7.8mm). OmniSec 4.1 fue el software utilizado. Como fase móvil se utilizó DMF 0.1%LiBr, con el sistema equilibrado a 70°C. Se realizaron análisis de las muestras en GPC utilizando HFIP (3g/L trifluoroacetato potásico) como fase móvil, 40°C y columnas de sílica modificada (PFG, tamaño partícula 7µm, porosidad 100 & 1000 Å) en Mainz, Alemania.

*Espectroscopía de infrarrojo (*FTIR). Los espectros de IR fueron medidos en un sistema Thermo Scientific Nicolet 380. Todas las muestras analizadas se encontraban disueltas en DMF. Los análisis se realizaron a 25°C.

Polarimetría. La quiralidad de los polímeros desprotegidos fue evaluada mediante con un polarímetro Jasco P-1020, midiendo cada muestra por triplicado (20scans/medida) en una celda de vidrio cilíndrica (ϕ 3.5x100mm). Las muestras se prepararon en ddH_2O a 10 mg/ml y se midieron a 25°C. Los datos se analizaron con el software Spectra Manager.

Resonancia magnética nuclear (RMN). Los espectros de ^{1}H, ^{13}C y DOSY fueron realizados en un sistema Bruker Advance AC-300 (300MHz) o AV500 (500MHz). Los espectros se hicieron en disolventes deuterados a 300K.

Cromatografía líquida-espectrometría de masas (*LCMS).* El equipamiento utilizado consta de un sistema Acquity UPLC (Ultra Performance Light Cromatography (Waters) con un detector PDA acoplado a un espectrómetro de masas Micromass ZQ Waters 400 LC Single quadrupole. Se utilizó una columna de fase reversa RP-18 Kinetex (2.6µm x100mm).

Microscopía de transmisión electrónica (TEM). Las muestras fueron adsorbidas en rejillas de cobre recubiertas por una película de

carbón de 200 mallas. Tras someter las rejillas a un proceso de glow-discharge, las muestras fueron depositadas y se realizó una tinción de contraste negativo con una disolución de acetato de uranilo al 1%. Las imágenes se adquirieron con un microscopio Zeiss operado a 60kV.

Dispersión de luz dinámica (DLS). El tamaño de partícula fue medido en un dispositivo Malvern Zetasizer Nano ZS equipado con un laser (532nm) a un ángulo de dispersión fijo de 90°. Las medidas se realizaron a 25°C.

Medidas de absorbancia o fluorescencia de ensayos in vitro o muestras ex vivo tratadas. Las medidas se realizaron en un equipo Victor^2 Wallac 1420 Multilabel HTS Counter Perkin Elmer (Northwolk, CT, EEUU) utilizando placas de 96 pocillos y las correspondientes longitudes de onda (emisión/excitación) propias de cada compuesto.

Ensayos celulares. Todos los procesos relacionados con el cultivo celular se llevaron a cabo en una cabina de flujo laminar recirculante vertical con seguridad biológica clase II (Telstar). En todo momento se utilizó material estéril.

Microscopía confocal de fluorescencia. Los estudios de internalización celular fueron hechos a través del Servicio de Microscopía Confocal del CIPF (Valencia). Las imágenes fueron adquiridas con un microscopio (invertido) láser confocal Leica, modelo TCS SP2 AOBS (Leica Microsystems Heidelberg GMBH, Mannheim, Alemania) usando un objetivo de inmersión de 63X Plan-Apochromat-Lambda Blue 1.4 N.A. La longitud de onda (λ) usada para excitar el fluorocromo fue: 488nm para el Oregon Green (OG), utilizando para ello un láser de argón. Las aperturas de los canales para la detección de la emisión del OG fueron: de 503 a 604nm. Las imágenes fueron tomadas bidimensionalmente y en pseudo color (255 niveles de color), con una resolución de 1024x1024 pixeles. Todas las imágenes fueron adquiridas bajo las mismas condiciones y los análisis de distribución de fluorescencia fueron hechos mediante el software de Leica “Leica Lite” versión 2.61.

Ensayos de imagen óptica in vivo. Para los estudios de biodistribución por fluorescencia se utilizó la plataforma IVIS®Spectrum equipado con el software Living Image®3.2 (Caliper Life

Sicences, Hopkinton, MA).

Ensayos mediante imagen por resonancia magnética (MRI). Los experimentos de biodistribución por MRI se realizaron en un espectrómetro horizontal Bruker Pharmascan (Bruker medical Bmbh, Ettlingen, Alemania) utilizando un imán superconductor de 7.0T, equipado con un resonador de volumen selectivo para 1H de 38mm y un inserto de gradientes Bruker de 90mm de diámetro. Los estudios fueron adquiridos en una consola Hewlett-Packard mediante el programa Paravision (Bruker medical Gmbh) operando sobre una plataforma Linux. El estudio fue realizado en el Instituto de Investigaciones Biomédicas "Alberto Sols" (CSIC/UAM), Madrid.

Ensayos por tomografía de emisión de positrones (PET). Para el estudio de biodistribución mediante PET, se utilizó un aparato Argus PET/CT (SEDECAL, Madrid) para la monitorización in vivo y se cuantificó la radiactividad *ex vivo* en un contador de centelleo gamma Cobra II auto-gamma. Los ensayos se realizaron en la unidad de Aplicaciones Biomédicas y Farmacocinéticas del CIEMAT, Madrid.

Dispersión de neutrones de ángulo pequeño (SANS). Los experimentos de SANS se llevaron a cabo en un instrumento D11 en el Institute Laue-Langevin (Grenoble, Francia) para determinar el tamaño y forma de los conjugados PGA-Doxy. Las muestras en disolución fueron preparadas con una concentración de conjugado de 10mg/mL en PBS deuterado 0.1M y se colocaron en células de cuarzo de 2mm de camino óptico, manteniendo una temperatura de 37 °C ($\pm$ 0.2). Estas condiciones permiten el estudio de los conjugados al pH, temperatura y fuerza iónica que experimentan los conjugados en los experimentos *in vivo.* El modelo FISH se utilizó para el análisis de los datos [20] .

3.2 Métodos más relevantes

3.2.1 Polimerización por apertura de anillo de N-α-carboxianhidridos.

Síntesis del monómero NCA-L-Glu (ɤ-bencil-L-glutamato N-Carboxianhidrido)

H-L-Glu(OBzl)-OH (71.7mmol, 1eq, 237.26g/mol) se añadió en un matraz de 500mL de dos bocas equipado con una columna de reflujo y un embudo de adición. El sistema fue purgado con nitrógeno. Después se añadió THF anhidro (recién destilado) (150mL) y el sistema se puso bajo agitación. A continuación, se adicionó gota a gota difosgeno (0.043mmol, 0.6eq, 1.6525g/cm^3, 197.83g/mol) diluido en THF anh. (10mL) mediante el embudo. La mezcla se dejó agitando durante 2h a 50^{o}C bajo flujo de nitrógeno. Después, la mezcla fue burbujeada con nitrógeno durante 2h para eliminar el HCl, colocando la salida del gas en una solución de sosa 1M. Luego el disolvente fue evaporado en un rotavapor hasta ¼ del volumen inicial. Se añadió etilacetato (16mL) y la mezcla se precipitó sobre hexano frío (500mL). El precipitado se aisló por filtración a vació y se lavó con hexano. A continuación, el producto fue recristalizado en tolueno anh. (60mL) y THF anh (30mL), añadiendo hexano gota a gota hasta inducir la cristalización. El matraz se dejó bajo atmósfera inerte a -20^{o}C durante 16h. Los cristales blancos se filtraron a vacío y se lavaron con hexano frío. El producto se secó a vacío. La recristalización fue realizada por triplicado. La identidad del producto se confirmó por RMN y punto de fusión (p.f.). Nota. La síntesis fue escalada hasta 34g de material inicial.

Síntesis de los iniciadores BF_4

nBuBF_4: Butilamina (2.7mmol, 73.14g/mol) se disolvió en dietileter (1mL), y se adicionó gota a gota el complejo $HBF_4.Et_2O$ (2.7mmol, 1.18g/cm^3, 161.93g/mol), dando lugar a la formación de una sal sólida blanca. El producto se secó a vació y se recristalizó en etilacetato.

Npt-BF_4: Neopentilamina (36.74mmol, 0.745g/cm^3, 87.16g/mol) fue adicionada gota a gota sobre 5mL del complejo $HBF_4{\cdot}Et_2O$ (34.5mmol, 1.18g/cm^3, 161.93g/mol), bajo agitación moderada, resultando en la formación de un sólido blanco. Tras secar el sólido a

vacío, se recristalizó por duplicado en etilacetato, lavando el sólido obtenido con hexano frío. El producto final se secó a vacío.

mPEG-BF_4: En un vial de 5mL, MeO-PEG(2000)-amine (0.3mmol, 1910g/mol) fue disuelto en THF (3mL) bajo agitación, y $HBF_4 \cdot Et_2O$ (0.3mmol, 1.18g/cm^3, 161.93g/mol) se añadió a la disolución gota a gota formando un sólido de color amarillo pálido. El disolvente se evaporó a vacío y el residuo se lavó por triplicado con hexano (hasta obtener un pH no acido). El sólido obtenido se secó a vacío.

Polimerización de N-carboxianhididridos. Síntesis de poli-γ-bencil-L-glutamato (PBLG)

Todo el material utilizado para la polimerización fue limpiado de forma exhaustiva antes de ser utilizado. Primero, el material se colocó en DMF y se aclaró con acetona, a continuación en H_2O_2 y finalmente aclarado con ddH_2O. Después, el material se secó durante 24h a 80°C. Todos los disolventes utilizados fueron destilados previamente y secados sobre tamiz molecular en atmósfera inerte (Ar). Los iniciadores se secaron a vacío previo uso y el monómero se sintetizó y recristalizó para usarlo de forma inmediata.

1g de monómero (γ-bencil-L-glutamato N-Carboxianhidrido (3.8mmol, 264g/mol) se colocó en un tubo Schlenk que se purgó con ciclos de vacío y argón. Bajo flujo de argón, DMF anhidro se añadió al tubo (concentración: 0.1g/mL). Una vez disuelto bajo agitación, el iniciador se añadió a la reacción. La reacción se dejó bajo agitación y atmósfera inerte, y se monitorizó por GPC y espectroscopia infrarroja. Cuando se detuvo la reacción, la solución se precipitó en dietileter frío (50mL). Tras centrifugar la mezcla (2600rpm, 4°C, 10min), se eliminó el sobrenadante y el sólido blanco se suspendió en ddH_2O y se liofilizó. El producto se analizó por GPC (DMF, 0.1%LiBr / HFIP) y por RMN-^{1}H.

Desprotección de PBLG

En medio ácido

En un matraz de fondo redondo, 100mg de PBLG se disolvieron en 3mL de TFA (el volumen de TFA debe ser suficiente para disolver el polímero y que no precipite tras la adición de HBr). Después, se añadieron gota a gota 2eq de HBr (48%v/v, 1.49g/cm^3, 81g/mol) por

grupo ácido carboxílico. Tras 5h en agitación, la solución se precipitó en dietileter frío obteniendo un sólido blanco que se recuperó por filtración a vacío. La mezcla se centrifugó (2600rpm, 4°C, 10min); el sólido blanco obtenido se lavó por triplicado con dietileter y se secó a vacío. A continuación, se purificó el producto por precipitación ácido-base ($NaHCO_3$/HCl 6M). Para obtener su forma sal, tras la última adición de NaHCO3 se realizó una diálisis o ultrafiltración. Una vez desalada la disolución, se liofilizó obteniendo el producto final. Nota: para la desprotección a mayor escala (>600mg), se necesitaron 16h para una desprotección completa.

En medio básico (única opción en caso de DB, TB)

Npt-$PBLG_n$, nBu-$PBLG_n$: En un matraz de fondo redondo se disolvió el x-$PBLG_n$ (5.1µmol, 9761g/mol, n=45 GA unidades) en THF (16mL) a temperatura ambiente. Luego, la solución se colocó a 4°C y se mantuvo bajo agitación. En un vial, se disolvieron 1.5eqde NaOH por grupo carboxilo (7.7µmol, 40g/mol) en 2mL de ddH_2O y se añadieron gota a gota a la disolución principal. La reacción se dejó bajo agitación constante durante 16h. Después, el THF se evaporó a vacío y el residuo se diluyó en ddH_2O para su purificación por ultrafiltración (Vivaspin®, 3000Da). La parte superior del tubo se liofilizó y el producto sólido blanco obtenido se caracterizó por RMN para comprobar la desprotección.

PEG-PGA_n: protocolo idéntico al anterior exceptuando el uso de 2eq de NaOH por grupo carboxilo.

3.2.2 Marcaje de los portadores poliméricos con sondas fluorescentes.

Oregon Green (OG)

PEG-PGA_n-PEG (TB). En un matraz de fondo redondo se disolvieron 14.4mg de TB_{200} (0.08mmol uds. GA, 1eq, MW ud. GA=102.4g/mol, 56.63%COOH) en 1mL de DMF anh. bajo flujo de N_2. Luego, se adicionó DIC (0.24mmol, 3eq, 0.806g/cm^3, 126.13g/mol) y se

dejó la reacción agitando 5min. A continuación, se añadió directamente HOBt (0.24mmol, 3eq, 135.1 g/mol). 10min después, se añadió al matraz de reacción OG-cadaverine ($1.6 \cdot 10^{-3}$mmol, 2%mol, 496.47g/mol). El pH del medio se ajustó a 8 con DIEA. La mezcla se dejó en agitación durante 24h protegida de la luz en atmósfera inerte. Se evaporó el disolvente a vacío y el residuo obtenido se disolvió en la mínima cantidad de $NaHCO_3$ 1M y se purificó a través de una columna PD-10 Sephadex™. La carga de OG se calculó mediante espectroscopia de fluorescencia midiendo la señal de cada fracción recogida de la columna. Las fracciones donde se encontró el producto fueron juntadas y liofilizadas.

Cyane5.5 (Cy5.5)

PEG-PGA_n (DB). En un matraz de fondo redondo se disolvieron 100mg de DB_{200} (PGA_{100}–PEG-SS-4TP, 0.72mmol, 1eq, MW ud. GA(forma sal sódica)=160.5g/mol) en 8mL de ddH_2O. Para un marcaje de 2%mol, se procedió a disolver en un vial aparte DMTMM·Cl^- (0.0217mmol, 0.03eq, 276.7g/mol) en 1mL de ddH_2O que se adicionó al matraz de reacción. Tras 10 min en agitación, Cy5.5-NH_2 (0.0144mmol, 0.02eq, 589.25g/mol) previamente disuelto en 7mL de ddH_2O se añadió a la reacción. El pH se ajustó a 8 ($NaHCO_3$ 1M). La reacción se monitorizó por TLC (MeOH). Tras 40h a temperatura ambiente, la reacción se liofilizó y el sólido azul obtenido se redisolvió en la mínima cantidad de ddH_2O y se purificó con una columna PD10 utilizando como eluyente ddH_2O. Las fracciones recolectadas se analizaron en un fluorímetro para calcular el porcentaje de marcaje. Las fracciones donde se encontró el producto se juntaron y liofilizaron. En este caso, la estabilidad del grupo 4TP se comprobó tras la obtención del producto final (test de absorbancia a 343nm).

DOTA / ^{68}GA

PGA_n: Para un porcentaje teórico de 10%mol: PGA_{100} (2.32mmol, 1eq, MW ud. GA=129g/mol) se colocó en un matraz de fondo redondo

y el sistema fue purgado bajo flujo constante de N_2. Tras su disolución en 20mL de DMF anh, se adicionaron 1.5eq de DIC (0.35mmol, 0.836g/cm^3, 126.20g/mol). 5minutos después, se añadieron 1.5eq de HOBt (0.35mmol, 135.10g/mol). Tras 10 minutos, el derivado DOTA-NH_2 (tert-butil 2,2´,2´´-(10-(2-(2aminoetilamino)-2oxoetil)-1,4,7-tetrazaciclododecano-1,4,7-triil)triacetato, 0.23mmol, 0.1eq, 614.82/mol) se disolvió en DMF anh. y se añadió a la reacción principal. El pH se ajustó a 8 con DIEA. Tras 48h en agitación a temperatura ambiente, la disolución se concentró a vacío y se procedió a la purificación del residuo mediante su precipitación en un exceso de acetona fría. El precipitado se recolectó tras centrifugar la mezcla (2600rpm, 4°C, 10min) y se secó a vacío. El porcentaje conjugado de DOTA se calculó tras el análisis del producto por RMN-^{1}H (D_2O).

La desprotección de los grupos t-butilo del DOTA se llevó a cabo en una mezcla TFA/H_2O/TIS (95:2.5:2.5 (v/v)), dejando la reacción bajo agitación durante 3h a temperatura ambiente. A continuación, se precipitó sobre un exceso de dietileter frío. El sólido obtenido se recuperó tras centrifugar la mezcla, se lavó y se secó a vacío. El porcentaje de desprotección se evaluó mediante análisis por RMN-^{1}H (D_2O).

3.2.3 Etiquetado de los portadores poliméricos con ligandos directores.

Transferrina

Tiolación de la transferrina (Tf_{tio})

En un matraz de fondo redondo, holo-transferrina humana (0.58mmol, 1eq, 78047g/mol) se disolvió a una concentración de 10mg/mL en PB pH=9. La disolución se incubó con un exceso molar de 76.2 de 2-iminotiolano (76.2molar exceso, 44mmol, 137.63g/mol) durante 1.5h en constante agitación y protegida de la luz. La purificación de la proteína se llevó a cabo con una columna Sephadex G25 utilizando PB pH=8 como eluyente. Cada fracción fue analizada por Nanodrop® (λ_{max}=220, 280nm, Ɛ=82.74 mM^{-1} cm^{-1}) y por el ensayo

Bradford (apéndice III). Las fracciones donde se detectó el producto se unieron y se analizó la concentración final de proteína por Nanodrop®. La cantidad de grupos –SH introducida se calculó tras el análisis por MS MALDI TOF. La proteína fue utilizada de forma inmediata para su conjugación.

Conjugación de la Tf_{tio}

En un matraz de fondo redondo, DB_{100}-Cy5.5 (1.63%mol Cy5.5, 8.4eq) se disolvió en 2mL de ddH_2O y se adicionó 1eq de Tf_{tio} (en disolución). La reacción se purgó bajo flujo de nitrógeno y se dejó en agitación constante 24h a temperatura ambiente y protegida de la luz. Después, se dejó 24h más a 4°C. Se tomaron alícuotas (20µL) para monitorizar la conjugación por SDS-PAGE (apéndice III). Cuando la reacción finalizó, el volumen fue reducido por ultrafiltración (Vivaspin® MWCO=2000Da) y purificado por FPLC. De las fracciones recolectadas se analizó su absorbancia por Nanodrop® para detectar la proteína conjugada y su fluorescencia (presencia de la sonda Cy5.5) mediante fluorimetría.

Angiopep-2

Modificación post-polimerización para introducir grupos sulfidrilo en el bloque polipeptídico. Espaciador entre el polímero y el ligando.

Para un 10%mol teórico: en un matraz de fondo redondo, PGA_{100}-DOTAtBu (1.06mmol, 1eq, 10%mol DOTA, MW ud.=188.7g/mol) se disolvió en 6mL de DMF anh. bajo flujo de N_2. Mediante un activación mediada por DIC se introdujo el grupo 3-aminopropano-1-tiol activado con el grupo 4TP: se adicionó DIC (0.159mmol, 0.075eq, 0.815g/cm^3, 126g/mol) a la disolución y 5 minutos después, HOBt (0.159mmol, 0.075eq, 135.13g/mol). Tras 10minutos de reacción, se añadió 3-(piridin-4-ildisulfanil)propan-1-amino (0.106mmol, 0.1eq, 1.012g/cm^3, 186.03g/mol) a la mezcla. El pH se ajustó a 8 con DIEA y la reacción se dejó bajo agitación a

temperatura ambiente durante 48h en atmósfera inerte. La purificación se realizó por precipitación en acetona fría. El sólido obtenido se recuperó tras centrifugar y desechar el sobrenadante. El sólido se secó a vacío y se caracterizó por RMN (D_2O). Se procedió a la desprotección del DOTA.

Conjugación de Angiopep-2 a la plataforma polimérica

Para la conjugación de Angiopep-2, se emplearon los mismos equivalentes de péptido que de espaciador introducido. Ej. 45 mg de PGA-$DOTA_{11\%}$-$Cys4TP_{6\%}$ (0.225mmol, 1eq, MW ud.=200.41g/mol) se disolvieron en tampón acetato de amonio 1501mM pH=5 (4mL). A su vez, el péptido (0.011mmol, 0.05eq, 2300g/mol) se disolvió en 3mL de tampón HEPES 10mM pH=7.4. Las dos soluciones se mezclaron (pH final =6) y se dejaron 16h bajo agitación. A continuación, la mezcla se purificó a través de una columna PD10. Las fracciones se analizaron por Nanodrop® y RMN (D_2O). La cuantificación del péptido conjugado se realizó por análisis de aminoácidos.

Péptido cíclico (cPEP)

Modificación post-polimerización para introducir grupos amino en el bloque polipeptídico. Espaciador entre el polímero y el ligando.

Para un 5%mol teórico: en un matraz de fondo redondo, PGA-DOTAtBu (0.53mmol, 1eq, 10%mol DOTA, MW ud.=188.7g/mol) se disolvió en 3mL de DMF anh. bajo flujo de N_2. Una vez disuelto, se añadió DIC (0.0397mmol, 0.075eq, 0.815g/cm^3, 126g/mol) y tras 5 minutos HOBt (0.0397mmol, 0.075eq, 135.13g/mol). 10min después, se adicionó N-Boc-etilamina (0.0265mmol, 0.05eq, 1.012g/cm^3, 160.21g/mol) a la reacción principal. El pH se ajustó a 8 con DIEA. La reacción se dejó bajo agitación constante y atmósfera inerte durante 48h. La purificación se realizó por precipitación de la mezcla en acetona fría. Tras recuperar el precipitado por centrifugación, se secó a alto vacío y se caracterizó por RMN D_2O). A continuación se procedió

a eliminar el grupo protector N-Boc de la amina introducida. Para ello, el producto (0.43mmol, MW ud.=161.69g/mol) se disolvió en una mezcla CH_2Cl_2:TFA (6:4, v/v) y se dejó bajo agitación constante durante 15 a temperatura ambiente. La solución se precipitó en dietileter frío. El sólido se recuperó, se lavó y se secó a vacío. La desprotección se comprobó por RMN.

Conjugación del cPEP a la plataforma polimérica

Tras activar con N-hidroxisuccinimida el grupo carboxilo del péptido, se procedió a la conjugación de éste utilizando los mismos equivalentes que del espaciador introducido en el bloque polipeptídico. Ej. 22.25mg de PGA-$DOTA_{2\%}$-$etilendiamina_{9\%}$ (0.1398mmol, 1eq, MW ud.=160.94g/mol) se disolvieron en PBS pH=7.4 (4mL). Después, se añadieron 13mg de cPEP-NHS (0.0126mmol, 0.09eq, 1033g/mol). La reacción se dejó 5h bajo agitación. A continuación, el producto se purificó por columna PD10 (ddH_2O) y las fracciones se analizaron por RMN (D_2O). La cuantificación del péptido conjugado se realizó por análisis de aminoácidos.

3.2.4 Síntesis, caracterización y evaluación de conjugados polímero-fármaco para el tratamiento de PAF:

3.2.4.1 PGA-X-Doxy

Síntesis de los conjugados PGA-X-Doxy

Proceso de derivatización de la doxiciclina (doxy-NH_2)

Doxicilina hidrocloruro (0.5000g, 512.94g/mol) fue añadida lentamente a una solución de H_2SO_4 conc. (1.75mL). Tras finalizar la liberación de gas, la solución fue precipitada en dietileter frío (100mL). El producto se recogió por filtración, se lavó con éter y se secó bajo flujo de N_2. El producto (542.12g/mol) se redisolvió en H_2SO_4 (5 mL), se enfrió a 0° C y se añadió $NaNO_3$ (1.56eq, 101 mg, 84.99g/mol) durante 10 min mientras la reacción se agitaba. Tras 3 horas a 0 ° C, la reacción se precipitó directamente en dietileter y la mezcla se filtró a vacío. El

precipitado se lavó con éter y se secó al aire, obteniendo un polvo naranja que se usó sin más purificación. El producto se analizó por RMN-^{1}H (MeOD). La nitración se puede producir en dos posiciones diferentes: orto-(C9) y para-(C7) respecto al grupo hidroxilo. C9 es preferente. El crudo (0.3634g) se disolvió en MeOH (5mL) y se añadió un 10% de Pd/C (25 mg). El matraz se purgó con H_2 y se dejó conectado a un globo de H_2. La reacción se dejó bajo agitación durante 2h. Después filtrar la mezcla a través de celite, la solución se diluyó con 7.5mL MeOH y se precipitó en éter dietílico previamente enfriado. Tras centrifugar (8000rpm, 4 °C, 5min), el éter se decantó y el sólido naranja se secó bajo flujo de N_2 y se analizó por RMN (MeOD) y MS MALDI TOF.

Síntesis de los conjugados PGA-CONH-Doxy. Acoplamiento vía DMTMM.

PGA en forma de sal sódica se colocó en un matraz de fondo redondo y se disolvió en ddH_2O. Para un 30%mol de activación de grupos carboxilo (15%mol de fármaco): en viales separados, doxy-NH_2 (0.6 eq, 557.53g/mol) y DMTMM·Cl (0.3eq, 276.77g/mol)) se disolvieron en ddH_2O y después se añadieron al matraz del PGA. La reacción se dejó bajo agitación 24h a temperatura ambiente y protegido de la luz. Después, la mezcla de reacción se liofilizó y se purificó a través de una columna G25 (ddH_2O). Las fracciones se analizaron por GPC/HPLC para identificar el producto.

Caracterización físico-química

La carga total de fármaco en el conjugado se realizó por espectroscopia UV (273nm, H_2O) teniendo como referencia una curva de calibrado del fármaco libre en las mismas condiciones. La determinación del contenido de fármaco libre en el conjugado se realizó mediante el análisis en LCMS. La estabilidad de los conjugados en condiciones hidrolíticas se llevó a cabo tras incubar los conjugados (concentración 6mg/mL) en medios con distinto pH (disoluciones de

PBS a pH=5.5 y 7.4), mimetizando las condiciones en áreas de inflamación y condiciones fisiológicas. Se tomaron alícuotas (100µL) a distintos tiempos a 37 °C durante 17 días que fueron analizadas por HPLC evaluando la pérdida de peso del conjugado (inyección directa) y la detección del fármaco liberado (previa extracción con MeOH y purificación en columna POROS 50R2). La estabilidad de los conjugados en plasma se llevó a cabo por dilución en plasma (concentración 6mg/mL) durante 24h a 37°C. De las alícuotas tomadas (100µL) se procedió a la precipitación de proteína con la adición de acetonitrilo. Los sobrenadantes se analizaron por HPLC para evaluar la presencia de fármaco. Los pellets fueron lavados y dicho lavado también se analizó con el mismo protocolo. La conformación en solución se determinó por experimentos de SANS y DLS, disolviendo los conjugados en PBS deuterado 0.1M a una concentración de 10mg/mL.

Evaluación biológica

Estudios de disrupción de fibrillas TTR de los conjugados in vitro

En condiciones estériles, se prepararon disoluciones madre en agua de todos los compuestos a una concentración equivalente de fármaco (3.36mM Doxy), se filtraron antes de su uso. Como controles se utilizó PGA, Doxy y Doxy-NH_2. Tras alicuotar las fibrillas de TTRL55P, se añadieron los conjugados y controles en una concentración de 6.7-veces de exceso molar de doxy (180µM). Todas las muestras fueron analizadas por TEM (tinción negativa con acetato de uranilo al 1%) y DLS tras 3 y 6 días para monitorizar la rotura de fibrillas.

Ensayos de hemólisis

Se prepararon disoluciones de PGA-X-Doxy, dextrano (74000g/mol) y poli(etilenimina) (Mn~ 60000, Mw~ 750000, 50% en peso en H_2O) con un rango de concentraciones entre 0-2mg/mL en PBS a pH 7.4, 6.5 y 5.5. Se sembraron (100µL) en placas estériles de 96 pocillos. Se extrajo sangre de ratones que se colocó en un tubo heparinizado en hielo. Los eritrocitos (RBC) se aislaron por

centrifugación (3000rpm, 10 min, 4°C). El plasma (sobrenadante) se descartó y los eritrocitos se lavaron tres veces con PBS. El sedimento (RBC) se dividió en partes iguales y se resuspendieron en disoluciones de PBS con los pHs descritos. De cada solución, se añadieron 100µL a las placas preparadas con los compuestos. Tritron X-1% w/v se usó como referencia del 100% de lisis y PBS como control de absorbancia. Las placas se incubaron 16h a 37°C, se centrifugaron (3000rpm, 10min). Cada sobrenadante se colocó en una nueva placa y la liberación de hemoglobina (Hb) se midió espectrofotométricamente (570nm). La liberación de Hb para cada muestra se expresó como porcentaje de la liberación producida respecto al Triton-X. PEI y dextrano representaron, respectivamente, el control positivo y el control negativo del ensayo.

Ensayos de biodistribución

Tras etiquetar el conjugado PGA-Doxy con una sonda fluorescente (Cy5.5) o con el complejo DOTA/Ga^{68}, se llevaron a cabo estudios de biodistribución mediante imagen óptica y tomografía por emisión de positrones (PET), respectivamente.

Biodistribución del conjugado PGA-CONH-Doxy-Cy5.5 por imagen óptica

PGA-CONH-Doxy-Cy5.5 se disolvió en suero salino (1.40mg conj/mL) y los animales (ratones Balb/c) fueron inyectados por vía intravenosa una dosis única de 100µL de la solución. Como controles, se emplearon ratones no inyectados. Los animales fueron anestesiados usando isofluorano (1 al 3%). Cinco ratones fueron monitorizados a la vez y la configuración de imagen se ajustó en función de la fluorescencia observada. La fluorescencia emitida por el conjugado se detectó, se digitalizó y se mostró superpuesta con una imagen del animal en escala de grises. La señal fluorescente se cuantificó como Eficiencia. A los distintos tiempos elegidos (0, 4 y 24h post-inyección) grupos de animales fueron sacrificados y se recolectó inmediatamente la sangre y los órganos principales (hígado,

pulmones, bazo, riñones, corazón y cerebro). Los órganos fueron analizados con la misma técnica (análisis *ex vivo*). Los órganos fueron pesados, congelados y almacenados a -80 °C para cuantificar la fluorescencia posteriormente.

Los órganos fueron homogenizados en tampón PBS pH=7.4 a una determinada concentración mediante un Ultraturrax (aprox. 1min, 13000rpm). La suspensión fue centrifugada (4000g, 1h, 4°C). Los sobrenadantes se recolectaron para medir la fluorescencia perteneciente al conjugado acumulado en cada tejido.

3.2.4.2 PEG-péptido RAGE

El péptido RAGE fue derivatizado añadiendo en su extremo N-terminal una glicina (PEP1) o el dipéptido glicina-cisteína (PEP2). Todos los péptidos fueron sintetizados por medio de síntesis en fase sólida (SPPS) a partir de aminoácidos N-Fmoc protegidos y caracterizados por HPLC, MS MALDI TOF y RMN.

Síntesis de los conjugados CXPX.

Síntesis de C1P1 y C2P1

NHS-PEG-NHS (0.014mmol, 1eq, 3023g/mol) se disolvió en DMSO anh. (4mL) en atmósfera inerte a temperatura ambiente. En un vial, PEP1 (0.03mmol, 2eq, 912.05g/mol) se disolvió en las mismas condiciones y se añadió a la solución de PEG. Después, se adicionó una cantidad catalítica de DMPA y el pH se ajustó a 8 con DIEA. La reacción se dejó agitando en atmósfera inerte durante 48h. El disolvente se eliminó bajo evaporación a vacío y el residuo, resuspendido en 1mL ddH_2O, se purificó por FPLC. Los conjugados se caracterizaron por RMN (D_2O) y MS MALDI TOF.

Síntesis de C1P2 y C2P2

4TP-SS-PEG-SS-4TP (0.052mmol, 1eq, 3400g/mol) se disolvió en tampón de acetato de amonio 10mM pH=7 a temperatura

ambiente. PEP2 (0.057mmol, 1.1eq, 1057.23g/mol) se disolvió en las mismas condiciones en 5mL de ddH_2O y se adicionó gota a gota durante 20min sobre la solución de PEG. La evolución de la reacción se monitorizó por UV (323nm) durante 15h en atmósfera inerte. A continuación, la reacción se liofilizó y el residuo se redisolvió en 1mL ddH_2O para su purificación por FPLC. Las fracciones de cada producto obtenido se juntaron y se desalaron mediante una columna PD10 (ddH_2O). Los conjugados caracterizaron por RMN (D_2O) y MS MALDI TOF.

Caracterización físico-química

La estabilidad de los conjugados CXPX bajo las condiciones de los ensayos in vitro se llevaron a cabo diluyendo los conjugados (15mM péptido) en medio de cultivo (DMEM, 10%FBS) y realizando incubaciones hasta 48h a 37°C. Se tomaron alícuotas (15µL) a distintos tiempos que fueron evaluadas por HPLC. La estabilidad en plasma se evaluó como en el se ha descrito previamente analizando las alícuotas por espectroscopia de masas MALDI TOF. La conformación en solución se determinó por DLS, realizando estudios de concentración (2-20mg/mL) en PBS 0.20M a 25°C. La afinidad de los conjugados por los agregados de TTR se evaluó por SPR, mediante el aparato BiacoreT100^{TM}, mimetizando las condiciones de los ensayos *in vitro*. Se inmovilizó la proteína en un chip CM5 y se hicieron pasar flujos de los distintos conjugados y péptidos realizando estudios de cinética.

Evaluación biológica

<u>Ensayo de actividad in vitro.</u>

Bajo condiciones estériles, los agregados de TTR L55P fueron disueltos en medio de cultivo (concentración 2µM). Se añadieron los conjugados y péptidos partiendo de sus disoluciones stock hasta obtener una concentración final 10µM péptido RAGE. La incubación se llevó a cabo durante 5h a 37°C bajo agitación constante. A continuación, los agregados tratados se incubaron en células (RN22)

durante 24 y 48h, y se evaluó la activación de caspasa-3 utilizando el test colorimétrico de CaspACE para ensayo en placas de 96 pocillos. El lisado celular obtenido también se utilizó para cuantificar la cantidad de proteína mediante el kit Bio-Rad, utilizando BSA como estándar. Con estos valores se normalizaron los datos obtenidos de la activación de caspasa-3.

Biodistribución del conjugado PEG-péptido RAGE.

Tras etiquetar el conjugado PEG-PEP1 con una sonda fluorescente (Cy5.5) se llevaron a cabo estudios de biodistribución mediante imagen óptica, repitiendo el protocolo descrito para PGA-Doxy-Cy5.5.

4. RESULTADOS

4.1 Obtención de nuevos transportadores poliméricos basados en el ácido poli-L-glutámico (PGA) (CAPÍTULO II)

Actualmente existe la necesidad de desarrollar portadores biodegradables con elevado Mw para aumentar las ventajas de la especificidad pasiva mediada por el efecto EPR. Los poliglutamatos son degradables por la enzima lisosomal catepsina B y actualmente se encuentran en estudio para aplicaciones tan diversas como el cáncer [7, 21, 22], los procesos isquémicos [23, 24] o el tratamiento de sepsis [25]. Como referencia, el conjugado PGA-paclitaxel (Opaxio^{TM}) se encuentra en fase III de ensayos clínicos [26, 27].

En el presente proyecto, se han diseñado nuevos portadores poliméricos basados en el ácido poli-L-glutámico con estructura definida, peso molecular (Mw) modulable y polidispersidad reducida (PDI<1.2) mediante la técnica de polimerización por apertura de anillo (ROP) de N-carboxi-anhídridos (NCA) [28, 29]. El proceso de síntesis implicó la optimización de la obtención del monómero (N-Carboxianhidrido-y-Bencil-L-glutamato), las condiciones de polimerización así como el proceso de desprotección de los grupos bencilo de los distintos portadores. Se han obtenido y caracterizado *homo-* y *co*-polímeros de bloque con polietilenglicol (PEG), para su posterior evaluación como vehículos de transporte para la liberación de fármacos.

Esta familia de *co*-polímeros de bloque anfifílicos se ha caracterizado mediante *técnicas físico-químicas* para confirmar su identidad y su conformación en solución; así como *biofísicas* para estudiar sus mecanismos de internalización celular en modelos *in vitro* mediante citometría de flujo y distribución celular por microscopía confocal; y su biodistribución *in vivo* mediante técnicas de imagen no invasiva (imagen óptica o resonancia magnética (MRI, magnetic resonance imaging)).

Todo el proceso ha sido patentado por el laboratorio de

Polímeros Terapéuticos dirigido por la directora de la presente tesis [30].

La propuesta del uso de sales no nucleófilicas como contraiones de las sales de amonio utilizadas como iniciadores del proceso de polimerización por ROP-NCA dio lugar a un proceso de reacción controlado, obteniendo grados de polimerización del bloque de poli-L-glutámico modulable (desde 10 a 800 uds.). Tras optimizar y escalar la síntesis del monómero, y el ajuste de parámetros como la temperatura, tiempo de reacción, el disolvente, la concentración y el ratio [monómero/iniciador], así como el uso distintos iniciadores (ej. PEG-NH_2, neopentilamina, n-butilamina), se obtuvo una familia de poliglutamatos lineares definidos (homopolímero, dibloque y tribloque, capítulo II) con baja polidispersidad (PDI<1.2). La velocidad de reacción se determinó por análisis directo del medio de reacción comprobando la desaparición de monómero por espectroscopia infrarroja.

Respecto a la desprotección de los grupos carboxilo de los poli-bencilglutamatos, distintos métodos fueron testados. Como métodos óptimos se determinó una desprotección ácida (HBr/TFA) para desproteger homopolímeros y una desprotección básica (NaOH aq./THF) la válida para cualquier poliglutamato pero en especial empleada en el caso de los dibloques / tribloques. Esta desprotección básica evita la degradación de los bloques de PEG sin modificar la estereoquímica de partida del bloque polipeptídico como pudo comprobarse al analizar el grado de rotación de luz polarizada.

La identidad de cada compuesto se determinó por GPC así como por RMN, la estructura secundaria (producto protegido o desprotegido) por dicroísmo circular confirmando la existencia de la hélice α. Los ensayos de viabilidad en la línea celular HUVEC determinó tolerabilidades por encima del 80% hasta concentraciones de 2mg/mL y los ensayos de citometría y microscopía confocal de los compuestos marcados con una sonda fluorescente (OG) confirmaron la internalización por endocitosis (CAPÍTULO III, IV).

4.2 Síntesis de portadores poliméricos capaces de atravesar la BHE (CAPÍTULO III, IV)

Una vez obtenidos los portadores poliméricos, se emplearon técnicas de bioconjugación para obtener sistemas capaces de cruzar la BHE gracias al transporte activo. Para ello, se conjugaron múltiples residuos dirigentes: holo-transferrina (Tf), anticuerpo monoclonal OX26 (mAOX26) y los péptidos Angiopep-2 [31-34] y CRTIGPCSVC (péptido cíclico, cPEP) [35, 36], a los *homo*- y *co*-polímeros de bloque sintetizados para comparar su biodistribución. En todos los casos se llevó a cabo la unión de estas biomoléculas, previamente derivatizadas y/o activadas con los grupos funcionales deseados, mediante puntos de unión telequélicos de la matriz polimérica, por ejemplo los puentes disulfuro. El número de residuos dirigentes conjugados al portador fue determinado por espectrometría de masas MALDI-TOF, ^{1}H-RMN o análisis de aminoácidos.

Dado que los estudios *in vivo* son más adecuados para evaluar la capacidad de transporte activo a través de la BHE, se llevó a cabo el etiquetado de los compuestos para estudios de biodistribución mediante técnicas de imagen no invasiva: (i) marcaje con sondas fluorescentes o en NIR (cyane5.5) para su monitorización a través de la plataforma IVIS®spectrum, (ii) marcaje con Gd para resonancia magnética de imagen (MRI) donde previamente el portador se derivatizó con el complejante DTPA y (iii) marcaje con Ga^{68} para análisis por tomografía por emisión de positrones (PET) previa derivatización del vehículo con DOTA. El porcentaje de sonda conjugado fue determinado con la técnica requerida (espectrómetro de fluorescencia, RMN-^{1}H).

Los ensayos de biodistribución fueron realizados en ratones Balb/c y en todos los casos los compuestos fueron inyectados vía intravenosa previa disolución en suero biológico a la concentración requerida para observar el nivel de señal necesario. Una vez realizada la monitorización *in vivo*, se procedió al sacrificio del animal para evaluar y cuantificar el porcentaje de compuesto existente en cada órgano así como en sangre.

Los poliglutamatos (homo, dibloque y tribloque) demostraron ser biocompatibles y no acumularse específicamente en ningún órgano, siendo eliminados vía renal. De los sistemas testados (FIGURE V. 1), se determinó que la técnica por detección de fluorescencia no aportaba la precisión requerida para determinar el contenido de vehículo dirigido que llegaba al cerebro, así como la transferrina y el anticuerpo monoclonal OX26 no fueron ligandos satisfactorios para tal fin. Los conjugados de los péptidos Angiopep-2 y CRTIGPCSVC fueron obtenidos mediante rutas de síntesis con menor problemática que los anteriores ligandos. Su evaluación *in vivo* no mostró acumulación significativa en el cerebro. Posiblemente los portadores fueron bombeados fuera del cerebro o los ligandos no estuvieran expuestos lo suficiente para su reconocimiento por los receptores de la BHE debido a la conformación en solución del sistema. Actualmente, nuevos sistemas poliméricos, utilizando PEG como punto de unión para los ligandos o poliglutamatos con otras arquitecturas (ej. estrella) están siendo evaluados con estos mismos ligandos para cruzar la BHE.

4.3 Obtención de conjugados polímero-fármaco para el tratamiento de PAF (CAPÍTULO V)

De forma paralela al desarrollo de los portadores poliméricos, tanto PGA como PEG han sido utilizados como polímeros de partida para la conjugación de agentes bioactivos para el tratamiento de PAF. El diseño racional del enlace polímero-fármaco se planteó como crucial para proporcionar los conjugados la estabilidad necesaria en circulación y la llegada a su diana terapéutica, así como mantener o incrementar la actividad natural de los compuestos bioactivos.

En el caso de la doxiciclina (doxy), se estudió la reactividad de los distintos grupos funcionales de la molécula para realizar su anclaje al polímero elegido, PGA, mediante un enlace éster (enlace lábil a pH). Se optimizaron las condiciones de reacción y se obtuvieron conjugados con distinta carga de fármaco conjugado (ωt%). A su vez, la doxy fue derivatizada introduciendo un grupo NH_2- en su anillo aromático para conjugarla mediante enlace amida al polímero y nuevamente se optimizó la reacción así como se obtuvieron conjugados con diferentes ωt%. Todos los conjugados fueron caracterizados (carga total de

fármaco, conformación en solución, ensayos de estabilidad en plasma y en condiciones hidrolíticas, estudios de cinética de liberación de fármaco) y su actividad *in vitro* como inhibidores de formación de fibrillas fue testada, eligiendo el candidato óptimo para los ensayos biológicos. Dicho conjugado fue etiquetado con una sonda fluorescente (Cy5.5) y con el complejo DOTA /Ga para estudiar su biodistribución *in vivo* así como sometido a ensayos preliminares de actividad en un modelo animal joven de PAF.

Respecto al péptido RAGE, se realizaron derivatizaciones de la secuencia inicial para obtener dos tipos de enlace al vehículo polimérico portador elegido, PEG: biodegradable (puente disulfuro) y no biodegradable (amida). La identidad de cada conjugado se confirmó por diversas técnicas físico-químicas así como se corroboró su capacidad para reconocer a la proteína por ensayos de unión, su conformación en solución y estabilidad en plasma. Se llevaron a cabo ensayos de actividad *in vitro* seleccionando el mejor candidato para los ensayos *in vivo*, del cual se realizaron estudios de biodistribución por marcaje fluorescente (Cy5.5) y ensayos preliminares de actividad en un modelo animal joven de PAF.

PGA-DOXY

La familia de conjugados PGA-x-Doxy demostró su estabilidad en plasma así como bajo las condiciones empleadas para la disrupción de fibrillas. Asimismo, la actividad *in vitro* observada para los conjugados fue mayor que para la doxiciclina libre a la misma concentración de fármaco. El conjugado con mejor perfil de actividad fue PGA-CONH-Doxy (FIGURA 3.), con una carga total de fármaco de 15-20ωt%, el cual resultó no ser hemolítico y poseer un tamaño de partícula de ≈ 12 nm (determinado por SANS, colaboración con Dr. Paul Cardiff Univ.) Tras su etiquetado con Cy5.5, la biodistribución del conjugado mostró una eliminación vía renal y no se acumuló de forma específica en ningún órgano. El mismo estudio mediante PET confirmó los resultados ya obtenidos, completando el estudio al determinar el $t_{1/2}$ del conjugado=0.98h .

Los conjugados PEG-péptido RAGE sintetizados (FIGURE V. 2.) incrementaron la estabilidad en plasma del péptido mejorando su

solubilidad. Exceptuando C2P2, el resto de conjugados mantuvo la capacidad del péptido para unirse a los agregados, así como mostraron una conformación en disolución estable y reproducible. En la evaluación de actividad *in vitro*, C2P1 (enlace amida entre el péptido y el PEG, proporción pep:PEG 2:1) fue seleccionado por su perfil para el posterior análisis *in vivo*. Tras su marcaje fluorescente, los estudios de biodistribución del péptido peguilado mostraron una eliminación renal del conjugado sin acumularse de manera específica en ningún órgano. La evaluación preliminar de actividad *in vivo* mostró resultados prometedores al no observarse daño a nivel histológico en los órganos donde ocurre la deposición fibrilar/reconocimiento agregados-receptor y apreciarse mejoras en el hígado, órgano en el que se sintetiza mayoritariamente la TTR.

5. CONCLUSION

La novedad y relevancia del presente trabajo radica en haber logrado los siguientes objetivos:

- la obtención y caracterización de una familia de poliglutamatos (homopolímero, dibloque, tribloque) mediante la optimización de los procesos de (i) polimerizacíon vía ROP-NCA a través de una nueva metodología (Mw elevados y pdi bajas) y (ii) desprotección del grupo protector bencilo (evitando subproductos de degradación). Esta metodología ha dado lugar a la generación de un Spin-Off (Polypeptide Therapeutic Solutions S.L.);

- diseño y obtención de portadores poliméricos para el cruce de la barrera hematoencéfalica para su aplicación en enfermedades neurodegenerativas mediante la unión de un ligando director contra el receptor transferrina;

- síntesis, caracterización y evaluación biológica de los primeros conjugados polímero-fármaco para el tratamiento de PAF. Estos conjugados puden considerarse como 'Fármacos Huérfanos' ya que no se dispone de tratamiento actual para esta enfermedad.

En la presente tesis se han empleado gran variedad de técnicas interdisciplinares: síntesis química, biología celular y modelos animales, abarcando así una extensa variedad de metodología aprendida. Finalmente cabe destacar la novedad y aplicabilidad del área de estudio y su importancia en el campo, avalada por los premios conseguidos, las dos patentes presentadas (una de ellas dando lugar a una Spin Off) y a los artículos en revistas internacionales que se esperan publicar en revistas de alto índice de impacto en los próximos meses.

6. BIBLIOGRAFIA

1. W. M. Pardridge, *Blood-brain barrier drug targeting: the future of brain drug development.* Mol Interv, 2003. **3**(2): p. 90-105, 51.
2. Pardridge, W.M., *Drug and gene targeting to the brain with molecular Trojan horses.* Nat Rev Drug Discov, 2002. **1**(2): p. 131-9.
3. R. Duncan, *Polymer conjugates as anticancer nanomedicines.* Nature Reviews Cancer, 2006. **6**(9): p. 688-701.
4. R. Duncan, H. Ringsdorf, and R. Satchi-Fainaro, *Polymer therapeutics--polymers as drugs, drug and protein conjugates and gene delivery systems: past, present and future opportunities.* Adv Polym Sci, 2006. **192**: p. 1-8.
5. R. Duncan, et al., *Polymer-drug conjugates: towards a novel approach for the treatment of endrocine-related cancer.* Endocr Relat Cancer, 2005. **12** Suppl 1: p. S189-99.
6. H. Maeda, T. Sawa, and T. Konno, *Mechanism of tumor-targeted delivery of macromolecular drugs, including the EPR effect in solid tumor and clinical overview of the prototype polymeric drug SMANC.* Journal of Controlled Release, 2001. **74**: p. 47-61.
7. M. J. Vicent, H. Ringsdorf, and R. Duncan, *Polymer therapeutics: Clinical applications and challenges for development.* Adv Drug Deliv Rev., 2009. **61**(13): p. 1117.
8. M.J. Vicent, et al., *Polymer conjugates as therapeutics: future trends, challenges and opportunities.* Exp Opin Drug Rev, 2008. **61**: p. 1220-1231.
9. www.esf.org.
10. Duncan, R., T.A. Connors, and H. Meada, *Drug targeting in cancer therapy: the magic bullet, what next?* J Drug Target, 1996. **3**(5): p. 317-9.
11. Duncan, R., *The dawning era of Polymer Therapeutics.* Nature Rev Drug Discov, 2003. **2**(5): p. 347-360.

12. F. Canal, J. Sanchis, and M.J. Vicent, *Polymer-drug conjugates as nano-sized medicines.* Curr opin Biotech, 2011. **22**(894-900).
13. F. Greco and M.J. Vicent, *Combination therapy: opportunities and challenges for polymer-drug conjugates as anticancer nanomedicines.* Adv Drug Deliv Rev, 2009. **61**(13): p. 1203-13.
14. Kabanov, A.V. and H.E. Gendelman, *Nanomedicine in the diagnosis and therapy of neurodegenerative disorders.* Prog. Polym. Sci., 2007. **32**(8-9): p. 1054-1082.
15. Pardridge, W.M., *Molecular Trojan horses for blood-brain barrier drug delivery.* Discov Med, 2006. **6**(34): p. 139-43.
16. Pardridge, W.M., *Blood-brain barrier drug targeting: the future of brain drug development.* Mol Interv, 2003. **3**(2): p. 90-105, 51.
17. M.J. Saraiva, et al., *Family studies of the genetic abnormality in transthyretin (prealbumin) in Portuguese patients with familiar amyloidotic polyneuropathy.* Ann NY Acad Sci, 1984. **43**: p. 86-100.
18. I. Cardoso and M.J. Saraiva, *Doxycycline disrupts transthyretin amyloid: evidence from studies in a FAP transgenic mice model.* The FASEB Journal, 2006. **20**: p. 234-239.
19. F. A. Monteiro, et al., *In vitro inhibition of transthyretin aggregate-induced cytotoxicity by full and peptide derived forms of the soluble receptor for advanced glycation end products (RAGE).* FEBS Lett, 2006. **580**(14): p. 3451-6.
20. Heenan, R.K., *FISH data analysis program.* Rutherford Appleton Laboratory, Didcot, U.K.
21. R. Duncan, *Targeting and Intracellular Delivery of Drugs*. Encyclopedia of Molecular Cell Biology and Molecular Medicine, ed. R. A. Meyers2006, Weinheim: Wiley-VCH Verlag GmbH & Co. KGaA.
22. M.J. Vicent and R. Duncan, *Polymer conjugates: nanosized medicines for treating cancer.* Trends Biotechnol, 2006. **24**(1): p. 39-47.
23. Mondragon, L., et al., *Modulation of cellular apoptosis with*

apoptotic protease-activating factor 1 (Apaf-1) inhibitors. J Med Chem, 2008. **51**(3): p. 521-9.

24. Vicent, M.J. and E. Perez-Paya, *Poly-L-glutamic acid (PGA) aided inhibitors of apoptotic protease activating factor 1 (Apaf-1): an antiapoptotic polymeric nanomedicine.* J Med Chem, 2006. **49**(13): p. 3763-5.
25. Vicent, M.J., et al., *Nanoconjugates as intracorporeal neutralizers of bacterial endotoxins.* J Control Release, 2009. **142**(2): p. 277-85.
26. Chipman, S.D., et al., *Biological and clinical characterization of paclitaxel poliglumex (PPX, CT-2103), a macromolecular polymer-drug conjugate.* Int J Nanomedicine, 2006. **1**(4): p. 375-83.
27. Sabbatini, P., et al., *A phase II trial of paclitaxel poliglumex in recurrent or persistent ovarian or primary peritoneal cancer (EOC): a Gynecologic Oncology Group Study.* Gynecol Oncol, 2008. **111**(3): p. 455-60.
28. H. R.Kricheldorf, *Polypeptides and 100 years of chemistry of alpha-amino acid N-carboxyanhydrides.* Angew Chem Int Ed, 2006. **45**(35): p. 5752-84.
29. J. Cheng and T.J. Deming, *Synthesis of polypeptides by ring-opening polymerization of alpha-amino acid N-carboxyanhydrides.* Top Curr Chem, 2012. **310**: p. 1-26.
30. M.J. Vicent, et al., *"Síntesis controlada de poliglutamatos con baja polidispersidad y arquitecturas versátiles"* N. de solicitud: P201131713, 2012.
31. van Rooy, I., et al., *Comparison of five different targeting ligands to enhance accumulation of liposomes into the brain.* J Control Release, 2011. **150**(1): p. 30-6.
32. Gabathuler, R., *Approaches to transport therapeutic drugs across the blood-brain barrier to treat brain diseases.* Neurobiol Dis, 2010. **37**(1): p. 48-57.
33. Ke, W., et al., *Gene delivery targeted to the brain using an Angiopep-conjugated polyethyleneglycol-modified polyamidoamine dendrimer.* Biomaterials, 2009. **30**(36): p.

6976-85.

34. Regina A., et al., *Antitumour activity of ANG1005, a conjugate between paclitaxel and the new brain delivery vector Angiopep-2.* Br J Pharmacol, 2008. **155**(2): p. 185-97.

35. Staquicini, F.I., et al., *Systemic combinatorial peptide selection yields a non-canonical iron-mimicry mechanism for targeting tumors in a mouse model of human glioblastoma.* J Clin Invest, 2011. **121**(1): p. 161-73.

36. D. Nathanson and P.S. Mischel, *Charting the course across the blood-brain barrier.* J Clin Invest, 2011. **121**(1): p. 31-3.

APPENDIX II. TABLE OF COMPOUNDS. CHEMICAL STRUCTURES AND NOMENCLATURE

CHEMICAL STRUCTURE	NAME (ABB.)	REF
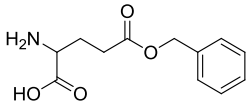	H-L-Glu(OBzl)-OH, Glu(Bz)NCA	**1**
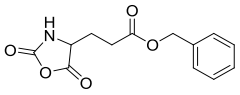	γ-Benzyl-L-Glutamate N-Carboxyanhydride (NCA monomer)	**2**
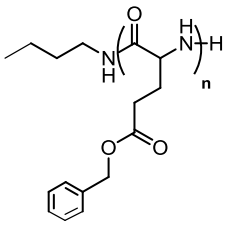	Poly-γ-benzyl glutamate (nBu-PGA$_n$, PBLGn)	**3**
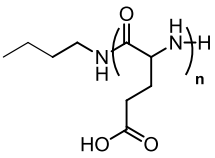	Poly-L-glutamic acid (nBu-PGAn)	**4**
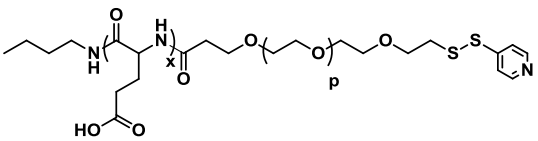	Diblock (DBn) (nBu-PGA$_n$--*b*-PEG$_p$-4TP, PGA$_n$-*b*-PEG$_p$)	**5**
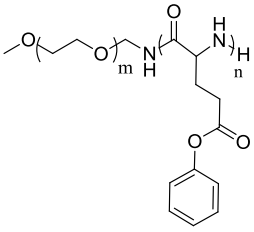	Poly(ethylene glycol)-*co*-poly(γ-benzyl L-glutamate) (protected DBn, PEG$_m$-*b*-PBLG$_n$)	**6**

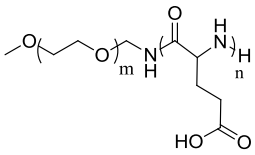	Diblock (DBn) (PEG_m-*b*-PGA_n)	**7**
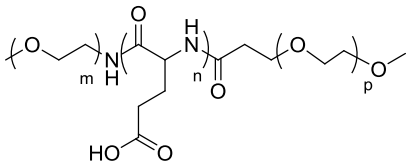	Triblock (TBn) (PEG_m-*b*-PGA_n-*b*-PEG_pOMe)	**8**
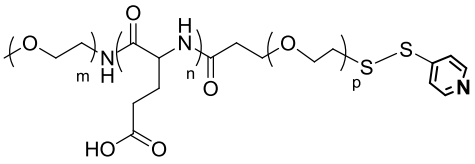	Triblock (TBn) (PEG_m-*b*-PGA_n-*b*-PEG_p-4TP)	**9**
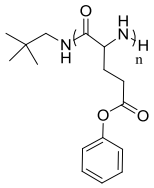	Poly-γ-benzyl glutamate (neo-PGA_n, PBLGn)	**10**
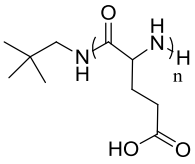	Poly-L-glutamic acid (neo-PGA_n)	**11**
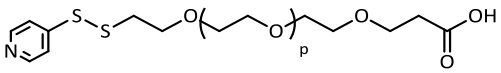	4-pyridyl disulfide-poly(ethylene glycol)-carboxyl 4TP-SS-PEG-COOH	**12**
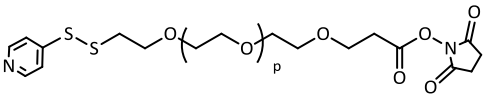	4-pyridyl disulfide-poly(ethylene glycol)-succinimide 4TP-SS-PEG-NHS	**13**

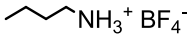	Tetrafluoroboran neopentylammon ium salt ($nBuBF_4$)	**14**
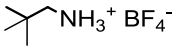	Tetrafluoroboran n-Butylammonium salt ($neoBF_4$)	**15**
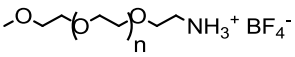	Tetrafluoroboran PEGammonium salt ($PEGBF_4$)	**16**
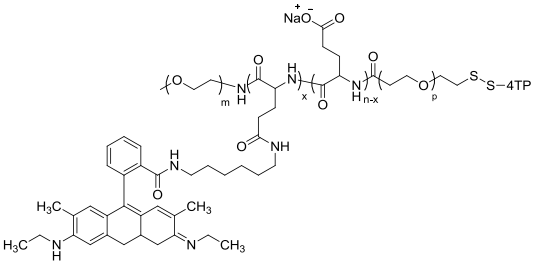	TBn-Rho (x%)	**17**
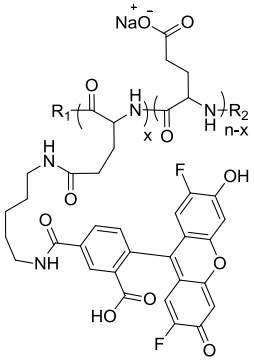	PGAn-OG (x%) PGAn : R1=nBu / neo, R2=H	**18**
	DBn-OG (x%) DBn : R1=nBu / neo, R2=PEG_p-4TP DBn : R1=$mPEG_m$, R2=PEG_p-4TP	**19**
	TBn-(OG)x TBO (x%) TBn : R1=$mPEG_m$, R2= PEG_p-4TP	**20**

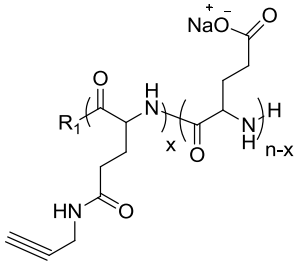	PGAn-(alkyne)x	**21**
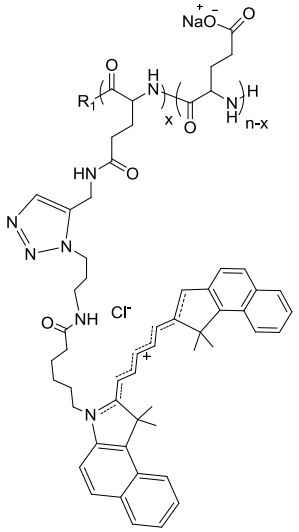	PGAn-Cy5.5 (x%) R1=nBu / neo	**22**
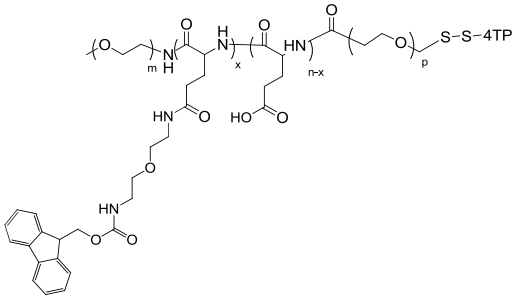	TBn- Fmoc diamine (x%)	**23**
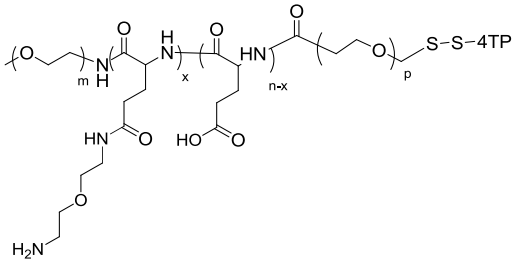	TBn-diamine (x%)	**24**

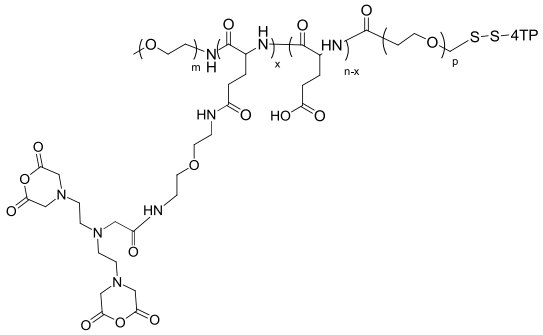	TB-diamine-DTPA (x%)	**25**
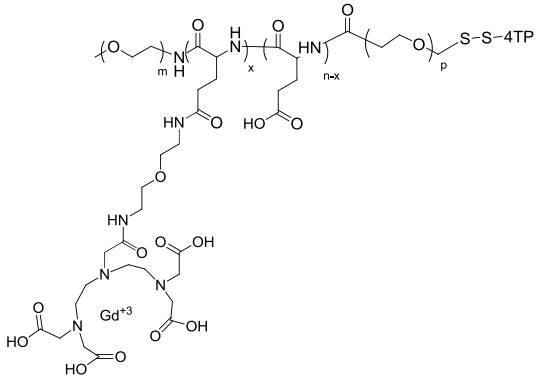	TB-diamine-DTPA/Gd (x%)	**26**
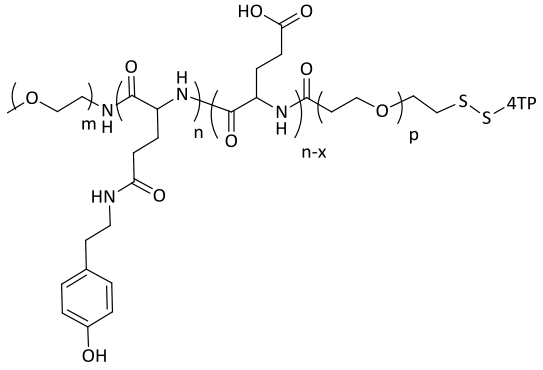	TBn-Tyramine (x%)	**27**

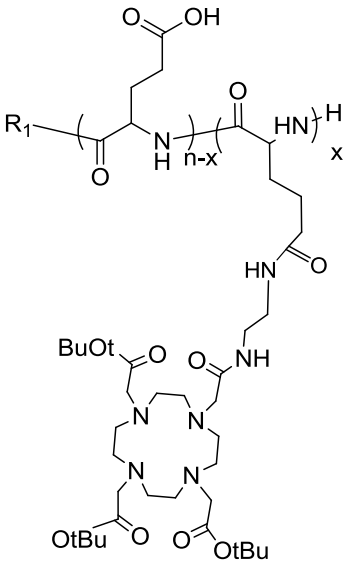	PGAn-DOTAtBu (x%) PGAn : R1=nBu / neo	**28**
	DBn-DOTAtBu (x%) DBn : R1=mPEG$_m$	**29**
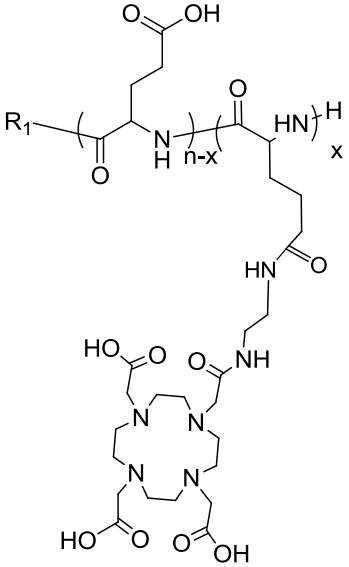	PGAn-DOTA (x%) PGAn : R1=nBu / neo	**30**
	DBn-DOTA (x%) DBn : R1=mPEG$_m$	**31**
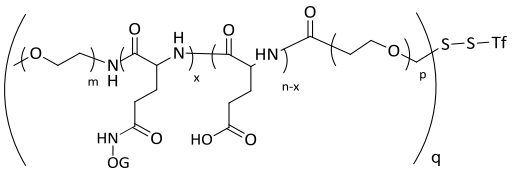	(TBn-(OG)x)q-Tf	**32**

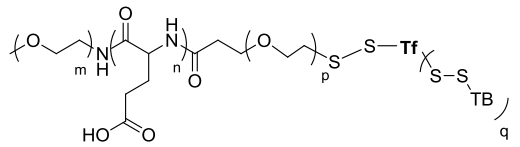	$(TB)_q$-Tf	**33**
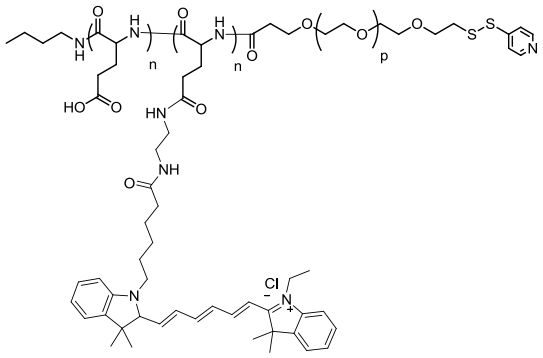	DB-Cy55	**34**
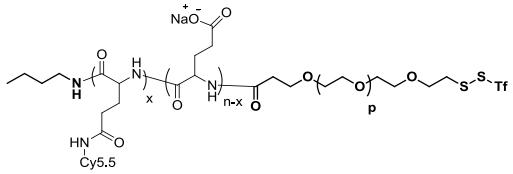	Tf-DB-Cy5.5	**35**
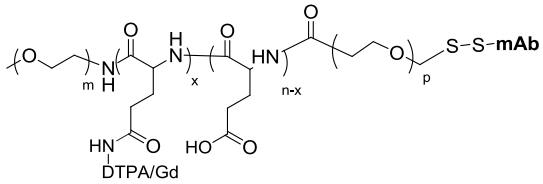	TB-DTPA/Gd-mAbOX26	**36**

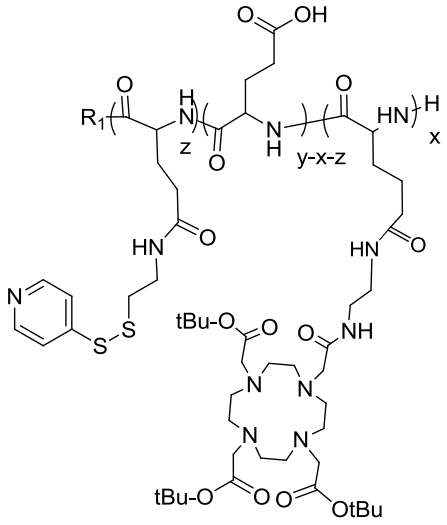	PGAn-(DOTAtBu)x-(4TP)z PGAn : R1=nBu / neo	**37**
	DBn-(DOTAtBu)x-(4TP)z DBn : R1=mPEG$_m$	**38**
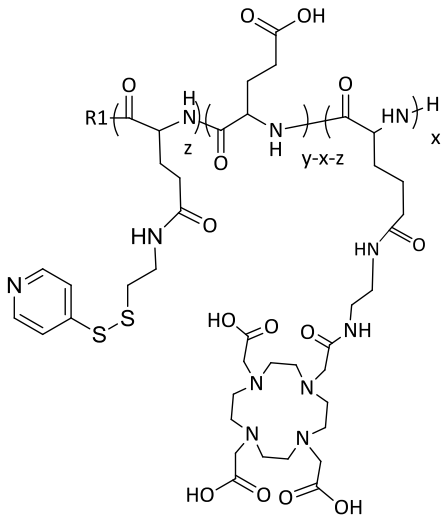	PGAn-(DOTA)x-(4TP)z PGAn : R1=nBu / neo	**39**
	DBn-(DOTA)x-(4TP)z DBn : R1=mPEG$_m$	**40**

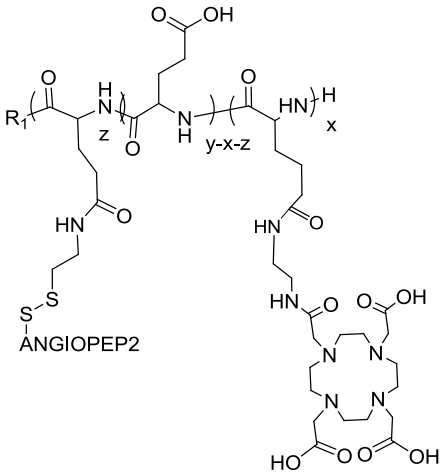	PGAn-(DOTA)x-(SS-Cys-Angiopep2)z R1=nBu / neo	**41**
	DBn-(DOTA)x-(SS-Cys-Angiopep2)z R1=mPEG$_m$	**42**
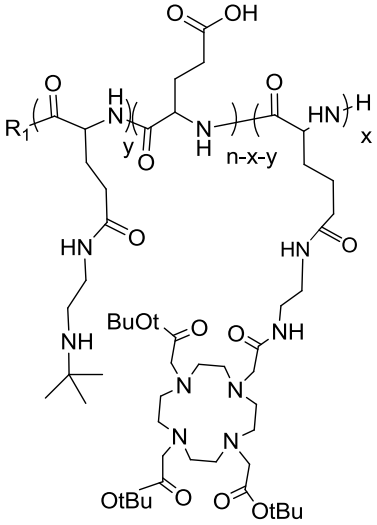	PGAn-(DOTAtBu)x-(BOC-diamine)z PGAn : R1=nBu / neo	**43**
	DBn-(DOTAtBu)x-(BOC-diamine)z DBn : R1=mPEG$_m$	**44**

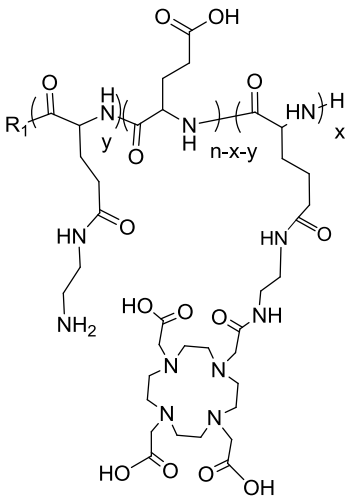 46	PGAn-(DOTA)x-(diamine)z PGAn : R1=nBu / neo	**45**
	DBn-(DOTA)x-(diamine)z DBn : R1=$mPEG_m$	**46**
	DBn-(DOTA)x-(cPEP)z DBn : R1=$mPEG_m$	**48**
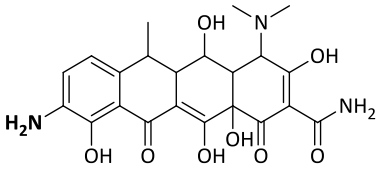	9-amino Doxycycline DOXY-NH_2	**49**
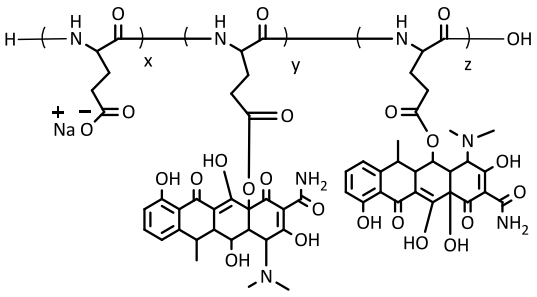	PGA-COO-Doxy	**50**
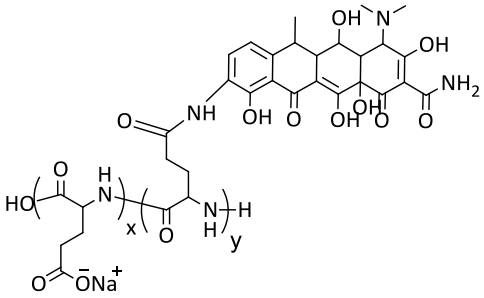	PGA-CONH-Doxy	**51**

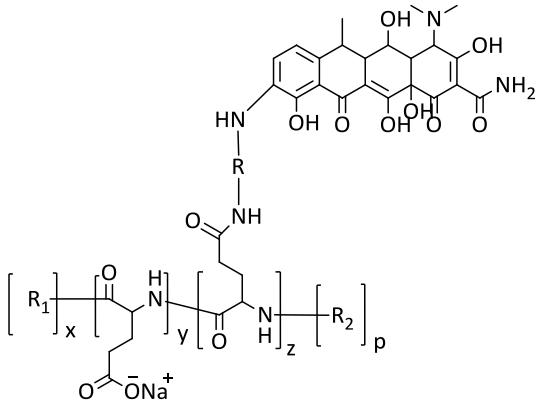	PGA-CONH-AA-Doxy (R= Gly-Gly, R = Leu-Gly)	**52**
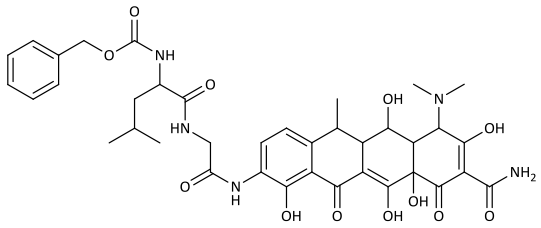	Bz-Leu-Gly-Doxy	**53**
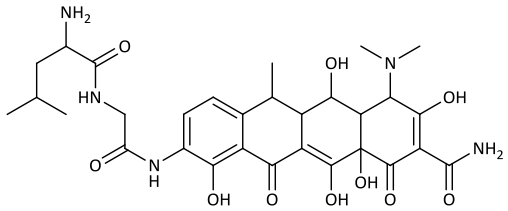	Leu-Gly-Doxy	**54**
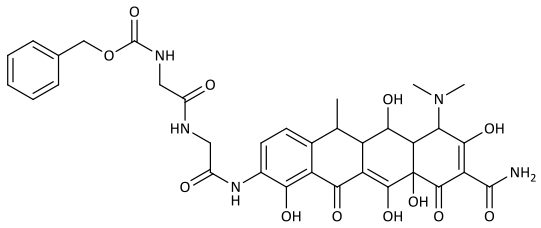	Bz-Gly-Gly-Doxy	**55**
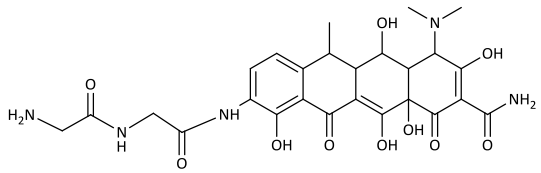	Gly-Gly-Doxy	**56**

RAGE peptide—Gly	PEP1	**57**
RAGE peptide-Gly-Cys	PEP2	**58**
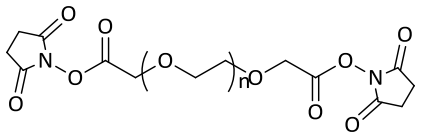	Succinimide-PEG-succinimide NHS-PEG-NHS	**59**
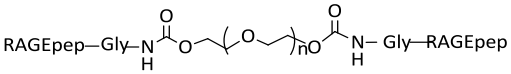	PEG-$(PEP1)_2$ C2P1	**60**
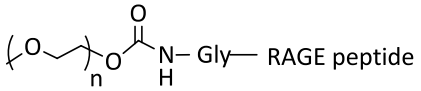	mPEG-PEP1 C1P1	**61**
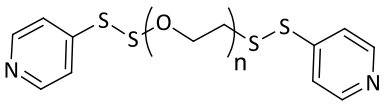	4TP-SS-PEG-SS-4TP	**62**
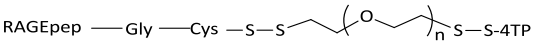	PEG-PEP2 C1P2	**63**
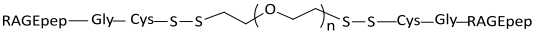	PEG-$(PEP2)_2$ C2P2	**64**
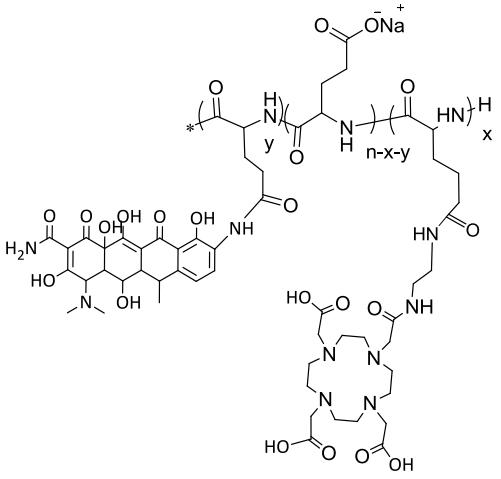	Doxy-PGA-DOTA	**65**

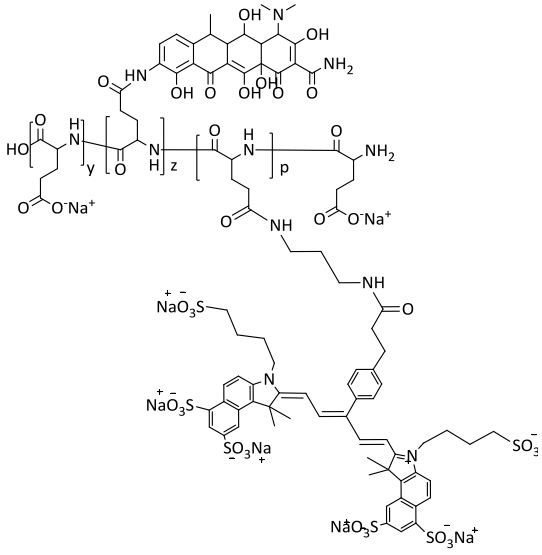	Doxy-PGA-Cy5.5.	**66**
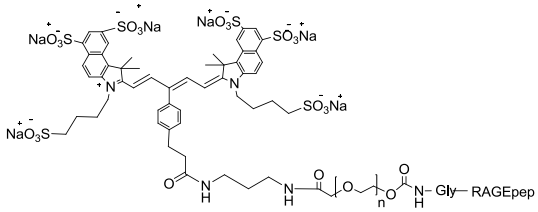	PEP1-PEG-Cy5.5	**67**

APPENDIX III. GENERAL METHODS AND PROTOCOLS.

1. TECHNIQUES FOR DRUG TRACKING, DRUG LOADING DETERMINATION AND LINKAGE STABILITY.

Polymer conjugate characterisation always entails development of techniques which enable drug detection in order to determine parameters such as total and free dug loading, kinetics of drug release or polymer-drug linker stability, etc. Most of the bioactive molecules are easily detected by their absorption in UV region or their fluorescent properties.

Reverse phase HPLC and LCMS are the most commonly used techniques for the identification and quantitative determination of the drug in physiological fluids and *in vitro* media.

High performance liquid chromatography, HPLC

Main characteristic of chromatography is its ability to separate substances from each other due to their different distribution between a mobile and a stationary phase [1]. Among the compendium of techniques using this principle, high performance liquid chromatography (HPLC) is the most important analytical technique used during the various steps of drug development and manufacturing. Methodology bases stems from separation, identification and quantification of the compounds present in a solution.

A high pressure pump is required to force the mobile phase (liquid) through the column (stationary phase, solid) at typical flow rates of 0.5-2mL/min. Once sample is injected, it goes through the column and, depending on the stationary phase, components are eluted. Then, they are detected by systems e.g. UV and/or fluorescence measurement devices, among others (see section of LCMS in appendix III). Detector examines the flow of liquid form the column and a chromatogram with peaks corresponding to the different components is shown.

Reversed phase (RP) has been the stationary phase used herein. This separation mode is based on the solvophobicity of the analytes and their thermodynamic partitioning between the mobile and stationary phases. The stationary phase is typically made of spherical silica beads with C18 alkyl chains covalently bound to the surface, a hydrophobic matrix which is largely based on their polarity. Basically, molecules are bound to the hydrophobic matrix in an aqueous buffer (polar) and eluted from the matrix using a gradient of organic solvent (non-polar). The elution process can be either isocratic, i.e. performed with a constant solvent composition, or gradient based, i.e. the solvent polarity is increased with time. If the analyte and the stationary phase are similar in chemical structure, intermolecular forces will favour the association. They will move more slowly through the column.

In this project, apart from the analytical HPLC for characterisation purposes, a preparative HPLC has been also used for purification of the synthesised peptides. Only difference lies on the column size for injection of higher amount of sample, and the collector device placed after the detector to recover the purified sample.

Mass spectroscopy (MS) and liquid chromatography-mass spectroscopy (LCMS)

As stated in section (a), alternatively HPLC can be also connected with other detectors such as a mass spectrometry (MS). Combination of both techniques is named LCMS, which provides high sensitivity and selectivity detection approach and potential identification of compounds in a mixture.

Briefly, MS provides structural data by measuring the weight of individual molecules in a sample. First, molecules are transformed into gas phase ions and these ionized compounds generate charged molecules or molecule fragments that are measured by their mass-to-charge ratios [2].

A MS instrument IS constituted by an ion source, a mass analyser and a detector. Vaporisation of the sample can be done by atmospheric pressure chemical ionisation (APCI) or electrospray ionization (ESI). Both are soft ionisation techniques that result in protonated or deprotonated molecules with low or no fragmentation. In this study, ESI mode was employed where sample molecules ionise in solution before they reach the source. On entering the evacuated source, they begin a desolvation process. There are two modes of detection: positive and negative ions. For a given compound M, the protonated $[M+H]^+$ ion, sodium and potassium adducts are commonly observed in detection of positive ions.

The mass analyser sorts the ions by their masses by means of electromagnetic fields [3]. In the LCMS utilised, a Single Quadrupole was used while there was a TOF (time of flight) for the MS device. Quadrupole mass analysers are four parallel metal rods where two of them have a direct current potential (U) applied while the others are linked to an alternating radio-frequency (rf) potential (V). The quadrupole acts as an m/z filter and by scanning values of U, V and rf the spectrum of m/z values can be passed to an ion detector. The TOF mass analyser is based on the time of flight of the ion through a drift tube. A direct relationship is observed between the m/z value and the time of flight.

LCMS applications comprise drug development, pharmacokinetic studies of pharmaceuticals and many investigations in bioanalysis. In this thesis, LCMS studies has been performed to detect free drug in the PGA-X-Doxy conjugates as well as to study if drug was released along the *in vitro* assays. LCMS system used was composed by an UPLC (ultra performance light chromatography), which retains the practicality and principles of HPLC while increasing the overall attributes of speed, sensitivity and resolution [4]. In UPLC the particle size in the stationary phase is decreased and consequently the flow rate of the mobile phase can be increased to attain faster separations and improve the resolution.

In addition, MS analysis has been carried out to identify the synthesised peptides and their PEGylated conjugates as well as monitoring their stability under different conditions. Doxy derivative was also characterised by this methodology.

Fast protein liquid chromatography, FPLC

As HPLC, FPLC is a liquid chromatography method base in the same principles explained (appendix III) and only it only differs in the use of a lower pressure (3-4MPa), although flow rates are relatively high (from 1 to 5mL/min) [5]. FPLC is generally applied to protein purification and allows purification scale up. FPLC columns design varies from ion exchange, gel filtration (size exclusion), hydrophobic interaction and affinity chromatography.

In the present thesis, FPLC column characteristics had been extrapolated for separating polymers conjugated to protein or peptides from the non-conjugated polymer or the free protein/peptide. In the case of RAGE pep conjugates, the cation exchange column was used. This resin is designed for the purification of large biomolecules such as PEG modified proteins. PEG is neutral and its conjugates exhibit lower average surface charge. Furthermore, PEGylation changes size of the protein. Both facts, larger size and lower charge contribute to separate reagents and products of the conjugation. By increasing the ionic force in the mobile phase, PEG, with one or two peptide molecules attached flow out of the column at different retention times.

Conformation in solution studies. DLS and SANS.

a) <u>Dynamic Light Scattering, DLS</u>

DLS is one form of spectroscopy, also namely Photon Correlation Spectroscopy (PCS). It is a useful non-invasive technique with well-established principles for determining size and size

distribution of molecules and particles in solution, typically in the submicron region [6]. It can be applied to a wide range of chemical engineering topics from simple macromolecule size measurements to critical phenomena and even monitoring aggregation kinetics.

When light contact the particles, a speckle pattern consisted of areas of bright light and dark areas appear. This is explained by the constructive (bright patch) or destructive (dark zone) interference by the surrounding particles with the scattered light. If in addition, particles are moving in a gas or liquid phase as defined by the Brownian motion, the constructive and destructive phase addition of the scattered light will cause the bright and dark areas to grow and diminish the intensity, i.e. the intensity appears to fluctuate. DLS measures the rate of intensity fluctuation and then uses this to calculate the size of the particles.
Relationship between the particle size and its velocity due to Brownian motion is defined in the Stokes-Einstein equation (equation 1) [7]. The hydrodynamic radius, R_h, is determined from the translational diffusion coefficient, D (in m^2s^{-1}). The radius measured in DLS is a value referred to how a particle diffuses within a fluid, therefore a "hydrodynamic" radius and it corresponds to a sphere that has the same translational diffusion coefficient as the particle. D depends not only on particle size but also on other factors as its surface structure or the ionic strength of the medium.

Sample preparation for DLS measurement either by filtration or centrifugation is a critical step to remove dust and artefacts from the solution. In our experiments, once conjugates were in solution they were filtered previous lyophilisation and then resuspended in known volumes of filtered solvent. Samples were measured, then filtered (0.02μm filters) and measured again.

In this study, DLS reported the size distribution of the PEGylated peptides as well as the PGA-X-Doxy conjugates. In a different scenario (chapter V.), DLS was useful to determine size reduction of the fibrillar TTR once the protein was incubated with the PGA-X-Doxy conjugates.

b) Small angle neutron scattering, SANS

SANS uses neutron scattering at small scattering angles to elucidate the structure in solution of compounds at length scales from 1 to 1000Å. This non-invasive methodology does not require use of chemical modification such as fluorescence labelling that could themselves affect the solution conformation In the subject that concerns us, this advanced technique helps to better understand the global and local structure of polymer drug conjugates in solution [8-10], owning the capability of elucidates the influence of drug type or loading on the solution conformation. For the analysis, physiological conditions can be reproduced (temperature, pH, ionic strength).

Our purpose in SANS analysis was based on the identification of possible differences in solution conformation of the doxy conjugates depending on their drug loading.

2. PROTOCOLS

Bradford Protein Concentration Assay

Background

The Bradford protein assay is one of several simple methods commonly used to determine the total protein concentration of a sample [12] . The method is based on the proportional binding of the dye Coomassie to proteins. Within the linear range of the assay (~5-25 mcg/mL), the more protein present, the more Coomassie binds. Furthermore, the assay is colorimetric; as the protein concentration increases, the colour of the test sample becomes darker. Coomassie absorbs at 595 nm. This dye appears to bind most readily to arginyl and lysyl residues of proteins (not to the free amino acids). This specificity can lead to variation in the response of the assay to different proteins, which is the main disadvantage of the method. The protein concentration of a test sample is determined by comparison to that of a series of protein standards known to reproducibly exhibit a linear absorbance profile in this assay. Although different protein standards can be used, we have chosen the most widely used protein as our standard - Bovine Serum Albumin (BSA).

There is no interference from cations nor from carbohydrates such as sucrose. However, detergents such as sodium dodecyl sulfate and triton x-100 can interfere with the assay, as well as strongly alkaline solutions.

Protocol

Solutions needed to perfom the test were:

- Bovine Serum Albumine (BSA) solution. Stock: 2mg/mL (To be prepared with PBS 0.1M).
- Bradford solution from Bio Rad Protein Assay. Keep in dark at 4°C.
- PBS 0.1M

The samples and stocks were maintained at 4°C during the experiment. For the calibration curve dilutions, 6 eppendorf tubes

were prepared and numbered as indicated in the table below. PBS amount required was placed in each eppendorf. Then, 100µL of the BSA stock was added in the tube 6. For the tube 5, the quantity required (70µL) was taken from the tube number 6. For the tube 4, 71.4µL were taken from the tube 5. For the tube 3, 50µL were taken from the tube4. Same protocol was followed until tube 2.

Tube number	Conc. BSA (mg/mL)	Vol. PBS (µL)	Vol. BSA (µL)
1	0	100	0
2	0.25	50	50
3	0.5	50	50
4	1	28.6	71.4
5	1.4	30	70
6	2	0	100

The samples were vortexed for 2 or 3 seconds and centrifuged (10000rpm, 4°C 12 min) and supernatants were placed into new epperdorfs. Samples were diluted with PBS to several concentrations to avoid possible saturation in measurements (1:10, 1:2, 1:3,…). Final volume of each sample was 20µL.

In a 96 well plate, 10µL sample or BSA were placed and then mixture with 200µL of the Bradford reagent. Plate was incubated at RT for 5min in the dark and subsequently, absorbance at 595nm using a UV-visible spectrophotometer was measured. Protein amount was determined using the calibration curve of BSA.

SDS-PAGE gel analysis of polymer-protein/peptide conjugates

Background

To determine either protein covalent conjugation to the polymeric carriers (i.e. TB-S-S-Tf, DB-S-S-Tf, etc) or complete purification from the non-conjugated protein, SDS-PAGE (Sodium Dodecyl Sulphate Polyacrilamide Gel Electrophoresis) technique was exploited, extensively reviewed elsewhere [13-15].

SDS-PAGE is based on molecule separation through their differences on size, shape or isoelectric point. The gel is a cross linked polymer matrix used to act as a support and promote the separation of the compounds.

Samples under evaluation are first denatured at high temperature exposure and afterwards negatively charged their mixture with an anionic detergent such as SDS, which denatures secondary and non-disulfide-linked tertiary structures and applies a negative charge to each protein in proportion to its mass. This loading buffer also contains a tracking dye, bromophenol blue, that is intercalated in presence of determined amino acids, allowing visualization of the protein. Once acrylamide gel is ready, samples mixed with a loading buffer are loaded in the wells of the gel and the transference process starts. It is applied an electric current to the gel which promotes protein migration through the matrix to the anode. As a pattern, a molecular weight marker is also run with the samples, making possible to evaluate the molecular weight of our samples and therefore helping to protein identification.

Protocol

Briefly, acrylamide gel assembly was performed as follows. Percentage of acrylamide was adapted depending on the desired band of MW. For Tf conjugates, 6% was used.

Samples and standards must be loaded in the gel at the same protein concentration, i.e. sample (a) with a concentration of protein = 20ug/µL. In 1.5mL eppendorfs, sample mixtures were prepared (sample + LB). Then, samples were heated for 7min at 95°C. Afterwards, samples were loaded into the gel.

Reagents recipes:

*LAMELY BUFFER (LB5X):*0.25M TRIS pH=6.8, 30% sacarose, 10%SDS, 0.5%bromophenol blue, 0.5M DTT. In the present work, tested samples presented disulphide bonds between the protein and the polymeric carrier. Therefore denaturing conditions with a LB without DTT were studied in parallel to the DTT original one.

RUNNING BUFFER 10X: for 1L of final volume, 144g/L glycine and 30.27g/L TRIS base were dissolved under strong agitation. Afterwards, buffer was autoclaved and store for further use.

RUNNING BUFFER 1X: 100mL of buffer 10X were diluted in 895mL of ddH_2O and 5mL of SDS 20% were added. After well mixing, solution was used.

GEL: Gel construction is divided in two steps due its two different parts. First, the *resolving buffer* that is on the bottom part of the gel. It is made of 5.79mL H_2O, 2.5mL TRIS buffer pH=8.8 1.5M, 1.5mL AA/Bis40%,0.1mL SDS 10%, 0.1mL APS 10% and 0.01mL TEMED. Mixture should be performed in this order and polymerisation starts immediately. Secondly, the *staking buffer* which is composed by of 2.42mL H_2O, 1mL TRIS buffer pH=6.8 0.5M ,0.5mL AA/Bis 40%, 0.04mL SDS 10%, 0.04mL APS10% and 0.004mL TEMED, which follows the same pattern.

Protocol

Two glass plates (outer and inner) were assembled into the casting frame, which was fitted into the casting stand. System was tested to not have any leakage and the mixture of resolving buffer was

added, followed by 50µL of butanol. 10-15min later, polymerisation had occurred and butanol was removed. Then, stacking buffer was added and immediately, the adequate plastic comb was placed. Once polimerisation finished, the plastic comb was removed and the two glasses with the gel were placed into the clamping frame and electrode assembly. After that, it was introduced in the electrophoresis box filled with running buffer 1X. The denaturalized samples mixted with the loading buffer were carefully loaded into the wells of the gel in a known order, as well as a molecular weight standard. Gel was run with constant current (90 V) 10min and after current was increased until 150V until it was observed the desired MW in the standard well.

Once the electrophoresis was finished, device was disconnected and dismounted. Gel was carefully detached from the glasses and buffer was removed with ddH_2O washes. For gel stainining, coomasie blue solution was incubated for 1h with the gel under constant agitation. For remove excess of stain and observe only sports belonging to the protein, gel was then incubated with a strong destain solution (10% HAcOH, 30% MeOH). Gel was photographed and analysed with Gel DocXR software.

Western Blot

The western blot (WB) or immunoblot is an analytical technique used to detect specific proteins in a given sample (i.e. from a tissue homogenate, cellular extract, polymer-protein conjugate solution, etc). By means of gel electrophoresis, first proteins are separated by the length of the polypeptide (denaturing conditions). In a second step, the proteins are then transferred from the gel to a membrane (typically nitrocellulose or PVDF), where they are detected through incubation with antibodies specific to the target protein.

In the present work, WB was useful to determine BBB crossing of TB-Tf. Brain homogenates were analysed by this technique for human Tf presence in rat brains after i.v. administration of TB-Tf.

Methodology

Gel electrophoresis has been already detailed in section IV.3.2.2.1. For WB analysis, Coomasie blue staining is not performed.

After all sample containing was perfectly visualised by electrophoresis, they were transferred to a membrane. This procedure is named electroblotting. The transference uses the same bases than SDS-PAGE technique although WB applies electric current in transversal direction instead in vertical, promoting protein migration out of the gel to the membrane. After complete migration to the membrane support, effectiveness is checked by its staining with coomasie or Ponceaus S dyes. Ponceau S is more common due to its higher sensitivity and, as it is water soluble facilitates stain removal. Afterwards, membrane is blocked. This step prevents non-specific binding by placing the membrane in a solution of BSA or non-fat dry milk (NFDM), with Tween 20. This protein in solution binds the membrane in all the places where there were no protein transferred from the gel, helping to reduce the noise in the WB result and eliminating positive false results.

After blocking the membrane, a incubation with a primary antibody is carried out. This antibody has to recognize only the protein of interest and bind it. Once incubation has been performed, membrane is rinsed and exposed to the secondary antibody which will bind the primary Ab. This second Ab is directly related with the animal specie which produced the first one, i.e. an anti-mouse secondary Ab will bind only any mouse-sourced primary antibody. Furthermore, secondary Ab bears biotin or an enzyme as alkaline phosphatase or horseradish peroxidase (HRP) with the aim of showing an enhanced signal to recognize the primary Ab. HRP-linked secondary Ab is the most exploited methodology where after the addition of quimioluminiscent agent (a substrate called luminal), a reaction occurs producing a luminescent signal proportional to the initial amount of the protein of interest. To capture that signal, the membrane is placed below a sensitive photographic film which captures the final image of the antibodies bound to the blot. Band densities of the different lanes can be directly compared providing information of the relative abundance of the protein of interest.

Reagents preparation

TRANSFER BUFFER: for 1L of final volume, 6g of TRIS BASE, 3.1g of boric acid were dissolved under agitation in 1L of ddH_2O.

BLOCKING BUFFER: 5g of non-fat dry milk were dissolved in 100mL of 0.05% Tween20.

Protocol

The PVDF membrane Thermo Scientific 0.45 µm (9x7cm) was placed in methanol for 1min for its activation. After quick drying, it was dropped in a box with transfer buffer. "sandwich" device was mounted following the order: a sponge on top of the black cassette (negative), three whatman paper (10x7cm), acrylamide gel, membrane, three whatman paper (10x7cm) (at this point air bubbles were removed), other sponge and finally the "sandwich" was closed (positive pole). Device was collocated inside the transfer box and electroblotting started at 4100mA for 2h at 4°C. The protein transference occur from the negative to the positive pole, e.g. from the gel to the membrane. A magnetic stirring bar was placed inside the box to allow agitation of the buffer.

Once the transference was finished, membrane was stained with Ponceau S for 5min under constant agitation. The proteins of interest were observed and after the membrane was washed with 0.025% PBS Tween 20 to remove the dye.

Afterwards, membrane blocking was performed by introducing it in blocking buffer in agitation during 1h at RT. Primary antibody used was transferrin (12A6), a mouse monoclonal antibody raised against transferrin of human origin. Ab was diluted in the blocking buffer 1:5000 and incubated 16h at 4ºC. Then, membrane was washed per duplicate with 0.05% PBS/Tween 20 for 10min. Incubation with a secondary Ab anti-mouse was performed for 2h at RT and again membrane washed with the same procedure.

Membrane was incubated 1min with ECL and then, cover immediately with a transparent film/cling wrap and then, exposed to X-ray film in the dark and revealed. Exposition time was optimised in order to be able to observe the desired signals.

BIBLIOGRAPHY

1. L. R. Snyder, J. J. Kirkland, and J.L. Glajch, *Practical HPLC method development.* 2nd ed.; John Wiley & Sons, Inc.: New York, USA, 1997.
2. Fenn, J.B., et al., *Electrospray ionization for mass spectrometry of large biomolecules.* Science, 1989. **246**(4926): p. 64-71.
3. A. El-Aneed, A. Cohen, and J. Banoub, *Mass spectrometry, review of the basics: Electrospray, maldi, and commonly used mass analyzers* Appl Spectrosc Rev, 2009. **44**: p. 210-230.
4. www.chromatographyonline.com, *Ultra Performance Liquid Chromatography (UPLC): an introduction.* Separation Sci Red, 2005: p. 8-14.
5. Sheehan, D. and S. O'Sullivan, *Fast protein liquid chromatography.* Methods Mol Biol, 2004. **244**: p. 253-8.
6. http://www.malvern.com.
7. Teraoka, I., *Polymer solutions: an introductionto physical properties.* John Wiley & Sons, Inc., 2002.
8. V. Gimenez, et al., *Demonstrating the importance of polymer-conjugate conformation in solution on its therapeutic output: Diethylstilbestrol (DES)-polyacetals as prostate cancer treatment.* J Control Release, 2012. **159 (2)**: p. 290-301.
9. A. Paul, et al., *Drug mimic induced conformational changes in polymer-drug conjugates characterized by Small Angle Neutron Scattering.* Biomacromolecules, 2010. **11**: p. 1978-1982.
10. A. Paul, M. J. Vicent, and R. Duncan, *Using small-angle neutron scattering to study the solution conformation of N-(2-hydroxypropyl)methacrylamide copollymer-doxorubicin conjugates.* Biomacromolecules, 2007. **8**: p. 1573-1579.
11. Heenan, R.K., et al., *SANS2d at the ISIS Second Target Station*, in *ICANS-XVII*

*17th Meeting of the International Collaboration on Advanced Neutron Sources*April 25-29, 2005: Santa Fe, New Mexico.

12. Bradford, M.A., *A rapid and sensitive method for the quantitation of microgram quantities of protein utilizing the principle of protein-dye binding.* Anal Biochem, 1976. **72**(248-254).

13. Bonifacino, J.S., *Electrophoresis and Immunoblotting.* Curr Protoc Cell Biol, 2011. **52**: p. 6.0.1-6.0.3.

14. Laemmli, U.K., *Cleavage of structural proteins during the assembly of the head of bacteriophage T4.* Nature, 1970. **227**(5259): p. 680-5.

15. O'Farrell, P.H., *High resolution two-dimensional electrophoresis of proteins.* J Biol Chem, 1975. **250**(10): p. 4007-21.

[APPENDIX III.]